MyosinVa and dynamic actin oppose minus-end directed microtubule motors to drive anterograde melanosome transport.

Christopher Lewis Robinson BSc (Hons)







Abstract

The intracellular transport of organelles and vesicles is thought to utilise both microtubules and actin filaments, which mediate long and short-range transport, respectively. Melanosomes, synthesised in melanocytes, are a convenient model organelle to study intracellular transport, since they are visible using brightfield microscopy. They are believed to be transported from the perinuclear area to the actin cortex along microtubules, and then captured by the myosin-Va/melanophilin/Rab27a complex which traffics them along actin filaments to the plasma membrane.

In contrast, data presented here demonstrate that anterograde melanosome transport relies only upon the actin cytoskeleton. Myosin-Va null melanocytes were used to test the importance of microtubules and actin on long-range organelle transport. In these cells, melanosomes cluster around the perinuclear area, but disperse into peripheral dendrites upon re-introduction of the myosin-Va gene. When this assay was repeated in the absence of microtubules, melanosomes still dispersed indicating that microtubule-based motors are not necessary for long-range anterograde trafficking. However, depolymerising F-actin, or freezing actin dynamics with latrunculin A or jasplakinolide inhibited the dispersion of pigment granules in myosin-Va null cells melanocytes and induced a clustered phenotype in WT melanocytes. This effect was abolished if microtubules were absent, suggesting that microtubules are only required for retrograde transport whilst dynamic actin is essential for anterograde melanosome transport. Moreover, when Kif5B was forcibly recruited to the melanosome membrane via an inducible dimerisation system, the melanosomes dispersed abnormally.

An siRNA knockdown screen of over 120 actin binding proteins identified several proteins including formin-1, Arpc1b, cofilin-1, γ-actin and spire1/2, which appear to be necessary for maintaining peripherally dispersed melanosomes. This evidence further underlines the importance of the actin cytoskeleton, rather than the microtubule network as previously thought, for the anterograde trafficking of melanosomes.

Contents

Acknowledgements xiv

Declaration xv

Abbreviations xvi

1 Introduction **1**

1.1 Modeling Intracellular Cargo Transport 2

1.1.1 Pigmented cells are excellent models for studying organelle transport 2

1.1.2 Melanogenesis 9

1.1.3 Defective lysosome related organelle trafficking leads to a number of syndromes 15

1.2 Microtubules and their associated molecular motors facilitate long-range organelle transport 17

1.2.1 Microtubules are dynamic tracks for kinesin and dynein 17

1.2.2 The kinesin superfamily 23

1.2.3 Role of kinesin in microtubule dynamics 31

1.2.4 Cytoplasmic Dynein 32

1.3 The actin cytoskeleton 38

1.3.1 Actin structure 38

1.3.2 Actin dynamics 39

1.4 The melanosome cooperative capture model 49

1.4.1 The tripartite complex 50

1.4.2 Evidence for long-range microtubule-dependent melanosome transport 56

1.5 Aims 57

2 Methods **58**

2.1 Cell Culture . . . 59

2.1.1 Murine Melanocytes . . . 59

2.1.2 NIH 3T3, HEK 293A and HeLa cell lines . . . 59

2.1.3 Melanophore cell culture . . . 60

2.1.4 Preparing and Thawing Cells Stocks . . . 60

2.1.5 Transfections . . . 60

2.2 Molecular Biology . . . 63

2.2.1 PCR . . . 63

2.2.2 Cloning . . . 64

2.2.3 Generating fusion proteins . . . 67

2.2.4 Generating adenoviral vectors . . . 70

2.2.5 Reverse-transcription PCR (RT-PCR) . . . 71

2.2.6 qRT-PCR . . . 72

2.3 Biochemistry . . . 76

2.3.1 Western Blotting . . . 76

2.3.2 Melanosome Purification . . . 78

2.4 Microscopy . . . 79

2.4.1 Fixed-cell Microscopy . . . 79

2.4.2 Live-cell Microscopy . . . 81

2.4.3 Image Analysis . . . 83

3 Identifying the long-range anterograde melanosome transporter **90**

3.1 Introduction . . . 91

3.2 Aims . . . 94

3.3 Results . . . 95

3.3.1 Determining the localisation of Kif5B in melanocytes via fluorescence microscopy . . . 95

3.3.2 Kif5B is not enriched in purified melanosomal fractions . . . 98

3.3.3 siRNA mediated knockdown of Kif5B did not result in melanosome clustering . . . 100

3.3.4 Evaluating kinesin isoform expression in wildtype melanocytes via RT-PCR . . . 103
3.3.5 Optimising the nocodazole dose murine melanocytes can tolerate . 107
3.3.6 Standardising cell shape enables precise quantification of melanosome distribution. . . . 112
3.3.7 Treating wildtype melanocytes with cytochalasin D induces partial melanosome clustering . . . 118
3.3.8 Treating wildtype melanocytes with latrunculin A closely mimics the melan-dilute phenotype . . . 123
3.3.9 A dynamic actin network is necessary to maintain peripherally dispersed melanosomes at steady state . . . 130
3.3.10 Nanomolar doses of JK and LatA are sufficient to perturb the actin cytoskeleton. . . . 134
3.4 Discussion . . . 139
3.4.1 Kif5B could not be detected on the melanosome membrane . . . 139
3.4.2 The melanosome distribution of melanocytes following Kif5B knockdown is identical to that of wildtype cells . . . 142
3.4.3 Depolymersing F-actin in wildtype melanocytes with CytD induces melanosomes to partially cluster . . . 142
3.4.4 Intermediate filaments may play a role in the morphology of the microtubule network and actin cytoskeleton . . . 144
3.4.5 Both sequestering G-actin or stabilising F-actin in wildtype melanocytes drives minus-end directed melanosome transport . . . 145
3.4.6 Standardising melanocytes does not affect melanosome distribution 147

4 Myosin-Va and F-actin work in opposition to microtubule-based motors to drive long-range melanosome transport 149

4.1 Introduction . . . 150
4.2 Aims . . . 152
4.3 Results . . . 153
4.3.1 Anterograde melanosome transport is not inhibited by noc treatment in murine melanocytes . . . 153

4.3.2 Treating *Xenopus laevis* melanophores with noc does not inhibit anterograde melanosome transport 156
4.3.3 Optimising the rescue assay using micropattern chips 159
4.3.4 Anterograde melanosome transport is enhanced following noc treatment 167
4.3.5 Forcibly recruiting Kif5B to the melanosome membrane in melan-dilute cells results in their abnormal distribution 171
4.3.6 Perturbing actin dynamics inhibits anterograde melanosome transport 180
4.3.7 CytD washout experiments indicate that actin regrows rapidly from the plasma membrane 184
4.3.8 Microtubules are required for retrograde melanosome transport . . 193
4.4 Discussion 199
4.4.1 Identifying melan-dilute cells expressing GFP-myosin-Va based on their fluorescence intensity 199
4.4.2 Noc treating cells has no affect on long-range anterograde melanosome transport 199
4.4.3 A dynamic actin cytoskeleton is crucial for anterograde melanosome transport 201
4.4.4 F-actin predominantly regrows from the plasma membrane after CytD treatment and is concomitant with melanosome redispersion 202
4.4.5 Investigating long-range melanosome transport using activatable motors shows Kif5B is inefficient at translocating this cargo 203
4.4.6 Microtubules are required for minus-end directed melanosome transport 204
4.4.7 Summary 205

5 Several actin-binding proteins play a role in melanosome transport 207

5.1 Introduction 208
5.2 Aims 209
5.3 Results 210
5.3.1 An siRNA screen revealed several actin-binding proteins are important for maintaining peripherally dispersed melanosomes 210

5.3.2 SMIFH2 and CK666 drug treatments do not perturb melanosome distribution . . . 218
5.3.3 Formin-1 and Arc1b knockdown does not grossly affect F-actin morphology . . . 221
5.3.4 Identifying the formin-1 isoform(s) expressed in murine melanocytes 223
5.3.5 Investigating the sub-cellular localisation of actin-binding proteins important for maintaining peripherally dispersed melanosomes . . . 226
5.3.6 Spire1 and spire2 are involved in anterograde melanosome transport 231
5.3.7 Several other actin binding proteins also appear to affect melanosome distribution . . . 234
5.4 Discussion . . . 243
5.4.1 Linear actin cables are necessary for anterograde melanosome transport . . . 243
5.4.2 $\gamma-$actin and cofilin-1 knockdown confirm the results from LatA and JK treatment . . . 245
5.4.3 Arpc1b is necessary for anterograde actin-dependent melanosome transport . . . 246
5.4.4 A number of actin-binding proteins may contribute to long-range anterograde melanosome transport . . . 247
5.4.5 F-actin is nucleated by the centrosome . . . 250
5.4.6 Summary . . . 251

6 Summary **255**

7 Appendix **260**

Bibliography **283**

List of Figures

1.1 Melanophores can cluster or disperse their melanosomes in response to chemical stimuli 5

1.2 Melanophilin from zebrafish and frog contains a predicted PKA phosphorylation site not present in the mouse or human protein 5

1.3 Myosin-Va, Mlph and Rab27a null melanocytes exhibit clustered pigment granules compared to the wildtype cells 6

1.4 Different melanosome biogenesis pathways 11

1.5 The eumelanin biosynthetic pathway 13

1.6 The structure of microtubules 19

1.7 The γ-TuRC complex 21

1.8 The structure of kinesin-1 25

1.9 Kinesin-1 motor and neck domains 25

1.10 Proposed models for how kinesin translocates along microtubules 27

1.11 The catalytic cycle of kinesin-1 29

1.12 The structure of kinesin-1 tetramer 30

1.13 The structure of cytoplasmic dynein 33

1.14 The catalytic cycle of dynein 35

1.15 The dynactin complex 37

1.16 Actin treadmilling 40

1.17 Formin mediated actin nucleation 41

1.18 Schematic outlining the exon and domain structure of the 6 different formin-1 isoforms 43

1.19 The domain structure of Spire 44

1.20 The Arp2/3 complex 46

1.21 The structure of non-muscle myosin-II 48

1.22 The cooperative capture model 50
1.23 The Rab cycle 52
1.24 Myosin-Va structure 53
1.25 Myosin-Va catalytic cycle 54
1.26 The structure of melanophilin and the tripartite complex 55

2.1 Vector maps depicting how KIF△MD was generated 68
2.2 Manually calculating the pigment ratio 86
2.3 Calculating the average distance of actin from the plasma membrane 88

3.1 Kif5B could not be detected on the melanosome membrane via immunofluorescence microscopy 97
3.2 Kif5B is not enriched in melanosomal fractions 99
3.3 Knocking down KIF5B induced clustering of mitochondria but not melanosomes 102
3.4 Comparing the expression of KIF5B and KIF3A-C in murine melanocytes and NIH3T3 cells 104
3.5 Comparing the expression profile of all known KIF isoforms in murine melanocytes and NIH3T3 cells via RT-PCR 105
3.6 Treatment with 1μM noc for 1 hour is sufficient to deplete melanocytes of microtubules 110
3.7 Live cell imaging confirms the microtubule network becomes significantly depolymerised after 1 hour in the presence of 1μM noc 111
3.8 Standardising melanocyte morphology allow precise quantification of melanosome distribution 115
3.9 Melanosomes remain peripherally dispersed in wildtype melanocytes after noc treatment 116
3.10 Noc treatment does not affect melanosome distribution in melan-dilute cells at steady state 117
3.11 Micromolar doses of cytochalasin D induce melanosomes to cluster. 119
3.12 Cytochalasin D specifically depolymerises F-actin. 121
3.13 Micropattern chip analysis reveals that CytD induces statistically significant melanosome clustering compared to the vehicle control 122

3.14 High (5μM - 0.5μM) doses of LatA for 30 minutes cause melanosomes to cluster, but also disrupts cell morphology 124
3.15 Low (50nM - 25nM) doses of LatA for 16 hours induces perinuclear melanosome clustering without affecting cell morphology 126
3.16 Actin density in melan-a cells remains largely unaffected by 10nM-50nM LatA treatment for 16 hours 127
3.17 Treating standardised melan-a cells with 25nM LatA for 16 hours results in a clustered phenotype 128
3.18 A sub-population of standardised melan-a cells treated with LatA exhibit asymmetric clustering 129
3.19 High (500nM) doses of JK cause cell death after 4 hours 131
3.20 Melan-a cells treated with low (10-50nM) doses of JK exhibit melanosomes that are aggregated around the perinuclear area 132
3.21 Standardised wildtype melanocytes treated with 10nM JK for 16 hours phenocopy melan-dilute cells 133
3.22 FACS data reveals that 25nM LatA is sufficient to deplete cells of quantifiable amounts of F-actin 135
3.23 10nM JK for 30 minutes is sufficient to inhibit F-actin turnover 137

4.1 Melan-leaden cells transfected with MLPH-GFP could be rescued after treatment with either DMSO or noc 155
4.2 *Xenopus laevis* melanophores can disperse their melanosomes in the absence of microtubules 158
4.3 The fluorescence intensity of antibody stained cells is not a reliable indicator of whether they have been transfected with myosin-Va-GFP 160
4.4 Total population of melan-dilute cells transfected with GFP-myosin-Va . . . 161
4.5 Reducing autofluorescence by imaging melanocytes live does not help determine if a cell is expressing GFP-myosin-Va based on fluorescence intensity 163
4.6 Staining with Alexa-568 secondary antibodies reduces autofluorescence and allows for transfected cells to be identified based upon their fluorescence intensity. 165

4.7 Total population of melan-dilute cells transfected with GFP-myosin-Va and stained with Alexa-568 secondary antibodies 166
4.8 Melan-dilute cells transfected with GFP-myosin-Va rescued to the same extent regardless of whether microtubule were present 169
4.9 Partial cell collapse does not skew either PDR or line plot measurements . 170
4.10 Outline of the constructs used for the inducible dimerisation experiments . . 173
4.11 The distribution of melanosomes forcibly coupled to Kif5B appears abnormal 174
4.12 Depolymersing microtubules blocks the accumulation of Kif5B-motor and myosin-Va-tail at the dendritic tips 177
4.13 Depolymersing microtubules blocks the accumulation of Kif5B-motor at the dendritic tips 178
4.14 Myosin-Va-tail alone cannot redistribute pigment granules in melan-dilute cells 178
4.15 Forcibly recruiting myosin-Va-motor to melanosome membranes in melan-dilute cells leads to normal pigment granule dispersion 179
4.16 Perturbing the actin cytoskeleton inhibits long-range anterograde melanosome transport 181
4.17 LatA treatment does not affect myosin-Va targeting to the melanosome membrane 182
4.18 JK treatment appears to disrupt myosin-Va targeting to the melanosome membrane 183
4.19 CytD washout from melan-a cells indicates that actin regrows from the plasma membrane 185
4.20 CytD washout from melan-dilute cells reveals actin regrowth is much faster compared with melan-a cells 187
4.21 CytD washout from melan-leaden cells reveals actin regrows from the plasma membrane on a similar timescale to the melan-a cells 189
4.22 Quantification of actin dispersion during CytD washout experiments. 190
4.23 Monitoring CytD washout live shows cortical actin recovers within 3-6 minutes whilst melanosomes redisperse within 30 minutes. 192
4.24 CB-D does not appear to inhibit retrograde organelle transport 196
4.25 Cilliobrevin D does not inhibit retrograde melanosome transport 197

4.26 Depolymerising microtubules inhibits retrograde melanosome transport induced by JK 198
4.27 Dynamic actin is required to oppose minus-end directed microtubule-dependent melanosome transport 206

5.1 An siRNA knockdown screen revealed several actin-binding proteins are important for maintaining peripherally dispersed melanosomes 214
5.2 Transfecting melanocytes with individual, rather than pooled, oligonucleotides targeting γ-actin, formin-1, Arpc1b and cofilin-1 resulted in different levels of melanosome clustering 215
5.3 qRT-PCR revealed that the siRNA oligonucleotides used are effective in knocking down their respective mRNA targets 216
5.4 Both formin-1 and Arpc1b are effectively knocked down at the protein level by at least 1 of the 4 oligonucleotides tested. 217
5.5 Treating wildtype melanocytes with SMIFH2 or CK666 does not phenocopy formin-1 and Arpc1b knockdown 220
5.6 Knocking down formin-1 and Arpc1b does not grossly affect actin morphology 222
5.7 Determining the specific isoform(s) of formin-1 expressed in murine melanocytes 224
5.8 Investigating the sub-cellular localisation of formin-1 using antibody labelling 228
5.9 Investigating the sub-cellular localisation of Arpc1b using antibody labelling 229
5.10 Investigating the sub-cellular localisation of formin-1 and Arpc1b using fusion proteins 230
5.11 Knocking down both spire1 and spire2 in wildtype melanocytes results in melanosome clustering 232
5.12 Quantification of the extent of melanosome clustering caused by knock down of spire1 and spire2 233
5.13 Example images from the two siRNA screens showing phenotypes arising from knocking down certain actin-binding proteins. 242
5.14 Formin-1, spire1/2, Apr2/3 and cofilin-1 complex create a dynamic F-actin network with filament barbed ends subtly polarised towards the plasma membrane 252

5.15 Following formin-1 or spire1/2 knockdown, F-actin is more randomly polarised, resulting in retrograde microtubule-dependent transport being favoured 253

5.16 Following Arpc1b knockdown, F-actin filaments become shorter, resulting in retrograde microtubule-dependent transport being favoured 254

7.1 Murine melanocyte cell lines used in this study 281

7.2 GFP-myosin-Va intensitiy Vs melanosome dispersion radius 282

List of Tables

1.1 Components of the BLOC and AP-3 complexes 14

2.1 Volumes used for passaging tissue culture cells 59
2.2 Reagents used for plasmid DNA transfection 61
2.3 Reagents used for siRNA transfection. 62
2.4 Thermocycler setting used for routine PCR. 63
2.5 Thermocycler settings used for site-directed mutagenesis. 63
2.6 Agarose gel components 66
2.7 Thermocycler setting used to sub-clone formin-1 into pENTR-EGFP-C2. . . 69
2.8 Primer and probe sequences for qRT-PCR targets. 73
2.9 Components of SDS-PAGE gels 76
2.10 Microscope settings used for acquisition of micro-pattern chips. 84
2.11 Dilutions of cell stains and antibodies used for immunofluorescence and western blotting 89

3.1 Summary of the expression levels of KIF isoforms from murine melanocytes and NIH 3T3 cells determined by RT-PCR 106
3.2 Percentage of membrane, stress fibre and mesh actin which makes up the immobile fraction in melan-a and melan-leaden cells after treatment with either 0.1% DMSO or 10nM JK for 30 minutes, calculated from the one-phase association fit data given in Figure 3.23b.ii, c.ii, d.ii & e.ii. The percentage of actin making up the mobile fraction is given in brackets. 138

5.1 Determining the specific isoform(s) of formin-1 expressed in murine melanocytes 225
5.2 - Results from the initial siRNA screen for actin-binding proteins involved in maintaining peripherally dispersed melanosomes in wildtype cells. . . . 235

5.3 - Results from the second siRNA screen to identify actin-binding proteins involved in maintaining peripherally dispersed melanosomes in wildtype cells. 239

7.1 Primers used in the KIF RT-PCR screen. 261

7.2 siRNA sequences used to test the involvement of actin-binding proteins in melanosome transport. 265

Acknowledgements

First and foremost I wish to thank my supervisor, Dr Alistair Hume, for his guidance and support during the past four years, without which this project would not have been possible. I am also especially grateful for the time he spent reading and commenting on this thesis. I would also to thank my co-supervisor Dr Sally Wheatley for her input.

Thanks also to Dr Richard Evans for his efforts developing the micropattern assay, his support discussing experiments, and, of course, his humour (and the many discussions about cars) as well as Deb Briggs for all her practical help in the lab (and industrious cloning abilities). You were both great to work with.

I would also like to extend my thanks to everyone in the lab, each of whom has helped me in some way, and more generally to the entire School of Life Science.

I would also like thank the following people for their contribution to this project:

Dr Emma King and Ian Ward for their help with widefield microscopy and Tim Self for his help with confocal microscopy (all University of Nottingham).

Dr Andy Bennett for access to his qRT-PCR instrument along with Nikki De Vivo and Monika Owen for their helpful guidance on sample prep and setting up the equipment (all University of Nottingham).

Dr Vince Hearing (National Institutes of Health) for kindly gifting the anti-tyrosinase antibody used in Chapter 3.

Dr Christina Wiesner and Stefan Linder (both University Medical Center Eppendorf) for gifting the KIF5B construct used in Chapter 3 and 4.

Prof David Stephens (University of Bristol) for his suggestions regarding Kif5B reagents.

Declaration

I declare that this thesis and the work presented in it are my own and has been generated by me as the result of my own original research, under the supervision of Dr Alistair Hume at the University of Nottingham, with the following exceptions:

- Samples for FACS analysis in Chapter 3 were prepared by Dr Alistair Hume, and FACS performed by Dr David Onion.
- GFP-myosin-Va, GFP-myosin-Va-MD-FKBP, GFP-myosin-Va-TD-FRB and KIF5B-1-810-FKBP construct used in Chapter 4 were generated by Deb Briggs.
- The positive control A/C heterodimeriser experiment where GFP-myosin-Va-motor was recruited to GFP-myosin-Va-tail in Chapter 4 was carried out by Dr Richard Evans.

Christopher Robinson, September 2015.

Abbreviations

ADF	Actin Depolymersing Factor
ADP	Adenosine Diphosphate
AMP	Adenosine Monophosphate
AP	Adaptor Protein
APS	Ammonium Persulfate
ATP	Adenosine Triphosphate
BLOC	Biogenesis of Lysosome-related Organelle Complex
BSA	Bovine Serum Album
cAMP	Cyclic AMP
CB-D	Ciliobrevin D
CHS	Chediak-Higashi Syndrome
CHX	Cyclohexamide
CLASP	Cytoplasmic Linker Associated Protein 1
CytD	Cytochalasin D
DAD	Diaphanous Autoregulatory Domain (relating to formin)
DAPI	4',6-diamidino-2-phenylindole
DCT	Dopachrome Tautomerase
DMEM	Dulbeco's Modified Eagle Medium
DHC	Dynein Heavy Chain
DHICA	5,6-dihydroxyindole-2-carboxylic aciod
DOPA	3,4-dihydroxyphenylalanine

DMSO Dimethyl Sulfoxide

EB End-binding Protein

ELC Essential Light Chain (relating to NMM)

EM Electron Microscopy

F-actin Filamentous Actin

FBS Fetal Bovine Serum

FH Formin Homology

FYVE Fab1/YOTB/Vac1/EEA1 (relating to Spire)

G-actin Globular Actin

GAP GTPase Activating Protien

GBD GTPase-binding Domain (relating to formin)

GC γ-Tubulin Complex

GDI Rab GDP Dissociation Inhibitor

GDP Guanosine Diphosphate

GEF GTPase Exchange Factor

GEP GTPase Exchange Protein

GMP Guanosine Monophosphate

GMP-PMP Guanosine 5'-(β, γ-imido)triphosphate (non-hydrolysable GTP analogue)

GPCR G-protein Coupled Receptor

GS Griscelli Syndrome

GTP Guanosine Triphosphate

HPS Hermansky-Pudlak Syndrome

IC Intermediate Chain (relating to dynein)

JK Jasplakinolide

JMY Junction Mediating Regulatory Protein

KHC Kinesin Heavy Chain

KIND Kinase Non-Catalytic C-Lobe Domain (relating to Spire)

KIF Kinesin superfamily protein

Kif5B Protein encoded by the KIF5B gene

KLC Kineisn Light Chain

LatA Latrunculin A

LC Light Chain (relating to dynein)

LIC Light Intermediate Chain (relating to dynein)

LRO Lysosome-related Organelle

MAP Microtubule-associated Protein

MD Motor Domain

Mel Melatonin

Mlph Melanophilin

αMSH αMelanocyte Stimulating Hormone

MT Microtubules

MTOC Microtubule Organising Centre

MyoVa MyosinVa

NMM Non-muscle Myosin

NPFs Nucleation Promoting Factors

Noc Nocodazole

PBS Phosphate Buffered Saline

PDR Pigment Dispersion Radius

PFA Paraformaldehyde

Pi Inorganic Phosphate

PKA Protein Kinase A

PKC Protein Kinase C

PMA Phorbyl 12-myristate 13-acetate

REP Rab Escort Protein

RGGT Rab Geranylgeranyl Transferase

RILP Rab Interacting Lysosomal Protien

RLC Regulatory Light Chain (relating to NMM)

SDS-PAGE Sodium Dodecyl Sulphate - Polyacrylamide Gel Electrophoresis

SKIP Sif and Kinesin Interacting Protein

+TIPs Microtubule Plus-End Tracking Proteins

γ-TuRC γ-Tubulin Ring Complex

TYR Tyrosinase

TYRP1/2 Tyrosinase-related Protein-1/-2

Utr Utrophin

WASH WASP/Scar Homology

N-WASP Neural-WASP

WASP Wiskott-Aldrich Syndrome Protein

WAVE WASP-family Verprolin Homology

WCA WASP Homology, Connector Region and Acidic Peptide

WH1/2 WASP Homology-1/-2

WHAMM WASP Homolog Associate with Actin Membranes and Microtubules

Chapter 1

Introduction

1.1 Modeling Intracellular Cargo Transport

The fact that cells are able to transport membrane bound cargo was first reported over two centuries ago by the Italian botanist Bonaventura Corti from observations of the green algae *Chara* (Corti, 1774). The precise spatiotemporal regulation of both organelles and vesicles is now recognised as a crucial process for the viability of all eukaryotic cells. For example, it is essential that the mammalian oocyte extrudes one set of chromosomes before fertilisation can take place, which is achieved by transporting one of the meiotic spindles to the cell cortex (McNally, 2013). In secretory cells, such as those of the immune system, not only do lytic granules need to be transported to the plasma membrane in order to kill pathogens (Kurowska et al., 2012) but the Golgi apparatus must also be precisely orientated such that secretions are directed towards the correct part of the membrane (Yadav and Linstedt, 2011). Mitochondria are also known to move to areas of high metabolic demand in neuronal cells (Sheng and Cai, 2012), whilst areas which contain large numbers of stationary mitochondria may promote axon branching (Spillane et al., 2013). Furthermore, the distribution of lysosomes has also been shown to change in response to cell starvation (Korolchuk et al., 2011).

Likewise, the transport of vesicles also makes possible a number of essential processes such as endocytosis, phagocytosis and exocytosis (Doherty and McMahon, 2009; Flannagan et al., 2012; Jahn and Fasshauer, 2012; Wu et al., 2014), as well as the localisation of mRNA molecules, which allows cells to spatiotemporally regulate the concentration of a particular protein (Besse and Ephrussi, 2008).

1.1.1 Pigmented cells are excellent models for studying organelle transport

Cells that are specialised to synthesis the black pigment eumelanin within single membrane-bound organelles termed melanosomes (Marks and Seabra, 2001) are highly useful to study organelle transport, since unlike other organelles and vesicles they can be monitored using brightfield or phase contrast microscopy. This has the advantaged of not relying on the over-expression of fluorescent fusion proteins to mark the organelles, which can perturb normal cellular function.

Two melanosome-containing cell types exist which are routinely used to study organelle transport: melanophores, a type of chromatophore found in the dermis, epidermis and scales of ecotherms (Andreas and Nilsson, 2011) and melanocytes - mammalian cells found in the

lower epidermis as well as hair follicles (Cichorek et al., 2013).

Both melanophores and melanocytes are derived from neural crest cells (Budi et al., 2008), although they serve different functions. While melanophores are capable of transferring their pigment granules to neighbouring keratinocytes (discussed further in section 1.1.1.3), they also function as chromatophores which are instrumental in providing camouflage for the animal. To achieve this, melanophores have evolved mechanisms to cluster and disperse their melanosomes which causes a lightening or darkening of the animal's skin (Nilsson and Wallin, 1997). This process has been shown to occur over reasonably short time scales, with pigment dispersion taking only 15 minutes in the melanophores of some fish, such as the black tetra (*Gymnocorymbus ternetzi*), allowing the animal to quickly adapt to environmental changes (Rodionov et al., 1991).

In contrast, mammalian skin cannot undergo rapid colour change. Therefore melanocytes fulfill a different biological function to melanophores - namely providing the surrounding keratinocytes with mature, darkly pigmented melanosomes which form a cap around the nucleus, thereby causing the skin to tan which protects the organism's DNA against damage from UV irradiation (Ando et al., 2012). Therefore, although fast bi-directional transport has been observed in mammalian melanocytes (Wu et al., 1998), it is unlikely to be a prerequisite for melanocyte function, since skin tanning is a much slower process compared to the colour changes observed in many cold-blooded animals. Therefore, although kinesin and dynein are thought to be responsible for the bi-directional transport of pigment granules in both melanophores and melanocytes (as discussed in section 3.1), it is possible that melanophores have evolved mechanisms to increase the speed of this process.

1.1.1.1 Melanophores as model cells to study organelle transport

Melanophores have long been used as a model cell type in which to study organelle transport due to the fact that pigment granules can be stimulated to undergo rapid anterograde or retrograde transport via chemical treatment (Figure 1.1). This phenomenon was first observed in 1917 when frog skins treated with bovine pineal extracts became lighter in colour (McCord and Allen, 1917), due to aggregation of the melanosomes, with the chemical responsible for this effect later identified as melatonin (5-methoxy N-acetyltryptamine)(Lerner et al., 1960).

Melatonin, synthesised from the amino acid tryptophan in the pineal gland (Pevet, 2002),

exerts it effect through three different G-protein coupled receptors (GPCRs): Mel_{1a} and Mel_{1b} (also designated $MT_1$and MT_2, respectively), which are expressed in mammals, birds, fish and amphibia and Mel_{1c}, which is expressed only in birds, fish and amphibia (Reppert et al., 1995). Upon binding to the melatonin receptor, melatonin stimulates the activation of Gi protein, which causes a reduction in intracellular cAMP via inhibition of adenylate cyclase (White et al., 1987; Hurley, 1999; Sugden and Rowe, 1992). Reduction in intracellular cAMP also has the effect of reducing protein kinase A (PKA) activity (Tasken and Aandahl, 2004). It has been suggested that phosphorylation of melanophilin by PKA may inhibit dynein from binding the melanosome membrane (at least in cells where melanosome distribution is sensitive to cAMP levels), since melanosomes in zebrafish melanophores containing a truncated version of melanophilin tended to remain clustered due to the effect of dynein (Sheets et al., 2007). Interestingly, zebrafish melanophilin contains two predicted PKA phosphorylation motifs (R-R-X-S/T; Ubersax and Ferrell Jr 2007) which are lacking from either human or mouse melanophilin - organisms whose melanosome distribution is insensitive to intracellular cAMP concentration (see Figure 1.2). Other evidence also indicates that PKA can directly phosphorylate the light intermediate chain of dynein, a minus-end directed motor protein which is essential for the retrograde transport of a large number of different cargo, including melanosomes (as discussed in section 1.2.4). Phosphorylation of this motor has also been shown to cause the dispersion of lysosomes and late endosomes, thereby suggesting the phosphorylation of dynein can regulate individual organelle distribution (Scherer and Vallee, 2011). It has also be shown that the phosphatase PP2A plays a role in melanosome clustering, since the overexpression of this protein leads to the aggregation of pigment granules in *Xenopus laevis* melanophores (Reilein et al., 1998).

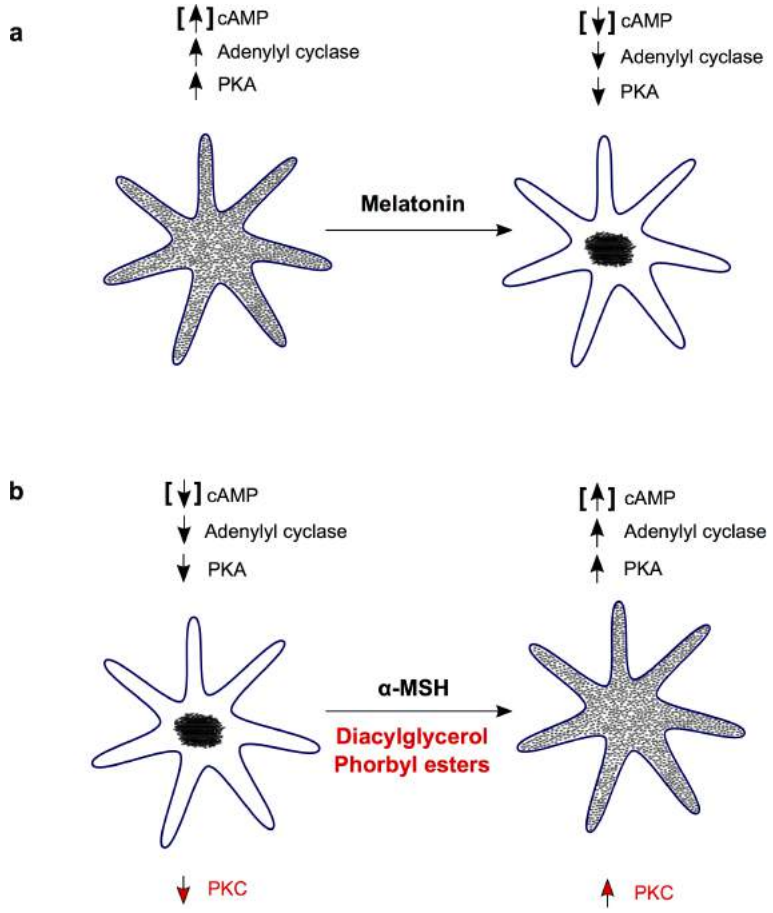


Figure 1.1 - Melanophores can cluster or disperse their melanosomes in response to chemical stimuli. (a) Treatment of melanophores with melatonin causes a decrease in intracellular cAMP concentration through the inhibition of adenylyl cyclase. This in turn inhibits protein kinase A (PKA), which requires cAMP to be active. In this situation, the action of phosphatases dominates allowing retrograde molecular motors to attach to the melanosome membrane, leading to clustering of the organelles. (b) Conversely, treatment of melanophores with αMSH leads to adenylyl cyclase activation and a concomitant increase in intracellular cAMP concentration. PKA therefore becomes active, phosphorylating its target proteins which inhibit retrograde motors from binding the melanosome membrane, resulting in organelle dispersion. Alternatively, treating melanosomes with diacylglycerol or phorbyl esters which activate protein kinase C (PKC) also leads to dispersion of the pigment granules. [↑] = high concentration, [↓] = low concentration, ↑ = high activity, ↓ = low activity.

```
Dr   HDEEHMDASEAQRYKQMRKTKRLLSVHPMDLEID-DYAVHSRRQSVQYIHDDRGQRNDLE 226
Xt   EDEDLIDSAEAQRYNMMRKTKRKLSVHPYDFDMDSEYSTQSRRQSMQLSP--TLEQDVFK 238
Mm   DGD--LDTEARDQPLNSKKKKRLLSFRDVDFEEDSDHLVQPCSQTLGLSS-VPESAHSLQ 224
Hs   DGEPGSEAQAQAQPFGSKKK-RLLSVHDFDFEGDSDDSTQPQGHSLHLSS-VPEARDSPQ 225

Dr   YNSEIYHQHQQRMNRRKSLDRFSRPDDGLYS--ENRMVRARSLSKINSSMAPRQIYLDTS 284
Xt   SFSERPSTGRDATSQKESLIAEADLASMFHHILQEQGQNAASPEQEFSTEVRLTVNSRRL 298
Mm   SLSGEPYSEDTTSLEPEGLEETGARALGCHPSPEVQPCSPLPSGEDAHAELDSPAASCKS 284
Hs   SLTDESCSEKAAPHKAEGLEEADTGASGCHSHPEEQPTSISPSRHGALAELCPPGGSHRM 285
```

Figure 1.2 - Melanophilin from zebrafish and frog contains a predicted PKA phosphorylation site not present in the mouse or human protein. Melanophilin from zebrafish (*Danio rerio*; Dr) contains 2 predicted PKA phosphorylation sites (R-R-X-S/T), while the protein from frog (*Xenopus tropicalis*; Xt) contained 1 such site (outlined in red boxes). However, neither human (*Homo sapiens*; Hs) or mouse (*Mus musculus*; Mm) melanophilin contained this PKA phosphorylation site, suggesting it may be unique to species which can cluster and disperse their melanosomes in response to intracellular cAMP levels. Figure adapted from Sheets et al. 2007.

Conversely, treating melanophores with αMSH (melanocyte stimulating hormone) induces the dispersion of pigment granules. αMSH binds to the melanocortin 1 receptor

(MC1R) - a GPCR which, when activated, stimulates adenylyl cyclase via the protein Gs, resulting in an increase in intracellular cAMP (Mas et al., 2003). This is turn drives the dispersion of melanosomes through the inhibition of retrograde forces. Alternatively, melanosome dispersion in melanophores can also be triggered through a protein kinase C (PKC) dependent pathway (Sugden and Rowe, 1992), which is itself activated by diacylglycerol and phorbyl esters (Newton, 1995). The fact that the pigment granules contained within melanophores can be made to rapidly cluster and disperse in response to external chemical stimuli therefore make them an excellent model system in which to study organelle transport.

1.1.1.2 Melanocytes as a model cell type to study organelle transport

The melanophores of fish, birds and amphibia have been extensively used as a model for organelle transport, due to the ease of invoking melanosome transport by treatment with either melatonin or αMSH. However, mammalian melanocytes are perhaps even better models for understanding how organelle transport is regulated, not least because they are more representative of membrane trafficking in human cells.

Additionally, over 50 different loci in mouse have been shown to affect coat colour (Jackson, 1991). Of these, 3 loci in particular have been extensively studied since mutants are not defective for either melanosome biogenesis or melanin synthesis, but rather the transport of these organelles is inhibited. This results in a phenotype whereby the pigment granules clump around the perinuclear area (Figure 1.3), which manifests itself at the organismal level as a greying of the coat colour in C57BL/6 mice since melanosomes are not transferred into neighbouring keratinocytes (Ando et al., 2012).

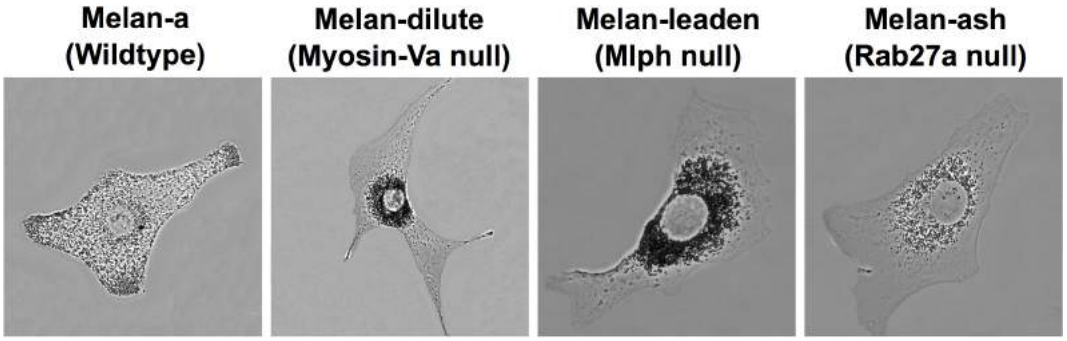


Figure 1.3 - Myosin-Va, Mlph and Rab27a null melanocytes exhibit clustered pigment granules compared to the wild-type cells. Immortalised melanocytes from C57BL-6 mice have melanosomes which are dispersed throughout the cell in wildtype background, but clustered around the perinuclear area if either the motor protein myosin-Va, the effector protein melanophilin (Mlph) or the small GTPase Rab27a are absent.

The best studied of these 3 loci is the *dilute* locus, located on mouse chromosome 9, for

which over 200 mutations have been identified that result in the clustering of melanosomes and the lightening of the coat colour in black mice (Strobel et al., 1990). The *dilute* locus encodes the actin-based motor protein myosin-Va (Mercer et al., 1991), which must therefore play some role in trafficking melanosomes to the melanocyte plasma membrane. The second locus involved in regulating melanosome transport is *ashen*, which is also found on mouse chromosome 9 (Lane and Womack, 1979). The small GTPase Rab27a which has been shown to be the product of the *ashen* locus (Wilson et al., 2000). This protein localises to the melanosome membrane (Hume et al., 2001; Lopes et al., 2007) and is required for the targeting of myosin-Va (Wu et al., 2001). Finally, the *leaden* locus which resides on mouse chromosome 1 (Silvers, 1979), is also crucial for melanosome transport. The product of this locus is melanophilin (Mlph), which links Rab27a and myosin-Va and is therefore also required for the correct targeting of myosin-Va to the melanosome membrane (Matesic et al., 2001; Provance et al., 2002; Nagashima et al., 2002; Strom et al., 2002), as described in section 1.4.1.

Transfecting *dilute*, *ashen* or *leaden* melanocytes with myosin-Va, Rab27a or Mlph, respectively, leads to the melanosomes redistributing throughout the cytoplasm (Evans et al., 2014; Hume et al., 2001, 2007), thus providing a clear assay via which to study melanosome transport.

1.1.1.3 Melanocyte and keratinocyte co-cultures can be used to study the melanosome transfer process

In mammals, the ultimate end-goal for melanosomes is to reach the melanocyte plasma membrane and subsequently be transferred into neighbouring keratinocytes where they form a cap around the nucleus, thus protecting the animal against UV irradiation. In theory all of the attributes which make melanocytes an excellent model to studying organelle transport also make these cells useful for investigating the process of organelle transfer from one cell to another. In practice, however, relatively little is know about this process, although at least four different mechanisms have been hypothesised.

Early studies proposed that the transfer process was mediated by cytophagocytosis - whereby melanocyte dendrites packed with melanosomes are engulfed by keratinocytes. This view was mainly supported by electron microscopy which showed cross-sectional images of melanocyte dendrites surround by a keratinocyte (Mottaz and Zelickson, 1967; Okazaki et al., 1976).

Electron microscopy, along with time-lapse video microscopy, have also show that filopodia extending from melanocytes make contact with keratinocytes and serve as conduits for individual melanosomes to pass through (Scott et al., 2002).

More recently, evidence has been provided which supports two alternative theories regarding the transfer of melanosomes to keratinocytes. The first is the 'shedding' mechanism, which suggests that a small number of melanosomes are concentrated into a packet which buds off from the melanocyte and is phagocytosed by the keratinocyte. Two main lines of evidence support this model. Firstly, Ando et al. showed via scanning electron microscopy (SEM) that melanosomes were packaged into globular 'sacs' of membrane at the ends of melanocyte dendrites which then pinched off. These 'pigment globules' were found in the culture medium (when melanocytes and keratinocytes were co-cultured) and could be purified. When purified pigment globules were added to keratinocytes SEM was again used to show microvilli wrapping around the melanosome packages, which were subsequently phagocytosed by the keratinocyte. Inhibition of the protease activated receptor-2 (PAR-2), which is known to play a role in keratinocyte phagocytosis (Sharlow et al., 2000), prevented melanosome uptake (Ando et al., 2012). Secondly, Wu et al. co-cultured melanocytes and keratinocytes from the transgenic Holy mouse (where the melanocyte plasma membrane is labelled red and the keratinocyte membrane green) and used time-lapse fluorescence microscopy to show red pigment globules being internalised by the keratinocytes. Pigment shedding did not occur in the absence of keratinocytes - indicating they must be fundamental to the process (Wu et al., 2012).

Finally, Tarafder et al. most recently suggested a fourth mechanism whereby melanocytes exocytose individual melanosomes which are then endocytosed by the keratinocyte. Three different pieces of evidence support this model. Firstly, when melanocytes and keratinoyctes were co-cultured melanin cores that were devoid of any membrane (as determined by transmission electron microscopy) were found in the growth media, suggesting they had lost their membrane during exocytosis. Secondly, TEM was again used to show that melanosomes in keratinocytes were surrounded by a single membrane, in keeping with single melanin cores being endocytosed. Finally, the membranes surrounding the melanin cores in keratinocytes were shown to be distinct from those in melanocytes, since they were no longer positive for TYRP1 (see section below for further details), which in melanocytes acts as a melanosome membrane marker. This further suggests that single melanosomes are exocy-

tosed from melanocytes (causing them to lose their membrane) and subsequently endocytosed by keratinocytes (causing them to gain a keratinocyte-derived membrane).

Melanophores have also been shown to transfer their melanosomes to surrounding cells in order to bring about permanent darkening of the skin in *Xenopus laevis* (Aspengren et al., 2006). In this study, since no keratinocytes cell lines from *Xenopus laevis* exist, fibroblasts were used instead. It was found that when melanophores were co-cultured with fibroblasts, melanosome transfer took place, although cell-cell contact did not appear to be necessary. To investigate the melanosome transfer mechanism, melanocytes were stained with the lipophilic dye 1,1'-dioctadecyl-3,3,3',3'-tetramethylindocarbocyanine perchlorate (Dil) which marks cellular membranes red. Dil appeared to be transferred to fibroblasts, where it co-localised with melanosomes. This finding was backed up by electron microscopy data showing that melanosomes in fibroblasts were surrounded by a double membrane. It is therefore possible that melanophores exocytose melanosomes as membrane-bound organelles which are then endocytosed by the fibroblasts.

1.1.2 Melanogenesis

Melanosomes are classed as lysosome-related organelles (LROs), since they share common features with lysosomes including an acidic lumen and the expression of lysosomal hydrolases and LAMP-1/2 (Dell Angelica et al., 2000). The fact that melanosomes can be considered a secretory organelle, since they extrude melanin into neighbouring keratinocytes, also suggests they are similar to other LROs, such as cytotoxic granules (Stinchcombe and Griffiths, 2001) or platelet dense granules (McNicol and Israels, 1999).

There are at least two potential pathways via which melanogenesis may occur (Figure 1.4). In the first pathway, stage I premelanosomes arise from the endoplasmic reticulum (ER), which is supported by mass spectrometry data (Basrur et al., 2003). This showed several ER proteins including the HSP70 molecular chaperone binding immunoglobulin protein (BiP), the enzyme protein disulphide isomerase (PDI), calreticulin and the transmembrane protein calnexin were all present in stage I and stage II premelanosomes. In the second pathway, stage I premelanosomes arise from endosomes, which is supported by immunogold labelling experiments which detect the endosomal protein EEA1 in premelanosomes (Raposo et al., 2001).

The structural protein Pmel17 is a type I integral membrane protein and a product of the

silver locus (Dunn and Thigpen, 1930). It possesses a large lumenal domain containing a partial repeat sequence required for amyloid fibril formation, along with a single membrane spanning domain and short cytoplasmic domain (Theos et al., 2005, November). Pmel17 is crucial for melanogenesis to occur, with *silver* C57BL/6 mice appearing grey in colour, similar to *dilute* mice. Pmel17 is co-translationally translocated as a 100kDa protein into the ER (Leonhardt et al., 2010), where it is post translationally modified by the addition of mannose residues via sialyltransferases, which increase its size to 120kDa (Theos et al., 2005, October). After trafficking to the Golgi, these mannose residues are further modified, and the luminal portion of the molecule is cleaved by the proprotein convertase furin, either in the trans-Golgi or in the endocytic pathway, since mutating the cleavage site consensus sequence of this protein prevented release of the luminal domain (Berson et al., 2003). The 85kDa luminal protein is then delivered to the premelanosomes in an adaptor protein (AP)-1 or AP2-dependent manner, where it aggregates to form striations (Valencia et al., 2006). Melanin (whose synthesis is described in section 1.1.2.1) is then deposited on these striations in stage II and III melanosomes, leading to the formation of mature organelles (Raposo and Marks, 2002).

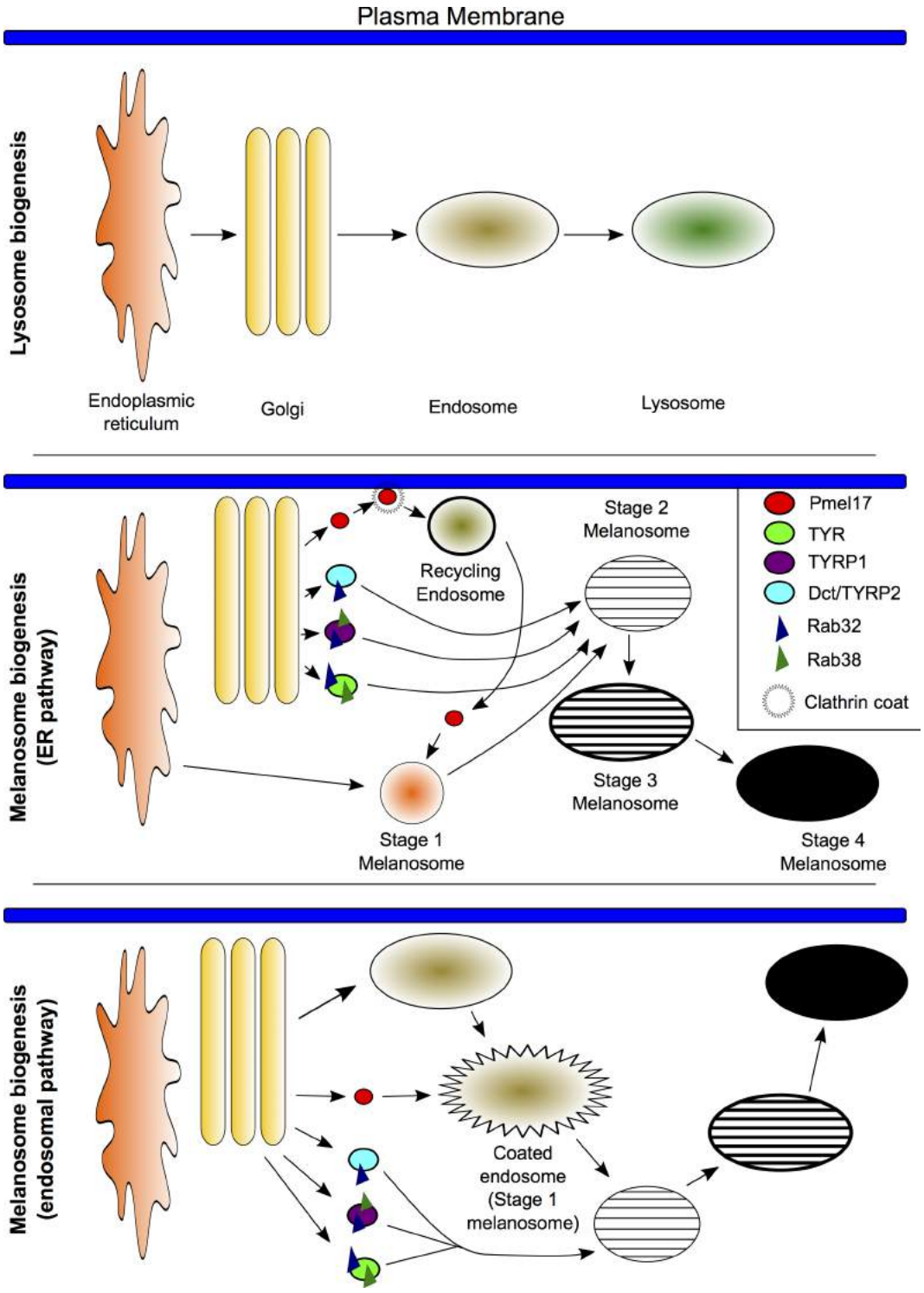


Figure 1.4 - Different melanosome biogenesis pathways. While lysosomes are known the arise from endosomes, there are at least two possible pathways for the biogenesis of melanosomes. The first pathway suggests that stage I melanosomes are formed directly from the ER. The structural protein Pmel17 is trafficked to these premelanosomes via recycling endosomes. Additional proteins required for melanin biosynthesis are then trafficked from the Golgi to these compartments to form stage II melanosomes. As melanin gradually becomes synthesised as deposited onto the striations formed from Pmel17, stage III and stage IV melanosomes are generated. The second pathway suggests that melanosomes arise from endosomes. Pmel17 is initially trafficked to endosomes from the Golgi, which differentiates them into stage I melanosomes. Additional proteins are then trafficked to these organelles (as in the first pathway) to generate stage II, III and IV melanosomes. Adapted from Dell'Angelica, 2003.

Another important process for melanogenesis to progress is the trafficking of tyrosinase

(TYR), tyrosinase-related protein-1 (TYRP1) and dopachrome tautomerase (Dct/TYRP2), which are collectively involved in the synthesis of eumelanin (as discussed in the section below), from the trans-Golgi network to stage II melanosomes (Hearing, 2005). It is known that the trafficking of both TYR and TYRP1 occurs in a Rab32/Rab38 dependent manner, since 'chocolate' or 'cht' mice with a Rab38^{G19V} mutation have a brown coat colour, resembling a similar (albeit weaker) phenotype to that of TYRP1 deficient mice. When Rab32 is knocked down in cht melanocytes, the resulting pigment deficiency is much more dramatic, and little TYR or TYRP1 is detected in the melanosomes, suggesting Rab32 and Rab38 are functionally redundant (Wasmeier et al., 2006). Meanwhile, TYRP2, mutations in which leads to the phenotype 'slaty', due to the resulting grey coat colour of the mouse (Costin et al., 2005), appears to be dependent only on Rab32 for trafficking. siRNA knockdown of this GTPase in human MNT1 cells lead to the complete loss of TYRP2, while knockdown of Rab38 had no effect (Bultema et al., 2012).

1.1.2.1 The melanin biosynthetic pathway

Melanin is synthesised from the amino acid tyrosine, which is thought to pass through the melanosome membrane using an amino acid transporter, since the rate of tyrosine uptake can be saturated at high concentrations and is temperature dependent, consistent with this uptake mechanism (Potterf et al., 1996). The first step in the biosynthesis of melanin is the hydroxylaion of L-tyrosine by TYR, the rate limiting enzyme in the process, to form the transient intermediate 3,4-dihydroxyphenylalanine (DOPA). TYR then catalyses the oxidation of DOPA to form DOPAquinone, which spontaneously forms DOPAchrome through the intermediate cycloDOPA (Potterf and Hearing, 1998; Ebanks et al., 2009; Kondo and Hearing, 2011). TYRP2 is then responsible for the formation of 5,6-dihydroxyindole-2-carboxylic acid (DHICA), a tautomer of DOPAchrome (Palumbo et al., 1991). Finally TYRP1 catalyses the oxidation and polymerisation of DHICA to form eumelanin (Figure 1.5).

There is also evidence to suggest that melanosome pH also regulates melanin synthesis, since melanosomes from lighter human skin having a more acidic lumen and reduced TYR activity compared to melanosomes purified from darker skin (Fuller et al., 2001). Vacuolar ATPases are thought to play a major role in controlling the pH of the melanosome lumen, while increased level of cAMP positively regulate their expression (Cheli et al., 2009). However, there is an ongoing debate regarding the necessity of an acidic lumen for successful

melanin synthesis, with some studies, such as claiming this is the case (Puri et al., 2000), while others have shown that melanin synthesis can occur in the presence of vacuolar ATPase inhibitors which block melanosome acidification (Ancans et al., 2001).

As expected, melanin synthesis and hence melanogenesis can also be regulated through levels of UV radiation reaching the epidermis. αMSH is known to drive the expression of tyrosinase during exposure to high levels of UV irradiation through binding the melanocortin 1 receptor (Le Pape et al., 2008). Melanin levels can also be increased through an alternative pathway whereby the tumour suppressor protein p53, which is also upregulated upon cellular stimulation with UV light (Hall et al., 1993), binds to and activates promoters for both TYR and TYRP1, causing an increase in their expression levels (Nylander et al., 2000).

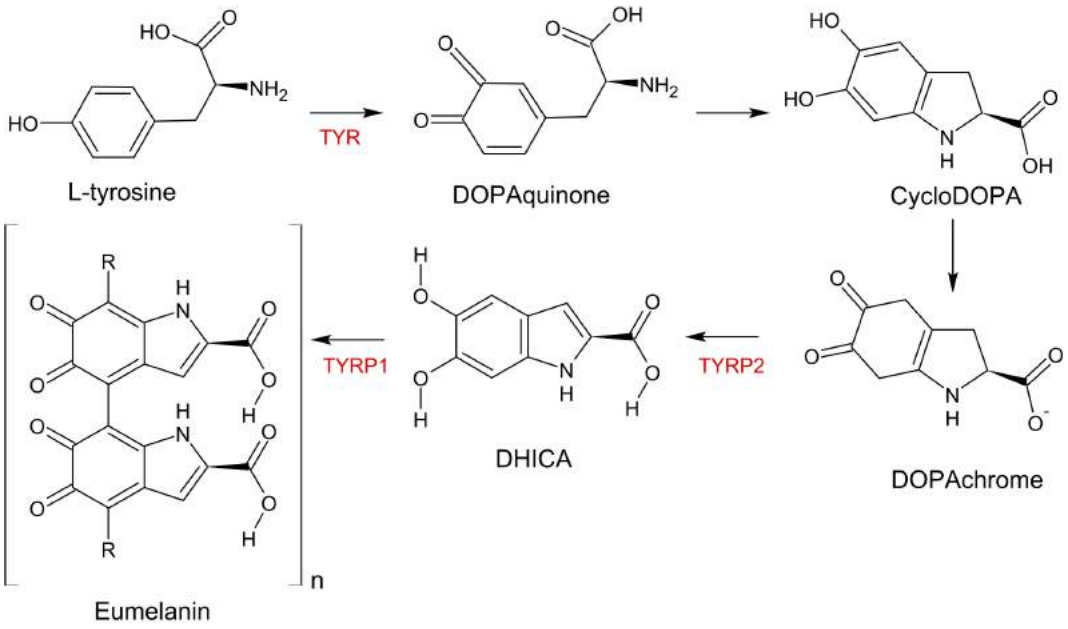


Figure 1.5 - The eumelanin biosynthetic pathway. Melanin is synthesised from the amino acid L-tyrosine. Initially tyrosinase (TYR) catalyses the oxidation of tyrosine to DOPAquinone - the rate limiting step in melanin biosynthesis. DOPAchrome is then spontaneously formed via the intermediate cycloDOPA. Tyrosinase related protein-2 (TYRP2), also know as DOPAchrome tautomerase then catalyses the production of 5,6-dihydroxyindole-2-carboxylic acid (DHICA). Finally tyrosinase related protein-1 catalyses the further oxidation of DHICA to eumelanin polymer. Adapted from Kondo and Hearing, 2011

1.1.2.2 BLOC and AP-3 components are also required for melanogenesis

Proteins which make up the three Biogenesis of Lysosome Related Organelle Complexes (BLOCs), as well as the adaptor protein complex AP-3, have also be shown to play a role in both the biogenesis and trafficking of lysosome related organelles. Defects in one of these complexes results in Hermansky-Pudlak Syndrome (HPS), an autosomal recessive disorder which is characterised by albinism and severe bleeding/prolonged bleeding time after injury

due to an inability synthesise either melanosome or platelet dense granules, respectively (Hurford and Sebastiano, 2008). Components of these complexes are given in Table 1.1.

Defects in BLOC1 components leads to an accumulation of stage I melanosomes, as well as a large number of vesicles which lack any striations. Defects in both BLOC2 and BLOC3 components also leads to an accumulation of stage I melanosomes, as well as novel 'stage IA' melanosomes which contain striations but lack any pigment. Finally, mutations in AP-3 prevent melanosomes maturing beyond stage III (Wei, 2006).

Complex	**Subunits**	**Gene**	**Mouse strain**	**Human disease**	**Function**
BLOC1	Pallidin	Pldn	Pallid	?	Binds syntaxin 13 (Huang et al., 1999)
	Cappucino	cno	Cappuccino	?	AP-3 independent melanogenesis (Gwynn et al., 2000)
	Muted	mu	Muted	?	Unknown
	BLOS3	BLOC1S3	Reduced pigmentation	HPS-8	Unknown
	Dysbindin	DNTBP1	Sandy	HPS-7	Binds α- and β-dystrobrevin (Benson et al., 2001)
	Snapin	SNAPIN	?	?	Potentially mediates interaction with dynein (Cai et al., 2010)
	BLOS1	BLOC1S1	?	?	Unknown
	BLOS2	BLOC1S2	?	?	Unknown
BLOC2	HPS3	HPS3	Cocoa	HPS-3	Unknown
	HPS5	HPS5	Ruby eye-2	HPS-5	Unknown
	HPS6	HPS6	Ruby eye	HPS-6	Unknown
BLOC3	HPS1	HPS1	Pale ear	HPS-1	Unknown
	HPS4	HPS4	Light ear	HPS-4	Unknown
AP-3	β3A	AP3B1	Pearl	HPS-2	Vesicle trafficking to lysosomes (Yang et al., 2000)
	δ	APS3D1	Mocha	?	Unknown
	μ3	AP3M1	?	?	Unknown
	σ3		?	?	Unknown

Table 1.1 - Components of the BLOC and AP-3 complexes, defects in which affects the biogenesis of LRO. Adapted from Wei, 2006.

1.1.3 Defective lysosome related organelle trafficking leads to a number of syndromes

Whilst HPS can be caused through the defective biogenesis of LROs, this condition may also manifest itself through defective trafficking of the mature organelles. For example, mutations within the Rab geranylgeranyl transferase (RGGT) gene gives rise to the *gunmetal* mouse, which exhibits a diluted coat colour along with prolonged bleeding times compared to wildtype C57B/6J mice, attributable to platelet defects (Swank et al., 1993). Biochemical evidence showed that in *gunmetal* mice, although total Rab27a levels are similar to WT mice, the membrane bound fraction is greatly reduced - suggesting RGGT is necessary for the prenylation and subsequent membrane targeting of this GTPase (Detter et al., 2000). Since RGGT is critical for the prenylation of many different Rabs (Watanabe et al., 2008), some of which will be required for the biogenesis/trafficking of organelles, this offers an explanation for the defects observed in the *gunmetal* mouse.

Chediak Higashi syndrome (CHS) is another severe, often fatal, disorder which results from defects in LRO trafficking. CHS, which is equivalent to the *beige* phenotype in mouse, is caused by mutations with the lysosomal trafficking regulator protein LYST (Nagle et al., 1996). Defects in this protein lead to giant LROs which are unable to reach the plasma membrane to secrete their contents, resulting in albinism, increased bleeding and neurological dysfunction (Introne et al., 1999), as well as immune disorders due to defects in T-cells releasing cytotoxic granules, reduced macrophage activity and reduced antigen presentation in B cells (Baetz et al., 1995; Faigle et al., 1998; Stinchcombe et al., 2000). The molecular mechanism by which mutations in LYST result in enlarged LROs is not well understood, partly due to its large size (13.5kb), which makes detecting mutations and research on the protein difficult (Certain et al., 2000). However, while the trafficking of proteins to LROs appears normal in cells lacking LYST, the organelles frequently fuse together, causing them to become enlarged (Stinchcombe et al., 2000). These organelles may have limited ability to be transported by molecular motors due to their large size, and are also frequently destroyed by the cell which recognises them as 'foreign' (Zelickson et al., 1967).

Finally Griscelli syndrome (GS) is another disorder which can lead to defects in the trafficking of LROs, resulting in very severe phenotypes in some cases. Three types of GS are know to occur. GS type 1 is caused by mutations within the MYO5A gene encoding the actin-based motor protein myosin-Va (Pastural et al., 1997), which leads to albinism along

with along with neurological defects (Dessinioti et al., 2009) and is therefore the human equivalent of the *dilute* phenotype in mouse. GS type 2 occurs due to mutations in the gene encoding the small GTPase Rab27a and results in albinism, immune deficiency, (which are unique to GS type 2), and some neurological defects (Shati et al., 2013), making it equivalent to the *ashen* phenotype in mouse. Finally, GS type 3 occurs due to mutations within the MLPH gene encoding the effector protein melanophilin. This is the least severe form of GS, resulting only in albinism (Tomita et al., 2004) and is similar to the *leaden* phenotype in mouse.

The large number of different phenotypes in which either the trafficking of LROs, including melanosomes, is disrupted therefore makes mouse melanocytes an attractive model in which to study the molecular mechanisms governing organelle transport.

1.2 Microtubules and their associated molecular motors facilitate long-range organelle transport

In 1965, when studying the axoneme of cilia from the protozoon *Tetrahymena pyriformis*, a protein was discovered which both bound to microtubules and acted as an ATPase (Gibbons and Rowe, 1965). The protein was termed dynein (from the Greek dyne, meaning 'force') and was the first microtubule-based motor protein to be identified. Later a cytoplasmic analogue of axonemal dynein was purified from calf brain (Paschal et al., 1987), which has since been shown to participate in retrograde microtubule-dependent transport of cargo and is required for a large number of processes from endocytosis to maintaining correct Golgi morphology (Roberts et al., 2013).

Two decades later brought the discovery of another protein translocator, isolated from the supernatant of a giant squid axon, which was able to induce microtubule movement in an ATP-dependent fashion when it was fixed to a glass coverslip (Vale et al., 1985). Named kinesin, from the Greek *kinein*, meaning 'to move', this microtubule-dependent transporter was found to be just one of a large family of kinesin motor proteins, the majority of which are responsible for the anterograde movement of cargo and play a fundamental role in a wide variety of cell processes from the transport of organelles, mRNA and protein/lipid complexes to organising mitosis and meiosis. These two classes of long-range microtubule-dependent transporters are therefore thought to complement each other in order to precisely orchestrate the intracellular transport of cargo.

1.2.1 Microtubules are dynamic tracks for kinesin and dynein

Fibrils running through both the flagella as well as the mitotic spindle were documented well over 100 years ago, but it was not until the 1950s and 1960s with the advent of electron microscopy that their existence was finally proved (Manton and Clarke, 1952; Fawcett and Porter, 1954). These hollow structures, 25nm in diameter, where termed 'microtubules', (Ledbetter and Porter, 1963). Soon after, studies using radioactive colchicine showed this drug bound most strongly to cells and structures known to be rich in microtubules, such as sea urchin egg, mitotic spindles and brain tissue. Colchicine was found to bind a 6S protein, proposed to be the subunit of microtubules (Borisy and Taylor, 1967) and afterward given the name 'tubulin' (Mohri, 1968).

1.2.1.1 Microtubule structure and assembly

Soon after the discovery that microtubules were composed of a 110, 000 dalton dimer called tubulin, it was demonstrated that this protein actually exists as two different isoforms, since depolymerising microtubules through heating led to two 55, 000 dalton monomers named A-tubulin and B-tubulin (now termed α-tubulin and β-tubulin) which were soluble at different pH values (Stephens, 1970). Although α- and β- tubulin were found to be present in equal quantities in microtubules, and therefore assumed to exist as a heterodimer (Bryan and Wilson, 1971), this was difficult to prove conclusively, as techniques such as SDS-PAGE caused the non-covalently bound dimers to separate into their constituent monomers which ran as a single band. Eventually, by using the cross-linking reagent DTDI which forms intradimer bonds specifically within the tubulin dimer, it was demonstrated by SDS-PAGE that tubulin does indeed exist as a heterodimer, since the 3 possible dimers, $\alpha\alpha$, $\beta\beta$, and $\alpha\beta$ migrate differently (Luduena et al., 1977).

Each tubulin monomer is able to bind a single molecule of GTP (Weisenberg et al., 1968). Early research into microtubule formation concluded that GTP hydrolysis was an absolute requirement (Gaskin et al., 1974; Olmsted and Borisy, 1975). Further research showed that although both α- and β- tubulin must be bound to GTP in order to polymerise (Brouhard and Sept, 2012), GTP hydrolysis is not necessary, since microtubules were shown to be able to form in the presence of the non-hydrolysable GTP analogue GMP-PNP and were indistinguishable from those formed in the presence of GTP (Arai and Kaziro, 1976). However, microtubules grown in GMP-PMP failed to depolymerise, suggesting that the intrinsic GTPase activity of tubulin is necessary for microtubule dynamics (as discussed in section 1.2.1.3).

Tubulin dimers assemble into protofilaments which further bind longitudinally to form the complete microtubule structure (Figure 1.6). Although cryoEM has revealed that microtubules can contain between 8 and 17 protofilaments (Pierson et al., 1978; Aamodt and Culotti, 1986), typically they contain 13 protofilaments (Chretien et al., 1992). Normally, α-tubulin makes lateral contact with another α-tubulin monomer in the microtubule (and likewise β-tubulin contacts another β-tubulin), which is presumably the strongest linkage. However, the 13 protofilament configuration necessitates the existence of a weak seam, whereby lateral contacts between α-tubulin and β-tubulin is required for two of the protofilaments (Mandelkow et al. 1986; see Figure 1.6). Microtubules are orientated such that α-tubulin is

always towards the minus-end of the filament, whilst the β-tubulin is orientated towards the plus-end, thus giving the microtubules polarity (Fan et al., 1996). Since the minus-end of microtubules are almost always orientated toward the microtubule organising centre (MTOC) at the cell centre (as discussed in below in section 1.2.1.2), this polarity also aids microtubule motor proteins in trafficking cargo to the correct sub-cellular destination.

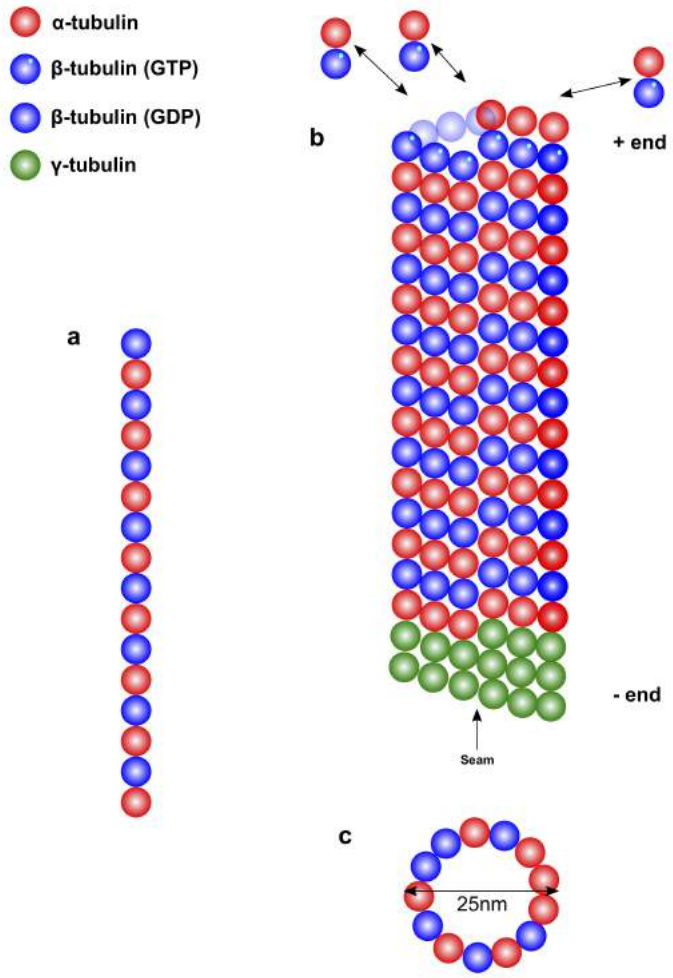


Figure 1.6 - The structure of microtubules. (a) Protofilaments are formed from α/β tubulin dimers with β-tubulin always pointed towards the + end of the filament. **(b)** γ-tubulin along with additional capping proteins form the major nucleation site for microtubules. At least one complete layer of GTP-bound tubulin at the + end is necessary to maintain microtubule integrity, and if this is lost microtubule catastrophe results. **(c)** Cross section of a microtubule showing that 13 protofilaments usually make up a complete microtubule, which is 25nm in diameter. Adapted from Conde and Caceres, 2009.

1.2.1.2 Microtubule nucleation

Growth of new microtubules from individual tubulin dimers is slow and energetically unfavorable until a 6-12 tubulin dimer seed has formed (Voter and Erickson, 1984; Flyvbjerg et al., 1996; Leguy et al., 2000) after which time the microtubule formation rate is greatly en-

hanced. *In vitro*, the rate of microtubule polymerisation is proportional to the concentration of GTP-tubulin (Johnson and Borisy, 1977), but *in vivo* cells have developed mechanisms to generate microtubule seeds such that high tubulin concentrations need not be maintained for rapid microtubule polymerisation to occur (described below). The centrosome, which consists of a pair of centrioles surrounded by pericentriolar material, normally positioned near the cell centre by the action of cytoplasmic dynein during interphase (Burakov et al., 2003), is the major MTOC and the site from which the majority of microtubules radiate out. γ-tubulin has been shown to be enriched at the centrosome in a number of different organisms (Zheng et al., 1991; Stearns et al., 1991) and has been implicated as an essential molecule for microtubule nucleation (Oakley et al., 1990).

When γ-tubulin was purified it was found to be part of a much larger complex devoid of either α- or β-tubulin. Electron microscopy revealed that the complex was ring shaped, resulting in the name γ-tubulin ring complex (γ-TuRC; Zheng et al., 1995). This 2.2MDa complex is made up of at least 6 different components (not including γ-tubulin): γ-tubulin complex protein 2 (GCP2), GCP3, GCP4, GCP5, GPC6 and NEDD1. However, more recently two smaller proteins termed mitotic-spindle organizing protein associated with a ring of γ-tubulin-1/2 (MOZART1/2) have been identified (Hutchins et al., 2010), suggesting that other as yet unknown components of this complex may exist.

At the core of γ-TuRC are three proteins, γ-tubulin, GCP2 and GCP3 which collectively make up the complex termed γTuSC, so called because it dissociates from γTuRC under high salt conditions (Zheng et al., 1995). The γ-TuSC complex has been shown via both electron and fluorescence microscopy to be a V-shaped structure (Choy et al., 2009; depicted in Figure 1.7), whilst 8Å cryoEM images of γ-TuSC oligomers (purified from *Saccaromyces cerevisiae*, which only express the γ-TuSC components) demonstrate that this structure is composed of 13 γ-tubulin molecules per turn - matching the typical number of protofilaments found in microtubules generated *in vivo (Kollman et al., 2010).* This finding led to the 'template' model, whereby the 6.5 γ-TuSC complexes per helical turn are scaffolded by the remaining components of the γ-TuRC complex in order to form a cap which mimics a microtubule seed, allowing for energetically favorable addition of free α/β tubulin dimers (see Figure 1.7). However, since GCP4, 5 and 6 can each directly bind γ-tubulin, it is possible that these proteins are directly incorporated into the ring structure, rather than simply acting as a scaffold (reviewed by Kollman et al., 2011).

Of great importance to normal cell function is the fact that microtubules are anchored at their minus ends to the MTOC, since if this was not the case organelle and vesicle transport mediated by plus- or minus-end directed motor proteins would fail to reach the correct subcellular location. Ninein appears to be a crucial attachment factor, since cells expressing a truncated construct of this protein showed gross defects in their ability to regrow microtubules after washout of the microtubule depolymerising agent nocodazole (Delgehyr et al., 2005). Delgehyr et al. also presented further microscopic and biochemical evidence to suggest that, while the C-terminus of ninein binds the centriole, the N-terminus makes contact with γ-tubulin, suggesting that ninein forms a bridge between the centriole and γ-TuRC in order to anchor microtubules at the MTOC.

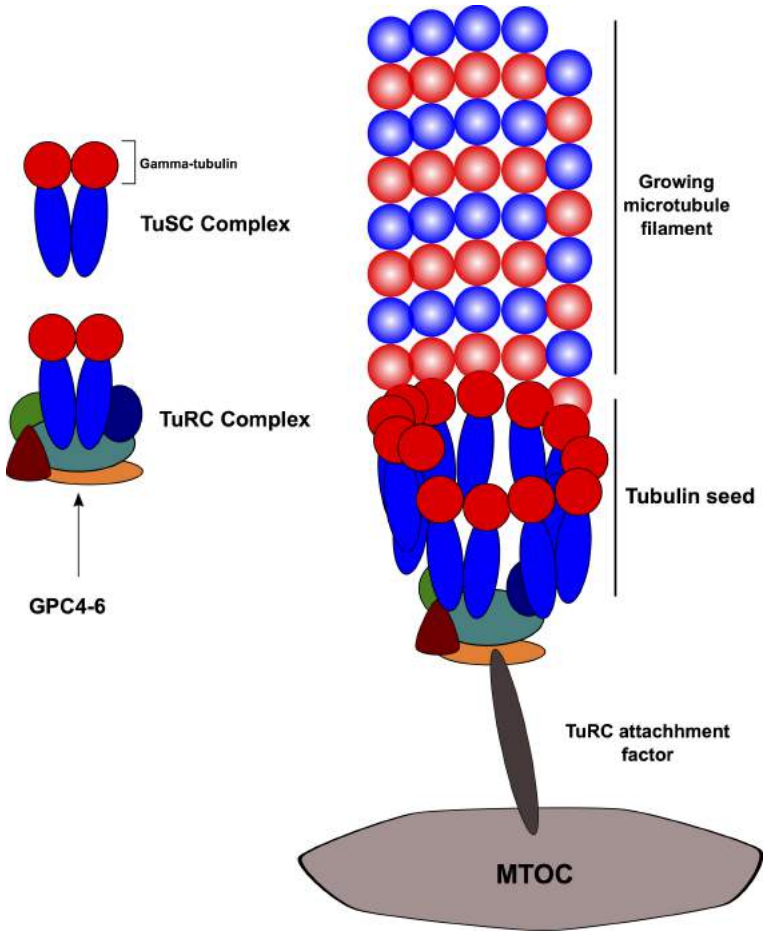


Figure 1.7 - The γ-TuRC complex. The γ-TuRC complex is made up of γ-TuSC (composed of γ-tubulin, GCP2 and GCP3) along with GPC4-6, thought to act as a scaffold for γ-TuSC. Recent evidence suggests GPC4-6 may also be incorporated into a ring structure in order to seed microtubules. The γ-TuRC complex also acts to link microtubules to the MTOC through TuRC attachment factors such as ninein. Adapted from Kollman et al., 2011.

1.2.1.3 Microtubule dynamics

An important feature of microtubules is the fact they are highly dynamic; switching between periods of growth, known as 'rescue', and periods of depolymerisation, known as 'catastrophe' with both processes collectively referred to as 'dynamic instability' (Mitchison and Kirschner, 1984). Since each round of microtubule growth and catastrophe consumes large quantities of GTP, this phenomenon requires a large amount of energy. Despite this, it is a highly conserved process across a wide number of species and cell types, most likely because in the absence of microtubule turnover, which allows for the spatial reorganisation of these filaments (Gundersen and Bretscher, 2003), severe membrane trafficking defects would result.

Of fundamental importance to the integrity of microtubules is the GTP-tubulin cap found at the plus-end. This was first demonstrated by the fact that breaks in the middle of microtubule filaments quickly caused the entire structure to depolymerise, suggesting a reliance on the ends of microtubules for stability (Mitchison and Kirschner, 1984). Hydrolysis of tubulin-GTP to tubulin-GDP, (as occurs for the bulk of the tubulin dimers making up a microtubule filament) is thought to cause the tubulin dimer to undergo a conformational change, which should cause each of the protofilaments to become curved, rather than straight (Mandelkow et al., 1991; Hyman et al., 1995). However, since the tubulin dimers are bound to neighbouring dimers in the microtubule lattice, this conformational change is prevented from happening and instead energy from GTP hydrolysis is stored as stress within the microtubule lattice, which unchecked would drive the microtubule toward spontaneous disassembly (Caplow et al., 1994; Tran et al., 1997). Loss of the GTP-cap, which has shown to be a minimum of 1 layer thick (13 tubulin dimers; Caplow and Shanks, 1996), appears to allow the stress in the protofilaments to be released, resulting in curved filaments which can be visualised via cryoEM (Müller-Reichert et al., 1998).

Aside from the GTP-cap, cells express a large number of different microtubule associated proteins (MAPs) which also have roles in promoting either microtubule rescue or catastrophe. One of the most effective proteins for driving microtubule assembly is XMAP215 (Xenopus microtubule-associated protein 215), which is able to bind electrostatically to microtubules and diffuse along its length, facilitating the delivery of tubulin dimers to the growing-plus end and stabilising the molecules there so they are incorporated into the growing structure with high frequency (Brouhard et al., 2008). This, at least *in vitro*, enables up

to 10 times faster growth rates, compared with diffusion-limited microtubule assembly, although since the reaction is reversible XMAP215 can also promote microtubule disassembly, given the correct conditions (Gard and Kirschner, 1987). Another class of MAPs, known as microtubule plus-end tracking proteins (+TIPs) also specifically bind the growing plus-ends of microtubules, which results in enhanced stability. Some proteins, such as CLASPs (cytoplasmic linker associated proteins) achieve this through connecting the microtubule with the cell cortex (Komarova et al., 2002). Meanwhile, other plus-end tracking proteins, such as EB (end-binding) 1 and EB3 appear to function to stabilise the formation of tubulin sheets (Vitre et al., 2008) as well as sheet closure to form the tubule, suggesting EB proteins can also stabilise the weak microtubule seam (Sandblad et al., 2006). Several possible hypotheses have been proposed for how EB proteins recognise the microtubule plus-end, including that they recognise tubulin sheets which have not yet undergone folding to form the completed tubule (Vitre et al., 2008), or that they recognise the GTP-cap (Zanic et al., 2009). However, more recent date from cryoEM images of microtubules bound to the fission yeast homolog of EB1, Mal3, showed this protein binds at the corner of four tubulin dimers (except at the microtubule seam), with GTP-tubulin promoting high affinity binding (Maurer et al., 2012).

1.2.2 The kinesin superfamily

Since the initial discovery of kinesin-1 in 1985, over 50 different kinesin isoforms have so far been identified, based upon the fact they all feature a conserved motor domain. Most kinesin motors utilise microtubules as 'tracks' in order to deliver cargo to specific sub-cellular areas, as discussed in detail below.

The kinesin superfamily of translocases can be sub-divided into at least 15 different families, based upon their gene sequences (Lawrence et al., 2004), but may also be grouped according to where the motor domain is located within the kinesin heavy chain. N-kinesins (which make up the majority of kinesins), have the motor domain located at the N-terminus and migrate towards the microtubule plus-ends; C-kinesins, which have the motor domain located at the C-terminus, translocate towards the microtubule minus-end whilst M-kinesin, which have the motor domain located centrally within the heavy chain, act to depolymerise microtubules (Hirokawa et al., 2009).

Functionally, kinesin motors have been implicated in the transport of a diverse range of

subcellular cargo - especially in neurons, where these fast, processive motors are crucial for transporting organelles and vesicles across the large (up to several meters in some species) distances typically found in these cell (reviewed by Hirokawa et al., 2009). As further discussed in section 1.4, kinesin-1 has also been implicated in the transport of lysosome-related organelles, including melanosomes (Hara et al., 2000; Vancoillie et al., 2000b).

1.2.2.1 The structure of kinesin-1

Kinesin-1, encoded by the KIF5A, KIF5B and KIF5C genes, is the archetypal kinesin, and the best studied of the superfamily. In its most basic form, kinesin-1 is a homodimer consisting of two heavy chains of 960 amino acids (Figure 1.8). The conserved $\sim$340 amino acid N-terminal motor domain, whose crystal structure was solved a decade after the motors discovery (Kozielski et al., 1997), is responsible for binding to the microtubule, as well as hydrolysing ATP (Yang et al., 1990). The β-phosphate of ATP is held tightly into a pocket formed of 4 different motifs: a Walker A P-loop motif (^{86}GQTSSGKT^{93}), switch-1 (^{199}NEHSSR^{204}), switch-2 (^{232}DLAGSE^{237}) and finally ^{14}RFRP^{17} (residue numbering according to the *Mus musculus* KIF5B sequence)(Marx et al., 2005). Meanwhile, alanine scans of the motor domain have revealed that mutations in basic residues (notably Arg278, Lys252, Lys240, Lys256, Lys281, Lys159, Arg284 and Lys141) and hydrophobic residues (Leu248 and Tyr274) result in a decreased affinity for microtubules (Woehlke et al., 1997). Moreover, mutating the acidic residues Glu250, Glu270, Asp279, Glu170, Glu311, Aps140 to alanine resulted in an increased affinity for microtubule, suggesting that the interaction between microtubules and the kinesin motor domain is mainly mediated though ionic interactions between positively charged residues in the motor and negatively charged residues in the microtubule.

Each motor domain is followed by a highly conserved 15 amino acid α-helical neck linker domain necessary for force generation (described in section 1.2.2.2) (Rice et al., 1999). This domain is made up of heptad repeats $(abcdefg)_n$, with amino acids in the 'a' and 'd' positions being mostly non-polar. This results in the coil having a hydrophobic surface, which mediates dimerisation (Thormählen et al., 1998)(Figure 1.9).

The neck domain, which functions to tether the two motor domains together as well as enhance the stall force of kinesin (Jaud et al., 2006) is followed by a flexible hinge region of approximately 50 amino acids whose sequence is poorly conserved between species and

which is thought to be largely unstructured. To attempt to understand the importance of this region, a series of deletion mutants were generated and it was found that removing the hinge results in a 4-fold reduction in kinesin-1 gliding velocity, possibly due to defects in the chemo-mechanical coupling of the motor domains (Grummt et al., 1998).

The bulk of the kinesin heavy chain is made up of a long (60-80nm) 'stalk' domain, which features a long coiled-coil region, through which the two heavy chain monomers dimerise. Several unstructured regions are also present which introduce kinks into the stalk and make it very flexible (Coy et al., 1999; Woehlke and Schliwa, 2000). This flexibility allows the C-terminus of the heavy chain to make contact with the N-terminal motor domain, resulting in autoinhibition (Dietrich et al., 2008), as discussed further below.

A globular tail domain responsible for binding kinesin light chain (KLC) (described in section 1.2.2.3) is located at the C-terminus of the molecule. The amino acid sequence of this domain is poorly conserved between different kinesin motors, suggesting it differs depending on the cargo each specific isoform of kinesin transports.

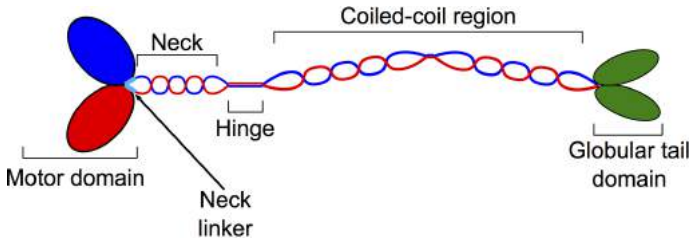


Figure 1.8 - The structure of kinesin-1. Kinesin-1 is composed of two identical heavy chains. The ~340 amino acid motor domain is situated at the N-terminus is followed by a short, flexible 15 amino acid neck linker which is responsible for force generation and the neck domain which tether the two motor domains together. A flexible hinge region, which is important for maintaining optimal gliding velocity, separates the motor/neck domains from the long coiled-coil region which is approximately 80nm long. At the C-terminus of the motor is the globular tail domain which can directly bind some cargo. It also functions to prevent unnecessary ATP hydrolysis by interacting with the motor domain to bring about autoinhibition of the motor in the absence of cargo. Adapted from Woehlke and Schliwa, 2000.

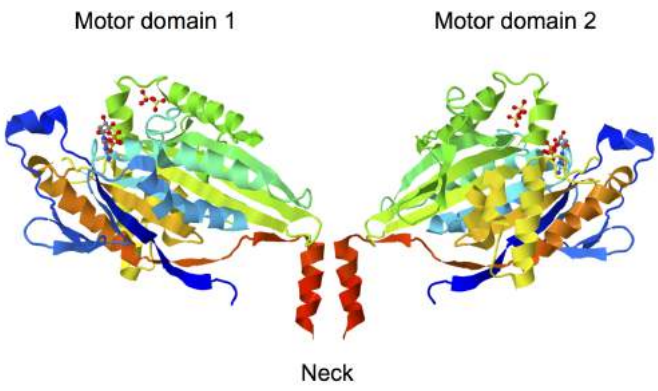


Figure 1.9 - Kinesin-1 motor and neck domains. The structure of human kinesin-1 motor and neck domains, solved using X-ray crystallography. Hydrophobic residues within the neck domain mediate binding of the two α-helical coils. PDB ID: 1MKJ (Sindelar et al., 2002).

1.2.2.2 Translocation and force generation mechanisms of kinesn-1

Kinesin-1 is a fast, processive and powerful motor; generating approximately 6-8pN of force while translocating towards the plus-ends of microtubules at speeds of up to 1μm s^{-1} and traveling approximately 800nm on average before dissociating from the filament, given optimal conditions *in vitro* (Howard et al., 1989; Block et al., 1990; Hunt et al., 1994).

At least 3 different hypotheses have been proposed for how kinesin-1 is able to translocate rapidly and processively along microtubules without falling off: the asymmetric hand-over-hand model, the symmetric hand-over-hand model and the inchworm model. In the asymmetric hand-over-hand model, the molecule moves in a similar manner to a person walking, with the lagging motor domain (or 'foot') needing to detach from the microtubule while the leading motor remains attached, swing forwards in front of the leading motor and re-bind, before the process repeats. In the symmetric hand-over-hand model it is theorised that the entire motor rotates 180^o about the leading motor, which it uses as a pivot, in order to move along the microtubule. In the inchworm model the lagging motor domain takes a short 8nm step and ends up parallel to the leading head (reviewed by Asbury, 2005) (Figure 1.10).

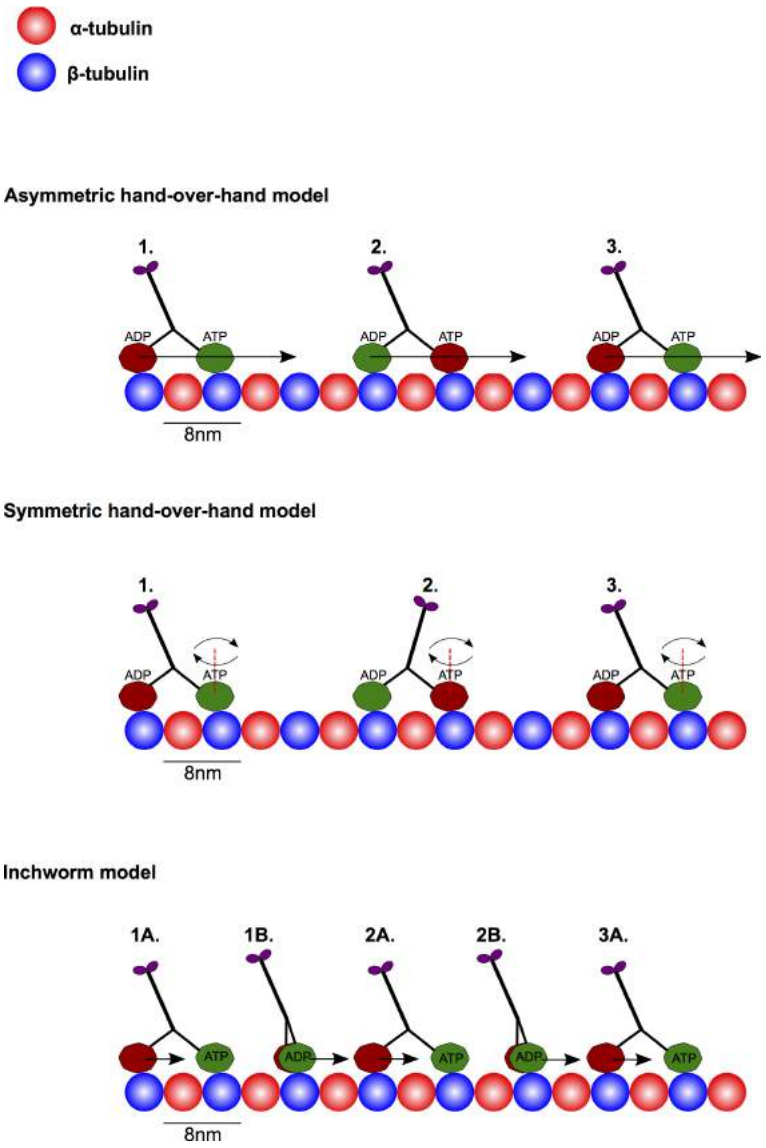


Figure 1.10 - Proposed models for how kinesin translocates along microtubules. In the asymmetric hand-over-hand model the lagging head swings forward by 16nm, passing the original leading head, thus moving the motor stalk forward by 8nm. In the symmetric hand-over-hand model the motor pivots by 180º about the leading head, which also has the effect of moving the motor stalk forward by 8nm. In the inchworm model, each head moves by only 8nm, rather than 16nm as proposed by the other two models. Moreover, the lagging head always remains behind the leading head, which results in the motor 'shuffling' along the microtubule. Adapted from Asbury, 2005.

The symmetric hand-over-hand model was proved to be incorrect, since when kinesin was rigidly attached to coverslips using biotin-avidin so it was impossible for the molecule to rotate, microtubule sliding was not inhibited (Hua et al., 2002). Moreover, since single molecule fluorescence experiments have demonstrated that the two motor domains advance in approximately 16nm steps (17.3 $\pm$3.3nm), this strongly favours the asymmetric hand-over-hand model (Yildiz et al., 2004), as the inchworm model requires the heads to advance in 8nm increments.

The asymmetric hand-over-hand model implies that the two heads can communicate with each other, since the leading motor domain must remain bound to the microtubule as the

lagging head moves forward to avoid the molecule dissociating from the filament (Asbury, 2005). The kinesin-1 motor domain binds the microtubule strongly in the presence of ATP or no-nucleotide, and weakly in the presence of ADP (Klumpp et al., 2004), therefore suggesting a mechanism exists to control the catalytic cycle of each head.

The 15 amino acid neck linker has been shown to be extremely important in controlling this cycle and thereby increasing the processivity of kinesin-1. Structural studies have revealed that the motor domain contains a hydrophobic 'switch' and 'docking' sites, which facilitate the binding of ATP and the neck linker, respectively. Neck linker binding is necessary to bring about ATP binding through invoking a conformational change in the switch region. When it is tightly bound to the lagging head, as in step 4 of Figure 1.11, this causes internal strain, preventing the forward neck linker from easily contacting the docking site and thus preventing the binding of ATP (Rosenfeld et al., 2003; Klumpp et al., 2004; Dogan et al., 2015).

Meanwhile fluorescence resonance energy transfer (FRET) and electron paramagnetic resonance (EPR) experiments have identified that a conformational change within the 15 amino acid neck linker domain is also crucial to facilitate the stepping of the kinesin motor. In the absence of ATP, the neck linker appears unstructured, but becomes rigid upon ATP binding the motor domain (Rice et al., 1999). This has the effect of throwing the lagging head forward (as in step 2 and 7 of Figure 1.11), forcing the motor to progress along the microtubule.

In the absence of cargo it would be wasteful for kinesin to continue translocating along the microtubule since ATP would be unnecessarily hydrolysed. To prevent this from happening, kinesin-1 is able to utilise its long stalk to allow the C-terminal tail to contact the motor domain. The conserved IAK motif in the tail region is known to play an important role in autoinhibition (Hackney and Stock, 2000), while a more recent 2.2Å crystal structure of the kinesin-1 motor-tail complex has revealed that binding of the tail results in the two heads becoming tethered together, preventing ADP release and blocking the catalytic cycle from progressing (Kaan et al., 2011).

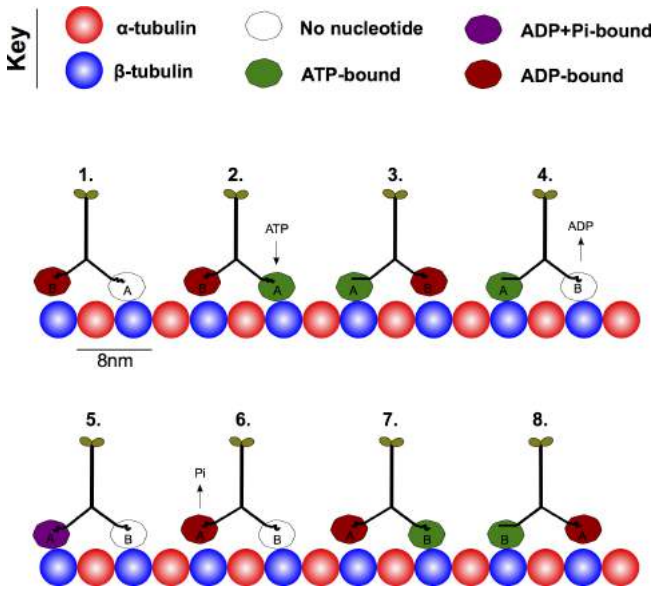


Figure 1.11 - The catalytic cycle of kinesin-1. The kinesin motor domain remain strongly attached to microtubules in the ATP-bound/no nucleotide state, whilst weakly attached in the ADP-bound state. Therefore in step 1, the lagging head in the ADP-bound state is free to move forward, while the leading head remains firmly attached to the microtubule. In step 2, binding of ATP to the leading head brings about a conformational change which throws the lagging head forward (step 3). In step 4, ADP diffuses from the now leading head, resulting in both heads becoming strongly attached to the microtubules. ATP is then hydrolysed in ADP+Pi (step 5). Diffusion of Pi away from the lagging head (stage 6) allows the head to detach from the microtubule and the catalytic cycle repeats. It is thought that internal strain prevents both heads binding ATP at the same time, since the simultaneous hydrolysis to ADP would result in the motor detaching from the microtubule. Adapted from **Rosenfeld et al., 2003; Klumpp et al., 2004**

1.2.2.3 Linking kinesin-1 to cargo

Although the number of different kinesin isoforms is large, it is dwarfed by the number of different cargos that kinesin must recognise. Kinesin motors can therefore utilise various adaptor proteins, called kinesin light chains (KLC) to help them achieve this specificity, although direct binding to the kinesin heavy chain (KHC) can also occur (Hirokawa et al., 2009).

KLCs, which are approximately 560 amino acids in length, contain an N-terminal coiled-coil heptad repeat region, approximately 100 amino acids in length that is predicted to form an α-helical coil in order to mediate binding to the α-helical coil of KHC tail, and 5 tetracopeptide repeat domains (TPRs; each 34 amino acids in length), which are responsible for binding to a variety of proteins (Gindhart and Goldstein, 1996; Diefenbach et al., 1998; Verhey et al., 1998). Purified kinesin-1 from HeLa cells exists either as a dimeric (KHC only) or tetrameric (KHC and KLC) complex (DeLuca et al., 2001), indicating that there is a 1:1 binding stoichiometry between KHC and KLC (Figure 1.12).

KLC has also been shown to be involved in the transport of some organelles, including the rough endoplasmic reticulum (RER) along with the Golgi complex (Woźniak and Allan,

2006). Lysosomes are also thought to be attached to KHC in a KLC-dependent manner. In this case, the only known GTPase to bind the organelle is Arl8, whose expression level affects the positioning of lysosomes (Bagshaw et al., 2006; Hofmann and Munro, 2006). Through the use of affinity chromatography, it has been shown that the effector protein SKIP (SifA and kinesin-interacting protein) is able to bind Arl8 (Rosa-Ferreira and Munro, 2011). In this case KLC2 mediates binding of SKIP to kinesin-1 (Dumont et al., 2010).

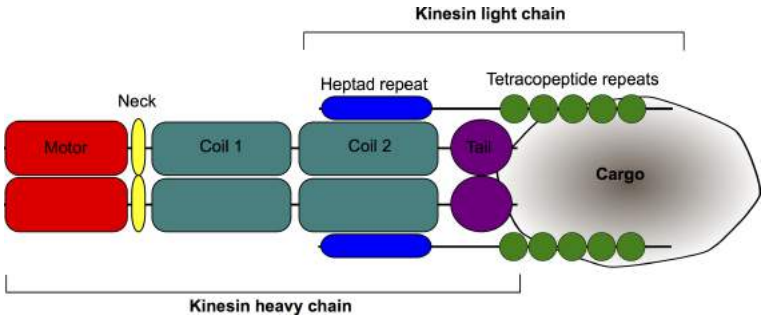


Figure 1.12 - The structure of kinesin-1 tetramer. Kinesin-1 tetramer is composed of two ∼960 amino acids heavy chains (KHC) as described in section 1.2.2.1 and two 560 amino acid kinesin light chains (KLC) which mediate binding to cargo. KLC contain an α-helical coiled coil region which binds the stalk region of KHC, while 5 tetracopeptide repeat domains are responsible for binding cargo. Adapted from Verhey et al., 1998.

Cargo may also be attached to the KHC in a KLC-independent fashion. Studies have convincingly demonstrated that kinesin-1 is required for the trafficking of mitochondria through the use of KIF5B$^{-/-}$ mouse embryos. Labelling these organelles with MitoTracker showed they were tightly clustered around the perinuclear area, but upon microinjection of KIF5B vector into the cells, the mitochondria re-dispersed throughout the cytoplasm (Tanaka et al., 1998). The mechanism through which mitochondria attach to kinesin-1 was elucidated through several experiments. Firstly genetic screens in *Drosophila melanogaster* were carried out which identified the effector protein milton (Stowers et al., 2002), which binds directly to the KHC. Through the use of both milton and KHC truncation mutants, it was found that the N-terminal portion of milton (residues 1-450) binds to residues 810-891 of KHC (Glater et al., 2006). Secondly the mitochondrial GTPase miro was identified as a potential milton binding protein through a yeast-2-hybrid screen (Giot et al., 2003). This was confirmed when mutations in *Drosophila* miro were found which prevented the mitochondria from being transported along the axon (Guo et al., 2005), and further experiments with truncation mutants showed that residues 1-750 of milton are important for binding miro (Glater et al., 2006).

Finally, kinesin-1 may also bind cargo directly, without the need for either KLC or other

adaptor proteins. When the C-terminal fragment of the KHC (residues 814-963 (human numbering)) was used as bait in a yeast-2-hybrid screen the results showed this fragment could directly bind the synaptosome-associated protein SNAP25, as well as SNAP23 (Diefenbach et al., 2002). The binding region of SNAP25/23 was mapped to residues 1-84, a region composed of heptad repeats, suggesting that a coiled-coil mediates binding to KHC.

1.2.3 Role of kinesin in microtubule dynamics

Although kinesins are mainly thought of as cargo transporters, a number of isoforms have been shown to regulate microtubule dynamics since they are able to depolymerise these structures. The kinesin-13 family, comprising of KIF2A, KIF2B and KIF2C/MCAK, which do not transport cargo and have their motor domain in the middle of the molecule, rather than at the N-terminus (Hirokawa et al., 2009), are the amongst the most well studied microtubule depolymerases. MCAK, for example is known to weakly bind microtubules and diffuse along their length until they reach the end of a filament, where upon they catalyse the removal of tubulin dimers in an ATP-dependent fashion (Hunter et al., 2003). MCAK appears to preferentially bind curved protofilaments (a hall mark of microtubules already undergoing depolymerisation), which may be one mechanism to ensure it only catalyses the disassembly of microtubules which have already lost their GTP-cap and have therefore undergone catastrophe (Moores et al., 2002). A member of the kinesin-8 family, KIF18A, also depolymerises microtubules in a length-dependent manner, with long filaments disassembled faster than shorter filaments. Since KIF18A is a processive plus-end directed motor protein, it's possible that the microtubule acts a 'sink', so the longer the filament, the more KIF18A molecules will accumulate at the plus-end, resulting in faster depolymerisation rates (Varga et al., 2006). KIF18A may therefore play an important role in regulating microtubule length, since budding yeast lacking this protein featured abnormally long filaments (Cottingham and Hoyt, 1997). Finally, the 17kDa protein stathmin, which is well studied due to the fact it is overexpressed in some cancer cells (Murphy and Cassimeris, 2006), acts through a completely different mechanism to bring about microtubule catastrophe. Since stathmin has two tubulin binding sites, it was originally postulated that the protein sequestered free tubulin dimers, thus preventing their incorporation into the growing microtubule (Belmont and Mitchison, 1996). However, recently it has been demonstrated that stathmin also stabilises curved protofilaments (Gupta et al., 2013), which results in microtubule catastrophe.

1.2.4 Cytoplasmic Dynein

Unlike kinesin, for which a large number of heavy chain isoforms have been discovered, there is only one major isoform of cytoplasmic dynein (hereafter referred to as dynein), which functions to transport cargo in a retrograde fashion towards the MTOC (Paschal et al., 1987). Moreover, it can also play a role in reorganising the microtubule network through positioning of the mitotic spindle (Rosenthal, 2013), making dynein of vital importance for the correct functioning of animal cells.

1.2.4.1 Structure

Like kinesin-1, dynein functions as a homodimer, although it is much larger complex with a molecular weight of 1.6 MDa (Allan, 2011). The dynein heavy chain is, as its name suggests, the highest molecular weight component of the motor at approximately 532 kDa. It comprises the small, C-terminal microtubule-binding domain at the end of a 10nm anti-parallel coiled-coil stalk (Gee et al., 1997), a AAA+ ATPase ring and a buttress, which were identified through electron microscopy and sequence analysis (Carter, 2013). The linker, important in force generation as discussed further below, sits across the AAA+ ring, with the N-terminal tail coming out from AAA1 at a 90^o angle to the linker (Roberts et al., 2012a).

Five additional subunits are also bound either directly or indirectly to the dynein heavy chain - all as dimers. Directly bound to the tail of the heavy chain is the intermediate chain (IC) of 74 kDa and the light intermediate chain (LIC) of 59 kDa. Three different light chains, LC7/Roadblock, LC8 and Tctex1 - each between $\sim$10 and $\sim$13 kDa, indirectly bind the heavy chain through the intermediate chain (Pfister et al., 2006). In mammals, two genes encode each of these five accessory proteins, and they can also be differentially spliced or phosphorylated, suggesting they play a major role in the recruitment of specific cargo (reviewed in (Allan, 2011). For example, lysosomes require IC for attachment (Cai et al., 2010), while endosomes require LIC (Bielli et al., 2001) and ribonucleoproteins depend on LC8 to bind dynein (Navarro et al., 2004). However, there is also evidence to suggest that these accessory proteins may also play a structural role, since in the absence of LIC the heavy chain aggregates, rather than forming a dimer, when it is assembled from recombinant proteins *in vitro*. See Figure 1.13 for a diagram of the dynein heavy chain and accessory proteins.

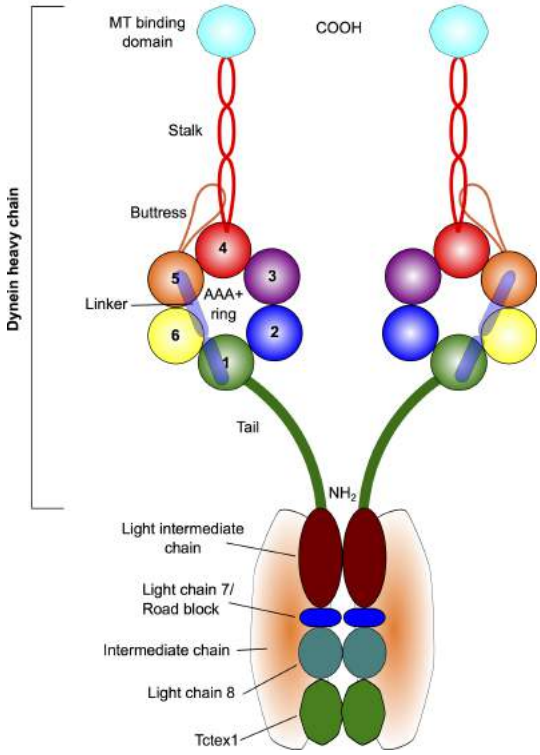


Figure 1.13 - The structure of cytoplasmic dynein. Cytoplasmic dynein consists of a C-terminal microtubule-binding domain which is attached to the end of 10nm stalk, which connects it to the AAA+ ATPase ring. The buttress which emerges from AAA5 and connects to the stalk is thought to confer support to the structure. Meanwhile the linker arm changes conformation depending on the ATP-binding state of the AAA+ ring. This conformation change is transferred through the stalk to the motor domain to allow the molecule to translocate along microtubules. Bound to the N-terminal tail of dynein are a number of addition proteins that either mediate binding to cargo directly, or binding to dynactin - an accessory complex required for the correct functioning of dynein. Adapted from Allan, 2011 and Schmidt et al., 2012.

1.2.4.2 Force generation

Dynein generates force of approximately 7pN (Gennerich et al., 2007) through rounds of ATP hydrolysis, followed by release of Pi and ADP (Trokter et al., 2012). This begins with the microtubule binding domain attached to the microtubule filament, which results in the opening of the ATP binding pocket in AAA1, the main catalytic site of the dynein motor (Kon et al., 2004; Imamula et al., 2007). As expected, this domain contains a Walker motif which mediates binding to ATP that diffuses into the pocket (Walker et al., 1982; Cho et al., 2008), resulting in the microtubule binding domain detaching from the filament (Kon et al., 2009). The long-range communication that must occur to allow this (the microtubule binding domain and the AAA1 domain are approximately 25nm apart) is thought to be mediated through sliding of the coiled coil stalk to which the microtubule binding domain is attached to the AAA+ ring, since fixing the stalk in different registries alters both the microtubule

and ATP binding affinities of the complex (Gibbons et al., 2005; Kon et al., 2009). CryoEM experiments, have demonstrated that ATP docking into the AAA1 catalytic site appears to bias the linker arm to become kinked, due to a flexible hinge region, contacting AAA1 and AAA2 (Roberts et al., 2012b). Reorienting the linker pushes the microtubule binding domain forward by approximately 8nm (Reck-Peterson et al., 2006), and weak binding to tubulin occurs. ATP hydrolysis and the release of inorganic phosphate strengthens the interaction of the motor and filament and causes the linker to straighten. ADP then diffuses away from the AAA1 domain, allowing the catalytic cycle to repeat (Figure 1.14). Whilst AAA2, 3 and 4 can also bind ATP, these nucleotide binding sites are non-catalytic. Nevertheless, mutations in the ATP binding motifs in these domains do negatively impact on dynein's processivity, suggesting nucleotide binding may provide structural support to the motor (Kon et al., 2004). Meanwhile, AAA5 and 6 do not possess any nucleotide binding motifs. It is thought that they play a structural role, helping to transmit the conformational changes in the AAA1 and microtubule binding domain, and acting as an anchor point for the buttress in the case of AAA5 (Cho and Vale, 2012).

It seems intuitive to imagine that, as is the case for kinesin-1, some communication between the two dynein heavy chains is required to ensure that the two catalytic cycles are asynchronous to ensure at least one of the microtubule binding domains is strongly attached to the microtubule filament at all times. However, experiments where each DHC have been tagged with a different colour fluorophore have demonstrated this is not necessarily the case, with little coordination observed between the two monomers (Qiu et al., 2012). The fact that dynein spends most of its time bound to tubulin during its catalytic cycle, only detaching when bound to ATP, may help explain why the motor does not fall off microtubule filaments more frequently (it can travel up to 1.5μm, the equivalent of $\sim$125 steps before detaching; similar to kinesin-1).

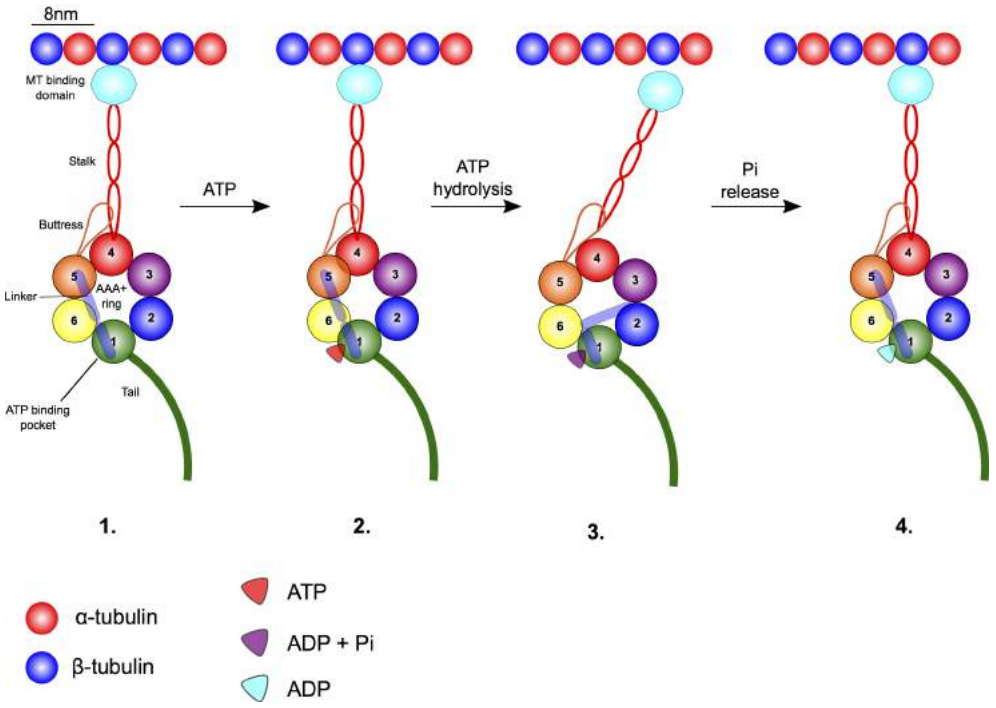


Figure 1.14 - The catalytic cycle of dynein. Dynein remains bound to microtubules in the absence of nucleotide (stage 1), and strongly bound once ATP diffuses into the nucleotide binding pocket of AAA1 (stage 2). However, upon hydrolysis of ATP to ADP+Pi, the motor domain becomes weakly bound, allowing it to move towards the minus end (stage 3). Release of Pi from the nucleotide binding pocket once again allows the microtubule binding domain to reattach to the track (stage 4). Release of ADP allows the cycle to repeat. Adapted from (Roberts et al., 2012a)

1.2.4.3 Linking to cargo

Dynactin is the major multi-subunit complex which is required to link the dynein motor to cellular cargo. In total dynactin is composed of 11 different subunits and has a molecular weight of 1.2 MDa; making it almost as large as dynein itself (Schroer, 2004; see Figure 1.15 for a cartoon of the dynactin complex).

The largest component of the dynactin complex is the central rod which is approximately 40nm long and composed of 8 Arp1 (actin-related protein 1) molecules, which is visible through electron microscopy (Schroer et al., 1996). 2D chromatography revealed that dynactin also contains CapZ, and imaging of polyclonal antibodies against this protein using electron microscopy indicated that this subunit was always located at one end of the rod, marking it as the 'barbed' end (Schafer et al., 1994). Polyclonal antibody staining also revealed that p62 was located at the opposite end to CapZ.

The location of the other subunits of dynactin were deduced mainly through treatment of the complex with potassium iodide salt (KI), followed by gel filtration chromatography. Arp1 was mainly eluted as a monomer, but other higher-order complexes were also eluted and found to be composed of multiple subunits after analysis with SDS-PAGE. For example,

p150^{Glued}, p50 (dynamitin) and p24 were found to exist as a complex after KI treatment, with densitometry analysis of the SDS-PAGE gel revealing the subunits existed in a 2:4:2 stoichiometry. Furthermore, p62 was found to be associated with β-actin, p27 and p25 via this method, with a 1:1:1:1 stoichiometry (Eckley et al., 1999).

p150^{Glued} supports both microtubule binding through the N-terminal CAP-Gly domain which plays an important role in dynein function, since it serves to enhance processivity of the motor (King and Schroer, 2000). Dynein binds the dynactin complex through an interaction between the intermediate chain and p150^{Glued} (King et al., 2003), with an extensive region of p150^{Glued} (amino acids 217 - 811) thought to support intermediate chain binding (Vaughan et al., 2002; King et al., 2003). Meanwhile, p50/dynamitin is required to link the 24nm p150^{Glued} to the Arp1 rod. It has been shown that overexpression of p50 causes the detachment of p150^{Glued}/p24, thereby interrupting the function of dynein by decoupling it from its cargo (Echeverri et al., 1996).

Dynactin is a crucial linker between the dynein motor and a wide variety of cargo. For example, both p50 and p150^{Glued} appear to co-localise with melanosomes, suggesting these two dynactin components are important in pigment granule transport (Vancoillie et al., 2000), with more recent evidence suggesting that melanoregulin and RILP (Rab-interacting lysosomal protein), which are both localised on the melanosome membrane, from a complex with p150^{Glued}. Meanwhile, βIII spectrin, which is localised on Golgi membranes can bind the Arp1 rod (Holleran et al., 2001), while the ability of the CAP-Gly domain of p150^{Glued} to bind microtubules is necessary for anchoring these filaments at centrosomes (Quintyne et al., 1999). Therefore dynein and dynactin play a critical role in both organelle transport and cell division.

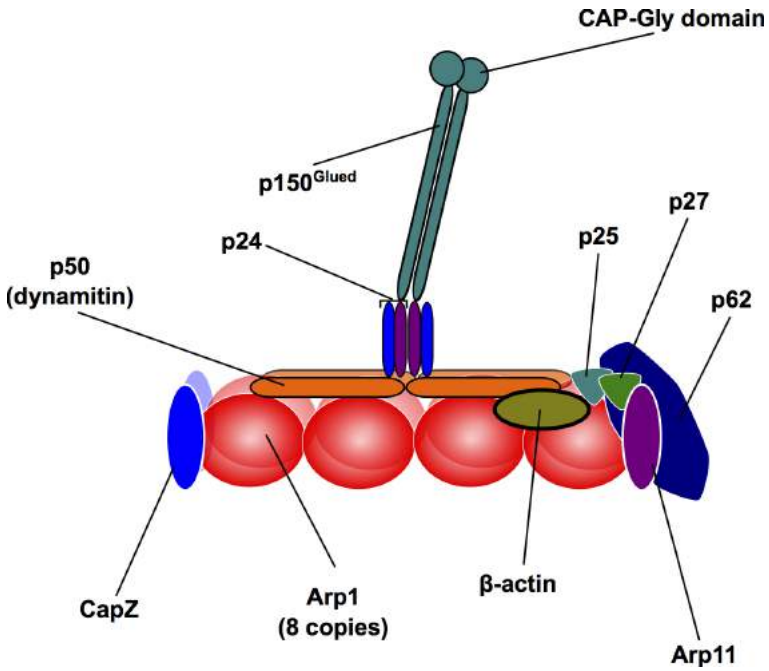


Figure 1.15 The dynactin complex. Dynactin is a large, 1.2 MDa complex which functions to both link many types of cargo to cytoplasmic dynein. It consists of a central 10nm rod composed of 8 copies of Arp1, the actin capping protein CapZ at the 'barbed' end of the rod and β-actin, p25, p27, p62 and Arp11 at the 'pointed' end. 4 copies of p50/dynamitin function to link the dimeric p24 & p150^{Glued} complex to the rod. p150^{Glued} plays a fundamental role, since it binds dynein, as well as some cargo - such as melanosomes. The CAP-Gly domain of p150^{Glued} also mediates binding to microtubules, therefore potential stabilising the interaction between dynein and its track, which may be important in maintaining long run-lengths. Adapted from Schroer, 2004.

1.3 The actin cytoskeleton

The existence of actin - first termed 'myosin-ferment' dates back well over 100 years, when it was isolated from muscle (Halliburton, 1887). Later, F.B. Straub, also using muscle tissue, again isolated this protein which was termed 'actin'. It was found to exist in two forms: non-viscous (globular actin) and viscous (filamentous actin), after the addition of KCl salt (Straub, 1942). Actin has since been recognised as one of the most abundant proteins in all eukaryotic cells, has a huge number of binding partners and is likewise involved in many processes that are essential for cell function.

1.3.1 Actin structure

Monomeric actin exists as 3 main 42 kDa isoforms - α, β and γ, which can be further sub-divided into α-skeletal, α-cardiac, α-smooth, β-cytoskeleton, γ-cytoskeleton and γ-smooth. They are encoded by six different genes (Acta1, Actc1, Acta2, Actb, Actg1 and Actg2, respectively; Perrin and Ervasti 2010). Despite the different functions of these isoforms, and their different expression patterns, they differ by only a few amino acids at the N-terminus, with each isoform sharing at least 93% sequence homology with every other isoform (Perrin and Ervasti, 2010).

Although the structure of G-actin has been solved via X-ray crystallography a number of times complexed with different actin-binding proteins, F-actin does not crystallise due to its flexible nature (Dominguez and Holmes, 2011). Therefore its structure has largely been deduced using electron microscopy, with cryoEM in particular providing high, 6.6Å resolution structures of F-actin, which are sufficient to observe the secondary structure of the protein (Fujii et al., 2010). This, and other studies, have shown that F-actin is composed of two chains which have counter-clockwise handedness and a periodicity of 36nm (Hanson and Lowy, 1963) which corresponds exactly to the step size of actin-based motors such as mysoin-Va (as detailed in section 1.4.1)(Walker et al., 2000).

Two different F-actin structures can be found in cells: linear and branched, which are found in different locations. For example, branched actin is required to form the lamellipodium; the mesh of actin located at the leading edge of cells which plays an important role in cell migration (Krause and Gautreau, 2014). The cell cortex, a band of actin which runs just underneath the plasma membrane and plays a largely structural role governing cell

shape (Salbreux et al., 2012), is also composed of branched actin due to the action of cross-linker proteins such as filamin, fimbrin and fascin (Stossel et al., 2001; Klein et al., 2004; Sedeh et al., 2010). Meanwhile, parallel bundles of linear actin filaments are required for the formation of filopodia - slender projections which emanate from the front of cells and are important for environmental sensing and therefore help direct cell migration (Mattila and Lappalainen, 2008). Stress fibres, which play a role in adhesion either to other cells or to a substrate via focal adhesion plaques are also composed of linear actin filaments, arranged in an anti-parallel configuration and cross-linked via protein such as α-actinin (Burridge and Wittchen, 2013). Evidence from the budding yeast *Saccharomyces cerevisiae* also suggests that linear actin cables are required to generate tracks along which myosin V can translocate cargo (Lo Presti et al., 2012).

1.3.2 Actin dynamics

The polymerisation of G-actin into F-actin is kinetically unfavorable until actin trimers are formed. These act as 'seeds', allowing the subsequent addition of G-actin monomers to occur much faster (Wegner and Engel, 1975), allowing the filament to elongate at speeds of up 5μm/s, given a higher enough concentration of G-actin (Pollard et al., 2000). G-actin is bound to ATP, since the ATPase activity of monomeric actin is weak. However, filamentous actin has much stronger ATPase activity, resulting in the hydrolysis of bound ATP to ADP+Pi. This results in very stable filaments, although as soon as Pi diffuses out of the binding pocket the actin filament becomes unstable (Korn et al., 1987). Coupled with the fact that the 'barbed' end of actin filaments is the major site of elongation, with up to 10 times faster addition of G-actin compared to the opposite 'pointed' end (Pollard, 1986), this leads to a phenomenon termed 'treadmilling', whereby the filament grows at the barbed end and depolymerises at the pointed end (see Figure 1.16).

The instability of non-muscle actin filaments which leads to rapid turnover is fundamental for normal cell function. Without this property, neither cell shape change nor cell migration would be possible. Likewise, dynamic actin tracks should lead to more effective transport of cargo by myosin motors, as actin filaments are typically short (0.2-3μm) and switching between static tracks is often not possible due to relatively low filament density (Cramer, 2008; Semenova et al., 2008). Given the importance of dynamic actin it is unsurprising that cells have evolved a large number of factors which control both assembly and disassembly

of linear and branched filaments, the best characterised of which are described below.

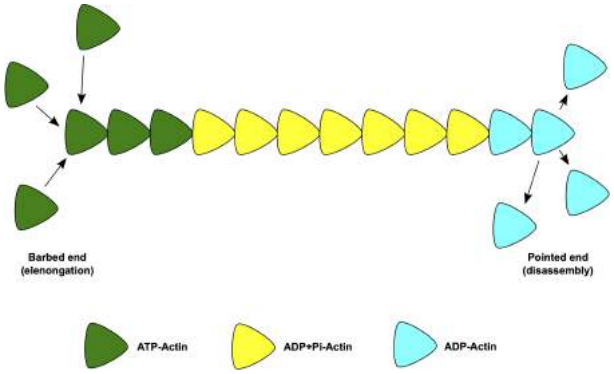


Figure 1.16 - Actin treadmilling. ATP-G-actin is able to polymerise into actin filaments, which occurs rapidly at the barbed end. However, the ATPase activity of F-actin is much higher than that of G-actin, resulting in the hydrolysis of ATP to ADP+Pi. F-actin bound to ADP+Pi is very stable, but release of Pi drives the filament to disassemble at the pointed end. Actin polymerisation at the barbed end, coupled with loss of G-actin subunits from the pointed end results in actin 'treadmilling' whereby the filament length remains approximately constant, but moves towards the pointed end.

1.3.2.1 Nucleation factors

Formins

Linear actin cables are largely generated by a family of nucleation factors termed formins, of which 15 different types exist in mammalian cells. All formins are characterised by the fact they contain a formin-homology 2 (FH2) domain, with the sequence of this region allowing these proteins to be organised into seven subclasses (diaphanous, formin-related proteins in leukocytes, inverted formins, dishevelled-associated activators of morphogenesis, formin homology domain proteins, delphilin and formins; Higgs and Peterson, 2005). Of these subclasses, diaphanous is the most well characterised. This protein contains a N-terminal GTPase binding domain (GBD) which can interact with the C-terminal diaphanous autoinhibitory domain (DAD), thus preventing the nucleation of filaments. This is relieved through binding of several GTPases, notably RhoA/B/C, to the N-terminal domain, which drives the FH1 and FH2 domain to adopt an active conformation (Lammers et al., 2005; Wallar et al., 2006). Other GTPase such as Rac, Rif and Cdc42 are also involved in regulating the actin nucleating capabilities of formins (Yayoshi-Yamamoto et al., 2000; Peng et al., 2003; Lammers et al., 2005; Pellegrin and Mellor, 2005). Moreover, the binding of these prenylated GTPases is also thought to be important for the localisation of formin, since they act to anchor the protein at the membrane (Maiti et al., 2012). The FH1 domain first binds profilin (a protein which complexes with ATP bound G-actin, preventing it from spontaneously incorporating into filaments) which serves to enhance the elongation rate (Chhabra and Higgs,

2007; Chesarone and Goode, 2009; Dominguez, 2009). The profilin-actin complex is then passed to the FH2 domain which incorporates G-actin onto the barbed end of the growing actin filaments, while profilin is released (Pruyne et al., 2002; Sagot et al., 2002). When the actin polymerisation rate of the yeast formin bni1 was measured and fitted to a model whereby the actin seed contained one, two or three actin monomers, the data best matched a seed contain two molecules of G-actin. It is therefore thought that the FH2 domain stabilises an actin-dimer in order to enhance filament nucleation (Pring et al., 2003).

The rate of elongation has been measured at around 100 G-actin molecules per second (Kovar and Pollard, 2004), which is around 15-fold faster than is possible using diffusion-limited elongation (Romero et al., 2004). Since formins remain tightly associated with the barbed end of actin filaments, it is also thought they enhance filament elongation by competing with capping proteins, such as α/β heterodimeric capping protein, which would otherwise block the addition of new G-actin (Zigmond et al., 2003).

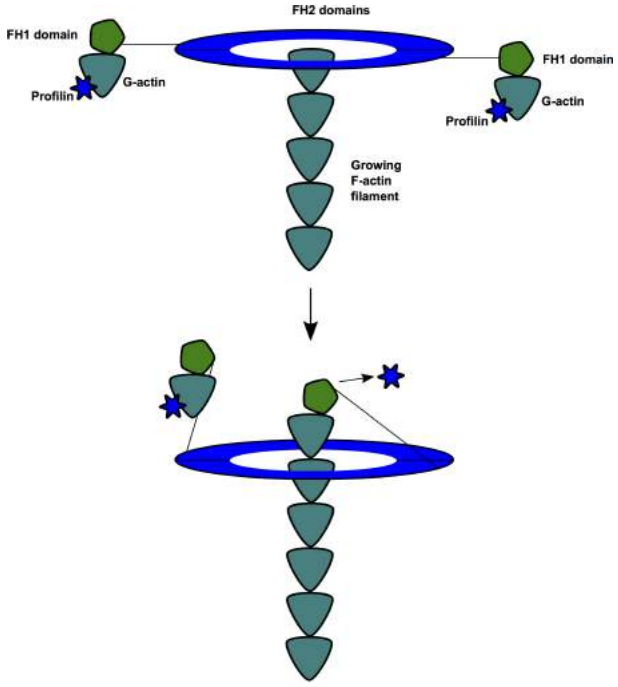


Figure 1.17 - Formin mediated actin nucleation. All formins contain both an FH2 domain which is required for actin nucleation at the barbed end of the actin filament and an FH1 domain which binds profilin-G-actin. Formins function as dimers, with the two FH2 domains creating a ring from which the newly generated filament emerges, while the FH1 domains deliver G-actin monomers to the FH2 domain. Adapted from (Campellone and Welch, 2010).

While diaphanous is the best characterised formin, formin-1 (beloning to the formin subclass) was the first such protein of this family to be discovered. To date 6 different splice isoforms of formin-1 have been identified in mouse (Kobielak et al., 2004; Dettenhofer et al., 2008), with the domain organisation of these isoforms outlined in Figure 1.18. Isoforms IA

and IB are almost 100% homologous, with formin-1 IB missing only a small 108bp stretch of DNA corresponding to exon 17. Likewise, isoforms IA and II are also nearly identical, with isoform II missing exon 5 (176bp) and exon 7 (118bp), while isoforms IB and II are 97.4% homologous. There is evidence to suggest that exon 2 is involved in binding microtubules, implicating formin-1 in mediating the interplay between both microtubule and actin cytoskeletons (Zhou et al., 2006).

On the other hand, formin-1 isoform IV is quite different from the other isoforms, since it is missing the large (1994bp) exon 2, and instead contains exon 6, known to encode an FH3 domain. Whilst for other formins this domain helps regulate the activation of the protein, since it can bind the C-terminal DAD domain to bring about autoinhibition, it is not thought that formin-1 possess a DAD domain, and therefore it remains unclear how the activity of any of the formin-1 isoforms is controlled (Schonichen and Geyer, 2010). However, compared with the other isoforms of formin-1, isoform IV has been relatively well studied, although conflicting evidence exists for the role this protein plays in cells. Originally, Kobielak et al. demonstrated by antibody labelling that formin-1 isoform IV localised to adherens junctions and went on to show that the protein was a binding partner of α-catenin using both yeast-2-hybrid and immuno pull-down techniques. However, more recently Dettenhofer et al. demonstrated that the antibody used in the Kobielak et al. study cross-reacted with F-actin, and that formin-1 isoform IV actually has microtubule and cytoplasmic localisation. While this group also provided evidence showing formin-1 plays a role in cell spreading and focal adhesion formation, other evidence indicates that formin-2, which is highly similar to formin-1 (Leader and Leder, 2000), also plays a role in the long-range transport of transferrin-containing vesicles (Schuh, 2011).

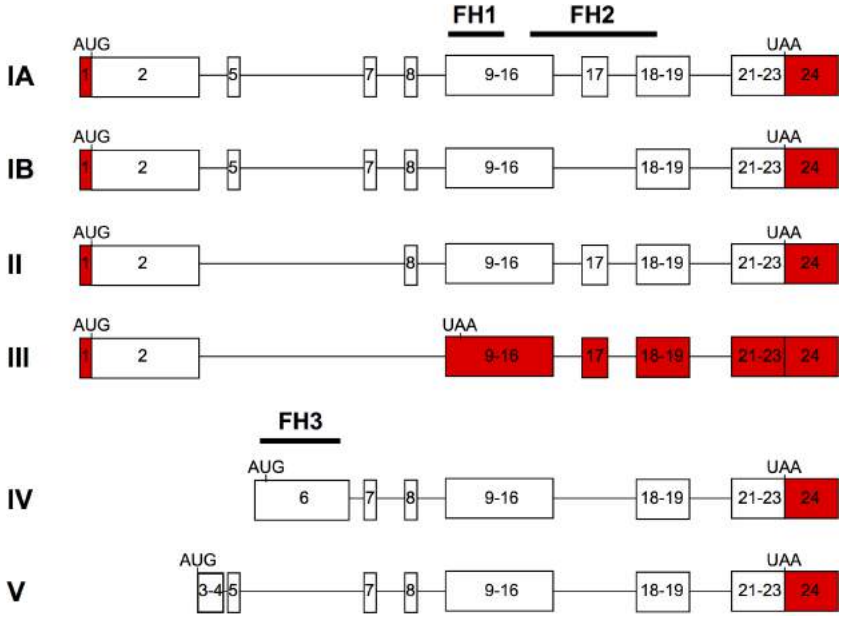


Figure 1.18 - Schematic outlining the exon and domain structure of the 6 different formin-1 isoforms. Each numbered box represents a different exon within the formin-1 gene that can be alternatively spliced to give rise to the 6 different isoforms. Red boxes indicate that no open reading frame exists for that exon, and hence it is not translated. Formin-1 isoform IA = 1466aa; IB = 1430aa; II = 1368aa; III = 627aa; IV = 1204aa; V = 850aa. Adapted from Wang et al., 1997 and Kobielak et al., 2004.

Spire

Spire is another protein that nucleates linear actin cables through an alternative mechanism to formin. Rather than catalysing the addition of new G-actin monomers at the barbed end, Spire simply acts as a substrate to which up to 4 G-actin molecules can bind simultaneously, thus forming an actin seed. Once this actin seed has been generated, the addition of further monomeric actin then becomes kinetically favorable without the need for any other factors (Wegner and Engel, 1975). Spire achieves this as it contains 4 adjacent WH2 (WASP homology domain-2), each of which can bind a single a G-actin molecule (Paunola et al., 2002; Quinlan et al., 2005).

In addition to the WH2 domains, Spire also contains an N-terminal KIND (kinase non-catalytic C-lobe domain) and a C-terminal Fab1/YOTB/Vac1/EEA1 (FYVE) domain (see Figure 1.19). The KIND domain allows interaction with the C-terminus of formin-1 and formin-2, which may be important for its ability to nucleate actin filaments (Quinlan et al., 2007). Meanwhile the FYVE domain is involved in targeting Spire to membranes, since it interacts with PIP3 (Stenmark et al., 2002). As with formin-2, Spire has also been implicated in the long-range transport of vesicles (Schuh, 2011; Lagal et al., 2014).

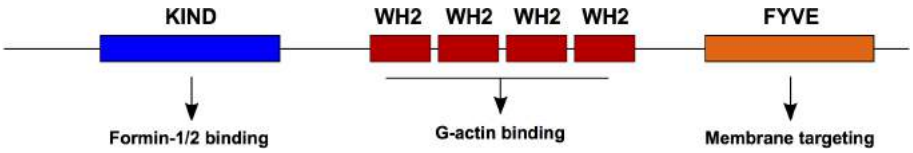


Figure 1.19 - The domain structure of Spire. Spire contains 4 WH2 domains, each of which can bind a single G-actin monomer. Thus, these molecules generate actin 'seeds', which when formed, allow the kinetically favorable addition of further G-actin monomers, thus resulting in the formation of an actin filament. The N-terminal KIND domain mediates binding to formin-1 and formin-2, while the FYVE domain interacts with lipid membranes. Adapted from (Campellone and Welch, 2010).

Arp2/3

Unlike Spire or formin which both generate linear actin cables, the Arp2/3 complex is uniques in its ability to nucleate branched actin filaments. Arp2/3 itself is a $\sim$220 kDa complex consisting of seven subunits in total: ARP2 (45kDa) and ARP3 (47kDa), both of which mimic the structure of G-actin, and ARPC1 (40kDa), ARPC2 (34kDa), ARPC3 (21kDa), ARPC4 (20kDa) and ARPC5 (16kDa) (Welch et al., 1997; Robinson et al., 2001).

Both X-ray crystallography and electron microscopy show that Arp2/3 enables the formation of branched actin filaments through ARPC2 and ARPC4 binding the mother filament, while ARP2 and ARP3 mimic an actin dimer, allowing a daughter filament to be nucleated at a 70º angle to the original filament (Rouiller et al., 2008; see Figure 1.20). Similar to G-actin ARP2 and ARP3 are also capable of binding ATP, which is essential for actin nucleation to occur (Goley et al., 2004). Also similar to filamentous actin, once ATP is hydrolysed by ARP2 (and possible ARP3), debranching occurs (Martin et al., 2006). The nucleotide state of the Arp2/3 therefore appears to be important for regulating the amount of branched F-actin.

A number of other proteins termed nucleation-promoting factors (NPFs) are also critical for the activity of Arp2/3 complex, which by itself only weakly nucleates the formation of branched actin filaments (Welch and Mullins, 2002). For example neuronal Wiskott-Aldrich syndrome protein (N-WASP) is a widely expressed and well characterised NPF that is able to activate the Arp2/3 complex. It consists of an N-terminal GBD, to which various GTPases such as Rac and Cdc42 can bind and in doing so relieve autoinhibition, thus activating the complex (Rohatgi et al., 2000). This allows the C-terminal portion of the molecule, which consists of a WCA domain (made up of an actin binding WH2 domain, a central region and an acidic Arp2/3 interacting region) to bind Arp2/3 directly, resulting in activation of the complex (Rohatgi et al., 1999). The WAVE (WASP-family verprolin homologue) family are

another type of NPF that are expressed in many different cells types (Takenawa and Suetsugu, 2007). WAVE exists as a complex with several other proteins including Sra1/PIR121, Nap1, Abi1, and HSPC300 which bind the N-terminal region, inhibiting the molecule (Suetsugu et al., 2006). The binding of both Rac and the adaptor NCK1 (non-catalytic region of tyrosine kinase adaptor protein 1) activates the molecule, allowing its C-terminal WCA domain to contact Arp2/3, resulting in enhanced actin nucleation (Eden et al., 2002). Other NPFs which contain a WCA domain include WASP and SCAR homologue (WASH), which is thought to be regulated through binding RhoA (Liu et al., 2009) and is necessary for membrane trafficking from endosomes to the *trans*-Golgi network (Derivery et al., 2009; Gomez and Billadeau, 2009). WASP homologue associated with actin (WHAMM) and the related JMY also contain C-terminal WCA domains and, as well as functioning as Arp2/3 activators, are known to play a role in ER-Golgi transport since they are able to bind microtubules (Campellone et al., 2008).

All NPFs described above are labelled class I, due to the fact they all contain C-terminal WCA domains which bind Arp2/3 in order to activate the complex. A second smaller class of NPFs activate Arp2/3 via a different mechanism compared to class I NPFs, albeit with lower potency. Class II NPFs mainly consist of cortactin and the related protein haematopoetic-specific protein 1 (HS1)(Dehring et al., 2011). Cortactin promotes branched actin filaments in two main ways. Firstly it is known to interact with N-WASP in order to increase its ability to activate Arp2/3 (Kowalski et al., 2005), and secondly it stabilises branched actin junctions (Ammer and Weed, 2008).

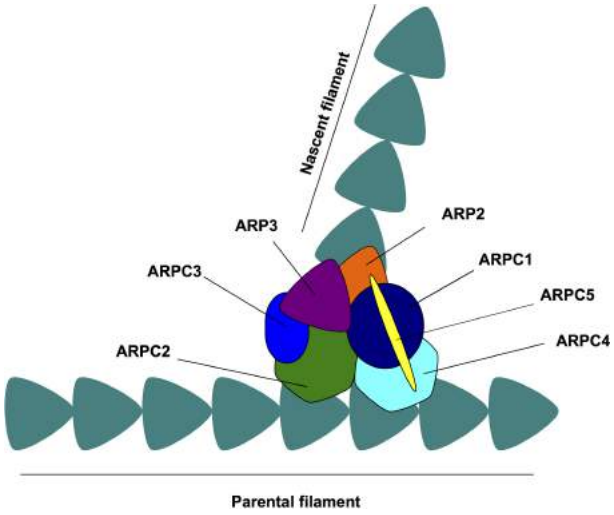


Figure 1.20 - The Arp2/3 complex. Arp2/3 is a 220 kDa complex consisting of ARP2 and ARP3 which mimic G-actin monomers, and ARPC1-5. ARPC2 and ARPC4 bind to the side of existing actin filaments, while ARP2 and ARP3 acts as a dimeric actin seed, facilitating the creation of new filaments at a 70º angle to the parental track. In this way Arp2/3 creates branched actin networks which are of primary important for driving cell motility and maintaining cell shape. Adapted from Rouiller et al., 2008

1.3.2.2 Disassembly factors

Although F-actin can spontaneously depolymerise through the hydrolysis of ATP, several proteins are also know to catalyse actin filament severing, such as actin depolymerising factor (ADF) and cofilin. These are small (15-20 kDa) proteins which play very similar roles in cells (Hotulainen et al., 2005) and contain 70% sequence homology. Two isoforms of cofilin are known to exist, with cofilin-1 expressed in most mammalian cell types, whilst cofilin-2 expression is restricted to muscle cells. Meanwhile ADF is expressed only in epithelial and endothelial cells (Vartiainen et al., 2002). Cryo-EM studies showed that the binding of ADF/cofilin to actin filaments changed its conformation by introducing a 5º twist in the helix which is sufficient to destabilise the filament and bring about actin severing (McGough et al., 1997).

Although ADF/cofilin functions to sever F-actin filaments, the generation of new barbed ends actually induce the formation of new tracks. Moreover, cofilin is able to nucleate actin filaments with a higher potency compared to ADF (Yeoh et al., 2002) and therefore these two proteins play an important role in governing actin dynamics.

Additionally, gelsolin is another protein which catalyses the severing of F-actin - cutting filaments with nearly 100% efficiency, making it more potent than either ADF or cofilin (Selden et al., 1998). The protein binds to the sides of actin filaments, inducing a kink which is thought to be the basis for severing to occur. After cutting, gelsolin remains bound

to the barbed end of the filament, thus preventing further elongation (Sun et al., 1999).

1.3.2.3 Non-muscle myosin-II

Myosins make up a large superfamily of actin-binding proteins which hydrolyse ATP to generate force. While over 35 different classes of myosin motors have so far been identified based on their gene sequence, class-II myosins comprise the largest group with up to 22 different isoforms expressed in some vertebrates (Odronitz and Kollmar, 2007). This group of motor proteins can be split into muscle and non-muscle types. Although the structure and function of muscle and non-muscle myosin-II is very similar they are regulated differently, with muscle myosin-II requiring troponin and tropmyosin, while non-muscle myosin-II depends on phosphorylation (discussed further below) (Conti and Adelstein, 2008). For brevity only non-muscle myosin-II (NMM-II) will be further discussed further here.

NMM-II is a hexameric complex comprising two 230 kDa heavy chains, two 20 kDa regulatory lights chains (RLC) and two 17 kDa essential light chains (ELC)(Vicente-Manzanares et al., 2009). The heavy chains contain a globular motor domain at the N-terminus which binds ATP and actin, followed by a lever arm which is required for force generation since it facilitates movement of the motor domain (Holmes, 2008). A long α-helical coiled coil follows the globular head and lever arm which mediates dimerisation of the two heavy chains. NMM-II can then associate with other NMM-II complexes through the coiled-coil domain to generate bipolar filaments which can slide actin filaments past each other (Figure 1.21).

Activity of NMM-II depends on the phosphorylation of RLC at serine19. In the dephosphorylated state, the myosin heads interact and become orientated in such a way that actin-binding is not favored. Upon phosphorylation of the RLC, the motor domains no longer interact and instead bind actin, resulting in increased ATPase activity and force generation (Wendt et al., 2001). Additional phosphorylation at threonine18 has been shown to further enhance the ATPase activity of NMM-II (Ikebe et al., 1986). Several kinases mediate phosphorylation of thr18/ser19 including myosin light chain kinase (MLCK), Rho-associated coiled coil-containing kinase (ROCK) and citron kinase (Matsumura, 2005), while dephosphorylation occurs via myosin light chain phosphatase (MLCP)(Griffith et al., 1987). Meanwhile the ELC binds the lever arm and functions to stabilise it (Ushakov, 2009).

NMM-II is involved in several essential cellular processes. For example myosin-II mediated actin contraction at the trailing edge, coupled with actin polymerisation in the lamel-

lipodium at the leading edge results in cell migration (Anderson et al., 1996). Similarly, myosin is also necessary to mediate contraction of the actin-ring to bring about cytokinesis (Wu and Pollard, 2005). The motor protein also has a role in the formation of focal adhesions as well as stress fibres, both of which are absent in NMM-II null cells (Even-Ram et al., 2007). Interestingly, there is also *in vitro* evidence to suggest that myosin-II can act to depolymerise F-actin. CryoEM microscopy was used to show that after the addition of low concentrations of myosin-II (10:1 ratio of actin:myosin-II) to thick actin bundles the result was thin, flexible bundles and in some cases individual filaments. Doubling the myosin-II concentration led to almost no actin bundles remaining. Moreover, even individual filaments had been depolymerised, leading to actin monomers being visible (Haviv et al., 2008). These findings suggest that myosin-II may also play a role in actin turnover by first depolymerising actin bundles such as stress fibres, followed by individual filaments to free G-actin.

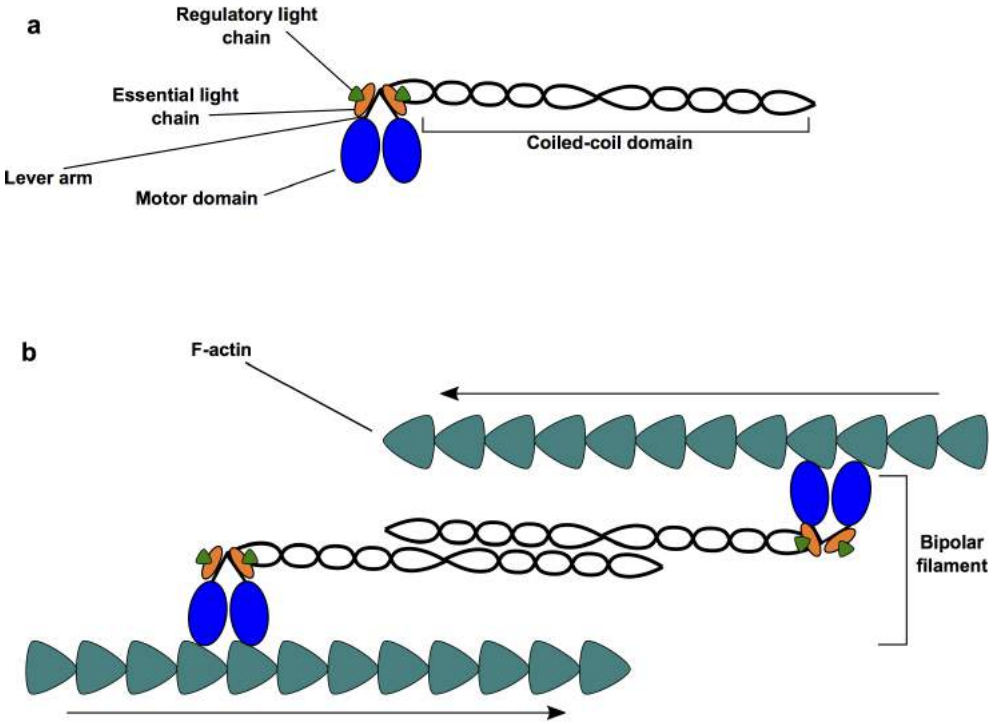


Figure 1.21 - The structure of non-muscle myosin-II. (a) Myosin-II is composed of two actin-binding motor domains which are tethered together via its coiled-coil domain. Phosphorylated regulatory light chain binds is required to relieve autoinhibition between the motor domain and the tail while the essential light chain stabilises the complex **(b)** Myosin-II forms bipolar filaments again through interactions between the coiled-coil domain. As the motor domains catalyses ATP, this causes actin filaments to slide past each other, producing tension and driving cell motility. Adapted from Vicente-Manzanares et al., 2009.

1.4 The melanosome cooperative capture model

The cooperative capture model states that long-range anterograde melanosome transport happens in two stages. Firstly the melanosome are trafficked bi-directionally along microtubules via kinesin and dynein. Once the pigment granules reach the cell periphery they then undergo myosin-Va-melanophilin-Rab27a dependent 'capture' and become tethered to the dense actin cortex (Wu et al., 1998)(Figure 1.22).

Brightfield video microscopy was used to show that melanosomes move bi-directionally in the periphery of *dilute* melanocytes, while treating the cells with nocodazole caused the movement to cease; demonstrating that this bi-directional transport is microtubule-dependent. Additionally the average transport velocity and path length of the melanosomes were measured in both wildtype and *dilute* melanocytes and found to be 60% slower and 50% shorter in the presence of myosin-Va. Furthermore, when myosin-Va tail was overexpressed (blocking myosin-Va function in a dominant-negative fashion) this induced melanosomes to cluster around the perinuclear area. These experiments, combined with observations from electron micrographs that actin filaments are randomly polarised and therefore not thought able to support long-range transport, gave rise to the hypothesis that myosin-Va retards melanosome transport and functions to tether these organelles at the cell periphery. Observations that the distribution of other organelles such as the endoplasmic reticulum, lysosomes and lytic granules are affected in cells lacking myosin-Va has led to the predication that this cooperative capture model is applicable to other types of cargo besides melanosomes (Dekker-Ohno et al., 1996; Klein et al., 1994; Griffiths, 1996).

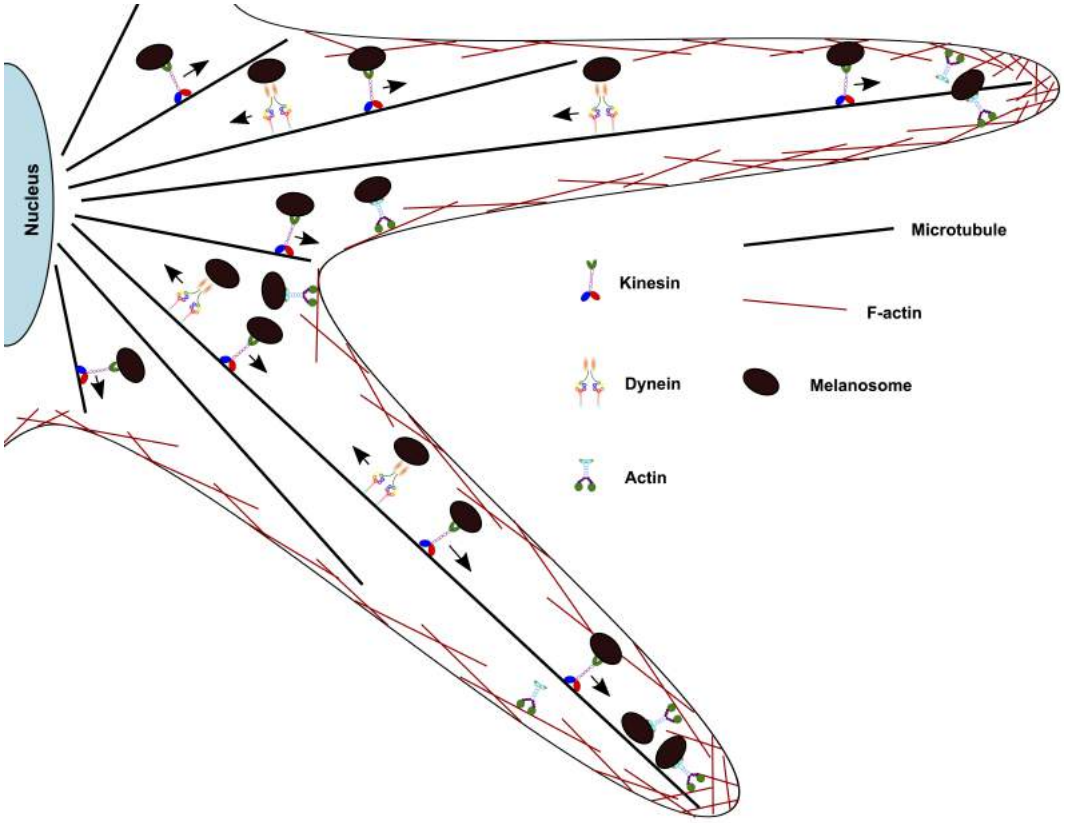


Figure 1.22 - The cooperative capture model. The cooperative capture model, based upon observation from *dilute* melanocytes, suggests that melanosomes are formed around the perinuclear area, and then move bi-directionally on microtubules under the influence of kinesin and cytoplasm dynein. Once they reach the periphery of the cell, where the concentration of F-actin and myosin-Va is greatest, the myosin motors 'capture' the pigment granules, and tether them. They then transport the melanosomes the short remaining distance to the plasma membrane, where they are transferred into neighbouring keratinocytes. Adapted from Wu et al. 1998.

1.4.1 The tripartite complex

Rab27a

Rab proteins are small GTPases (∼25 kDa) which are important for the intracellular trafficking of organelles and vesicles. These proteins act as molecular switches, cycling between GTP and GDP-bound conformations, which determines whether they are able to recruit various effectors such as adaptor proteins, tethering factors and molecular motors (reviewed by Stenmark, 2009). Individual Rab isoforms, of which there are over 60 predicted in the human genome (Seabra et al., 2002), are uniquely localised to different organelle membranes. Post-translational prenylation - the attachment of either a 15 carbon farnesyl or 20 carbon geranylgeranyl lipid via a thioether bond to cysteine residues at the C-terminus of Rabs - is crucial for this targeting to occur (Leung et al., 2006). 3 classes of prenyltransferases exist: farnesyltransferase and geranylgeranyl transferase type-I which act on the CAAX motif, and geranylgeranyltransferase type-II which prenylates both cysteine residues in proteins ending

in either CC or CXC motifs (Casey and Seabra, 1996). In addition, Rab escort protein (REP) is required to bind unprenylated Rab proteins, present it to the geranylgeranyl transferase and then chaperones it to the target membrane (Alexandrov et al., 1994).

Melanosomes, along with other lysosome related organelles and secretory vesicles use the small GTPase Rab27a in order to recruit effector molecules and motor proteins that regulate their transport (Hume et al., 2001). In the case of Rab27a, a di-geranylgeranyl modification, catalysed by the heterodimeric enzyme Rab geranylgeranyl transferase (RGGT) (Larijani et al., 2003), is required to allow Rab27a to associate with melanosome membranes. Along with prenylation, Rab27a must also be in its GTP-bound configuration in order to be successfully targeted to the melanosome membrane. The exchange of GDP for GTP is carried out by the exchange factor Rab3GEP. The loss of this protein disrupts the melanosomal localisation of Rab27a and causes perinuclear clustering of the pigment granules which is highly reminiscent of the *ashen* phenotype, whilst transfection of Rab3GEP-GFP restores the wild-type phenotype (Figueiredo et al., 2008; Tarafder et al., 2011). Since Rabs have low intrinsic GTPase activity additional factors termed GTPase activating proteins (GAPs) are needed to 'switch off' Rabs by increasing the GTPases hydrolysis rate. In the case of Rab27a, EPI64 has been identified as one possible GAP, since overexpression of this protein leads to aggregated melanosomes and a decrease in GTP-Rab27A, while expression of mutant EPI64 leads to normal levels of GTP-Rab27a and peripherally distributed pigment granules compared to control melan-a cells (Itoh and Fukuda, 2006).

One further class of protein, Rab GDP dissociation inhibitors (Rab GDIs) are required to extract GDP-Rab from the membrane. These proteins therefore play an important role in the recycling of Rabs and complete their catalytic cycle (Figure 1.23) (Soldati et al., 1993).

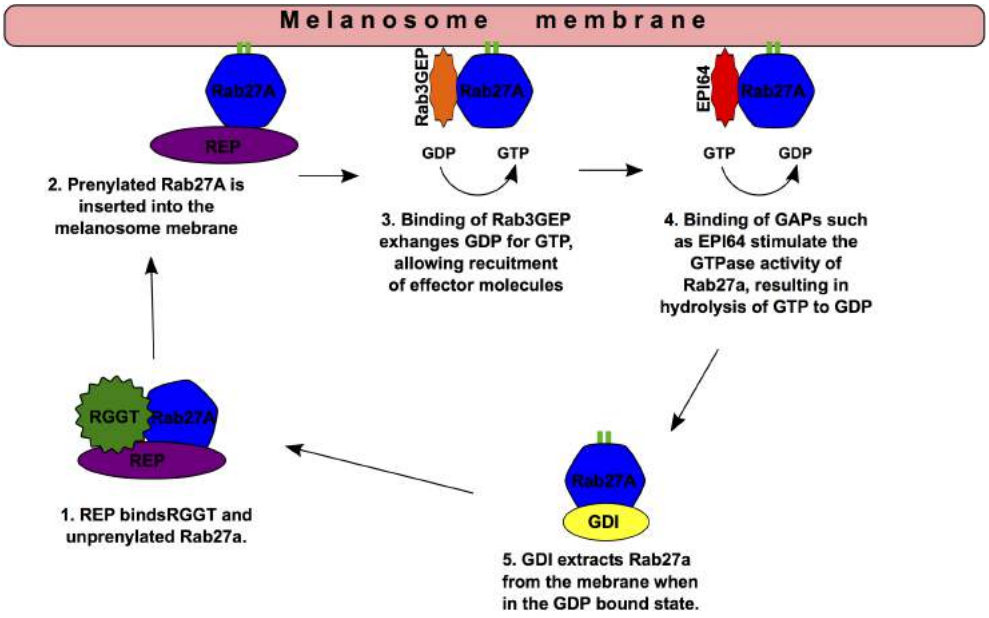


Figure 1.23 - The Rab cycle. (1) Initially, unprenylated Rab27a is bound by the Rab escort protein (REP) and prenylated by the Rab geranylgeranyl transferase complex. **(2)** Prenylated Rab27a can insert into the melanosome membrane. **(3)** Rab27a is loaded with GTP via the Rab3GEP protein - the GTP exchange complex for this Rab. In the GTP-bound state, Rab27a can then recruit effector proteins such as melanophilin. **(4)** To 'switch off' Rab27a, GTPase activating proteins, such as EPI64, stimulate the intrinsic GTPase activity of Rab27a thus bringing about the hydrolysis of GTP to GDP. **(5)** GDP-bound Rab27a is extracted from the melanosome membrane via GDP dissociation inhibitors (GDIs).

Myosin-Va

Myosin is a class of motor protein that utilises energy released from ATP hydrolysis to transport cargo towards the plus-end (or barbed-end) of actin filaments (Sakamoto et al., 2008), with the exception of myosin VI, which is minus-end directed (Buss et al., 2004). As with kinesin, there are a large number of myosin isoforms (the human genome encodes 40 myosin genes; Berg et al., 2001) which are organised into approximately 35 different classes (Odronitz and Kollmar, 2007).

However, unlike kinesin it has been well documented how melanosomes binds myosin, and the specific isoform required for melanosomal transport has been identified as myosin-Va (Hume et al., 2007). Myosin-V, with the exception of myosin II is the most well characterised myosin motor protein. Structurally it is similar to kinesin, with a motor domain at the N-terminus which binds actin and ATP, an α-helical neck domain which is required to generate the power stroke, and a tail domain that mediates both dimerisation with another myosin molecule, and attachment to cargo through various adaptor proteins (Figure 1.24; Hammer and Sellers, 2012). An alternatively spliced version of myosin-Va is expressed in pigment granule-containing cells that contains the protein sequence encoded by exon F which is required for the motor to interact with the EFBD of Mlph (Au and Huang, 2002).

Like kinesin-1, myosin-V is a two-headed motor and experiments involving labelling each head domain using quantum dots with a different emission profile and imaging with TIRF microscopy show that myosin V moves processively along actin filaments in a hand-over-hand stepping manner (Figure 1.25) (Warshaw et al., 2005; Hodges et al., 2007), the speed of which is comparable to kinesin, at approximately 400 nm s−1 (Cheney et al., 1993). However, myosin-V also has a high duty ratio (0.85; Forgacs et al., 2009), which is defined as the time the motor spends in contact with its track, which is partly why it is thought to behave mainly as a tether.

The neck domain of myosin-V contains 6 IQ motifs, each of which bind a molecule of calmodulin which functions to stabilise the neck domain and make it more rigid (Trybus, 2008). The neck domain is highly elongated compared with kinesin which allows myosin V to take large steps of 36 nm, as shown by optical trapping experiments (Rief et al., 2000), which matches the periodicity of actin.

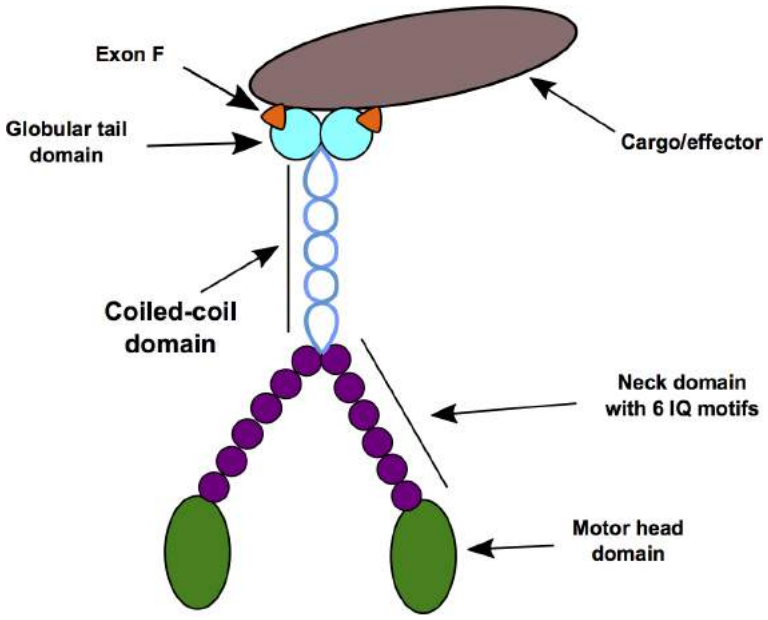


Figure 1.24 - Myosin-Va structure. Myosin-Va is a dimeric protein with each heavy chain weighing approximately 210 kDa. The motor domain is situated at the N-terminus, followed by a neck domain containing 6IQ motifs, each of which are capable of binding calmodulin which gives the neck rigidity. This region is responsible for the 36nm step size of the motor. After a long coiled-coil domain, the C-terminus of myosin-Va comprise a globular tail domain and (in the case of melanocyte-specific myosin-Va), the region encoded by exon F which is important for binding melanophilin. Adapted from Hammer and Sellers, 2012.

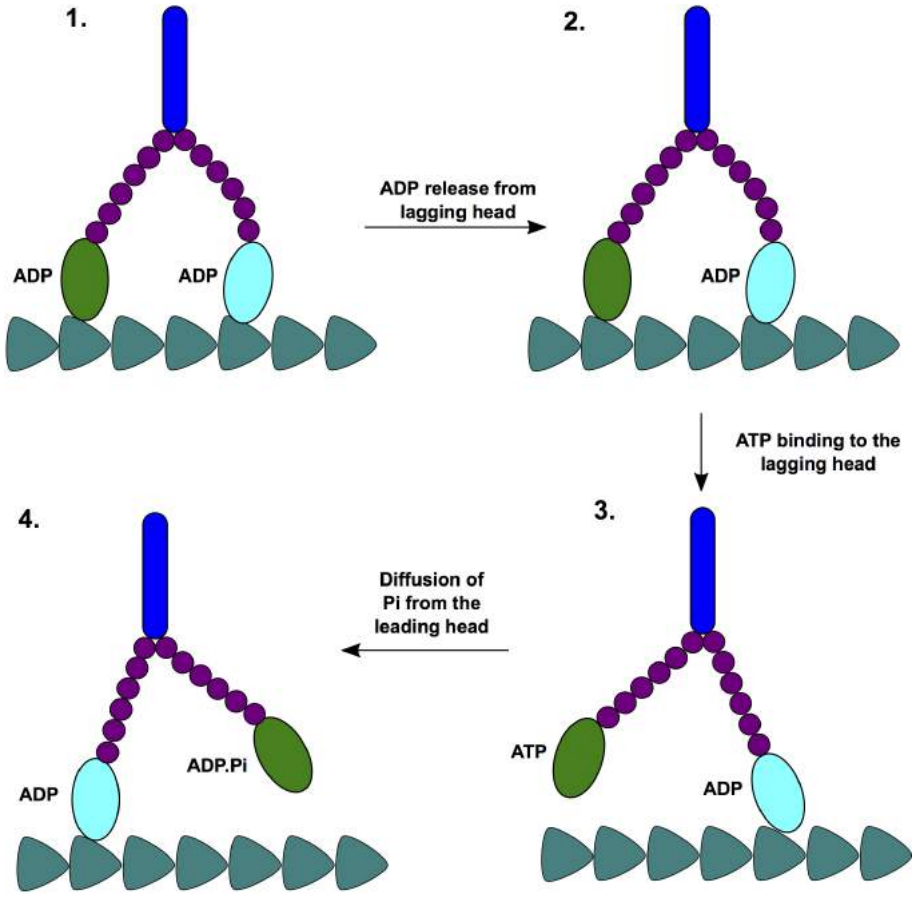


Figure 1.25 - Myosin-Va catalytic cycle. **(1)** Both motor domains are in the ADP-bound state, meaning they are strongly attached to the actin filament. The leading head is in the pre-powerstroke conformation. **(2)** Internal strain promotes ADP release from the lagging head. **(3)** Following the binding of ATP to the lagging head the motor undergoes the 'powerstroke', whereby the lagging head moves forward to become the new leading head. (4) ATP is hydrolysed to ADP+Pi and subsequently Pi diffuses from the leading head, causing both heads to again become strongly attached to the actin filament. Each step results in the lagging motor domain moving forwards by 72nm, thus moving the coiled-coil region forward by 36nm. Adapted from Hodges et al., 2007.

Melanophilin

Once Rab27a has been loaded with GTP and inserted into the melanosome it is able to recruit a number of effector molecules of which melanophilin (also known as Slac2-a), a 590 amino acid (65 kDa) protein is most important for pigment granule transport. Mutations in the melanophilin (Mlph) gene, or knockdown of the protein, leads to clustered melanosomes (Matesic et al., 2001; Hume et al., 2007).

Yeast two-hybrid experiments have shown that melanophilin can interact with GTP-Rab27a but not with Rab27T23N, which is thought to be either GDP-bound or nucleotide free (Hume et al., 2001; Strom et al., 2002). Truncation experiments have also demonstrated that only the first 150 amino acids of melanophilin, which contain two synaptogamin homology domains and a zinc finger domain, are required for binding Rab27a (Hume et al., 2006).

After the first 150 amino acids of Mlph which are important for Rab27a binding, the

central 250 amino acids of the molecule contains a globular tail binding domain (GTBD) and exon F-binding domain (EFBD), of which the latter is crucial for binding the myosin-Va motor, while the GTBD, although not essential for myosin-Va binding, functions to stabilise the interaction. Moreover, a small coiled-coil region within the C-terminus of melanophilin is also important for the interaction with myosin-Va, since Mlph1-466 did not bind the motor protein, whereas Mlph1-483 did (Hume et al., 2006).

The C-terminal portion of Mlph (aa 400-590) is also capable of binding F-actin. This region has been implicated in prolonging the run-length of myosin-Va, whilst simultaneously reducing the motor's velocity (Sckolnick et al., 2013). It has also been suggested that the C-terminal portion of Mlph enhances the ability of myosin-Va to tether melanosomes at the cell periphery (Kuroda et al., 2003). Figure 1.26 details the structure of Mlph and the tripartite complex.

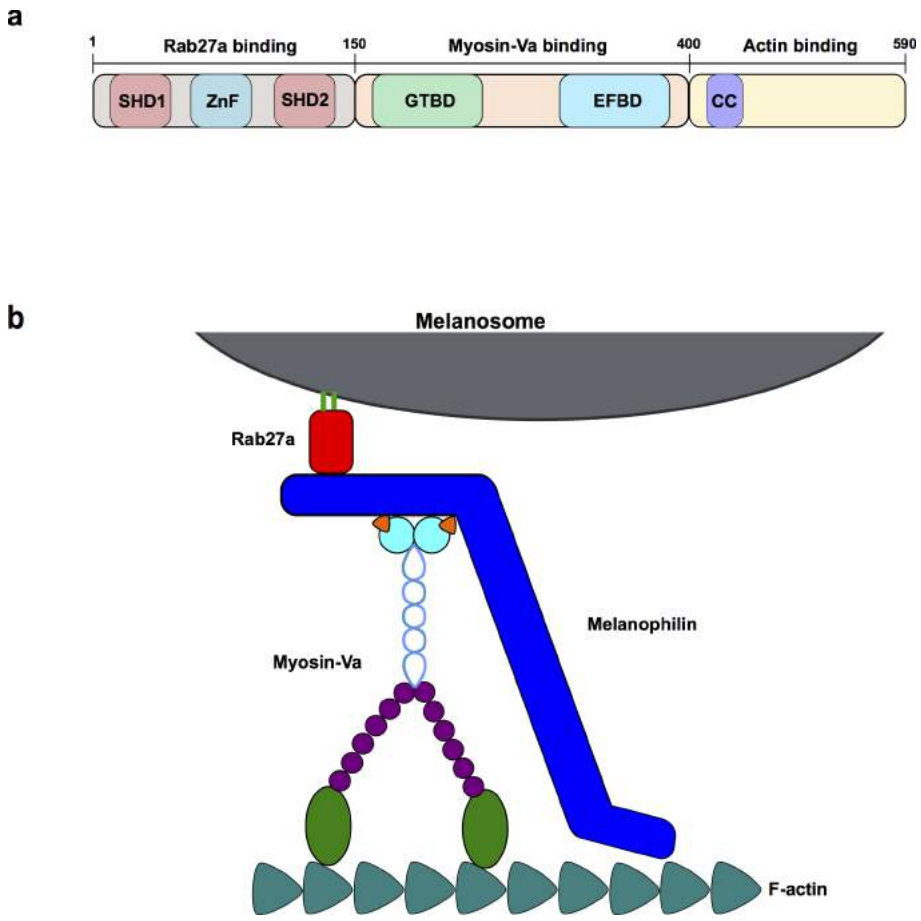


Figure 1.26 - The structure of melanophilin and the tripartite complex. **(a)** Melanophilin consists of an N-terminal Rab27a binding domain (aa 1-150), followed by a myosin-Va binding domain (aa 151-400), of which the EFBD region is most important, and finally a C-terminal actin binding domain (aa 401-590), of which the small coiled-coil region has been demonstrated to be important for binding myosin-Va. **(b)** The tripartite complex - Rab27a is bound to the melanosome membrane and recruits melanophilin, which in turn binds the globular tail domain of myosin-Va. Melanophilin is also though to make contact with the actin filament, reducing the velocity of myosin-Va whilst increasing its run length. Adapted from Hume et al., 2006 and Sckolnick et al., 2013.

1.4.2 Evidence for long-range microtubule-dependent melanosome transport

In addition to the evidence from Wu et al. showing that bi-directional melanosome movement appears to be microtubule-dependent, Aspengren et al. also demonstrated that when microtubules were depleted in *Xenopus laevis* melanophores the treatment prevented aggregation of melanosomes. Meanwhile, it was found that while some cells pretreated with melatonin were able to re-distribute their pigment granules normally when incubated with α-MSH and nocodazole, the melanosomes in other cells remained clustered around the nucleus (Aspengren et al., 2006).

Evidence suggesting that microtubules are fundamental for the normal trafficking of melanosomes in both mouse and frog cells fits with the observation that microtubules radiate out from the MTOC at the cell centre with the plus-end oriented towards the plasma membrane, meaning they form very efficient tracks to support organelle and vesicle transport. On the other hand, F-actin filaments are randomly orientated in cells which makes long-range actin-based transport seem very unlikely (Woolner and Bement, 2009).

While kinesin has been implicated in long-range melanosome transport in both frog and fish melanophores (Tuma et al., 1998; Nilsson et al., 1996), as well as mammalian melanocytes (Vancoillie et al., 2000b; Hara et al., 2000), there is no clear consensus for which isoform performs this role although kinesin-1 and kinesin-2 are the best candidates to date. Moreover, although there is a large amount of evidence describing how myosin-Va binds melanosomes, the molecular mechanism governing the attachment of pigment granules to kinesin is still lacking. Finally, it is also unclear how melanosomes are passed from kinesin-based transport to myosin-based transport. Therefore, further research is still necessary in order to answer these questions.

1.5 Aims

Murine melanocytes are an excellent cell type in which to model intracellular transport for several reasons. Firstly a number of mutant cells lines exist whereby melanosomes adopt a clustered distribution compared to wildtype cells. This is particularly useful since it allows the possibility of add-back experiments which can help dissect which motor proteins and accessory factors are involved in melanosome transport. Secondly their pigment granules can be observed in brightfield without the need for fluorescent dyes which are often problematic, since they require transfection, may co-localise with other organelles, and easily photobleach - limiting the amount of time cells may be imaged for. Thirdly, these cells are very thin ($\sim 1 \mu$m) meaning melanosomes essential move in two dimensions, making the acquisition of three-dimensional images unnecessary.

However, despite the promise of melanocytes as a tool for understanding how intracellular organelle trafficking is regulated, there is still a lack of clear evidence describing the exact molecular mechanisms that govern long-range pigment granule transport. Although several experiments have shown that microtubules are necessary for the anterograde melanosome transport there is still debate over which kinesin isoform(s) are involved. Therefore, the foremost aim of this study was to identify which long-range transporter facilitates the anterograde trafficking of melanosomes from the perinuclear area to the plasma membrane.

Additionally, this study also aimed to identify the molecular mechanisms through which attachment of melanosomes to their long-range transporter is mediated as well as to elucidate how pigment granules are transferred from microtubule-based transport to actin-based transport. It is hoped that by answering these 3 main questions melanocytes will be able to better serve as a model for how other organelles are trafficked within mammalian cells.

Chapter 2

Methods

2.1 Cell Culture

2.1.1 Murine Melanocytes

All melanocyte cell lines derived from non-agouti/black C57BL/6 mice were maintained in RPMI-1640 medium (Sigma), supplemented with 10% (v/v) FBS (Gibco), 100 units penicillin/ml (Sigma), 172μM streptomycin (Sigma) and 200nM PMA (complete medium) and incubated at 37ºC with 10% CO_2.

Melanocytes were passaged when 80-90% confluent by incubating cells in 0.05% trypsin and 0.02% EDTA (Sigma) in 1X PBS (Lonza) for 2-3 minutes at 37ºC. Cells were detached from the plastic by gentle agitation of the flask, before quenching the trypsin by the addition of complete RPMI-1640 medium (see Table 2.1 for volumes used). The cell suspension was transferred to a sterile 25ml Sterilin tube and centrifuged at 1500g using a Heraeus Biofuge Primo centrifuge (Thermo Scientific) fitted with a 45º fixed-angle rotor for 5 minutes, after which time the pellet was re-suspended in at least 5ml complete RPMI-1640 medium. Melanocytes were typically split 1 in 5, into either T25 (Nunc) or T75 (Corning) filter cap flasks containing 4ml or 20ml complete RPMI-1640 medium, respectively.

Flask/Plate	1x Trypsin/EDTA	RPMI to Quench
T-25 (Nunclon)	2ml	3ml
T-75 (Corning)	7ml	8ml
6-well (Nunclon)	2ml	3ml
24-well (Nunclon)	500µl	500µl
10cm dish (Corning)	7ml	8ml

Table 2.1 - Volumes used for passaging tissue culture cells.

2.1.2 NIH 3T3, HEK 293A and HeLa cell lines

NIH 3T3, HEK 293A and HeLa cells were maintained in DMEM (Sigma), supplemented with 10% (v/v) FBS and 1% (v/v) 100x penicillin/streptomycin (complete medium) and incubated at 37ºC with 10% CO_2.

NIH 3T3, HEK 293A and HeLa cells were passaged as described above and typically split 1 in 10 into T25 or T75 filter cap flasks containing 4ml and 20ml complete DMEM medium, respectively.

2.1.3 Melanophore cell culture

Melanophores were grown in 0.7X L-15 medium (Lonza), supplemented with 10% FBS, 1% penicillin/streptomycin and 5μg/ml insulin (complete medium) and incubated at 27^{O}C. Melanophores were grown in standard cell culture flasks, as used for the other cell lines in this study.

2.1.4 Preparing and Thawing Cells Stocks

To prepare cells stocks, 90-100% confluent cells were trypsinised and re-suspended in complete medium (as described in section 2.1.1), supplemented with 7.5% (v/v) DMSO, to give a final concentration of 1×10^{6} cells/ml. 1ml aliquots of cells were transferred to cryogenic tubes (Thermo Scientific) and cooled to -80ºC at a rate of approximately 1ºC/minute via the use of a cryogenic freezing container (Thermo Scientific) filled with isopropyl alcohol. Cryogenic vials were then transferred into liquid nitrogen for long-term storage.

To thaw cryogenically frozen cell stocks, vials were removed from liquid nitrogen and placed in a 37ºC water bath until the medium was completely defrosted. The cell suspension was then immediately transferred to a 25ml Sterilin tube, and 4ml complete medium was added drop-wise to every 1ml cell suspension. Cells were then centrifuged as outlined in section 2.1.1 and the pellet resuspended in 5ml complete medium. The entire cell suspension was then transferred to a T25 filter cap flask. Cells were incubated for 24 hours at 37ºC in 10% CO_2, after which time the cells were washed in 1X PBS to remove any cells which had failed to adhere to the plastic and the medium replaced with fresh. Melanocytes were typically passaged 2-3 times before use, whereas HeLa, HEK293A and NIH 3T3 cells were used after reaching 80-90% confluency.

2.1.5 Transfections

2.1.5.1 Plasmid DNA

Cells were seeded at the required density for the culture plate used (shown in Table 2.2) and left to spread for at least 5 hours, but typically overnight, prior to transfection with plasmid DNA. Fugene 6 (Promega) was diluted in optiMEM (Gibco) in an Eppendorf tube, mixed by inversion, and subsequently incubated at room temperature for 5 minutes. Plasmid DNA was then added, mixed by inversion, and incubated at room temperature for a further

15 minutes (see Table 2.2 for quantities of reagents used). The original growth medium was then aspirated from the cells and replaced with the transfection mixture. Cells were then incubated at 37ºC with 10% CO_2 for between 3 and 16 hours, after which time the transfection mixture was replaced with complete RPMI-1640/DMEM. Typically, cells were then incubated for between 24 and 72 hours to allow expression of the plasmid DNA.

Plate	**Cells seeded (per well) Melanocytes**	**Cells seeded (per well) HEK293A**	**Plasmid DNA (per well)**	**Fugene 6 (per well)**	**OptiMEM**
24-well (Nunc)	3×10^4	2×10^4	500ng	1.5µl	300µl
6-well (Corning)	3×10^5	2.5×10^5	2,500ng	7.5µl	1,000µl
35mm dish (MatTek)	1×10^5	N/A	2,500ng	7.5µl	1,000µl

Table 2.2 - Reagents used for plasmid DNA transfection.

2.1.5.2 siRNA

Cells were seeded and allowed to spread as described in section 2.1.5.1. siRNA (Sigma/Dharmacon) and oligofectamine (Invitrogen) were diluted separately with optiMEM (Gibco) and incubated at room temperature for 5 minutes, after which time the siRNA and oligofectamine dilutions were mixed by pipetting and incubated for a further 5 minutes at room temperature (see Table 2.3 for quantities of reagents used). OptiMEM was then added to a final volume as shown in Table 2.3, and the exhausted medium aspirated from the cells and replaced with the transfection mixture.

Cells were incubated at 37ºC with 10% CO_2 for between 3 and 16 hours, after which time the transfection mixture was replaced with complete growth medium. Cells were then typically incubated for 72-96 hours in order to allow the mRNA to be knocked down. If the target protein was found to have a slow turnover rate and was not significantly depleted after 96 hours, a double knock down was carried out. In this procedure cells that had already been transfected with siRNA were trypsinised and split 1 in 5, as outlined in section 2.1.1, before being re-transfected with siRNA as described above.

Plate	Cells seeded (per well)	siRNA (per well)		Oligofectamine (per well)		Final volume optiMEM
96-well (Corning Costar)	3.5×10^3	50ng	Diluted in 50µl optiMEM	0.4µl	Diluted in 12µl optiMEM	100µl
24-well	2×10^4	250ng		1.5µl		300µl
6-well	2.5×10^5	1,100ng		10µl		1000µl

Table 2.3 - Reagents used for siRNA transfection.

2.2 Molecular Biology

2.2.1 PCR

PCR primers were designed to flank the gene sequence to be amplified, and synthesised by either Sigma (routine PCR) or MWG Biotech (qRT-PCR only). For routine PCR the following was added to a 200μl thin-walled PCR tube (in the order stated): 38μl Milli-Q water, 5μl 10X Taq Polymerase Buffer (NEB), 2μl 10mM dNTPs (Promega), 5 units Taq Polymerase (NEB), 1.5μl 10μM 5' primer, 1.5μl 3' primer, 1μl 10ng/μl cDNA template. The PCR reaction was mixed by gently pipetting several times, briefly centrifuged, and then subjected to the following PCR cycles using a Sensoquest thermocycler:

Temperature (^{O}C)	Time (mins)	Cycles
95	3	1
95	1	25
55	1	25
72	1 minute per kb	25
72	10	1

Table 2.4 - Thermocycler setting used for routine PCR.

If the DNA was to be used for downstream applications, such as cloning, Pfu and 10X Pfu buffer (Promega) were used instead of Taq Polymerase, since Pfu is a higher fidelity polymerase due to its proof-reading capabilities. Therefore the possibility of introducing mutations into the amplified DNA during each PCR cycle is minimised.

2.2.1.1 Site-directed Mutagenesis

For site-directed mutagenesis, primers were designed to mutate a maximum of 3 base-pairs. At least 20bp of complementary sequence were included either side of the mutagenic base-pairs to ensure the primers would still anneal tightly to the template DNA. The PCR reaction was set-up exactly as described above in section 2.2.1, with Pfu enzyme always being used. The following cycles were then used:

Temperature (^{O}C)	Time (mins)	Cycles
95	3	1
95	1	18
55	1	18
72	1.5 minutes per kb	18
72	10	1

Table 2.5 - Thermocycler settings used for site-directed mutagenesis.

In order to degrade any parental plasmid DNA that would not contain the mutation(s), 16μl PCR reaction with mixed with 2μl NEB buffer 2 and 1μl DpnI restriction enzyme (NEB). The reaction was incubated for 1 hour at 37^{O}C and the DpnI then heat inactivated for 20 mins at 80^{O}C. The linear PCR product was then transformed into competent DH5α *E. coli* cells (generated according to Chung et al. 1989 and stored at -80^{O}C until required), and the circular plasmid DNA purified as described in sections 2.2.2.2 and 2.2.2.3.

2.2.2 Cloning

2.2.2.1 Preparing agar plates

To prepare agar plates, 1.5% w/v agar was added to the LB medium prior to autoclaving. Once cooled to approximately 55ºC the appropriate antibiotic was added (50μg/ml kanamycin; 100μg/ml ampicillin) mixed by inverting, and then poured into petri dishes and allowed to harden. Agar plates were inverted and stored at 4ºC until required.

2.2.2.2 Bacterial transformations

For each transformation a 50μl aliquot of competent DH5α *E. coli* cells was defrosted on ice for 30 minutes, after which time 200ng of plasmid DNA (in 3μl total volume) to be transformed was added and gently mixed by flicking the Eppendorf tube. Cells were incubated on ice for a further 30 minutes and then heat-shocked by incubating the cells at 42ºC for 60 seconds, followed by rapidly cooling on ice for at least 2 mins. 250μl sterile LB medium (1% w/v tryptone, 0.5% w/v yeast extract, 1% w/v NaCl adjusted to pH 7.0 with 1M NaOH) was then added and the cells kept at 37ºC for 90 minutes in a shaking incubator (200 rpm).

Agar plates spread with transformed DH5α *E. coli* cells were inverted and incubated at 37ºC for approximately 18 hours to allow the growth of colonies.

2.2.2.3 Inoculating Overnight Cultures & Miniprep

LB medium was prepared and the appropriate antibiotic added, as described above. 5ml was transferred to a sterile Sterilin tube and a single colony from an agar plate was picked using a sterile 200μl pipette tip which was then ejected into the Sterilin tube under aseptic conditions. The Sterilin tube(s) were then placed in a shaking incubator (200 rpm) and left for approximately 18 hours at 37ºC to allow the *E. coli* cells to multiply.

To extract the plasmid of interest from the *E. coli* cells, the overnight cultures were centrifuged at 4, 000 rpm, at room temperature, using an Eppendorf 5804 centrifuge to pellet the cells. The supernatant was discarded and plasmid DNA extracted from the pellet using a NucleoSpin plasmid extraction kit (Machery Nagel) and following the manufacturer's instructions. DNA was always eluted using 50μl elution buffer supplied with the kit.

2.2.2.4 DNA Quantification

The concentration and quality of the plasmid DNA was quantified using a NanoDrop 2000 instrument (Thermo Scientific), with elution buffer used as the blank. The quality of plasmid DNA was assessed using the 260nm/280nm ratio, with a value of 1.8 being accepted as 'pure' DNA.

2.2.2.5 Agarose Gel Electrophoresis

The DNA to be analysed was mixed with an appropriate quantity of 6X DNA loading buffer (40% sucrose, 0.25% bromophenol blue in Milli-Q water) and MilliQ water in order to dilute the DNA loading buffer to a final 1X concentration.

To analyse DNA, an agarose gel was prepared according to Table 2.6. 1X TBE buffer was prepared from 1.08% w/v Tris base, 0.55% w/v boric acid, 0.0585% EDTA w/v in dH_2O, adjusted to pH8.0) in a conical flask and mixing until dissolved.

Components of the agarose gel (except ethidium bromide) were placed in a conical flask and heated in a microwave over until dissolved. After heating the gel mix was cooled to approximately 50ºC and ethidium bromide then added, mixed well, and the agarose poured into an appropriately sized casting tray such that the gel was approximately 5mm thick. After inserting a comb to give the required number of lanes the gel was left at room temperature until solid. The casting tray was then placed into the corresponding tank filled with 1X TBE buffer, the comb removed and 10μl of the sample loaded into each well. The gel was run using 80mA of current until the dye front reached the end of the gel, which was then imaged using a GelDoc system.

2.2.2.6 Restriction Digest

Restriction endonucleases, along with the appropriate buffers, were obtained from either NEB or Promega. Irrespective of the restriction endonuclease(s), the following was always

used per reaction: up to 1μg plasmid DNA, 1μl each restriction endonuclease, 2μl appropriate 10X buffer (as per manufacturer's recommendation), made up to 20μl total volume with MilliQ water. The reaction was incubated for between 2-16 hours at 37ºC, depending on enzyme activity. Heat inactivation of the enzyme was then carried out, if required, in accordance with the manufacturer's instructions. The efficacy of the digest was the assessed by running 10% of the reaction volume on a agarose gel, as described above.

2.2.2.7 Ligaton

In order to ligate a gene of interest into a vector, both pieces of DNA were digested with the same pair of restriction endonucleases, as described above. The digests were then purified using a PCR cleanup kit (Machery Nagel) and following the manufacturer's instructions. This ensured small fragments of DNA released from the vector would be removed, thereby preventing the vector from re-ligating to itself. It also served to remove excess salt from the restriction digest buffer which again may also interfere with the ligation reaction.

Subsequently, 50ng digested vector was ligated to an amount of insert calculated using the formula $x = \frac{3 \times I \times 50}{P}$, where x = ng of insert, I = insert size (in bp), and P = vector size (in bp). The DNA was mixed with 1 unit T4 DNA ligase (Promega), 2μl 10x DNA ligase buffer (Promega) and MilliQ water to give a total reaction volume of 20μl, and incubated at 16ºC for 18 hours, after which time it was transformed into DH5α *E. coli* cells and plasmid DNA extracted by miniprep, as outlined in sections 2.2.2.2 and 2.2.2.3 above. The efficacy of the ligation was assessed by restriction digest and subsequently visualising the banding pattern on an agarose gel, as described in sections 2.2.2.6 and 2.2.2.5.

If the ligation failed to work, the cleaned-up vector was dephosphorylated using shrimp alkaline phosphatase (SAP)(NEB), after the restriction digest. 1μg vector was mixed with 2 units SAP and 2μl 10X SAP buffer and the reaction volume made up to 20μl with MilliQ water. The reaction was incubated for 30 minutes at 37ºC, and the SAP then heat inactivated by incubating at 65ºC for 30 minutes. The ligation was then carried out as described above.

Component	1% agarose gel	1.5% agarose gel	3% agarose gel
DNA length	>1kb	<1kb	<300bp
Agarose	1g	1.5g	3g
1X TBE buffer	Make up to 100ml		
Ethidium bromide	4μl		

Table 2.6 - Agarose gel components. Weights and volumes indicated are for 100ml gel.

2.2.2.8 Sequencing

All DNA sequencing was performed by sending 600ng plasmid DNA in 6μl total volume to SourceBioscience. Where possible, stock primers supplied by SourceBioscience were used. Otherwise, primers were diluted to 3.2pM using MilliQ water and 10μl sent per sequencing reaction.

2.2.3 Generating fusion proteins

2.2.3.1 KIF5B-YFP-$\triangle$MD

KIF5B in pEYFP-N1 vector was kindly gifted by Christina Wiesner and Stefan Linder, Institute for Medical Microbiology, Virology and Hygiene, University Medical Centre Eppendorf, Hamburg. KIF5B-YFP was initially sub-cloned into a pEGFP-N1 vector using existing EcoRI (5') and SalI (3') sites and following the protocols in sections 2.2.2.6, 2.2.2.7, 2.2.2.2 and 2.2.2.3 to digest, ligate, transform and subsequently mini-prep KIF5B-EGFP.

To remove the motor domain to generate KIF5B-GFP-ΔMD, a second EcoRI site was introduced 1050bp after the motor domain using site-directed mutagenesis (described in section 2.2.1.1) using the following primers (mutagenic base pairs in bold):

5'ATGAAAAAGAAAAAGAAAAA**GAATTC**AT**G**CTGCGGAACACTATTCAGTG3'

3'CACTGAATAGTGTTCCGCAG**C**AT**GAATTC**TTTTTCTTTTTCTTTTTCAT5'.

Vector maps illustrating this procedure are shown in panel a and b in Figure 2.1).

The mutated plasmid was then digested with EcoRI as described in section 2.2.2.6 for 2 hours in order to excise the motor domain. The truncated plasmid was then ligated as described in section 2.2.2.7. Next, the vector was transformed into competent E. coli cells as described in section 2.2.2.2 and once the DNA was purified using a mini-prep kit (section 2.2.2.3) the vector was once again digested with EcoRI for 2 hours and subsequently run on a 1% agarose gel (section 2.2.2.5) to ensure the plasmid was of the correct size, indicating the motor domain had been successfully removed. Finally, the following primers were used to sequence the KIF5B-GFP-ΔMD clone to ensure it was free of mutations (see panel c of Figure 2.1 for binding locations): (F1) 5'-CCGGACTCAGATCTCGAGCT-3'; (F2) 5'-TCAATTATGATCAGAAGTCTC-3'; (F3) 5'-GATCAGGAAAAGAGCAGAAAA-3'.

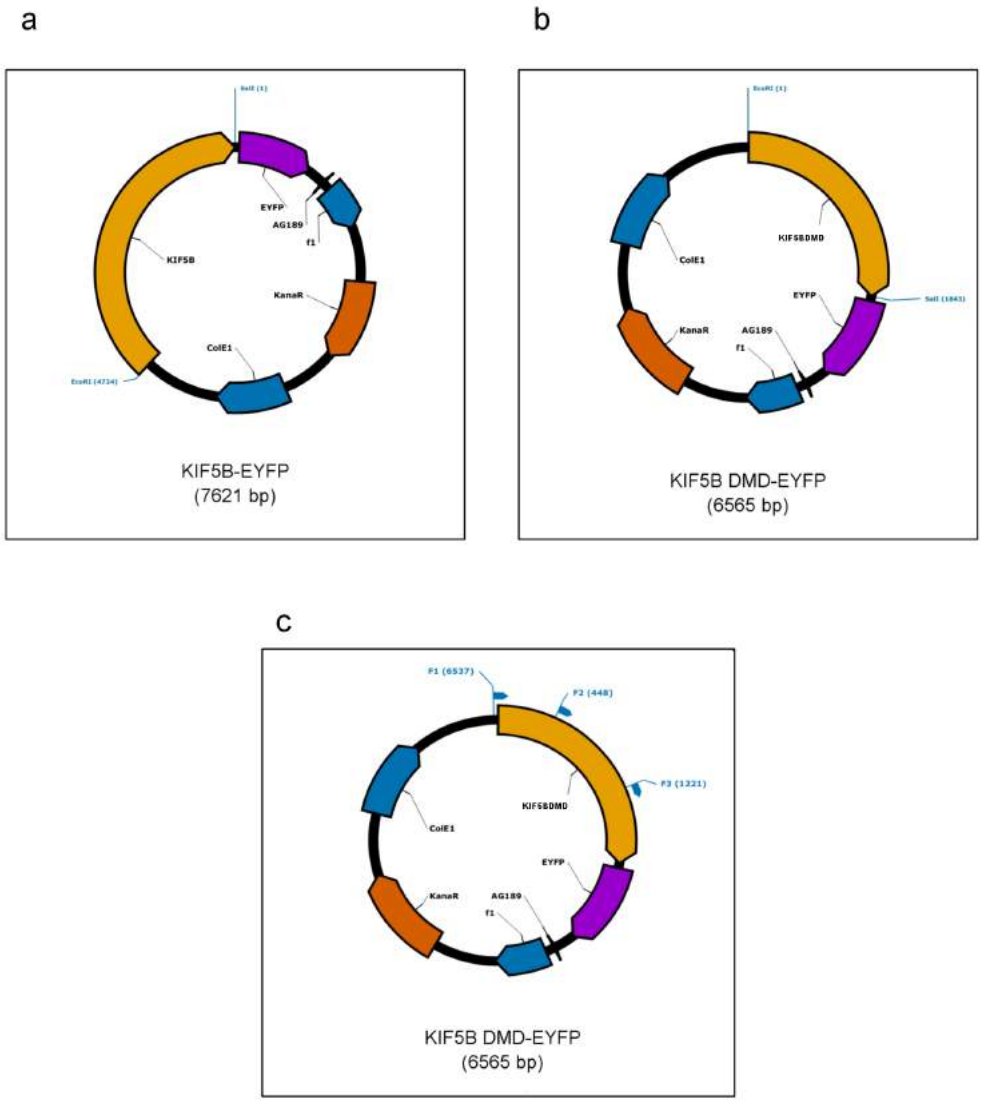


Figure 2.1 - **Vector maps depicting how KIF△MD was generated**. **(a)** The original KIF5B-YFP vector, kindly gifted by Stefan Linder, with the positions of the EcoRI and SalI restrictions sites shown. **(b)** The vector after truncation of the motor domain. **(c)** Positions at which the sequencing primers bind. The size of the vector is given underneath each map.

2.2.3.2 KIF5B-1-810-GFP

To generate the KIF5B-1-810-GFP mutant, a NotI site was introduced into the KIF5B coding sequence after the first 2430bp, using site-directed mutagenesis. Primers used were (mutagenic base-pairs are in bold):

5'-AAACTCTTTGTTCAGGACCTG**A**GC**GG**C**CG**CAGTTAAAAAGAGTGCTGAGAT-3'

3'-ATCTCAGCACTCTTTTTAACT**GCG**G**CC**GC**T**CAGGTCCTGAACAAAGAGTTT-5'

DNA was then digested with NotI and SacII to release the KIF5B encoding region, loaded onto an agarose gel and then separated from the vector using electrophoresis. The band

corresponding to KIF5B was excised from the gel and purified using a gel extraction kit (Machery Nagel) and following the instructions supplied. An EGFP-N1 vector was digested with NotI and SacII and KIF5B1-810 ligated into it as described above (sections 2.2.2.6 and 2.2.2.7).

2.2.3.3 KIF5B-GFP-FKBP

FKBP was excised from its vector by digest with NotI and SalI. KIF5B-1-810-GFP was also digested with these endonucleases (as described in sections 2.2.2.6). The DNA was then purified and FKBP ligated into the KIF5B-1-810-GFP vector as described in section 2.2.2.7)

2.2.3.4 GFP-MyosinVaMD-FKBP & GFP-MyosinVaTD-FRB

To generate GFP-MyosinVaMD-FKBP (motor domain), FKBP was ligated to myosin after amino acid 920 as described in the section above. Likewise GFP-MyosinVa-TD-FRB (tail domain) was generated by sub-cloning the melanophilin binding tail domain of myosin-Va into an FKBP-rapamycin-binding (FRB) domain containing vector. For details, see Evans et al., 2014.

2.2.3.5 Formin-1-GFP and Arpc1b-GFP

The *Mus musculus* formin-1 gene (obtained from addgene, clone number 19320) was cloned into a pENTR-EGFP-C2 vector by introducing a 5'EcoRI and 3'BamHI site via PCR, using the following primers: foward: 5'-GATCGAATTCATGGAAGGCACTCACTGCA-3'; reverse: 5'-GATCGGATCCTTAGTTGGTGGCCACGCTG-3'. PCR cycler setting used:

Temperature	Time (minutes)	Cycles
95	3	1
95	1	18
55	1.5	18
72	12	18
72	10	1

Table 2.7 - Thermocycler setting used to sub-clone formin-1 into pENTR-EGFP-C2.

The PCR product was purified using a PCR clean-up kit (Machery Nagel), and the vector and PCR product digested with EcoRI and BamHI (NEB) as described in section 2.2.2.6.

The digested PCR product and vector were again purified and ligated together as described in section 2.2.2.7.

To verify that the insert had been taken up correctly, and no mutations had been introduced into the plasmid, the following formin-1 specific primers were used to sequence the vector: EGFP C F: 5'-GATCACATGGTCCTGCTG-3'; Fmn1.1: 5'-GGACACTGATCTTGAAGG-ACC-3';Fmn1.2: 5'-GAGAAGAAGCCAACCCCCCAG-3';Fmn1.3: 5'-ACCAGGCTGC-TATCCTACATC-3';Fmn1.4: 5'-TCCTCCGCCAGGACTTGCACC-3'; Fmn1.5: 5'-ATCT-TAGCTCTCATTCTGGCT-3'.

The *Mus musculus* Arpc1b gene was cloned into a pENTR-EGFP-C2 vector by introducing a 5' EcoRI and 3' BamHI sites, using the following primers: forward: 5'-GATCGAATTCAT-GGCCTACCACAGCTTCC-3'; reverse: 5'-GATCGGATCCTCATTTGATTTTCAGGTCC-3'. The Arpc1b gene was then cloned into the vector using the same protocol as the formin-1 gene.

2.2.4 Generating adenoviral vectors

To produce adenoviral vectors, the gene of interest was initially sub-cloned from the original vector into a pENTR vector (gateway expression vector; ThermoFisher Scientific). This was achieved by excising the gene using an appropriate pair of restriction enzymes and ligating into the pENTR vector (digested with the same restriction endonuclease pair) with DNA ligase (see sections 2.2.2.6 and 2.2.2.7). The gene of interest was then transposed into a pAD destination vector by incubating 150ng pENTR vector with 150ng pAD destination vector, 2μl LR clonase (Life Technologies) and the volume made up to 10μl with TE buffer pH 8.0 (1M Tris, 0.5M EDTA in MilliQ water) for 1 hour at 25ºC. Subsequently, 3μl was transformed into competent DH5α *E. coli*, as described in section 2.2.2.2. Colonies obtained were used to inoculate overnight cultures (described in section 2.2.2.3), and the pAD plasmid was purified as described in section 2.2.2.3. The portion of the pAD containing the gene of interest was sequenced to ensure it had been taken up correctly and was free of any mutations, and the pAD then transformed into HEK 293A cells, as described in section 2.1.5.1, which had been seeded onto a 6-well plate and allowed to spread for at least 5 hours.

The HEK 293A cells were checked after 72 hours using a Zeiss Axiovert S100 inverted microscope to assess if they were fluorescent in the appropriate channel, which was a strong indicator that the cells were producing adenovirus. For each of the wells where it appeared

that the cells were producing adenovirus they were detached from the plastic by vigorously flowing medium over them, and the suspension transferred to a 10cm dish and made up to 10ml with complete DMEM. Cells were incubated for up to 10 days until plaques formed, indicating cell death caused by the adenoviral infection was occurring. At this point, cells were mechanically detached from the plastic by agitation and flowing medium over them, and the suspension transferred to a 15ml falcon tube. The cells were subjected to 3 freeze-thaw cycles in order to lyse them, whereby the cells were subjected to -80ºC for 30 mins, and then 37ºC for 15 mins. After the final cycle, the lysate was centrifuged at 3000g for 15 minutes at room temperature using a Eppendorf 5804 swinging-bucket centrifuge to pellet cell debris. The supernatant was harvested under sterile conditions and aliquoted into 1ml fractions which were stored at -80ºC until required. 100μl of this 'crude' adenovirus stock was then used to infect an 80% confluent dish of HEK 293A cells, and the process repeated in order to generate a high titer stock.

2.2.5 Reverse-transcription PCR (RT-PCR)

2.2.5.1 Obtaining Starting Material

Cells were grown to confluency as described in section 2.1 and then 1x10^7cells harvested, pelleted and washed in 1X PBS. Cell pellets were kept on ice and and mRNA extracted using an RNeasy kit (Qiagen) and following the instructions provided. Cells were lysed by passing them through a sterile 25G needle fitted to an RNase free syringe 10 times. mRNA was typically eluted using 30μl of elution buffer provided with the kit. The concentration and quality of the RNA obtained was quantified using a NanoDrop 2000 instrument (Thermo Scientific), with a 260/280 ratio of 2.1 being accepted as 'pure' RNA.

2.2.5.2 First Strand Synthesis

mRNA was reverse-transcribed into cDNA using the Moloney Murine Leukemia Virus Reverse Transcriptase (M-MLV RT) kit (Promega). 2μg of mRNA and 1μg random primers were placed in an RNase free 200μl PCR tube and gently mixed by pipetting. The tubes were then placed in the thermocycler and subjected to the following cycle - 70ºC, 5 mins; 0ºC, 3 mins, in order for the primers to anneal to the mRNA (rapidly cooling to 0ºC prevented secondary structure from forming within the RNA that could prevent the subsequent reverse transcription step).

The following was then added to the tube (in the order listed): 5μl M-MLV 5X reaction buffer, 1.25μl 10mM dATP, 1.25μl 10mM dGTP, 1.25μl 10mM dTTP, 1.25μl 10mM dCTP, 25 units recombinant RNasin ribonuclease inhibitor, 200 units M-MLV reverse transcriptase (or equivalent volume of DEPC water for -RT control) and DEPC water to a total volume of 25μl. The reaction volume was mixed gently by pipetting, spun down briefly and then incubated at 42ºC for 60 mins using the thermocycler, which allowed the reverse transcriptase to reverse transcribe the mRNA to cDNA. cDNA was stored at -80ºC until required.

2.2.5.3 Generating Primers Sequences

Primers were designed using the Primer-BLAST tool supplied by NCBI (Ye et al., 2012). This tool allowed for the automated generation of primer pairs that matched user-specified criteria. Primers were only selected if they spanned an exon-exon junction, produced a product between 100bp and 500bp in length, and did not anneal to any other targets within the mouse genome according to a BLAST search. Primers were synthesised by Sigma-Aldrich, re-hydrated using MilliQ water to 100μM and stored at -20ºC until required.

2.2.5.4 Second Strand Synthesis

cDNA was amplified as described in section 2.2.1 and visualised on a 1.5% agarose gel, as described in section 2.2.2.5. As the quality of the DNA was not important, since it would not be used for any down-stream applications, Taq DNA Polymerase was used.

2.2.6 qRT-PCR

The DNA sequence of both the primers and the probe for each qRT-PCR target (with the exception of formin-1, for which no suitable primers/probes could be found) were automatically generated using Primer Express software (Life Technologies), and synthesised by MWG. Since a TaqMan assay was used, probes were modified to contain 5'-FAM (dye) and 3'-TAM (quencher). Progression of the PCR reaction causes FAM and TAM to become separated (due to the exonuclease action of the polymerase) preventing TAM from quenching the fluorescence from FAM meaning that it can be detected. Sequences of the primers/probes used are as follows:

Primers were diluted to 10μM with MiliQ water whilst probes were diluted to 10μM with the supplied qPCR probe dilution buffer (10mM Tris-HCl; pH 8; 1mM EDTA). In the case of formin-1, a TaqMan assay was purchased from Applied Biosystems (Assay ID: Mm01327668_m1).

Melanocytes were seeded onto 6-well plates (as described in section 2.1), allowed to spread overnight, and then transfected in triplicate with NT siRNA (5'-CAUAGAACACUG-CACGUGA-3'); γ-actin oligonucleotide #1 (5'-GGAGAAGAGUUACGAGCUG-3'); Aprc1b oligonucleotide #2 (5'-GAACAAGGACCGUACACAG-3'); cofilin-1 oligonucleotide #2 (5'-GGUGGCAGCG-CCGUCAUUU-3') and formin-1 oligonucleotide #1 (5'-GGACAAACC-UGAACAAUUU-3') as described in section 2.1.5.2. 96 hours after siRNA transfection, cells were harvested and the pellet washed twice in 1X PBS (described in section 2.1), before RNA was extracted (described in section 2.2.5.1) and cDNA generated (described in section 2.2.5.2).

For qRT-PCR the cDNA was initially diluted 1:4, giving 100μl total volume, henceforth termed 'neat cDNA'. 5μl from each +RT sample were pooled into a single tube, and diluted 1:4, 1:16, 1:64, 1:256 for a standard curve, in order to generate a reference sample. The neat cDNA was then diluted 1:8 to give the final 'working cDNA' dilution. All dilutions were performed using DEPC treated MiliQ water.

For formin-1, the following reagents were added per well of a 96-well plate: 10μl TaqMan Fast 2X PCR Master Mix (Life Technologies); 1μl formin-1 TaqMan assay mix (containing forward/reverse primers and FAM/TAM probe); 3μl working stock cDNA; 6μl DEPC treated water. For all other targets, the following reagents were added per well of a 96-well plate: 6.5μl TaqMan Fast 2X PCR Master Mix (Life Technologies); 0.4μl forward primer (10μM);

Target	Forward Primer	Reverse Primer	Probe
γ-actin	CCCTAGCACC-TAGCACGATGA	GCCACCGATC-CAGACTGAGT	ATTAAGATCATTG-CTCCCCCTGAGCGC
Arpc1b	GTGCAGGATCT-TCTCTGCCTATATC	TCCCCAAAG-GGCATCTTG	AACGGCCAGCCCC-TACACCGTG
Cofilin-1	CCCCTCAAGA-GCAAAATGATCT	GCTTGATTCCT-GTCAGCTTCTTC	TGCCAGCTCCAAG-GATGCCATCA
GAPDH	GTGTCCGTCG-TGGATCTGA	CCTGCTTCACC-ACCTTCTTGA	CCGCCTGGAGAAA-CCTGCCAAGTATG

Table 2.8 - Primer and probe sequences for qRT-PCR targets.

0.4μl reverse primer (10μM); 0.25μl probe (10μM); 3μl working stock cDNA; 2.45μl DEPC water. For each sample, 3 technical repeats were performed. Subsequently, the 96-well plate was sealed with an optically clear adhesive film, briefly centrifuged, and then qRT-PCR performed using a StepOnePlus Real-Time PCR system (Applied Biosystems) using the default 'fast' mode, which performs a run in 40 minutes. For each siRNA knockdown performed the extracted cDNA was probed by all 5 primer/probe pairs, such that if knocking down one particular gene affected the levels of another gene, this would be detected.

The StepOne software automatically set a threshold for the qRT-PCR reaction curves after the run had finished, allowing CT values (the cycle number where the threshold was reached) to be exported as an MS Excel file. Initially the slope, intercept and R^2values were calculated for the standard curve. The following manipulations were performed to generate a 'quantity value' for each CT value. Firstly:

$$\frac{(CT - I)}{S} \tag{2.1}$$

where I = the intercept value from the standard curve and S the slope value.

Secondly:

$$10^{LQ} \tag{2.2}$$

where LQ is the product of equation 2.1.

Thirdly, the mean quantity values from equation 2.2 were normalised to non-targeting siRNA control values by:

$$Q \times (\frac{1}{MNT}) \tag{2.3}$$

Where Q is the product of equation 2.2 and MNT is the mean non-targeting quantity values from the 9 total repeats (3 technical repeats of 3 biological repeats) after performing equations 2.1 and 2.2.

Finally, the product of equation 2.3 was normalised to results from obtained for the GAPDH primer/probe by:

$$\frac{GOIP}{GP} \tag{2.4}$$

where GOIP is the normalised quantity value for the gene of interest primer and GP is the normalised quantity value for the GAPDH primer.

2.3 Biochemistry

2.3.1 Western Blotting

2.3.1.1 Preparing Gels

Gels were prepared by mixing components outlined in Table 2.9 in the order they appear (ammonium persulfate (APS) (Fisher Scientific) was made fresh on the day the gels were prepared) and pouring between front plates and 1.5mm spacer plates, using the BioRad Mini-PROTEAN Tetra Cell casting frames.

	8%	10%	12%
Stacking Gel			
ddH_2O	3.65ml		
40% Acrylamide	625µl		
1M Tris pH 6.8	625µl		
10% Ammonium Persulfate	50µl		
10% SDS	50µl		
TEMED	5µl		
Separating Gel			
ddH_2O	5.3ml	4.8ml	4.3ml
40% Acrylamide	2ml	2.5ml	3ml
1.5M Tris pH 8.8	2.5ml	2.5ml	2.5ml
10% Ammonium Persulfate	100µl	100µl	100µl
10% SDS	100µl	100µl	100µl
TEMED	6µl	4µl	4µl

Table 2.9 - Components of SDS-PAGE gels.

2.3.1.2 Western Blot Sample Preparation

Cells, typically grown on a 6-well tissue culture plate, were harvested as described in section 2.1 and then washed in 1X PBS. Cells were then re-suspended in 200µl ice cold RIPA buffer (50mM Tris-HCl pH7.4, 1% NP-40, 0.5% Na-deoxycholate, 0.1% SDS, 150mM NaCl, 2mM EDTA) supplemented with 1 protease inhibitor tablet (Roche) per 10ml for at least 20 minutes on ice in order to lyse them. After protein quantification (see section 2.3.1.3), 5 volumes of sample (containing 25µg total protein) were boiled at 95^{O}C for 10 minutes with 1 volume of 6X protein loading buffer (375mM Tris-HCl pH 6.8, 6% SDS, 48% glycerol, 9% β-mercaptoethanol, 0.03% bromophenol blue).

2.3.1.3 Protein Quantification

A BioRad DC protein assay (based on the Bradford assay whereby an absorbance shift from Coomassie Brilliant Blue occurs in the presence of protein) was used to measure the protein concentration of samples. Using a 96-well plate, 5µl of sample was mixed with 20µl BioRad DC reagent A, and subsequently mixed with 200µl BioRad DC reagent B. Samples were incubated at room temperature for between 15 and 60 minutes before Abs750nm was taken using an LT-4000 microplate reader (Labtech). Samples from melanocytes were centrifuged at 700g for 10 mins at 4ºC and the supernatant collected prior to protein quantification, in order to remove melanin, since this pigment interfered with the absorbance reading. A standard curve containing at least 6 points, was generated simultaneously by serially diluting BSA (usually to 1.0, 0.8, 0.6, 0.4, 0.2, 0.1 mg/ml), from which the protein concentration of the samples could be calculated.

2.3.1.4 Electrophoresis

Gels were placed in a Mini-PROTEAN Tetra Cell tank (BioRad) containing running buffer (25mM Tris, 192mM glycine, 0.1% SDS) and samples loaded, along with 5µl protein molecular weight standards (Geneflow) per gel. Samples were run using 35mA current until the dye front had reached the bottom of the gel (typically ~90 minutes).

2.3.1.5 Transferring to Membrane

Protein was transferred to PVDF membrane using the Geneflow wet transfer system. PVDF membrane was activated by soaking in 100% methanol for 15 seconds and then incubating in transfer buffer (25mM Tris, 192mM glycine, 10% methanol) for 2 minutes. The gel was layered on top of the PVDF membrane and sandwiched between 3M filter paper pre-soaked in transfer buffer before placing in the Geneflow cassette. The cassette was then placed in the tank with the PVDF membrane closest to the cathode and immersed with ice cold transfer buffer. Transfer took place at 4ºC, using either 155V for 3 hours, or 30V for 18 hours.

2.3.1.6 Blocking and Antibody Staining

The PVDF membrane was initially blocked with 5% MARVEL in 1X PBS for 1 hour at room temperature to reduce non-specific antibody binding. The membrane was then incu-

bated with the primary antibody in 1% MARVEL in 1X PBS-Tween-20 (0.1%) for 16 hours at 4ºC. Subsequently, the membrane was washed (3x rinse, 3x 10 minutes, 3x rinse) using 1X PBS-Tween-20 and incubated with the secondary antibody in 1% MARVEL in 1X PBS-Tween-20 for 1 hour at room temperature. Washes were then repeated as for the primary antibody. See Table 2.11 for antibody dilutions used.

2.3.1.7 Image Acquisition

To image the fluorescent signal from the PVDF membrane it was carefully placed face down on the glass scanning area of a Licor Odyssey instrument that had been pre-wetted with 1X PBS-Tween-20, so as to avoid air bubbles becoming trapped between the glass and the membrane. ImageStudio 3.0 software was used to interface with the scanner and acquire the image, using the following settings: resolution - 85μm; quality - medium; offset - 0mm. The channel intensities were adjusted for each scan so that the bands were never saturated.

2.3.2 Melanosome Purification

1.8×10^7melan-a cells were spun down and washed in 1X PBS as described above in section 2.2.5.1. Melanocytes were re-suspended in 1ml sonication buffer (50mM Tris-HCl pH 7.2, 0.1mM DTT, and protease inhibitor tablet) and lysed by sonicating on ice for 3x30 second bursts with 30 seconds recovery between each burst. The lysate was centrifuged at 700g for 10 mins at 4ºC to pellet nuclei. The supernatant was then centrifuged at 17,000g for 30 mins at 4ºC to pellet heavy organelles (including melanosomes). The supernatant from the 17,000g spin was then loaded on top of 2.0M sucrose in 10mM HEPES, pH 7.2, and centrifuged at 100,000g for 1 hour at 4ºC using a Beckman Coulter ultracentrifuge fitted with an SW41Ti (swinging bucket) rotor to further pellet dense organelles. Aliquots were retained at every stage of this protocol for analysis by western blot.

All aliquots were run on an 8% SDS-PAGE gel and transferred to PVDF membrane (as described in section 2.3.1). The membrane was then stained with Goat anti-kinesin-1 and Rabbit anti-tyrosinase as described in section 2.3.1 using the concentrations outlined in Table 2.11.

2.4 Microscopy

2.4.1 Fixed-cell Microscopy

2.4.1.1 Cell plating

For routine immunofluorescence where quantification of melanosome distribution was less important, cells were plated onto No. 1.5 thickness circular coverslips, 13mm in diameter (Scientific Laboratory Supplies). See Table 2.2 for cell densities used.

To facilitate the robust quantification of melanosome distribution within melanocytes, micropattern chips (CYTOO) were used to standardise cell size and shape, thus allowing an average pigment map to be generated. The micropattern chips featured discs of fibronectin, to which the cells adhered, which were printed onto glass coverslips treated with a cytophobic agent. Optimisation experiments showed that melanocytes spread and adhered best to fibronectin disks with an area of 1600μm^2 and therefore this size was used for all experiments requiring micro-patterned chips.

Individual micropattern chips were each placed in a single well of a 6-well tissue culture plate (Nunc) and melanocytes then trypsinised as described in section 2.1 and counted using a haemocytometer. For the CYTOO mini-chips used for fixed-cell microscopy (which contained 3,840 fibronectin discs into total), cells were diluted to 1x10^4/ml using complete RPMI-1640 medium and 2ml of the suspension was then pipetted into each well. Adding the correct number of cells was important in order to avoid multiple cells occupying a single fibronectin disk. The plate was then left in the cell culture hood for 10 minutes to allow cells to sediment onto the chip. After this time the plate was incubated at 37ºC with 10% CO_2 for 20 minutes to allow melanocytes to adhere to the fibronectin disks. The micropattern chips were then gently washed with complete RPMI-1640 medium until all cells that had not properly adhered were removed (typically 6-9 washes). Great care was taken to ensure that the micropattern chips did not dry out during the washing, since this was found to cause cell death. Therefore, cells on micropattern chips were washed by repeatedly aspirating 1ml medium and replacing with 1ml fresh medium. Cells were then allowed to spread for a minimum or 5 hours (but typically 16 hours) before use.

2.4.1.2 Fixing

Prior to fixing, growth medium was aspirated and cells gently washed in 1X PBS. Cells were then fixed by the application of 4% paraformaldehye (pH 7.0) in 1X PBS for 15 minutes at room temperature. Subsequently, cells were washed three times in 1X PBS and then incubated in 50mM NH_4Cl made up in 1X PBS (in order to quench aldehyde groups and reduce autofluorescence) for 10 minutes. Cells were again washed twice in 1X PBS and stored immersed in PBS at 4ºC until required.

2.4.1.3 Immunofluorescence

Fixed cells were incubated in 1X blocking buffer (0.5% BSA (Fisher Scientific), 0.05% saponin (Sigma) in 1X PBS) for at least 15 minutes in order to permeabilise cell membranes. Cells were then incubated in primary antibody in order to recognise the specific protein of interest (made up to the appropriate dilution as indicated in Table 2.11 using blocking buffer) for 1 hour. Subsequently, coverslips were washed 5 times using 1X PBS before being incubated with secondary antibody which recognised the primary antibody (made up as per primary antibody) for 30 minutes. Phalloidin was applied concurrently with the secondary antibody, if required. Coverslips were again washed 5 times in 1X PBS. If nuclear staining was required, coverslips were then immersed in 300nM DAPI in 1X PBS for 10 minutes, before undergoing 3 washes in 1X PBS. Coverslips were then inverted and mounted on glass slides using a gelvatol-based mounting media. All incubations were carried out at room temperature under humid conditions to avoid the cells drying out.

2.4.1.4 Image capture

For widefield microscopy, a Leica DMIRB inverted fluorescence microscope fitted with 63x 1.4 NA phase contrast objective, and ORCA HR digital camera (Hamamatsu) was used. Images were captured using Volocity software. The microscope was fitted with a range of standard excitation/emission filters including DAPI/FITC/TRITC/Cy5.

For confocal microscopy, a Zeiss LSM710 inverted microscope, fitted with a 63x 1.4 NA phase contrast objective, an environmental chamber heated to 37ºC and 405nm, 488nm, 561nm, 594nm, and 633nm laser lines was used. Additionally, this microscope was fitted with a perfusion system (built in-house), allowing up to 6 different buffers to be flowed over live cells during image acquisition.

2.4.1.5 Drug wash-out experiments

For end-point assays, melanocytes were seeded as per Table 2.2 and allowed to spread for at least 16 hours in complete RPMI-1640 growth medium. Subsequently, cells were incubated in either cytoskeleton inhibitor or 0.1% DMSO as a vehicle control (in complete growth medium) for 60 minutes at 37ºC with 10% CO_2. After this time, cells were either fixed immediately, using the protocol in section 2.4.1.3 or washed 5 times with complete growth medium to remove the cytoskeleton inhibitor or DMSO. For the washes, the exhausted medium was aspirated and replaced with fresh medium in which the cells were incubated for 30 seconds before the process was repeated. After the cells were washed they were incubated at 37ºC with 10% CO_2until ready to be fixed.

2.4.1.6 FACS experiments

2 x 10^4 melanocytes were seeded in 4-well plates, and incubated overnight in complete RPMI-1640 medium at 37ºC with 10% CO_2 to allow them to spread. Cells were then treated with either 0.1% DMSO, 25nM LatA or 500nM LatA for 1 hour. Subsequently, cells were detached from the plastic by incubating with 200μl 1X trypsin-EDTA in 1X PBS for 5 minutes at 37ºC followed by mechanical agitation. The trypsin was then quenched by the addition of 300μl complete RPMI-1640 medium. The cell suspension was then transferred to an Eppendorf tube and spun down (1500g, 5 minutes at room temperature) and the cell pellet washed by re-suspending in 1X PBS. The cell suspension was once again pelleted before being incubated in 100μl 100nM texas-red (TR) phalloidin in 1x PBS for 30 minutes. Cells were then spun down and the pellet washed in 1X PBS 5 times. 10,000 melanocytes per condition were analysed using a Beckman Coulter MoFlo XDP flow cytometer equipped with 561nm laser. Results were analysed using Weasel software (Walter and Eliza Hall Institute of Medical Research).

2.4.2 Live-cell Microscopy

2.4.2.1 Cell plating

For routine live-cell imaging where quantification of melanosome distribution was less important, cells were plated onto 35mm MatTek dishes (see Table 2.2 for cell densities used) and allowed to spread out overnight before use.

For live-cell experiments where robust quantification of the melanosome distribution was required, cells were seeded onto standard CYTOO chips, designed to fit the CYTOO live cell chamber. These chips were 19.5mm^{2}and contained 11,664 fibronectin discs that were also 1,600μm^2, as with the mini chips. Melanocytes were plated onto the standard CYTOO chips exactly as described in section 2.4.1.1, with the exception that cells were diluted to 2x10^4/ml.

2.4.2.2 Live washout of actin cytoskeleton inhibitors.

Cells were transfected with utrophin-RFP (binds F-actin) using an adenoviral vector and allowed to express for 24 hours. Cells were incubated in either cytoskeleton inhibitor or 0.1% DMSO in complete growth medium and incubated for 45 minutes at 37ºC with 10% CO_2. After this time, the chip was transferred to a CYTOO live cell chamber and connected to the perfusion system described in section 2.4.1.4. The chamber was run through with approximately 2ml of L-15 buffer, prewarmed to 37ºC, containing either 0.1% DMSO or cytoskeleton inhibitor and then allowed to equilibrate to the temperature of the microscope (37ºC) for 15 minutes in order to combat thermal drift during imaging. Cells were imaged every 3 minutes with a 561nm laser (also used for phase contrast images), using a Zeiss LSM710 confocal microscope fitted with a 63x 1.4NA oil immersion objective. Up to 5 different cells could be imaged for each time-point using the motorised stage. The autofocus system (a contrast-based method which used the fluorescence from the utrophin-RFP) was used to ensure cells remained in focus throughout the time course.

2.4.2.3 Mitotracker staining of mitochondria in living cells

Mitochondria were labeled using MitoTracker Green FM (Life Technologies). A 1mM stock solution was prepared using DMSO as a solvent, and this was diluted in complete RPMI-1640 to a final working concentration of 200nM. Cells were incubated in 200nM MitoTracker Green FM for 30 minutes, after which time it was aspirated and the cells washed twice in fresh RPMI-1640. Cells were imaged live immediately (as described below in section 2.4.1.4), as this particular molecular probe was not fixable, since it is dependent on the mitochondrial membrane potential.

2.4.2.4 Fluorescence Recovery after Photobleaching

2 x 10^4 melanocytes were seeded onto 35mm glass bottomed dishes (MatTek) and incubated overnight in complete RPMI-1640 medium with 10% CO_2 to allow them to spread. Cells were then transfected with GFP-β-actin plasmid DNA (see section 2.1.5.1 for method) and allowed to express protein for 48 hours. Prior to FRAP experiments, RPMI-1640 medium was replaced with L-15 supplemented with 10% FBS and 1% penicillin/streptomycin containing either 10nM JK or 0.1% DMSO and cells were incubated at 37ºC without CO_2 for 30 minutes. FRAP experiments were performed using a Zeiss LSM710 confocal microscope, equipped with a 63x 1.4 NA oil immersion objective. Three small (~6μm^2) regions of interest (ROIs) were selected using the Zen Black software, in order to simultaneously select areas corresponding to membrane, mesh and stress fibre actin. ROIs were then bleached using 30 iterations of a 5mw 488nm laser operating at 100% power. Images were recorded every 5 seconds for a total of 130 seconds. FRAP data was subsequently analysed using Zeiss' Zen 2011 software and normalised using Microsoft Excel.

2.4.2.5 Forced protein-protein dimerisation experiments

Melanocytes were plated onto 35mm MatTek dishes as described in section 2.4.2.1, allowed to spread overnight, and subsequently double transfected with FKBP and FRB constructs which were allowed to express for 48 hours. Prior to imaging, RPMI-1640 was replaced with prewarmed L-15 medium. Cells were imaged at T=0 using an LSM710 confocal microscope as described in section 2.4.1.4 and subsequently rapamycin analogue (A/C heterodimersier; Clonetech) was added to a final concentration of 0.5μM while cells were continually imaged.

2.4.3 Image Analysis

2.4.3.1 Micropattern Chips

Micropattern chips were fixed and stained as described in section 2.4.1.3. This microscope was fitted with a motorised stage, which allowed for the semi-automated acquisition of images. Between 25 and 100 cells were selected based on the criteria that they were a) singly occupying a fibronectin disk and b) had spread such that the cell filled the entire pattern. Their positions on the micropattern marked using the Zen Black software. Each marked cell

was then manually reviewed to ensure that it was correctly centered within the field of view of the microscope, and then all cells were automatically acquired by auto-focusing on the fluorescent fibronectin pattern (excitation = 633nm, emission = 650nm). Standard microscope settings were used (with the exception of gain) for every micropattern chip imaged, which are outlined in Table 2.10

Setting	Value
Image size	1024x1024 pixels
Bit depth	16-bit
Averages	4
Pix dwel	0.79μs
405 laser power	4%
488 laser power	2%
561 laser power	1%
633 laser power	2%

Table 2.10 - Microscope settings used for acquisition of micro-pattern chips.

All images were then aligned in ImageJ (Schneider et al., 2012) using a macro written by CYTOO (CellRef_démo_V2_1.ijm), using the fibronectin images as a reference. For the purposes of the macro, each pixel in all the micropattern chip images corresponded to 73.2nm, and a cutting size of 700 pixels was used.

The phase images were then inverted and thresholded such that only high-value pixels (corresponding to darkly pigmented melanosomes) were picked out, and a binary image generated. The ImageJ plugin 'Radial Profile Angle' (written by Philippe Carl, University of Strasbourg) was then used to quantify the distribution of the pixels corresponding to melanosomes. For this plugin, a droplet size of radius 320 pixels, which corresponded exactly to the radius of the fibronectin pattern, was used, coupled with an integration angle of 360º. The profile gave the mean melanosome distribution (an average of 360 radii around the circle) for each cell imaged. This data could then be used to generate line plots indicating the probability of finding pigment anywhere along the average radius of the entire population, along with scatter plots indicating the radius of a hypothetical circle which encapsulated 95% of the pigment for each cell imaged. The binary images could also stacked and averaged and a 'fire' lookup table applied in order to generated the pigment probability heat maps.

For statistical analysis or the PDR measurements the Mann-Whitney test was used to compared two datasets, whilst the Kruskal-Wallis ANOVA test was used to compare three or more

datasets. Line plots were compared using the Spearman's rank correlation coefficient.

2.4.3.2 Quantifying fluorescence intensity

To compare the fluorescence intensity of experimental cells to those of control cells (untransfected, stained with secondary antibody only), the plasma membrane of 10 control cells was selected using the free-hand drawing tool in ImageJ and the mean fluorescence within the ROI measured. 3 areas were also taken outside the cell and the average intensity of these areas were taken as the background. The background value was then subtracted from the cell value to give the final intensity measurement. The standard deviation of the fluorescence intensity for the control cells was calculated and experimental cells were considered to be expressing if their fluorescence intensity was greater than the average control cell intensity + 2SD units.

2.4.3.3 Quantifying microtubule and F-actin filaments

In order to estimate the number of microtubules or F-actin filaments present in a cell, images were analysed using the 'Area filter' option of the 'Image Edge' plugin in ImageJ (written by Thomas Boudier and Joris Meys). This gave a binary outline of the filaments, and the image was manually inspected to ensure that it conformed well to the original. If not, the 'deriche alpha value' (deriche is an edge detection algorithm, based upon the work of John F. Canny (Canny, 1986)), whose default was 1, was altered. Lowering the value made the edge detection more stringent (fewer filaments detected), whilst increasing it made it less stringent (more filaments detected).

The number of filaments was then measured using the 'Analyze particles' function, within the 'Analyze' menu of ImageJ. The default options were used (Size = 0-Infinity; Circularity = 0-1) whilst 'Masks' was selected from the 'Show' drop-down menu. Again, the masks displayed was manually inspected to ensure they conformed well to the binary outline.

2.4.3.4 Quantifying Actin Density

Melanocytes were fixed and stained with TR-phalloidin using the protocol given in section 2.4.1.3. All cells were stained using the same stock of TR-Phalloidin to minimise changes in staining intensity. Cells were then imaged using a Zeiss LSM710 confocal microscope,

equipped with a 63x 1.4 NA oil immersion objective using exactly the same settings for each image.

Actin density was quantified using ImageJ. Firstly, the area of each cell was calculated by either drawing around the plasma membrane using the free-hand selection tool, or using the method outlined in section 2.4.3.6. Secondly, the actin channel was thresholded (same threshold settings used for each image) to create a binary mask. The number of pixels corresponding to actin in the binary mask were counted by exporting the xy coordinates of the image. The number of pixels corresponding to actin was then normalised to the area of the cell.

2.4.3.5 Quantifying melanosome distribution in free growing melanocytes

The distribution of melanosomes in free growing cells was quantified in two different ways. In the first 'manual' method the melanosome distribution was determined by drawing around the plasma membrane of each cell using the 'polygon selection tool in ImageJ and the total area determined. Next, the same process was repeated for the bulk pigment (see Figure 2.2 for examples). The area occupied by the pigment was then divided by the total cell area to give a cell area:pigment area ratio, where values close to 1 indicate a WT phenotype (i.e. dispersed) whereas values close to 0 indicate a clustered phenotype.

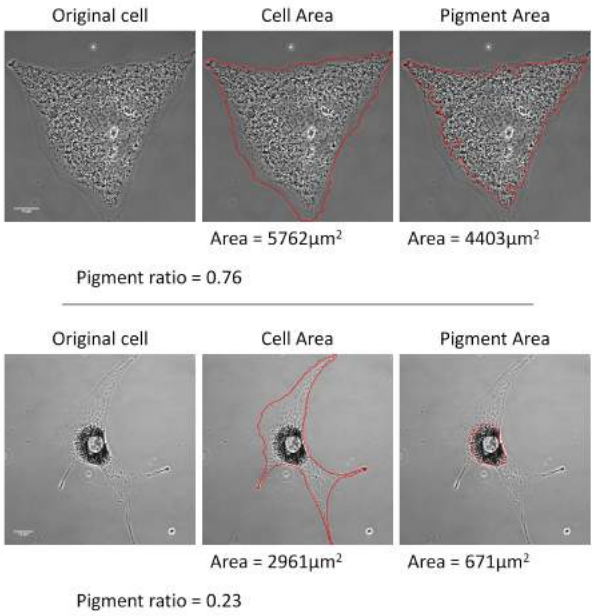


Figure 2.2 - Manually calculating the pigment ratio. Top panel = wildtype melan-a cell; bottom panel = melan-d1 cell. The red line in the 'cell area' column outlines the plasma membrane, whilst the red line in the 'pigment area' column encapsulates the bulk of the melanosomes, as visualised by phase contrast microscopy.

In the second method, the coverage index of a particular organelle or cellular component was measured by initially either drawing around the plasma membrane of the cell using the free hand selection tool in ImageJ, or, if the cell was stained with a volume marker such as actin, by thresholding on the intensity of the marker. The xy coordinates of the plasma membrane were then exported to MS Exel and the centre of the cell calculated using the formula:

$$x_{centre} = \frac{\sum x_i}{n} \qquad\qquad y_{centre} = \frac{\sum y_i}{n} \tag{2.5}$$

The distance from the cell centre to each plasma membrane coordinate was then calculated using formula 2.7. The object(s) of interest were then thresholded in ImageJ to generate a binary mask, and the xy coordinates of each white pixel exported. The distance from the cell centre to the object of interest was again calculated using formula 2.7. Finally the dispersion ratio was calculated by:

$$DR = \frac{\bar{CO}}{\bar{CPM}} \tag{2.6}$$

where $\bar{CO}$ = the average distance from the cell centre to the object(s) of interest and $\bar{CPM}$ = the average distance from the cell centre to the plasma membrane.

2.4.3.6 Measuring the average distance of actin to plasma membrane

To measure the average distance of actin to the plasma membrane, the actin image was initially thresholded using ImageJ to create a binary mask. The image was then re-thresholded until the entire cell area was filled with white pixels and the cell outline selected using the 'magic wand tool' (see Figure 2.3). The xy coordinates of every pixel corresponding to actin were then exported, as were the xy coordinates of the plasma membrane. The distance of each pixel corresponding to actin to every plasma membrane coordinate was then calculated using the distance formula:

$$d = \sqrt{(x_2 - x_1)^2 + (y_2 - y_1)^2} \tag{2.7}$$

For each coordinate corresponding to actin the smallest distance to the plasma membrane was found, allowing an average distance of the actin to the plasma membrane to be calculated.

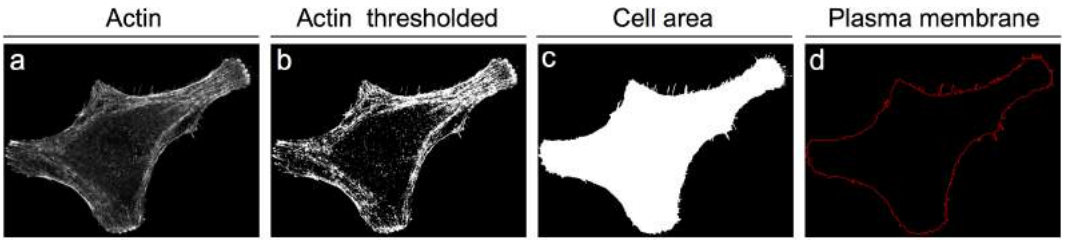


Figure 2.3 - Calculating the average distance of actin from the plasma membrane. Initially, the raw actin image was loaded into ImageJ **(a)**, and then thresholded to create a binary mask that faithfully represented the raw actin image **(b)**. The xy coordinates of each white pixel corresponding could then be exported using this mask. The raw actin image was then re-thresholded to create a binary mask of the entire area of the cell **(c)**, the outline of which **(d)** could then be used to generate the plasma membrane xy coordinates.

Primary Antibodies	Immunofluorescence	Western Blot	Supplier
Mouse anti-Tubulin	1 in 100	1 in 1,000	Calbiochem (cp06)
Mouse anti-GFP	1 in 100	1 in 1,000	Roche (11814460001)
Goat anti-GFP	1 in 100	1 in 1,000	Sicgen (A0020-200)
Goat anti-Kinesin-1	1 in 50	1 in 1,000	Everest Biotech (EB05492)
Rabbit anti-MyosinVa	1 in 50	1 in 1,000	Cell Signaling Technology (3402)
Goat anti-Rab27a	1 in 200	N/A	Sicgen (AB0023-200)
Rabbit anti-Tyrosinnase	N/A	1 in 1,000	Kindly gifted by Vincent Hearing, National Cancer Institute.
Rabbit anti-Arpc1b	1 in 100	1 in 300	Abcam (Ab99314)
Rabbit anti-Cofilin	1 in 100	1 in 1,000	GeneTex (GTX102156)
Goat anti-Formin-1	1 in 50	1 in 300	Santa Cruz (Y20)
Secondary Antibodies/Stains	**Immunofluorescence**	**Western Blot**	Supplier
Texas-red Phalloidin	100nM	N/A	Sigma (P1951)
DNaseI 594	1 in 1,000	N/A	ThermoFisher Scientific (D12372)
DAPI	300nM		
Alexa-647 Phalloidin	1 in 100	N/A	ThermoFisher Scientific (A22287)
Rabbit anti-Goat 488	1 in 500	N/A	ThermoFisher Scientific (A-11008)
Donkey anti-Goat 488	1 in 500	N/A	ThermoFisher Scientific (A-11055)
Donkey anti-Goat 568	1 in 500	N/A	ThermoFisher Scientific (A-11057)
Goat anti-Mouse 488	1 in 500	N/A	ThermoFisher Scientific (A-11029)
Goat anti-Mouse 568	1 in 500	N/A	ThermoFisher Scientific (A-11031)
Licor Donkey anti-Goat IR800	N/A	1 in 30,000	Licor (P/N 926-32214)
Licor Donkey anti-Mouse IR680	N/A	1 in 10,000	Licor (P/N 926-68072)
Licor Donkey anti-Rabbit IR680	N/A	1 in 30,000	Licor (P/N 926-68073)

Table 2.11 - Dilutions of cell stains and antibodies used for immunofluorescence and western blotting.

Chapter 3

Identifying the long-range anterograde melanosome transporter

3.1 Introduction

Previous research focusing on the mechanisms of anterograde melanosome transport in both melanophores and melanocytes have mainly concluded that kinesin, translocating along microtubule tracks, is crucial for this process. In particular, two isoforms of kinesin - kinesin-1 (encoded by the KIF5B gene) and the heterotrimeric kinesin-2 (encoded by KIF3A, KIF3B and KIF3C genes) have been attributed to melanosome transport.

Early experiments involved microinjecting antibodies raised against Kif5B into the clustered melanophores of the black tetra fish *Gymnocorymbus ternetzi*. Subsequently, cells were treated with caffeine to induce melanosome dispersion (as described in section 1.1.1.1). The results demonstrated that melanosomes within antibody treated melanophores remained aggregated, whilst melanosomes within control melanophores (injected with pre-immune serum) redispersed to the periphery (Rodionov et al., 1991). However, the antibody used in this study was raised against a conserved portion of Kif5B, and therefore cross-reacted with multiple different kinesin and kinesin-like isoforms (Wright et al., 1993; Johnson et al., 1994; Lombillo et al., 1995).

Other studies focused on the mechanism of melanosome transport in mammalian melanocytes have also concluded that Kif5B may be involved in this process. For example, one study used electron microscopy combined with immunogold labeling to visualise the intracellular localisation of anti-Kif5B antibody. This showed that a subset of melanosomes (29%) were positive for Kif5B, compared with 4% for the negative control where an irrelevant antibody was used (Vancoillie et al., 2000b). The authors also showed via immunogold labelling that the receptor for Kif5B, kinectin, was present on 14% of the melanosomes tested. However, the functional importance of this finding was not addressed and no attempt was made to investigate if additional isoforms of kinesin co-localised with melanosomes.

Another study also implicated Kif5B as being involved in melanosome transport in mammalian cells by knocking down the motor protein with antisense oligonucleotides on a patch of Guinea Pig skin which was simultaneously irradiated each day for a total of 14 days with UVB light. It was found that the skin was lighter in the patch treated with the antisense oligonucleotides against KIF5B compared with the control patch. When the skin was sectioned and imaged using electron microscopy very few melanosomes were present in the keratinocytes of the KIF5B antisense oligonucleotide treated skin, compared with the

control skin where melanosomes were abundant in the keratinocytes (Hara et al., 2000). However, no high magnification images of single melanocytes following KIF5B siRNA treatment were provided in order to show the distribution of melanosomes, which would be expected to clustered around the perinuclear area if Kif5B was indeed responsible for the long-range anterograde transport of these organelles. Since the study used melanosome content in keratinocytes as a readout of transport efficiency, it is possible that Kif5B knockdown affected the transfer of melanosomes into keratinocytes, rather than pigment granule trafficking within melanocytes.

More recently, Kif5B has also been shown to be involved in the anterograde transport of melanosomes in mouse melanocytes (Ishida et al., 2015). siRNA-mediated knockdown of the protein in wildtype melanocytes caused the melanosomes in 28%-38% of cells to become clustered (depending on the siRNA construct used), compared to 8% of cells treated with control siRNA. The authors also provided evidence suggesting that kinesin light chain-2 is responsible for linking Kif5B to melanosomes, since knockdown of this protein in wildtype melanocytes also caused cells to adopt a clustered phenotype in approximately 42% of cases.

Meanwhile, experiments utilising *Xenopus laevis* melanophores have concluded that heterotrimeric kinesin-2 is required for melanosome transport within these cells (Tuma et al., 1998). Western blot analysis using both anti-Xklp3 (raised against the tail domain of Xklp3, a *Xenopus* homolog of KIF3B) and anti-KAP115 (an accessory protein associated with kinesin-2) demonstrated that kinesin-2 co-purified with fractionated melanosomes. Kinesin-2 mutants were then generated where the motor head domain was replaced with GFP, and when this construct was microinjected into melanophores the melanosomes clustered around the MTOC. Lysosome transport remained unaffected by this dominant-negative kinesin-2 construct, suggesting this isoform of kinesin specifically drives pigment granule dispersion. Additionally, when SUK4 (a specific Kif5B antibody) was microinjected into melanophores plus-end directed transport of melanosomes still took place, while lysosomes clustered around the MTOC, indicating that conventional kinesin was not responsible for pigment granule transport in *Xenopus laevis*.

Kif5B and heterotrimeric kinesin-2 have also be implicated in the trafficking of organelles related to melanosomes, such as endosomes and lysosomes. For example, Kif5B was shown to be required to power the anterograde transport of lysosomes (Hollenbeck and Swanson, 1990; Rosa-Ferreira and Munro, 2011). In another study, kinesin-2 was also implicated

in anterograde lysosome and late endosome transport (Brown et al., 2005). In this work, HeLa cells were transfected with a dominant-negative version of KIF3A lacking the motor head, which caused late endosomes and lysosomes (stained with LAMP-1) to cluster around the perinuclear area. Other organelles, such as early endosomes, the Golgi and ERGIC (ER-Golgi intermediate compartment) remained unaffected by this treatment. In contrast, Kif16B has been implicated in the anterograde transport of early endosomes (Hoepfner et al., 2005). Kif16B is a homodimeric motor, with dimerisation shown to be cargo-dependent (Soppina et al., 2014). Interestingly, Hoepfner et al. showed that the small GTPase Rab5, which is associated with early endosomes, is necessary for the localisation of Kif16B to these organelles, although the two proteins do not directly interact. Instead, Rab5 is thought to recruit the phosphatidylinositol-3-OH kinase (PI3-K) hVPS34/p150 which functions to generate PIP3 at the early endosome membrane. The C-terminal PX domain of Kif16B then binds PIP3, thus linking the cargo and motor protein together. It is therefore plausible that the long-range anterograde transport of melanosomes may be driven by either Kif5B, kinesin-2 or (given the evidence that melanosomes arise from endosomes, as discussed in section 1.1.2) Kif16B.

While the majority of studies conclude that kinesin is a prerequisite for the long-range anterograde transport of melanosomes and related organelles, other experiments again using melanophores from *Gymnocorymbus ternetzi* appear to demonstrate that pigment granule transport can occur in a microtubule-independent fashion. When melanophores were depleted of microtubules with cold treatment combined with colchicine the melanosomes remained dispersed and continued to move at similar velocities to those in untreated cells (Schliwa and Euteneuer, 1978). Moreover, experiments where anterograde melanosome trafficking in *Xenopus* melanophores was monitored in the presence and absence of nocodazole showed that microtubule depletion had little effect on transport efficiency (Gross et al., 2002).

It is therefore important to further investigate if Kif5B is indeed responsible for the long-range anterograde transport of melanosomes in mammalian melanocytes, as has been previously suggested in the literature. This question forms the basis of the current chapter, and is addressed through a number of different techniques using wildtype mouse melanocytes at steady state.

3.2 Aims

The foremost aim of these experiments was to investigate which specific isoform(s) of the motor protein kinesin are required for long-range anterograde trafficking of melanosomes. Despite the fact the cooperative capture model was first hypothesised in 1998, this still remains an open question. A more complete understanding of how this process takes place is important, since this model is often used to describe how other cargo, such as cytotoxic T-cell granules or secretory vesicles budding from the Golgi are transported.

3.3 Results

3.3.1 Determining the localisation of Kif5B in melanocytes via fluorescence microscopy

In order to test whether Kif5B is involved in anterograde melanosome transport, an obvious first step was to determine if the motor localises to the melanosome membrane. To achieve this, wildtype murine melanocytes from C57BL/6 mice (henceforth referred to as melan-a cells) were transiently transfected with KIF5B-GFP and allowed to express for 72 hours before being fixed and antibody stained to amplify the GFP signal, as described in sections 2.1.5.1 and 2.4.1 using antibody concentrations given in Table 2.11. Empty EGFP-C2 vector was used as a negative control since GFP should be diffuse throughout the cytoplasm, while Rab27a-GFP was used a positive control, since it is known to localise specifically to melanosome membranes.

Kif5B did not appear to co-localise with melanosomes in any obvious way and instead seemed to be mainly located around the nucleus of the cells, with some diffuse staining throughout the cytoplasm (Figure 3.1c). However, Rab27a clearly localised to the melanosome membrane (Figure 3.1b), while GFP remained diffuse throughout the cell as expected (Figure 3.1a).

In order to functionally test the role of Kif5B as a melanosome transporter, a mutant version of this motor protein was generated which lacked the first 350 amino acids, corresponding to the motor domain (Kozielski et al., 1997). This construct, referred to as KIF5BΔMD, was generated according to the protocol in section 2.2.3.1. This mutant should act in a dominant-negative fashion; preventing kinesin from translocating along microtubules. Since the cooperative capture model states that melanosomes move bi-directionally along microtubules (Wu et al., 1998) it was hypothesised that if Kif5B is important for the anterograde transport of these organelles, expression of KIF5BΔMD should invoke clustering of the pigment granules, since minus-end directed motors would be allowed to dominate.

As a positive control for clustering, melan-a cells were transfected with a truncated version of melanophilin (MLPH1-266-GFP). This construct contains a Rab27a binding domain, allowing it to localise to the melanosome membrane, but lacks a myosin-Va binding domain - thus inducing melanosome clustering in a dominant-negative fashion (Hume et al., 2006) (Figure 3.1d).

When KIF5BΔMD-GFP was transfected into melan-a cells the construct neither induced perinuclear melanosome clustering, nor did the protein localise to the melanosome membrane (Figure 3.1e). Instead, the protein was either diffuse throughout the cytoplasm, similar to that of GFP alone or, in some cases, exhibited a tubular staining pattern - a phenomenon that was never observed with wildtype Kif5B-GFP. The observed staining pattern is highly reminiscent of microtubules, suggesting Kif5BΔMD-GFP was binding these filaments.

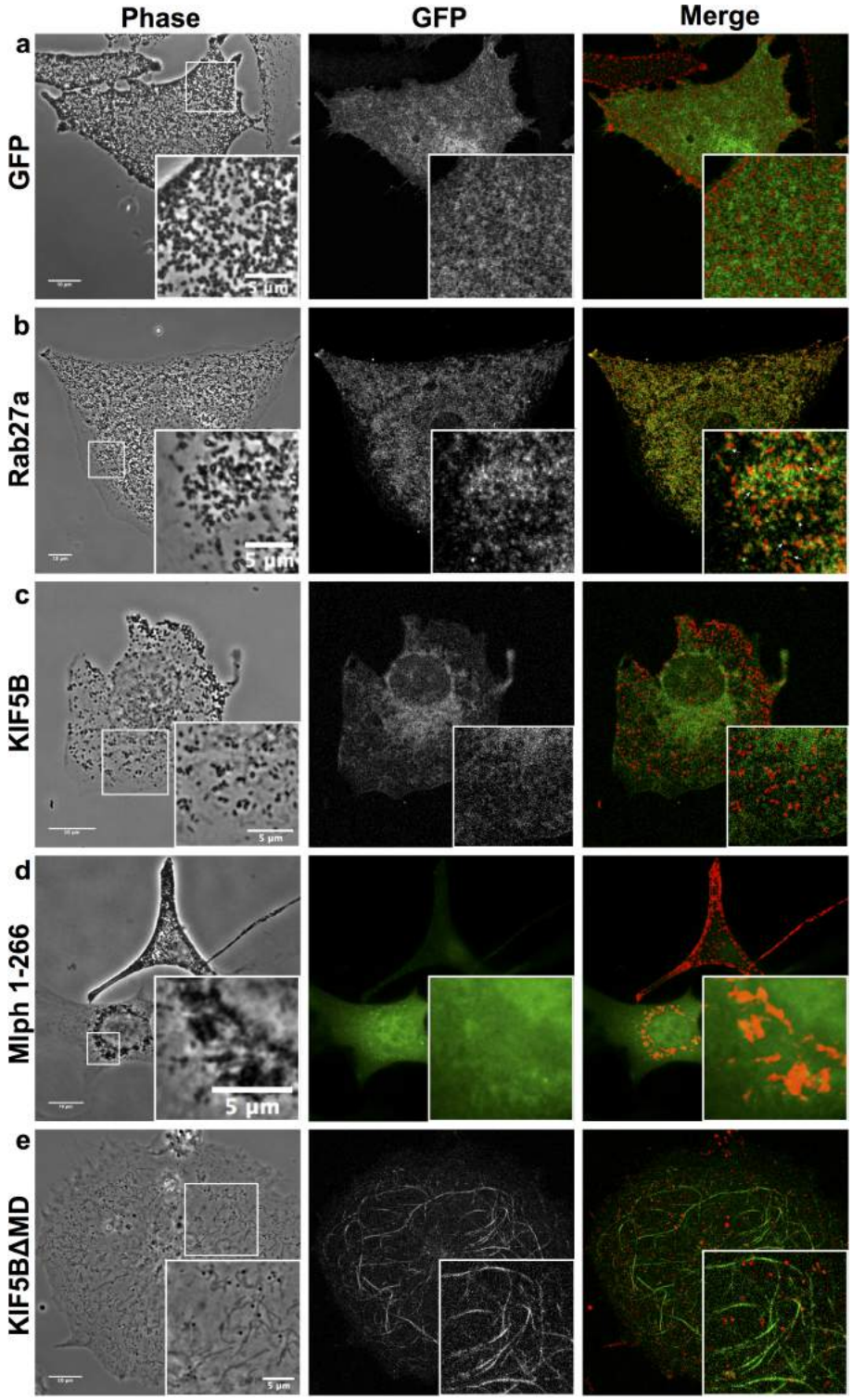


Figure 3.1 - Kif5B could not be detected on the melanosome membrane via immunofluorescence microscopy. (a) GFP was transfected into wildtype melanocytes as a negative control which does not localise to melanosomes. **(b)** Rab27a, a known melanosome marker, was transfected into melan-a cells as a positive control. Examples of melanosomes co-localising with Rab27a are highlighted with arrows in the merge panel **(c)** KIF5B-GFP was transiently transfected into melan-a cells to determine if the motor protein localises to melanosome membranes. **(d)** Mlph1-266 (which lacks the ability to bind myosin-Va) was used as a positive control for inducing perinuclear melanosome clustering. **(e)** Expression of KIF5BΔMD which lacks the motor domain, does not induce melanosomes to cluster. Cells were imaged using a confocal microscope, as described in section (2.4.1). For the merged images, fluorescent protein is coloured green, whilst melanosomes are false coloured red.

3.3.2 Kif5B is not enriched in purified melanosomal fractions

The number of kinesin motors that localise to the melanosome membrane at steady-state may be very small (<10), as suggested by Vancoillie et al. 2000b. It is therefore possible that immunofluorescence is simply not a sensitive enough technique to detect this fewer number of molecules. Therefore western blotting was used instead to test if Kif5B is specifically enriched in melanosomal fractions. Melan-a cells were harvested, lysed and the melanosomal fraction purified (as described in section 2.3.2) and analysed using western blotting (as described in section 2.3.1).

As expected, there are prominent bands for both tyrosinase (a melanosome marker) and Kif5B in the crude lysate (Figure 3.2a). Quantification of the bands (Figure 3.2b) indicate that for the post nuclear supernatant (PNS) fraction, where the nuclei have been removed by centrifugation, the levels of Kif5B remained constant, whilst there was a 60% decrease in tyrosinase levels compared to the crude fraction. For the nuclear pellet fraction, which should contain only nuclei, there was a 40% drop in tyrosinase compared with the crude fraction, whilst the amount of Kif5B is enriched by approximately 20%. Next, the PNS (theoretically containing the entire contents of the cell with the exception of nuclei) was centrifuged at higher speeds (17,000g for 30 minutes) in order to pellet heavy organelles, such as melanosomes. The vast majority of Kif5B was found in the supernatant, whilst, as expected, tyrosinase could not be detected in this fraction, since it was devoid of melanosomes. In the pellet, there was a prominent band for tyrosinase, with only a very weak band for Kif5B, demonstrating that whilst there was an enrichment of melanosomes in this fraction, there was not a concomitant enrichment of Kif5B.

When the pellet from the 17,000g spin was re-suspended, loaded onto a sucrose gradient (prepared as described in section 2.3.2 and centrifuged at 28,500g for 1 hour, a tyrosinase rich fraction was also collected at the bottom of the sucrose gradient (P28,500), although again, very little Kif5B could be detected, compared to either the crude or S17,000 fractions. These results are therefore in agreement with the Kif5B localisation results, shown in Figure 3.1, and suggest that Kif5B may not reside on the melanosome membrane, or if it does it is present in very low quantities meaning it could not be easily detected through either fluorescent microscopy of western blotting techniques.

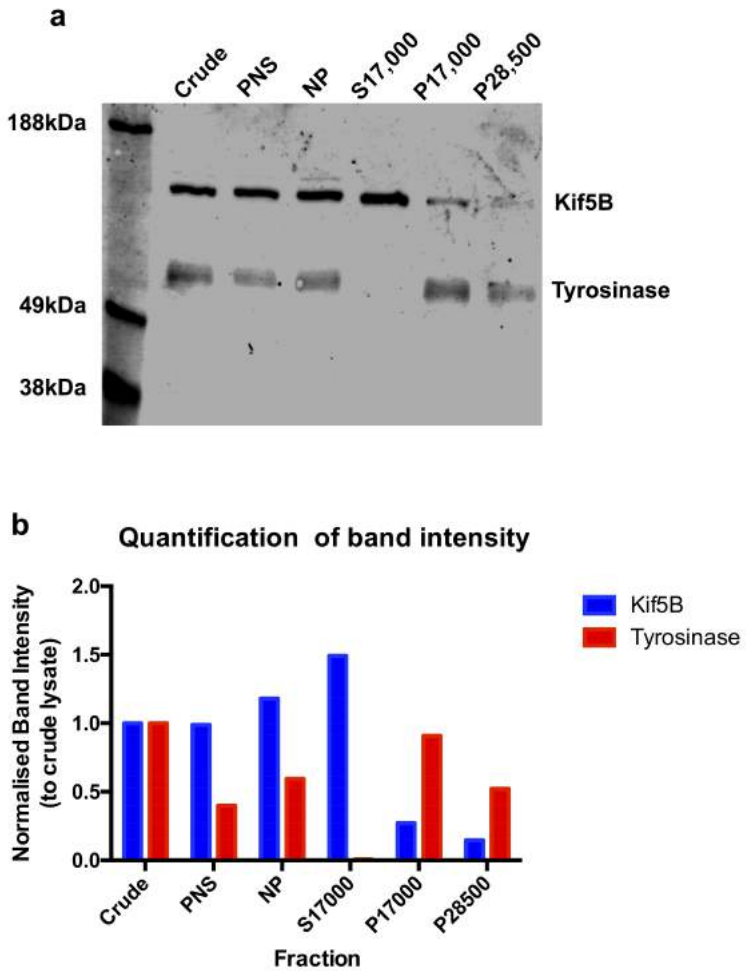


Figure 3.2 - Kif5B is not enriched in melanosomal fractions. **(a)** $1x10^7$ melan-a cells were lysed and fractionated. The sub-cellular localisation of either Kif5B or a melanosome marker (tyrosinase) was then investigated using western blotting of the different fractions. Crude = whole cell lysate; PNS = supernatant following 700g spin (10mins); NP = pellet following 700g spin (10mins); S17,000 = supernatant following 17,000g spin (30mins); P17,000 = pellet following 17,000g spin (30 mins); P28,500 = pellet following 28,500g spin (60mins) in 2M sucrose. Kif5B appears to be enriched in fractions containing light vesicles and organelles, since the majority of it was detected in the S17, 000 fraction. By contrast, tyrosinase is enriched in melanosomal fractions, since it was only detected in the P17,000 and P28,500 which correspond to dense cellular components, of which melanosomes are the most numerous in these cells. **(b)** Quantification of the band intensities from (a) with each fraction normalised to the crude lysate.

3.3.3 siRNA mediated knockdown of Kif5B did not result in melanosome clustering

Since Kif5B could not be detected on melanosomes using immunofluorescence and did not appear to be enriched in melanosomal fractions as demonstrated by western blotting another experimental approach was taken to investigate the importance of this motor protein in melanosome transport. Small interfering RNA (siRNA) was used to specifically knockdown the motor protein, which should cause retrograde transport to be favoured, and therefore melanosomes to become clustered, if the cooperative capture model is correct.

To knockdown Kif5B, melan-a cells were transiently transfected with KIF5B siRNA, while non-targeting (NT) siRNA was used as a negative control and Rab27a as a positive control (see section 2.1.5.2 for the protocol used). To confirm that the KIF5B siRNA was effectively knocking down Kif5B, mitochondria were stained for (see section 2.4.2.3), since it is well documented that these organelles are trafficked by this motor protein (described in section 1.2.2.3).

The results of this experiment show that Kif5B does indeed appear crucial for the anterograde transport of mitochondria, since in cells treated with KIF5B siRNA these organelles cluster tightly around the perinuclear area (Figure 3.3b; Mitotracker panel). In contrast, cells treated with either NT siRNA or RAB27A siRNA (Figure 3.3a & c, respectively) contained mitochondria that remained dispersed throughout the cytoplasm. However, the melanosomes remained dispersed after KIF5B siRNA treatment, compared to those in the RAB27A siRNA condition, where they exhibit a clustered phenotype. As expected, the melanosomes also remained dispersed in the NT siRNA control cells.

In order to quantify the levels of Rab27a and Kif5B following siRNA transfection, cells that had undergone identical treatment to those stained with MitoTracker for imaging were harvested, lysed and a sample run on a 10% SDS-PAGE gel for a western blot (as described in section 2.3.1 using antibody concentrations given in Table 2.11). The results indicate that both Kif5B and Rab27a are being effectively knocked down (Figure 3.3d & e, respectively). When the intensity of each of the bands was normalised to α-tubulin as a reference protein, it was seen that the levels of Kif5B were reduced by approximately 95% in the KIF5B siRNA treated cells, whilst Rab27a is depleted by around 70% in the RAB27A siRNA treated cells, compared to the levels in the negative control (Figure 3.3f).

Overall therefore, this is clear evidence that KIF5B siRNA does significantly attenuate

levels of Kif5B over a 72 hour period, and that this causes clustering of an organelle known to be transported by this motor protein. However, reduction in the levels of Kif5B do not appear to have any affect on the distribution of melanosomes.

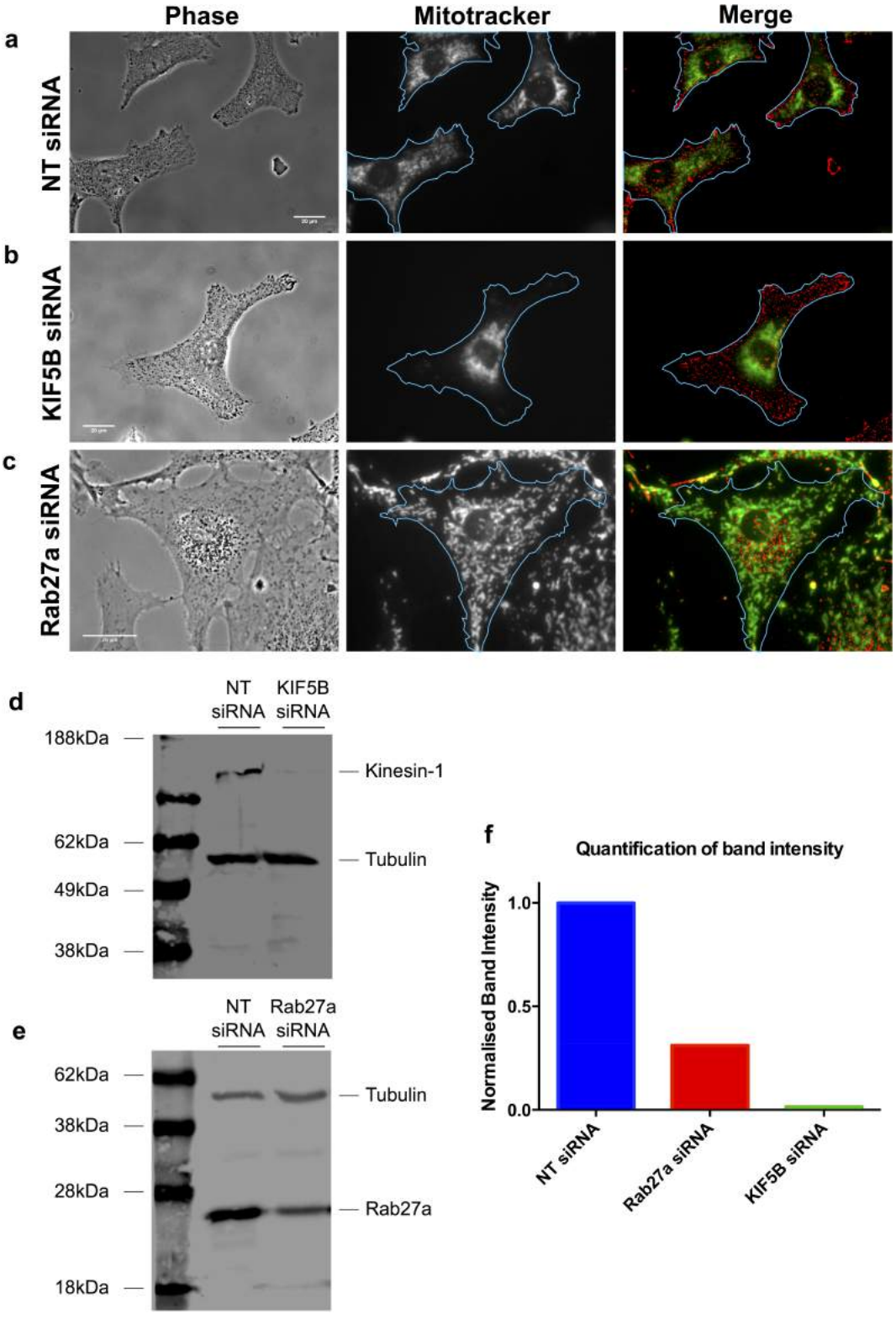


Figure 3.3 - Knocking down KIF5B induced clustering of mitochondria but not melanosomes. **(a)** In wildtype melanocytes transfected with non-targeting siRNA both melanosomes (red spots in the merge) and mitochondria (green spots in the merge) were evenly distributed throughout the cytoplasm. **(b)** Melan-a cells transfected with KIF5B siRNA exhibited clustered mitochondria, whilst melanosomes remained peripherally dispersed. **(c)** By contrast knocking down Rab27a induced clustering of melanosmes, but did not affect the localisation of the mitochondria. Western blotting showed that Kif5B was knocked down by approximately 95% compared with non-targeting levels **(d & f)**, whilst Rab27a was knocked down by approximately 70% **(e & f)**. Cell outlines (manually drawn from the phase image) are shown in light blue.

3.3.4 Evaluating kinesin isoform expression in wildtype melanocytes via RT-PCR

The above results show that Kif5B could not be detected on the melanosome membrane by either fluorescence microscopy or western blotting. Moreover this motor does not appear to play a major functional role in anterograde melanosome transport, since neither a dominant-negative construct lacking the motor-domain, nor siRNA-mediated knockdown of the protein lead to the perinuclear clustering of melanosomes. However, evidence from the literature suggests that melanosomes, at least in the melanophores of ectotherms, may be transported by kinesin-2 (Rogers et al., 1997; Tuma et al., 1998). Likewise, additional kinesin isoform such as Kif16B have also been implicated in the transport of related organelles such as early endsomes (Hoepfner et al., 2005). This opens up the possibility that kinesin isoforms other than Kif5B may be responsible for the anterograde transport of melanosomes in mammalian melanocytes.

To attempt to identify candidate motor proteins that may be involved in pigment granule transport a reverse transcription PCR (RT-PCR) screen was carried out to determine if any kinesin isoforms were specifically over expressed in murine melanocytes, which may be indicative of an involvement in melanosome transport.

mRNA was extracted from from both WT murine melanocytes (melan-ink cell line; Ha et al., 2007, which are genetically identical to the melan-a cells used in the rest of this study) as well as from a non-pigmented mouse fibroblast cell line (NIH3T3) and RT-PCR performed on it (see section 2.2.5 for protocol used). Initially only Kif5B and heterotrimeric kinesin-2 (KIF3A, KIF3B and KIF3C) motors, which have already been implicated in anterograde transport, were screened for. The results firstly indicate that all 4 genes are expressed in both cell types, since prominent bands of the expected size are apparent in the +reverse transcriptase (+RT) lanes, whereas for the -reverse transcriptase (-RT) lanes either no bands are visible or the signal is highly attenuated compared with the +RT condition (Figure 3.4).

Although RT-PCR is not considered a quantitative technique (it was chosen instead for its ability to screen a large number of genes relatively quickly), most variables such as the amount of cDNA template used, composition of the RT-PCR reaction mix, thermocycler settings, the amount of PCR reaction loaded onto the agarose gels and the thickness of the gel were kept constant. Therefore, although it is well documented that there is not always a good correlation between mRNA levels and protein expression (Vogel and Marcotte, 2012),

this could indicate at first glance a role for these isoforms in pigment granule transport, since it appears that the mRNA for each gene is more abundant in the melan-ink sample compared to the NIH3T3 sample. However, when GAPDH primers were used as a control to check if the signal from the NIH3T3 sample was comparable to that of the melan-ink sample, the band from the NIH3T3 sample was much weaker, which necessitated normalisation of the signal. After this operation was performed, each of the genes tested in the initial screen actually appear more highly expressed in the NIH3T3 cells, potentially implying these motors do not in fact play a significant role in melanosome transport.

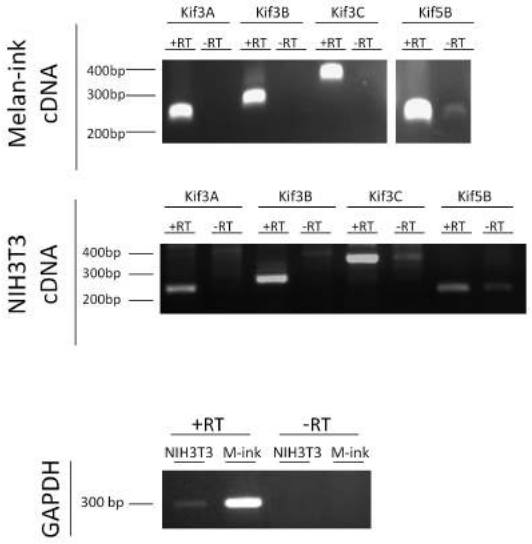


Figure 3.4 - Comparing the expression of KIF5B and KIF3A-C in murine melanocytes and NIH3T3 cells. RT-PCR on cDNA extracted from both wildtype melanocytes (melan-ink) and a non-pigmented mouse fibroblast cell line (NIH3T3) indicates that the KIF5B gene is highly expressed in melanocytes compared with NIH3T3 cells. KIF3A-C genes also appear more highly expressed in melanocytes compared with NIH3T3 cells. Expected band sizes are given in Table 7.1.

To check if any other kinesin isoforms are specifically up-regulated in melan-ink cells, a more extensive RT-PCR screen was carried out which included all other known kinesin isoforms. The results from this screen are given in Figure 3.5 and also summarised in Table 3.1 alongside the results from the initial screen. See Table 7.1 for a list of primers used in this RT-PCR screen.

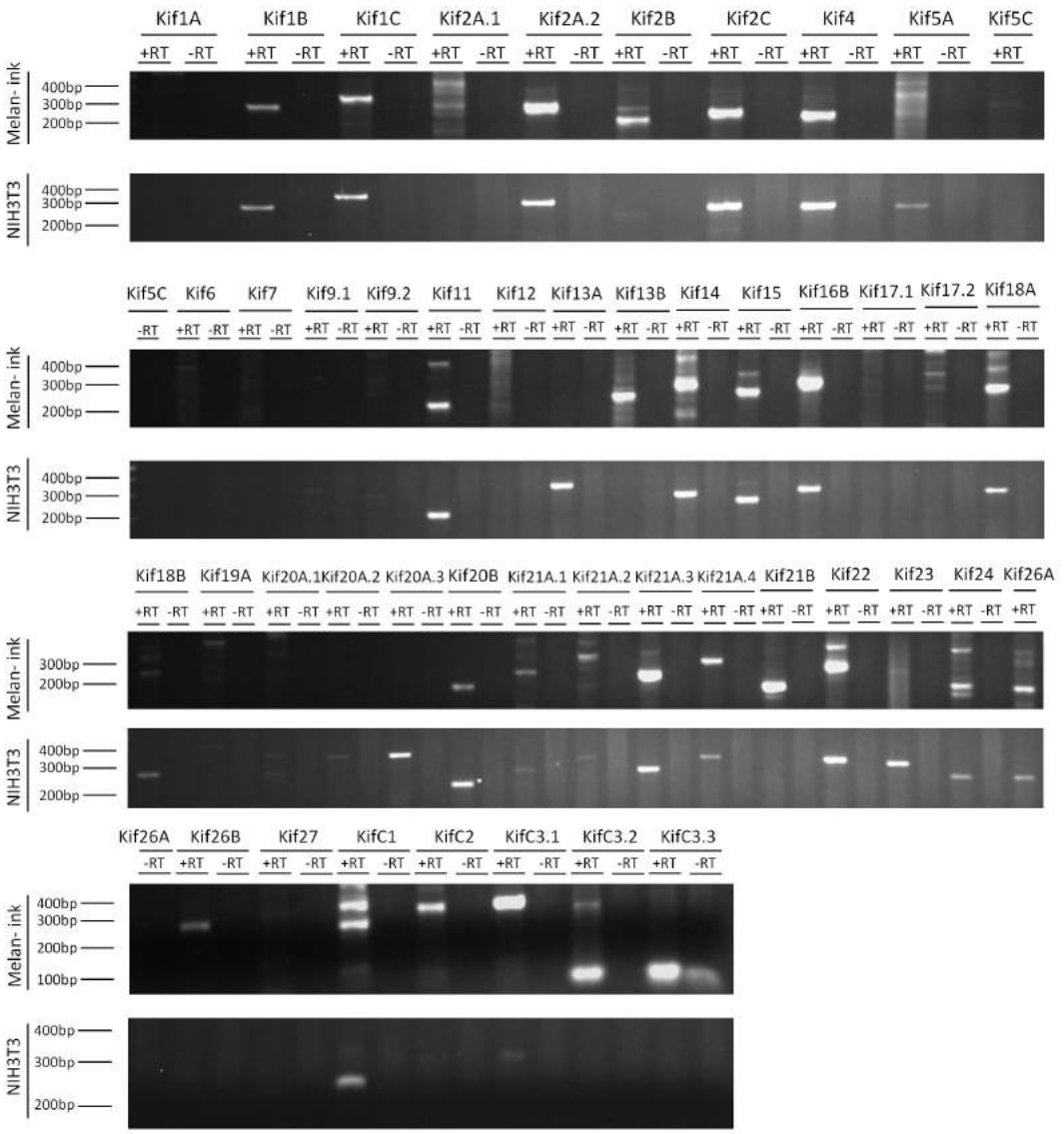


Figure 3.5 - Comparing the expression profile of all known KIF isoforms in murine melanocytes and NIH3T3 cells via RT-PCR. cDNA from both melan-ink and NIH3T3 cells was screened to detect which of all the major kinesin isoforms identified to date are expressed. The results indicate that there are some significant differences in the expression pattern between the two cell lines, notably KIFC3 isoforms KIF21B and KIF26B which appear to be highly expressed only in the melan-ink cells.

The results from the extended screen show that after normalising to GAPDH a majority of the kinesin isoforms appear more highly expressed in the NIH3T3 sample. However, this may simply be due to the difference in GAPDH expression level, which can vary between tissue types (Barber et al., 2005).

In total five genes, KIF6, KIF17.2, KIF21B, KIFC3.2 and KIFC3.3, appear more highly expressed in melan-ink cells compared with NIH3T3 cells, although differences in the expression level of KIF6 are insignificant, given the qualitative nature of this technique, as are the differences between KIF17.2 and KIF21B mRNA levels. However, KIFC3.2 and

KIFC3.3, which both encode a minus-end directed C-terminal kinesin (Dietrich et al., 2013), do appear significantly up-regulated in melanocytes compared with the fibroblast cell line. It was also apparent from this screen that KIF13A is completely absent from melanocytes, but well expressed in NIH3T3 cells, whilst the reverse is true for KIF13B.

Overall, whilst this evidence alone clearly cannot implicate a particular kinesin isoform as being involved in melanosome transport, it is nonetheless intriguing that two genes encoding a minus-end directed motor are so highly expressed specifically in melanocytes, potentially implicating them in the retrograde transport of melanosomes.

Gene	Expression in Melan-ink	Expression in NIH-3T3	Gene	Expression in Melan-ink	Expression in NIH-3T3
KIF1A	0.00	0.00	KIF17.1	0.00	1.33
KIF1B	0.16	20.47	KIF17.2	0.52	0.20
KIF1C	0.31	37.20	KIF18A	1.47	29.69
KIF2A.1	0.00	2.00	KIF18B	0.15	12.64
KIF2A.2	0.71	42.74	KIF19A	0.27	1.29
KIF2B	0.27	2.18	KIF20A.1	0.09	2.35
KIF2C	0.39	56.06	KIF20A.2	0.00	3.60
KIF3A	0.97	12.51	KIF20A.3	0.00	45.06
KIF3B	0.66	15.42	KIF20B	0.79	51.54
KIF3C	0.90	16.46	KIF21A.1	0.48	6.63
KIF4	0.40	53.65	KIF21A.2	0.77	4.16
KIF5A	0.11	11.46	KIF21A.3	3.14	48.51
KIF5B	1.19	8.52	KIF21A.4	1.59	14.73
KIF5C	0.00	0.36	KIF21B	3.11	2.19
KIF6	0.05	0.00	KIF22	3.09	60.15
KIF7	0.00	1.66	KIF23	0.31	44.42
KIF9.1	0.02	1.34	KIF24	1.32	18.09
KIF9.2	0.03	2.54	KIF26A	1.31	18.09
KIF11	1.53	46.36	KIF26B	0.69	2.78
KIF12	0.00	1.00	KIF27	0.21	2.57
KIF13A	0.00	46.25	KIFC1	2.44	36.84
KIF13B	1.78	0.65	KIFC2	2.00	9.47
KIF14	1.64	46.83	KIFC3.1	3.66	5.37
KIF15	1.93	44.15	KIFC3.2	3.34	0.00
KIF16B	2.97	43.54	KIFC3.3	4.22	0.00

Table 3.1 - Summary of the expression levels of KIF isoforms from murine melanocytes and NIH 3T3 cells determined by RT-PCR. Bands from the agarose gels given in Figures 3.4 and 3.5 were quantified in ImageJ and the values normalised to GAPDH expression. Blue rows indicate that expression was higher in melan-ink cells for that particular isoform, compared with the expression in NIH 3T3 cells.

3.3.5 Optimising the nocodazole dose murine melanocytes can tolerate

The results from the RT-PCR screen showed that only minus-end directed kinesin motors were significantly overexpressed in melanocytes, while immunofluorescence and western blot experiments could not detect Kif5B colocalising with melanosomes. Moreover, siRNA depletion does not significantly effect the steady-state intracellular distribution of these organelles. These observations are at odds with the accepted view of melanosome transport, exemplified by the cooperative capture model. Since cytoskeleton disrupting drugs have been previously used in the literature to investigate melanosome transport (Wu et al., 1998; Aspengren et al., 2006; Palmisano et al., 2008; Semenova et al., 2008), it was decided to adopt this approach here to investigate the mechanisms underpinning long-range anterograde melanosome transport. These treatments give the advantage of rapidly revealing the general contribution of motor proteins to organelle transport.

Initially the contribution microtubules make towards maintaining melanosome distribution at steady-state was tested. Therefore melanocytes were treated with the synthetic drug nocodazole (noc), a well known agent which inhibits the polymerisation of $\alpha\beta$ tubulin heterodimers into microtubules and thus induces depolymerisation of microtubules as these filaments turnover. It is widely used both because of its fast mode of action which sees microtubules depolymerise after approximately 20 minutes subsequent to cells being treated with a 1μg/ml dose (3.3μM), and because it is highly selective such that even when doses several log units greater than is necessary are used, no non-specific effects are observed. Furthermore, the effects of noc have been shown to be reversible, with cells recovering when the drug is washed out after exposure to 0.04μg/ml (133nM) noc for either 24, 48 or 72 hours (De Brabander et al., 1976). The binding of noc to tubulin monomers best fits a model whereby each tubulin monomer has two binding sites which differ in their affinity for the drug (Xu et al., 2002). The presence of GTP bound to the exposed β-tubulin subunit at the plus-end of microtubules is thought to be essential for microtubule growth. Noc is therefore thought to block the addition of new $\alpha\beta$ tubulin heterodimers onto the growing filament by increasing the GTPase activity of tubulin by approximately 5-fold (Mejillano et al., 1996).

Before this drug could be used to study the effects of depleting microtubules on the steady-state distribution of melanosomes, it was first necessary to optimise the dose required, so that the lowest concentration of noc could be used in order to minimise cytotoxicity and off-

target effects. Initially a range of noc concentrations between 10μM and 1μM were applied to melan-a cells for 60 minutes (Figure 3.6b-e), since this range is typical of that used in the literature (De Brabander et al., 1976). As a control, melan-a cells were also treated with 0.1% DMSO (vehicle control) to ensure that any observed effects were specific to noc (Figure 3.6a). To visualise the microtubules, cells were fixed as described in section 2.4.1.3 and then stained with an anti α-tubulin antibody and imaged as described in section 2.4.1, using antibody concentrations given in Table 2.11.

Unsurprisingly, the immunofluorescence results given in Figures 3.6b-e shows that the highest dose of noc tested was most effective at depolymerising microtubules. However, even the lowest concentration tested (1μM) was still highly effective, with only a very small number of fragmented microtubules remaining which are unlikely to support long-range transport.

In order to check cells were still healthy after noc treatment, the melanocytes were treated with 1μM noc for 2 hours, at which time the drug was washed out (described in section 2.4.1.5) and the cells allowed to recover for a further 90 minutes (Figure 3.6f). The results show that melanocytes are able to rapidly re-form their microtubule networks, such that it closely resembles the cytoskeleton of cells treated with 0.1% DMSO alone. Overall this suggests that treatment with 1μM noc for 2 hours is not cytotoxic.

Cells were also stained for F-actin using Texas-Red phalloidin (see section 2.4.1.3 for protocol) to demonstrate the specificity of noc. Whilst in the DMSO treated cells the phalloidin staining appears mainly at the plasma membrane, in the noc treated cells, this staining appears intense throughout the cytoplasm, and there also appears to be a greater number of stress fibres. Quantification (given in the top left hand corner of Figure 3.6a-f; performed as described in section 2.4.3.3) shows that the F-actin filament number vary slightly depending on the noc concentration, although this variability may be due to the difficulties in quantifying F-actin. For example, when filaments become more densely packed together it becomes more difficult to identify the individual filaments, due to the resolution limit of the microscope. However, it was clearly apparent that there was no affect on the steady-state melanosome distribution, regardless of the noc concentration used. This result suggests either microtubules are not required for the positioning of pigment granules, or that since the contribution from both anterograde (kinesin) and retrograde (dynein) motors have been lost, melanosomes simply remain stationary.

Therefore, a more informative experiment would be to understand if melanosomes can re-disperse in the absence of an intact microtubule network using an add-back experiment. This would require one of the clustered cell lines (*dilute*, *leaden* or *ashen*) to survive overnight treatments with noc - the length of time required for the missing gene to be expressed and melanosomes to re-disperse to the periphery. Therefore, melan-leaden cells were treated with either 1μM or 500nM noc for 16 hours. The results indicate that after overnight treatment with noc, cell morphology appears normal, despite the complete lack of a detectable microtubule network (Figure 3.7a.i & a.ii).

Finally, cells were imaged live to understand how rapidly the microtubule network was being depleted by noc treatment. Melan-a cells were seeded onto 35mm glass-bottomed Matek dishes and transiently transfected with α-tubulin-GFP (as described in section 2.1.5.1). Cells were imaged 48 hours later using a Zeiss LSM710 confocal microscope (described in section 2.4.2). Noc was added to a final concentration of 1μM and cells imaged every 10 minutes (Figure 3.7b.i-b.vi). They show that the majority of the microtubule network is depleted after only 10 minutes. Between 20 and 40 minutes, a small sub-population of filaments persist which appear to be more resistant to the noc, but after 60 minutes these microtubules have also been depleted.

Overall therefore, this set of optimisation experiments demonstrates that 1μM noc applied for 60 minutes is sufficient to deplete melanocytes of microtubules, and that cell morphology and melanosome distribution appeared very similar to the DMSO control even after 16 hours in the presence of the drug. Importantly, these experiments open up the possibility of add-back experiments in the presence and absence of microtubules to further investigate their role in melanosome trafficking.

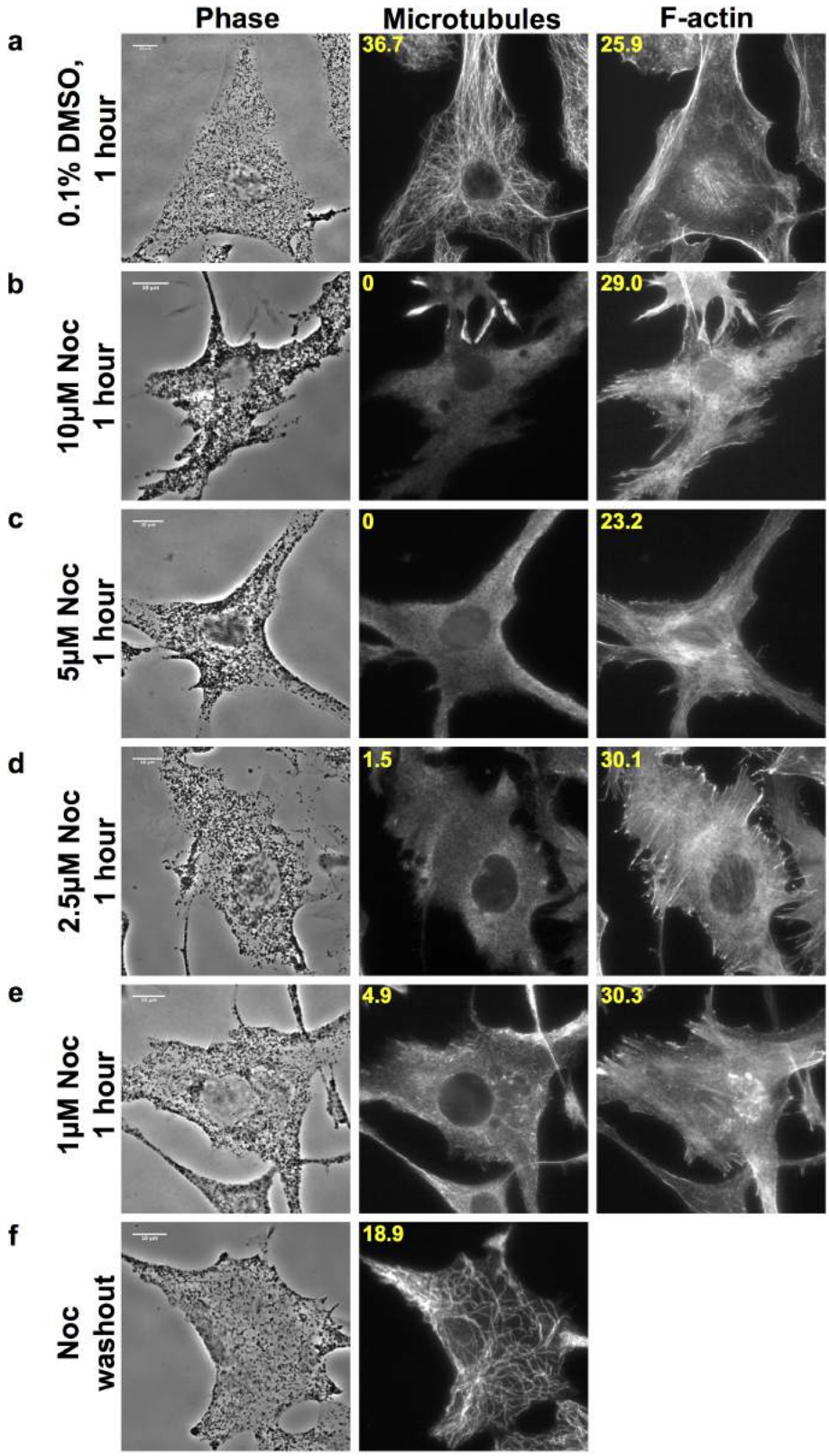


Figure 3.6 - Treatment with 1μM noc for 1 hour is sufficient to significantly deplete the microtubule network in melanocytes. **(a)** Melan-a cells treated with 0.1% DMSO for 1 hour had an intact microtubule network and actin cytoskeleton, as expected. **(b & c)** After 1 hour cells treated with either 10μM (b) or 5μM (c) noc for 1 hour had no observable microtubules remaining, although the actin cytoskeleton remained intact. **(d)** Treatment with 2.5μM noc for 1 hour was sufficient to depolymerise the vast majority of microtubules, compared with the control cells. **(e)** Treatment with 1μM noc caused a significant decrease in the total number of microtubules compared with the vehicle control. **(f)**. Melan-a cells were treated with 1μM noc for 2 hours after which time the drug was washed out and the cells allowed to recover for 90 minutes prior to fixing. Microtubules recovered to approximately half the density of the vehicle control in this time. Numbers in the top left hand corner denote the mean number of microtubules per 10μm^2. **a**, n=6; **b-e**, n=3; **f**, n=5.

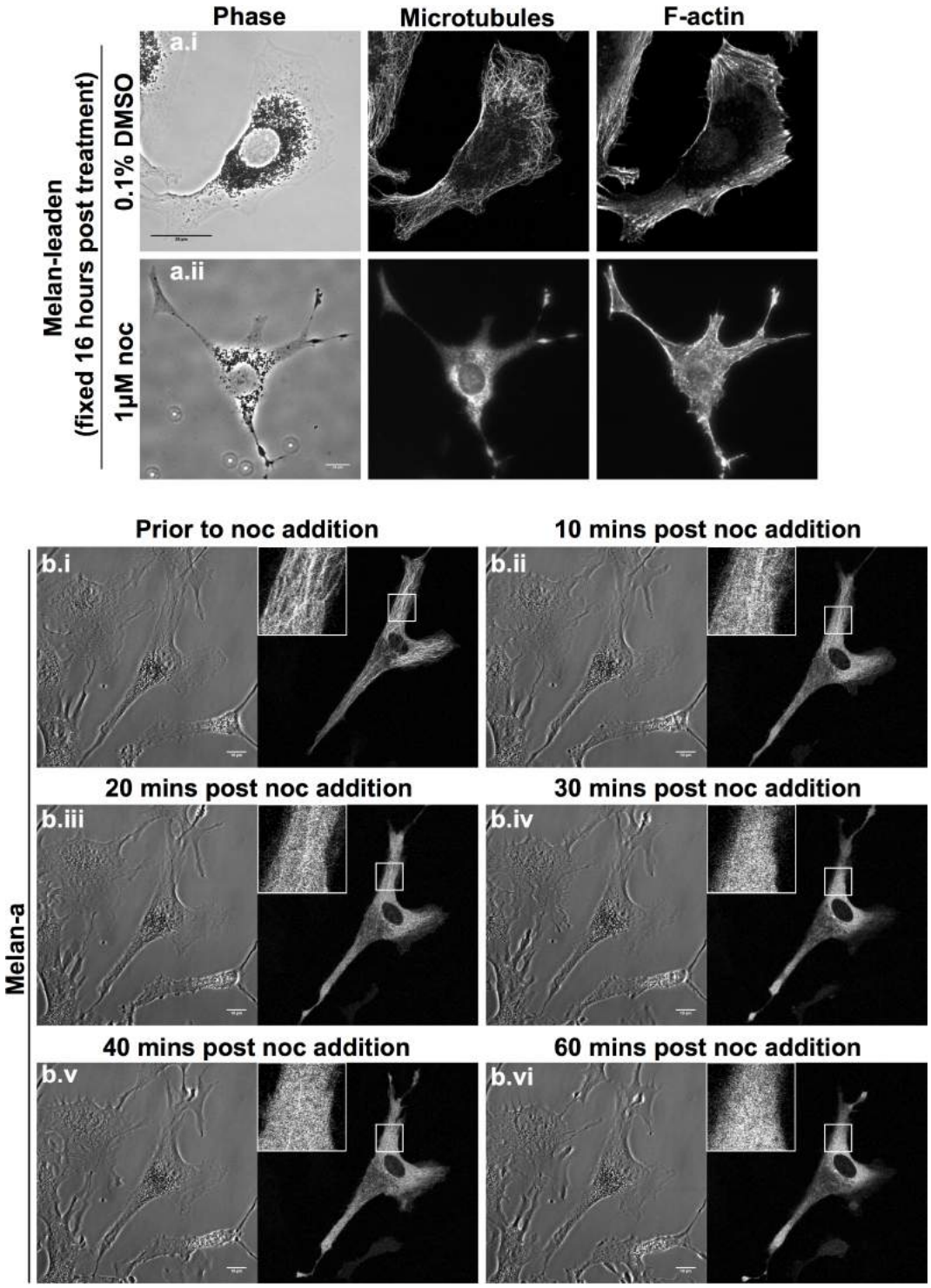


Figure 3.7 - Live cell imaging confirms the microtubule becomes significantly depolymerised after 1 hour in the presence of 1μM noc. (a.i-a.vi) Melan-a cells were transiently transfected with $\alpha-$tubulin-GFP 48 hours prior to imaging. Cells were then treated with 1μM noc during live cell imaging in order to estimate how long this concentration of drug took to depolymerise the microtubule network. **(b.ii)** Melan-leaden cells were treated with 1μM noc for 16 hours to confirm this did not disrupt melanosome localisation compared to the control cells (b.i), and was not cytotoxic.

3.3.6 Standardising cell shape enables precise quantification of melanosome distribution.

In previous studies melanosome distribution was quantified by calculating the area occupied by the bulk pigment and dividing by the area of the entire cell (described in section 2.4.3.5). This gives a value between 0 and 1, with lower values representing clustered cells, and higher values representing dispersed cells. However, although simple, this method is ultimately flawed since the experimenter must manually (and therefore subjectively) outline the bulk pigment. This is not always straightforward and may lead to a biased result, especially if efforts are not taken to perform the quantification 'blind'. Moreover, this method is time-consuming, which limits the total number of cells that can be quantified, thereby reducing the statistical power of the results. To combat these problems, a more rigorous method of assessing melanosome distribution was sought which would afford more accurate quantification as well as reduce experimenter bias.

To achieve this, melanocytes were seeded onto micropattern chips which had circular fibronectin patterns with an area of $1600\mu m^2$ printed onto a cytophobic glass coverslip (see section 2.4.3 for the protocol used). This resulted in the melanosomes seeded onto the chip adhering to the fibronectin and subsequently becoming constrained to the dimensions of the disc as they spread, thus allowing melanocyte size and shape to be standardised across all experiments. The exact distribution of melanosomes in each cell could then be quantified very precisely, without any experimenter bias, as described in section 2.4.3. Moreover, because both the image acquisition and the quantification could be automated to a large extent, a larger number of cells could be processed compared with the manual method, allowing for greater statistical power and the possibility to discern very subtle phenotypes that may otherwise be overlooked.

Example images of melan-a and melan-dilute cells are shown in Figure 3.8a & b, respectively. Corresponding 'pigment probability maps' are also shown (Figure 3.8c.i & c.ii). These represent the probability of finding pigment in one particular area of the cell as a colour (see the scale bar at the top right of each image) based on the average distribution of melanosomes from all the melanocytes imaged for each treatment (see section 2.4.3 for details on how these maps were generated). The data is also represented as a line plot (Figure 3.8d), which plots the probability of finding pigment at any given point along the average radius of the cell from the centre to the plasma membrane. Finally a scatter plot depicts

(for every cell imaged) the radius of a hypothetical circle which encapsulates 95% of the melanosomes within that cell, known as the pigment dispersion radius (PDR)(Figure 3.8e).

Constraining the melanocytes on micropatterns in this way allowed for precise quantification of the average melanosome distribution. Figure 3.8d shows that the average line plots for melan-a and melan-dilute cells have a completely different profile, whilst the scatter plot indicates the PDR for the melan-a cells is 19.9μm, while for the melan-dilute cells this is reduced to 11.7μm. This method therefore offers the possibility to rapidly and quantitatively detect subtle change in melanosome distribution after different treatments.

This approach was used to re-test the effect of overnight noc treatment on melanosome distribution, in order to understand if a subtle change in phenotype was previously overlooked using free growing melanocytes. Melan-a cells were allowed to spread on the patterns overnight, and then treated with either 0.1% DMSO or 1μM noc for a further 16 hours prior to fixing. The pigment probability maps reveal that while for the DMSO control the highest probability of finding pigment is in a band just underneath the plasma membrane, for the noc treated cells this band shifted slightly toward the cell centre (Figure 3.9c.i & c.ii). This is exemplified by the % pigment plot (Figure 3.9d), where the line representing noc treated cells tails off approximately 1μm before the line profile representing DMSO treated cells. However, the shape of the two profiles are very similar, resulting in the high Spearman's rank value of 0.798 (perfect positive correlation = 1, perfect negative correlation =-1). Meanwhile, the scatter plot (Figure 3.9e) shows that the PDR for DMSO treated cells is 20.2μm, while for the noc treated cells this is reduced to 19.2μm.

It was also of interest to understand if melanosomes were able to diffuse out from the perinuclear area in the absence of microtubules for extended periods of time, as has been reported for other organelles such as mitochondria (Tanaka et al., 1998), since if diffusion did occur it would be difficult to uncouple these effects from active transport in add-back experiments. To test this, melan-dilute cells were also seeded onto micropattern chips, allowed to spread overnight, and subsequently treated with either 0.1% DMSO or 1μM noc for 16 hours. The average pigment maps (Figure 3.10c.i & c.ii) indicate that pigment does not diffuse away from the perinucelar area after noc treatment, as both images appear equivalent. This is backed up by both the scatter plot (Figure 3.10d), which shows there is no significant difference between the mean PDR of cells treated with either DMSO or noc, and the line plot (Figure 3.10) where the profile after the two treatments appears very similar.

These experiments firstly demonstrate the power of using micropattern chips to determine melanosomes distribution compared with previous methods of quantification. Secondly they show that noc treatment has a small, albeit significant, effect on the distribution of melanosomes at steady-state, although this could be explained by partial collapse of the plasma membrane after microtubules were depolymerised. Finally, the observation that the phenotype of *dilute* melanocytes does not significantly change even after overnight treatment with noc opens up the possibility of add-back experiments to test the contribution of microtubules on long-range anterograde melanosome transport.

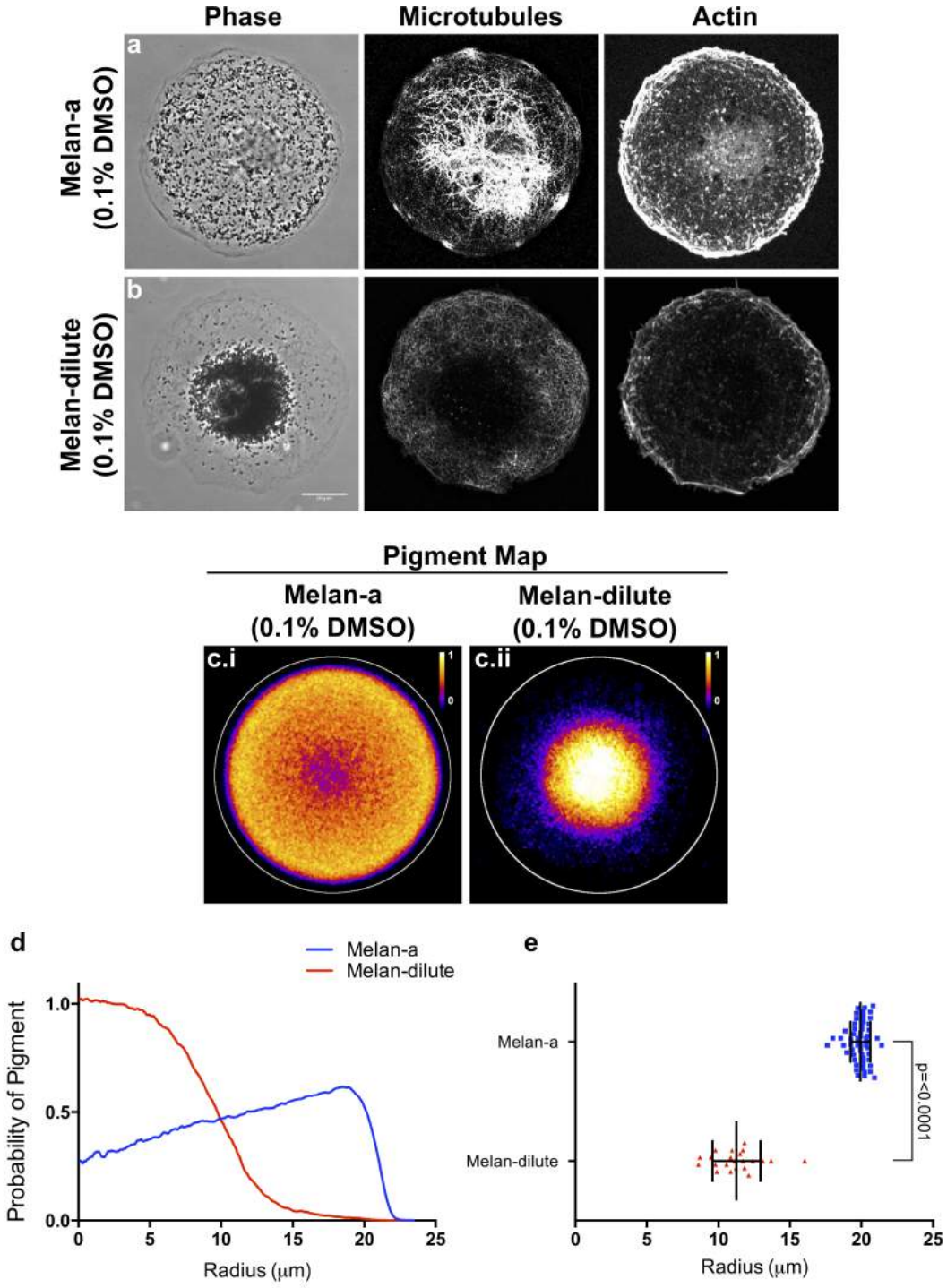


Figure 3.8 - Standardising melanocyte morphology allows precise quantification of melanosome distribution. Both melan-a **(a)** and melan-dilute **(b)** cells were seeded onto circular fibronectin patterns printed onto an otherwise cytophobic glass coverslip and allowed to spread overnight before fixing. Cells were then stained with an α-tubulin antibody and texas-red phalloidin to visualise microtubules and F-actin, respectively. **(c.i & c.ii)** Multiple images of cells were captured using a Zeiss LSM710 confocal microscope and aligned using ImageJ. A binary mask of the melanosomes was created for each image, and an average Z-projection performed to create an 'average pigment map' whereby black = 0% probability of finding pigment and white = 100% probability of find pigment in that area. **(d)** Average probability of finding pigment along a hypothetical radius of the circular cells. **(e)** Each spot represents the radius of a hypothetical circle encapsulating 95% of the total number of melanosomes in each cell imaged. Melan-a n=59; melan-dilute n=22. For **d**, Spearman's rank = -0.329. For **e**, statistical analysis was performed using a Mann-Whitney test.

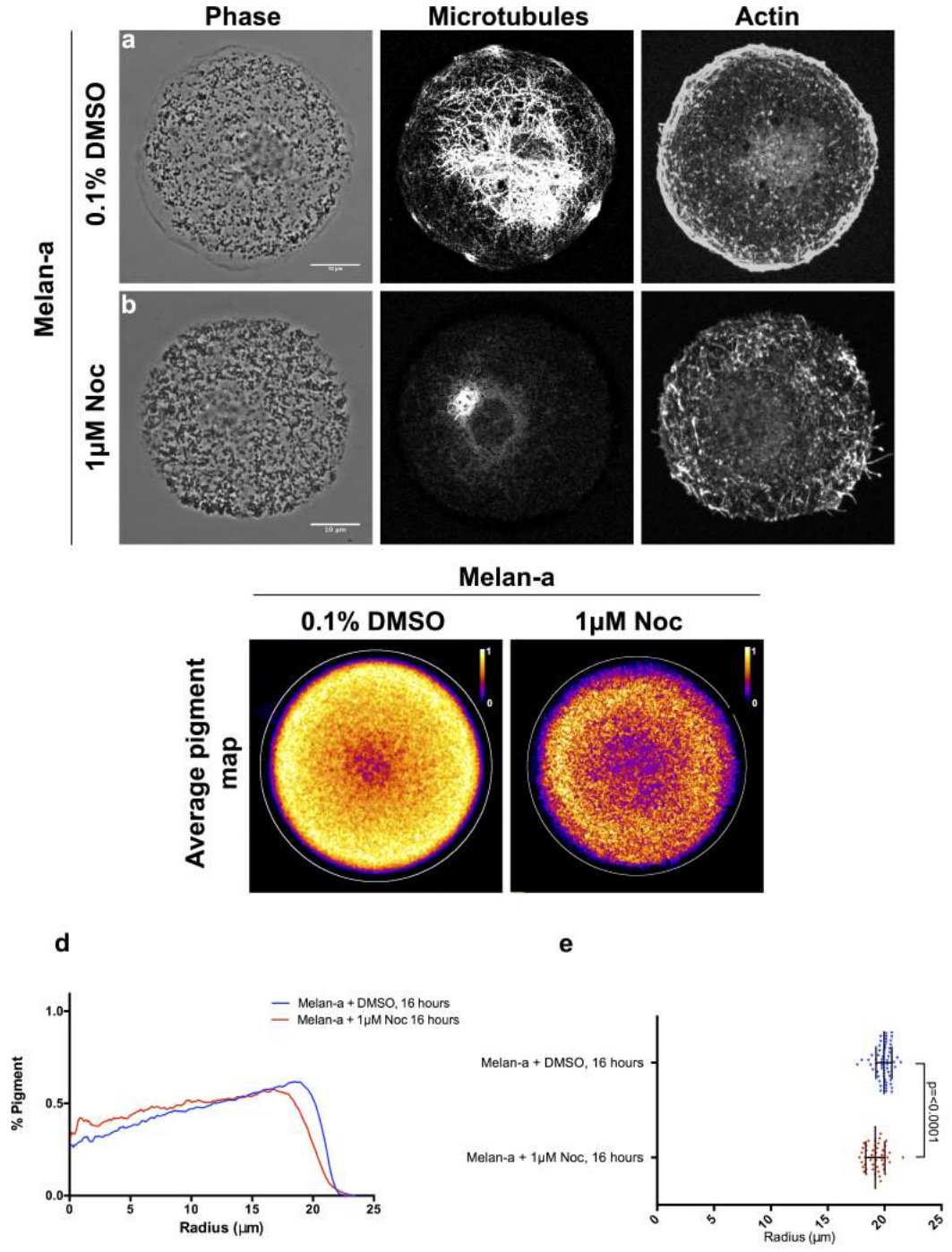


Figure 3.9 - Melanosomes remain peripherally dispersed in wildtype melanocytes after noc treatment. Wildtype melanocytes were allowed to spread overnight on micropattern chips before treatment with either 0.1% DMSO **(a)** or 1μM noc **(b)** for 16 hours prior to fixing. **(c.i & c.ii)** images of cells from each condition were acquired and virtually 'stacked' to create an average pigment map. White = 100% probability of finding pigment in that area; black = 0%. **(d)** Line plot depicting the probability of finding pigment along an average radius for the entire number of cells imaged. Spearman's rank value = 0.798. **(e)** Scatter plot depicting the radius of a hypothetical circle which encapsulates 95% of the pigment granules for each cell imaged. Melan-a + 0.1% DMSO, n=59; melan-a + 1μM noc, n=43. Statistical analysis was performed using a Mann-Whitney test.

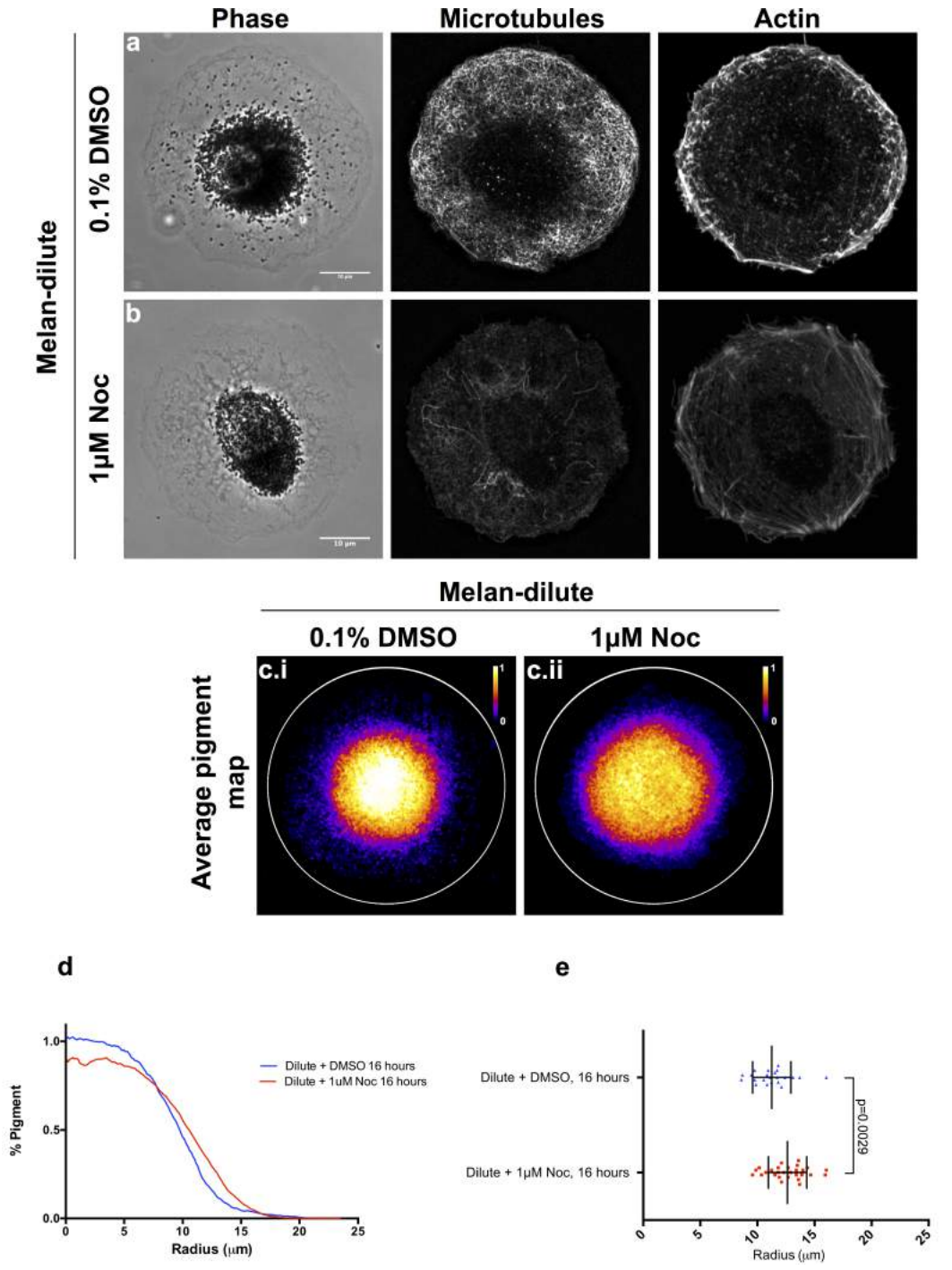


Figure 3.10 - Noc treatment does not affect melanosome distribution in melan-dilute cells at steady state. Melan-dilute cells were allowed to spread on micropattern chips for 16 hours before treatment with either 0.1% DMSO, n=22 **(a)** or 1μM noc, n=28 **(b)** for 1 hour prior to fixing. **(c & d)** A number of images of cells were then imaged and virtually 'stacked' to create an average pigment map. White = 100% probability of finding pigment in that area; black = 0% probability. The figure in the lower right hand corner indicates the total number of cells imaged. **(d)** Line plot depicting the probability of finding pigment along an average radius for the entire number of cells imaged. Spearman's rank value = 0.992. **(e)** Scatter plot depicting the radius of a hypothetical circle which encapsulates 95% of the pigment granules for each cell imaged. Statistical analysis was performed using a Mann-Whitney test.

3.3.7 Treating wildtype melanocytes with cytochalasin D induces partial melanosome clustering

The results from noc treating both wildtype and clustered melanocytes indicate that depleting microtubules does not dramatically influence melanosome distribution. It was therefore of interest to test what contribution the other major cytoskeleton protein - actin, makes towards maintaining peripherally dispersed melanosomes.

To test this, wildtype melanocytes were initially treated with the drug cytochalasin D (CytD), a well known and widely used agent for disrupting F-actin which binds to the barbed end of the actin filament, preventing the incorporation of further G-actin molecules (Cooper, 1987). As with the noc optimisation experiments, in order to reduce cytotoxic effects, the lowest dose required to deplete F-actin was optimised by treating cells with 10μM, 5μM, 1μM and 100nM CytD for 1 hour before fixing the cells and staining with texas-red phalloidin to visualise any remaining F-actin (Figure 3.11b-e). These concentrations and times were chosen, since they were similar to those used in previously published literature (Peng et al., 2011; Shoji et al., 2012). The results show that with the highest dose tested, the majority of the melanosomes were clustered around the perinuclear area, whilst the actin network had collapsed into a number of aggregates dispersed throughout the cytoplasm, compared with the DMSO treated cells where filamentous actin was still present (Figure 3.11a). Treatment with 10μM CytD for 1 hour also caused the cell membrane to partially collapse, which is similar to that previously reported by Schliwa, 1982 after treatment of BSC-1 cells with 3.6μM CytD for 45 minutes.

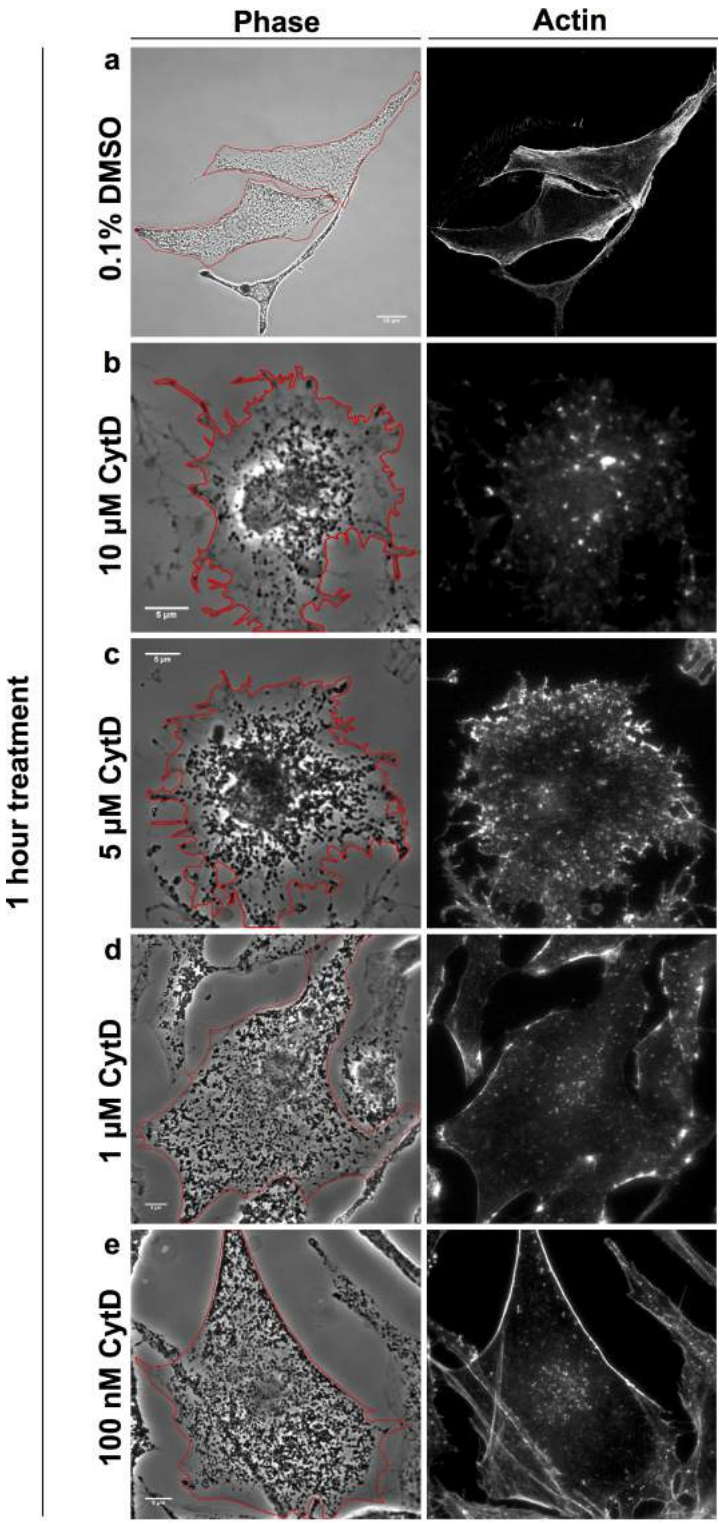


Figure 3.11 - Micromolar doses of cytochalasin D induce melanosomes to cluster. **(a)** Melan-a cells treated with 0.1% DMSO for 1 hour appeared wildtype, with the melanosomes dispersed throughout the cytoplasm and actin mainly concentrated under the plasma membrane. **(b)** Treatment with 10μM CytD for 1 hour caused the melanosomes to cluster at the cell centre, whilst the actin became concentrated into a number of foci that were distributed throughout the cytoplasm. **(c)** Treatment with 5μM CytD led to a similar phenotype as in (b), with melanosomes clustered around the perinuclear area. However, actin foci were smaller and mainly located close to the plasma membrane. **(d)** Treatment with 1μM CytD for 1 hour was not sufficient to induce melanosome clustering and the actin was filamentous, as in the vehicle control, rather than concentrated into foci. **(e)** The resulting phenotype after treatment with 100nM CytD for 1 hour was not distinguishable from that of the vehicle control. Red outline shows the location of the plasma membrane.

When the concentration of CytD was halved to 5μM (Figure 3.11c), the melanosomes still tended to cluster around the perinuclear area while the actin continued to appear to exist mainly in a number of foci. However, they were smaller compared with the 10μM CytD treatment, and mainly distributed towards the periphery of the cell, rather than throughout the cytoplasm. As previously reported, it does not appear that total actin content has been reduced significantly by 5μM CytD compared with the DMSO control (Kolega et al., 1991), and therefore CytD at concentrations below 10μM for 1 hour may simply be functioning to reorganise the actin, rather than deploymerise it.

When the CytD concentration was reduced to 1μM, melanosomes no longer accumulated around the perinuclear area but instead aggregated into small clumps in many cases (Figure 3.11d). The number of actin foci was reduced compared to treatment with higher doses of the drug, and F-actin was present below the plasma membrane, indicating this dose of CytD was not completely effective in depolymerising F-actin over the length of time it was applied. Reducing the dose of drug even further to 100nM (Figure 3.11e) did not have any noticeable effect on either the appearance of the actin cytoskeleton, the distribution of melanosomes, or the cell morphology, compared with the DMSO treatment.

To ensure that CytD was specifically depolymerising F-actin, cells were treated with either 5μM CytD or 0.1% DMSO for 1 hour, and subsequently the integrity of both actin and microtubules were investigated via immunofluorescence (Figure 3.12). As expected, actin filaments were no longer present after this treatment, compared with the DMSO control, whilst the microtubule network remained intact. The microtubule staining actually appeared stronger after CytD treatment, suggesting that microtubule formation may be promoted as a consequence of F-actin depolymerisation, perhaps in order for the cell to try and compensate for the loss of structural support the actin cytoskeleton provides, although this phenomenon has not been reported in the literature. However, since the cell membrane collapses to some degree as a result of CytD treatment, it is also possible that the staining intensity increases simply due to the microtubules being packed closer together.

In order to quantitatively determine the effect of CytD treatment on melanosome distribution, melan-a cells were seeded onto micropattern chips before treatment with either 5μM CytD or 0.1% DMSO for 1 hour (Figure 3.13a & b). Melanosomes on the constrained cells appear to aggregate into 'local clusters' after CytD treatment which tend to be predominantly distributed a short distance from the plasma membrane. This is evidenced in the line plot

(Figure 3.13c) which shows a peak in the probability of finding pigment 2μm closer to the perinuclear area compared with the DMSO treated cells. The peak in pigment probability is also more prominent for the CytD treated cells compared to the control cells, which is most likely due to the aggregated melanosomes. Comparing the pigment probability maps after treatment with either 5μM CytD or 0.1% DMSO for 1 hour (Figure 3.13a & b), it also appears that the melanosomes are more clustered after CytD treatment, an observation that is reflected in the scatter plot (Figure 3.13d). This suggests an important role for F-actin in maintaining peripherally dispersed melanosomes at steady-state.

When melan-a cells were constrained on micropattern chips and subsequently treated with 5μM CytD, it was also noticeable that the majority of the actin foci were located at the plasma membrane. When the distribution of actin in melan-a cells constrained on the micropattern chips was quantified (see section 2.4.3.6), it was found that the actin is on average significantly closer to the plasma membrane after CytD treatment (Figure 3.13e), compared to the DMSO control.

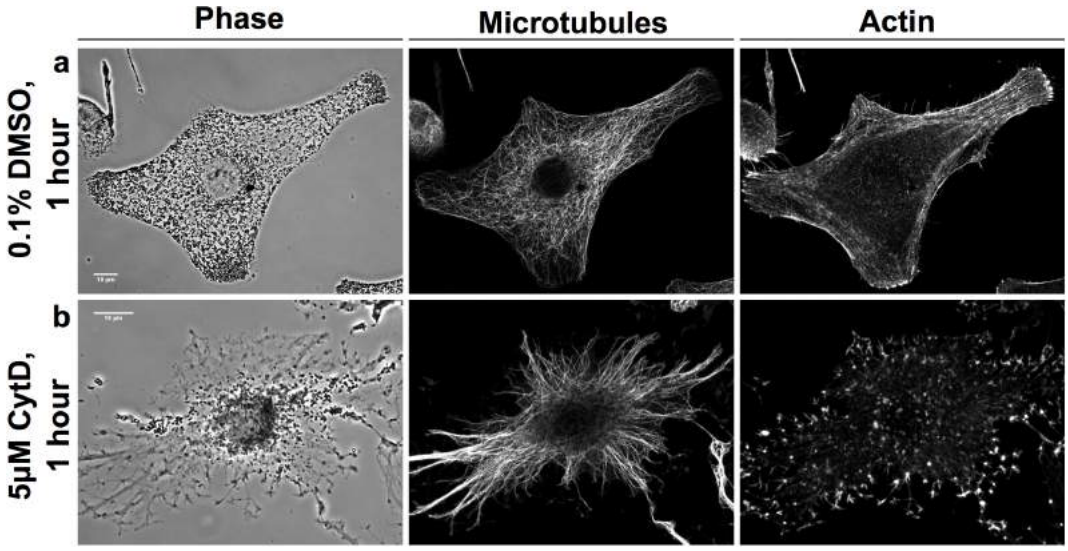


Figure 3.12 - Cytochalasin D specifically depolymerises F-actin. **(a)** Melan-a cells treated with 0.1% DMSO for 1 hour had a prominent microtubule network running throughout the cytoplasm, whilst F-actin was mainly concentrated under the plasma membrane. **(b)** After treatment with 5μM CytD for 1 hour F-actin was no longer present and instead a large number of actin foci were observed. The microtubule network was clearly still intact, demonstrating that CytD was specifically targeting F-actin.

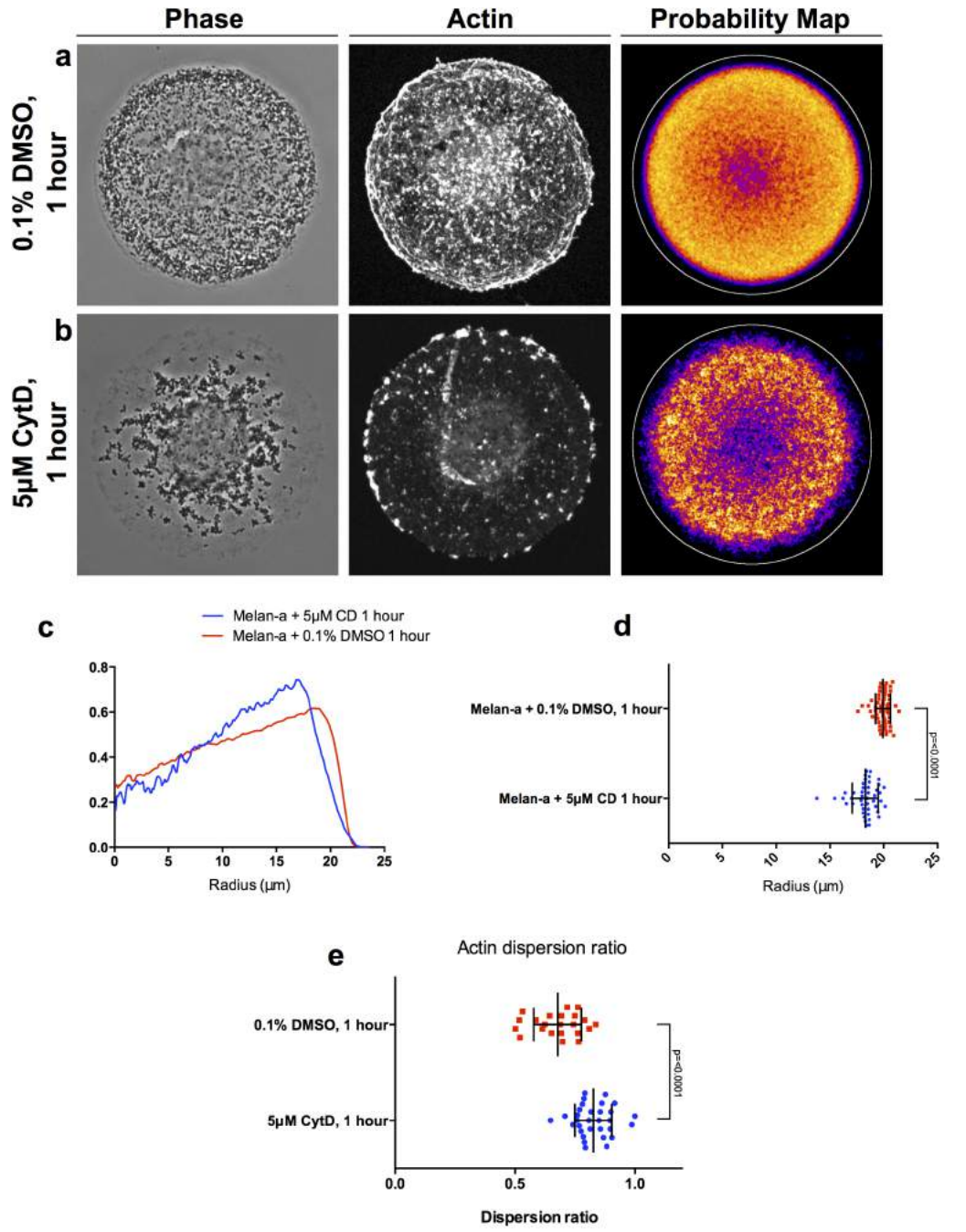


Figure 3.13 - Micropattern chip analysis reveals that CytD induces statistically significant melanosome clustering compared to the vehicle control. **(a)** Melan-a cells seeded onto micropattern chips and treated with 0.1% DMSO for 1 hour had well dispersed melanosomes and very prominent actin staining. **(b)** Melanosomes in cells treated with 5μM CytD were mostly found in small clusters, with the average pigment map showing that melanosomes are likely to be found in a ring between 10.3μm and 18.3μm from the cell centre. 5μM CytD treatment was sufficient to deplete actin filaments as only actin foci remained, which were concentrated almost exclusively at the plasma membrane. White circles drawn on the average pigment maps indicate the outline of the fibronectin pattern (diameter = 46μm). **(c)** The line plot of pigment probability against cell radius shows that following treatment with 0.1% DMSO, the highest probability of finding pigment is at 19.2μm radius, whilst following 5μM CytD treatment this is reduced to 17.3μm. Spearman's rank value = 0.869 **(d)** The scatter plot of the PDRs for each cell imaged indicates that CytD induces statistically significant clustering of the melanosomes. Mean PDR after DMSO treatment = 19.9μm (n=59) Vs. 18.3μm after CytD treatment (n=45); p=<0.0001 (Mann-Whitney significance test). **(e)** The actin dispersion ratio (see section 2.4.3.5 for methods) shows that the mean distance of actin from the cell centre increases following treatment with 5μM CytD from 0.68 (DMSO treatment; n = 22) to 0.84 (CytD treatment; n =33); p=<0.0001 (Mann-Whitney significance test).

3.3.8 Treating wildtype melanocytes with latrunculin A closely mimics the melan-dilute phenotype

Treating melan-a cells with 5μM CytD for 1 hour resulted in the partial perinuclear clustering of melanosomes, compared to control cells treated with 0.1% DMSO. Since previous data showed melanosomes do not move by diffusion (Figure 3.10), it is therefore likely that an active retrograde force is responsible for this clustering. In this case, it is reasonable to postulate that if melanocytes are incubated with CytD for longer periods of time, this force will continue to transport melanosomes towards the perinuclear area. However, when the length of time melanocytes were incubated with the drug was increased to attempt to more convincingly recapitulate the melan-dilute phenotype, this resulted in cell death (data not shown). Meanwhile, overnight incubations with 1μM-100nM CytD did not induce significant clustering (similar to Figure 3.11e). Since it is possible that cell death from CytD treatment is happening because of cytotoxic effects of the drug at these high concentrations, it was decided to test a more potent actin inhibitor, which would allow for lower doses to be used.

Latrunculin A (LatA) perturbs the actin cytoskeleton by sequestering actin monomers, rather than capping existing actin filaments, and has been shown to be much more potent than CytD, with LatA having a Kd of 0.2μM (Pring et al., 2002) whilst CytD has been estimated to have a Kd of between 2.6μM - 18μM, depending on the concentration of Ca^{2+} and Mg^{2+} ions present (Goddette and Frieden, 1985).

To test whether LatA caused a more substantial redistribution of melanosomes compared to CytD treatment, melan-a cells were initially treated with either 0.1% DMSO, 5μM, 1μM or 500nM LatA for 30 minutes (Figure 3.14a, b, c & d). As when high doses of CytD were applied for 1 hour (Figure 3.11), this caused melanosomes to cluster around the perinuclear area, but also caused the cell membrane to collapse, resulting in a dispersion ratio that was not significantly different from that of wildtype melanocytes treated with 0.1% DMSO for 30 minutes (Figure 3.14e). Melanocytes were not able to tolerate high (1-5μM) doses of LatA for longer than 30 minutes, since this concentration of LatA appeared to be cytotoxic, causing cells to detach from the cover glass.

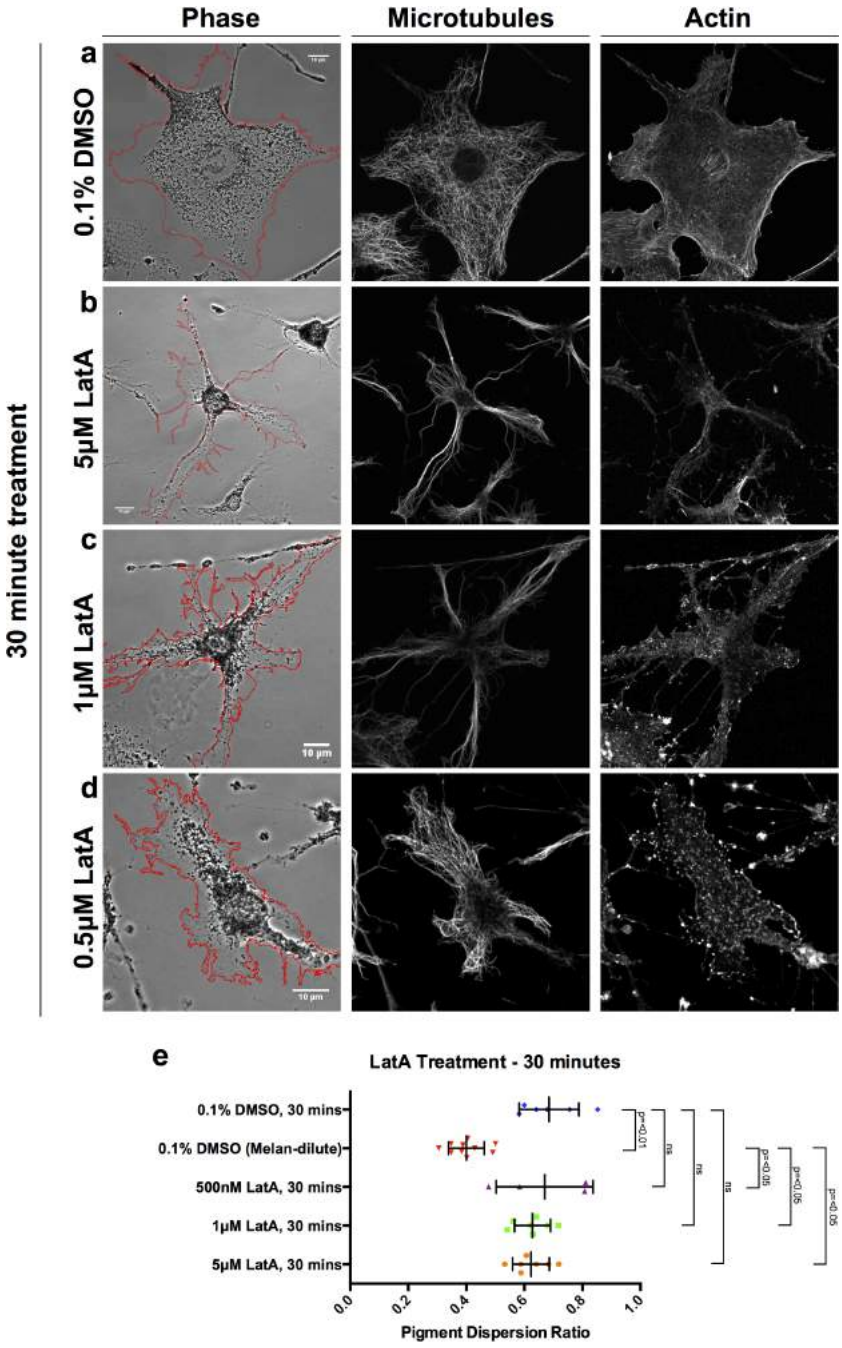


Figure 3.14 - High (5μM - 0.5μM) doses of LatA for 30 minutes cause melanosomes to cluster, but also disrupts cell morphology. (a) Melan-a cells treated with 0.1% DMSO for 30 minutes had dispersed melanosomes, normal morphology, and an intact actin cytoskeleton and microtubule network. After treatment with either 5μM LatA **(b)**, 1μM LatA **(c)** or 500nM LatA **(d)**, the melanosomes tended to aggregate at the cell centre, although these treatments also caused the cell membrane to collapse. Actin foci, which were distributed throughout the cytoplasm, were apparent after treatment with either 1μM or 500nM LatA, but not after treatment with 5μM LatA. **(e)** Quantification of the pigment dispersion ratio shows that none of the LatA treatments caused statistically significant melanosome clustering compared with the DMSO treated melan-a cells (Kruskal-Wallis ANOVA test). Red outlines indicate the location of the plasma membrane.

Therefore, cells were treated with much lower concentrations of LatA (between 10-50nM), which allowed cells to be incubated with the cytoskeleton inhibitor for at least 16 hours without causing cell death (Figure 3.15b-d).

Although these doses did not appear sufficient to deplete cells of the structural F-actin that

is required to convey mechanical support to the melanocytes (since actin staining was still prominent) the melanosome distribution was greatly affected. After treatment with 10nM LatA, the melanosomes appeared to form small clumps that were spread throughout the cytoplasm. Whilst the dispersion ratio was reduced compared to the melan-a cells treated with 0.1% DMSO, the result was not statistically significant (Figure 3.15e). However, when melanocytes were treated with 25nM LatA for 16 hours the result was dramatic clustering of the melanosomes around the perinuclear area and a reduction in the dispersion ratio that was highly significant when compared to the vehicle control treated melanocytes. The application of 50nM LatA caused a very similar effect, with the dispersion ratios of cells treated with either 25nM or 50nM LatA for 16 hours not significantly different. Moreover, the amount of F-actin remaining after treatment with either 10nM, 25nM or 50nM LatA for 16 hours appeared similar to that remaining after treatment with 0.1% DMSO (Figure 3.16; see section 2.4.3.4 for methods). In contrast to the prediction of the cooperative capture model, this suggests that melanocytes do not rely on the myosin-Va-melanophilin-Rab27a tripartite complex binding F-actin in order to maintain peripherally dispersed melanosomes, as the actin cytoskeleton appears largely unaffected by overnight treatments of 25-50nM LatA.

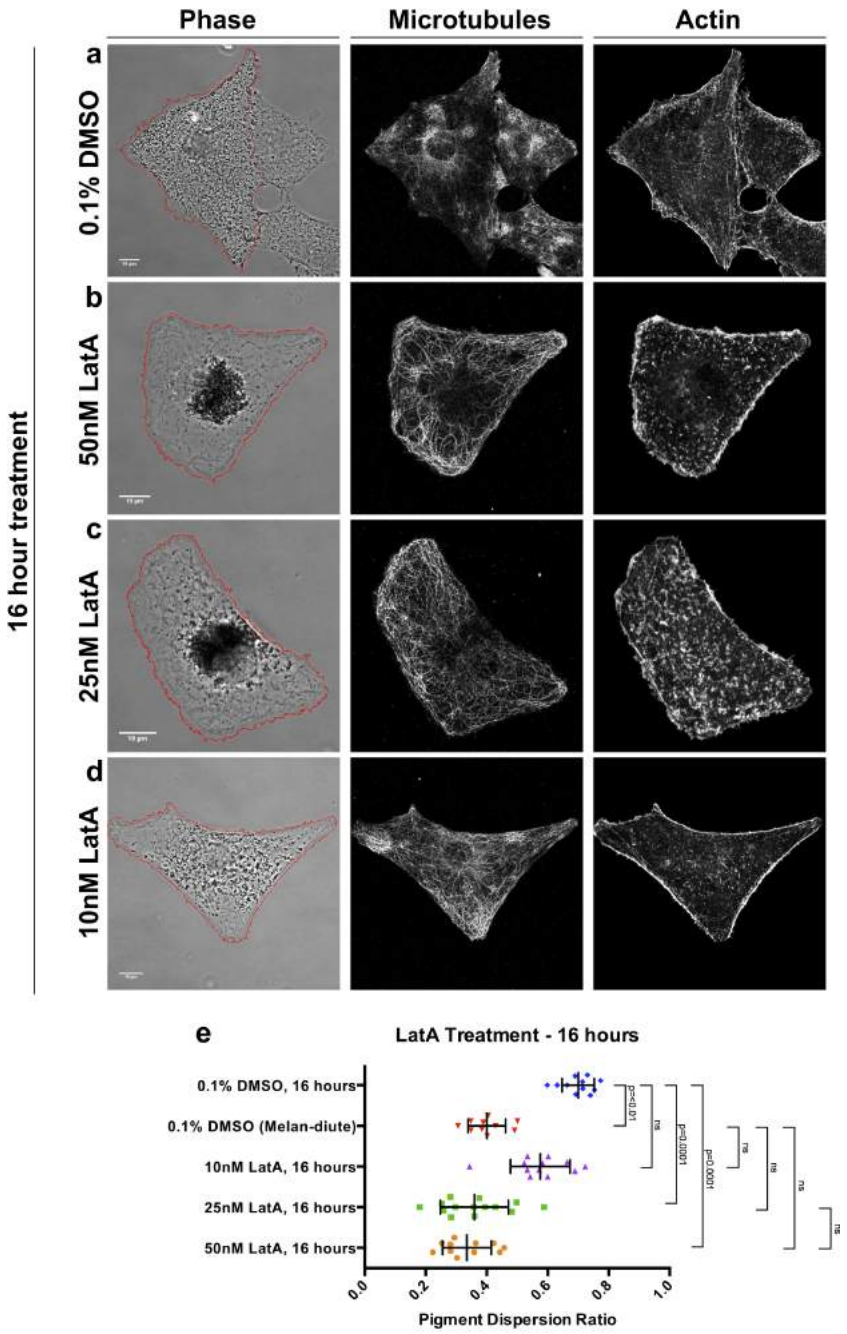


Figure 3.15 - Low (50nM - 25nM) doses of LatA for 16 hours induces perinuclear melanosome clustering without affecting cell morphology. (a) Melan-a cells treated with 0.1% DMSO for 16 hours had dispersed melanosomes, the cell morphology appeared normal, and the actin cytoskeleton and microtubule network were both intact. After treatment with either 50nM **(b)** or 25nM **(c)** LatA for 16 hours, the melanosomes were tightly clustered at the cell centre, whilst neither the morphology of the cell, nor the appearance of the actin cytoskeleton or microtubule network looked appreciably different from the vehicle control. **(d)** After treatment with 10nM LatA for 16 hours the melanosomes were much more dispersed compared with (b) or (c), although still more clustered compared to the vehicle control. **(e)** Statistical analysis of the pigment dispersion ratio (PDR) following LatA treatment showed that treatment with 10nM LatA Vs vehicle control was not statistically significant, whilst treatment with either 25nM or 50nM LatA Vs vehicle control was significantly different (p=<0.0001). The PDR of melan-a cells treated with either 25nM or 50nM LatA was not statistically different from vehicle treated melan-dilute cells, whilst the PDR of melan-a cells treated with 25nM LatA Vs melan-a cells treated with 50nM LatA was not significantly different either. Statistical analysis was performed using the Kruskal-Wallis ANOVA test. Red outlines indicate the location of the plasma membrane.

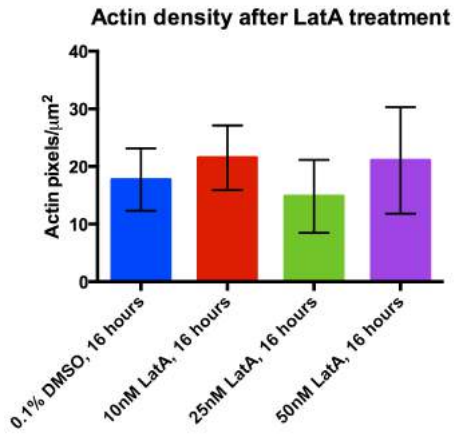


Figure 3.16 - Actin density in melan-a cells remains largely unaffected by 10nM-50nM LatA treatment for 16 hours. Actin density was calculated from immunofluorescence images as described in section 2.4.3.4. Neither treatment with 10nM LatA (n=12), 25nM LatA (n=15) or 50nM LatA (n=11) caused actin density to change significant compared with the 0.1% DMSO treatment (n=12) when analysed using a Kruskal-Wallis ANOVA test.

To more precisely quantify the effect of LatA on the distribution of melanosomes in wild-type melanocytes, cells were seeded onto micropattern chips and then incubated with 25nM LatA - the lowest dose that led to the redistribution of pigment around the perinuclear area in free growing melanocytes (Figure 3.17c), for 16 hours. As with the free growing cells, this treatment induced the clustering of melanosomes whilst the actin cytoskeleton clearly remained intact (Figure 3.17a & b). When the extent of the pigment clustering as a result of LatA treatment was analysed, the mean PDR was statistically different compared with the DMSO treated melan-a cells ($p=<0.0001$), but also significantly different also from the mean PDR of the melan-dilute cells ($p=<0.05$)(Figure 3.17c). When the line plot (Figure 3.17d) from the LatA treated melan-a cells was analysed using a Spearman correlation it was found that it closely mimicked the melan-dilute line plot, whilst it was negatively correlated with the line plot from the DMSO treated melan-a cells (see Figure 3.17 legend for values).

One possible explanation for the mean PDR and line plot of the LatA treated melan-a cells not being even more similar to that of the DMSO treated melan-dilute cells could be that for many of the cells imaged, the pigment did not cluster in the centre of the cell, but rather aggregated in a polarised fashion (Figure 3.18). However, when this hypothesis was tested by excluding the data from the asymmetrically clustered cells from the analysis, the results were almost identical (Figure 3.17c & d).

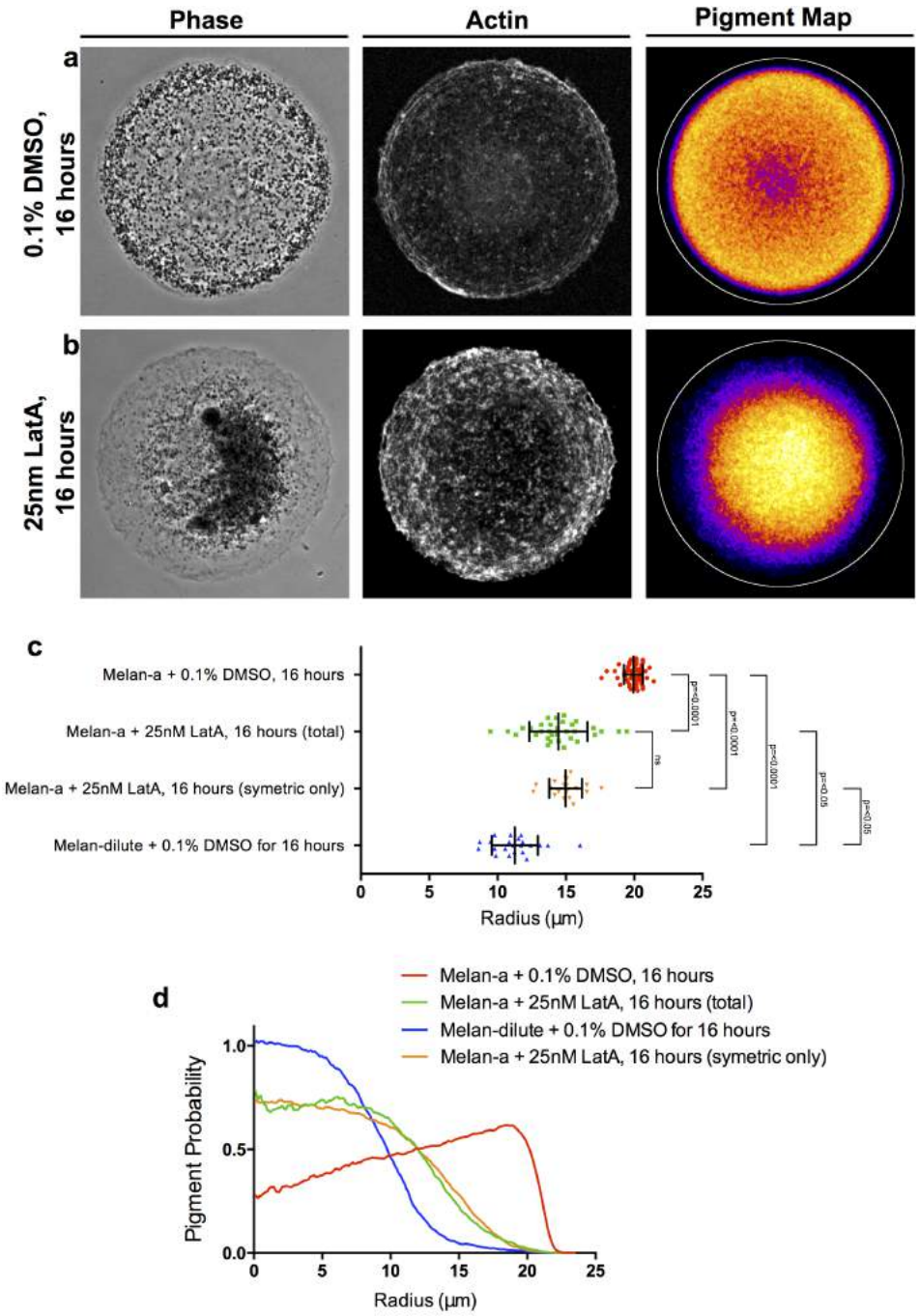


Figure 3.17 - Treating standardised melan-a cells with 25nM LatA for 16 hours results in a clustered phenotype. (a) Melan-a cells that were seeded onto micropattern chips to standardise cell size and shape and subsequently treated with 0.1% DMSO for 16 hours had well dispersed melanosomes, whilst the morphology of the actin cytoskeleton appeared normal. **(b)** Standardised melan-a cells treated with 25nM LatA for 16 hours had tightly clustered melanosomes around the perinuclear area, with the probability map indicating that the greatest chance of finding melanosome was at the cell centre. The morphology of the actin cytoskeleton appeared similar to that of the vehicle control cells. **(c)** The mean PDR of LatA treated melan-a cells (14.5μm, n=33) was statistically different (p=<0.0001) from that of the DMSO treated melan-a cells (mean PDR = 19.9μm, n=59). Removing asymmetrically clustered cells did little to change the mean PDR (15.0μm; n=19) which was not significantly different from the total population of LatA treated melan-a cells. The mean PDR of LatA treated melan-a cells was still significantly different (p=<0.05) from that of DMSO treated melan-dilute cells (mean PDR = 11.3μm; n=22). In each case a Kruskal-Wallis ANOVA test was used. **(d)** The line plot of pigment probability against radius for the total population of LatA treated melan-a cells correlated very well to that of th**e** DMSO treated melan-dilute cells (0.945 using Spearman's rank test). As expected, there was a negative correlation between LatA treated and DMSO treated melan-a cells (-0.329). Removing asymmetrically clustered cells (see Figure 3.18) did not affect the line plot.

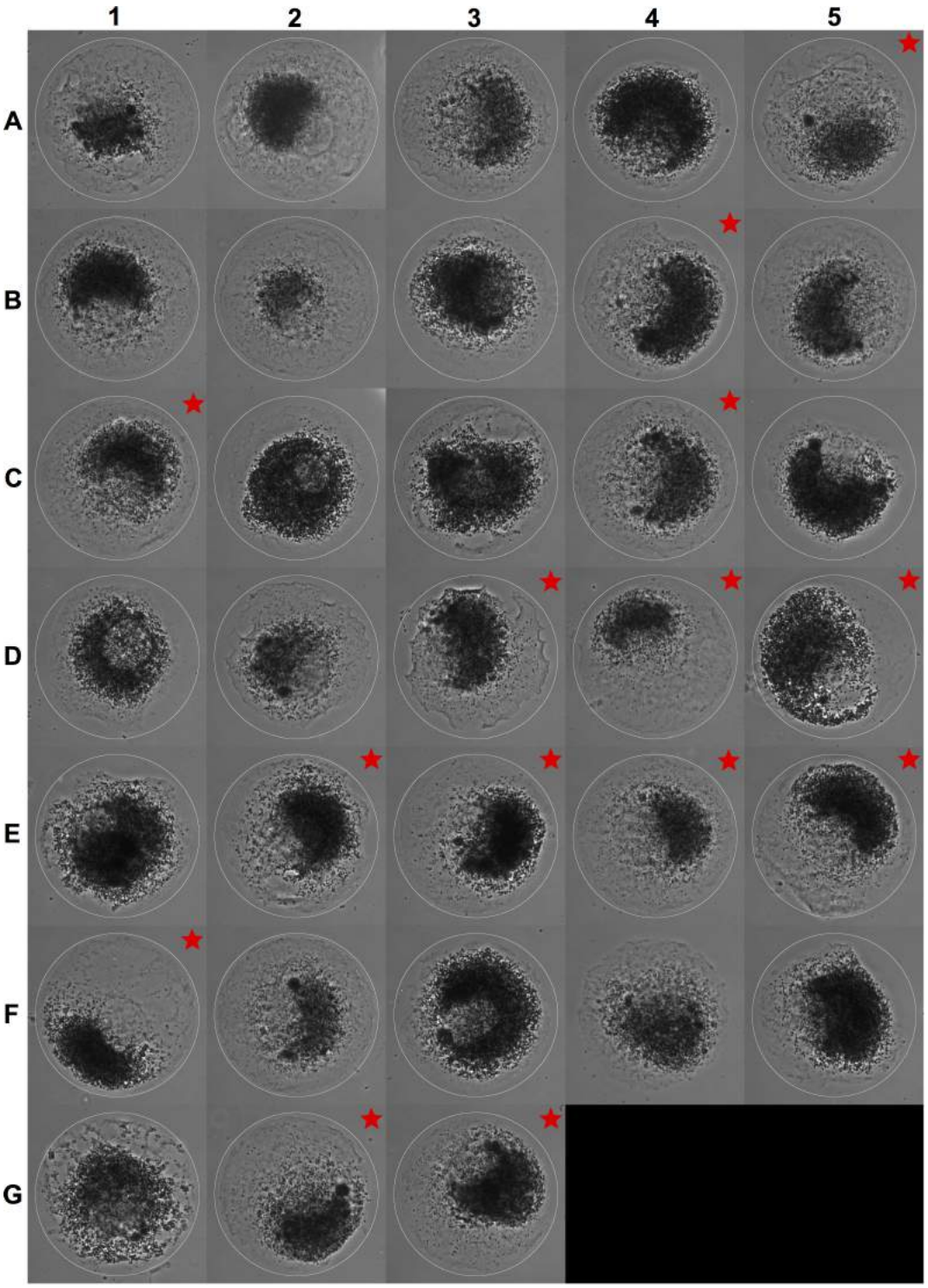


Figure 3.18 - A sub-population of standardised melan-a cells treated with LatA exhibit asymmetric clustering. Following treatment with 25nM LatA for 16 hours, a sub-population of melan-a cells, which had been seeded onto a micro-pattern chip to standardise cell size and shape appeared to have clustered asymmetrically. In this case the centroid of the pigment was not positioned at the cell centre, but rather near the plasma membrane. Such cells are highlighted with a red star at the top righthand corner of the image. White circles represent the outline the fibronectin pattern, the radius of which is 23μm.

3.3.9 A dynamic actin network is necessary to maintain peripherally dispersed melanosomes at steady state

Overnight treatment of melan-a cells with low doses of LatA was shown to be sufficient to cause melanosomes to tightly cluster around the perinuclear area, despite no significant change in F-actin morphology compared with DMSO treatment. These results indicate that F-actin's role in maintaining peripherally dispersed melanosomes is more complex than simply providing a structural scaffold to which myosin-Va can attach to tether pigment granules, since plenty of structural actin remains after 25nM LatA treatment.

To further test the possibility that F-actin plays a greater role in melanosome transport than simply fulfilling a structural role to allow myosin-Va to tether melanosomes, jasplakinolide (JK) was used as a tool to freeze actin dynamics (Holzinger, 2009). Importantly, JK has also been previously shown not to inhibit myosin-Va translocation along actin filament *in vitro* (Semenova et al., 2008). It is therefore a very useful drug to test the importance of actin dynamics on melanosome transport, since if actin is only important for facilitating the tethering of melanosomes at the plasma membrane, JK should not affect the distribution of pigment in wildtype melanocytes, as myosin-Va binding would remain unaffected.

Initially, as with the other drugs used in this study, a range of doses of JK were applied to wildtype melanocytes in order to optimise the dose and avoid cytotoxic effects. Similar to LatA, JK appeared to be very potent, and when micromolar doses (1-5μM) were applied to melan-a cells for 1 hour it caused cell death (data not shown). Even a 500nM dose applied for 4 hours caused the cells to round up and partially detach from the glass coverslip (Figure 3.19). Therefore, as with LatA, low nanomolar doses were tested for 16 hours (Figure 3.20) in order to minimise cytotoxic effects. 50nM JK was sufficient to cause melanosomes to tightly cluster at the cell centre (Figure 3.20b), although this dose caused the cells to partially collapse. Moreover, the actin appears to have been reorganised into an aggregate that is located around the perinuclear area, although since JK competes for the same binding site as phalloidin (Bubb et al., 1994), it is likely that fine actin structures cannot be visualized. Application of 25nM JK for 16 hours (Figure 3.20c) also induced melanosomes to cluster around the perinuclear area, and likewise the formation of actin aggregates, but partial collapse of the cell membrane was still observed. However, when the dose of JK was reduced even further to 10nM (Figure 3.20d) the actin no longer aggregated at the centre of the cell, but instead formed dramatic stress fibres which ran through the entire cytoplasm.

The bulk of the melanosomes were still tightly clustered at the cell centre, phenocopying the melan-dilute cells. Reducing the dose of JK 10-fold to 1nM (Figure 3.20e) both ablated the clustering effect and no longer induced the formation of actin stress fibres, indicating that this is a dose-dependent phenomenon.

In order to more precisely quantify melanosome clustering, melan-a cells were seeded onto micropattern chips and treated with either 0.1% DMSO or 10nM JK for 16 hours (Figure 3.21a & b). As with the free-growing cells, this induced the pigment granules to aggregate around the cell centre, although the constrained cells lacked F-actin stress fibers. The line plot (Figure 3.21c) mimics that of the melan-dilute profile very closely (see legend of Figure 3.21 for Spearman's rank correlation), indicating how closely the JK treated wild-type melanocytes phenocopy the myosin-Va null cells. Meanwhile the scatter plot (Figure 3.21d) shows the mean radius which encapsulates 95% of the pigment granules is 14.0μm for JK treated melan-a cells, which is not significantly different from the melan-dilute mean (11.3μm).

When the two pigment maps are compared in Figure 3.21, as well as the obvious difference in melanosome distribution it also appears there is less total pigment on average in the JK treated cells. This is also the case when comparing the average pigment maps of other cells that have undergone different drug treatments, such as in Figure 3.9 and 3.13. Conceptually it is hard to image how total melanosome content would be reduced by these treatments, since these cells do not shed melanosomes when cultured in isolation. Moreover, melanosomes have shown to be extremely stable, as discussed in section 3.4.5.

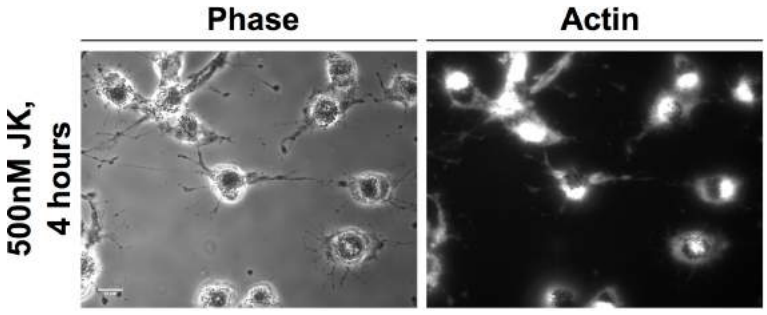


Figure 3.19 - High (500nM) doses of JK cause cell death after 4 hours. Melan-a cells incubated with 500nM JK rounded up and detached from the glass coverslip after 4 hours.

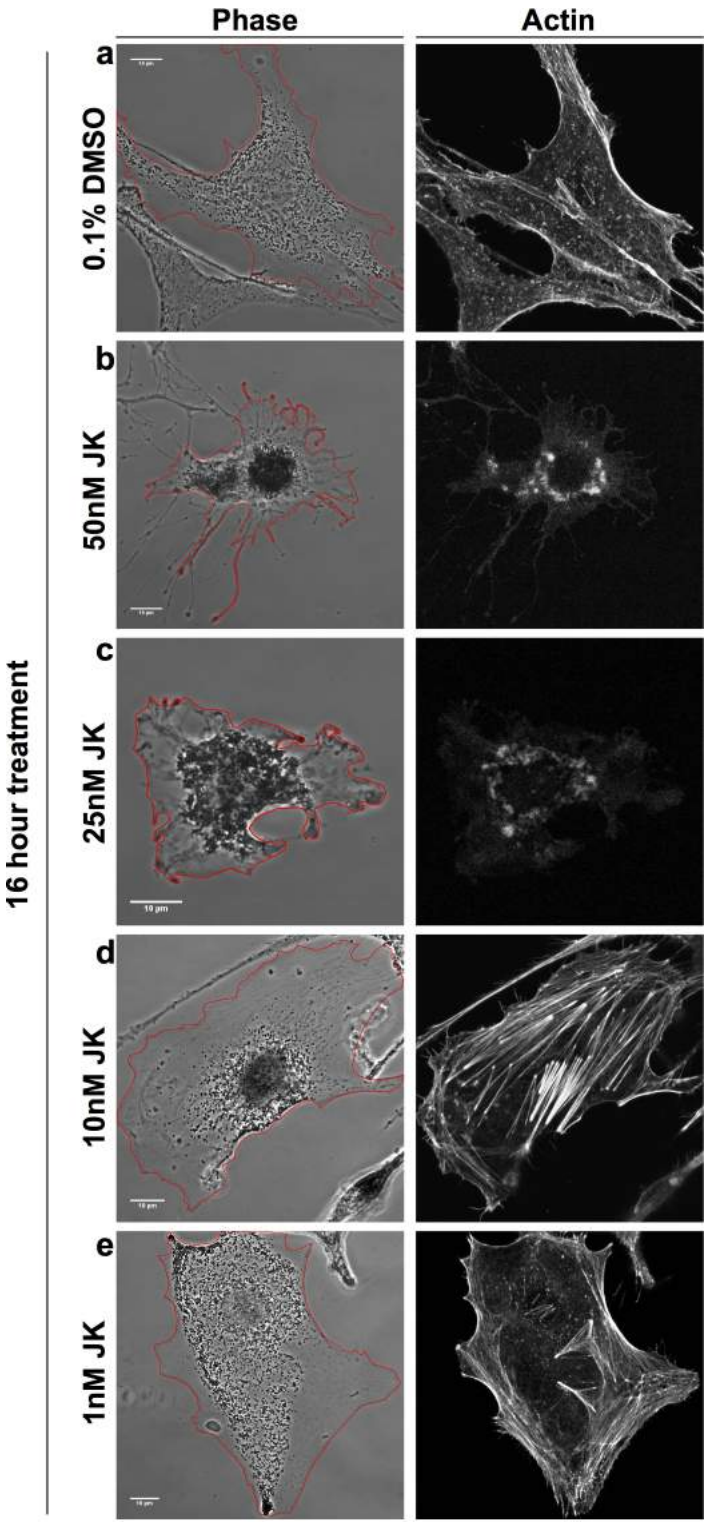


Figure 3.20 - Melan-a cells treated with low (10-50nM) doses of JK exhibit melanosomes that are aggregated around the perinuclear area. Melan-a cells were treated with either 0.1% DMSO for 16 hours as a control **(a)** or with 50nM **(b)**, 25nM **(c)**, 10nM **(d)** or 1nM **(e)** JK for 16 hours. Red outlines indicate the location of the plasma membrane.

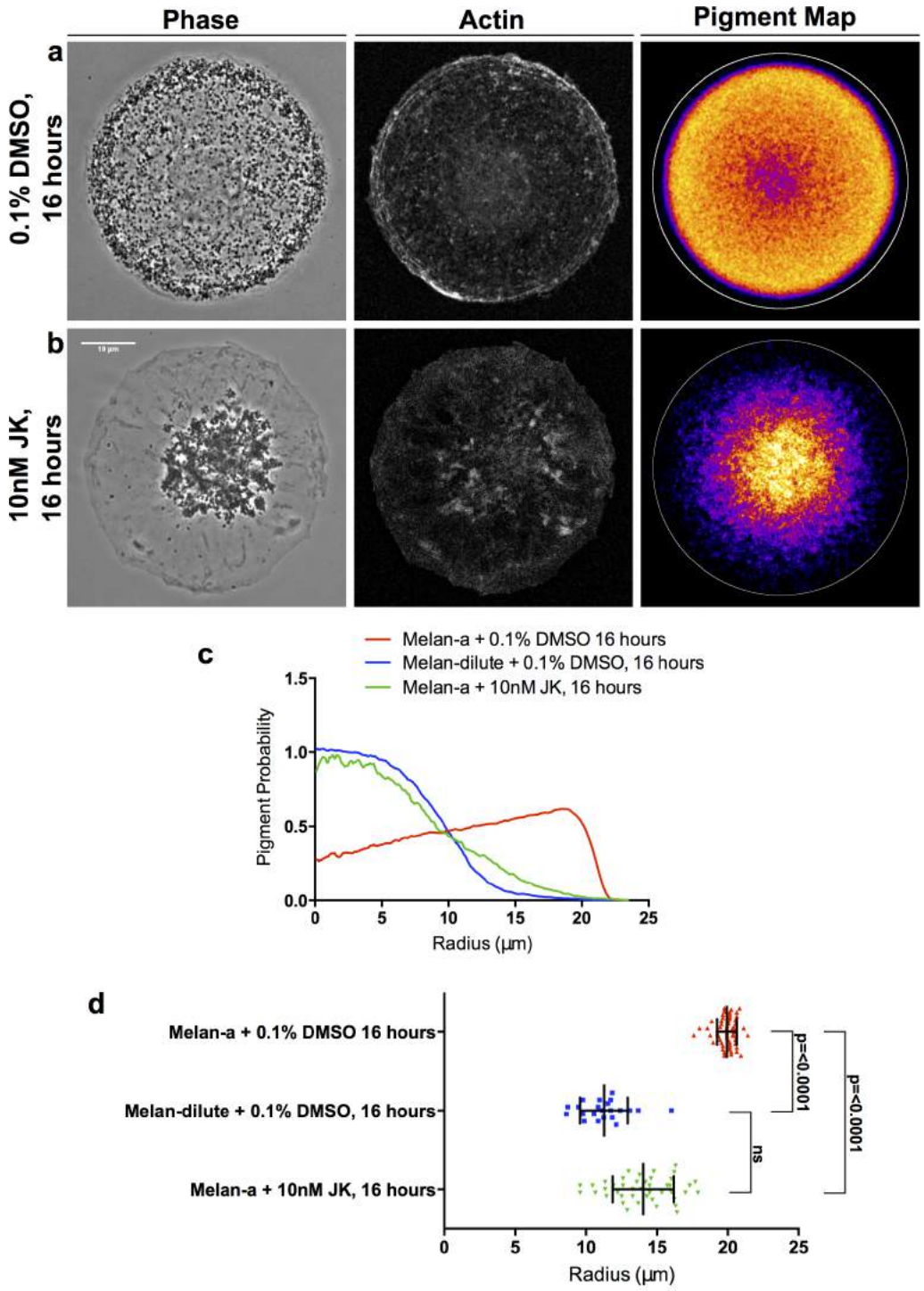


Figure 3.21 - Standardised wildtype melanocytes treated with 10nM JK for 16 hours phenocopy melan-dilute cells. (a) Melan-a cells which had been seeded onto micropattern coverslips to standardise their size and shape were treated with 0.1% DMSO for 16 hours as a vehicle control. **(b)** Standardised melan-a cells were treated with 10nM JK for 16 hours which caused the pigment granules to become redistributed around the perinuclear area, with the pigment map showing there is a very low probability of finding melanosomes outside this area. Phalloidin staining indicates the F-actin has been reorganised into a number of aggregates that are mainly found at the cell centre. **(c)** The line plot of pigment probability against cell radius shows that there is a very good correlation between the profile of melan-dilute cells and JK treated melan-a cells (0.996) whilst there is a negative correlation between vehicle control treated melan-a cells and JK treated melan-a cells (-0.325). Correlation analysis was performed using Spearman's rank test. **(d)** The mean PDR of vehicle treated melan-a cells = 19.9μm (n=59); vehicle treated melan-dilute = 11.3μm (n=22); JK treated melan-a cells = 14.0μm (n=43). There is no statistical difference between vehicle treated melan-dilute cells and JK treated melan-a cells using Kruskal-Wallis ANOVA test.

3.3.10 Nanomolar doses of JK and LatA are sufficient to perturb the actin cytoskeleton.

Since only very low concentrations of LatA were needed to have a large effect on the steady state distribution of pigment granules in wildtype melanocytes, it was important to determine if this drug was actually having an influence on the actin cytoskeleton. This was not possible using laser-scanning confocal microscopy, since the resolution limit (~200nm in xy and ~500nm in z) precludes the detection of single actin filaments (particularly in a dense cellular environment), which are 7nm in diameter (Cooper, 2000). Moreover, the low-throughput nature of confocal microscopy meant that determining whether the overall fluorescence intensity from phalloidin-staining was decreasing following LatA treatment was extremely difficult.

Therefore, flow-cytometry was used to determine whether 25nM LatA was sufficient to perturb F-actin, or if an off-target effect could explain why the melanosomes were clustering. Melan-a cells were treated with either 0.1% DMSO (negative control), 500nM LatA (positive control) or 25nM LatA for 60 minutes, fixed and subsequently stained with texas-red phalloidin and the fluorescence intensity of 10,000 cells measured (see section 2.4.1.6 for protocol used). Whilst the mean fluorescence intensity (MFI) of unstained cells treated with 0.1% DMSO is 19.9, the MFI of control cells stained with TR-phalloidin was 1848.6. As expected, after treatment with 500nM LatA the MFI dropped very dramatically to 567.3 - a decrease of 69%. However, it was found that when cells were treated with 25nM LatA the drop in MFI, whilst modest, was still quantifiable, since this value decreased to 1742.8 - a reduction of 6% compared to the control cells (Figure 3.22). The flow cytometry method therefore demonstrates that low nanomolar doses of LatA are indeed capable of depolymerising a small amount of F-actin which may be responsible for the observed melanosome clustering.

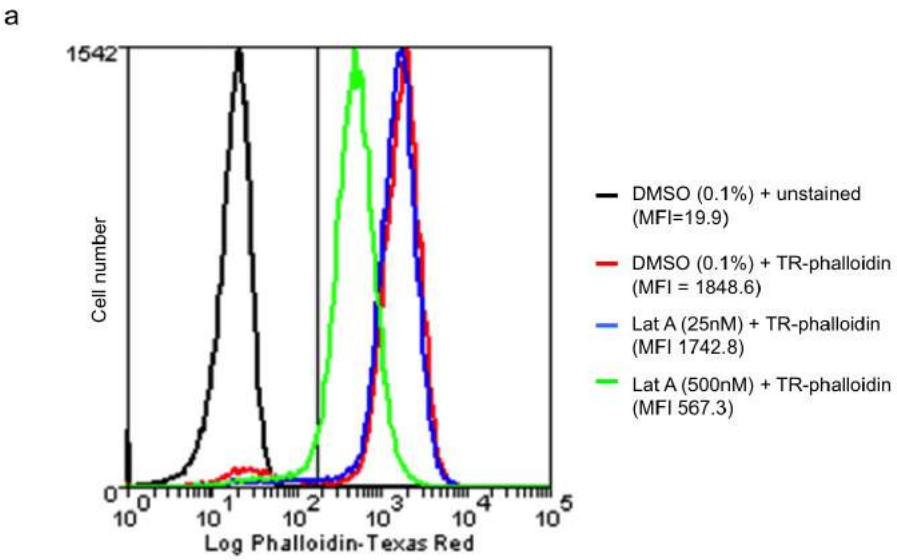


Figure 3.22 - FACS data reveals that 25nM LatA is sufficient to deplete cells of quantifiable amounts of F-actin. Melan-a cells were treated with either 0.1% DMSO, 25nM LatA or 500nM LatA for 1 hour and then stained with texas-red phalloidin or left unstained as a control (see section 2.4.1.6 for methods). 10, 000 cells were then analysed using a MoFlo fluorescence cytometer. Cells were treated with drug and stained by Alistair Hume, whilst FACS and subsequent data analysis was performed by David Onion.

As with LatA treatment, incubating cells with very low (10nM) doses of JK for 16 hours was found to be sufficient to induce melanosome clustering (Figure 3.20). To test if these low doses are sufficient to freeze actin dynamics melan-a cells were transfected with β-actin-GFP and 48 hours post transfection treated with either 0.1% DMSO or 10nM JK for 30 minutes. Actin dynamics were then investigated via fluorescence recovery after photobleaching (FRAP), as described in section 2.4.2.4. Three different types of actin were tested: cortical actin, stress fibres and the actin mesh, examples of which are shown in Figure 3.23a. The FRAP curves were then fitted using a non-linear one-phase association fit in order to calculate the percentage of actin that was in the immobile fraction (Table 3.2).

When the actin dynamics of melan-a cells that had been treated with 0.1% DMSO were investigated (Figure 3.23b.i & b.ii), recovery was initially very rapid for each of the 3 different actin types tested. After approximately 10 seconds the speed of recovery decreased sharply and increased much more gradually for the remaining 110 seconds. Mesh actin recovered the most, followed by stress fibres with membrane actin recovering the least. When melan-a cells were treated with 10nM JK for 30 minutes and the FRAP experiment repeated (Figure 3.23c.i), recovery was again initially very rapid for approximately 3 seconds, after which time it rapidly plateaued (likely due to the diffusion of free G-actin into the bleach area). It was found that actin recovery in JK treated cells was greatly attenuated compared with that

of the DMSO treated cells, with the amount of membrane, stress fibre and mesh actin in the immobile fraction increasing by 30.7%, 35.0% and 105.2%, respectively (summarised in Table 3.2).

Interestingly, when actin turnover in melan-leaden cells was quantified after treatment with 0.1% DMSO (Figure 3.23d.i) it appeared to be less dynamic compared with that of the wildtype melanocytes, with the amount of cortical, stress fibre and mesh actin in melan-leaden cells that was in the immobile fraction increasing by 9.4%, 6.5% and 57.7%, respectively, compared with the wildtype cells. Treating melan-leaden cells with 10nM JK for 30 minutes (Figure 3.23e.i) had much less of an effect on actin turnover compared with the wildtype cells, with the amount of cortical, stress fibre and mesh actin in the immobile fraction increasing by only 1.2%, 21.9% and 6.1%, respectively (summarised in Table 3.2). Whilst it is therefore clear that very low doses of JK, even when applied for short periods of time, can dramatically reduce actin dynamics in wildtype melanocytes, these results also suggest that melanophilin plays some role in regulating actin turnover dynamics.

Overall, this data indicates that very low nanomolar dose of JK are indeed sufficient to perturb actin dynamics, and that this rapid turnover is fundamental for maintaining peripherally dispersed melanosomes in wildtype mouse melanocytes.

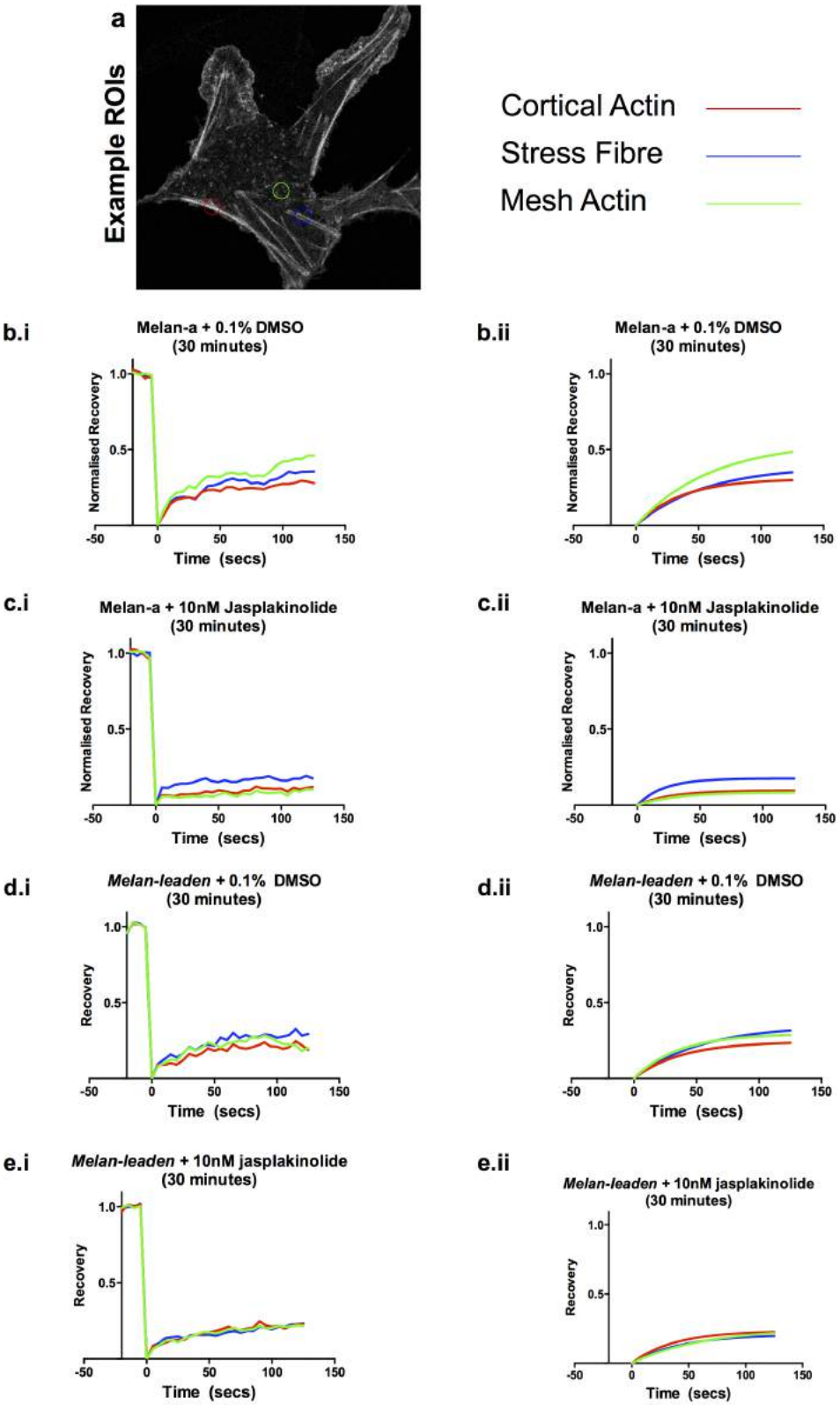


Figure 3.23 - 10nM JK for 30 minutes is sufficient to inhibit F-actin turnover. **(a)** Example bleach areas for cortical actin, stress fibres and meshwork actin. **(b.i)** Normalised FRAP curves for melan-a cells treated with 0.1% DMSO for 30 minutes. n=9. **(c.i)** Normalised FRAP curves for melan-a cells treated with 10nM JK for 30 minutes. Recovery for each type of actin structure has been greatly attenuated compared with b.i. n=10. **(d.i)** Normalised FRAP curves for melan-leaden cells treated with 0.1% DMSO for 30 minutes. n=8. **(e.i)** Normalised FRAP curves for melan-leaden cells treated with 10nM JK for 30 minutes. Recovery of actin was not as greatly affected by JK treatment for melan-leaden cells compared with melan-a cells. n=10. **b.ii**, **c.ii**, **d.ii** and **e.ii** show data in b.i, c.i, d.i and e.i, respectively, fitted with a one-phase association curve, allowing the percentage of actin making up the mobile/immobile fraction to be calculated.

Table 3.2 Percentage of membrane, stress fibre and mesh actin which makes up the immobile fraction in melan-a and melan-leaden cells after treatment with either 0.1% DMSO or 10nM JK for 30 minutes, calculated from the one-phase association fit data given in Figure 3.23b.ii, c.ii, d.ii & e.ii. The percentage of actin making up the mobile fraction is given in brackets.

	Melan-a 0.1% DMSO	**Melan-a 10nM JK**	**Melan-leaden 0.1% DMSO**	**Melan-leaden 10nM JK**
Membrane	69.21% (30.79%)	90.41% (9.59%)	75.71% (24.29%)	76.59% (23.41%)
Stress fibre	61.02% (38.98%)	82.38% (17.62%)	65.01% (34.99%)	79.27% (20.73%)
Mesh	44.64% (55.36%)	91.60% (8.40%)	70.41% (29.59%)	74.70% (25.30%)

3.4 Discussion

3.4.1 Kif5B could not be detected on the melanosome membrane

Initially, experiments designed to answer the question of whether Kif5B is required for anterograde melanosome transport focused on transfecting melanocytes with KIF5B-GFP in order to observe the sub-cellular localisation of this protein. In many cases the staining pattern was either diffuse, or appeared localised around the perinuclear area, similar to results published by Vancoillie et al. 2000b. However, in some cases (particularly when the KIF5B$\triangle$MD was transfected into melanocytes), the staining pattern appeared reminiscent of microtubules. This phenomenon has previously been reported in the literature, since early studies found that when the C-terminal portion of kinesin heavy chain was expressed in CV-1 cells, it co-localised specifically with microtubules (Navone et al., 1992). More recent studies also confirmed biochemically that the C-terminal region of kinesin can bind microtubules by incubating fragments of the motor's tail with microtubules and performing spin-down assays (Hackney and Stock, 2000). It is now understood that the binding between kinesin-tail and microtubules is largely electrostatic in nature, as when positively charged arginine residues in the tail (892-RKRYQQEVDRIKEAVRSKNMARR-914[1]) were mutated to alanine, the construct had a 25-fold lower affinity for microtubules (Seeger and Rice, 2010). Since the C-terminus of α/β-tubulin is known to have a strong negative charge due to a number of aspartic acid and glutamic acid residues (Redeker et al., 1992), it is believed that electrostatic interaction between aspartic and glutamic acid residues - the 'E-hook' region - and the arginine residues from the C-terminal portion of the kinesin heavy chain mediate the binding of these two proteins (Moua et al., 2011).

However, it should be stated that no experiments were performed to test whether the KIF5B-GFP construct was capable of cargo binding. In future work, at least two different experiments could be performed to check this. Firstly, it should be determined if Kif5B-GFP is localising to organelles that are known to be transported by this motor, such as lysosomes or mitochondria. Secondly, an informative experiment would be to express only the Kif5B tail as a GFP-tagged construct. This smaller protein fragment would still be capable of marking the melanosome membrane (if Kif5B does indeed localise to these organelles) but should be more abundantly expressed by melanocytes, making detection via immunofluorescence

[1] numbering from human KIF5B

methods easier. Kif5B tail also has the advantage that it lacks the microtubule motor domain, which may perturb the localisation to the melanosome membrane.

An RT-PCR screen to detect which of all the major kinesin isoforms are expressed in mouse melanocytes compared with a non-pigmented fibroblast cell line (NIH3T3) revealed that 3 isoforms, KIF13B, KIFC3.2 and KIFC3.3 isoforms were over-expressed specifically in melanocytes, as were KIF17.2 and KIF21B to a much lesser extent. However, expression of the housekeeping gene GAPDH, to which all KIF bands were normalised, was much more abundant in melanocytes compared with the NIH3T3. Why this should be is unclear, although it could be speculated that since GAPDH is involved in the glycolytic pathway which ultimately generates ATP for the cell, melanocytes may up-regulate this enzyme (and others involved with ATP synthesis), to provide energy for trafficking melanosomes - a process which does not occur in NIH3T3 cells. If this screen were to be repeated, it would therefore be wise to use another method of normalising band intensities, such as spiking the sample with a known quantity of control DNA. Moreover, it would also be useful to use a more quantitative method such as qRT-PCR.

Despite KIF5B expression appearing weaker in the melanocytes compared with a non-pigmented cell line after normalisation, it was still highly expressed compared to the expression level of most of the KIF genes tested. This result, along with the evidence in the literature that suggests Kif5B may be important for the anterograde transport of melanosomes in mammals (Hara et al., 2000; Vancoillie et al., 2000b) meant it was a strong candidate to investigate further. However, there are of course other possibilities for why KIF5B should be highly expressed in melanocytes. For example, it was observed that melanocytes contain a large number of mitochondria, which were often visible even using phase contrast microscopy. Since it is well documented that mitochondria are transported by Kif5B, this may also explain why KIF5B mRNA is highly expressed.

Melanocyte fractionation experiments were also carried out in order to understand if Kif5B was localised to melanosomes. These studies revealed that the majority of Kif5B was found in the supernatant after the cell lysate was centrifuged at 17,000g for 30 minutes (S17,000). In this case the supernatant would have contained mostly low-density vesicles that would not have pelleted at the relatively slow speeds used. Only a very small amount of Kif5B was detected in the pellet after the 17,000g spin, which corresponds to denser organelles such as melanosomes, whilst the amount of tyrosinase (a known melanosome

marker) detected was large. However, it should be stated that while tyrosinase is a good melanosome marker, it is not a membrane protein. Therefore, it may be possible that Kif5B is simply detaching from the melanosome membrane during sample preparation which would explain why it is most abundant in the S17,000 fraction. Therefore, for future experiments a better marker for melanosomes would be the membrane-bound GTPase Rab27a. Alternatively, as proposed above for the localisation of Kif5B via immunofluorescence methods, organelles known to be positive for Kif5B such as lysosomes or mitochondria could be purified in order to test whether Kif5B can still be detected on their membranes via western blotting.

Several other KIF genes that could also potentially play a role in melanosome transport (based on current reports in the literature) were also identified by this screen. For example, prominent bands corresponding to the three subunits of kinesin-2 (KIF3A/3B/3C) along with KIF16B, and KIFC3 were observed. As discussed in Chapter 1 and section 3.1, there is already evidence which implicates kinesin-2 in the transport of melanosomes in melanophores (Tuma et al., 1998; Gross et al., 2002), and therefore this motor may also play a role in melanosome transport in mammalian cells. When KIF3A-GFP and KIF3B-GFP were transiently transfected into melan-ash cells these constructs only weakly associated with the melanosomes (data not shown). It would therefore be of interest to repeat this experiment in a future study using the KAP3 (KIF3C) subunit as a readout of kinesin-2 localisation. This protein may more efficiently target melanosomes due to the fact it does not contain a microtubule binding domain like KIF3A or KIF3B which may be one reason these constructs were not found to colocalise with melanosomes. This approach of using the tail domain, rather than the full length motor, could also be extended to other kinesin isoforms. KIF16B, a member of the kinesin-3 family, also appeared to be highly expressed in melanocytes. Since this motor has previously been implicated in early endosome transport as discussed in section 3.1, it is possible it also has a role in melanosome trnasport, since these organelles are thought to arise from endosomes. Likewise, KIF5A mRNA (another member of the kinesin-1 family) was also detected in melanocytes, despite the fact it is only thought to be expressed in neurones (Kanai et al., 2000). It would therefore be interesting to to employ some of the approaches used in this chapter to understand more fully if these kinesin isoforms also have a role in melanosome transport.

It was also of interest that KIFC3, a minus-end direct motor, was found to be up-regulated

in melanocytes, since there is evidence to show melanosome do cluster (possible in a microtubule-dependent fashion) when treated with actin inhibitors. KIFC3 has previously been implicated in the minus-end directed transport of the Golgi (Xu et al., 2002) and peroxisomes (Dietrich et al., 2013). It is therefore plausible that this motor could act cooperatively with (or even instead of) dynein to traffic melanosomes towards the perinuclear area. However, the focus of this study is the anterograde transport of melanosomes. Therefore, whilst this motor may be important for melanosome trafficking, its role in this process should be investigated further in future work.

3.4.2 The melanosome distribution of melanocytes following Kif5B knockdown is identical to that of wildtype cells

In order to investigate the functional importance of Kif5B on the distribution of melanosomes in wildtype melan-a cells, the protein was knocked down by transfection with KIF5B siRNA oligonucleotides. 72 hours post transfection there was no apparent change in melanosome distribution, compared to non-targeting siRNA oligonucleotides.

To ensure the KIF5B siRNA was actually knocking down Kif5B, the experiment was repeated and mitochondria stained for. These organelles were clustered around the nucleus following KIF5B siRNA transfection whereas in control cells transfected with non-targeting siRNA they were dispersed throughout the cytoplasm - strongly suggesting that the KIF5B siRNA was effectively disrupting the translation of Kif5B. This was subsequently confirmed by performing a western blot on cells which had been treated with either KIF5B or non-targeting siRNA, which showed a ~95% reduction in the level of Kif5B in KIF5B siRNA treated cells compared with non-targeting siRNA. Overall therefore, taking the results from these experiments with those from the localisation studies, it appears that, contrary to the published data, Kif5B does not play any obvious role in the long-range anterograde transport of melanosomes, and that in its absence the phenotype of the melanocytes is identical to that of the wildtype cells.

3.4.3 Depolymersing F-actin in wildtype melanocytes with CytD induces melanosomes to partially cluster

Treating wildtype melanocytes at steady-state with 5-10μM CytD for 1 hour had the effect of reducing the pigment coverage index in both the free growing and standardised cells,

indicating that the actin cytoskeleton is very important for maintaining the dispersed phenotype. Following treatment with 5-10μM CytD, the remaining actin cytoskeleton no longer appears filamentous, but rather concentrated into a number of asters. The formation of these structures has been previously reported and is thought to be driven by CytD weakening the cytoskeleton, thus allowing myosin II to translocate F-actin (and in particular stress fibres) into these foci (Kolega et al., 1991; Verkhovsky et al., 1997). Furthermore, it has also been reported by Verkhovsky et al. that total actin content is not reduced by CytD treatment, and instead the drug functions only to reorganise the actin into aggregates.

One potential explanation for the observation that CytD treatment induces pigment granule clustering is that the myosin-Va-Mlph-Rab27a tripartite complex is necessary for tethering melanosomes to F-actin bundles, which are densest near the plasma membrane (Figure 3.12). Therefore either depolymerising F-actin or reorganising it into asters will result in loss of tethering at the plasma membrane and the melanosomes will consequently be transported towards the cell centre via minus-end directed molecular motors, as proposed by Wu et al.. If this model is correct, it would be expected that the pigment granules would colocalise with the actin asters in the majority of cases, since CytD should not perturb myosin-Va binding F-actin. However, in most cases, as highlighted in Figure 3.13, for example, large actin asters and clusters of melanosomes occupy distinct spatial areas, suggesting that pigment granule clustering is likely not due to an impairment of melanosome tethering to the cortical actin.

Another explanation for pigment granule clustering may be that the plasma membrane tends to collapse following treatment with 5-10μM CytD - a phenomenon also observed by Kolega et al.. However, when melanocytes were plated on micropattern chips the cells' morphology remained unchanged after treatment with CytD, potentially due to the extra support afforded by the fibronectin. Partial clustering of the pigment granules was still observed, thus ruling out the possibility that plasma membrane collapse is the only driver of melanosome aggregation.

Since neither the loss of myosin-Va tethering melanosomes to cortical actin, nor plasma membrane collapse due to CytD treatment are able to explain the resulting clustered phenotype observed this suggests myosin-Va and actin play a more complex role in melanosome trafficking than previously thought.

3.4.4 Intermediate filaments may play a role in the morphology of the microtubule network and actin cytoskeleton

When wildtype melanocytes were treated with noc it became apparent that this not only affected the microtubule network (as expected), but also resulted in the actin cytoskeleton changing morphology. For example, in Figure 3.9, the thick band of cortical actin is lost following noc treatment, and the actin cytoskeleton instead appears more punctate. Likewise, when melan-a cell were treated with F-actin inhibitors, such as CytD, the microtubule network usually changed morphology, with filaments often appearing to bundle together, possible to compensate for the lack of structural support from the actin cytoskeleton. Even myosin-Va null cells appeared to have a different actin cytoskeleton organisation compared to wildtype cells, with cortical actin often appearing thicker in melan-dilute cells.

There is evidence in the literature to suggest that intermediate filaments (IFs) may be responsible for this coordination between the microtubule network and the actin cytoskeleton. For example, it was observed by electron microscopy several decades ago that IFs form parallel arrays with microtubules in fibroblasts (Goldman, 1971), with vimentin IFs in particular localising to stable, detyrosinated microtubules (Gurland and Gundersen, 1995). Moreover, when cells were treated with colchine to disrupt microtubules, the morphology of the IFs was also disrupted, since they became aggregated and clustered around the perinuclear area. There is also evidence to suggest IFs localise to actin filaments. For example, actin and IFs have been co-purified from smooth muscle lystate (Hubbard and Lazarides, 1979), while double staining fibroblasts for both actin and IF showed there was significant overlap between these two filaments (Green et al., 1986). Furthermore, when cultured keratinocytes were treated with CytD, the resulting actin foci were also positive for IFs (Green et al., 1987).

Given this evidence it is therefore possible that interplay between the actin and microtubule networks following treatment with cytoskeleton inhibitors may be mediated through IFs. It has also been shown that in myosin-Va null axons, IFs have an altered distribution, potentially accounting for the difference in actin cytoskeleton morphology in melan-dilute cells compared with wildtype melanocytes (Rao et al., 2002). However, a thickening of the actin coretx was also apparent in cells treated with low does of actin inhibitors, such as LatA, which caused the melanosomes to cluster around the perinuclear area. In this case it could be speculated that melanosomes themselves convey structural support to the cell when they are dispersed, and therefore the the actin cytoskeleton must adapt when they cluster. IFs

were not investigated in this study, and it would therefore be of interest to investigate the role these filaments play in regulating melanosomes transport in future work.

3.4.5 Both sequestering G-actin or stabilising F-actin in wildtype melanocytes drives minus-end directed melanosome transport

Free-growing melanocytes treated with 0.5-5μM LatA for 30 minutes appeared to exhibit a similar phenotype to melan-a cells after 5-10μM CytD treatment, with melanosomes clustering at the cell centre. Similar to when high concentrations of CytD were applied to melanocytes, collapse of the plasma membrane also occurred after 0.5-5μM LatA treatment, most likely due to the loss of structural F-actin. This phenomenon was so prominent that despite the fact melanosomes tightly cluster at the cell centre following 0.5-5μM LatA treatment, the PDR was similar to that of wildtype DMSO treated melanocytes. These gross effects are likely due to the higher potency of LatA compared with CytD, since LatA has shown to more effectively depolymerise the actin cytoskeleton (Wakatsuki et al., 2001). A lack of any actin asters after treatment with either 1μM or 5μM LatA also suggests that F-actin is being more effectively depolymerised by this drug compared with CytD.

When free-growing wildtype melanocytes were treated with much lower doses of LatA (10nM - 50nM), both the cell morphology and the appearance of the actin cytoskeleton appeared very similar to that of the vehicle control, even when cells were treated for long periods of time (up to 16 hours). However, wildtype melanocytes treated with 25nM LatA for 16 hours were found to phenocopy the melan-dilute cells, since melanosomes were tightly clustered at the cell centre. This result firstly highlights the importance of actin *per se* in maintaining peripherally dispersed melanosomes and also provides further evidence that myosin-Va is unlikely to be involved in tethering melanosomes to cortical F-actin, since this was still abundant after 25nM LatA treatment (as demonstrated by immunofluorescence data). However, flow cytometry revealed that total F-actin content was very slightly depleted after LatA treatment, implying that some component of the actin cytoskeleton is indeed responsible for maintaining peripherally dispersed melanosomes at steady-state.

To further investigate the role of actin in maintaining peripherally dispersed melanosomes, melanocytes were treated with JK which is known to both stabilise F-actin through inhibiting its turnover, as well as induce the polymerisation of actin into amorphous aggregates (Bubb et al., 1994). As with LatA, high nanomolar doses for relatively short (4 hours) periods of

time caused extensive morphological changes to the melanocytes, whilst the cells tolerated very well low (10nM) doses for up to 16 hours. Doses higher than 10nM JK induced the formation of amorphous masses of actin which accumulated at the cell centre, similar to that reported by Bubb et al., 2000, whilst treatment with 10nM JK appeared to induce the formation of a number of stress fibres. Along with the changes to the actin cytoskeleton, low nanomolar doses of JK also induced the clustering of melanosomes at the cell centre, providing yet more evidence that the actin cytoskeleton plays a vital role in maintaining dispersed melanosomes, as well as further dispelling the hypothesis that myosin-Va is required to tether melanosomes to F-actin, since it has been show that JK does not affect binding of the motor to actin filaments (Semenova et al., 2008).

Standardising melanocyte size and shape through the use of micropatterns and repeating the LatA or JK treatments resulted in a similar clustering phenotype as observed with the free growing cells. However, following treatment with LatA, the melanosomes often clustered in an asymmetrical fashion, with the centroid of the cluster located near the plasma membrane, rather than at the cell centre. This phenomenon was not observed after free growing cells were treated with LatA or JK, and nor after standardised melanocytes were treated with JK. It is unclear why some cells exhibit asymmetric clustering, although since there is evidence to suggest that microtubules are implicated in retrograde melanosome transport, one possibility is that is caused by displacement of the MTOC. It has been previously shown that disrupting microtubules in mouse embryonic fibroblast cells by treatment with either noc or taxol resulted in the displacement of the MTOC from the cell centre in circular shaped cells (Hale et al., 2011). Whilst this study also revealed that latrunculin B had little effect on MTOC position, it is possible that LatA has a greater effect on the microtubule network which might account for the observed asymmetric clustering effect.

When the two pigment maps are compared in Figure 3.21, as well as the obvious difference in melanosome distribution it also appears there is less total pigment on average in the JK treated cells. This is also the case when comparing the average pigment maps of other cells that have undergone other other drug treatments, such as in Figure 3.9 and 3.13. Conceptually it is hard to image how total melanosome content would be reduced by these treatments, since these cells do not shed melanosomes when cultured in isolation. Moreover, melanosomes have been shown to be extremely stable, retaining their size, shape and ultrastructural features even after boiling in 6M HCl for 72 hours (Borovansky et al., 1977). It is

therefore unlikely that melanosomes are being degraded by these drug treatments. Rather, the apparent decrease in pigment is most probably due to an artifact stemming from the need to generate a binary mask in order to produce the average pigment maps (as described in section 2.4.3).

Overall, the results from JK treatment indicate that actin turnover is highly important for maintaining peripherally dispersed melanosomes. Moreover, data from experiments where cells were treated with LatA also confirm the importance of a dynamic actin cytoskeleton, since these low doses of drug selectively deploymerise only actin with relatively fast turnover kinetics. Therefore, it appears that melanosomes cluster when the actin cytoskeleton is perturbed not because myosin-Va is no longer capable of tethering the organelles to cortical actin, but rather due to the inhibition of the dynamic reorganisation of the actin cytoskeleton.

3.4.6 Standardising melanocytes does not affect melanosome distribution

Quantifying the melanosome distribution was initially performed by manually drawing around first the cell membrane and then the bulk pigment and taking a ratio of the two areas. However this method is both subjective and time consuming. Therefore to attempt to analyse melanosome distribution more quantitatively, cell size and shape was standardised by plating them on micropattern chips which allowed for the pigment to be quantified using an ImageJ plugin. This method was highly objective, reproducible, semi-high throughput and very quantitative, and allowed for subtle phenotypes to be detected. Whilst it is possible that constraining the cells in this manner could alter the distribution of melanosomes or cause transport defects, it was found that the distribution of pigment granules for wildtype and mutant (clustered) melanocytes were almost identical to that of the unconstrained cells. Furthermore, when the cytoskeleton was highlighted with phalloidin or anti-tubulin antibodies its morphology appeared normal. Moreover, melanocytes *in situ* are always highly constrained by the surrounding keratinoyctes. It must therefore be concluded that neither the melanocytes themselves, nor the melanosome distribution, is altered by the constraint imposed on them by the fibronectin patterns of the chips.

Summary

Overall, the results presented in this chapter indicate that a dynamic actin cytoskeleton is crucial for maintaining peripherally dispersed melanosomes at steady state. This is at odds with the accepted model of melanosome transport, exemplified by the cooperative capture model, which states that stable cortical actin is vital for maintaining dispersed melanosomes, as found in melan-a. Furthermore, these experiments also suggest that Kif5B does not localise to melanosomes, nor is it vital for maintaining the wildtype phenotype. This has been shown through siRNA mediated knockdown of the motor, as well as transfecting cells with dominant-negative mutants lacking a motor domain - neither of which altered the distribution of melanosomes in melan-a cells.

Finally, these experiments demonstrate that cells are viable when treated with either 1μM noc, 25nM LatA or 10nM JK for at least 16 hours. Treatment with noc did not affect the pigment granule distribution in either melan-a or melan-dilute, allowing the possibility to test the importance of microtubules in anterograde melanosome transport using add-back experiments.

Chapter 4

Myosin-Va and F-actin work in opposition to microtubule-based motors to drive long-range melanosome transport

4.1 Introduction

Results from the previous chapter are at odds with the cooperative capture model proposed by Wu et al., 1998. Firstly, the myosin-Va/melanophilin/Rab27a tripartite complex bound to F-actin does not appear to tether pigment granules. When melanocytes were incubated with JK, which stabilises actin filaments but does not interfere with myosin-Va's ability to act as a melanosome tether, pigment granules were found to cluster around the perinuclear area. Secondly, depleting these cells of microtubules did not alter the melanosome distribution, while Kif5B could not be detected associating with melanosomes, nor was any evidence found that it is functionally involved in maintaining peripherally dispersed pigment granules. Taken together, these results indicate that myosin-Va and F-actin play a much larger role in facilitating melanosome transport than previously thought.

Reports in the literature have provided evidence that myosin-Va may act as a transporter in a similar way to kinesin. For example, experiments using the axoplasm from squid axons demonstrated that organelle transport was actin-dependent since movement was inhibited by treatment with actin-binding proteins such as DNaseI and gelsolin (Kuznetsov et al., 1992). However, since this research was carried out *in vitro* the results may not be applicable to live cells.

While myosin-Va is mainly regarded as either a tether or short-range cargo transporter in mammalian cells, the *Saccharomyces cerevisiae* analogue, myo2, has well known roles in the trafficking of a number of organelles. For example, mutations in the myo2 gene cause defects in vesicle trafficking, resulting in cells which are unable to form buds along with an accumulation of vesicles in the cytoplasm (Johnston et al., 1991). Later experiments concluded that peroxisome trafficking was also regulated by the myo2p motor protein. Cells that were double labelled for actin and peroxisomes showed these two structures co-localised, while temperature-sensitive myo2p mutants caused peroxisome movement to cease at the non-permissive temperature (Hoepfner et al., 2001). Moreover, the integral peroxisomal membrane protein Inp2p was identified as the receptor for myo2p, since Inp2p knockout cells exhibited peroxisome transport defects (Fagarasanu et al., 2006). Golgi trafficking was also shown to be myo2p-dependent, with this motor required for trafficking the Golgi into the bud (Rossanese et al., 2001). More recently it has also been confirmed that mitochondria are transported via myo2p, with mutations in the cargo binding region of the motor blocking

the accumulation of these organelles in the bud (Förtsch et al., 2011).

While myo2p translocating on actin filaments in *Saccharomyces cerevisiae* has been well documented, these organisms appear to have simpler actin networks compared to mammalian cells which may explain how this phenomenon is possible. However, there is evidence to suggest that myosin-V is also capable of long-range microtubule-independent transport of vesicles in mammalian cells (Schuh, 2011). These experiments showed that the transport of myosin-Vb/Rab11/transferrin-positive vesicles was unaffected by treatment with noc which depolymerised the microtubule network, but was frozen completely by treatment with CytD which depolymerised the actin cytoskeleton. Moreover, experiments using *Xenopus* melanophores indicated that freezing actin-dynamics with JK treatment prevented the melanosomes from dispersing (Semenova et al., 2008), again suggesting that the actin cytoskeleton plays a more complex role in organelle transport than simply providing a substrate to which myosin-V can bind and tether cargo.

The results of the above experiments set a clear precedent for the important role myosin-V and the actin cytoskeleton may have in long-range organelle trafficking. The results of the previous chapter demonstrated that actin dynamics, rather than microtubules, are important for maintaining dispersed melanosomes at steady state in murine melanocytes. It was therefore of interest to understand the role myosin-Va and F-actin plays in the active transport of these organelles. This question was addressed through add-back experiments (where the MYOVA, MLPH or RAB27A gene was transfected into *dilute*, *leaden* or *ashen* melanocytes, respectively, to induce melanosome to disperse) in combination with the drug treatments detailed in the previous chapter.

4.2 Aims

From the experiments described in the previous chapter it is apparent that dynamic actin is crucial for maintaining peripherally dispersed melanosomes in wildtype melanocytes at steady state. Furthermore, it is was shown that depleting microtubules has no affect on the melanosome distribution, either in melan-a or melan-dilute cell lines. The major aim of this set of experiments is to therefore further test the cooperative capture model by investigating whether microtubules are required for long-range melanosome transport. A secondary aim is to understand the role of the microtubule network in regulating the retrograde transport of melanosomes in wildtype melanocytes.

4.3 Results

4.3.1 Anterograde melanosome transport is not inhibited by noc treatment in murine melanocytes

From the noc optimisation experiments described in the previous chapter it is clear that depleting cells of microtubules does not affect the melanosomal distribution. Furthermore, these experiments demonstrated that microtubules are not crucial for cell survival (at least for periods up to 16 hours). These findings therefore opened up the possibility to perform add-back assays to test the involvement of microtubules in long-range anterograde transport.

These experiments involve transiently transfecting mutant (clustered) melanocytes with adenovrius which will express the missing gene in order to drive redistribution of the pigment granules to resemble the wildtype phenotype. It is preferable to use adenovirus as an expression vector, since exogenous protein can be detected after much shorter time periods compared with plasmid transfections, limiting the amount of time cells must spend in the presence of noc (or other inhibitors). This therefore reduces any cytotoxic effects which they may elicit.

Melan-leaden cells have already been shown to survive for at least 16 hours in the absence of an intact microtubule network at steady state (Figure 3.7a.ii), and therefore these cells were initially used to test if melanosome transport could take place in the absence of these filaments. To this end, melan-leaden cells were treated with either 0.1% DMSO or 1μM noc for 1 hour and then infected with GFP-MLPH adenovirus (see section 2.2.4 for methods regarding how the adenovirus expression vector was generated). This pretreatment of 1μM noc, which has been shown to be sufficient to completely depolymerise the vast majority of the microtubules in the cell (Figure 3.7b), ensured that at no time should it be possible for microtubule-dependent transport to take place in the presence of a functional Rab27a-melanophilin-myosin-Va tripartite complex. Cells were allowed to express Mlph-GFP for 16 hours post infection, before they were fixed, stained for GFP (to detect weakly expressing Mlph-GFP) and α-tubulin and subsequently imaged (as described in sections 2.4.1.2, 2.4.1.3 and 2.4.1.4, respectively).

As expected from previous results, treating untransfected melan-leaden cells with either 0.1% DMSO or 1μM noc for 16 hours did not cause a change in pigment distribution (Figure 4.1a, b & e). However, surprisingly melanosomes in cells transfected with MLPH-GFP

were able to redisperse, regardless of whether the microtubule network was intact or not (Figure 4.1c, d & e). These findings are therefore in direct contrast with the cooperative capture model, since they suggest that microtubules may not be fundamental to the long-range anterograde transport of melanosomes.

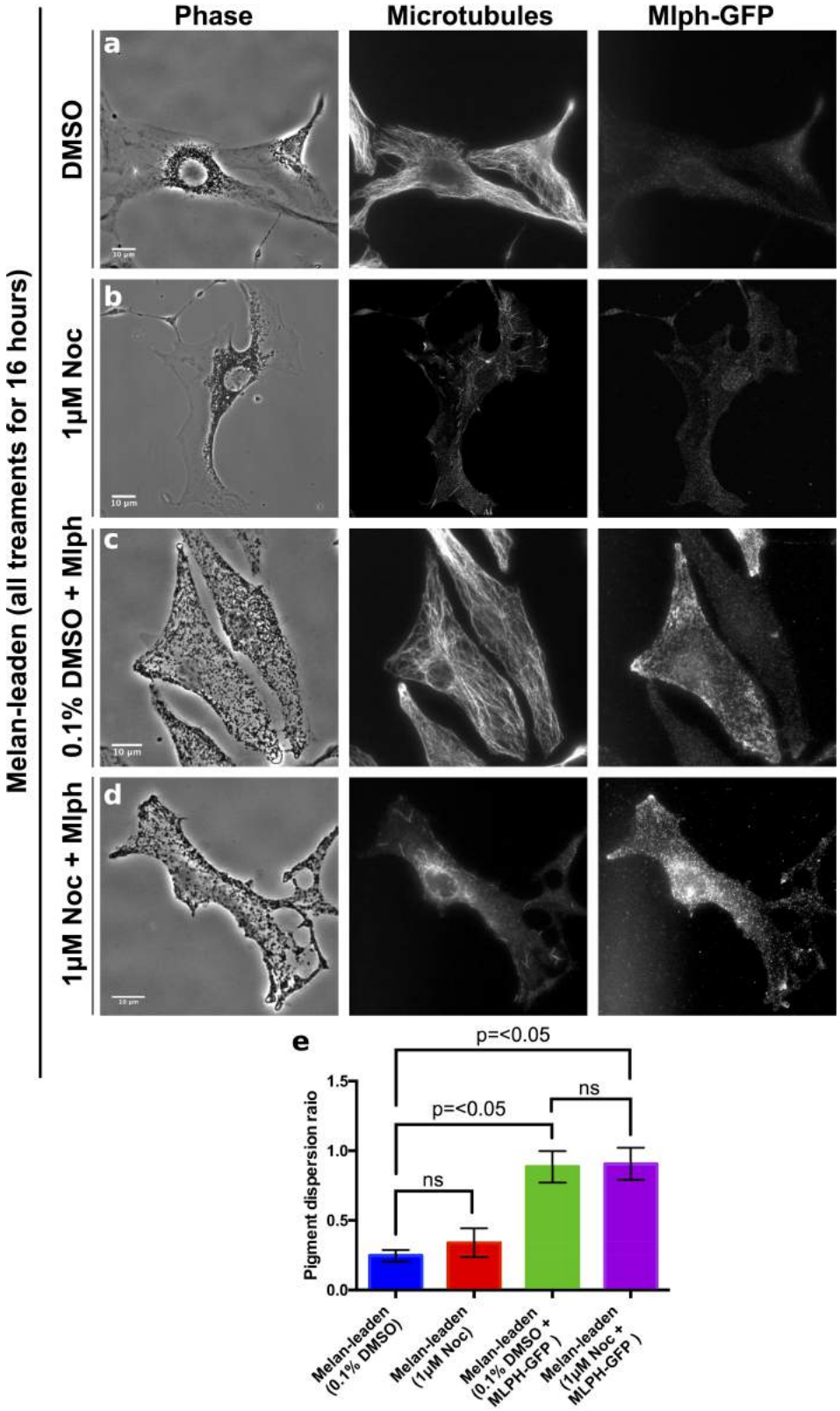


Figure 4.1 -Melan-leaden cells transfected with MLPH-GFP could be rescued after treatment with either DMSO or noc. Melan-leaden cells, pretreated with either 0.1% DMSO or 1μM noc, were transfected with MLPH-GFP using an adenoviral vector and allowed to express for 16 hours in the continued presence of either DMSO or noc. Melanosomes appear to be able to undergo long-range transport regardless of whether microtubules are intact or not. a, n=4; b, n=4; c, n=7; d, n=6. Statistical analysis was performed using a Kruskal-Wallis ANOVA test.

4.3.2 Treating *Xenopus laevis* melanophores with noc does not inhibit anterograde melanosome transport

There have been several reports in the literature since the early 1990s that implicate kinesin-II, translocating along microtubules, as the driver of long-range melanosome transport in *Xenopus laevis* melanophores. It was therefore of interest to understand if melanosomes in these cells were also able to undergo long-range anterograde transport subsequent to noc treatment. This is made simpler by the fact these cells offer an advantage over murine melanocytes, since the distribution of their melanosomes can easily be manipulated by the application of either melatonin (induces clustering) or αMSH (induces dispersion).

Xenopus laevis melanophores were cultured as described in section 2.1.3 and approximately 2x10^4 cells seeded onto 20mm glass coverslips placed into 4-well plates (using the same method described for mammalian cells in section 2.1.1). Cells were left overnight to spread and then subjected to the treatments outlined in Figure 4.2 before being fixed and stained for microtubules and F-actin.

Following treatment with 0.1% DMSO for 1 hour, the melanosomes appeared to have a dispersed distribution, as expected, with a mean pigment ratio of 0.78 (Figure 4.2a & e). Microtubules were clearly intact and radiated out from the MTOC to the plasma membrane, while the actin cytoskeleton appeared to be concentrated at the cortex. When 10nM melatonin was applied for 1 hour melanosomes became tightly clustered around the perinuclear area, reducing the mean pigment ratio to 0.15 (Figure 4.2b & e). Although microtubule staining appears comparable to the DMSO treated cells, the actin staining seems more intense, particularly just underneath the plasma membrane. It is therefore possible that the melanosomes afford the cells structural support when they are dispersed, and this must be compensated for when they cluster by increasing the thickness of the cortical actin band.

Next, melanophores were initially subjected to 10nM melatonin for 1 hour in order to cluster the pigment granules. After this time, DMSO was added to a final concentration of 0.1%, in the continued presence of 10nM melatonin, for a further 1 hour. Finally, melatonin was replaced with 100nM αMSH and the cells incubated for a further 60 minutes (in the continued presence of 0.1% DMSO) in order to induce the dispersion of the pigment granules (Figure 4.2c). This experiment was then repeated, with the exception that 1μM noc was used instead of 0.1% DMSO in order to depolymerise the melanophores' microtubule network (Figure 4.2d). Remarkably the results show that the final pigment ratio is not significantly

different regardless of whether the melanosomes redispersed in the presence of 0.1% DMSO or 1μM noc (Figure 4.2e).

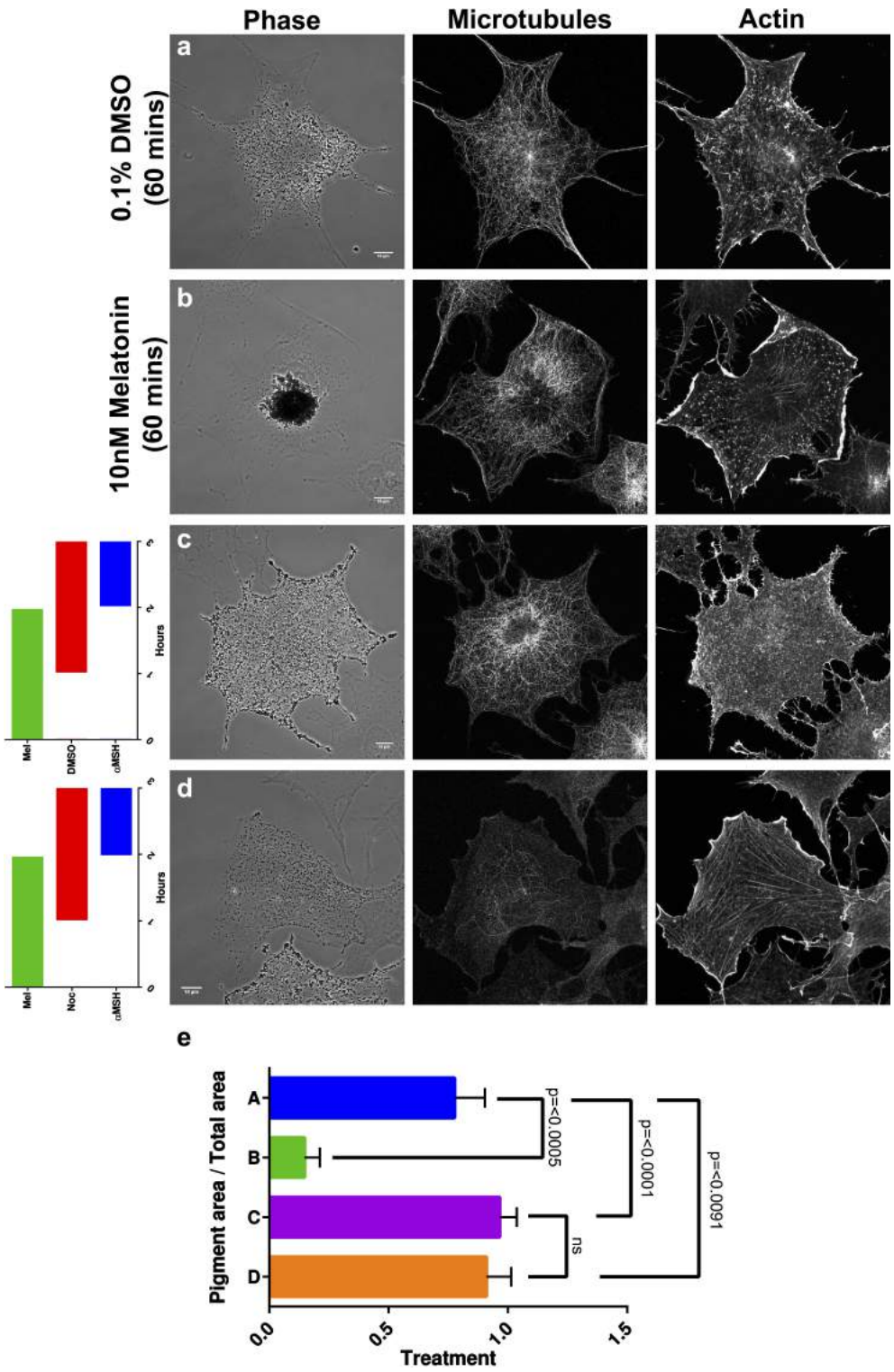


Figure 4.2 - ***Xenopus laevis*** **melanophores can disperse their melanosomes in the absence of microtubules.** **(a)** Melanosomes within wildtype melanophores treated with 0.1% DMSO for 60 minutes were evenly dispersed throughout the cell. **(b)** After treatment with 10nM melatonin (Mel) for 60 minutes, the pigment granules redistributed to form a tight cluster at the cell centre. **(c)** Melanosomes were initially clustered with 10nM melatonin for 60 minutes and then treated with 0.1% DMSO for a further 60 minutes. Melatonin was then replaced with 100nM αMSH, which caused the melanosomes to become peripherally dispersed after 60 minutes. **(d)** Melanosomes were again clustered by treating the melanophores with 10nM melatonin. The microtubule network was then disrupted by incubating the cells with 1μM noc for 60 minutes. After this time the melatonin was replaced with 100nM αMSH and the cells incubated for a further 60 minutes in the continued presence of noc. **(e)** Quantification of the melanosome distribution after each treatment. For a, n=10; b, n=8; c, n=11 and d, n=12. Pair-wise comparisons between a & b, a & c, a & d and c & d were performed using a Mann-Whitney significance test.

4.3.3 Optimising the rescue assay using micropattern chips

Following on from the experiments described in sections 4.3.1 and 4.3.2, it was important to more precisely quantify the rescue process in the presence and absence of microtubules in order to understand if depolymerising microtubules has any quantifiable impact on the resulting melanosome distribution. To do this, melan-dilute cells were plated onto micropattern chips, allowed to spread for 5 hours, and then pretreated with either 0.1% DMSO or 1μM noc for 1 hour. Cells were then infected with GFP-myosin-Va adenovirus and allowed to express the construct for 16 hours before being fixed and stained with anti-GFP and anti-α-tubulin antibodies to detect exogenous GFP-myosin-Va and endogenous microtubules, respectively.

Despite antibody staining, signal from GFP-myosin-Va was found to be very weak (Figure 4.3a). When the PDR for the total population of cells imaged was plotted (Figure 4.3c), the points were spread across a large range from 10.2μm to 21.3μm. The simplest explanation for this is that some cells were not being transfected and therefore skewing the data. To test this, control cells were setup in parallel that were not infected and stained only with secondary antibody. The mean fluorescence intensity of the control cells was then calculated. Any cell from the population infected with GFP-myosin-Va adenovirus was said to be truly expressing only if it had an intensity of greater than 2SD units compared to the control value (see section 2.4.3.2). However, any such attempt to excluded non-expressing cells based upon their fluorescence intensity resulted in little difference in mean PDR compared to the total population (an increase from 15.3μm to 16.2μm was observed, meaning that statistically there was no significant difference between the total and expressing populations (Figure 4.3c)). Meanwhile, the line profile between the total population and non-expressing excluded population appeared very similar, exemplified by the high Spearman's rank value of 0.901 (Figure 4.3d). Furthermore the average pigment maps for the two populations were very similar (Figure 4.3b.i and b.ii), again suggesting a more robust method of removing non-expressing cells was required. The total population of cells imaged is given as a montage in Figure 4.4 to demonstrate the difficulties identifying expressing (and therefore rescued) cells based upon their fluorescent intensity.

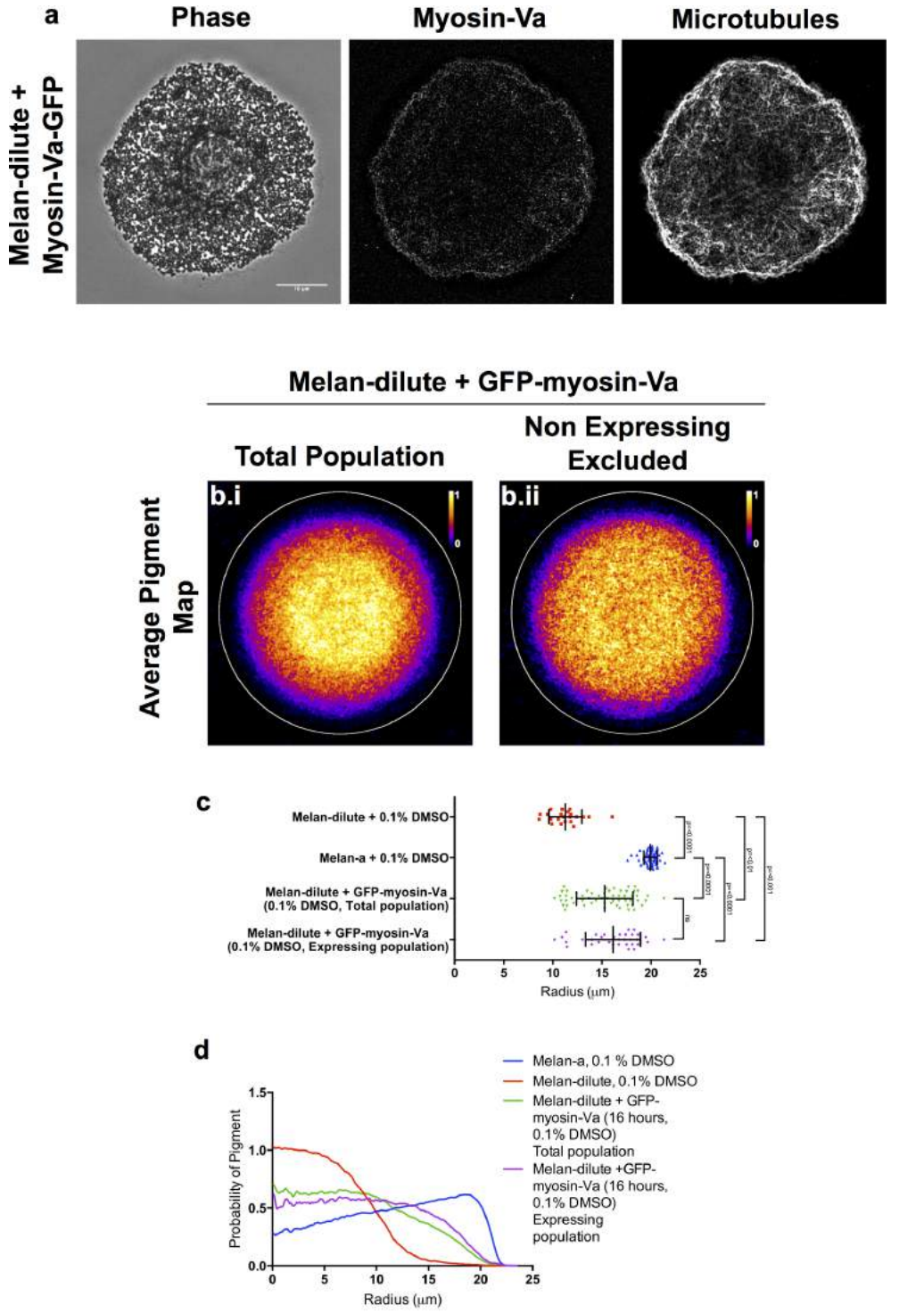


Figure 4.3 - The fluorescence intensity of antibody stained cells is not a reliable indicator of whether they have been transfected with myosin-Va-GFP. (a) Melan-dilute cells transfected with myosin-Va-GFP had dispersed melanosomes, although the fluorescent signal was very weak, despite antibody staining with anti-GFP. Based on fluorescence intensity alone it was not possible to distinguish between transfected (rescued) cells and control cells (untransfected melan-dilute cells stained with secondary antibody only). **(b.i)** The average pigment map from the total population of cells imaged showed a hybrid phenotype between melan-a and melan-dilute (see Figure 116). **(b.ii)** When non-expressing cells were removed by only including cells whose fluorescence intensity was at least 2SD units greater than the average intensity of the control cells the average pigment map still appeared similar to that of the total population. **(c)** Scatter plot depicting the radius of a hypothetical circle which encapsulates 95% of the pigment granules for each cell imaged. The average pigment radius of the non-expressing excluded population (n=58) changed little compared with that of the total population (n=34). Statistical analysis was performed using a Kruskal-Wallis ANOVA test. **(d)** Line plot depicting the probability of finding pigment along an average radius for the entire number of cells imaged. As with the scatter plot, the line profile of both the total population and non-expressing excluded population were very similar. Spearman's rank correlation was calculated as 0.901 for these two populations.

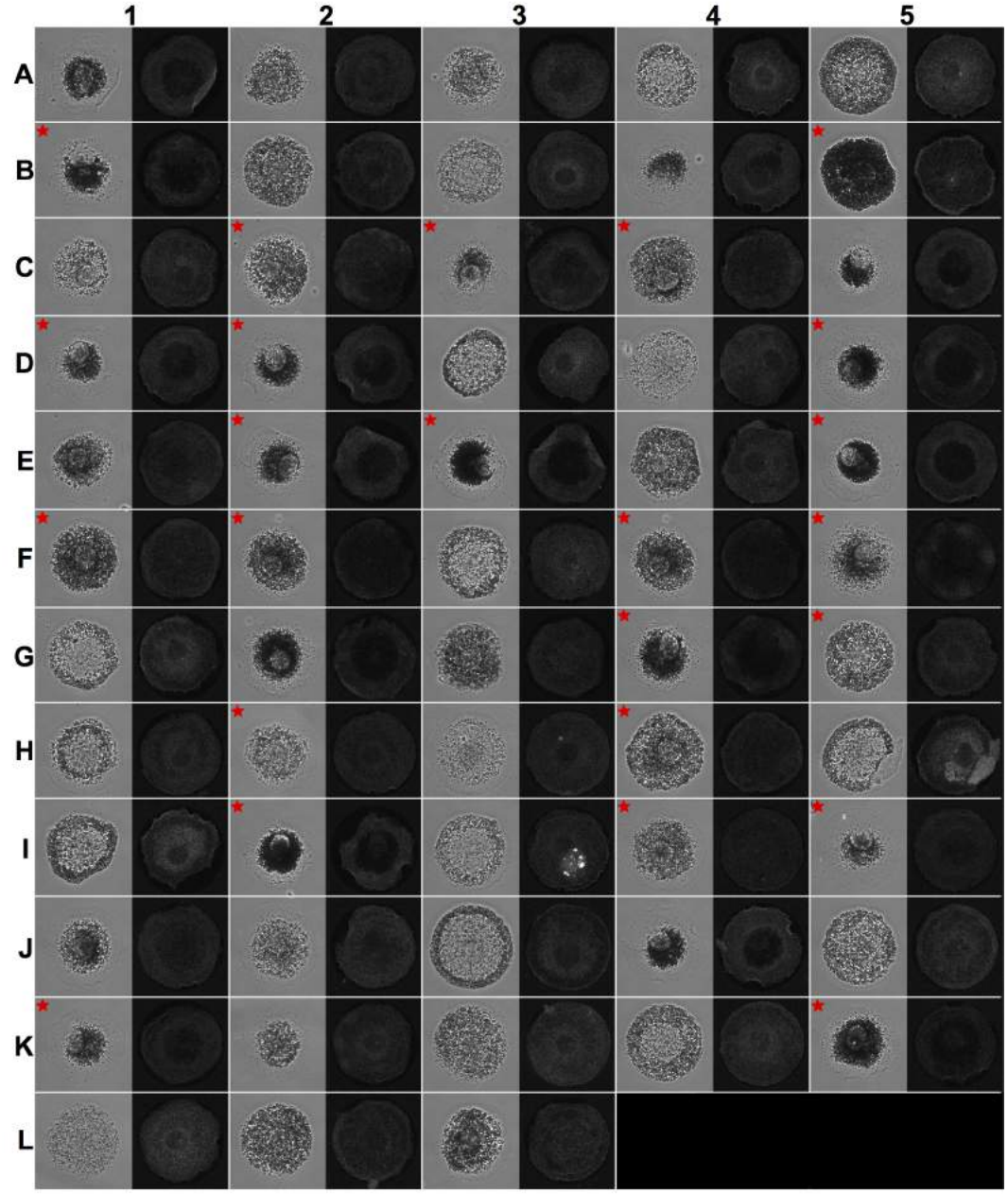


Figure 4.4 - Total population of melan-dilute cells transfected with myosin-Va-GFP. Montage of the total population of melan-dilute cells transfected with GFP-Myosin-Va and subsequently stained with anti-GFP primary and Alexa 488 secondary antibodies. Red stars in the upper left hand corner of each panel indicate the cell is untransfected when compared to the control staining, using the protocol described in section 2.4.3.2.

Since the high background was most likely due to autofluorescence caused by fixing the cells, a phenomenon that has been previously documented (Del Castillo et al., 1989), it was reasoned that if the cells were imaged live, autofluorescence should be reduced which may allow untransfected cells to be more reliably excluded based upon their fluorescence intensity. For live cell imaging melan-dilute cells were seeded onto standard sized micropattern chips and subsequently transfected with GFP-myosin-Va of left untransfected as a negative

control. Cells were allowed to express protein for 16 hours and prior to imaging the micropattern chip was placed into a live cell imaging chamber, which allowed for buffer to be perfused over the cells during acquisition (see 2.4.1.4 for the protocol used). Exactly the same imaging settings were used for both the infected and uninfected cells and the fluorescence intensity of the uninfected cells was again used to establish the background level in order to exclude any melan-dilute cells not expressing GFP-myosin-Va (as described in section 2.4.3.2). However, when average pigment maps were generated for the total population and expressing population there appeared to be little difference between the two (Figure 4.5a.i & a.ii), as with the fixed cell imaging described above. Moreover, the scatter plot and line plot (Figure 4.5c & d) also show there is no statistical difference between the two populations with the PDR for the 'expressing' population only increasing by 1.5μm over the PDR for the total population. The total population of cells imaged is given as a montage in Figure 4.5b. A fire look up table was applied to make visualising the fluorescent signal easier, since it was extremely weak. A smaller number of cells were imaged for the live cell experiment, since the live cell imaging chamber had a reduced surface area for imaging compared to the micropattern coverslips used for fixed-cell imaging. Furthermore, because cells needed to be bathed in buffer during imaging this reduced the quality of the phase contrast images (as can be seen in Figure 4.5b) which could potentially impact the results, since high quality phase contrast images were need to accurately compute the PDR for each cell. These problems therefore ruled out live cell imaging as a viable way to solve the problem of accurately detecting which melanocytes had been transfected based upon fluorescence intensity alone.

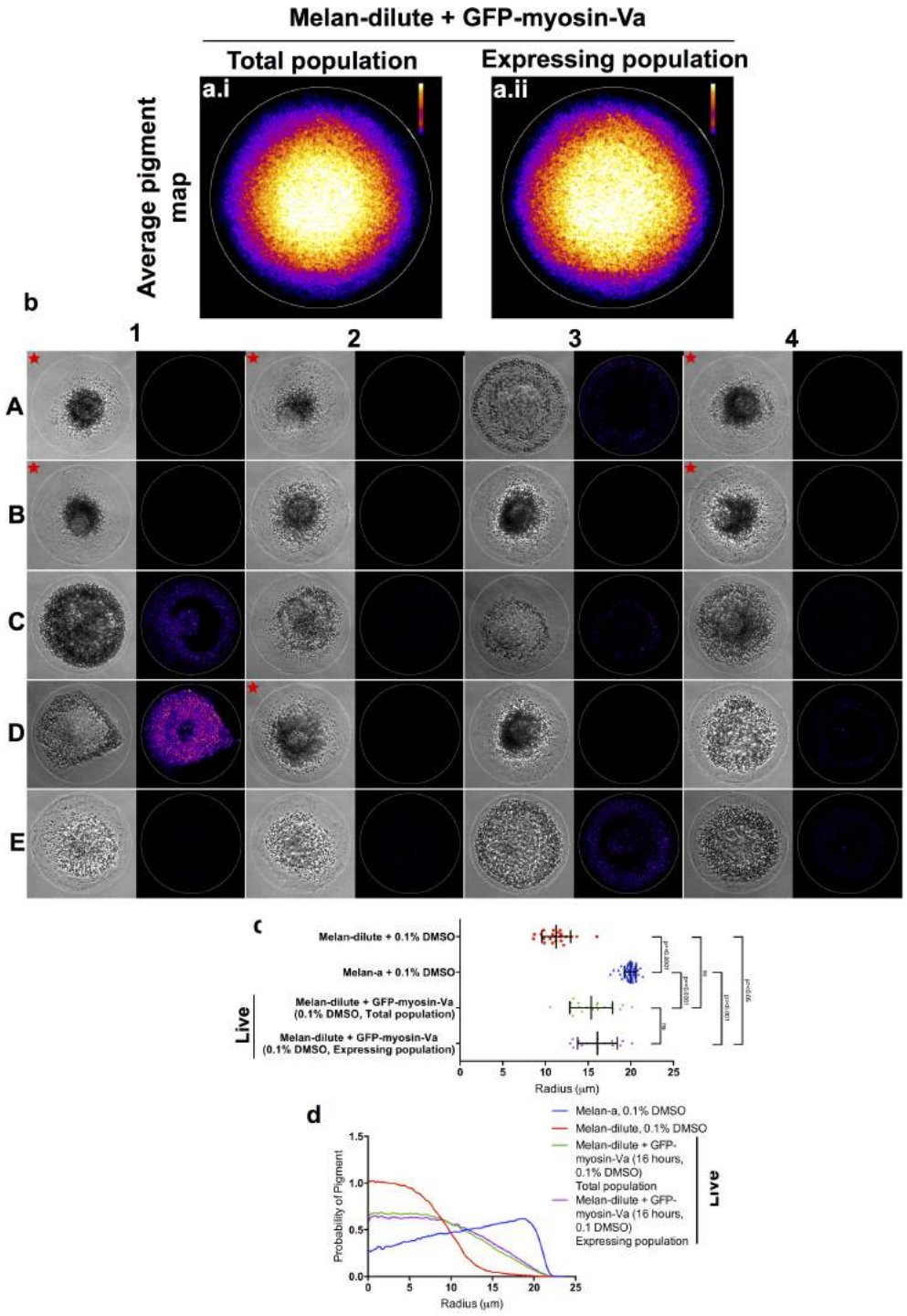


Figure 4.5 - Reducing autofluorescence by imaging melanocytes live does not help determine if a cell is expressing GFP-myosin-Va based on fluorescence intensity. Cells were imaged live in order to reduce autofluorescence that could be causing false positives. However, this caused additional problems, since the quality of the phase image obtained was poor, and also the number of cells that could be imaged was low compared with fixed samples, due to a reduced surface area available for live cell imaging. **(a.i)** The average pigment map for the total population of cells imaged (n=20) appears *dilute* in phenotype. **(a.ii)** Including only cells that have a fluorescence intensity at least 2SD units greater than that of the untransfected control cells (n=14) did not alter the average pigment map. **(b)** Montage of the total population of melan-dilute cells transfected with GFP-myosin-Va. Red stars in the upper left hand corner of each panel indicate the cell is untransfected when compared to the control staining. **(c)** The scatter plot indicates the average pigment dispersion ratio is halfway between that of the melan-dilute and melan-a cells and does not change significantly when 'non expressing' cells are excluded. Statistical analysis was performed using a Kruskal-Wallis ANOVA test **(d)** The line plot also shows that the pigment probability profile is both halfway between that of the wildtype and clustered cells does not change when non expressing melanocytes are excluded (Spearman's rank between total population and 'expressing' population = 0.996).

It was therefore decided to switch back to imaging fixed cells, but in order to try and reduce any possible autofluorescence, (which was always much more apparent in the green channel, compared to the other channels used for imaging) an Alexa-568 labelled secondary antibody was used instead of the Alexa-488 labelled secondary used previously to detect the anti-GFP antibody.

This small change meant that the correlation between fluorescence intensity and the level of rescue observed became much stronger, and when the average pigment maps were generated for the two populations they appeared very different (Figure 4.6a.i and a.ii). The scatter plot shows the average PDR for the total population is 15.5μm - very similar to the value shown in Figure 4.3c. However, when only cells which had a significantly higher fluorescent intensity in the red channel compared with the control cells were included (as calculated by the method described in section 2.4.3.2), this increased to 20.1μm (Figure 4.6b), meaning that the population was not significantly different from the melan-a cells, which had an average PDR of 19.9μm. The line plot also shows that the profile of the expressing population of cells infected with GFP-myosin-Va adenovirus closely follows that of the melan-a cells. Meanwhile the plot for the total population of melan-dilute cells infected with GFP-myosin-Va adenovirus appears more similar to the melan-dilute line (Figure 4.6c). Comparing the montages of the total cells imaged (Figure 4.7) also shows there is a much better correlation between the level of rescue and the intensity of the fluorescence. For example, out of a total of 31 cells included in the expressing population, only 2 have a clustered phenotype (D2 and G9).

Therefore, simply by changing the colour of the secondary antibody in order to avoiding imaging in the green channel which was subject to autofluorescence from the paraformaldehye fixative, very weak fluorescence signals could be reliably detected with very little background, which allows robust identification of cells expressing an exogenous fluorescent protein.

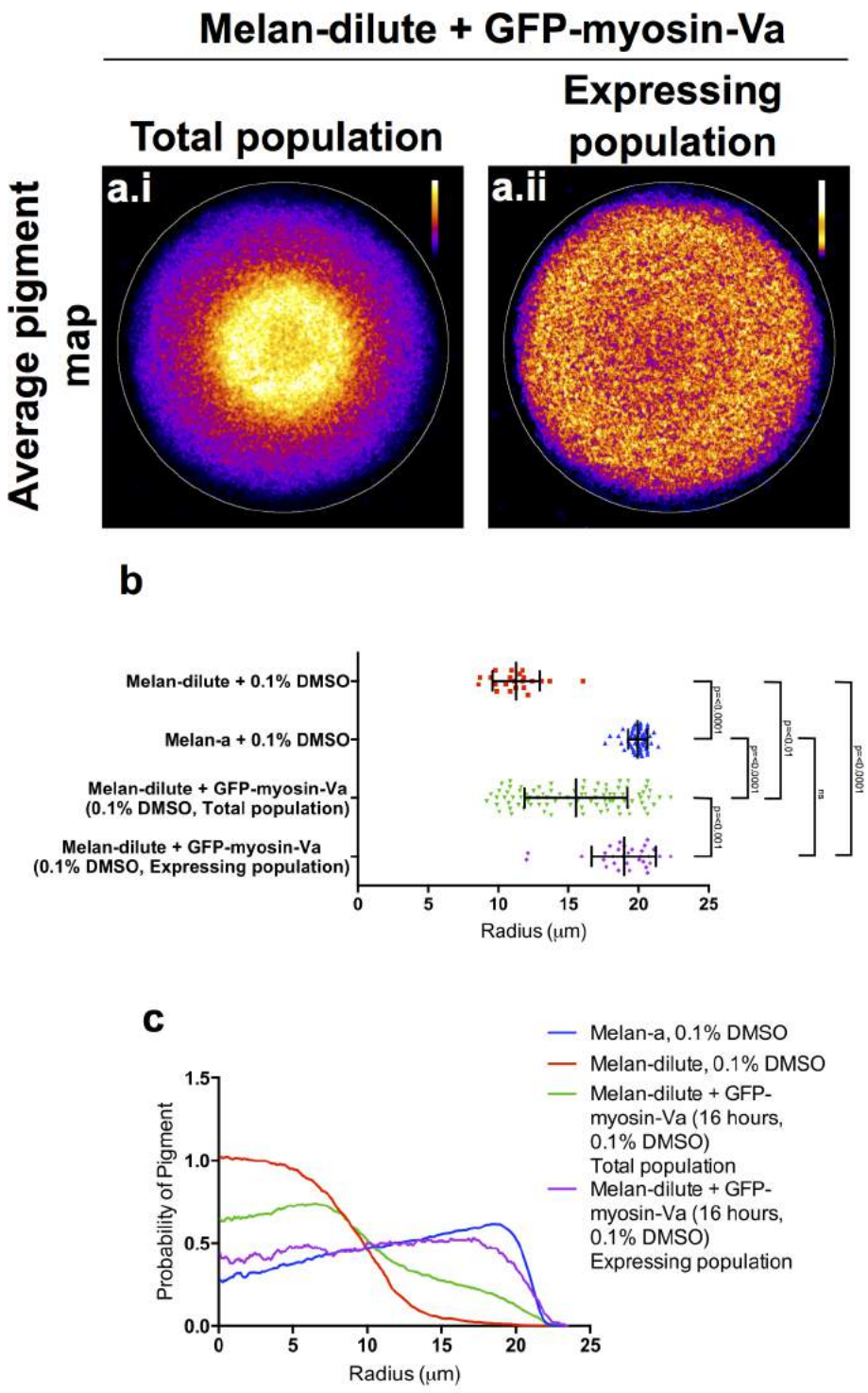


Figure 4.6 - Staining with Alexa-568 secondary antibodies reduces autofluorescence and allows for transfected cells to be identified based upon their fluorescence intensity. Cells were stained instead with a secondary antibody conjugated with Alexa-568, since there appeared to be less autofluorescence in this channel. This approach made it possible to differentiate between transfected and untransfected cells based upon their fluorescence intensity when compared to secondary antibody only stained cells. **(a.i)** Average pigment map of the total population of melan-dilute cells transfected with GFP-myosin-Va adenovirus and allowed to express for 16 hours prior to fixing (n=87). **(a.ii)** Average pigment map with non-expressing cells (based up their fluorescence intensity) removed (n=31). **(b)** The scatter plot shows removing non expressing cells has a large impact on the average pigment dispersion ration, which is no longer significantly different from that of the wildtype cells (statistical analysis performed using Kruskal-Wallis ANOVA test). **(c)** When non-expressing cells were excluded the pigment probability line plot for melan-dilute cells transfected with GFP-myosin-Va is very similar to that of the wildtype cells (Melan-a Vs non-expressing excluded = 0.730; Melan-a Vs total population =-0.240, using Spearman's correlation).

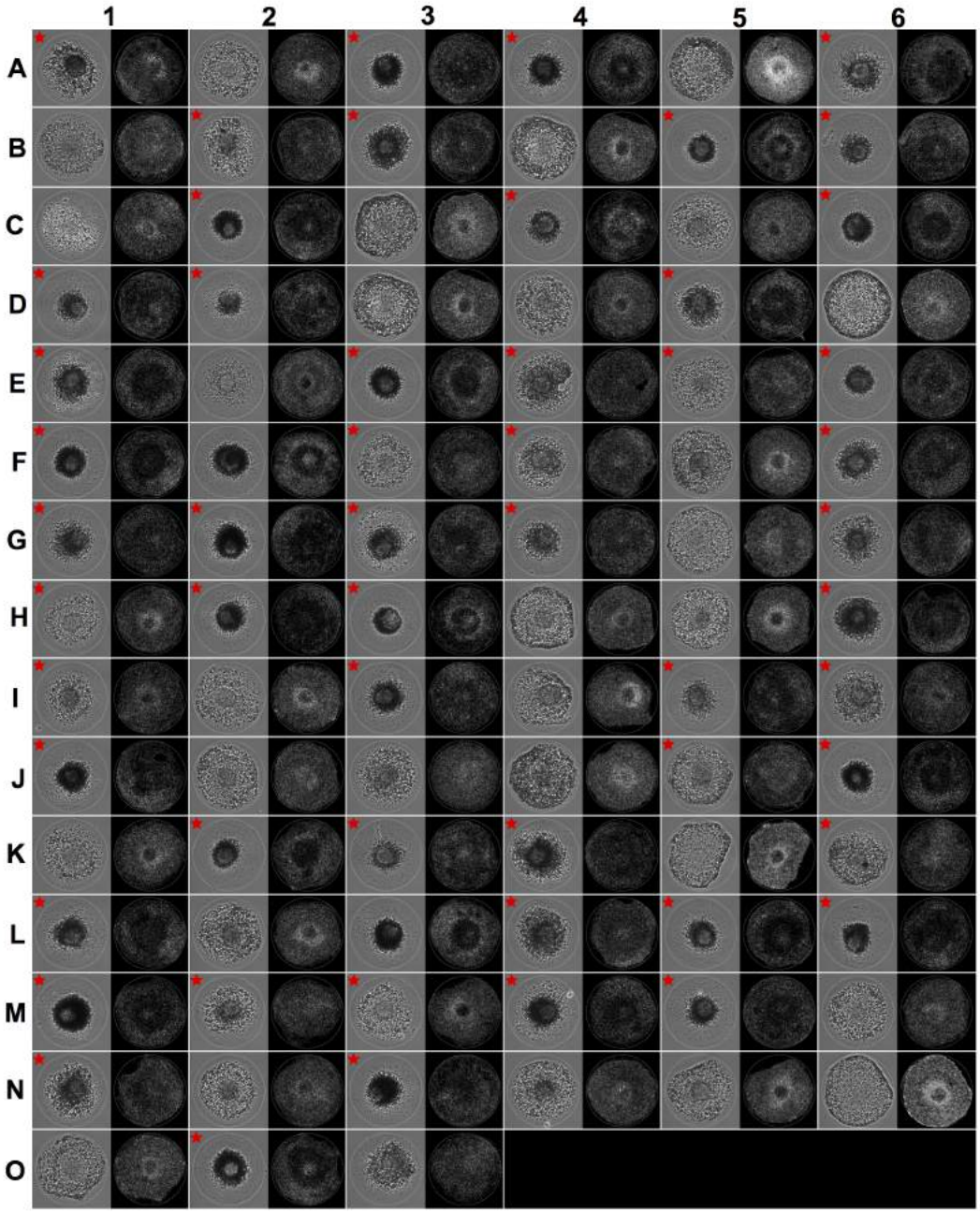


Figure 4.7 - Total population of melan-dilute cells transfected with GFP-myosin-Va and stained with Alexa-568 secondary antibodies. Montage of the total population of melan-dilute cells transfected with GFP-myosin-Va adenovirus and subsequently stained using Alexa-568 conjugated secondary antibodies against anti-GFP, instead of Alexa-488 secondary antibodies, as used previously. Red stars in the upper left hand corner of each panel indicate the cell is untransfected when compared to the control cells (untransfected, stained with secondary antibody only).

4.3.4 Anterograde melanosome transport is enhanced following noc treatment

The experiments described in sections 4.3.1 and 4.3.2 both indicate that deploymerising the microtubule network does not inhibit the anterograde transport of melanosomes from the perinuclear area to the plasma membrane. Following on from these results, it was important to more precisely quantify melanosome distribution after rescue +/- noc to understand if there are any subtle differences between the two treatments which may indicate a role for microtubules. Melan-dilute cells were therefore seeded onto micropattern chips, allowed to spread for 5 hours, and then treated with either 0.1% DMSO or 1μM noc for 1 hour. Subsequently, melanocytes were infected with GFP-myosin-Va adenovirus, and allowed to express for 16 hours before fixing and staining using an Alexa-568 conjugated secondary antibody to amplify the GFP signal.

Melanosomes still appear to rescue normally when constrained on the micropatterns, even in the presence of 1μM noc which is sufficient to destroy the microtubule network (Figure 4.8a & b). Furthermore, the pigment probability maps appear to show that the transport of melanosomes is actually somewhat enhanced when microtubules are depleted (Figure 4.8c & d). This is in agreement with the scatter plot which shows the PDR for rescued cells treated with 0.1% DMSO is 19.0μm, whilst for cells treated with 1μM noc this value increases to 19.9μm (Figure 4.8e; see figure legend for statistical comparisons). Meanwhile, the line plot corresponding to melan-dilute cells infected with GFP-myosin-Va adenovirus and treated with 1μM noc overlaps almost perfectly with the line corresponding to melan-a cells (blue). There is also strong overlap between these two profiles and that of rescued cells treated with 0.1% DMSO (Figure 4.8f; see figure legend for Spearman's rank values).

When melan-dilute cells seeded onto micropattern chips were rescued in the presence of 1μM noc, the overall cell size appeared smaller (Figure 4.8a & b) - possibly due to the lack of structural support from microtubules. This effect was also observed when melan-a cells were treated with 1μM noc for 16 hours (Figure 3.9). When this effect was quantified, it was found that the melan-dilute cells were on average 1486μm^2, whereas the micropatterns are 1650μm^2. Since the PDR and line plot measurements are normalised to the micropattern, not the individual cells, it is therefore possible this reduction in cell size is skewing the quantification. To check this, the quantification of randomly selected cells was repeated and the PDR and line plot measurements normalised to the actual cell size instead (Figure

4.9). The quantification shows there is very little difference between the two measurements, suggesting that small changes in cell size do not significantly skew the PDR and line plot measurements.

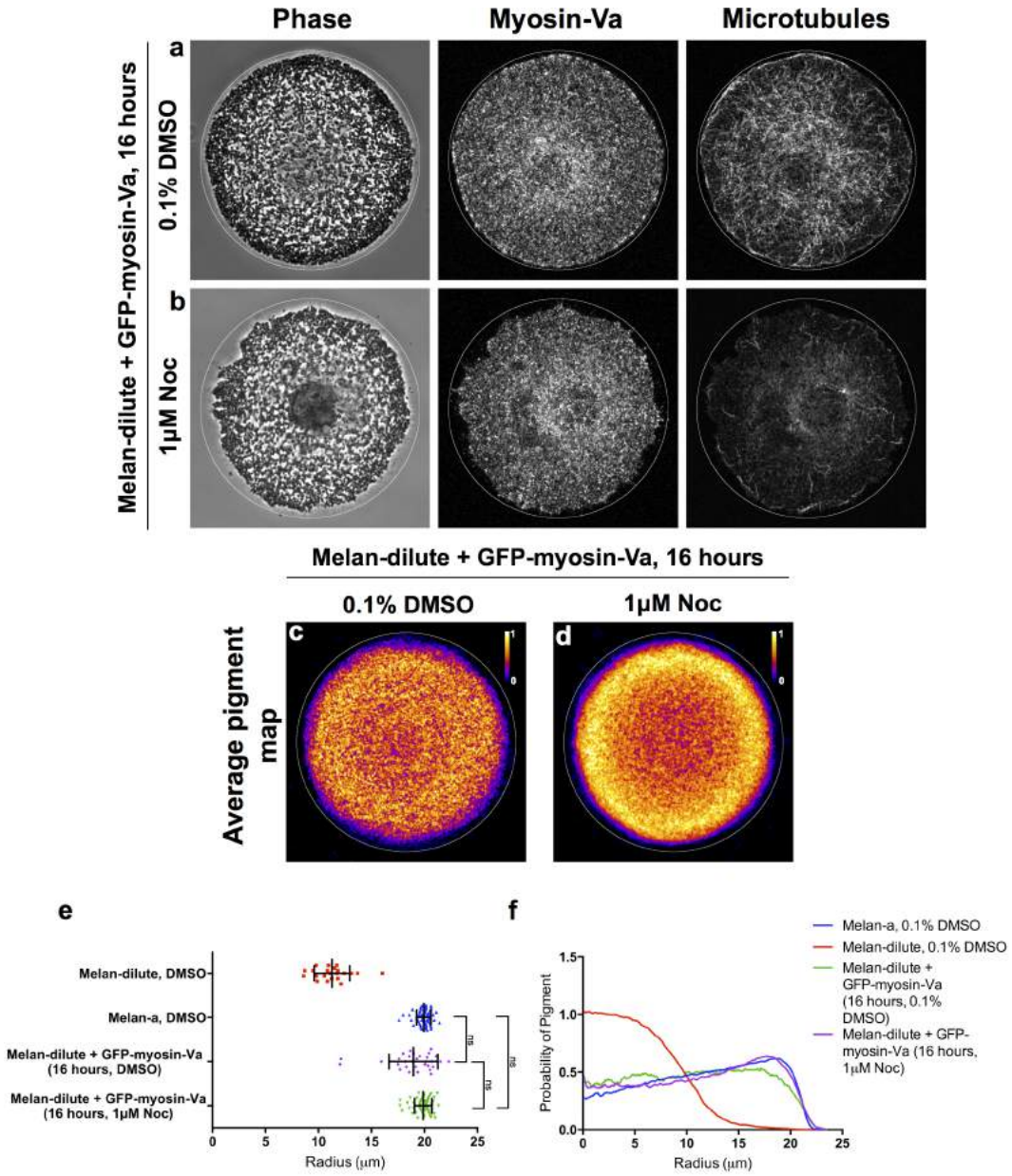


Figure 4.8 - Melan-dilute cells transfected with GFP-myosin-Va rescued to the same extent regardless of whether microtubules were present. Melan-dilute cells constrained on micropatterns were infected with GFP-myosin-Va adenovirus in the presence of either 0.1% DMSO **(a)** or 1μM noc, which was sufficient to significantly depolymerise the microtubule network **(b)**. Rescue of the pigment granules occurred regardless of microtubule integrity. The average pigment maps show that the rescue is slightly enhanced in cells treated with noc **(d)** compared with DMSO **(c).** However the scatter plot **(e)** shows that when pigment granule distribution is analysed using a Kruskal-Wallis ANOVA test there is no significant difference between the PDR of cells treated with either 0.1% DMSO or 1μM noc. **(f)** The line plot reconfirms this finding, showing the pigment probability profile is almost identical for GFP-myosin-Va expressing melan-dilute cells treated 1μM noc when compared to the wildtype profile. Melan-a Vs melan-dilute + GFP-myosin-Va, 0.1% DMSO = 0.730; Melan-a Vs melan-dilute + GFP-myosin-Va, 1μM noc = 0.960; Melan-dilute + GFP-myosin-Va, 0.1% DMSO Vs melan-dilute + GFP-myosin-Va, 1μM noc = 0.740 (Spearman's correlation). Melan-dilute + DMSO, n=28; Melan-a + DMSO, n=59; melan-dilute + myosin-Va-GFP + DMSO, n=31; melan-dilute + GFP-myosin-Va, n=56.

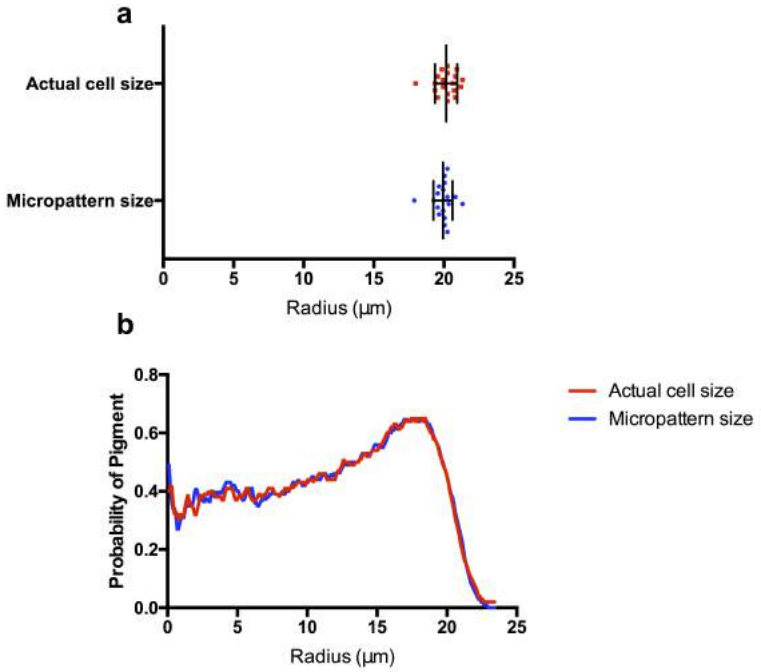


Figure 4.9 - Partial cell collapse does not skew either PDR or line plot measurements. Melan-dilute cells transfected with myosin-Va GFP in the presence of 1μM noc were found to be on average 11% smaller than the total area of the micropattern to which the PDR and line measurements are normalised, which may skew the results. However, when the PDR and line plot data were normalised to the individual cell size there was almost no difference compared to the data normalised to the micropattern. Mean PDR (actual cell size) = 20.2μm; (micropattern size) = 19.9μm. There is no significant difference between the two data sets (Mann-Whitney statistical test). n=19.

4.3.5 Forcibly recruiting Kif5B to the melanosome membrane in melan-dilute cells results in their abnormal distribution

The evidence presented in section 4.3.4 implies that myosin-Va alone must be capable of transporting melanosomes from the perinuclear area to the plasma membrane, since these organelles dispersed only when this motor was expressed, regardless of microtubule integrity. Since other evidence presented in this study also suggests that Kif5B is not involved in melanosome transport, it was therefore of interest to understand whether the resulting phenotype would appear wildtype if Kif5B was forcibly linked to this motor protein; currently the best candidate in the literature for the transporter responsible for long-range anterograde melanosome trafficking in mammalian melanocytes.

In order to target Kif5B to the melanosome membrane, the FKBP-FRB inducible dimerisation system was employed. This system makes use of the fact that the macrolide anti-fungal drug rapamycin is able to force the interaction of the 12 kDa FK506 binding protein (FKBP) and a 100 amino acid domain from mTOR (mammalian target of rapamycin) kinase, known as both mTOR and FRB (FKBP-rapamycin binding domain)(Banaszynski et al., 2005). In this study an analogue of rapamycin, termed A/C heterodimeriser (also known as AP21967), was used, since it inhibits mTOR kinase with much lower potency compared to rapamycin (Edwards and Wandless, 2007).

To utilise this inducible dimerisation system, 3 different constructs were generated (see section 2.2.3 for methods): KIF5B-GFP-1-810-FKBP (which should not be able to bind other organelles, since amino acids 810-891 are required for both KLC binding; Verhey et al., 1998 and direct binding to cargo; Diefenbach et al., 2002), mCherry-myosin-Va-FRB-tail fragment and GFP-myosin-Va-FKBP-motor (see Figure 4.10a.i for a schematic diagram and Figure 4.10a.ii & a.iii for cartoons of how these complexes should assemble when expressed in cells). Initially, KIF5B-GFP-1-810-FKBP (hereafter referred to as Kif5B-motor) and mCherry-myosin-Va-FRB-tail (hereafter referred to as myosin-Va-tail) were co-transfected into melan-dilute cells using adenovirus. Myosin-Va-tail should bind endogenously expressed melanophilin at the melanosome membrane, and upon addition of A/C heterodimeriser (see section 2.4.2.5 for protocol) the FKPB and FRB domains are forced to dimerise resulting in recruitment of Kif5B-motor, thus making the motor 'activatable' over a short time period (a few minutes). This system gives the advantage of being able to observe the affect of the motor protein on melanosome transport almost immediately, rather

than having to image the cells for several hours whilst fusion proteins are expressed, which can cause phototoxicity which may skew the results.

6×10^4 melan-dilute cells were seeded onto a 35mm glass-bottomed Matek dish and allowed to spread for 5 hours before being infected with either Kif5B-motor and myosin-Va-tail, GFP-Myosin-Va-FKBP motor (hereafter referred to as myosin-Va-motor) and myosin-Va-tail or myosin-Va-tail alone (to serve as a negative control), as described in section 2.1.5.1. Constructs were allowed to expressed for 48 hour before being imaged live using a Zeiss LSM710 confocal microscope as described in section 2.4.2. Cells were imaged before addition of A/C heterodimeriser (to a final concentration of 500nM), and then every 3 minutes for up to 90 minutes subsequent to the addition of the drug.

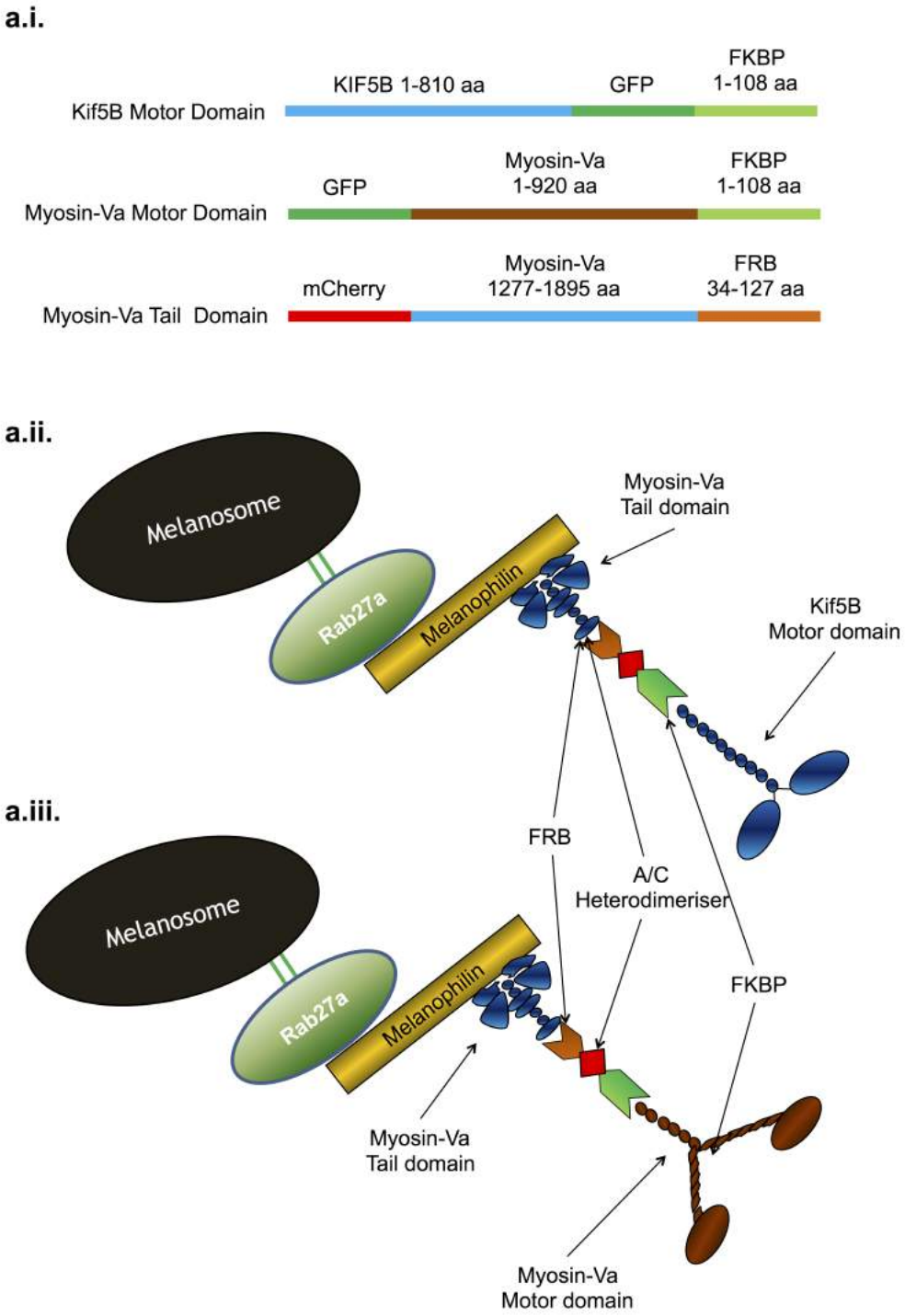


Figure 4.10 - Outline of the constructs used for the inducible dimerisation experiments

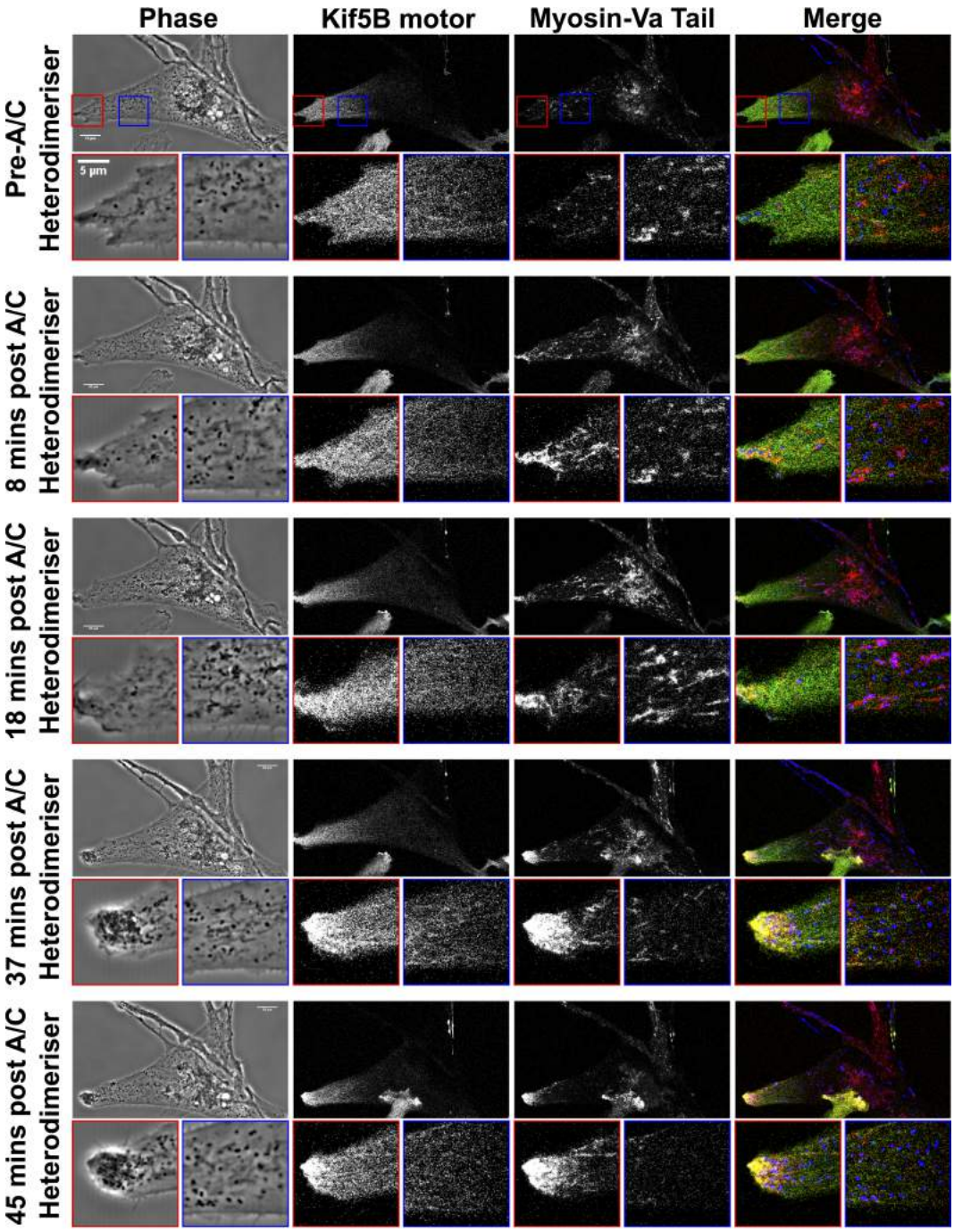


Figure 4.11 - The distribution of melanosomes forcibly coupled to Kif5B appears abnormal. Melan-dilute cells were co-transfected with Kif5B-motor and myosin-Va-tail, allowing Kif5B-motor to be forcibly recruited to the melanosome membrane upon addition of A/C heterodimeriser. This caused an abnormal accumulation of melanosomes at the dendritic tips after approximately 30 minutes. Melanosomes could also be observed translocating along what appeared to be microtubules at 18 minutes post A/C heterodimeriser. In the merged panels, Kif5B-motor is depicted in green, myosin-Va-tail in red and melanosomes in blue.

Initially, melanosomes are clustered around the perinuclear area, as expected for melan-dilute cells, whilst the Kif5B-motor appears to mainly localise to the dendritic tips of the cell (Figure 4.11 and Supplementary Movie 1 & 2). Upon addition of A/C heterodimeriser, the bulk of the pigment remains clustered around the perinuclear area throughout the time course. However, a small fraction of melanosomes are transported out to the dendritic tips,

where they accumulate (see red-framed zooms). There is also a concomitant increase in fluorescence intensity from the Kif5B-motor and myosin-Va-tail, indicating that Kif5B-motor is transporting a small subset of melanosomes via attachment through the myosin-Va-tail. It also appeared that Kif5B-motor was teasing myosin-Va-tail along structures which resembled microtubules, which is particularly apparent in the blue-framed zooms of the myosin-Va tail and merged panels at 18 mins post A/C heterodimeriser.

To test that the accumulation of melanosomes and myosin-Va-tail at the dendritic tips was due to the action of Kif5B-motor, the experiment was repeated after cells had been treated with either 0.1% DMSO or 1μM noc for 60 minutes. As before, when A/C heterodimeriser was added to cells with an intact microtubule network there was a small accumulation of Kif5B-motor, myosin-Va-tail and melanosomes at the dendritic tips after 1 hour (Figure 4.12a & b). However, when A/C heterodimeriser was added to cells pretreated with noc, no such accumulation at the dendritic tips was observed, and instead Kif5B-motor (presumably freely diffuse within the cytoplasm due to the lack of microtubules) was recruited to the melanosomes, which remained clustered around the perinuclear area (Figure 4.12c & d and Supplementary Movie 3 & 4). This was quantified by measuring the accumulation of fluorescence at the dendritic tips from Kif5B-motor during the time course in cells pretreated with both 0.1% DMSO and 1μM noc (Figure 4.13e & f).

Conversely, when myosin-Va-motor and myosin-Va-tail were double transfected into melan-dilute cells and the experiment repeated (Figure 4.15 and Supplementary Movie 5), all of the melanosomes in the cell were gradually transported from the perinuclear area and became evenly distributed throughout the cytoplasm such that it resembled a wildtype cell after just 70 minutes.

When melan-dilute cells were transfected only with myosin-Va-tail (as a negative control) and then treated with A/C heterodimeriser as in the previous experiments, there was no gross change in melanosome distribution after 60 minutes (Figure 4.14), indicating that the A/C heterodimerise itself does not invoke melanosome transport. Overall, these experiments demonstrate that melanosome transport from the perinuclear area to the plasma membrane can occur over a 60 minute time period in mouse melanocytes when mediated by myosin-Va (similar to the time scale observed for *Xenopus laevis* melanophores). Moreover, they also demonstrate that when Kif5B is forced to transport melanosomes, the resulting phenotype is abnormal, with only a minority of the melanosomes accumulating in the dendritic tips,

whilst the majority of the pigment granules remain clustered around the perinuclear area.

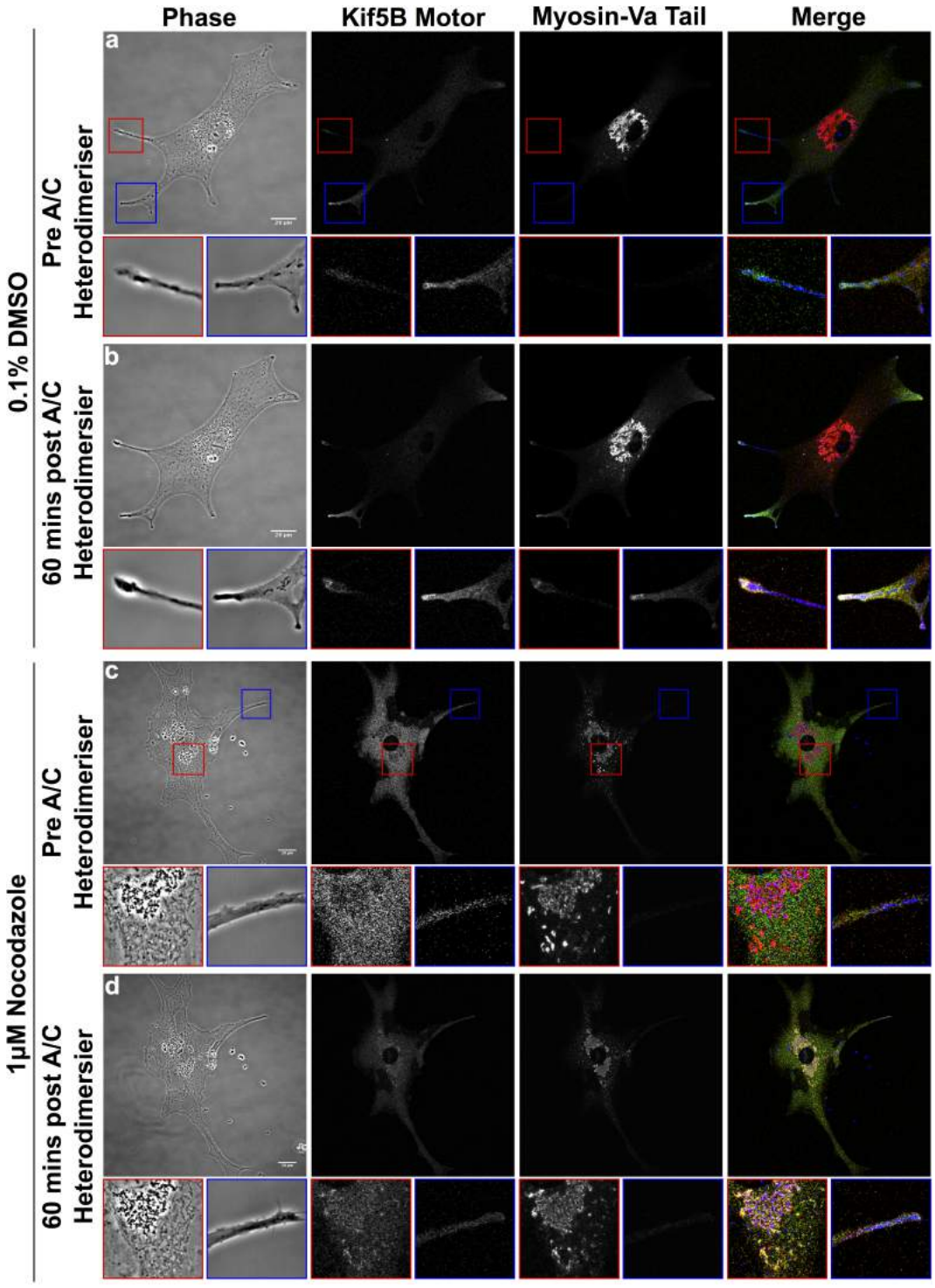


Figure 4.12 - Depolymersing microtubules blocks the accumulation of Kif5B-motor and myosin-Va-tail at the dendritic tips. **(a)** Prior to treatment with A/C heterodimeriser, melanosomes in melan-diute cells transfected with Kif5B-motor and myosin-Va-tail and treated with 0.1% DMSO were mainly clustered around the perinuclear area as expected. **(b)** 60 minutes post addition of A/C heterodimeriser, a small subset of melanosomes appeared to be transported to the ends of dendritic tips whilst the bulk pigment (marked by myosin-Va-tail) remained clustered.

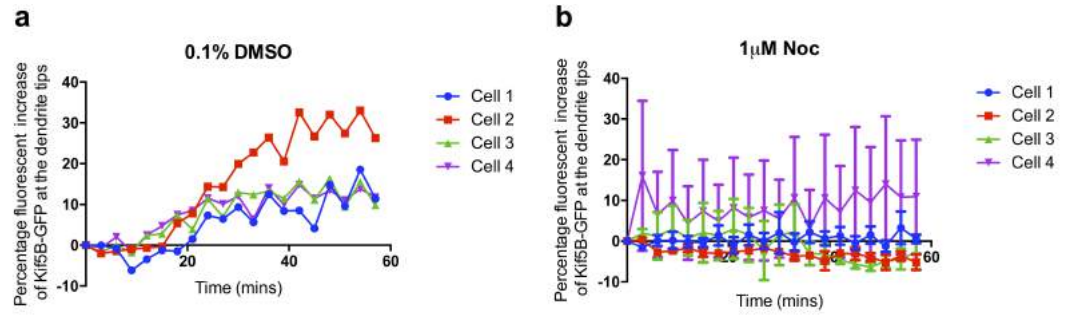


Figure 4.13 - Depolymersing microtubules blocks the accumulation of Kif5B-motor at the dendritic tips. (a) Addition of A/C heterodimeriser to cells expressing Kif5B-motor and myosin-Va-tail and treated with 0.1% DMSO led to an overall increase in fluorescence signal from the dendritic tips after 60 minutes. **(b)** No such increase in fluorescence was oberved in the dendritic tips if cells were treated with 1μM noc prior to the addition of A/C heterodimeriser. Quantification performed on cells shown in Figure 4.12.

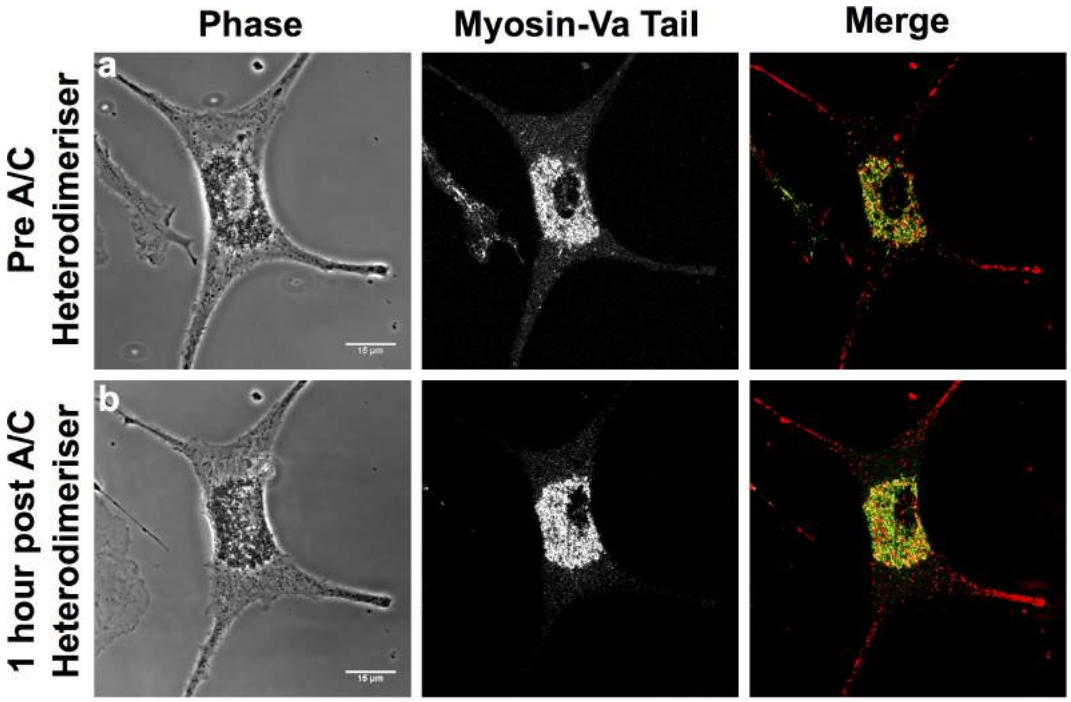


Figure 4.14 - Myosin-Va-tail alone cannot redistribute pigment granules in melan-dilute cells. As a negative control, melan-dilute cells were transfected with m-Cherry-myosin-Va-tail alone. As expected, melanosome distribution did not change following the addition of A/C heterodimeriser, demonstrating that the presence of the heterodimeriser itself does not influence melanosome distribution.

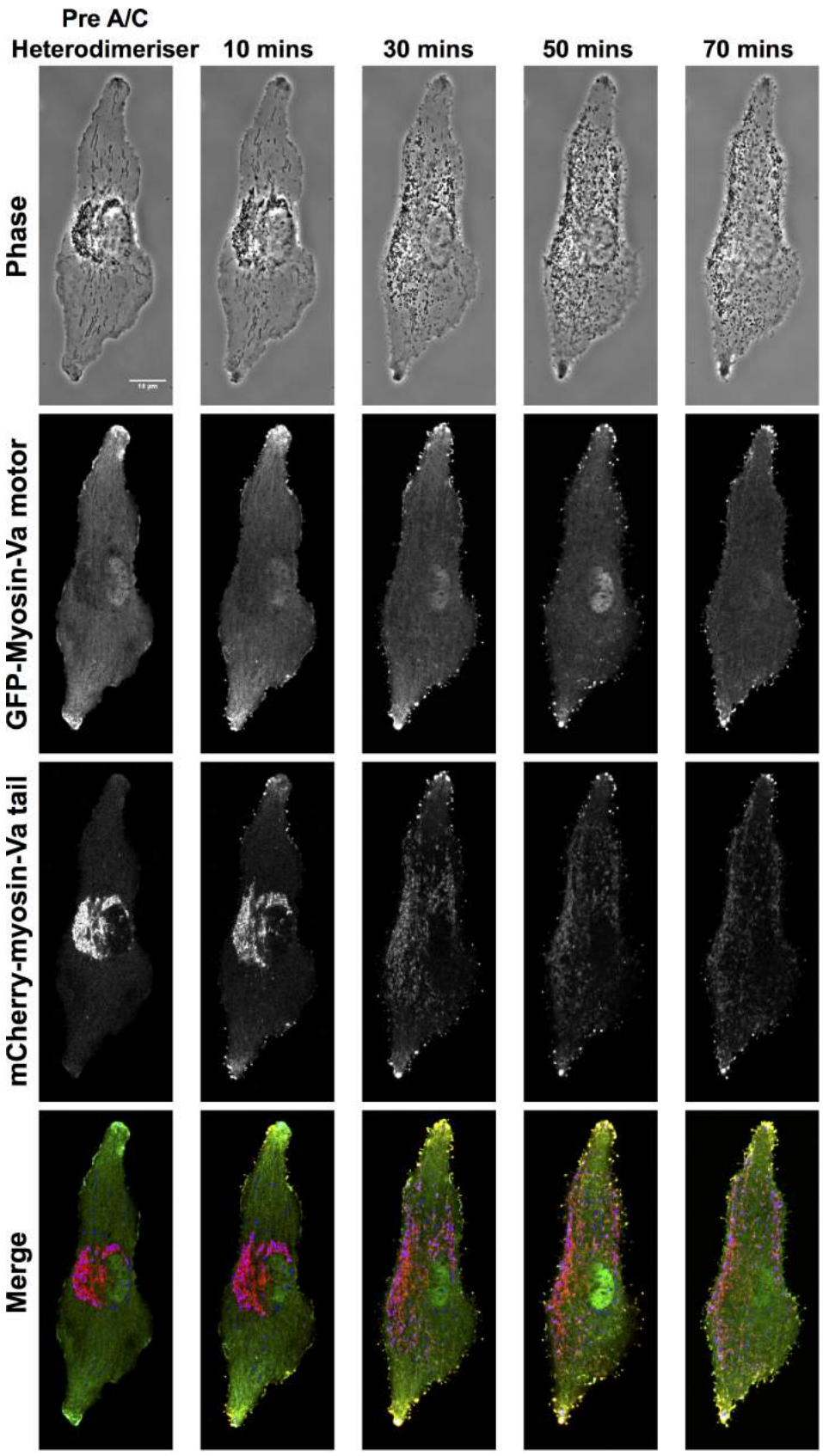


Figure 4.15 - Forcibly recruiting myosin-Va-motor to melanosome membranes in melan-dilute cells leads to normal pigment granule dispersion. Melan-dilute cells were co-transfected with myosin-Va-motor and myosin-Va-tail, allowing the myosin-Va-motor to be forcibly recruited to the melanosome membrane upon addition of A/C heterodimeriser. This caused the pigment granules to spread out from the perinuclear area *en masse*, with cells appearing rescued after apprximately 70 minutes. In the merged panels, myosin-Va-motor is depicted in green, myosin-Va-tail in red and melanosomes in blue. Data was acquired by Richard Evans.

4.3.6 Perturbing actin dynamics inhibits anterograde melanosome transport

The results described in section 3.3.9 and 3.3.10 strongly suggest that a dynamic actin cytoskeleton plays a vital role in maintaining peripherally dispersed melanosomes at steady-state. Therefore the next obvious question was whether perturbing the actin cytoskeleton also inhibits long-range anterograde transport of pigment granules. To test this, melan-dilute cells were seeded onto micropattern chips, allowed to spread for 16 hours, and then treated with either 10nM JK, 25nM LatA or 0.1% DMSO for 60 minutes. Cells were then infected with either GFP-myosin-Va or GFP alone (as a negative control) using adenovirus and allowed to express the protein for 16 hours before fixing.

As expected, melan-dilute cells treated with 0.1% DMSO and subsequently infected with GFP-myosin-Va were completely rescued (Figure 4.16c, e & f), whereas melanosomes in cells infected with GFP alone remained clustered around the perinuclear area (Figure 4.16d, e & f). However, treatment with either 10nM JK or 25nM LatA greatly attenuated long-range anterograde transport of the melanosomes (Figure 4.16a, b, e & f), with JK being most effective in blocking rescue. Therefore these results strongly suggest that even very subtle perturbation of the actin cytoskeleton with low doses of either LatA or JK is sufficient to almost completely inhibit long-range anterograde transport of melanosomes.

In order to test whether LatA or JK treatment was not simply inhibiting anterograde pigment granule transport by blocking myosin-Va targeting to the melanosome membrane, free-growing melan-dilute cells treated with either 0.1% DMSO, 25nM LatA (Figure 4.17) or 10nM JK (Figure 4.18) for 1 hour and the cell then infected with GFP-myosin-Va for 16 hours before fixing and staining with an anti-GFP antibody. The results demonstrate that the GFP-myosin-Va spots and melanosomes still appear in similar spatial areas after treatment with LatA, indicating that it is likely that myosin-Va can still target to the melanosome membrane. However, colocalisation between GFP-myosin-Va and melanosomes was less apparent after treatment with 10nM JK, although published data indicates that melanosomes are still transported *in vitro* by myosin-Va in the presence of this drug (Semenova et al., 2008). It is therefore possible that whilst a large fraction of myosin-Va gets miss-targetted in cells after JK treatment the melanosomes still retain a small population of myosin-Va motors, albeit at numbers which make them undetectable via immunofluorescence microscopy.

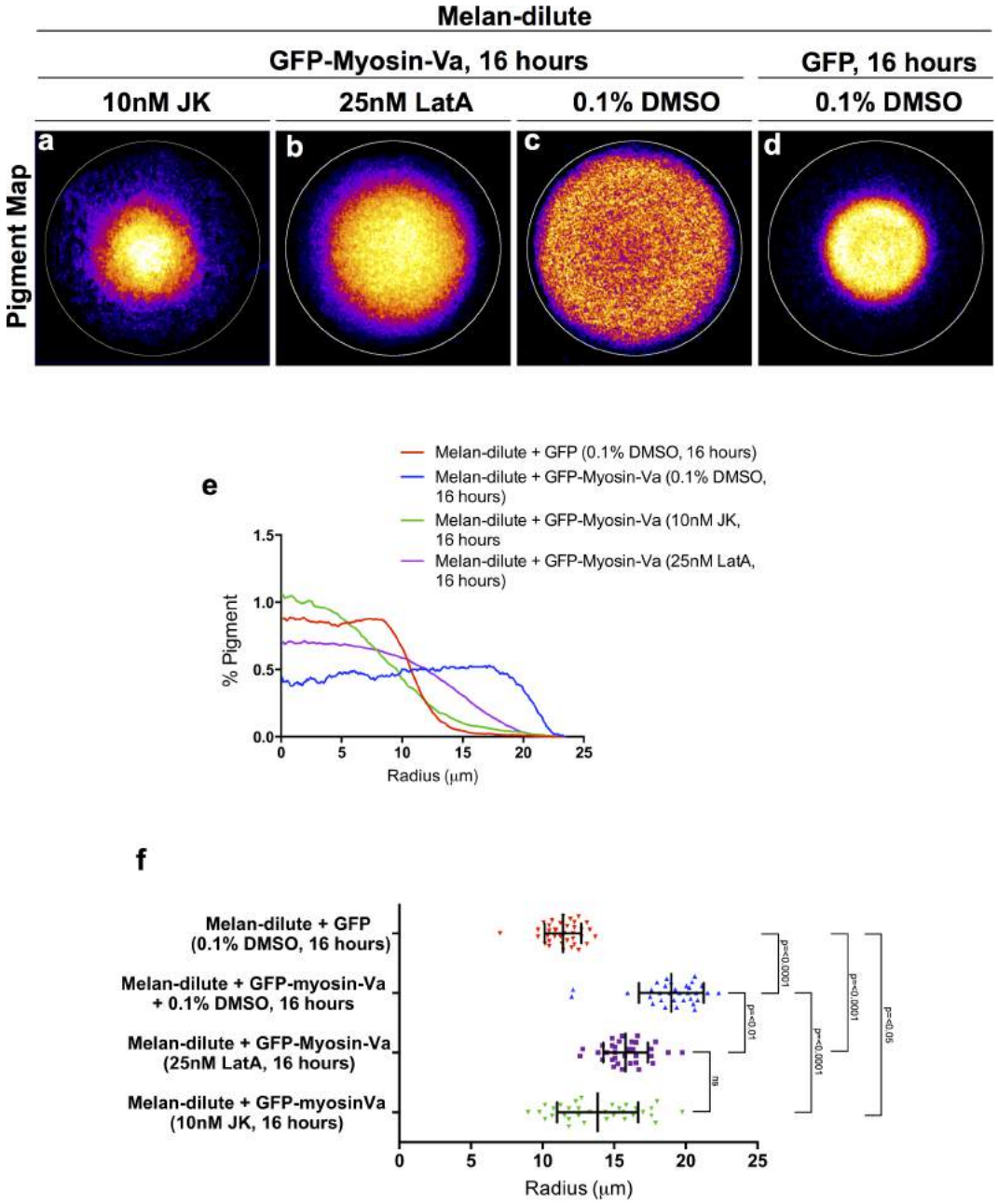


Figure 4.16 - Perturbing the actin cytoskeleton inhibits long-range anterograde melanosome transport. Melan-dilute cells were treated with either 10nM JK, n=33 **(a)**, 25nM LatA, n=33 **(b)**, or 0.1% DMSO, n=32 **(c)** for 1 hour before being infected with GFP-myosin-Va adenovirus and allowed to express for 16 hours prior to fixing and staining with anti-GFP antibody to amplify the weak signal from the GFP-myosin-Va fusion protein. **(d)** As a negative control melan-dilute cells were treated with 0.1% DMSO and infected with GFP adenovirus and allowed to expressed for 16 hours, n=37. **(e)** Line plot displaying the average probability of finding pigment at any given cell radius for each condition tested. Spearman's rank correlation shows: **a** Vs **b** = 0.997; **a** Vs **c** = 0.031; **a** Vs **d** = 0.958; **b** Vs **c** = 0.032; **b** Vs **d** = 0.956; **c** Vs **d** = 0.037. **(f)** Scatter plot indicating the PDR for each cell imaged. Mean PDR for **a** = 13.9μm; **b** = 15.8μm; **c** = 19.0μm; **d** = 11.4μm. Statistical analysis was performed using a Kruskal-Wallis ANOVA test.

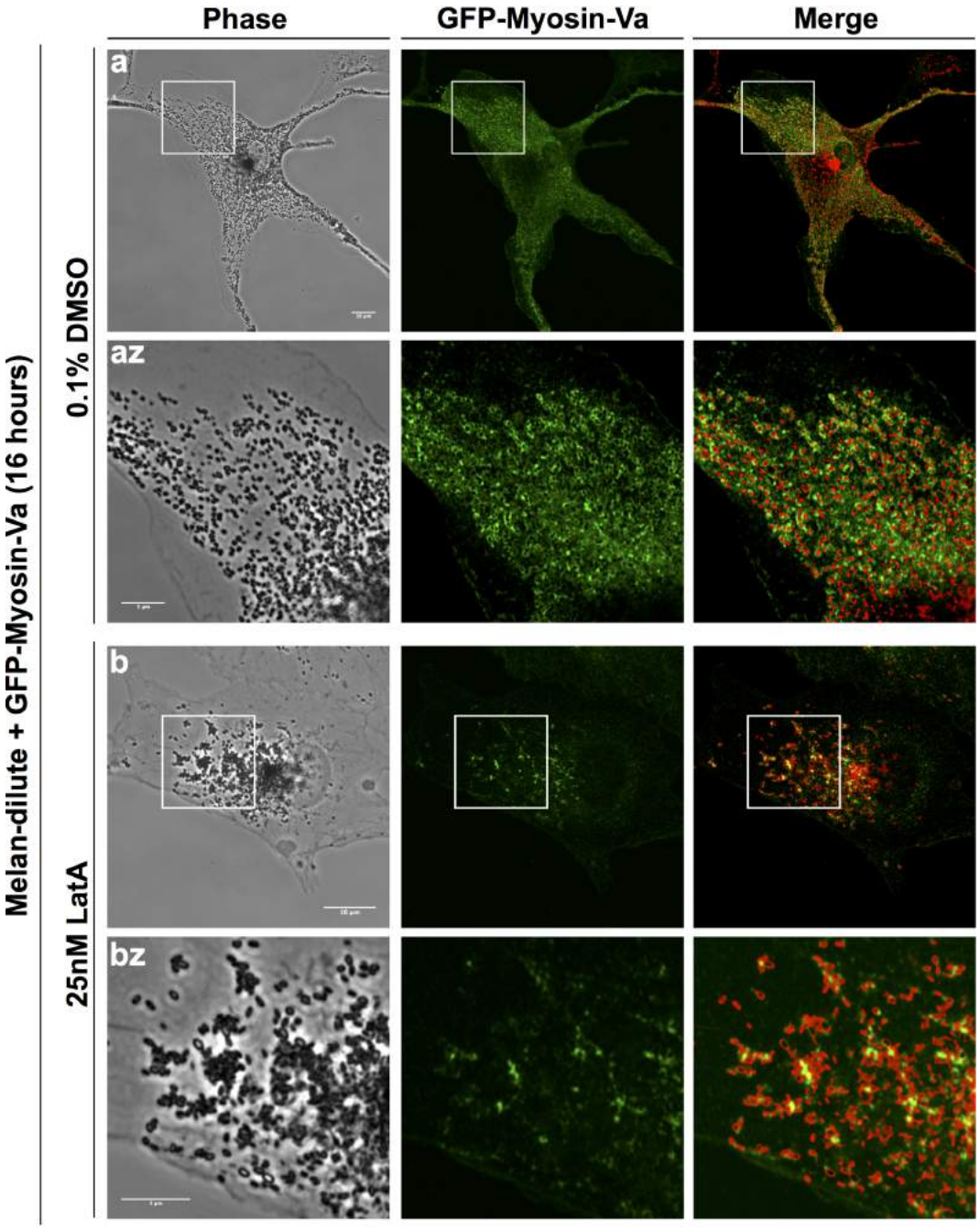


Figure 4.17 - LatA treatment does not affect myosin-Va targeting to the melanosome membrane. **(a)** In melan-dilute cells transfected with myosin-Va-GFP and treated with 0.1% DMSO for 16 hours myosin-Va targets to the melanosomes, forming rings around the organelles in many cases. **(az)** Higher magnification images of the cell areas in (a) encapsulated by the white boxes. **(b)** In melan-dilute cells transfected with myosin-Va-GFP and treated with 25nM LatA for 16 hours myosin-Va can be detected at the melanosome membrane in the majority of cases. **(bz)** Higher magnification image of the cell area in (b) encapsulated by the white box. For merged images green = myosin-Va, red = pigment granules. Cells were stained with anti-GFP antibody to amplify the weak signal from the GFP-myosin-Va fusion protein.

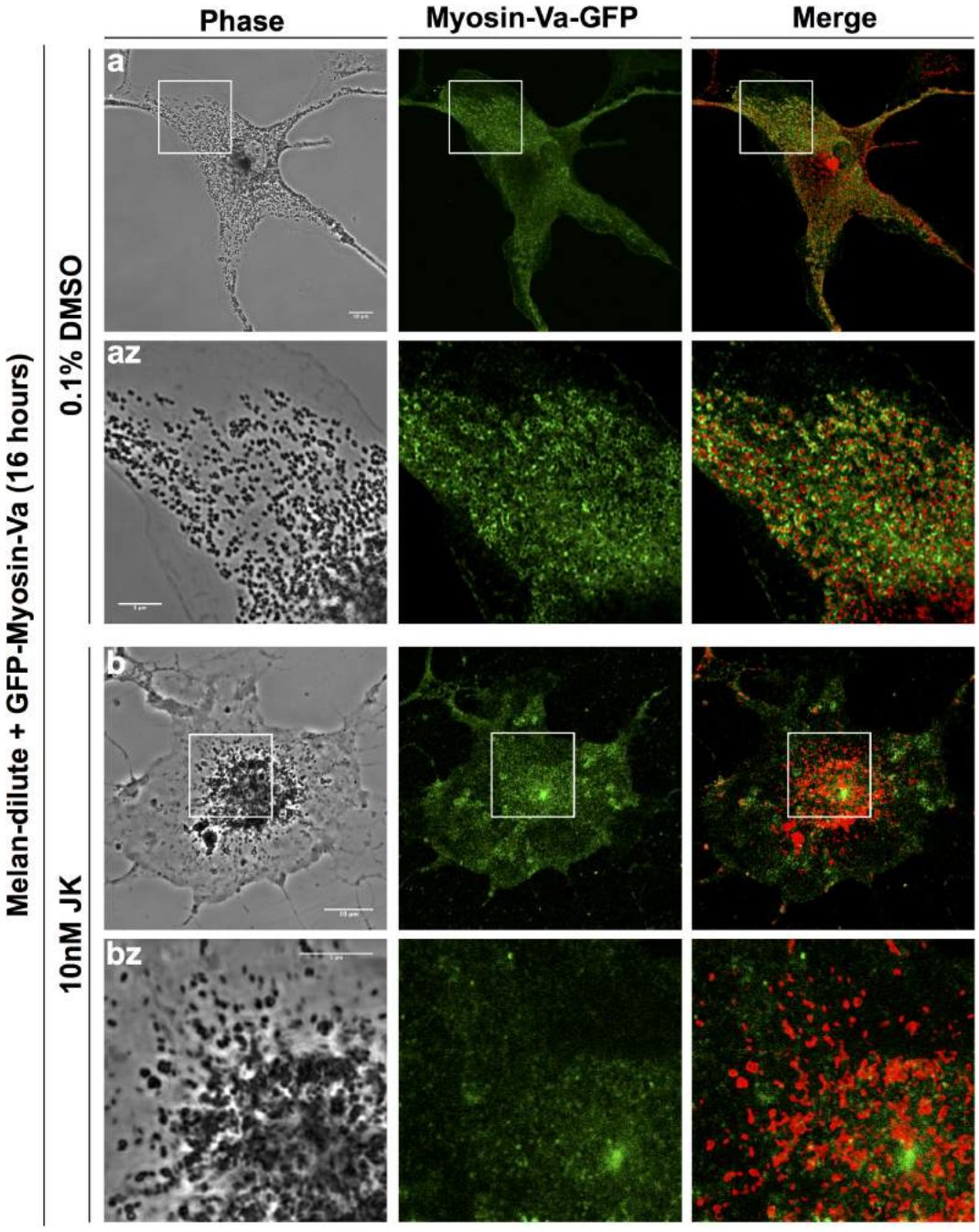


Figure 4.18 - JK treatment appears to disrupt myosin-Va targeting to the melanosome membrane. **(a)** In melan-dilute cells transfected with myosin-Va-GFP and treated with 0.1% DMSO for 16 hours myosin-Va targets to the melanosomes, forming rings around these organelles in many cases. **(az)** Higher magnification images of the cell areas in (a) encapsulated by the white boxes. **(b)** In melan-dilute cells transfected with myosin-Va-GFP and treated with 10nM JK for 16 hours myosin-Va can no longer be detected on the majority of melanosomes. **(bz)** Higher magnification image of the cell area in (b) encapsulated by the white box. For the merged images green = myosin-Va, red = pigment granules. Cells were stained with anti-GFP antibody to amplify the weak signal from the GFP-myosin-Va fusion protein.

4.3.7 CytD washout experiments indicate that actin regrows rapidly from the plasma membrane

Since the above results appear to indicate that the actin cytoskeleton plays a key role in the anterograde trafficking of melanosomes, the next question was to understand by what mechanism the actin cytoskeleton is able to support melanosome transport. The accepted model for melanosome transport is that microtubules are important for long-range trafficking, whilst actin is crucial for tethering melanosomes (Wu et al., 1998). However, this hypothesis is not compatible with the data presented in this study, since wildtype melanocytes whose actin was stabilised by low doses of JK exhibit clustered melanosomes, strongly resembling the *dilute* phenotype, which should not be the case if myosin-Va simply acts as a tether. Dynamic actin must therefore be facilitating anterograde melanosome transport by an as yet undetermined mechanism.

To gain some mechanistic insight into why the actin cytoskeleton is so important for anterograde melanosome transport, melan-a, melan-dilute and melan-leaden cells were incubated with 5μM CytD for 1 hour to invoke the formation of actin foci and induce the melanosomes to cluster (in the case of melan-a cells). These mutant cells were chosen in order to investigate if the loss of either myosin-Va or melanophilin affects how the actin behaves, since both of these proteins are know to have actin-binding regions. After CytD treatment the drug was washed out of the cells, and they were then fixed at regular intervals and stained with phalloidin so that the actin regrowth could be monitored (experimental procedure described in section 2.4.1.5).

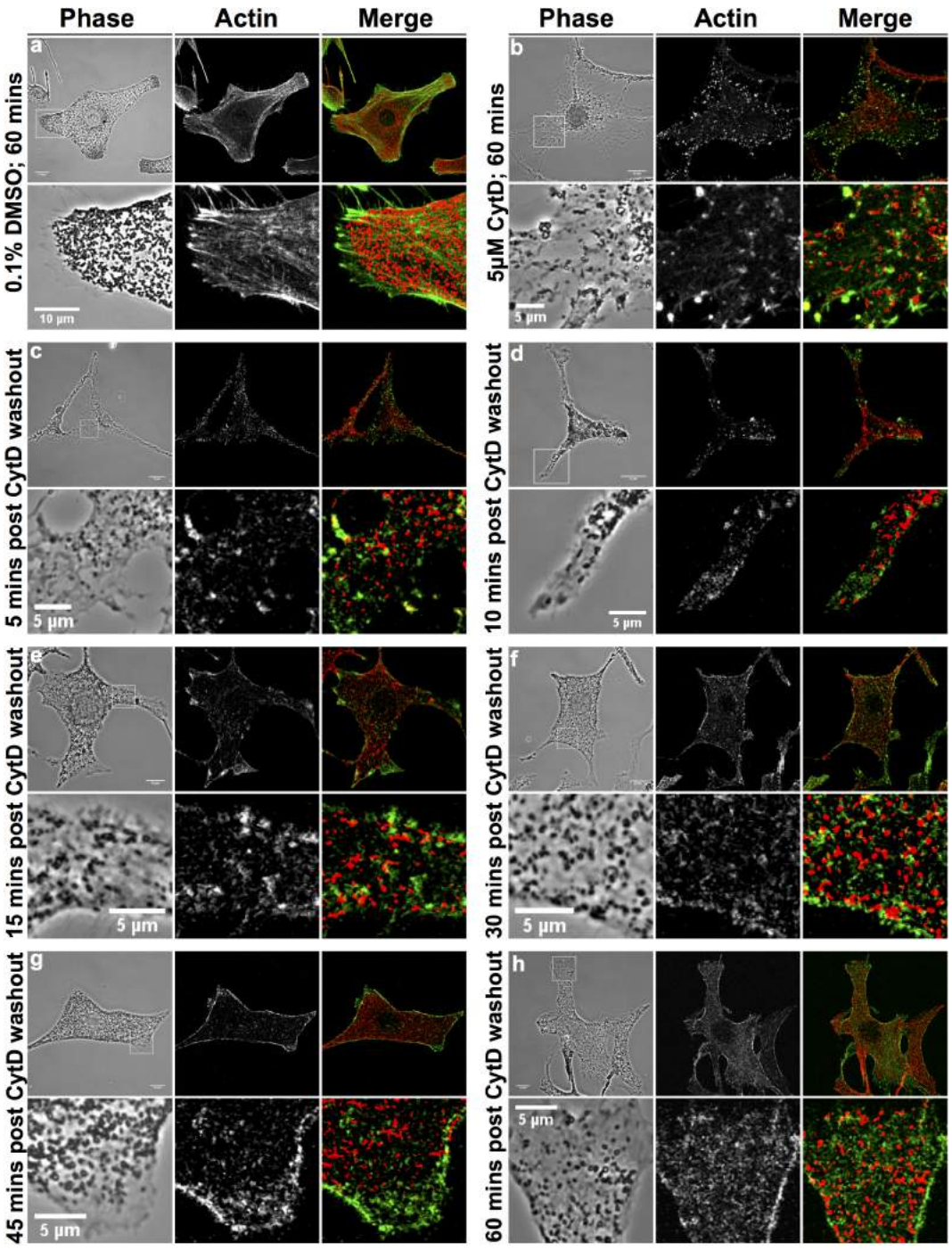


Figure 4.19 - CytD washout from melan-a cells indicates that actin regrows from the plasma membrane. **(a)** Melan-a cells treated with 0.1% DMSO for 60 minutes. **(b)** Melan-a cells treated with 5μM CytD for 60 minutes and subsequently fixed immediately or, CytD was washed out and the cells fixed after 5 mins **(c)**, 10 mins **(d)**, 15 mins **(e)**, 30 mins **(f)**, 45 mins **(g)** or 60 mins **(h)** post washout. Lower panels show higher magnification images from the area encapsulated by the white box in the above panel.

In control melan-a cells (treated with 0.1% DMSO, 60 minutes), actin was mainly localised in a thick band underneath the plasma membrane (Figure 4.19a) that likely plays a structural role, providing mechanical support (Charras et al., 2006). However, as seen previously (Figure 3.11) upon treatment with 5μM CytD for 60 minutes, this thick band of cortical actin is completely depolymerised and forms aggregates of actin that are dispersed

throughout the cytoplasm (Figure 4.19b). Some of these actin foci are found just underneath the plasma membrane, but they do not appear to co-localise with the pigment granules in the majority of cases. Quantification of actin localisation (Figure 4.22a; see section 2.4.3.6 for the method of quantifying mean distance of actin to the plasma membrane) shows that for control cells treated with 0.1% DMSO for 60 minutes the average distance of actin from the plasma membrane is very short. However, following treatment with 5μM CytD for 60 minutes it becomes redistributed throughout the cell (as denoted by the large SD) and is on average much further from the plasma membrane. At 5 minutes post CytD washout the actin foci still persist but they appear to have largely cleared from the cell centre and have migrated closer to the plasma membrane (Figure 4.19c). This is also reflected in the quantification, where the average distance of actin to the plasma membrane is very similar to that of the control cells. At 10 minutes post CytD washout, the actin spots have been further cleared from the cell centre, with the remaining aggregates almost entirely residing just underneath the plasma membrane (Figure 4.19d). Interestingly the total amount of actin also seems to have been reduced, suggesting the aggregates in the middle of the cell may have been de-ploymerised. At 15 minutes post CytD washout, a very thin band of cortical actin starts to appear (Figure 4.19e). It is at this time point that the actin is closest to the plasma membrane, according to the quantification in Figure 4.22a, since almost no actin foci persist at the cell centre. The partial re-formation of cortical actin coincides with the melanosomes becoming more peripherally dispersed throughout the cytoplasm, as well as the cell becoming more spread out. By 30 minutes post CytD washout, the cortical actin has become more prominent (Figure 4.19f), and by 45 minutes post washout it runs unbroken under the entire membrane (Figure 4.19g). Finally, at 60 minutes post CytD washout, the cortical actin has largely reformed and the phenotype of the cell appears similar to the DMSO control (Figure 4.19h).

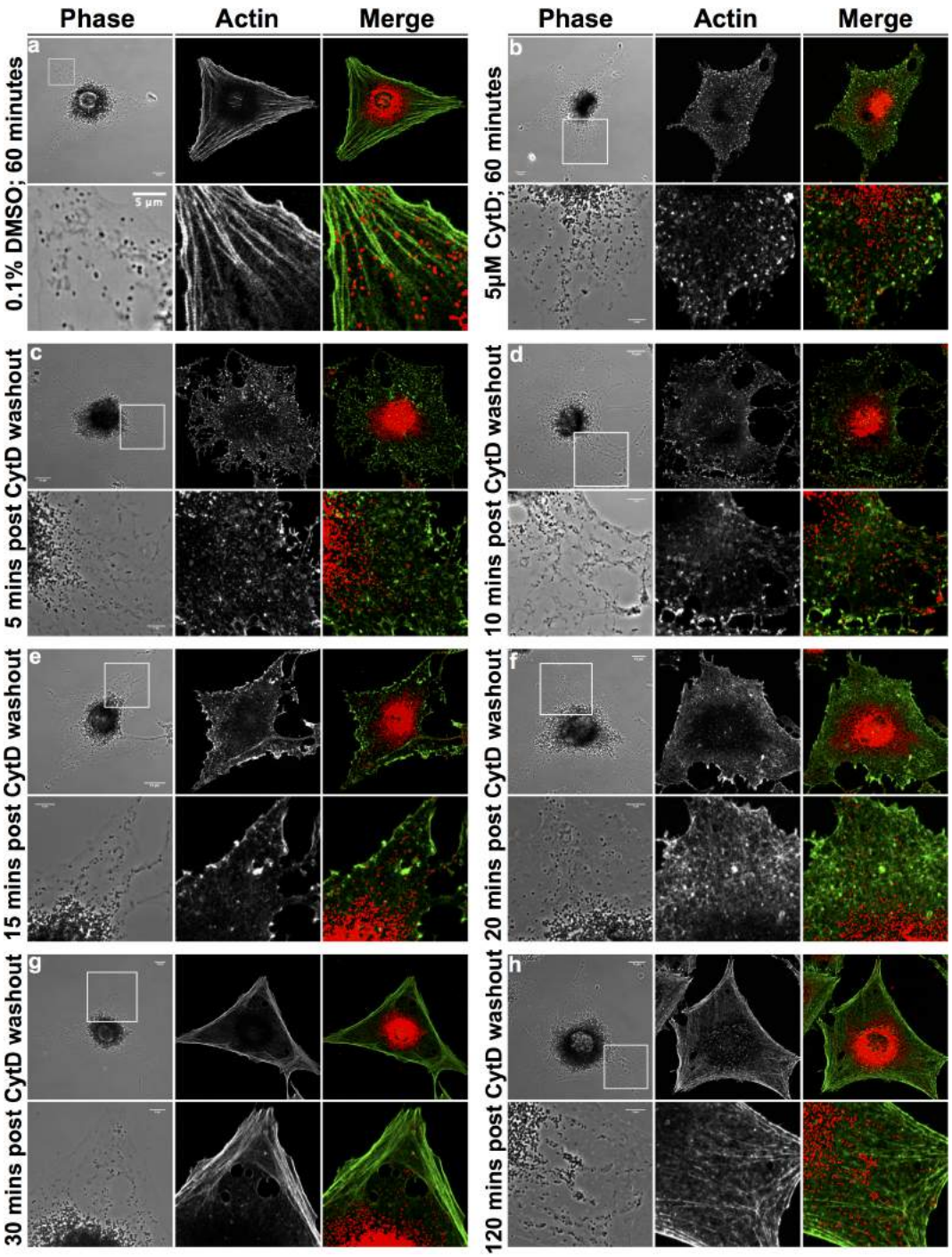


Figure 4.20 - CytD washout from melan-dilute cells reveals actin regrowth is much faster compared with melan-a cells. **(a)** Melan-dilute cells treated with 0.1% DMSO for 60 minutes. **(b)** Melan-dilute cells treated with 5μM CytD for 60 minutes and subsequently fixed immediately or, CytD was washed out and the cells fixed after 5 mins **(c)**, 10 mins **(d)**, 15 mins **(e)**, 20 mins **(f)**, 30 mins **(g)** or 120 mins **(h)** post washout. Lower panels show higher magnification images from the area encapsulated by the white box in the above panel.

The CytD washout experiment was next repeated using melan-dilute cells to test if any differences in actin regrowth could be detected that might be attributable to the loss of myosin-Va. The first noticeable difference is that there are many more stress fibres running underneath the plasma membrane in the DMSO treated control cells compared with the melan-a

cells (Figure 4.20a), which causes the average distance of the actin from the plasma membrane in the melan-dilute cells to be much greater than in the melan-a cells (Figure 4.22b) at steady state. When melan-dilute cells were treated with 5μM CytD for 60 minutes and fixed immediately, the actin foci appeared to be mainly localised close to the plasma membrane (Figure 4.20b). The quantification shows that, in contrast to the results with the melan-a cells, the average distance of actin from the plasma membrane decreased following CytD treatment compared with the DMSO control. At 5 minutes post CytD washout the actin spots appear more homogeneously spread throughout the cytoplasm (Figure 4.20c), but by 15 minutes post washout, the majority of the actin is once again localised just under the plasma membrane (Figure 4.20e). At 30 minutes post drug washout the actin network appears to have completely reformed (Figure 4.20g), and looks similar to that of the control melan-dilute cells (Figure 4.20a). By contrast, actin in the melan-a cells at 30 minutes post CytD washout still appeared fragmented and not representative of the actin cytoskeleton of the DMSO treated cells (compare Figure 4.19a with Figure 4.19e). At 120 minutes post CytD washout, the actin in the melan-dilute cells does not look markedly different than at 30 minutes post washout, except for an increase in stress fibres running through the cytoplasm, which caused the average distance of the actin from the plasma membrane to increase slightly (Figure 4.20h). These results therefore suggest that myosin-Va is working as an F-actin depolymerise in these cells, resulting in the actin cytoskeleton taking longer to reform after CytD treatment in the wildtype cells compared with the melan-dilute cells.

Similar results to that of the melan-dilute cells were obtained when the CytD washout experiment was repeated using melan-leaden cells. In the control cells, the thickness of the cortical actin is very similar to that of the melan-leaden (Figure 4.21a & Figure 4.22c), and following 5μM CytD treatment for 60 minutes the actin foci were located close to the plasma membrane (Figure 4.21b). Post CytD washout, the actin reformed with a kinetic that was somewhere between that of the melan-a and melan-dilute cells, since after 30 minutes the actin spots appeared to have fused to form a contiguous band under the membrane (Figure 4.21f) which was similar to the result observed for the melan-a cells after 45 minutes post CytD washout (Figure 4.19g) while the actin had reached this stage of regrowth after just 15 minutes in the melan-dilute cells (Figure 4.20e). By 1 hour post CytD washout, the average distance of the actin to the plasma membrane was very similar to that in the melan-dilute cells (Figure 4.22c), although the SD was much smaller, suggesting that most of the actin

was localised underneath the membrane, whereas in the melan-dilute cells more of the actin was distributed throughout the cytoplasm.

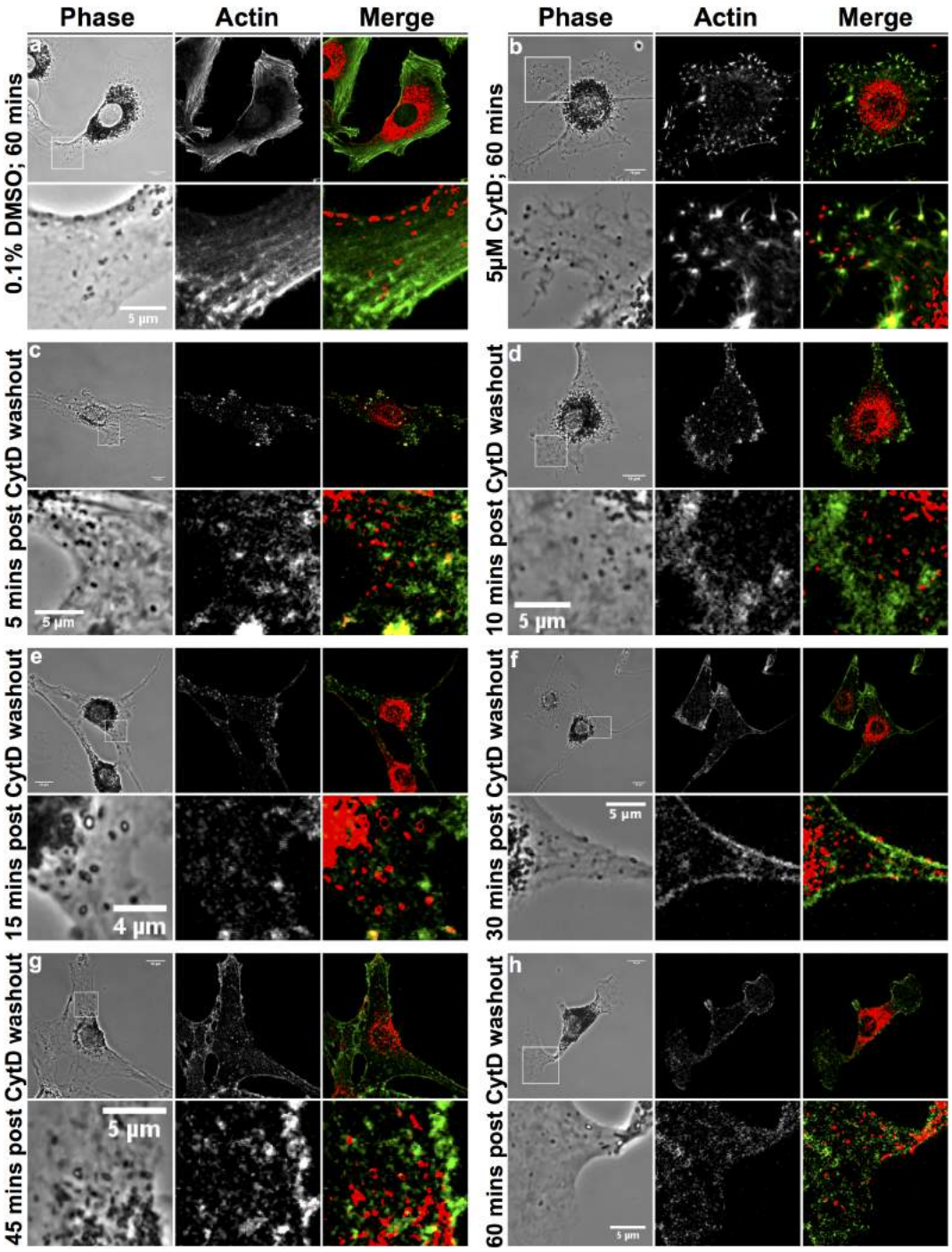


Figure 4.21 - CytD washout from melan-leaden cells reveals actin regrows from the plasma membrane on a similar timescale to the melan-a cells. **(a)** Melan-leaden cells treated with 0.1% DMSO for 60 minutes. **(b)** Melan-leaden cells treated with 5μM CytD for 60 minutes and subsequently fixed immediately or, CytD was washed out and the cells fixed after 5 mins **(c)**, 10 mins **(d)**, 15 mins **(e)**, 30 mins **(f)**, 45 mins **(g)** or 60 mins **(h)** post washout. Lower panels show higher magnification images from the area encapsulated by the white box in the above panel.

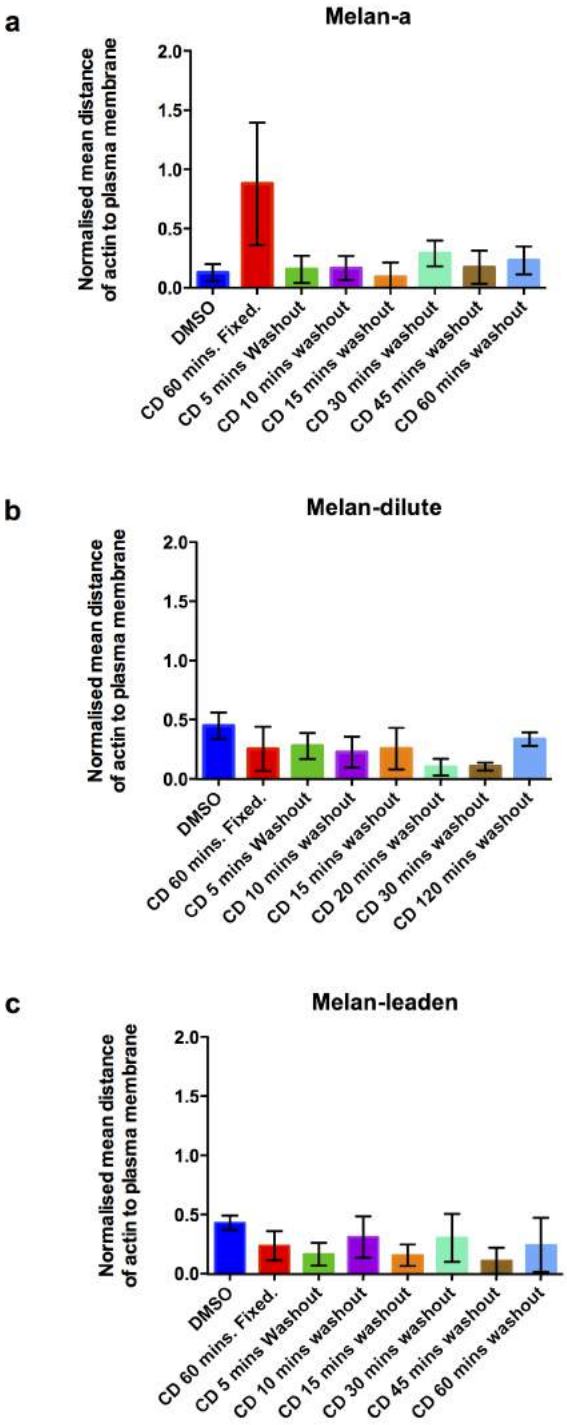


Figure 4.22 - Quantification of actin dispersion during CytD washout experiments. (a) Average dispersion ratio of actin in melan-a cells during CytD washout. CytD treatment caused the formation of actin foci which are spread throughout the cytoplasm, giving a large dispersion distance which is quickly reduced post CytD washout. n=10 (DMSO, CytD 60 mins then fixed and 5 mins post CytD washout); 7 (10 and 15 mins post CytD washout); 8 (30 and 45 mins post CytD washout); 9 (60 mins post CytD washout). **(b)** Average dispersion ration of actin in melan-dilute cells during CytD washout. The dispersion ratio immediately after CytD treatment decreased, in contrast to the melan-a cells, indicating that the majority of the remaining actin is located near the plasma membrane. n=11 (DMSO); 6 (CytD 60 mins then fixed); 7 (5 and 10 mins post CytD washout); 6 (15 mins post CytD washout); 5 (20 mins post CytD washout); 6 (30 mins post CytD washout); 7 (120 mins CytD washout). **(c)** Average dispersion ratio in melan-leaden cells during CytD washout is similar to that of the melan-dilute cells. n=13 (DMSO); 10 (CytD 60 mins then fixed); 8 (5 mins post CytD washout); 9 (10 mins post CytD washout); 11 (15 mins post CytD washout); 10 (30 mins post CytD washout); 7 (45 mins post CytD washout); 8 (60 mins post CytD washout).

To further assess both actin regrowth and melanosome redistribution during CytD washout, wildtype melanocytes were transfected with utrophin-GFP which was allowed to express for 48 hours and subsequently treated with 5μM CytD for 1 hour. The drug was then washed out using a perfusion system, thus allowing the recovery to be monitored live, as described in section 2.4.1.5 (Figure 4.23 and Supplementary Movie 6). Actin asters which are prevalent throughout the cytoplasm at the beginning of the time course (Figure 4.23a) disappear very quickly, and after just 3 minutes most appear to have been reorganised into cortical F-actin (Figure 4.23b). This represents a kinetic approximately 5 fold faster compared with the results shown in Figure 4.19. As the time course progresses, the band of cortical actin appears to increase in thickness and by 9 minutes, this too has reformed to a great extent (Figure 4.23d). By 18 minutes post washout the pigment granules have fully dispersed (Figure 4.23g), which is again faster than that observed in Figure 4.19. After 18 minutes, cortical actin staining increases slightly until approximately 30 minutes (Figure 4.23j), after which time there is little change in phenotype. Melanosome dispersion is complete after approximately 30 minutes and is concomitant with the clearing of the actin asters observed at the beginning of the time course and regrowth of cortical actin.

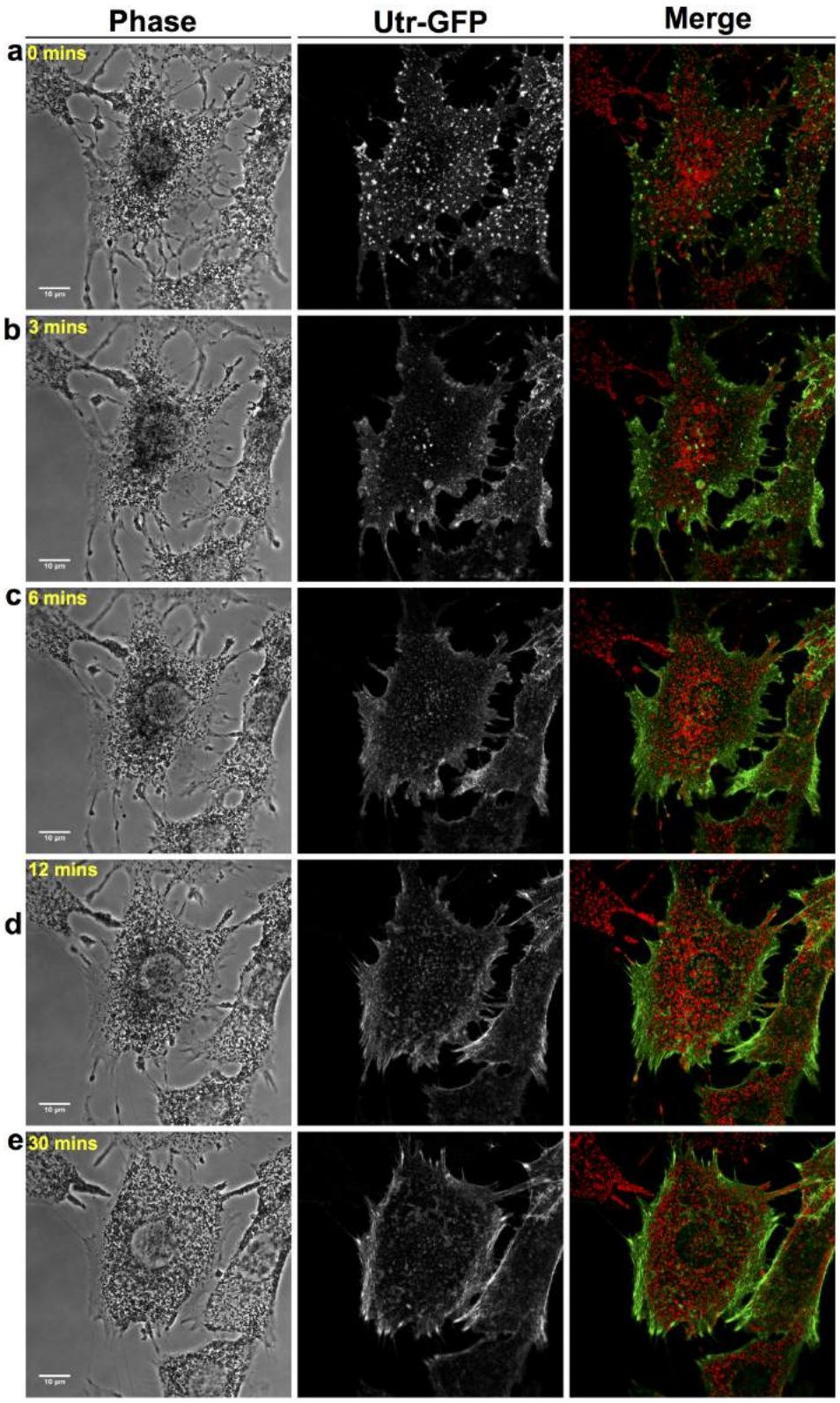


Figure 4.23 - Monitoring CytD washout live shows cortical actin recovers within 3-6 minutes whilst melanosomes re-disperse within 30 minutes. Melan-a cells, transfected 24 earlier with utrophin-GFP adenovirus, were treated with 5μM CytD in complete RPMI-1640 media for 1 hour. Subsequently the chip was transferred to a CYTOO chamber, placed on the microscope stage, and the cells incubated with 5μM CytD in L-15 media for 10 minutes to allow the chamber to equilibrate with the stage in order to minimise thermal drift. Cells were then continuously perfused with 0.1% DMSO in L-15 media to washout CytD, whilst being imaged live. **a** = 0 mins; **b** = 3 mins; **c** = 6 mins; **d** = 12 mins; **e** = 30 mins. Actin asters disappear within the first 3 minutes after initial perfusion, and after 6 minutes cortical F-actin has almost completely reformed. Melanosomes appear to have completely redispersed after 30 minutes.

4.3.8 Microtubules are required for retrograde melanosome transport

The results from the rescue assays given in sections 4.3.1, 4.3.2 and 4.3.4 all indicate that microtubules do not play a significant role in anterograde melanosome transport. Meanwhile, perturbing the actin cytoskeleton, as detailed in sections 3.3.7, 3.3.8, 3.3.9, 3.3.10, 4.3.6 and 4.3.7 always results in robust clustering of the pigment granules around the perinuclear area, suggesting a retrograde force dominates in these conditions. Since several reports from the literature suggest that cytoplasmic dynein plays a key role in the retrograde transport of melanosomes, as well as many other organelles (Rogers et al., 1997; Byers et al., 2000; Vancoillie et al., 2000; Firestone et al., 2012; Ohbayashi et al., 2012), it was of interest to test this assertion.

Cilliobrevins are a group of small molecules based around benzoyl dihydroquinazolinone which have been shown to inhibit the motor domain of cytoplasmic dynein (Firestone et al., 2012). These compounds were first discovered via a high-throughput screen to find inhibitors of the Hedgehog signaling pathway, whereby it was noticed that some of these compounds reduced the size and number of primary cillia. It was also found that accumulation of a transcription factor, Gli2, which normally localises at the tips of cilia when the Hedgehog pathway is activated, is increased upon treatment with ciliobrevin compounds; indicating it may affect intraflagellar transport. To test this, *Xenopus* melanophores whose melanosomes were initially dispersed were incubated with different ciliobrevin analogues and then treated with melatonin to drive melanosome clustering. The results showed that ciliobrevin D (CB-D) most effectively blocked the retrograde transport of melanosomes in a dose-dependent (and reversible) manner - further suggesting this drug functions to inhibit cytoplasmic dynein. This was then further confirmed through the use of *in vitro* assays, whereby the gliding velocity of microtubules powered by dynein was greatly diminished in the presence of CB-D, compared to the DMSO control.

Firestone et al. then sought to determine the mechanism through which (CB-D) inhibits dynein function. Co-localisation experiments initially demonstrated that the targeting of both dynein and dynactin to structures such as the kinetochore was normal in both the presence and absence of CB-D and immunofluorescence microscopy further demonstrated that the microtubule network was not disrupted by this drug. Furthermore, co-sedmentation assays revealed that binding between ADP-dynein and microtubules was not weakened in the presence of CB-D, since cytoplasmic dynein was still pulled down with microtubules when

incubated with this drug, even at relatively high concentrations (50μM). However, ciliobrevin D was found to effectively block the ATPase activity of dynein in a dose-dependent manner, suggesting a mechanism for how it blocks retrograde transport.

To test the efficacy of CB-D, melan-a cells that had been transfected with Rab1a-GFP for 48 hours in order to mark the Golgi (whose morphology is known to be dependent on dynein; Yadav et al., 2012) were treated with either 25μM or 50μM (similar to the highest doses used by Firestone et al.) CB-D, 0.1% DMSO (negative control), or 2μM noc for 2 hours (positive control). When cells were treated with 0.1% DMSO for 2 hour, Rab1a-GFP appeared to mark the Golgi which was visible as a ring around the nucleus, but upon treatment with noc this structure appeared to spread out. However, when the cells were treated with either 25μM or 50μM CB-D (Figure 4.24c and d, respectively), Rab1a-GFP remain clustered around the nucleus, similar to the DMSO treatment.

This observation is backed up by the quantification of the dispersion ratio of Rab1a-GFP, which shows that treatment with 2μM noc for 2 hours caused this value to increase by 50% (from 0.4 to 0.6), compared with the DMSO treatment (Figure 4.24e). By contrast, treatment with 25μM or 50μM CB-D for 2 hour did not affect the dispersion ratio, suggesting that CB-D was not effectively inhibiting dynein.

Since no clear conclusions could be drawn regarding the efficacy of CB-D from the application of the drug on melan-a cells at steady state, the ability of CB-D to inhibit retrograde melanosome transport was tested by treating melan-a cells overnight with either 0.1% DMSO, 10nM JK or 10nM JK in the presence of 25μM CB-D (the highest concentration the cells could tolerate for this length of time). As expected, pigment granules in the JK treated cells appeared clustered around the perinuclear area compared with the control cells (Figure 4.25a Vs b). However, CB-D treatment did not prevent the melanosomes from clustering, since pigment granules in these cells were still found to be distributed around the perinuclear area (Figure 4.25c). Quantification of the pigment dispersion ratio further shows that there is no difference in phenotype between cells treated with 10nM JK and those treated with 10nM JK in the presence of 25μM CB-D (Figure 4.25d).

The above results suggested that either CB-D was ineffective at inhibiting dynein, or that another minus-end direct motor protein besides dynein was involved in the retrograde transport of melanosomes. Since several other microtubule-associated minus-end directed motor proteins are known to exist and it was therefore decided to adopt the approach of establishing

if microtubules *per se* were necessary for melanosome clustering. To test this melan-a cells were seeded onto micropattern chips and allowed to spread overnight before being treated with either 0.1% DMSO, or 1μM noc for 1 hour to deploymerise the microtubule network. Subsequently, cells were treated with 10nM JK in the continued presence of either DMSO or 1μM noc for a further 16 hours. For the cells that were pre-treated with DMSO, and therefore had an intact microtubule network, normal clustering of melanosomes was observed (Figure 4.26b). However, when the microtubule network was no longer intact, retrograde transport of melanosomes appeared to be perturbed, since little clustering of the pigment granules was observed (Figure 4.26c). Instead, treatment with both noc and JK induced 'localised clustering' of melanosomes, where pigment granules clump together but are not transported to the perinuclear area. The scatter plot most clearly demonstrates the importance of microtubules on the retrograde transport of melanosome, with cells treated with 0.1% DMSO + 10nM JK having a mean PDR of 11.3μm, whilst cells treated with 1μM noc and 10nM JK had a mean PDR of 17.9μm (Figure 4.26f). The difference between the different phenotypes is also clearly apparent in the pigment probability plot (Figure 4.26c) with the lines corresponding to 10nM JK and 10nM JK + 1μM noc having very different profiles. The pigment probability maps (Figure 4.26b & c) also highlight the differences in melanosome distribution after these treatments, with the map in Figure 4.26b resembling that of a melan-dilute population while the map in Figure 4.26c is similar to a melan-a population.

Overall it is clear from these results that the majority of retrograde melanosome transport is indeed microtubule dependent, as suggested by current literature, although the identity of the motor(s) involved is not clear.

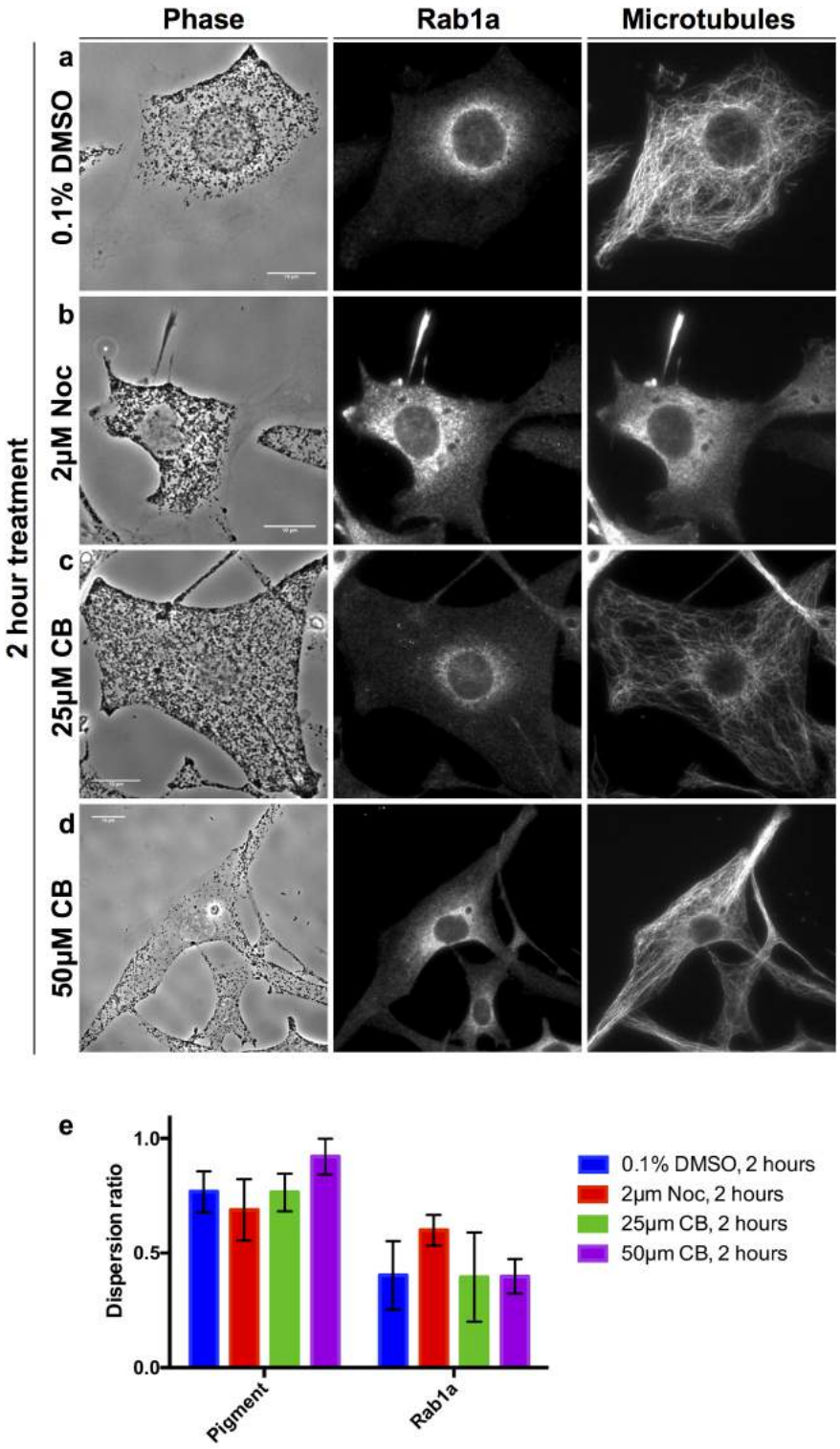


Figure 4.24 - CB-D does not appear to inhibit retrograde organelle transport. Melan-a cells were transfected with Rab1a-GFP 48 hours prior to imaging. Although this protein should mark the Golgi, the staining pattern appears more reminiscent of the ER, an organelle also reliant on dynein and kinesin for its morphology. **(a)** Melan-a cells were treated with 0.1% DMSO for 2 hours. **(b)** Melan-a cells were treated with 2μM noc for 2 hours which caused the ER to disperse compared to the vehicle control. Treatment with either 25μM **(c)** or 50μM **(d)** CB-D did not result in the dispersion of either the melanosomes or the ER. **(e)** Quantification of the dispersion ratio of both melanosomes and Rab1a-GFP shows that neither noc, nor either dose of CB-D tested, had a statistically significant effect compared to DMSO treatment (Kruskal-Wallis one-way analysis of variance test).

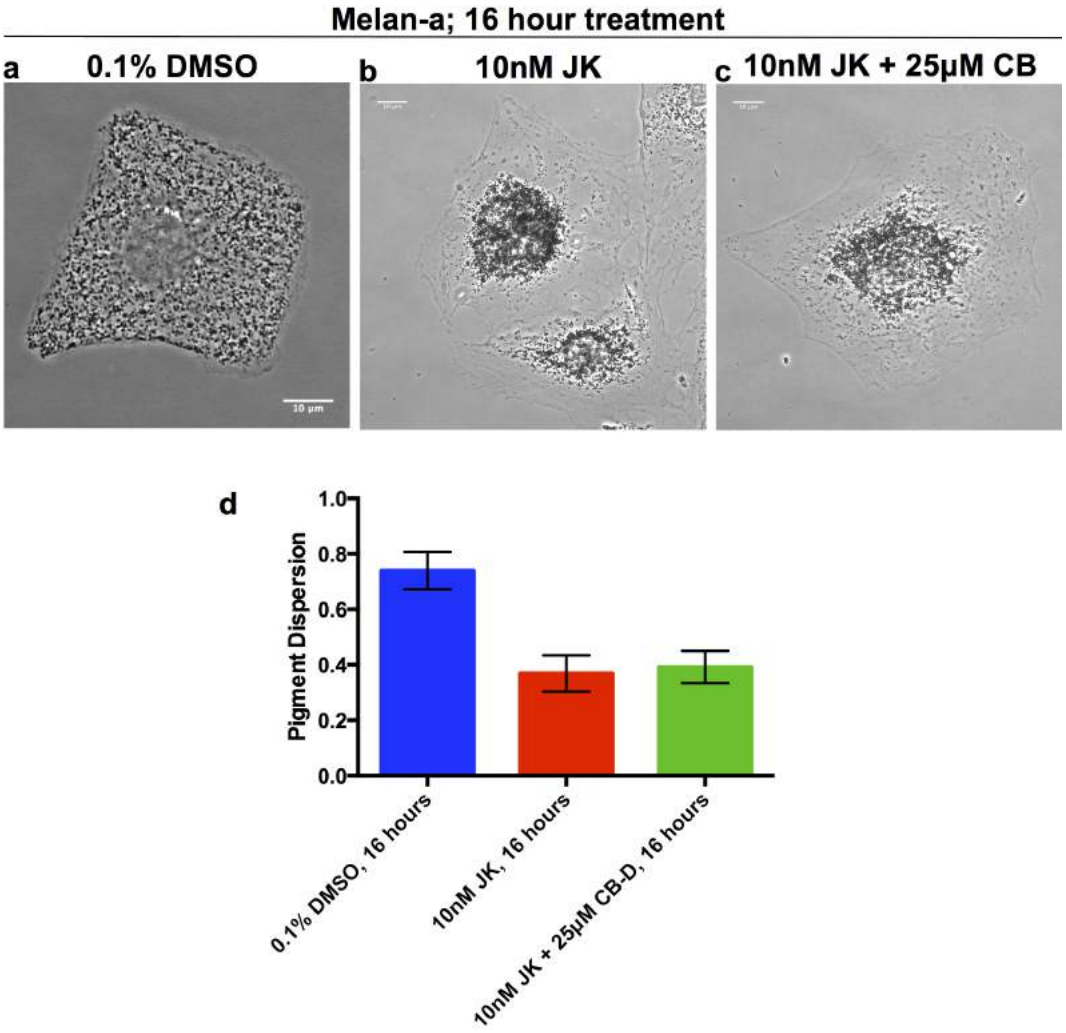


Figure 4.25 - Cilliobrevin D does not inhibit retrograde melanosome transport. **(a)** Melan-a cells treated with 0.1% DMSO for 16 hours. **(b)** Melan-a cells were treated with 10nM JK for 16 hours to induce pigment clustering. **(c)** Melan-a cells were treated with 10nM JK and 25μM CB-D for 16 hours. Clustering of the pigment granules at the cell centre still occurs despite the presence of the dynein inhibitor. **(d)** Quantification of pigment dispersion after treatment outlined in (a), (b) and (c). Pigment dispersion following treatment with 10nM and 25μM CB-D is not significantly different from that following treatment with 10nM JK alone (Kruskal-Wallis one-way analysis of variance test).

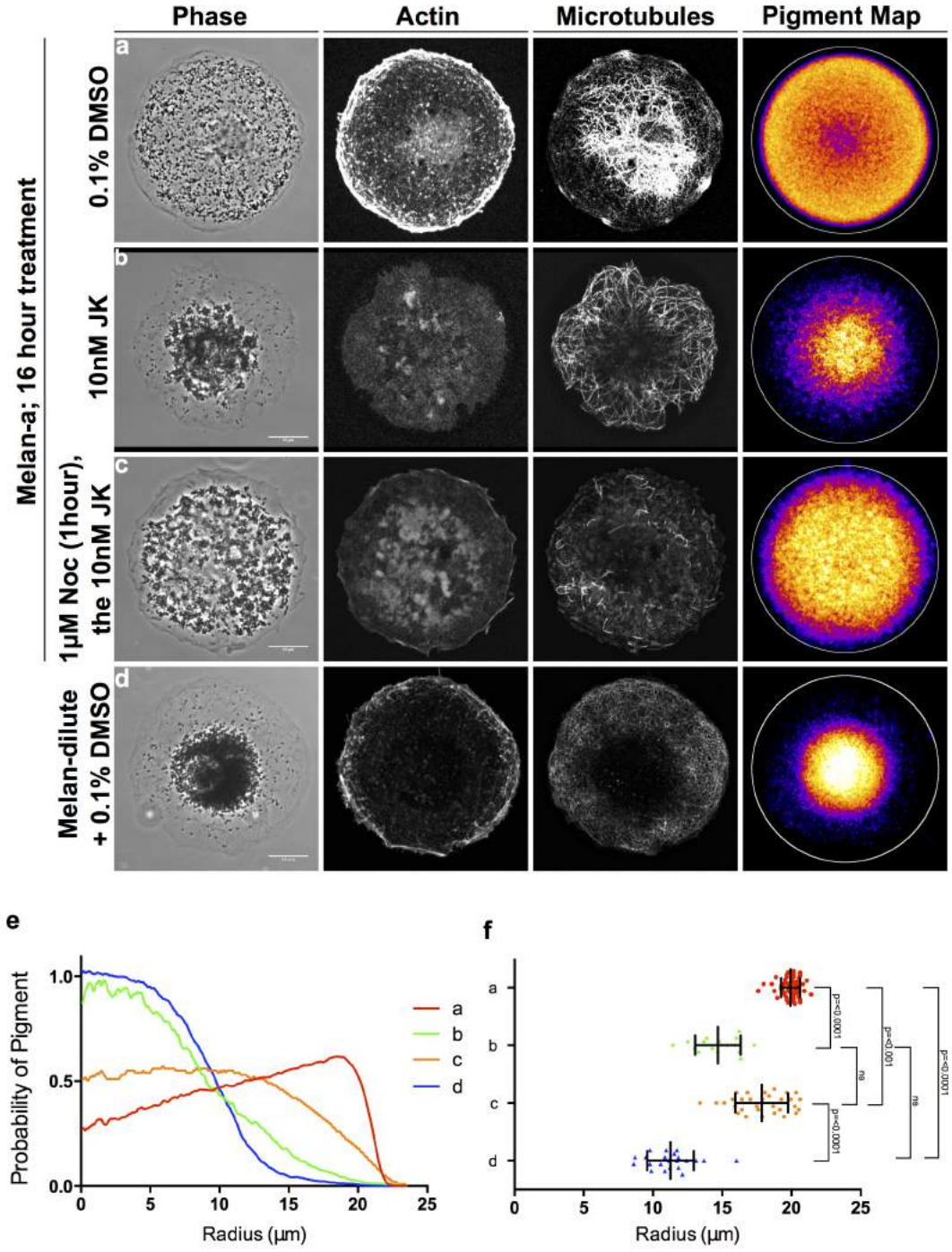


Figure 4.26 - Depolymerising microtubules inhibits retrograde melanosome transport induced by JK. Melan-a cells seeded onto micropattern coverslips to standardise cell size and shape and subsequently treated with either 0.1% DMSO **(a)** or 10nM JK **(b)** for 16 hours. **(c)** Standardised melan-a cells were pre-treated with 1μM noc to depolymerise microtubules and then treated with 25nM LatA for 16 hours. **(d)** Melan-dilute cells seeded onto micro-pattern chips were treated with 0.1% DMSO for 16 hours. **(e)** Line plot showing probability of finding pigment Vs. cell radius with labeling corresponding to treatments outlined in (a-d). a Vs b = -0.325; a Vs c = -0.109; a Vs d = -0.329; b Vs c = 0.806; b Vs d = 0.996; c Vs d = 0.799 (Spearman's rank test). **(f)** Scatter plot showing mean PDR for each cell imaged with labeling corresponding to treatments outlined in (a-d). a Vs b (p=<0.0001); a Vs c (p=0.001); a Vs d (p=0.0001); b Vs c (ns); b Vs d (ns); c Vs d (p=<0.0001). Statistical analysis performed using a Kruskal-Wallis ANOVA test.

4.4 Discussion

4.4.1 Identifying melan-dilute cells expressing GFP-myosin-Va based on their fluorescence intensity

In order to draw meaningful conclusion from add-back experiments where GFP-myosin-Va was transfected into melan-dilute cells to induce melanosome re-dispersion in the presence and absence of cytoskeleton inhibitors, it was crucial to find a robust method for determining which cells were truly expressing fusion protein in order to avoid skewing the results. The most straightforward way to achieve this was by using fluorescence as a marker of transfection. However, since the cells exhibited autofluorescence, especially in the green (488nm) channel, combined with the fact that GFP-myosin-Va was very weakly expressed, this method was ultimately unreliable. When cells were imaged live to try and avoid the autofluorescence caused by the paraformaldehye fixative, known to be responsible for this phenomenon (Clancy and Cauller, 1998), it was still often very difficult to distinguish expressing cells (which had rescued) from non-expressing cells (which remained clustered) based upon fluorescence intensity. Imaging live also reduced the quality of the phase image, which could potentially also skew the melanosome distribution analysis. One solution for avoiding autofluorescence was to use a secondary antibody conjugated to a 568nm Alexa dye in order to probe for the GFP-myosinVa protein. This simple switch from 488nm to 568nm secondary antibodies meant that it was possible to accurately differentiate between melan-dilute cells that were expressing the GFP-myosin-Va construct (whose pigment granules should therefore be dispersed), and cells which had not been transfected (and whose melanosomes should therefore remained clustered). There was a weak positive correlation between the level of fluorescence intensity of GFP-myosin-Va expressing cells and the PDR, suggesting that melanosome transport can occur in the presence of only a relatively small number of myosin-Va molecules (see Figure 7.2).

4.4.2 Noc treating cells has no affect on long-range anterograde melanosome transport

Initial experiments in the previous chapter indicated that a) Kif5B did not appear to play a role in mediating melanosome transport and b) that cells could survive for over 16 hours in the absence of an intact microtubule network, which is similar to previously published results

where cell survival has been examined (Blajeski et al., 2002; Diederich et al., 2012; Frost et al., 2013). Therefore, rather than testing each kinesin isoform individually (e.g. by siRNA-mediated knockdown) to determine if its loss induced clustering in wildtype melanocytes, melanocytes could be treated with noc to test the importance of microtubules (and by implication kinesin) on long-range melanosome transport.

Surprisingly, when clustered melan-leaden cells were transfected with MLPH-GFP melanosomes were still able to fully disperse even in the presence of noc. To ensure that there was no possibility that microtubule-mediated transport was playing a role in the redispersion of these granules, cells were treated with noc 60 minutes prior to infection and the cells incubated with the drug for the entire time course.

This experiment was then repeated using melan-dilute cells to ensure the result was repeatable across multiple cell lines. Cells were also plated onto micropattern chips to standardise their size and shape so that the affect of depolymersing the microtubule network on anterograde melanosome transport could be more precisely quantified. In direct contrast to the predictions of the cooperative capture model, melanosome transport was found to actually be slightly enhanced by noc treatment, although this was not statistically significant. These add-back experiments therefore provide clear evidence that kinesin is not absolutely required for the anterograde transport of pigment granules, and instead imply that myosin-Va must be capable of driving long-range transport.

However, it should be emphasised that a small population of microtubules could be detected by antibody labelling in some cells following noc treatment. This is likely due to post-translational modifications, such as glutamylation or acetylation which cause microtubules to become insensitive to noc treatment (Palazzo et al., 2003; Wloga et al., 2010). Therefore, should these experiments be repeated cells should be subjected to cold plus noc treatments to ensure all microtubules are depolymerised (Schliwa and Euteneuer, 1978). It should, however, also be noted that the regime of 1μM noc treatment for 60 minutes as used in this study did block minus-end directed melanosome transport (as discussed further in section 4.4.6), suggesting this treatment is sufficient to functionally inhibit microtubule to a large extent.

4.4.3 A dynamic actin cytoskeleton is crucial for anterograde melanosome transport

From the initial optimisation experiments described in the previous chapter using wild-type melanocytes at steady-state, a dynamic actin cytoskeleton appeared to be vital in order to maintain peripherally dispersed melanosomes. To further test the importance of a dynamic actin cytoskeleton on the anterograde transport of melanosomes, melan-dilute cells were treated with JK and subsequently transfected with GFP-myosin-Va. Melanosomes failed to redisperse in the JK condition, indicating that actin dynamics may play a crucial role in anterograde pigment granule transport. Likewise, treatment with LatA prior to transfection with myosin-Va also inhibited anterograde melanosome transport in melan-dilute cells. Taken together, these results strongly suggest that the rapid turnover of some actin structures is required for pigment granule transport. This is exemplified by the fact that low nanomolar doses of LatA also inhibit anterograde melanosome transport. At these very low concentrations, this drug is likely to specifically target only the most dynamic actin structures, since these would use relatively large amounts of G-actin compared to more stable F-actin structures over the same time period.

The fact that either stabilising actin through treatment with JK, or inhibiting the turnover of dynamic actin with LatA almost completely inhibits anterograde melanosome transport suggests that myosin-Va is not simply trafficking melanosomes along very long actin filaments, similar to how kinesin translocates along microtubules, but rather that the motor utilises many actin tracks which are constantly being reorganised in order to allow trafficking of melanosomes from the cell centre to the periphery. Why such dynamic rearrangement of the actin cytoskeleton is necessary for melanosome transport is an intriguing question. It is very likely that the complex meshwork of actin filaments sterically hinder these large organelles, which are often up to 500nm in diameter (Hume et al., 2002). Therefore, one hypothesis to explain why inhibiting actin turnover blocks melanosome transport is that the actin meshwork must constantly be remodeled in order to allow the melanosomes to more easily pass through.

However, if this is the case, it could also be argued that a static actin meshwork should likewise block minus-end directed transport - a process which is clearly uninhibited by treatment with JK or LatA. One possible reason why this is not the case may be due to the difference in stall force between the two motor proteins, with the value for myosin-Va being much smaller

(1.5-3pN; Ali et al. 2011) compared with dynein (7pN; Gennerich et al. 2007), if dynein is indeed involved in retrograde melanosome transport.

4.4.4 F-actin predominantly regrows from the plasma membrane after CytD treatment and is concomitant with melanosome redispersion

Treatment with 5μM CytD induced the formation of actin asters in melanocytes - an event which was found to be reversible if the drug was washed out. This allowed the possibility to monitor the regrowth of actin to attempt to elucidate a mechanism for how anterograde melanosome transport is achieved. Subsequent to manual CytD washout, the actin asters distributed throughout the cytoplasm appeared to become depolymerised over the course of approximately 45 minutes, which coincided with the reformation of cortical actin. As both the cortical and mesh actin reformed, the melanosomes began to redisperse towards plasma membrane, strongly suggesting that a normal actin cytoskeleton is necessary for long-range anterograde melanosomes transport.

The results from the manual CytD washout from wildtype melanocytes were mirrored to a large extent by the live cell washout experiment using a perfusion chamber. Here, although the actin recovered much more quickly, most likely due to the drug being washout out more effectively by the perfusion system, the same pattern is observed, with cortical actin recovering first, followed by cytoplasmic mesh actin. It was also observed that along with the actin recovering more quickly, the melanosomes redisperse more quickly too; thus providing further evidence that melanosome redispersion relies on the integrity of the actin cytoskeleton.

When the CytD washout experiment was carried out in melan-dilute cells the amount of time required for actin regrowth to occur appeared to decrease compared with the melan-a cells, with an almost continuous band of cortical actin reforming after just 20 minutes. However, when melan-leaden cells were used for the CytD washout time-course the results were very similar to those of the melan-a cells (manual washout), with cortical actin beginning to reform after approximately 60 minutes.

The difference in actin regrowth kinetics between melan-a, melan-dilute and melan-leaden cells appear to suggest that myosin-Va retards the regrowth of actin, since it is only melan-dilute cells which have a fast rate of actin reformation. *In vitro* evidence does suggest that

myosin-V is capable of depolymerising actin filaments when it is present at high enough concentrations (Ishikawa et al., 2003), indicating it is possible that this motor may work in opposition to actin polymerising factors such as formin and Arp2/3, which are known to be involved in the formation of the actin cortex (Bovellan et al., 2014).

4.4.5 Investigating long-range melanosome transport using activatable motors shows Kif5B is inefficient at translocating this cargo

While the add-back experiments involving noc treatment are useful for demonstrating that microtubules are not important for anterograde melanosome transport, it is entirely possible that microtubule are used for transporting these organelles when the network is intact. In order to test this, melan-dilute cells were transfected with an activatable version of Kif5B whereby the motor domain can be forced to dimerise with myosin-Va tail through the addition of A/C heterodimeriser. This system has been used previously in the literature to probe the role of motor proteins in the transport of organelles such as peroxisomes (Kapitein et al., 2010).

The Kif5B motor domain was rapidly recruited to the melanosome membrane, but after 60 minutes, the bulk pigment remained located in the perinuclear area, whilst a small number of melanosomes were transported along microtubules by Kif5B and accumulated in the dendritic tips of the melan-dilute cells. Repeating this experiment in the presence of noc resulted in the recruitment of diffuse Kif5B motor to the melanosome membrane (presumably due to a lack of microtubules to which the motor head could bind), thus demonstrating the FKBP/FRB dimerisation system was effective at inducing the binding of two proteins. By contrast, when the myosin-Va motor domain was forced to bind myosin-Va tail all the melanosomes were gradually redispersed from the perinuclear area to the cell periphery after approximately 60 minutes.

It was observed that even prior to the the addition of A/C heterodimeriser, the myosin-Va motor construct was detected at the cell periphery. This could be taken as evidence that the cooperative capture model, which predicts myosin-Va should localise to the cell periphery where it acts as a melanosome tether, is correct. However, it is more likely that a fraction of the total myosin-Va motor pool is simply binding to an actin-rich area of the cells, especially given that when this experiment was repeated in the presence of noc, melanosomes still

dispersed to the same extent, and over a very similar timescale (Evans et al., 2014).

Overall, these experiments demonstrate that Kif5B is actually incapable of transporting the bulk population of melanosomes. According to the cooperative capture model, active kinesin should have transferred the pigment granules from the perinuclear area and onto microtubules, but this was not observed. These experiments also showed that myosin-Va is capable of transporting the melanosomes from the perinuclear area to the periphery in just 60 minutes - a very similar timescale to that required for clustered melanosomes in melanophores to completely disperse following treatment with αMSH in the presence of noc.

4.4.6 Microtubules are required for minus-end directed melanosome transport

There is evidence in the literature which suggests that dynein is crucial for minus-end directed melanosome transport (Nilsson and Wallin, 1997; Byers et al., 2000; Vancoillie et al., 2000a; Reilein et al., 2003). The evidence presented in this study also indicates that the microtubule network plays a vital role in allowing melanosomes to cluster, since destroying this network prior to inducing pigment clustering effectively prevented retrograde melanosome transport.

However, there is a growing pool of evidence to suggest that minus-end directed kinesin motors, of which KIFC3 is the best studied, also play a significant role in retrograde cargo trafficking. One study showed KIFC3 to be involved in maintaining the perinuclear localisation of the Golgi complex, a process normally thought to be carried out by dynein (Harada et al., 1998), when cells were deprived of cholesterol (Xu et al., 2002). There is evidence that cholesterol is required to link dynein to the membranes of late endosomes, since when it binds ORP1L, this protein is able to stabilise the dynein-HOPS-RILP-Rab7 complex which tethers the minus-end directed motor to the membrane (van der Kant et al., 2013). It is therefore possible that when cholesterol levels are reduced, KIFC3 compensates for the loss of dynein on the Golgi membrane and becomes the dominant minus-end directed motor.

KIFC3 has also been identified as a peroxisome-associated protein (Dietrich et al., 2013), although in this case it is thought to inhibit dynein-mediated peroxisome transport, rather than facilitate retrograde transport. Nevertheless, since several other isoforms of minus-end directed kinesins are known to exist (Hirokawa et al., 2009), and since KIFC3 was found

to be overexpressed in melanocytes compared to NIH3T3 cells in this study (see section 3.3.4) it would be important to test their involvement in retrograde melanosome transport in future studies. For example, LatA or JK treatment of cells pretreated with either siRNA against minus-end direct KIFs or NT siRNA could demonstrate if these motors are involved in retrograde melanosome transport.

4.4.7 Summary

Building upon the results of the previous chapter, evidence presented here demonstrates that a dynamic actin cytoskeleton, rather than a microtubule network, is crucial for long-range anterograde melanosome transport. Partially depleting the actin cytoskeleton with nanomolar doses of LatA, or inhibiting actin turnover with JK prevented melanosomes for dispersing, whilst depleting the microtubule network with noc had no effect on the anterograde trafficking of the pigment granules. Furthermore, when Kif5B was forcibly recruited to the melanosome membrane using the FKBP-FRB inducible dimerisation system it resulted in an unusual phenotype whereby only a small fraction of total pigment granules were trafficked to the dendritic tips, while the bulk pigment remained clustered.

However, microtubules were found to be necessary for retrograde melanosome transport, since no clustering was observed when wildtype cells were treated with noc, followed by JK to induce pigment granule aggregation. This finding, along with the fact that melanosome transport actually appears slightly enhanced in the absence of microtubules suggest that myosin-Va and microtubule-associated retrograde motors oppose one another, rather than cooperate to mediate melanosome transport. This is summarised in Figure 4.27.

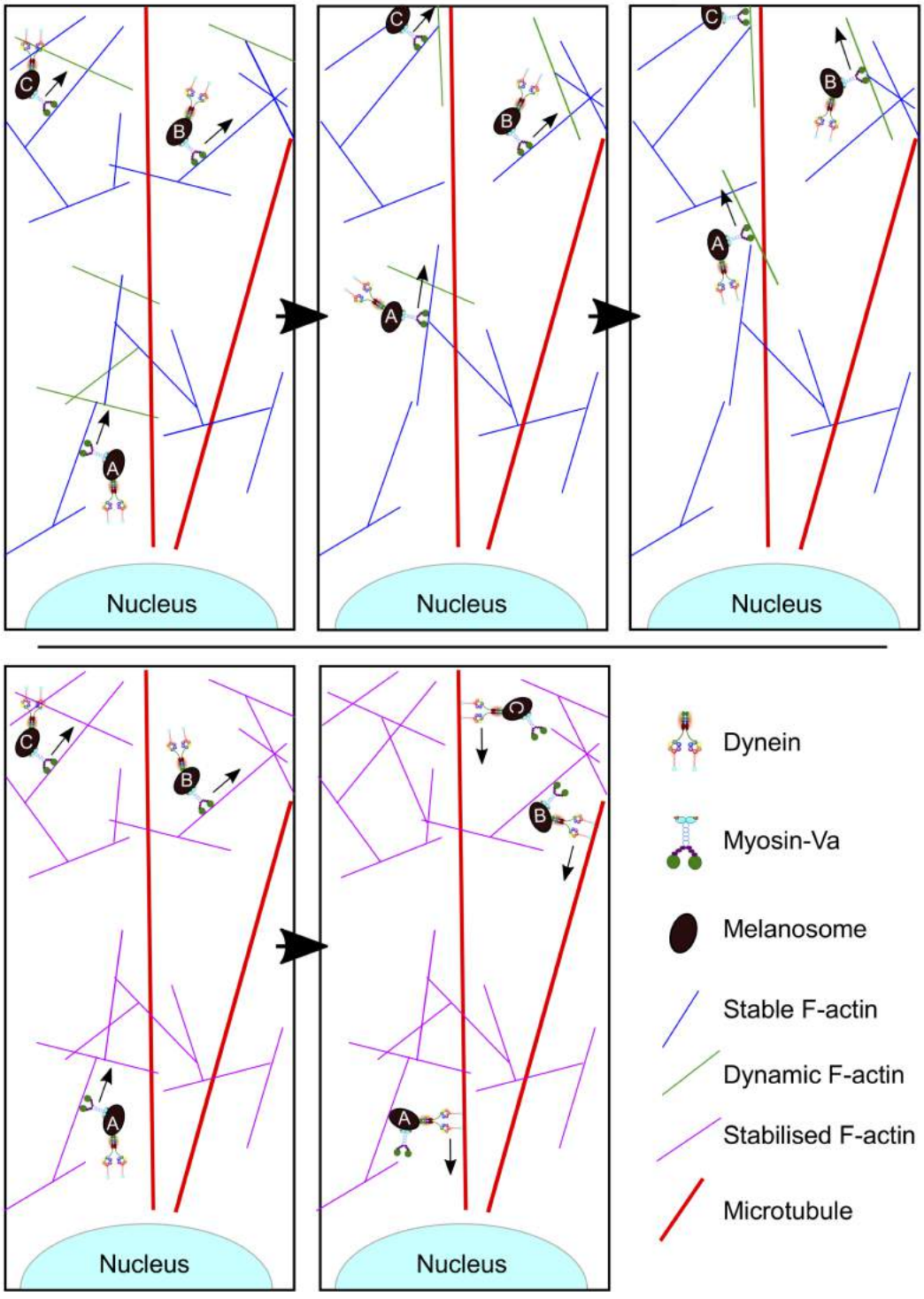


Figure 4.27 - Dynamic actin is required to oppose minus-end directed microtubule-dependent melanosome transport. (Upper panels) Melanocytes contains a large number of stable actin filaments which have a slow turnover rate, and a small number of dynamic filaments with a much faster turnover rate. It is hypothesised here that dynamic F-actin is necessary for myosin-Va to overcome roadblocks and also facilitates track switching. **(Lower panels)** When dynamic actin filaments are either stabilised (i.e. by JK treatment) or removed (i.e. by LatA treatment) myosin-Va can no longer overcome roadblocks. Therefore, minus-end directed motors, such as dynein, are utilised to backtrack the melanosomes which over time leads to these organelles clustering around the perinuclear area in a microtubule-dependent manner.

Chapter 5

Several actin-binding proteins play a role in melanosome transport

5.1 Introduction

Results from the previous chapter demonstrated that dynamic actin is crucial for the long-range anterograde transport of melanosomes whilst only retrograde transport appears microtubule-dependent. Since actin dynamics are governed by a large number of proteins, it is likely that a subset of these play a role in melanosome transport.

There is already some evidence to suggest that actin-binding proteins do indeed play a role in organelle and vesicle trafficking. For example, Pfender et al. demonstrated that the F-actin nucleators spire1 and spire2 cooperate to drive the position of the spindle pole during meiosis in mouse oocytes, since transport was inhibited in cells treated with RNAi against these proteins. This resulted in oocytes that were unable to asymmetrically divide - a crucial event since defects in this process cause polyploid embryos and pregnancy loss. Furthermore, fluorescence microscopy showed that formin-2 (Fmn2) colocalised with spire1/2, and that Fmn2$^{-/-}$ mice also suffered from polyploid embryos and pregnancy loss characteristic of failed oocytes division (Pfender et al., 2011a).

Fmn2 and spire1/2 have also been implicated in the transport of Rab11a/transferrin positive vesicle in mouse oocytes. Again, cells treated with RNAi against spire1/2 exhibited transport defects compared to control cells, as did oocytes taken from Fmn2$^{-/-}$ mice. Microscopy data showed that these actin nucleators were present both at the plasma membrane, as well as colocalsied to the Rab11a/transferrin vesicles. These findings led to the hypothesis that spire/formin generate short, randomly polarised actin cables through which vesicles are connected in a global mesh. Meanwhile, myosin motors translocating along linear actin cables generated by spire/formin located at the plasma membrane are thought to constantly pull the mesh, and therefore the vesicles, towards the cell periphery. In this way, even randomly polarised actin can support the directed movement of vesicles towards the plasma membrane (Schuh, 2011).

While the Arp2/3 complex is well known to control cell shape and migration, Zhou et al. have also recently described a role for Arp2/3 in the trafficking of vesicles in intestinal epithelial cells. Specifically, ARPC3, which is required for activation of the Arp2/3 complex via NPFs (Gournier et al., 2001), resulted in defects in the distribution of the retromer complex and also inhibited the internalisation of CD36 positive structures (Zhou et al., 2015).

Since melanosomes are visible using brightfield microscopy, this allowed the possibility

to conduct a semi-high throughput screen to test if any known actin-binding proteins caused defects in organelle trafficking in these cells. To this end, 122 siRNA targets were generated and subsequently transfected into wildtype melanocytes in order to determine which, if any, actin-binding proteins are responsible for maintaining peripherally dispersed melanosomes.

5.2 Aims

The results of this study have so far implicated a dynamic subpopulation of F-actin and myosin-Va, rather than microtubules and kinesin, as playing the dominant role in the long-range anterograde trafficking of melanosomes in murine melanocytes. Since the actin cytoskeleton is modified by a large number of different proteins, the aim of the next set of experiments was to elucidate potential molecular mechanisms governing long-range myosin-Va-dependent organelle trafficking.

5.3 Results

5.3.1 An siRNA screen revealed several actin-binding proteins are important for maintaining peripherally dispersed melanosomes

To attempt to identify potential molecular players that are important for maintaining the steady state distribution of melanosomes in melan-a cells, an siRNA knockdown screen was carried out. It was reasoned that, as with the drug treatments, knocking down any proteins that have a role in regulating the anterograde trafficking of melanosomes should result in a clustering phenotype, as retrograde forces would be allowed to dominate. The siRNA screen targeted well know actin-binding proteins, such as members of the formin and spire families and their molecular regulators such as RhoGTPases, the constituents of the Arp2/3 complex and actin severing proteins such as cofilin. The screen also included a number of targets which were found to bind Rab27a in a previous study (Booth, 2012), and therefore could potentially be involved in melanosome transport (see Table 7.2 for a full list of proteins knocked down along with the siRNA sequences used).

Of the 122 genes screened, 4 candidates genes were identified where transfecting melan-a cells with the corresponding siRNA repeatedly led to melanosome clustering. These genes were ACTG1, encoding γ_{cyto}-actin (hereafter referred to as γ-actin); APRC1B, encoding Actin Related Protein 2/3 Complex, Subunit 1B; FMN1, encoding formin-1 and CFL1, encoding cofilin-1 (Figure 5.1).

The initial siRNA screen utilised a pool of 4 different oligonucleotide sequences per target. Therefore to test the specificity of the knockdown and ensure there was minimal chance that the observed clustering was caused by off-target effects, wildtype melanocytes were transfected with the individual oligonucleotides targeting ACTG1, ARPC1B, CFL1 and FMN1 to check this still resulted in melanosome clustering. Three separate dishes of melanocytes were transfected with each oligonucleotide sequence (see section 2.1.5.2 for methods) and three fields of cells from each dish imaged (Figure 5.2a-f shows example fields for each oligonucleotide). Melanocytes from these images were then manually scored as being either 'clustered' (fully resembling the *dilute* phenotype), 'dispersed' (fully resembling the wildtype phenotype) or 'intermediate phenotype' (cells contained both dispersed and clustered melanocytes) (Figure 5.2g-k).

The results of this analysis indicated that of the 4 genes tested, silencing the FMN1

gene most effectively induced melanosome clustering, since each individual oligonucleotide tested lead to 20-30% clustered cells and 40% cells of 'intermediate phenotype'. Silencing the ARPC1B gene produced the next greatest effect, although in this case only 30% of cells were of intermediate phenotype, whilst very few appeared completely clustered. Knockdown of cofilin-1 and γ-actin with the individual oligonucleotides produced the weakest effect, with only 2 of the 4 oligonucleotides targeting cofilin-1 producing any effect (intermediate phenotype only) whilst 3 of the 4 oligonucleotides targeting γ-actin caused between 20 and 60% of cells to adopt an intermediate phenotype.

To further confirm that the resulting phenotype observed after knockdown of either FMN1, APRC1B, CFL1 or ACTG1 genes was due to silencing of the gene, rather than an off-target effect, melanocytes were transfected with the most effective single oligonucleotide from the previous experiment (FMN1 oligo #1; ARPC1B oligo #2; CFL1 oligo #2; ACTG1 oligo #1) and qRT-PCR performed on the extracted mRNA (see section 2.2.6 for methods). After double normalising the data firstly to levels of GAPDH expression and secondly to the levels of the gene of interest in the non-targeting siRNA control, it was found that levels of the 4 target genes were decreased by 75% (FMN1), 93% (ARPC1B) and 84% (CFL1 and ACTG1) after siRNA transfection (Figure 5.3a-d). However, these results also appear to show that the knockdown of one gene can cause an increase in the expression levels of another. For example, knockdown of FMN1 seemed to result in an increase in APRC1B, whilst knockdown of CFL1 caused a rise in ACTG1 expression levels. The levels of GAPDH in each of the knockdowns appeared to be variable (Figure 5.3e) which will have impacted on the quantification since these values are used for the first round of data normalisation. As with the RT-PCR performed in chapter 3, it would therefore be beneficial to find a different gene than GAPDH with which to normalise the data, should these experiment be repeated.

Whilst qRT-PCR data indicates that the siRNA oligonucleotides are affecting the levels of the corresponding mRNA, it cannot show if there is also a change at the protein level. Therefore in order to verify that siRNA transfection also depletes cells of the corresponding protein, western blotting was used to detect protein levels in the the lystate of cells transfected with either targeting or non-targeting siRNA. Western blotting was initially used to detect levels of formin-1, since FMN1 oligonucleotides produced the greatest effect in terms of melanosome clustering. However, when the formin-1 antibody was tested on the lysate from untransfected wildtype melanocytes, no band corresponding to this protein was detected

(Figure 5.4a).

To test the efficacy of the formin-1 antibody further, HEK293A cells (chosen because they are well known to express high levels of exogenous protein) were either mock transfected, or transfected with either empty GFP vector or a formin-1-GFP (isoform 1B) construct for 72 hours and the cell lysate used for western blotting (Figure 5.4a). A band of approximately 100 kDa was detected in the lysate of mock transfected HEK293A (which is of lower molecular weight than expected for full-length formin-1, but may correspond to an alternative splice isoform), as well as a ~200 kDa band in the lystate of HEK293A cells transfected with full-length formin-1-GFP, suggesting the antibody does bind formin-1, but that the concentration of protein is too low in the melan-a cells.

As the formin-1 antibody failed to detect endogenously expressed formin-1 in melanocytes, HEK293A cells expressing formin-1-GFP were instead used as a proxy, since it was reasoned that if the formin-1 siRNA could knockdown the fusion protein, it would also be effective against endogenous protein. Therefore HEK293A cells were initially transiently transfected with formin-1 siRNA oligonucleotides (described in section 2.1.5.2) and then transfected with formin-1-GFP plasmid 24 hours later (described in section 2.1.5.1). 96 hours after plasmid DNA transfection, the cells were harvested and the lysate run on a western blot (Figure 5.4b). The results indicated that oligonucleotides #1 and #2 are most effective at knocking down the protein (Figure 5.4c), which is in keeping with the results shown in Figure 5.2, where these two oligonucleotides led to a higher percentage of fully clustered melanocytes. With FMN1 oligonucleotides #3 and #4 around 40% of the formin-1 protein remained compared with levels in the non-targeting control cells, whereas only 10% of protein remained after treatment with oligonucleotides #1 and #2.

Since the Arpc1b oligonucleotides produced the next greatest effect in terms of melanosome clustering (Figure 5.2h), HEK293A cells were transiently transfected with Aprc1b-GFP, and 24 hours later transfected with ARPC1B siRNA. As with the previous experiment, cells were again left for 96 hours before harvesting and performing a western blot on the cell lysate. The blot showed that oligonucleotide sequence #1 was most effective, knocking down almost 100% of Arpc1b compared with the non-targeting control (Figure 5.4d & e). Oligonucleotide #2 reduced the level of protein by approximately 60%, but oligonucleotides #3 and #4 were not effective, with protein levels actually increasing above those found in the control cells. This result was unexpected, since oligonucleotide sequences #3 and #4 led to similar

levels of partially clustered melanocytes as oligonucleotides #1 and #2 (Figure 5.2). However, the bands in Figure 5.4d are very faint, which may impact on the quantification. It would therefore be necessary to perform these experiments several more times so a mean relative expression value after siRNA treatment can be calculated.

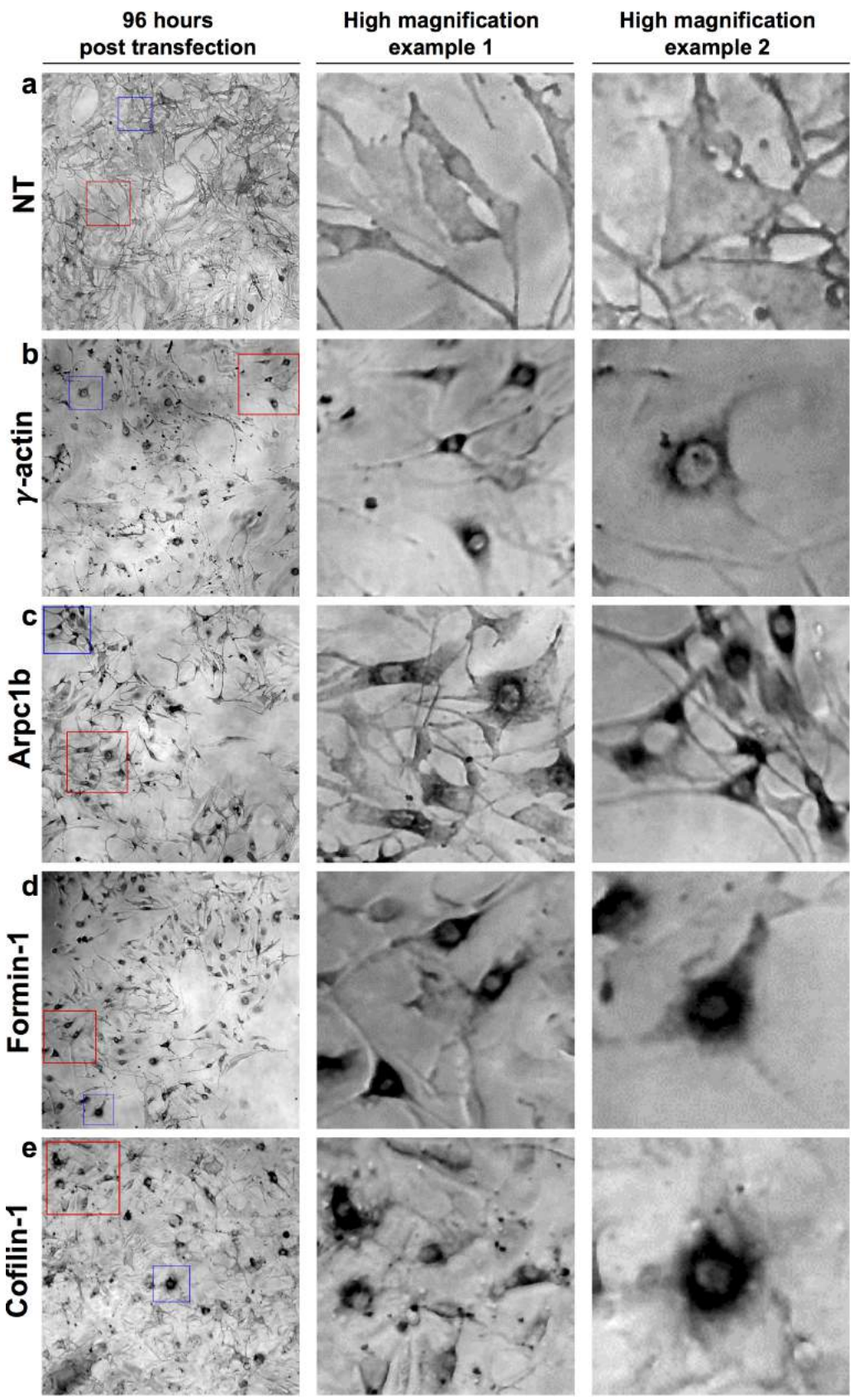


Figure 5.1 - An siRNA knockdown screen revealed several actin-binding protein are important for maintaining peripherally dispersed melanosomes. Wildtype melanocytes were transfected with either control siRNA **(a)** or with a pool of 4 oligonucleotides designed to specifically knockdown either γ-actin **(b)**, Arpc1b **(c)**, formin-1 **(d)** or cofilin-1 **(e)**. Melanocytes were then left for 96 hours prior to imaging. Melanosomes remained dispersed after transfection with control siRNA, but in all other cases the majority of cells exhibited a clustered phenotype which mimics the melan-dilute cells. Red squares correspond to high magnification example 1; blue squares correspond to high magnification example 2.

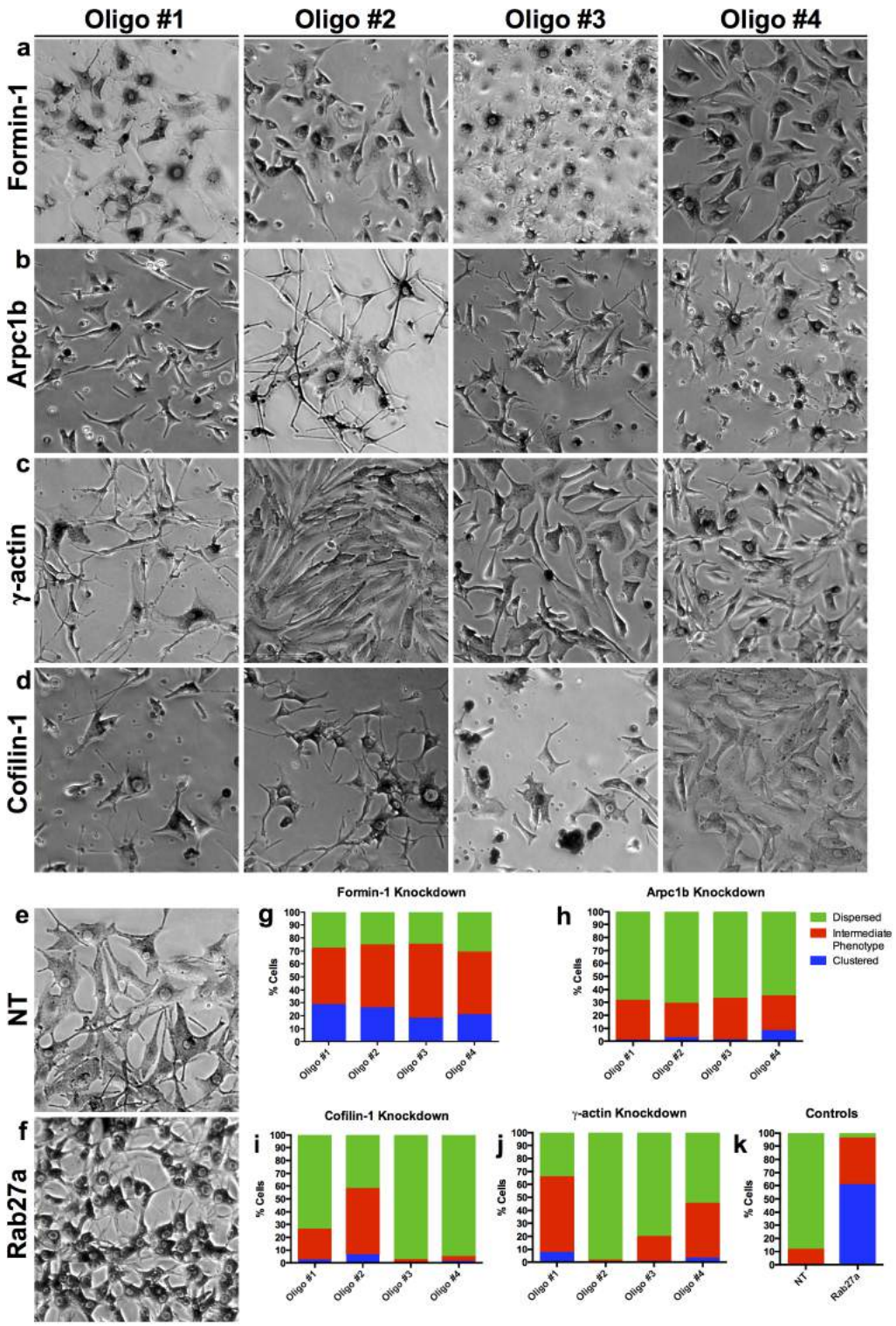


Figure 5.2 - Transfecting melanocytes with individual, rather than pooled, oligonucleotides targeting γ-actin, formin-1, Arpc1b and cofilin-1 resulted in different levels of melanosome clustering. (a-f) Wildtype melanocytes were transfected with the individual oligonucleotides making up the siRNA pool that cells were transfected with in Figure 5.1 and left for 96 hours prior to imaging. **(g-k)** Quantification of the images shown in a-f. Melanocytes were transfected in triplicate and three fields of cells for each transfection were imaged and subsequently scored based on the number of cells exhibiting either a fully clustered, fully dispersed, or intermediate phenotype (whereby approximately 50% of melanosomes were clustered whilst the remaining 50% remained dispersed). The number of cells scored are as follows: FMN1 knockdown - oligo#1 = 271; oligo#2 = 258; oligo#3 = 359; oligo#4 = 470. ARPC1b knockdown - oligo#1 = 206; oligo#2 = 245; oligo#3 = 376; oligo#4 = 398. ACTG1 knockdown - oligo#1 = 172; oligo#2 = 1012; oligo#3 = 560; oligo#4 = 755. CFL1 knockdown - oligo#1 = 227; oligo#2 = 277; oligo#3 = 134; oligo#4 = 855. RAB27A knockdown = 520; non-targeting control = 452.

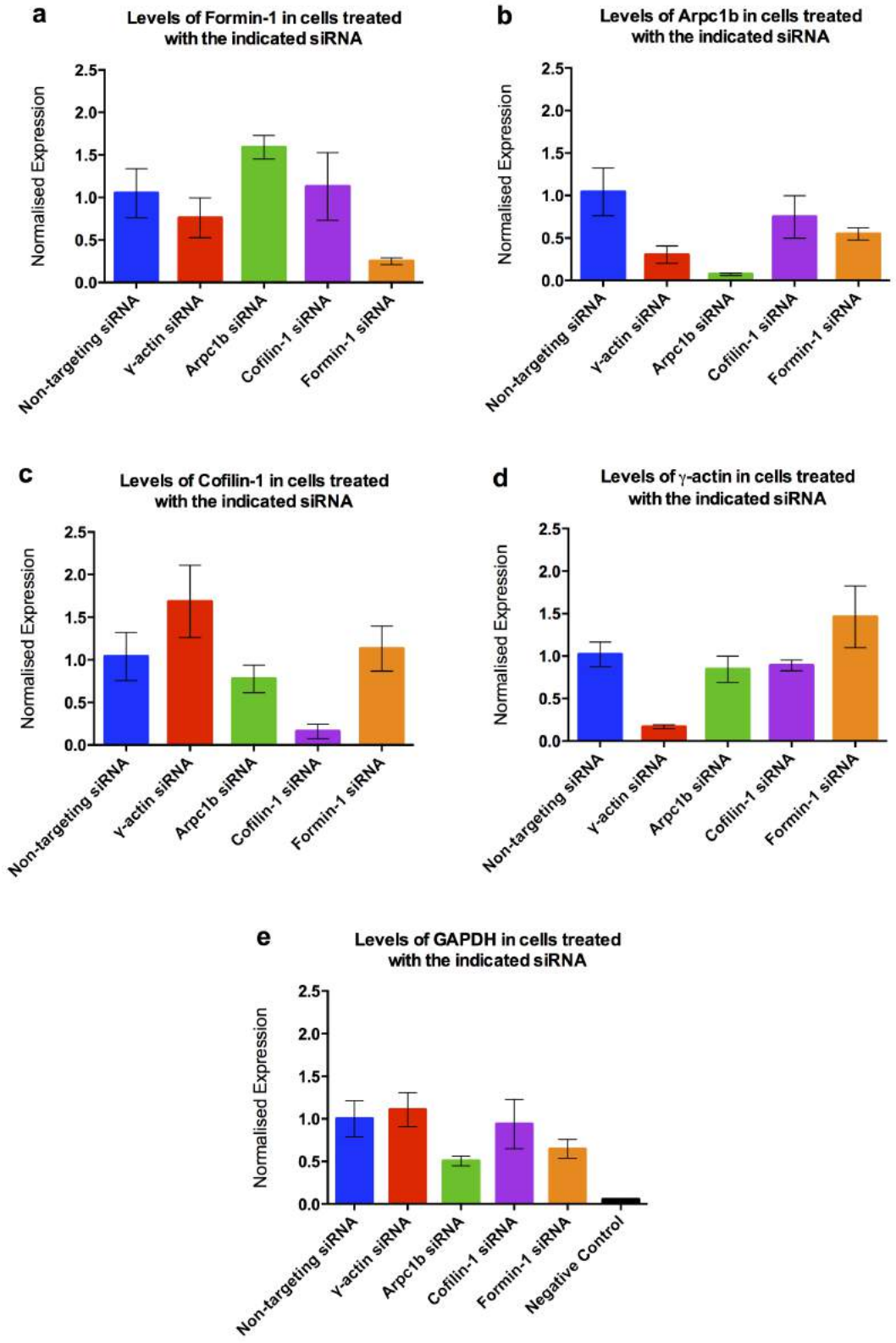


Figure 5.3 - qRT-PCR revealed that the siRNA oligonucleotides used are effective in knocking down their respective mRNA targets. Wildtype melanocytes were transfected with either FMN1 oligo#1; ARPC1B oligo#2; CFL1 oligo#2, ACTG1 oligo#1 or non-targeting siRNA in triplicate, left for 96 hours, and mRNA then prepared as described in sections 2.2.5.1 and 2.2.5.2. qRT-PCR was then performed as described in section 2.2.6. Results were double normalised firstly to GAPDH and then to the non-targeting siRNA, as described in section 2.2.6.

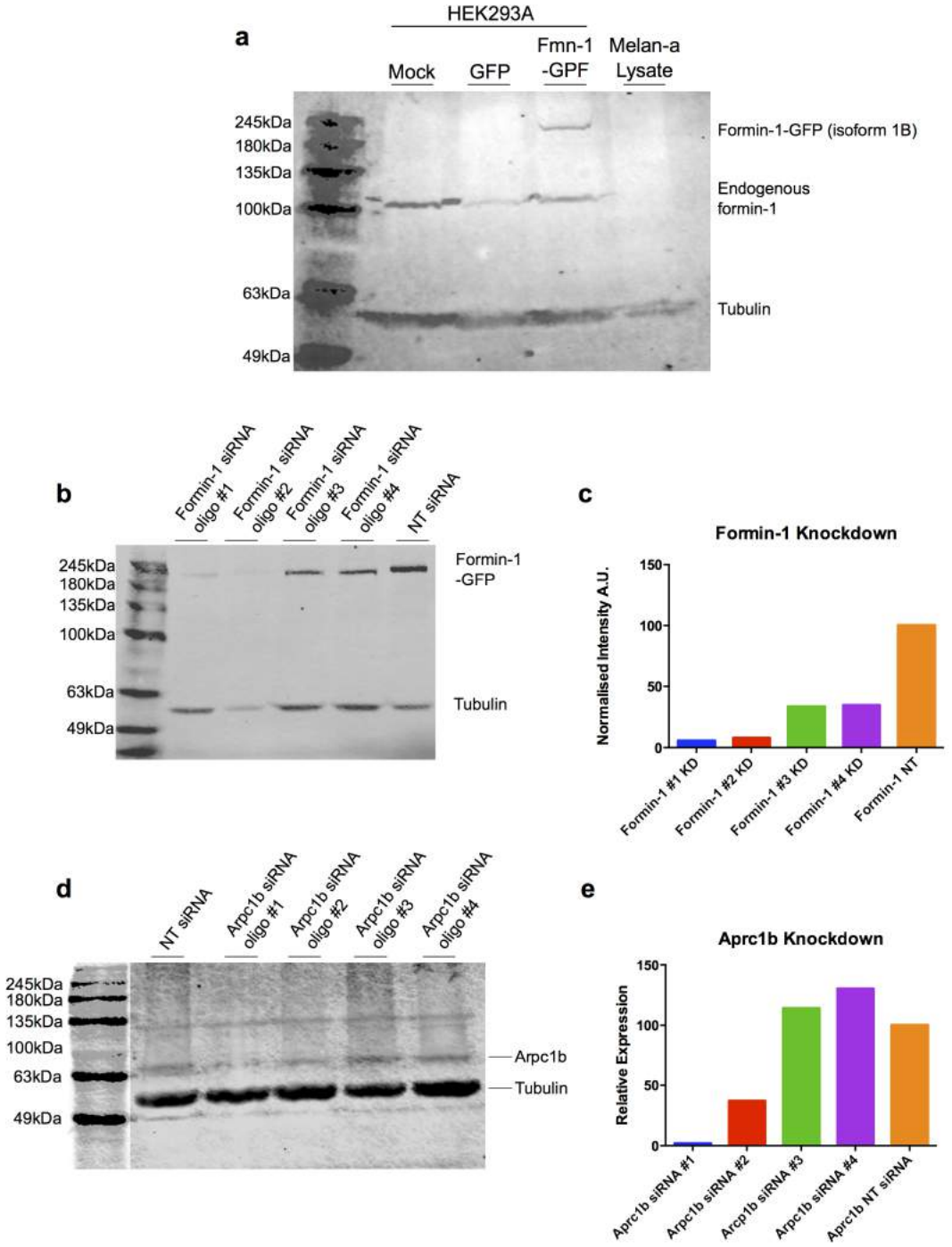


Figure 5.4 - Both formin-1 and Arpc1b are effectively knocked down at the protein level by at least 1 of the 4 oligonucleotides tested. (a) HEK293A cells were transfected with either empty GFP vector, formin-1-GFP or mock transfected, as described in section 2.1.5.1 and allowed to express for 72 hours. Approximately $1x10^7$ HEK293A cells and $1x10^7$ wildtype melanocytes were harvested as described in section 2.1, and then run on an 8% SDS-PAGE gel ($25\mu g$/lane) and subsequently transferred to a PVDF membrane as described in section 2.3.1. The membrane was stained with goat-anti formin-1 and mouse-anti tubulin primary and donkey-anti goat/goat-anti mouse Licor secondary antibodies at the concentrations given in Table 2.11 using the protocol described in section 2.3.1. Whilst a band for endogenous formin-1 could be detected in the HEK293A cells, no matching band could be detected in the melanocyte lysate. **(b & d)** HEK293A cells were transfected with the indicated siRNA oligonucleotides, followed by formin-1-GFP (b) or Arpc1b-GFP (d) constructs 24 hours later. Cells were harvested 120 hours after the initial siRNA transfection and the lysate used for a western blot as described for (a). Both gels were stained with goat-anti GFP and mouse-anti tubulin primary antibodies and donkey-anti goat/goat-anti mouse secondary antibodies at the concentrations given in Table 2.11. **(c & e)** gives quantification of (b & d) based upon band density, normalised to tubulin.

5.3.2 SMIFH2 and CK666 drug treatments do not perturb melanosome distribution

In order to investigate the loss of formin-1 on melanosome distribution via a mechanism other than siRNA knockdown, melan-a cells were treated with SMIFH2. This is a small molecule (377.2 daltons) which was discovered to effectively inhibit the FH2 domain of formin after screening over 10,000 different compounds (Rizvi et al., 2009a). The drug works by reducing the affinity of the FH2 domain for actin, which both decreases the rate of actin polymerisation, as well as increasing the rate of actin depolymerisation at the barbed end (since formin acts as protective cap). As SMIFH2 binds the FH2 domain (the defining domain of formin), it should therefore be effective against all types of formin, and has been shown to inhibit actin polymerisation in organisms as diverse as fission yeast and mouse NIH 3T3 cells.

SMIFH2 was applied to melan-a cells for 16 hours at a range of concentrations (6μM - 25μM; Figure 5.5), with higher doses tested causing cell death, consistent with the reported LD50 value in NIH 3T3 of 28μM after a 24 hour treatment period (Rizvi et al., 2009b). However, despite the IC50 value for SMIFH2 on mDia1 reported as 15μM, the melanosome distribution in melan-a cells following 25μM SMIFH2 treatment did not appear significantly different from that of the vehicle control (Figure 5.5a). Melanocytes also retained their wild-type phenotype when the dose was reduced further (Figure 5.5d-f), whereas 25nM LatA was sufficient to induce a clustered phenotype, as expected (Figure 5.5b). The fact that the phenotype of the melan-a cells treated with SMIFH2 remained unchanged compared to the DMSO control was surprising, since it was expected that this drug, known to inhibit the highly conserved FH2 domain present in all formins, would cause gross morphological defects. Further experiments to test the efficacy of SMIFH2 in melanocytes are therefore needed before any conclusion can be drawn from these results. For example, since it is known that formin is involved in stress fibre formation, the numbers of these structures in cells treated with either SMIFH2 or DMSO could be used as a readout for the efficacy of the molecule. Alternatively, since formin is known to be involved in filopodia formation, inducing filopodia to form via the overexpression of Cdc42, for example (Mattila and Lappalainen, 2008), is another potential assay to test if SMIFH2 is inhibiting formin activity.

siRNA mediated knockdown of Arpc1b, but not any other components of the Arp2/3 complex, also affected melanosome transport. Therefore to determine if Arp2/3 itself was

playing a role in pigment granule distribution, or if Arpc1b might be acting independently of this complex through an alternative pathway, wildtype melanocytes were treated with CK666. This is another small molecule (296.3 daltons) which selectively inhibits the Arp2/3 complex (Hetrick et al., 2013). It achieves this by blocking the activation of the complex by binding at the interface of Arp2 and Arp3 and preventing these subunits from undergoing the necessary conformational change required to mimic an actin-dimer after Arp2/3 binds an NPF. CK666 does not, however, interfere with Arp2/3 binding actin filaments. Therefore, the rate of branched actin disassembly will be dependent not only on the concentration of CK666, but also the natural turnover rate of the actin cytoskeleton. Due to the conserved structure of Arp2/3 (for example there is 67% homology between the amino acid sequence of human and *Saccharomyces cerevisiae* Arp2), CK666 should also effectively inhibit the complex across a broad range of species.

As with the SMIFH2 experiments, melan-a cells were treated with a range of doses of CK666 for 16 hours, all of which were greater than the reported IC50 of 7μM. However, none of the doses tested resulted in either clustered melanosomes, or any noticeable change in melanocyte morphology compared with the DMSO treated control cells (Figure 5.5g-j). Again, it is not clear if the drug is efficiently inhibiting activation or the Arp2/3 complex, and therefore, as with SMIFH2, further work is required to test this before any conclusions can be drawn. For example, since Arp2/3 is known to be required for lamellipodia formation and therefore plays a role in cell migration (Suraneni et al., 2012), monitoring the distances melanocytes migrate after treatment with either CK666 or DMSO over time (e.g. 24 hours) could provide an assay to determine the efficacy of this drug. Alternatively FRAP experiments focusing on the lamellipodium or actin meshwork in melanocytes treated with CK666 or DMSO could also demonstrate if this drug is inhibiting Arp2/3, since actin turnover should be reduced if this protein is non-functional.

If CK666 was found to be effectively inhibiting the formation of branched actin, this would be a very interesting result, since taken together with the siRNA knockdown data for the 6 other subunits of the Arp2/3 complex, it would indicate that Arpc1b may have a role in melanosome transport that is independent of actin nucleation.

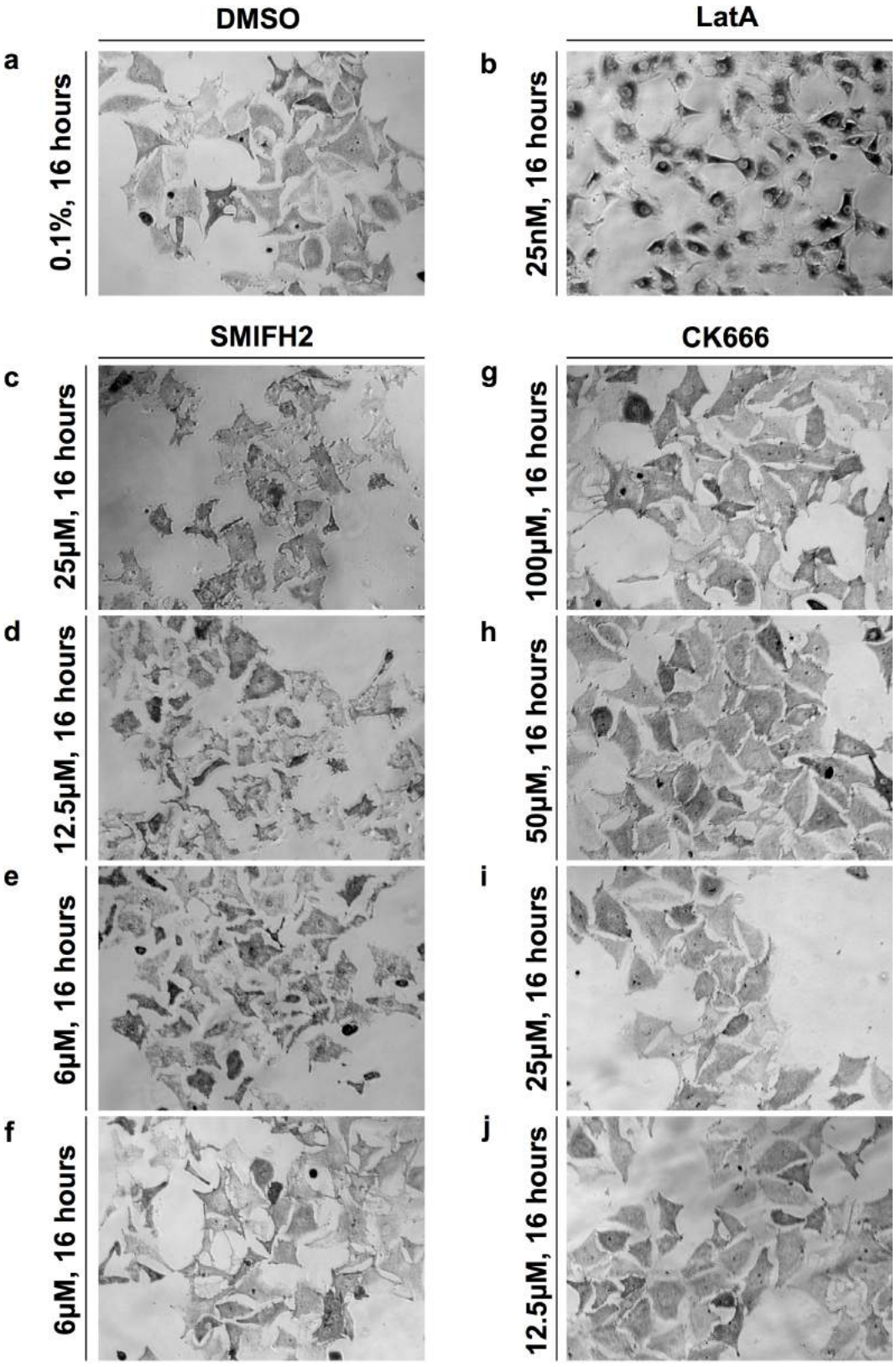


Figure 5.5 - Treating wildtype melanocytes with SMIFH2 or CK666 does not phenocopy formin-1 and Arpc1b knockdown. Wildtype melanocytes were treated with either 0.1% DMSO as a vehicle control **(a)**, or 25nM LatA as a positive control which resulted in clustering of melanosomes around the perinuclear area **(b)**. Wildytype melanocytes were treated with the indicated concentration of either SMIFH2 **(c-f)** or CK666 **(g-j)** for 16 hours. However, even at the highest concentrations of drug that were tolerated by the cells, the melanosomes remained dispersed.

5.3.3 Formin-1 and Arc1b knockdown does not grossly affect F-actin morphology

To attempt to understand the reason why both formin-1 and Arpc1b appear to be so crucial for maintaining dispersed melanosomes, wildtype melanocytes were transfected with oligonucleotides and the cells then stained with phalloidin to highlight the actin cytoskeleton. They were then subsequently imaged to determine if the loss of formin-1/Arpc1b resulted in any obvious defects compared with untreated cells which may account for the clustering phenotype. Cells that were transfected with FMN1 oligonucleotides (Figure 5.6c.i & c.ii) had an actin cytoskeleton which had characteristics of both melan-a (Figure 5.6a.i & a.ii) and melan-dilute cells (Figure 5.6b.i and b.ii), since while formin-1 knockdown cells had a relatively thick actin cortex similar to the *dilute* melanocytes, as well as actin puncta distributed throughout the cytoplasm, as in the wildtype cells.

On the other hand, melanocytes transfected with ARPC1B oligonucleotides (Figure 5.6d.i & d.ii) had an actin cytoskeleton that appeared different from both the wildtype and *dilute* melanocytes. Firstly the actin cytoskeleton in Arpc1b knockdown cells had a very thin cortex, which is unusual for cells with clustered melanosomes. Secondly, the actin in these cells was organised into a large number of long linear filaments that run throughout the cytoplasm, almost resembling microtubules.

High magnification images of Arpc1b and formin-1 knockdown cells were also used to more accurately quantify the pigment granule distribution (using the method described in section 2.4.3.5), since this had previously only been achieved by scoring low magnification fields of cells (as in Figure 5.2). This quantification revealed that formin-1 and Arpc1b knockdown reduced the PDR such that it is not significantly different from melan-dilute cells (Figure 5.6e) which again demonstrates the importance of these two proteins in anterograde melanosome transport.

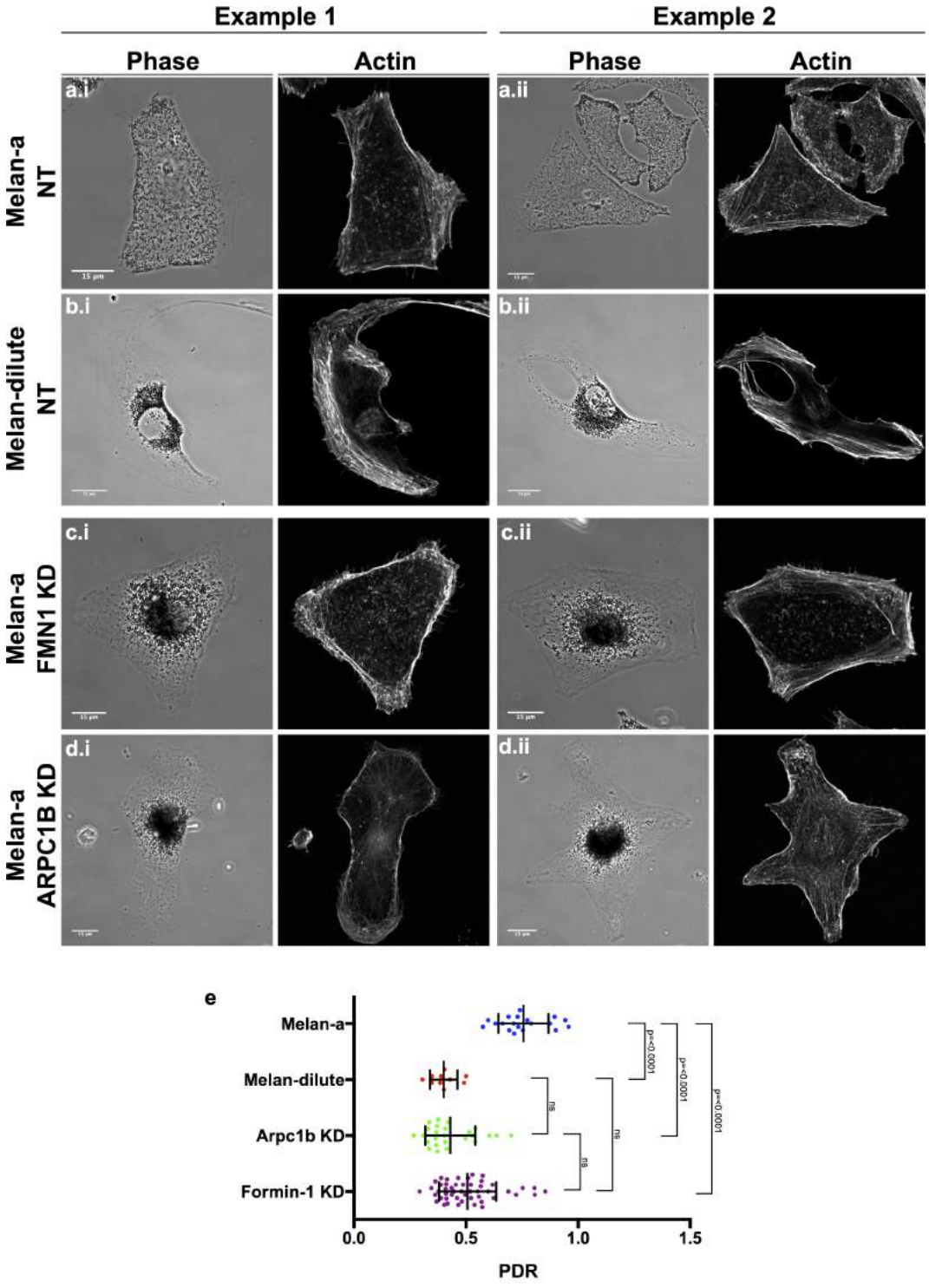


Figure 5.6 - Knocking down formin-1 and Arpc1b does not grossly affect actin morphology. (a.i & a.ii) NT melan-a. **(b.i & b.ii)** NT melan-dilute. **(c.i & c.ii)** FMN1 KD. **(d.i & d.ii)** ARPC1B KD. **(e)** Comparison of the pigment coverage index from melan-a and melan-dilute cells, and after melan-a cells were transfected with FMN1 and ARPC1B siRNA. Statistical analysis was performed using Kruskal-Wallis ANOVA test. Melan-a, n=19; melan-dilute, n=10; Aprc1b KD, n=25; formin-1 KD, n=49

5.3.4 Identifying the formin-1 isoform(s) expressed in murine melanocytes

Evidence from the FMN1 siRNA knockdown experiments strongly suggest that formin-1 plays an important role in facilitating long-range anterograde melanosome transport. At least four different splice isoforms of formin-1 are known to exist (Jackson-Grusby et al., 1992). However, the siRNA used to knockdown the protein covers a sequence that is conserved across all isoforms. Therefore to attempt to establish which isoform(s) of formin-1 are expressed in mouse melanocytes, four different primer pairs were designed that would give unique banding patterns in an RT-PCR screen (Table 5.1). In order to simplify the screen, isoform III was not tested (since it does not contain an FH1 or FH2 domain), and nor was the truncated isoform V.

The banding observed (Figure 5.7) strongly suggests that isoforms IA, II and IV are expressed in mouse melanocytes, although there was not a perfect correlation between observed and expected banding patterns. For example, an extra band of 300bp was observed using primer pair A and B, a band of 620bp instead of 2013bp observed for primer pair C, and two extra bands of 1100bp and 1500bp observed for primer pair D.

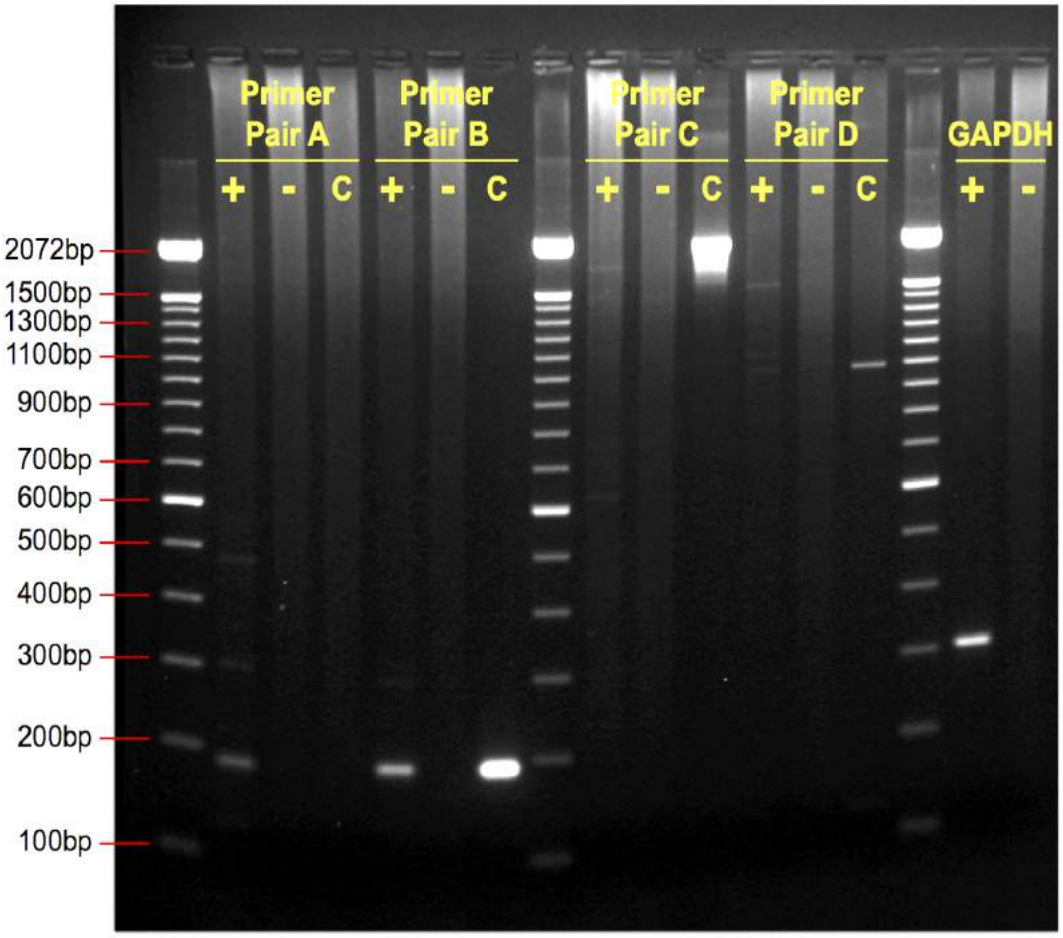


Figure 5.7 - Determining the specific isoform(s) of formin-1 expressed in murine melanocytes. Observed bands for primer pair A = 190bp, 300bp and 480bp; pair B = 190bp and 300bp; pair C = 620bp and 1900bp; pair D = 1100bp, 1200bp 1500bp. + = +reverse transcriptase, - = -reverse transcriptase, C = positive control (10ng/reaction formin-1 isoform IB clone).

	Expected expression pattern			
Hypothetical formin-1 isoforms expressed	**Pair A**	**Pair B**	**Pair C**	**Pair D**
Formin-1 isoform IA only	480	300	2121	-
Formin-1 isoform IB only	480	192	2013	-
Formin-1 isoform II only	186	192	1719	-
Formin-1 isoform IV only	-	192	1719	990
Formin-1 isoforms IA & IB	480	300 & 192	2121 & 2013	-
Formin-1 isoforms IA & II	480 & 186	300 & 192	2121 & 1719	-
Formin-1 isoforms IA & IV	480	300 & 192	2121	990
Formin-1 isoforms IB & II	480 & 186	192	2013 & 1719	-
Formin-1 isoforms IB & IV	480	192	2013	990
Formin-1 isoforms II & IV	186	192	1719	990
Formin-1 isoforms IA, IB & II	480 & 186	300 & 192	2121, 2013 & 1719	-
Formin-1 isoforms IA, IB & IV	480	300 & 192	2121 & 1719	990
Formin-1 isoforms IA, II & IV	480 & 186	192	2013 & 1719	990
Formin-1 isoforms IA, IB, II & IV	480 & 186	300 & 192	2121 & 2013 & 1719	990
Bands observed (approximate sizes):	190, 300 & 480	190 & 300	620 & 1900	1050, 1100 & 1500

Table 5.1 - Determining the specific isoform(s) of formin-1 expressed in murine melanocytes. Hypothetical sizes of the bands expected, if the indicated formin-1 isoforms are present. Primer sequences used were:
Pair A - 5'-TCTGAGGAAGCTTCCGAAAAA-3'; 5'-TACTAATGCGTGCTCACCCCG-3'
Pair B - 5'-CCCAAACTCAAAGACGTCAAA-3'; 5'-CAGCTTCCTCAAATCCTTTAG-3'
Pair C - 5'-ATCACAGCTCCACCCCAGCAC-3'; 5'-CAGCTTCCTCAAATCCTTTAG-3'
Pair D - 5'-GAGGAAGTCATTTGGGTCCGT-3'; 5'-GCTCTGGTCAGGGCTTTTGG-3'

5.3.5 Investigating the sub-cellular localisation of actin-binding proteins important for maintaining peripherally dispersed melanosomes

Since understanding precisely where a protein localises to in the cell is often key to revealing its function(s), the sub-cellular localisation of formin-1 and Arpc1b was investigated using specific antibodies against each of the two proteins. Melan-a cells were treated with both non-targeting or formin-1 (oligonucleotide #1) siRNA for 96 hours and then stained with a formin-1 antibody. Whilst evidence in the literature suggests that formin-1 isoform IV localises to the plasma membrane (Kobielak et al., 2004), antibody staining was mainly diffuse (Figure 5.8a), with only very weak staining at the plasma membrane in a limited number of cases (Figure 5.8b). When formin-1 was knocked down, the staining pattern was still diffuse (Figure 5.8c & d), similar to that observed in the control cells. Moreover, the total amount of staining did not appear to be reduced in these knockdown cells, suggesting that this antibody has high levels of non-specific staining, since it was expected that little antibody staining would be observed.

When the experiment was repeated using an Arpc1b antibody a similar result was observed (Figure 5.9). Both in the non-targeting siRNA control cells (Figure 5.9a & b) and the Arpc1b knockdown cells (Figure 5.9c & d), the antibody staining produced a punctate pattern throughout the cytoplasm. Moreover, as with the formin-1 knockdown cells, the staining intensity did not appear to decrease in the Aprc1b knockdown condition, which suggests that this antibody also has high levels of non-specific staining.

In order to avoid relying on antibody staining to localise formin-1 and Arpc1b, formin1-GFP and Arpc1b-GFP constructs were transiently transfected into wildtype melanocytes and allowed to express for 48 prior to fixing and imaging. Again formin-1 appeared to be distributed homogeneously throughout the cytoplasm (Figure 5.10b) similar to the expression pattern of GFP alone. Since cytoplasmic depletion has previously been necessary to reveal that another formin member, mDia1, also binds the plasma membrane (Geron et al., 2013), cells were treated with 0.05% saponin to permeabilise them, prior to fixing (Figure 5.10c). In the majority of cases this did not alter the distribution of the fusion protien, suggesting it was either anchored to the cytoskeleton and unable to diffuse out, or that the saponin treatment was insufficient to allow the formin protein to diffuse out. However, the latter is unlikely, given that permeabilisation with this concentration of saponin was routinely used throughout

this study in order to allow antibodies (which are of higher molecular weight compared with formin-1-GFP) to diffuse into the cell for immunofluorescent staining. Moreover, 0.05% saponin treatment was sufficient to allow GFP alone to diffuse out of the cells (data not shown).

In a very small number of cases formin-1-GFP in saponin permeabilized cells formed a number of puncta which were distributed in close proximity to melanosomes (Figure 5.10d. However, these observations were very rare, and it was not possible to determine if formin-1 is binding the melanosome membrane from this data. It would nonetheless be of interest to overexpress formin-1-GFP in melanocytes and subsequently purify the melanosomes, which could then be run on a western blot to investigate if formin-1 is associated with the melanosome membrane or not (similar to the experiment described in section 3.3.2).

Despite Arpc1b being a well established component of the Arp2/3 complex, which has previously been shown to have a punctate staining pattern in mouse fibroblasts (Johnston et al., 2008), when melan-a cells were transfected with Aprc1b-GFP the protein also appeared to be expressed diffusely throughout the cytoplasm (Figure 5.10e). While a greater signal intensity was observed around the nucleus, this is most simply explained by the fact the cells are thicker at the centre; signal in the GFP control cells also increased in a similar manner at the cell centre (Figure 5.10a).

The lack of a punctate expression pattern may simply be due to the overexpression of the protein masking this localisation pattern. However, it could also be possible that this isoform of Arpc1 contributes to melanosome transport by a mechanism that is independent of the Arp2/3 complex - especially since knocking down the other subunits of the complex, or even Arpc1a, did not result in melanosome clustering.

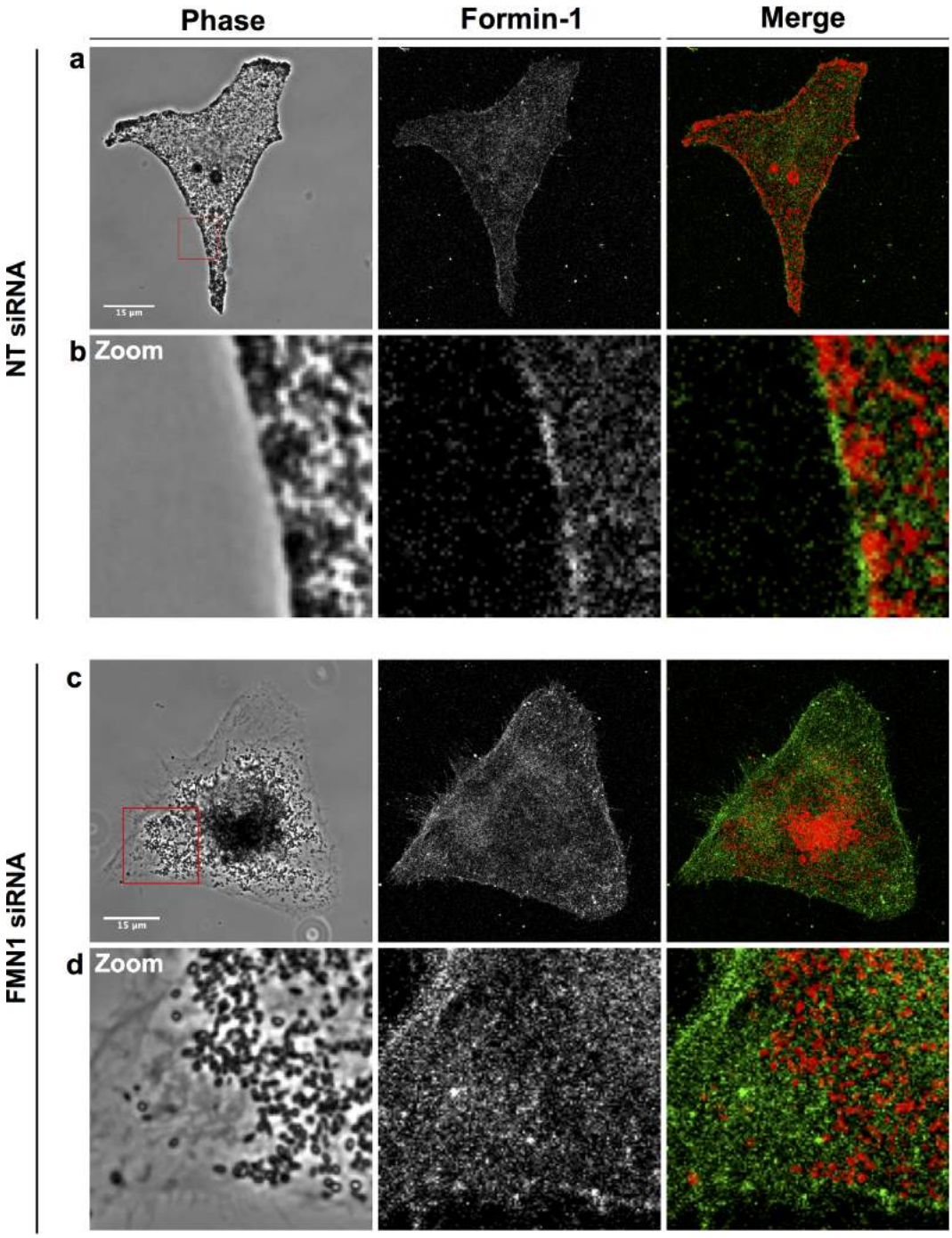


Figure 5.8 - Investigating the sub-cellular localisation of formin-1 using antibody labelling. **(a)** Melan-a cells treated with NT siRNA for 96 hours were stained with goat-anti formin-1 antibody, 1 in 100. **(b)** High magnification image of the portion of the cell encapsulated by the red box in (a). **(c)** Melan-a cells were treated with FMN1 oligonucleotide #1 for 96 hours and stained with antibody as in (a). **(d)** High magnification image of the portion of the cell encapsulated by the red box in (c).

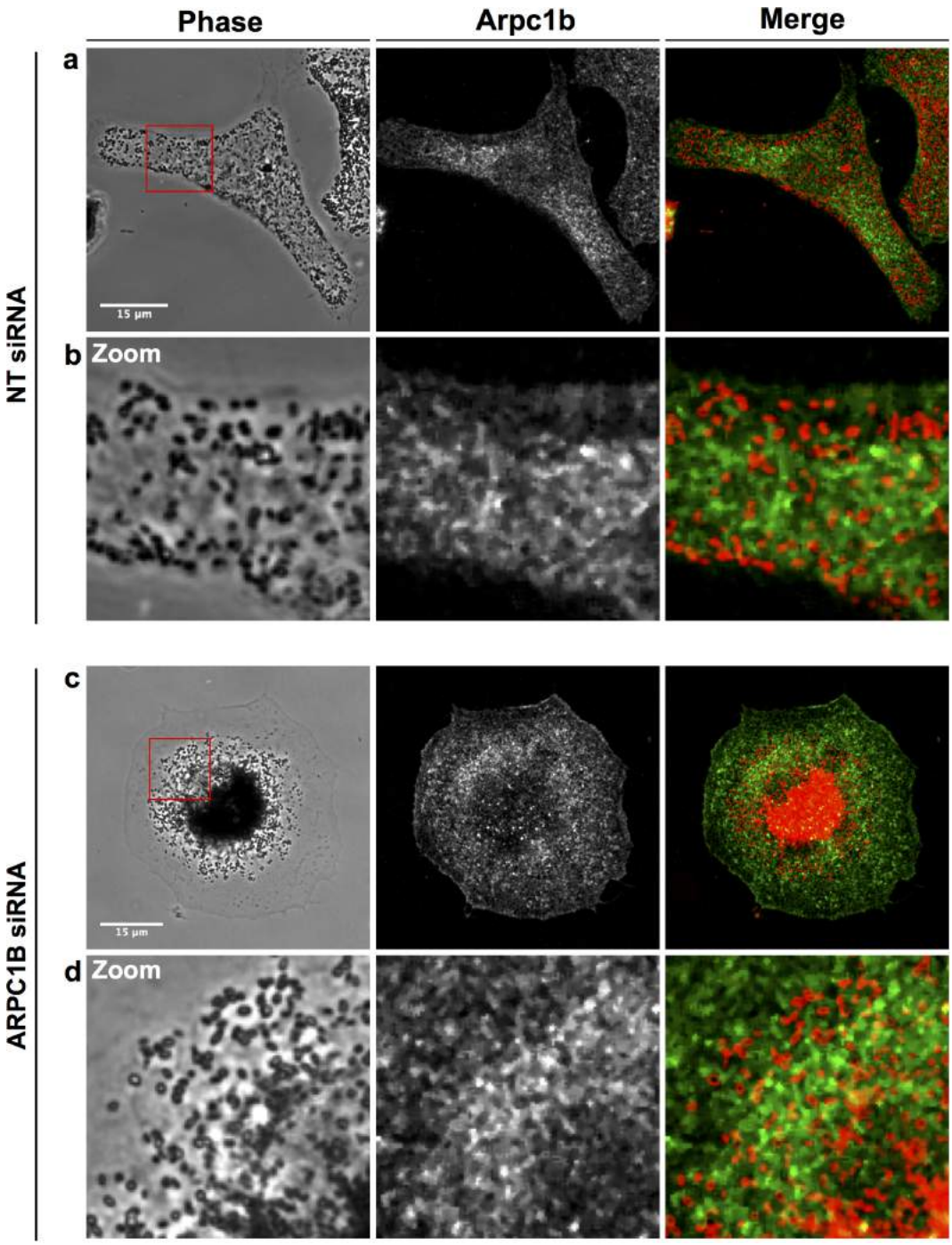


Figure 5.9 - Investigating the sub-cellular localisation of Arpc1b using antibody labelling. **(a)** Melan-a cells treated with NT siRNA for 96 hours were stained with rabbit-anti Arpc1b antibody, 1 in 100. **(b)** High magnification image of the portion of the cell encapsulated by the red box in (a). **(c)** Melan-a cells were treated with APRC1B oligonucleotide #2 for 96 hours and stained with antibody as in (a). **(d)** High magnification image of the portion of the cell encapsulated by the red box in (c).

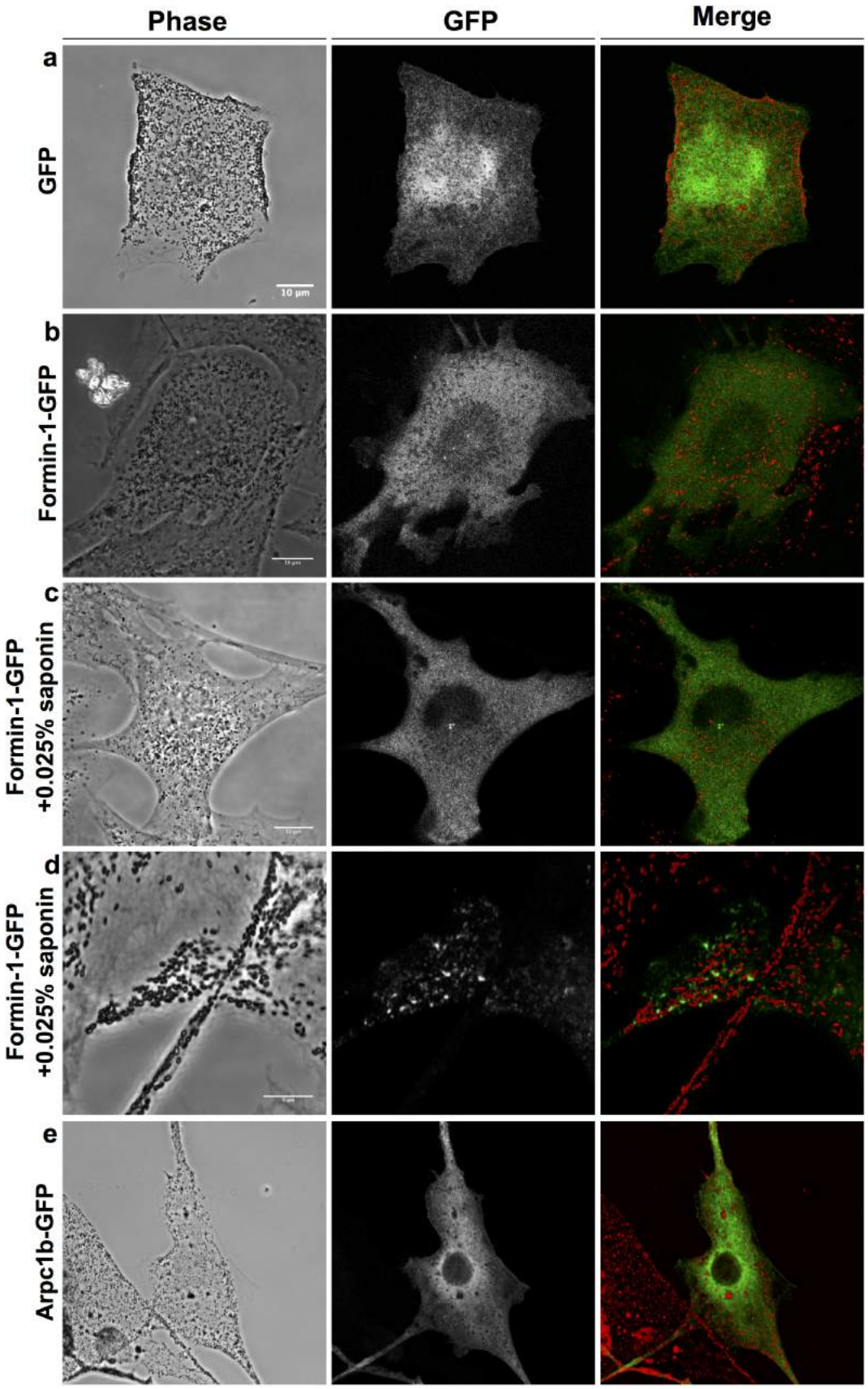


Figure 5.10 - Investigating the sub-cellular localisation of formin-1 and Arpc1b using fusion proteins. **(a)** GFP negative control **(b)** Formin-1-GFP **(c)** Formin-1 GFP in permeablised cells (0.05% saponin 5 mins prior to fixing). **(d)** In rare cases formin-1-GFP in permeablised cells was organised into puncta which were distributed with close proximity to melanosomes. **(e)** Arpc1b-GFP in melan-a. All constructs were allowed to express for 48 hours after transfection before cells were permeabilised and fixed.

5.3.6 Spire1 and spire2 are involved in anterograde melanosome transport

Whilst knockdown of FMN1 led to marked melanosome clustering, knockdown of either spire1 or spire2, two proteins also known to nucleate linear actin cables, did not appear to change the distribution of melanosomes (Figure 5.11a-h). These actin nucleators have both been implicated in the actin-dependent transport of vesicles (Schuh, 2011) and the meiotic spindle (Pfender et al., 2011b) in mouse oocytes. However, Pfender et al. demonstrated that there was redundancy between spire1 and spire2, so it was decided to knockdown both of these actin nucleators simultaneously to understand if this induced melanosomes to cluster similar to the formin-1 knockdown.

Since it was impossible to establish from the brightfield images (Figure 5.11a-h) which of the 4 different oligonucleotides for spire1 and spire2 were most effective at knocking down the protein, every combination of spire1 and spire2 oligonucleotides were tested to determine if any led to melanosome clustering (Figure 5.11i-x). Melanocytes were manually scored as either 'clustered' (represented the *dilute* phenotype) or 'dispersed' (represented the wildtype phenotype). The percentage of clustered cells for each combination is given in Figure 5.12.

Knocking down both spire1 and spire2 simultaneously resulted in clustered melanosomes for a number of combination tested. For example, knocking down spire1 oligonucleotide #4 and spire2 oligonucleotide #2 resulted in approximately 50% of cells adopting a clustered phenotype (Figure 5.11p and Figure 5.12d), as does knocking down spire1 oligonucleotide #3 and spire2 oligonucleotide #4 (Figure 5.11w and Figure 5.12f). These results therefore suggest that a second nucleator of linear actin cables also plays a role in maintaining peripherally dispersed melanosomes (and possibly also the long-range anterograde trafficking of these organelles), along with formin-1 and potentially the Arp2/3 complex.

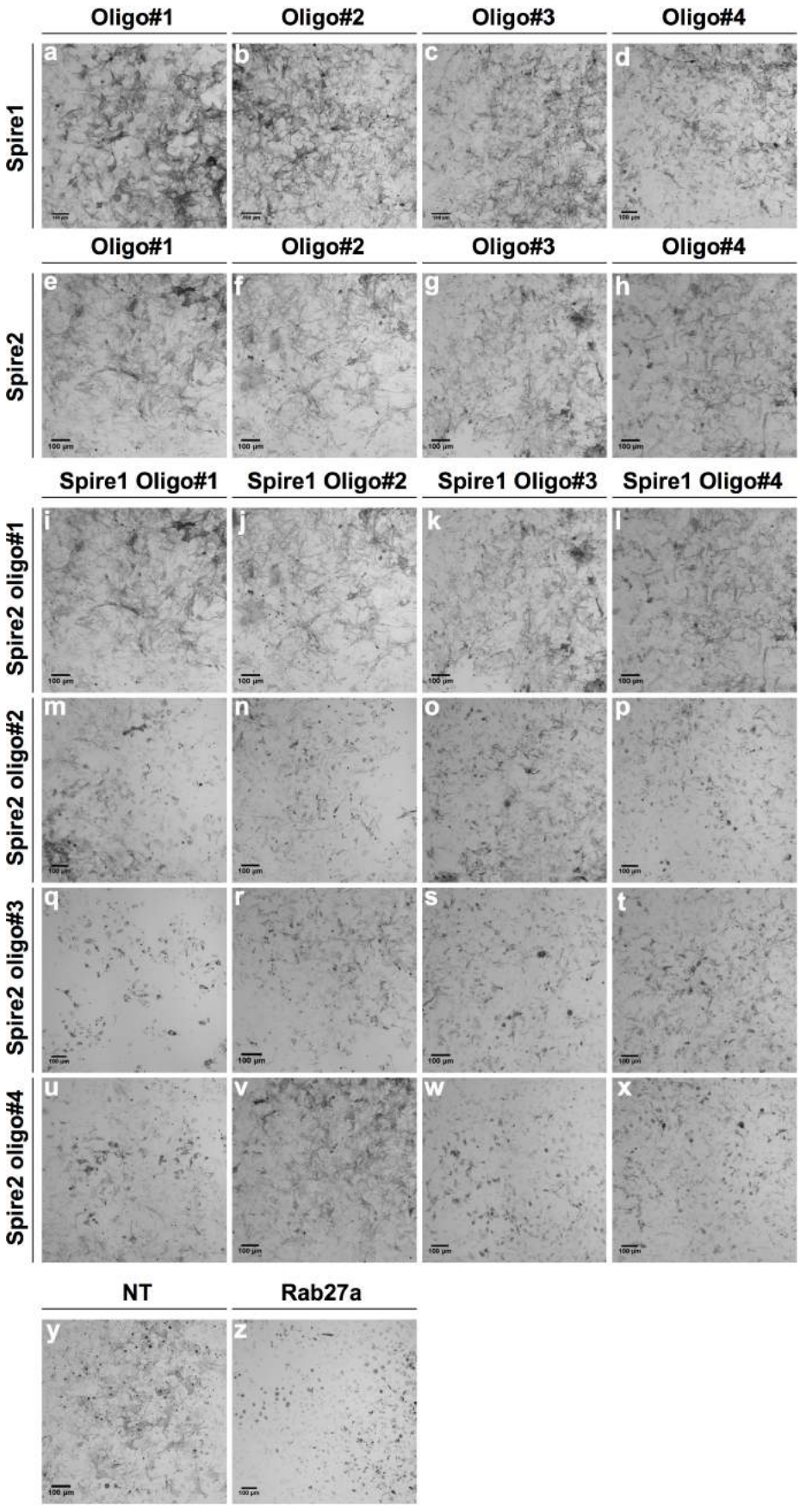


Figure 5.11 - Knocking down both spire1 and spire2 in wildtype melanocytes results in melanosome clustering. Individual spire1 and spire2 oligonucleotides did not cause melanosome clustering **(a-h)**. However, in a number of cases when melanocytes were double transfected with both spire1 and spire2 oligonucleotides, melanosomes appeared clustered around the perinuclear area after 96 hours **(i-x)**.

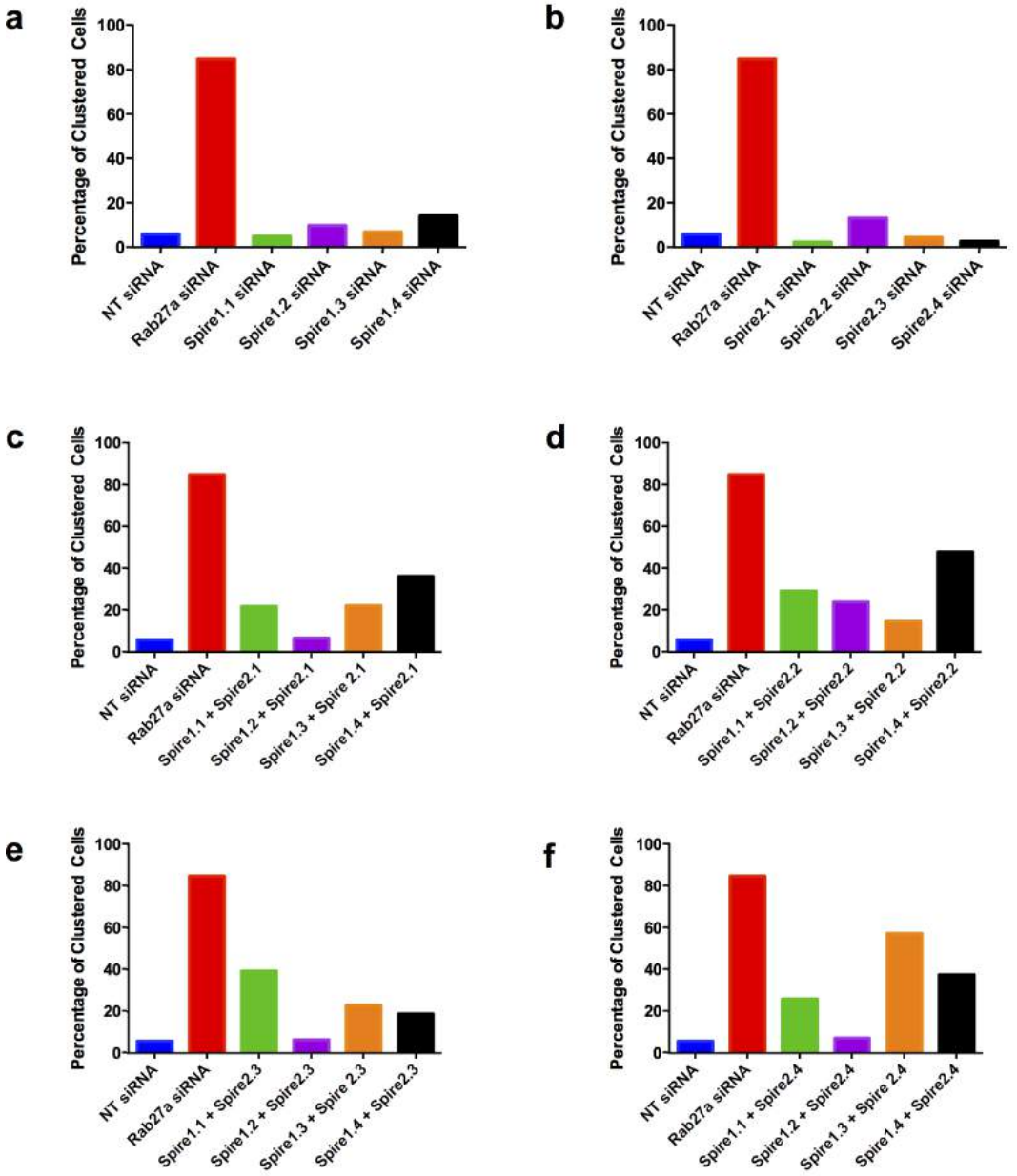


Figure 5.12 - Quantification of the extent of melanosome clustering caused by knock down of spire1 and spire2. Melanocytes transfected with spire1 and spire2 oligonucletoides (Figure 5.11) were scored as either clustered or dispersed and the percentage of clustered cells given for each condition.

5.3.7 Several other actin binding proteins also appear to affect melanosome distribution

Although the siRNA screen of 122 actin binding proteins revealed that silencing only FMN1, ARPC1B, ACTG1 and CFL1 genes resulted in wildtype melanocytes adopting a phenotype similar to melan-dilute cells, knockdown of 16 other genes led to more subtle 'partially clustered' phenotypes (Table 5.2 and 5.3). For example, melan-a cells transfected with TMOD1, TMOD3 and TMOD4 siRNA caused redistribution of some of the melanosomes to the perinuclear area (Figure 5.13D-F), with this effect being most acutely observed after TMOD4 knockdown. TMOD3 knockdown also led to cells becoming very spindly and smaller in size compared to the control cells (Figure 5.13A), whilst treatment with TMOD1 siRNA resulted in only a slight redistribution of the melanosomes towards the perinuclear area in a subset of cells. Likewise, knockdown of FHOD1, LMOD1 and LMOD3 also partially mimicked the *dilute* phenotype and again resulted in cells adopting a spindly morphology (Figure 5.13G-I).

Melanocytes transfected with RHOA, RHOF, RHOU, RHOBTB2 and RAC2 also induced a *dilute* phenotype (Figure 5.13J-N), with RHOF and RHOU producing the strongest effect in terms of melanosome clustering, whilst transfection with RAC2 siRNA caused the cells to adopt a spindly morphology. On the other hand, transfecting melan-a cells with RHOBTB2 and RHOA siRNA elicited only a weakly clustered phenotype compared to the positive controls (Figure 5.13B & C). Moreover, transfecting the wildtype cells with IQGAP2 also caused them to become very spindly and induced partial melanosome clustering.

Perhaps unsurprisingly, given the results of LatA treatment on melanosome distribution shown previously, depleting the cells of ACTB (β-actin) invoked a partially clustered phenotype in WT melanocytes (Figure 5.13P). The actin-binding protein profilin may also have a role in maintaining normal melanosome distribution, since transfecting melan-a cells with profilin-specific siRNA also caused the melanosomes to partially cluster (Figure 5.13Q).

Finally, melan-a cells transfected with both ZYX and CAPZB siRNA produced partially clustered and spindly melanocytes, with the phenotype similar to TMOD3, RAC2 and IQGAP2 knockdown (Figure 5.13R & S).

Table 5.2 - Results from the initial siRNA screen for actin-binding proteins involved in maintaining peripherally dispersed melanosomes in wildtype cells.

Key:

Wildtype	Clustered	Partially Clustered	Depigm-ented	Spindly and clustered	Spindly and dispersed	Pavement-like and clustered	Pavement-like and dispersed

Gene	Repeat 1	Repeat 2	Repeat 3	Repeat 4	Repeat 5	Consensus
Non-targeting negative control	Wildtype	Wildtype	Wildtype	Wildtype	Wildtype	Wildtype
Positive control (MYO5A)	Partially Clustered	Partially Clustered	Clustered	Clustered	Partially Clustered	Partially Clustered
ACTG1	Clustered	Wildtype	Clustered	Partially Clustered	Partially Clustered	Partially Clustered
IQGAP2	Clustered	Wildtype	Partially Clustered	Wildtype	Partially Clustered	Partially Clustered
PFN1	Partially Clustered	Clustered	Partially Clustered	Clustered	Pavement-like and clustered	Partially Clustered
MSN	Spindly and clustered	Wildtype	Wildtype	Wildtype	Wildtype	Wildtype
MYH9	Wildtype	Wildtype	Spindly and dispersed	Wildtype	Wildtype	Wildtype
RHOC	Wildtype	Wildtype	Wildtype	Wildtype	Wildtype	Wildtype
SETP2	Wildtype	Wildtype	Spindly and dispersed	Wildtype	Spindly and dispersed	Wildtype
MTPN	Wildtype	Wildtype	Partially Clustered	Wildtype	Spindly and dispersed	Wildtype
TLN1	Wildtype	Spindly and clustered	Wildtype	Wildtype	Partially Clustered	Wildtype
CAPZB	Wildtype	Wildtype	Partially Clustered	Partially Clustered	Partially Clustered	Partially Clustered
COTL1	Wildtype	Wildtype	Wildtype	Spindly and dispersed	Spindly and dispersed	Wildtype
CORO1C	Wildtype	Wildtype	Wildtype	Wildtype	Spindly and dispersed	Wildtype
MYL6B	Wildtype	Wildtype	Wildtype	Wildtype	Wildtype	Wildtype
TMOD3	Wildtype	Depigmented	Partially Clustered	Partially Clustered	Partially Clustered	Partially Clustered
ACTR3	Wildtype	Wildtype	Depigmented	Wildtype	Wildtype	Wildtype

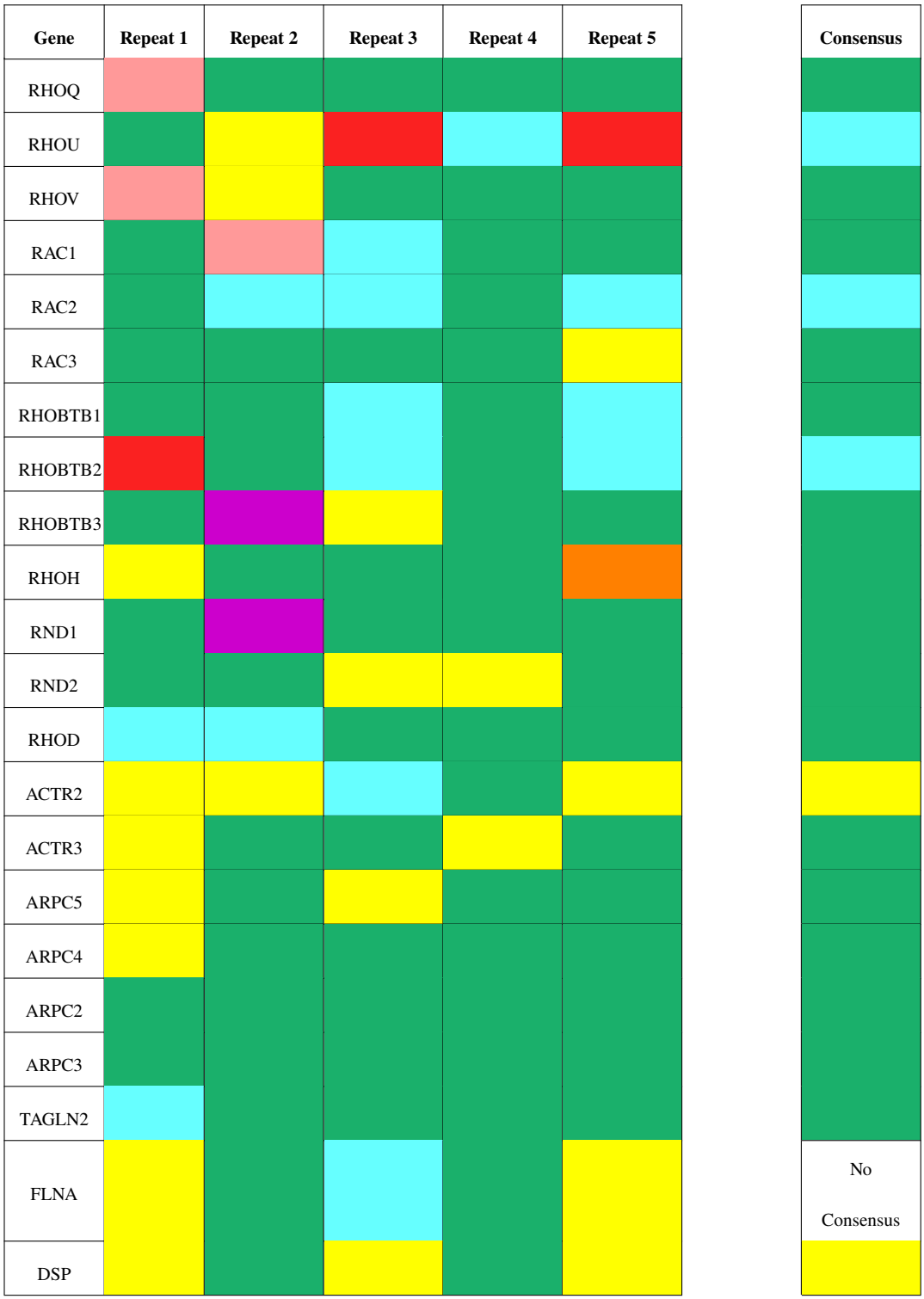
Key:

Wildtype	Clustered	Partially Clustered	Depigm-ented	Spindly and clustered	Spindly and dispersed	Pavement-like and clustered	Pavement-like and dispersed

Gene	Repeat 1	Repeat 2	Repeat 3	Repeat 4	Repeat 5	Consensus
ZYX						
DSTN						
EPB4.1L3						No Consensus
EPb4.1L2						
PP1CC						
RAP2A						No Consensus
CDC42						No Consensus
VASP						
ENAH						
DIAP2						
FMNL3						
DAAM1						
DAAM2						No Consensus
FMN1						
FMN2						
RHOA						
RHOF						
ROCK1						
SPIRE1						
SPIRE2						

Key:

Wildtype	Clustered	Partially Clustered	Depigm-ented	Spindly and clustered	Spindly and dispersed	Pavement-like and clustered	Pavement-like and dispersed



Key:

Wildtype	Clustered	Partially Clustered	Depigm-ented	Spindly and clustered	Spindly and dispersed	Pavement-like and clustered	Pavement-like and dispersed

Gene	Repeat 1	Repeat 2	Repeat 3	Repeat 4	Repeat 5	Consensus
PTMA						No Consensus
TPM1						
CFL1						
ACTB						
DIAP1						
DIAP3						No Consensus
FMNL1						
FMNL2						
FHOD1						
FHOD3						
RHOB						
ROCK2						
RHOJ						No consensus
RHOG						
RND3						
ARPC1B						
LMO2						

Table 5.3 - Results from the second siRNA screen to identify actin-binding proteins involved in maintaining peripherally dispersed melanosomes in wildtype cells.

Key:

Wildtype	Clustered	Partially Clustered	Depigmented	Spindly and clustered	Spindly and dispersed	Pavement-like and clustered	Pavement-like and dispersed

Gene	Repeat 1 (96 hours)	Repeat 2 (96 hours)	Repeat 3 (192 hours)	Consensus
Negative control				
Positive control (Rab27a)				
GRID2IP				
FHDC1				
INF2				
ARPC1A				
WAS				
WASL				
WASF1				
WASF2				
WASF3				
WASH				
WHAMM				
JMY				
CTTN				
HCLS1				
COBL				
LMOD1				

Key:

Wildtype	Clustered	Partially Clustered	Depigm-ented	Spindly and clustered	Spindly and dispersed	Pavement-like and clustered	Pavement-like and dispersed

Gene	Repeat 1 (96 hours)	Repeat 2 (96 hours)	Repeat 3 (192 hours)	Consensus
LMOD2				
LMOD3				
CTNNA2				
CTNNA1				
CTNNA3				
CTNNB1				
CDH1				
CDH2				
CDH3				
LRRC58				
ACTA1				
ACTG2				
ACTBL2				
JUP				
CTNND1				
VCL				
VIM				
NCKIPSD				
GSN				
CORO6				
CORO1A				
CORO1B				
CORO2A				

Key:

Wildtype	Clustered	Partially Clustered	Depigm-ented	Spindly and clustered	Spindly and dispersed	Pavement-like and clustered	Pavement-like and dispersed

Gene	Repeat 1 (96 hours)	Repeat 2 (96 hours)	Repeat 3 (192 hours)	Consensus
WIPF1				
NCK2				
PAK1				
TMOD1				
TMOD2				
TMOD4				
TPM2				
TPM3				
TPM4				

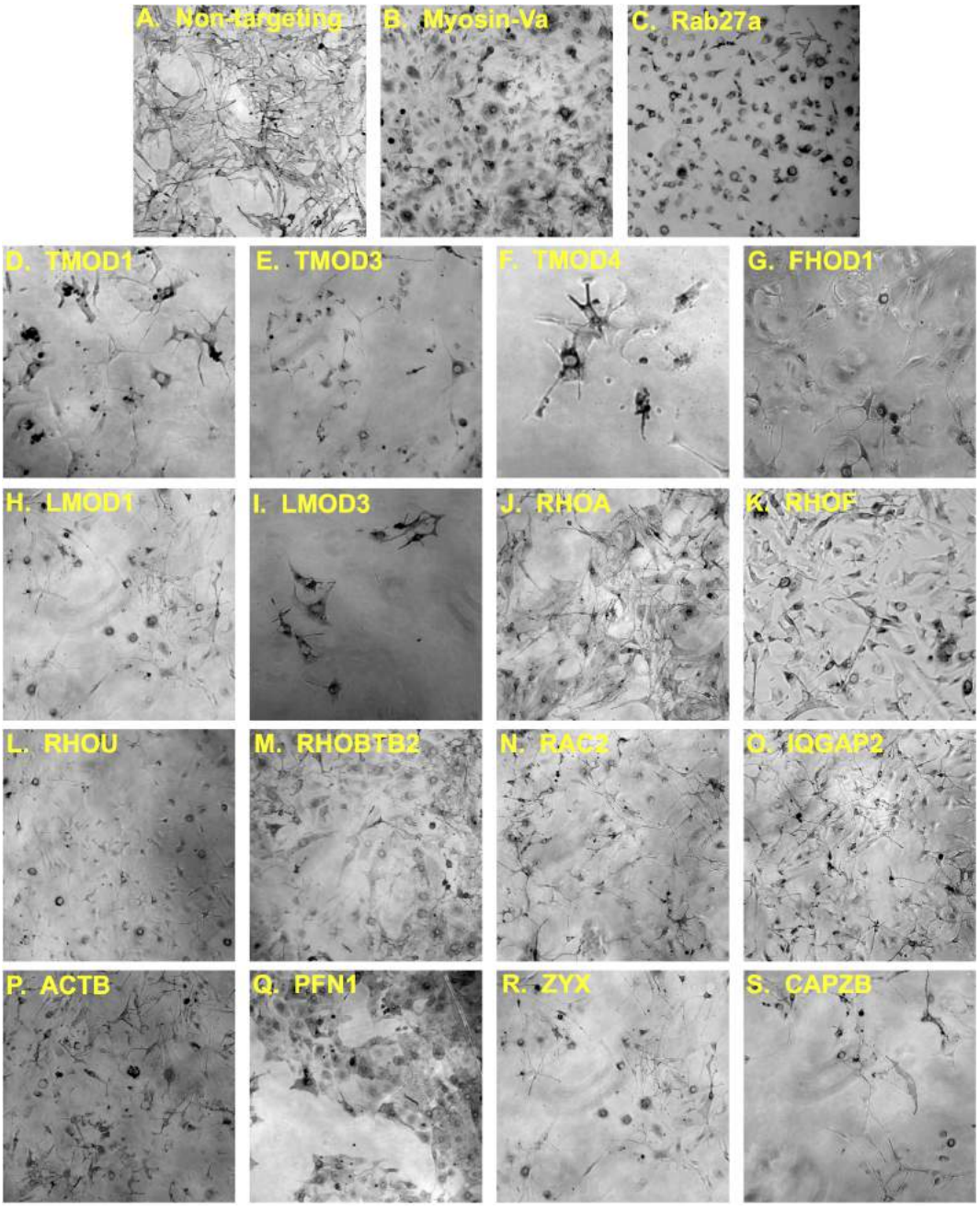


Figure 5.13 - Example images from the two siRNA screens showing phenotypes arising from knocking down certain actin-binding proteins.

5.4 Discussion

5.4.1 Linear actin cables are necessary for anterograde melanosome transport

An siRNA screen of actin-binding proteins revealed that depleting murine melanocytes of formin-1 caused the most significant melanosome clustering of all the siRNA targets tested. Since this family of actin nucleators generate unbranched F-actin (Pruyne et al., 2002) this strongly suggests that linear actin cables play a significant role in the long-range anterograde transport of melanosomes.

While it is well established in both budding and fission yeast that linear actin cables (nucleated by bnr1 and bni1; *Saccharomyces cerevisiae* or for3; *Schizosaccharomyces pombe*) are required to support the long-range transport of a number of organelles and vesicles such as peroxisomes, Golgi, mitochondria and mRNA to the polarised tip (Feierbach and Chang, 2001; Martin and Chang, 2006; Motegi et al., 2001; Rossanese et al., 2001; Yang and Pon, 2002), there is less evidence for such transport in mammalian cells. However, more recently published work is beginning to establish a precedent for transport along linear actin cables generated by formins in metazoan cells. For example, Geron et al. 2013 showed that exocrine secretion in pancreatic acinar cells requires linear actin cables, generated by the formin mDia1, in order to transport vesicles to apical plasma membrane, with this mechanism thought to be conserved in a number of other exocrine tissues.

That double knockdown of two other nucleators of unbranched actin, spire1 and spire2, also caused melanosome clustering further suggests that specifically linear actin cables may play an important role in either maintaining the wildtype dispersed phenotype, the anterograde transport of melanosomes, or both. Furthermore, there is evidence to suggest that spire1 and spire2 act together, along with formin-2, to bring about vesicle transport in mouse oocytes (Schuh, 2011). In this model spire1, spire2 and formin-2 localises to both the vesicle and plasma membrane where they nucleate unbranched actin filaments to generate a 'web' of actin, to which the vesicles are attached via myosin-V motors. As the myosin-V motors move towards the plus ends of the actin cables, the actin web, and the vesicles attached to it, gradually move *en mass* towards the plasma membrane. Given the similarity in molecular players identified in melanocytes, this serves as an attractive hypothesis for how melanosomes are being transported to the plasma membrane.

However, it could not be established whether a model similar to the one proposed by Schuh was responsible for melanosome transport, as it was not possible to determine the sub-cellular localisation of formin-1, since both antibody staining and transfection of a formin-1-GFP construct led to a diffuse staining pattern in the majority of cases. Moreover, formin-1 is not known to be an effector of any RhoGTPase, and therefore it is unclear how this actin nucleator would interact with either the melanosome or plasma membrane (Campellone and Welch, 2010). However one possible mechanism is via an interaction with spire (which is able to bind membranes via its C-terminal FYVE domain interacting with the membrane lipid phosphatidylinositol-3-phosphate Gaullier et al., 1998; Lee et al., 2005), which X-ray crystallography has shown is able to bind formin-1 and formin-2 through its N-terminal KIND domain (Vizcarra et al., 2011; Zeth et al., 2011). It is therefore possible that spire1 and spire2 knockdown only causes melanosome clustering by displacing formin-1. It would be of interest to determine if this is truly the case in a future study by, for example, generating a formin-1-FYVE construct which should bind membranes and testing whether transfecting this protein into spire1/2 double knockdown cells rescues the clustered phenotype.

Surprisingly, treating wildtype melanocytes with the broad formin inhibitor SMIFH2 appeared to have no effect on melanosome distribution despite the concentration used being well above the reported IC50 value. However, it was found that treating melanocytes with doses of SMIFH2 higher than 25μM for 16 hours caused cell death. One explanation may be that this drug was simply too broad acting, meaning that at the concentration of drug necessary to inhibit a large enough proportion of the total formin-1 molecules so as to mimic their knockdown quickly resulted in cell death as other essential formins needed for maintenance of the cytoskeleton would also be inhibited. It is of course also possible that at these high concentrations there may be significant off-target effects, resulting in SMIFH2 inhibiting other essential proteins. For example, Isogai et al., 2015 reported that rapid cell death occur when cells (U2OS, HEK293T and HCT116 cell lines were tested) were exposed to concentrations of SMIFH2 above 50μM , potentially due to downregulation of p53.

RT-PCR was used to attempt to determine which isoform(s) of formin-1 were being expressed in murine melanocytes. However, as with determining the protein's sub-cellular location, this also proved challenging due to the apparently low levels of formin-1 mRNA detected, and the strong homology between the 4 different isoforms tested. These preliminary results indicated that isoforms IA, II and IV are expressed in melanocytes. While it

has been reported that the expression pattern for the 6 different formin-1 isoforms does vary in mouse embryos (Chan et al., 1995), with the exception of isoform IV, which is thought to be involved in cell motility (Dettenhofer et al., 2008), it is not well understood if the other formin-1 isoforms also have specialised functions. The recent generation of FMN1$^{-/-}$ melanocytes (unpublished data) should help determine if one or more specific formin-1 isoforms are involved in melanosome transport, as it will open up the possibility for add-back experiments which should show which isoform(s) allow redistribution of the melanosomes towards the plasma membrane.

5.4.2 $\gamma-$actin and cofilin-1 knockdown confirm the results from LatA and JK treatment

The fact that ACTG1 and CFL1 knockdown caused melanosome to cluster around the perinuclear area is consistent with previous results, since depleting cells of γ-actin mimics LatA treatment, whilst depletion of the actin-severing protein cofilin-1 (resulting in increased actin stability) mimics JK treatment to a large extent.

That specifically knocking down the γ-cyto isoform of actin caused melanosome clustering may suggest it is used preferentially over other isoactins for supporting melanosome transport. This is consistent with results from the β-actin knockdowns performed, where only partial clustering was observed in a subset of cells. Published data indicates that β-actin is mainly localised at the leading edge of cells, where it is thought to play a role in cell migration, while γ-actin is more uniformly distributed throughout the cytoplasm (Otey et al., 1988; Hoock et al., 1991; Hill and Gunning, 1993; Peckham et al., 2001). Therefore one explanation for the apparent preferential use of γ-actin in melanosome transport may simply be due to its broader availability, which would be crucial for rapid turnover of actin filaments. Since a number of actin-binding proteins were also found to influence melanosome distribution (discussed below), its also conceivable that, despite almost identical primary amino acid structures (Perrin and Ervasti, 2010), one or more of these proteins preferentially binds γ-actin over β-actin - a phenomenon which has been reported for some actin-binding proteins such as annexin 5a (Tzima et al., 2000).

Interestingly, qRT-PCR data showed that depleting cells of γ-actin caused a concomitant increase in levels of cofilin-1. This suggests the possibility of a feedback mechanism whereby cofilin expression increases upon reduced levels of γ-actin in order to increase fila-

ment severing and therefore drive an increase in free G-actin monomers. It would therefore be of interest to understand if cofilin-1 levels also increase upon depletion of β-actin, or whether it is specific for γ-actin.

5.4.3 Arpc1b is necessary for anterograde actin-dependent melanosome transport

Knockdown of Arpc1b had a large effect on melanosome distribution, which therefore implicates Arp2/3 as playing an important role in pigment granule transport (since Arpc1b is one of the 7 subunits making up this complex). However, when the other subunits of Arp2/3 were knocked down no obvious disruption of melanosome distribution was seen, (although the knockdown efficacy was not confirmed with RT-PCR or western blotting). The same was true when cells were treated with ARPC1A siRNA (a closely related isoform). Furthermore, melanocytes remained wildtype after treatment with the Arp2/3 inhibitor CK666, even when high doses (approximately 10 times greater than the reported IC50 concentration) were used.

Recently, evidence has been published which suggests that Arpc1b may be involved in regulating the length of the actin filaments nucleated by the Arp2/3 complex (Abella et al., 2016). Abella et al. examined the ability of the vaccinia virus to produce F-actin tails after knocking down different subunits of the Arp2/3 complex. In controls cells, F-actin tails were 2.68 ± 0.03μm, whilst in cells transfected with Arpc1b siRNA this was reduced to 0.95 ± 0.02μm. Conversely, in cells transfected with Arpc1a siRNA, the tails increased in size to 4.66 ± 0.06μm. The speed the vaccinia viruses moved through the cytoplasm was also quantified and taken as a measure of the efficiency of actin nucleation. In control cells, vaccinia moved with an average speed of 0.17 ± 0.01μm s^{-1}, while in Arpc1b KD cells this decreased to 0.15 ± 0.01μm s^{-1} and in Arpc1a KD cells this value increased to 0.20 ± 0.002μm s^{-1}. Taken together, these results indicate that the Arpc1b isoform is necessary for Arp2/3 complex to efficiently nucleate relatively long actin filaments.

It is also possible that Arpc1b may be acting independently of the Arp2/3 complex to facilitate melanosome transport. Little research has been conducted on Arpc1b outside of its role as a component the Arp2/3 complex, although it has been shown that it can activate Aurora A via phosphorylation, and that its knockdown prevents cells from undergoing G2-M phase of the replication cycle, whilst knockdown of the closely related Arpc1a (69% homologous to Arpc1b at the protein level) did not (Molli et al., 2010). However, neither interrupting

the cell cycle with thymidine, or transfecting wildtype melanocytes with Aurora A siRNA led affected melanosome distribution (data not shown), which suggests that knockdown of Arpc1b does not induce melanosome clustering by interfering with the cell cycle.

5.4.4 A number of actin-binding proteins may contribute to long-range anterograde melanosome transport

Aside from formin-1, Aprc1b, γ-actin, cofilin-1, and spire1/2 whose knockdown robustly phenocopied the melan-dilute cells, transfecting wildtype melanocytes with siRNA against a number of other actin binding proteins was also found to cause partial clustering of the pigment granules.

For example, the knockdown of profilin-1 induced the partial clustering of pigment granules in the majority of melanocytes, consistent with the hypothesis that formin-1 plays a crucial role in the positioning of melanosomes, since profilin is known to increase the elongation rate of actin filaments nucleated by formins (Paul et al., 2008).

Several isoforms of formin, such as mDia1, are activated by RhoGTPase which bind to the GTPase-binding-domain (GBD) at the N-terminus of the formin, thus relieving autoinhibition resulting in the protein's activation (Watanabe et al., 1999). Interestingly, although it is unlikely that formin-1 is regulated by RhoGTPases in the same way as other formins, since this member of the formin family lacks a GTPase binding domain (Campellone and Welch, 2010), knockdown of a number of RhoGTPases also caused partial clustering of the pigment granules. In particular, silencing of the RHOU gene appeared to cause the strongest effect in terms of melanosome clustering. This protein is known to be involved in the formation of filopodia (Ruusala and Aspenstrom, 2008), which suggests it may either directly or indirectly influence the activity of myosin-V, which play a role in the formation of these structures (Wang et al., 1996). Furthermore it has also been shown to have a role in the disassembly of stress fibres, since overexpression of RhoU in NIH 3T3 cells reduced the number of stress fibres by approximately 90%, causing the cells to detach from the substrate and round up (Saras et al., 2004). However in melanocytes there was generally no correlation between stress fibre content and melanosome distribution, with both melan-a and melan-dilute melanocytes appearing to have arbitrary numbers of these structures. Moreover transfecting wildtype melanocytes with siRNA against zyxin was found to induce partial melanosome clustering. Knockdown of this protein should result in a decrease in

stress fibre numbers, since there is evidence to show it binds to and repairs stress fibres that have undergone damage (Smith et al., 2010). Taken together, it is therefore unlikely that the melanosome clustering observed after transfection with RHOU siRNA occurs due to an increase in stress fibres.

Although RhoU shares 57% sequence homology with Cdc42, transfecting melanocytes with siRNA targeting this protein did not perturb wildtype melanosome distribution. Since the major difference between these two proteins is that RhoU features a 46 amino acid N-terminal extension and a 21 amino acid C-terminal extension (Tao et al., 2001), it is possible that either of these two regions could play a role in maintaining peripherally dispersed melanosomes, for example, through the recruitment of an effector protein. The C-terminus of RhoU also contains a palmitoylation motif, which causes it to localise mainly at the plasma membrane, as opposed to the cytoplasm and perinuclear membranes as is the case for Cdc42 (Berzat et al., 2005). Therefore this difference in sub-cellular localisation may also explain why the loss of RhoU but not Cdc42 caused the pigment granules to cluster. Future studies should therefore focus on elucidating both the intracellular localisation of RhoU, as well as determining if the loss of either the activators of this protein such as Grb2 whose SH3 domain interacts with the N-terminal extension of RhoU (Shutes et al., 2004), or the proteins RhoU regulates, such as PAK1, JNK and Par6 (Chuang et al., 2007; Brady et al., 2009), also results in melanosome clustering.

Transfecting melanocytes with siRNA targeting the RHOA gene gave the next strongest effect in terms of pigment granule clustering. Although it is known that this protein does regulate formins, formin-1 lacks a GBD and therefore is not likely to be a substrate of RhoA. However, knockdown of FHOD1, an example of a formin that does contain a GBD (Campellone and Welch, 2010; Koka et al., 2003), and therefore is potentially regulated by RhoA, also caused partial melanosome clustering. While there was no effect from knockdown of the related formin FHOD3, it is possible that, as with spire, there is redundancy between these formins, and therefore double knockdown of these two proteins may be necessary to drive melanosomes to cluster. Likewise this redundancy may also explain why silencing of two other formins which are thought to be regulated by RhoGTPases, DAAM1 & DAAM2 (Campellone and Welch, 2010), did not cause pigment granule clustering.

Aside from regulating the activity of formins, RhoA is thought to control the actin cytoskeleton architecture through several other pathways. For example, the fact that it can

function to indirectly activate the Arp2/3 complex by acting upon NPFs, such as the WASH complex (Liu et al., 2009), may serve as one explanation for why clustering was observed upon silencing of the RhoA gene. Interestingly, levels of RhoA have been found to be elevated during interphase (Chircop, 2014), with the protein shown to be indispensable for the progression of mitosis in mouse embryonic fibroblasts (Melendez et al., 2011). Since, as discussed above, depleting cells of Arpc1b also blocks mitosis, this raises the possibility that melanosomes cluster before entering mitosis and that if the cell cycle is blocked, the *dilute* phenotype persists. Although this phenomenon has not be observed for melanosomes, it has been shown that endosomes and lysosomes appear to cluster around MTOC during mitosis in MDCK cells, with the distribution thought to be due to microtubule motors (Bergeland et al., 2001).

Transfecting wildtype melanocytes with RHOF siRNA led to similar mild clustering of the pigment granules as was observed after transfecting cells with RHOA siRNA. As with RhoU, it is thought that RhoF also plays a role in filopodia formation, although the evidence suggests this is achieved though collaboration with mDia1 (Goh et al., 2011), whose knockdown did not induce melanosome clustering. Finally, transfecting cells with RHOBTB2 siRNA also caused weak clustering of the pigment granules on several occasions, although there is little evidence that RhoBTB GTPases play any role in organizing the actin filaments (Aspenstrom et al., 2004). RhoBTB2 has, however, been shown to play a role in the anterograde transport of vesicles from the endoplasmic reticulum to the Golgi (Chang et al., 2006), although this trafficking was microtubule-dependent. Nevertheless, it would be of interest to determine the sub-cellular localisation of RhoBTB2 in a future study.

Despite it being reported that Rac2 expression is mainly restricted to haematopoietic derived cells (Didsbury et al., 1989; Shirsat et al., 1990), transfecting melanocytes with siRNA targeting this RhoGTPase was also found to cause weak clustering of the pigment granules. The fact that Rac2 is known to regulate the activity of both the Arp2/3 complex through WAVE, as well as cofilin (Sun et al., 2007), both of which have been implicated in melanosome transport in this study, offers a simple explanation as to why its knockdown results in melanosome clustering. Furthermore, transfecting cells with siRNA against the ubiquitously expressed Rac1 was also found to cause mild pigment granule clustering on some occasions, although depleting melanocytes of one of its effectors, IQGAP2, led to cells more repeatably adopting the *dilute* phenotype (see Table 5.2). This protein has been shown

to localise to filopodia, bind F-actin and importantly act as a molecular scaffold for Arp2/3 complex formation (Schmidt et al., 2003), which may explain why it affects melanosome distribution.

Several members of the tropomodulin family (TMOD1, TMOD3 and TMOD4), which are known to influence actin dynamics by capping the pointed ends of filaments (Rao et al., 2014), may also be important in anterograde melanosome transport, since transfecting melanocytes with siRNA targeting these genes also led to a partially clustered phenotype. Likewise, siRNA against CapZβ (encoded by the CAPZB gene), which is known to localise to the barbed ends of actin filaments where it regulates actin assembly (Li and Russell, 2013), also resulted in melanocytes adopting a spindly morphology, along with clustered melanosomes.

Interestingly, two proteins from the leimodin family (LMOD1 and LMOD3) which are structurally related to tropomodulin, but function as actin nucleators to generate linear actin cables (Chereau et al., 2008) also perturb the wildtype phenotype. It therefore appears that perturbing many of the major pathways through which actin is nucleated (via formin, spire or leimodin and potentially Arp2/3) results in at least partial clustering of the melanosomes, opening up the possibility that a large number of different proteins collaborate to bring about the anterograde transport of these organelles.

5.4.5 F-actin is nucleated by the centrosome

Recent work has demonstrated that the centrosome not only functions as a microtubule organising centre, but also as an actin organising centre (Farina et al., 2016). This was revealed when centrosomes from either Jurkat or HeLa cells were extruded into a buffer that supported actin nucleation, since previous buffers were found to inhibit this process. Centrosomes were also shown to serve as sites of actin nucleation *in vivo*, with a colour switch assay (where cells are first incubated with red G-actin, followed by green G-actin) being used to show that actin filaments were being nucleated *de novo.* The authors went on to demonstrate via both immunostaining and mass spectrometry that the Arp2/3 complex was present at centrosomes. Moreover, CK666 was found to block actin nucleation, while SMIFH2 had no affect on this process. WASH, an activator of Arp2/3, was also found to localise to the centrosome, and inhibition of this protein by blocking antibodies also inhibited actin nucleation, as did using centrosomes from cells that had been siRNA depleted of WASH. These findings therefore strongly suggest that the Arp2/3 complex is necessary for the centrosome's

ability to nucleate actin.

If the centrosome in melanocytes is also able to nucleate F-actin through a similar mechanism, this could have important consequences for melanosome transport, since the Arp2/3 nucleated actin filaments would radiate out from the perinuclear area with their barbed ends pointing towards the plasma membrane. These filaments could therefore serve as tracks for myosin-Va-dependent trafficking of melanosomes from the perinuclear area towards the cell periphery. Moreover, there is already *in vitro* evidence to suggest that myosin-Va is capable of both navigating through Arp2/3 mediated junction, as well as track switching from mother to daughter filaments, which would support this trafficking mechanism (Ali et al., 2007; Vilfan, 2008).

5.4.6 Summary

Results from this chapter further support a major role for F-actin in driving anterograde melanosome transport since knockdown of several actin-binding proteins induced the clustering of pigment granules around the nucleus. Formin-1 knockdown elicited the strongest effect of any of the proteins tested, with the recent isolation of melanocytes from a Fmn1$^{-/-}$ mouse whose melanosomes are also clustered backing up this finding (data not shown). Knockdown of Arpc1b, cofilin-1 and spire1/2 also induced pigment granules to cluster, further implicating dynamic actin as being fundamental for anterograde melanosome transport. For example, the partial clustering of melanosomes resulting from knockdown of the actin severing protein cofilin-1 mimics the results from JK treatment while the finding that γ-actin also appears important for the maintenance of dispersed pigment granules further suggests that a sub-population of dynamic actin is necessary for the anterograde trafficking of these organelles. However, further work is necessary to elucidate where these actin nucleators localise to in the cell and the mechanism by which they facilitate melanosome dispersion. A possible model explaining how formin-1, spire1/2, Arpc1b and cofilin-1 promote long-range actin-dependent melanosome transport is shown in Figures 5.14, 5.15 and 5.16.

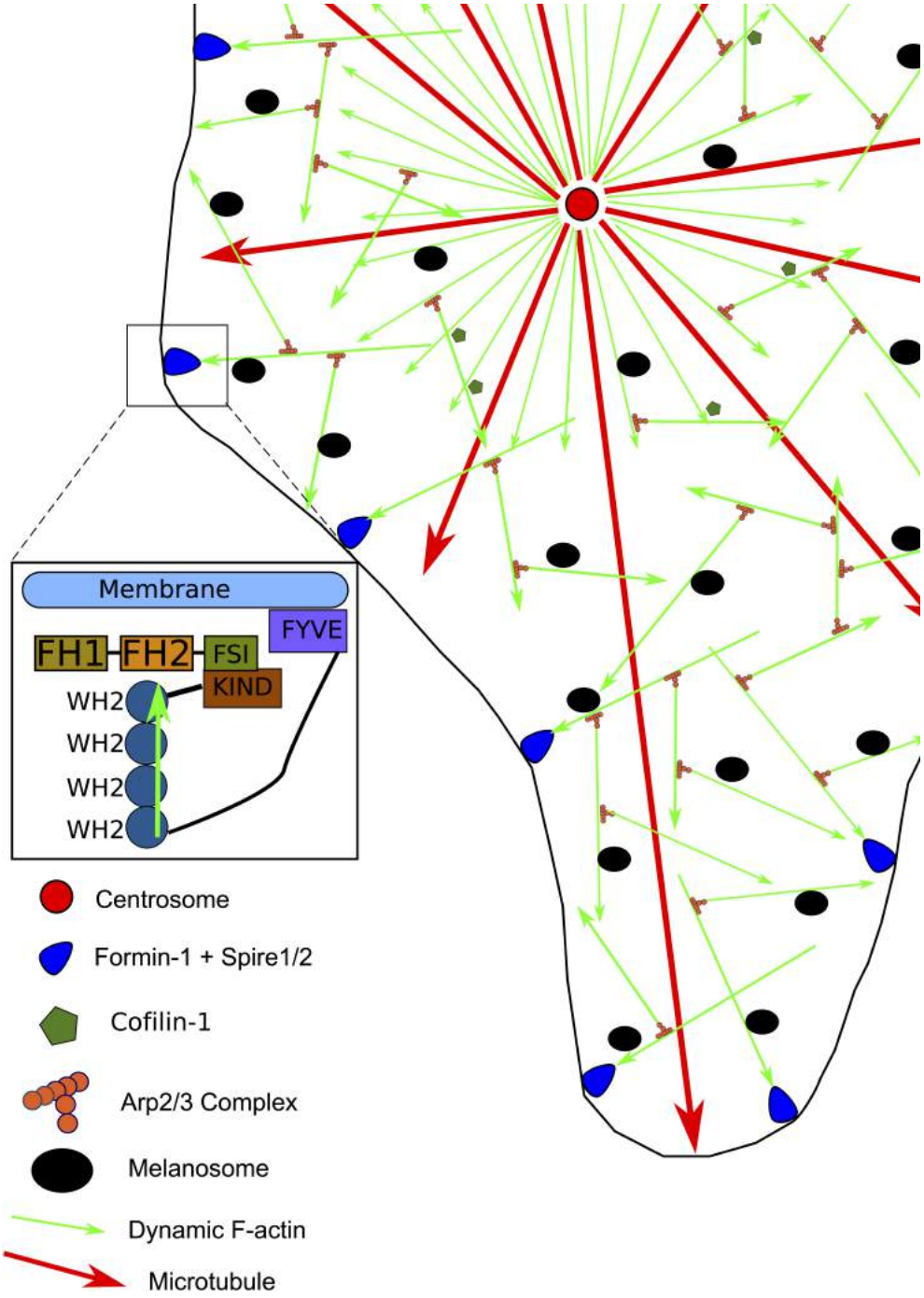


Figure 5.14 - Formin-1, spire1/2, Apr2/3 and cofilin-1 complex create a dynamic F-actin network with filament barbed ends subtly polarised towards the plasma membrane. In this model, spire1/2 is localised at the plasma membrane, where it recruits formin-1 via its KIND domain. Spire could then generate actin seeds, which are then elongated by formin. In this case, these complexes would be expected to generate linear actin cables that protrude into the cell, with the filament barbed ends pointed towards the plasma membrane (as observed by Geron et al., 2013). If the data published by Farina et al., 2016 is also applicable to melanocytes, this would result in linear actin cables generated at the centrosome via Arp2/3 complex radiating out from the cell centre with their barbed ends also pointing to the plasma membrane. Along with branched actin generated by the Arp2/3 complex, where the daughter filament is always at a 70º angle to the mother filament, this would in theory create an actin network that is subtly polarised towards the plasma membrane. Melanosomes may be returned to the perinuclear area either by retrograde microtubule-dependent transport (which myosin-Va is constantly opposing) or via actin filaments whose barbed ends are polarised towards the cell centre. However, because actin filaments are (on average) polarised towards the plasma membrane, given enough time every melanosome would be able to be trafficked from the perinuclear area to the cell periphery in an actin-dependent manner. Cofilin-1 is needed to continually sever actin filaments, thus keeping the actin network dynamic. Arrow heads represent the plus or barbed end of microtubules and actin filaments.

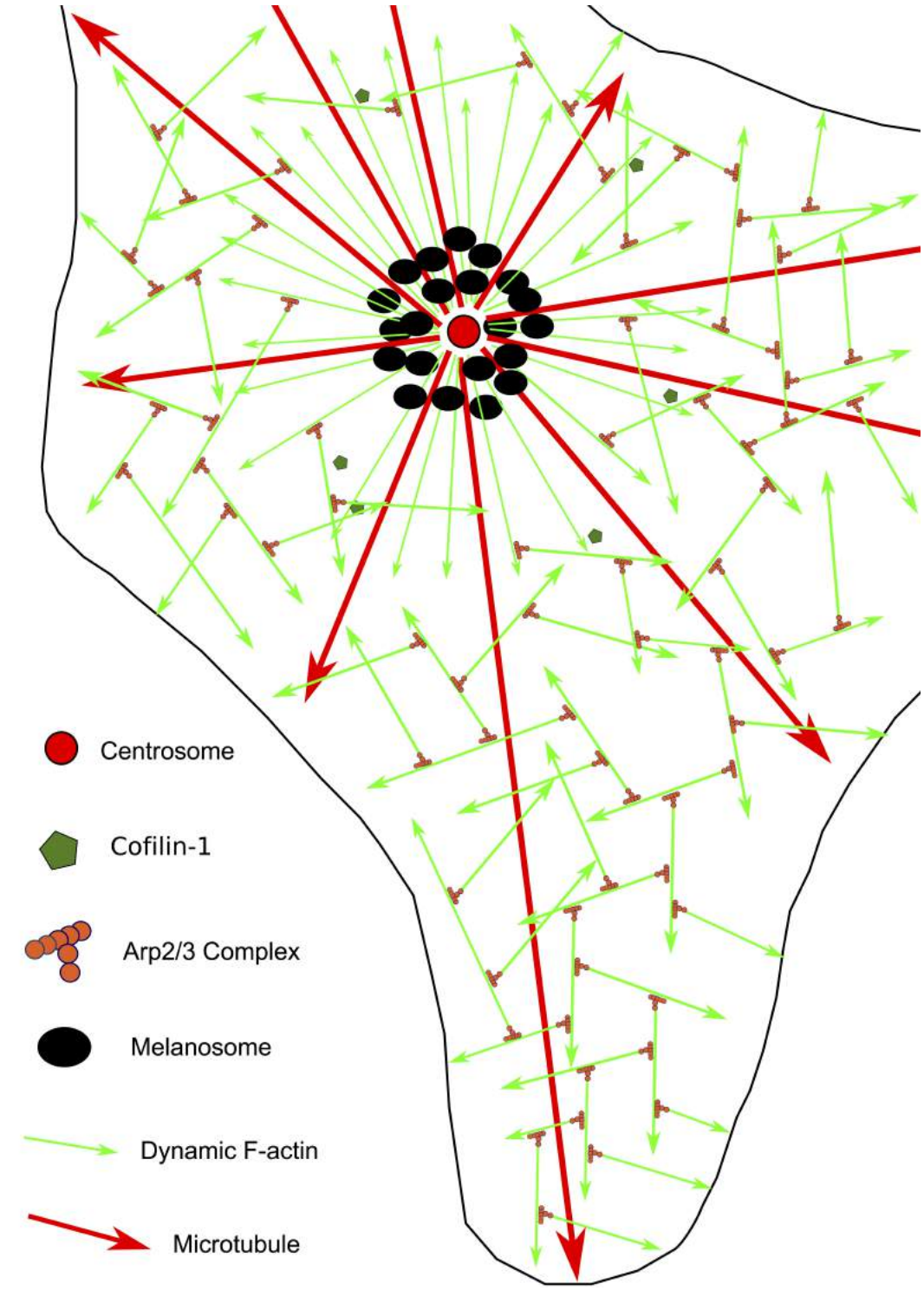


Figure 5.15 - Following formin-1 or spire1/2 knockdown, F-actin is more randomly polarised, resulting in retrograde microtubule-dependent transport being favoured. In cells lacking formin-1, or spire1/2 (which in this model is required for the localisation of formin-1 at the plasma membrane), the linear actin cables generated by these nucleators are lost. The Arp2/3 complex alone could in theory generate a highly branched actin network that is anchored to the centrosome-generated filaments, with some barbed ends polarised towards the periphery. However, without formin-1 and spire1/2, the actin network would on average be less polarised towards the plasma membrane compared to the wildtype cells. Moreover, in the absence of linear actin cables protruding into the cytoplasm from the plasma membrane, any myosin-Va trafficking melanosomes to the periphery would be forced to translocate along purely branched actin. This means the number of track changes the motor would be required to make to reach the cell cortex would be greater on average than in the wildtype cells, especially when the dynamic nature of the actin network is considered. This would increase the likelihood that the myosin-Va/melanosome complex would at some point detach and get trafficked to the cell centre in a microtubule-dependent fashion. Arrow heads represent the plus or barbed end of microtubules and actin filaments.

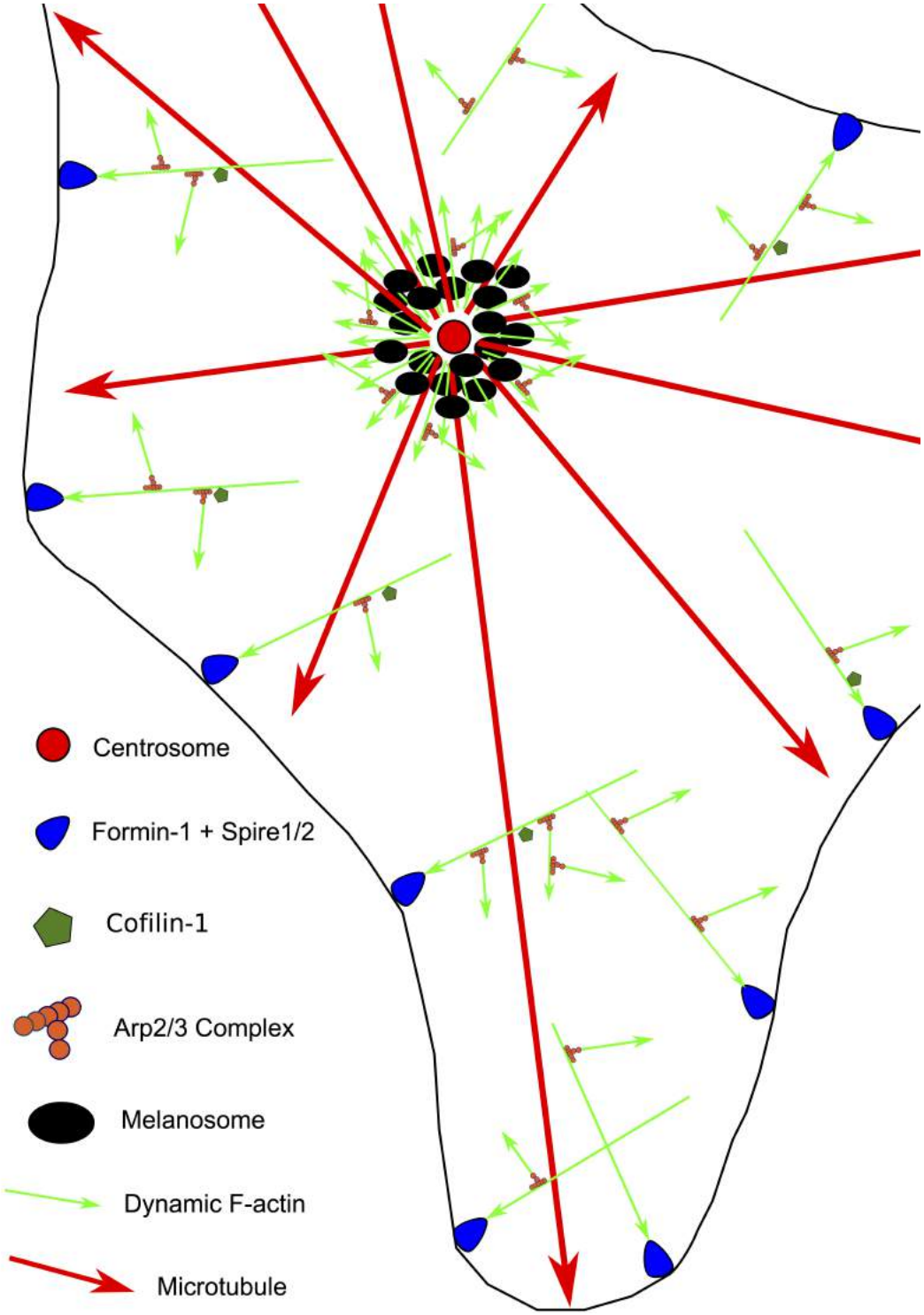


Figure 5.16 - Following Arpc1b knockdown, F-actin filaments become shorter, resulting in retrograde microtubule-dependent transport being favoured. If the data published by Abella et al., 2016 is also applicable to melanocytes, Arpc1b knockdown in these cells should result in actin filaments nucleated by the Arp2/3 complex becoming much shorter. In this case, the actin network would become less branched, and the number of 'dead ends' - where an actin cables nucleated by Apr2/3 do not cross paths with another filaments - would increase compared to the wildtype cells. This would increase the likelihood that the myosin-Va/melanosome complex detaches from the actin filament and becomes trafficked to the perinuclear area in a microtubule-dependent manner. Arrow heads represent the plus or barbed end of microtubules and actin filaments.

Chapter 6

Summary

This project had the original aims of identifying the isoform of kinesin responsible for anterograde melanosome transport, the mechanism by which this motor attaches to these organelles, and the process by which they are handed over from microtubule to actin-based transport. However, despite the widely held view that kinesin facilitates long-range anterograde organelle transport, the experiments described here indicate kinesin is not necessary for anterograde melanosome transport.

Initial experiments sought to determine the subcellular localisation of Kif5B, which has previously be implicated in melanosome transport within melanocytes (Hara et al., 2000; Vancoillie et al., 2000b). However, neither immunofluorescence nor western blotting were able to detect either exogenously or endogenously expressed Kif5B on the melanosome membrane. When the functional importance of this protein was tested by knocking it down in melan-a cells via siRNA, the melanosome distribution remained wildtype, although the mitochondria were found to cluster around the perinuclear area.

These experiments suggested that Kif5B was not responsible for the anterograde trafficking of melanosomes. Before individually testing the involvement of a large (>50) number of different kinesin isoforms in the transport of melanosomes, a more general approach was adopted whereby the relative contribution of the actin and microtubule networks on melanosome distribution was investigated. It was found that depolymerising the microtubule network did not alter the phenotype of wildtype melanocytes. By contrast, destroying the actin cytoskeleton caused the pigment granules to cluster around the perinuclear area. At first glance, this finding appears to support the cooperative capture model (proposed by Wu et al., 1998), which states that actin is required to tether the melanosomes at the periphery. However, when drugs were used to stabilise the actin cytoskeleton, rather than depolymerise it, the wildtype melanocytes were still found to phenocopy the melan-dilute cells, suggesting a dynamic actin network is vital to maintain dispersed melanosomes at steady-state.

Next, the contribution of microtubules in melanosome transport was investigate further by testing if they are required for the active long-range anterograde transport of these organelles. Melanosomes within clustered melan-dilute cells can be made to re-disperse over the course of 16 hours if these cells are infected with GFP-myosin-Va adenovirus. Therefore, *dilute* melanocytes were preteated with noc to depolymerise the microtubule network and subsequently transfected with GFP-myosin-Va. Surprisingly, the melanosomes were still able to re-disperse, implying that microtubules are not necessary for this process. Moreover, by

precisely quantifying melanosome distribution through the use of micropattern chips which standardise cell size and shape, it was found that anterograde transport was actually slightly enhanced in the absence of an intact microtubule network.

These 'add-back' experiments were then repeated to determine the contribution that the actin cytoskeleton plays in anterograde melanosome transport. Stabilising F-actin before transfecting *dilute* melanocytes with GFP-myosin-Va completely inhibited rescue, demonstrating the important role these filaments play in the active dispersion of melanosomes. Moreover, when wildtype melanocytes were treated with these actin inhibitors in order to cluster the melanosomes and the drug subsequently washed out, re-dispersion of the pigment granules coincided with the re-growth of the actin cytoskeleton, with cortical actin almost always recovering first.

The importance of the actin cytoskeleton on anterograde melanosome transport was further demonstrated when a number of actin-binding proteins such as formin-1, Arpc1b, cofilin-1, γ-actin and spire1/2 were identified through an siRNA screen to be important for maintaining peripherally dispersed pigment granules at steady state. Recently, melanocytes from a Fmn1$^{-/-}$ CJ57BL/6 mouse have been isolated and the melanosomes shown to be clustered around the perinuclear area, similar to the phenotype of melan-dilute cells. When these cells are transfected with GFP-formin-1, the melanosomes re-disperse to the periphery, confirming the involvement of this protein in pigment granule transport (data not presented in this study).

Formin-2, which is highly analogous to formin-1 (Leader and Leder, 2000), along with spire1 and spire2, was also found to be important for the long-range microtubule-independent trafficking of transferrin-containing vesicles (Schuh, 2011). These actin nucleators were shown to be present on the vesicle membrane and were important for nucleating short actin filaments through which the vesicles are tethered in a 'global mesh'. Formin and spire were also found to be localised at the plasma membrane, where they generate actin cables with their barbed ends orientated towards the membrane. These membrane-bound filaments guide myosin-V motors towards the cell periphery, and as they translocate they drag the actin-mesh (and therefore the transferrin vesicles) towards the membrane. Although there is no evidence that formin-1 or spire1/2 are present at the melanosome membrane, it could be theorised that these molecules are present at the plasma membrane where they help generate a subtly polarised actin network (as outlined in Figure 5.14), allowing myosin-Va to mediate antero-

grade melanosome transport. Futhermore, the Arpc1b isoform of Aprc1 may be required to ensure the Arp2/3 complex nucleates sufficiently long actin filaments in order to promote an overlapping actin cytoskeleton. This would mean that myosin-Va only rarely reaches the end of an actin track, detaches and subsequently gets transported back to the perinuclear area in a microtubule-dependent manner (as outlined in Figure 5.16).

While this study strongly suggests that Kif5B is not involved in melanosomes transport, other recent research argues the opposite is true. For example, recent findings from Ishida et al. show that transfecting wildtype melanocytes with KIF5B and KLC2 siRNA leads to clustering of the pigment granules. Moreover, their data also suggests that Rab1A is required to link Kif5B to the melanosome membrane (Ishida et al., 2015). However, when these experiments were replicated by Hume and colleagues, neither KIF5B nor Rab1A siRNA treatment caused the melanosomes to cluster in the majority of cases, in keeping with the data presented in this study. It is possible the method of quantifying the data, which was done by manually scoring cells as either 'clustered' or 'dispersed' in the Ishida et al. study may be one reason for their conclusions. Furthermore, no positive control for melanosome clustering, such as Rab27a or Mlph siRNA was used, making it difficult to interpret their findings.

In conclusion, the results from this study argue against the established 'cooperative capture' model of melanosome transport. Instead they show that melanosomes can disperse via an actin-dependent process that likely involves a number of actin-binding proteins which function together to promote a dynamic actin cytoskeleton which can oppose microtubules and support long-range anterograde organelle transport.

Chapter 7

Appendix

Table 7.1 Primers used in the KIF RT-PCR screen.

KIF Gene	NCBI Reference	Forward (5') Primer	Reverse (3') Primer	Expected band size (bp) if kinesin expressed
KIF1A	NM_008440.3	CCCAGGATGACCG-CGTTTCC	GTGAGGCGGGTAG-CTTGGCG	257
KIF1B	NM_008441.2	AGCTGCGCTCAGG-GAACCGTA	TCCCCGCTATCAG-AATCCGCGT	289
KIF1C	NM_153103.2	GGACACCAGCTGA-GGAGGGCA	GGACTTCCCAGCC-CCCGTCT	349
KIF2A.1	NM_008442.2	GTGGTGGCAGTCG-CCCTGAT	CGAATGGATTCC-TGGAACACTGCCC	331
KIF2A.2	NM_001145779.1	AAGCGCAGCGATG-GCCGAAT	CGTGCGCGTGCTG-AACCAAC	302
KIF2B	NM_028547.2	CCAACGGTCACGT-AGGCCCC	TCGGCGGCGCTTC-TCTCTCT	232
KIF2C	NM_134471.4	GAGTCGCTTCACG-CACGCCT	TGCGTTTTTGCT-TCGGGACCGT	268
KIF3A	NM_008443.3	TGGTGGTTAGGTG-CCGGCCT	GCAAAGATGGTCC-CATTGTAGCCT	245
KIF3B	NM_008444.4	GGTGCCAAAATC-AAGGCCATGGAGA	CGTGGATCTCGGC-CTTCACGG	280
KIF3C	NM_008445.2	GCGGAACAGAAAC-GCCGTGAAC	GGCACCAGTGGCT-GGAACCT	359
KIF4	NM_008446.2	GCACTCAGCATGC-CCTACGCC	CGGCGCTCACTCA-ACTTGGCT	259
KIF5A	NM_008447.4	GATATGTACTTT-GCCAGCAGCGGAG	GGCTGGGGCTAGG-GAGGGAAG	251

Continued on next page

KIF5B	NM_008448.3	GGCTCCCCTCGCT-TACCCCA	GGCATAAGGCTTG-GACGCGATCAT	213
KIF5C	NM_008449.2	AGCTGGCCCAGAA-AACGACGA	CTCGCGCTCACTG-GCGTTCA	323
KIF6	NM_177052.3	AGGCCACCAGCCT-GCAGGTAA	TGGCTTTGCTGG-TTGGGGCAG	202
KIF7	NM_010626.2	ACATCCGCAATCG-CGCCACA	TGTCGGGTCCGGA-GGCAGAG	342
KIF9.1	NM_001163569.1	GCCGGTGGCGTTA-GCTAAAATGG	CCGGCTCCTGTCT-GCCCGTA	312
KIF9.2	NM_010628.3	CGCCATCGCCTGC-TCATGGAATTT	TGTGTGACTGTT-GGAGGCCCAC	283
KIF11	NM_010615.1	AGGCCGGCAGGTT-TTGGCTC	TCCGTCAACCCTG-CAGTCCG	200
KIF12	NM_010616.2	CCTGCGTGTCCCC-TTCAGCG	CCTGGTGCCGTGG-TGTGCAT	211
KIF13A	NM_010617.2	ACCCCAAAGGGAG-CAGGCAGT	CTTTCAGCCGCTC-ACCCGCA	327
KIF13B	NM_001081177.1	GTTCATGGGCGCC-AGGGCTT	CCACGGCCAGCAC-ACTCCTC	229
KIF14	NM_001081258.1	GGCTGGAGACCGC-GCAAGAC	GGCTGGAGACCGC-GCAAGAC	280
KIF15	NM_010620.1	TGGAGAAGAGCAG-CGAGACCGT	TGCCACCAAGGGA-GTCCCGA	252
KIF16B	NM_001081133.2	TCGGCCTTGTTCC-CGTAGCA	GGCCGTCTCTGAG-GGGAGGT	306
KIF17.1	NM_010623.4	GGTGGCTTGCCTG-TCTCCCG	GCGCTCCTCATAC-TCCTCTCGGA	325
KIF17.2	NM_001190978.1	GGTGGCTTGCCTG-TCTCCCG	CAGCCGAGGATGG-CTCTCGGA	323

Continued on next page

KIF18A	NM_139303.1	GTGGAAAAGGCCA-CTTGCAAACGA	TGCTTGTGCTGCT-GTTCCTGGAG	287
KIF18B	NM_197959.2	CACAGCACCCCAC-GGATGCC	CTTGCGGCCCTTT-GCATCAGC	263
KIF19A	NM_001102615.1	ACAAGGGCTGTCC-CGTCCCA	CGGCTTGGTTGGG-GGCAACA	212
KIF20A.1	NM_001166406.1	CGCGTCCGTAGAA-GGCTCCTG	GTAGAGCCTGCTT-GTCCTCCAGA	350
KIF20A.2	NM_001166407.1	AGGACAAGGGAT-TGCGGCTGA	AGGTGTCCTCCAG-TAGAGCCTGC	338
KIF20A.3	NM_009004.4	GCTGCGCGGGTGG-GTAGAAG	CGCAGCCCTGATC-TTCCTGTCG	338
KIF20B	NM_183046.1	CGCCTCAAACCCT-GCGGCAA	TCTGTGCCACCTG-TCCAGAGC	203
KIF21A.1	NM_001109040.1	TGTCTGGCCCTCT-GGCACCT	GGAAGCGCCCGAA-TCTGAGTGTTT	254
KIF21A.2	NM_001109041.1	TTACACAGCCCGG-GGTCGGA	GCCCGAATCTGAG-ATGCTGCCTA	309
KIF21A.3	NM_016705.3	GCCACGCACTGCA-AGAAAACGAG	GCCCTTCTGCAAC-AGGTGCCA	252
KIF21A.4	NM_001109042.1	TTACACAGCCCGG-GGTCGGA	TGGGTTGATTAT-GCCTATGCTGCC	312
KIF21B	NM_001039472.1	GTGGTCTGCTGGC-CTTGGGC	GCGGGCCCGGTTG-GCATATT	212
KIF22	NM_145588.1	GGCAACCAGGGCAT-TCGGCT	GGTGCCAAGGCAT-GAGGCTGT	302
KIF23	NM_024245.4	GCAACTCATGAGC-CAGCCGC	TGGGGTGTTCCTG-CGGCAATG	283
KIF24	NM_024241.2	GCGCTATGCTGAC-CGGGTGAA	GGCTGGCCAAAGG-ATGGGCT	227

Continued on next page

KIF26A	NM_001097621.1	ACTCCTCTCCGGG-ATCCTTGCCT	CCCTGGAGCTGGG-AGCCGCA	220
KIF26B	NM_001161665.1	CCCCTCCCGGGAA-AGGACCC	GCCCACCCATGTG-GCGAGAC	265
KIF27	NM_175214.3	GCGCACACTGACC-GAGCATCAT	TGGCCACTGGAGG-GCGCTAT	420
KIFC1	NM_001195298.1	GGCGCAGAGGCCA-CCTTTGT	GAGCTGCAGTGTG-GCCCTGG	248
KIFC2	NM_010630.2	TCCCACCCAGAA-AAGCGGCG	GGGCTCCGTGTCC-ATGCCAG	312
KIFC3.1	NM_010631.2	TGTCTCCGCTAGG-CCGCTTG	CCACGCTGAGGGC-TCGACAC	317
KIFC3.2	NM_001145831.1	TCAGAGCTGTCAG-GGCGTGGA	ATGCCAAAGAGCC-GCCCACC	314
KIFC3.3	NM_001145832.1	CCAGCCCACGTTC-CCTACAGC	GGCTGCTCTCCTG-GCTGTGCT	326
Fmn1	NM_010230.2	ATGATAAAAGCC-AAGACGCCG	AACTTGATGATC-TTTTTGACT	172bp
Aprc1b	NM_023142.2	GACTGGGCCCCTG-AGAGTAA	TTGCACACCCACC-AGTCATT	230bp
Cfl	NM_007687	TAGGAGATGTGGG-GCAGACT	TTCATGCTTGAT-TCCTGTCAGC	233bp
ACTG1	NM_009609	TGGAAGAAGAAA-TCGCCGCA	GGTTTCAAACAT-TATCTGCGTCA	377bp

Table 7.2 - siRNA sequences used to test the involvement of actin-binding proteins in melanosome transport.
Protein names in bold were found to pull down with Rab27a in a TAP-tag experiment (Booth, 2012)

Gene	Protein	NCBI Reference	Sequence
KIF5B	Kinesin-1	NM_008448.3	UGAAUUGCUUAGUGAUGAATT[1]
ACTG1	**γ-actin**	NM_009609	#1 - GGAGAAGAGUUACGAGCUG #2 - GGCAUGGAGUCCUGUGGUA #3 - UAGAUGGACUGAGCAGGUG #4 - ACGAUGAAGAUUAAGAUCA
IQGAP2	**IQ motif containing GTPase activating protein**	NM_027711	#1 - CAGAACAAGUCGACGAAAU #2 - AGGCACACGUGGACCGUUA #3 - AAUCAUGGCUCACGGGAGA #4 - AGGUGAAAGUGAACGUGAA
PFN1	**Profilin 1**	NM_011072	#1 - GCAAAGACCGGUCAAGUUU #2 - CAAAGAAGGUGUCCACGGU #3 - CAAUGGAUCUUCGUACCAA #4 - GAAAUGUUCUGUGAUCCGG
MSN	**Moesin**	NM_010833	#1 - GCAAGCAGCUGUUUGACCA #2 - GCGCAAGCCUGACACCAUU #3 - GGCUGAAACUCAAUAAGAA #4 - GAGUACACCUCAUGUGGCA
MYH9	**Myosin heavy polypeptide 9 (non-muscle)**	NM_022410	#1 - GAGCGAGCCUCCAGGAAUA #2 - GCACCAAGCUCAAGCAGAU #3 - GAACCGAACUGGCCGACAA #4 - GAAGGUGGCUGCCUACGAU
Rhoc	**Ras homolog gene family member C**	NM_007484	#1 - GAAAGAAGCUGGUGAUUGU #2 - CUACAGGUCCGGAAGAAUA #3 - CUAUAUAGCCGACAUCGAA #4 - GAUCAGUGCCUUUGGCUAC
SEPT2	**Septin 2**	NM_010891	#1 - GCAGGAAAGUAGAGAAUGA #2 - GAUAGAGGCUUCGACUGUU #3 - UGAAGAGCAUAGCAUUAAA #4 - GCGAUACACAAUAAGGUGA

Continued on next page

[1] Gupta et al., 2008

Gene	Protein	NCBI Reference	Sequence
MTPN	**Myotrophin**	NM_008098	#1 - UGAAAUUGCUUCUGUCAAA #2 - GAAGGACUAUGUGGCUAAG #3 - GCUGAAAGGAGCAGAUAUU #4 - UCAUUAUGCUGCAGAUUGU
Tln1	**Talin 1**	NM_011602	#1 - GAUAGGCGCUCACAUCAAA #2 - GCACAGAGCCGAUUGAAUG #3 - GGAUGUAGCUGGUGGACUA #4 - UGACAAGGCCUGUGAAUUU
CAPZB	**Capping protein (actin filament) muscle Z-line**	NM_009798	#1 - GAUCUCCUGUCAUCUGUUG #2 - GUAUGACCCUCCUUUGGAA #3 - GUACUGCCCAUUACAAGUU #4 - GAAAGACGAAACUGUGAGU
COTL1	**Coactosin-like 1**	NM_028071	#1 - GCGAUCAGGGAGCAGAUUA #2 - GAGCAAAAGAUCCAAGUUU #3 - CCGACAAGACGCUGGUGAA #4- CGUACAACUUAGUGCGGGA
CORO1C	**Coronin-1C**	NM_011779	#1 -GAUCAAAUCCAUAAAGGAA #2 - GACCGAGCCUGUGGUGAUU #3 - CAAUUGCUCUCCAUGAAAU #4 - GAAAGUGCGAGCCCAUUAU
Myl6b	**Myosin light polypeptide 6B**	NM_172259	#1 - GUCCCGACGUGUAGACUUU #2 - AGGACCAGCUGGAGGAAUU #3 - GAACCGGGACCAAGGCACA #4 - AAGUGGUGAUCGAGUUUAA
Tmod3	**Tropomodulin 3**	NM_016963	#1 - ACAAAGACCGGGACGAUUA #2 - GUAACGGUGUCAACCAAGA #3 - CCAACGCGAUAACGAAGAA #4 - CCACGGGACCCUUUGAUAG
Actr3	**Actin-related protein 3**	NM_023735	#1 - AUACAGAGCCACAGUUUAU #2 - CAAGUUAUUACACACCAUA #3 - GUUCAACCAUGUUCAGGGA #4 - GGCGUCCUCUCUACAAGAA

Continued on next page

Gene	Protein	NCBI Reference	Sequence
Zyx	**Zyxin**	NM_011777	#1 - GUAUUGACCUGGAGAUUGA #2 - GGAGGGAGCACCAUAUUGU #3 - GGAUAAGAACUUUCAUAUG #4 - AGACGAGACUGUGCGAGUA
Dstn	**Destrin**	NM_019771	#1 - GAGUUCAGGUUGCGGAUGA #2 - GCAUGAGUAUCAAGCAAAU #3 - GUGCAUAGUCGUUGAAGAA #4 - CGACAUGAAAGUUCGGAAA
Epb4.1l3	**Erythrocyte protein band 4.1-like 3**	NM_013813	#1 - GAAACUGCCUUAACAAACG #2 - GCACGAGUGUGGGCAGUAU #3 - GAGUGGAGAUUAUGUUAGG #4 - GCACCAAACCAAUAUUAGU
Epb4.1l2	**Erythrocyte protein band 4.1-like 2**	NM_013511	#1 - GGGCAUCUCUCGAUUCAUA #2 - AAACAGAGAUGGUAACAAU #3 - GCACAAAGAAACAGAGUUG #4 - GUAAAGAGAUGUCACCGGG
Ppp1cc	**Protein phosphatase 1, catalytic subunit, gamma isoform**	NM_013636	#1 - GAACUUCUUUCUUCUCAGA #2 - GGAGUGUCCUUCACAUUUG #3 - UCAAUAGGAUCUACGGAUU #4 - GCAGUUAGUCACUCUGUUU
Rap2a	RAS related protein 2a	NM_029519	#1 - UGACAAAGAUGACCCAUGC #2 - GAAGUGUCCUCCAACGAAG #3 - GCGUGAAGCGGUAUGAGAA #4 - UUGCAGAAAUUGUGCGGCA
Cdc42	Cell division cycle 42	NM_009861	#1 - CGGAAUAUGUACCAACUGU #2 - GCAGUCACAGUUAUGAUUG #3 - GACUACGACCGCUAAGUUA #4 - UCUAGUAUGUUUCUCAGUG
Myo5a	Myosin-Va	NM_010864	#1 - GCAAGAUACUCCGUGAAUA #2 - GCACAAGCAUAUAUUGGUU #3 - GAACCUGAUUCUAGAACUA #4 - CAACACGUCUCGCCAGAAU

Continued on next page

Gene	Protein	NCBI Reference	Sequence
Vasp	Vasodilator-stimulated phosphoprotein	NM_009499	#1 - GGGCUACUGUGAUGCUUUA #2 - GGAGGACGCCAUACAGUUU #3 - CGGAUCAGCAGGUGGUUAU #4 - CCAGAGUGAACCUGUGAGA
Enah	Enabled homolog (*Drosophila*)	NM_001083121	#1 - GCAGAAAGAUUCAAGACCA #2 - GAGAACGACUAGAACGAGA #3 - GACAGAAGGCCUUGACUAU #4 - GGAUGGAACAAACGGAGUU
Diap2	Diaphanous homolog 2	NM_172493	#1 - GAUGACCGAUCUUUGAUUU #2 - CCUAGAUGCUUGUGUAAAU #3 - UACCAUCUGCUGUAUAAUA #4 - CCGCAUGCCAUACGAGGA
Fmnl3	Formin-like 3	NM_011711	#1 - GUAAAGAACUGCAUCGGUU #2 - CUUCGAAACUUCCUUAGUA #3 - GAUCUCACUUCGCACCAAU #4 - GAGAUUCGCCCUAGUGCUG
Daam1	Dishevelled associated activator of morphogenesis 1	NM_172464	#1 - GGACUGAAAUUGAUGAUAC #2 - GAAUUCAACCUGUUAUAGA #3 - GCACUGGGCGUUAUCGGGA #4 - GUCGUAAGAAUGUUGGUUA
Daam2	Dishevelled associated activator of morphogenesis 2	NM_001008231	#1 - GCAGAUCGCUUCCUCUAUG #2 - CCAUAAACAGGCUAAAUUA #3 - GAGAAGAGCGACAUUGAUC #4 - GCUAAAGCACCUAUCAGAA
Fmn1	Formin 1	NM_001043322	#1 - GGACAAACCUGAACAAUUU #2 - GAACGUGCCCAGUGCAUAA #3 - GCAGACGGAUAUAGUUUAG #4 - GGUGAGCACGCAUUAGUAA
Fmn2	Formin 2	NM_019445	#1 - GGACAGCGCUCACUCUAUA #2 - AGACAUGACUCUGGGAUUA #3 - CUACGGAGCAGGAGGAUUU #4 - GAGCAAGUCCGAUUCUAGA

Continued on next page

Gene	Protein	NCBI Reference	Sequence
Rhoa	Ras homolog gene family member A	NM_016802	#1 - GGUAAGACAUGCUUGCUCA #2 - GCAGGUAGAGUUGGCUUUA #3 - AAAACUAUGUGGCGGAUAU #4 - UGAAGCAGGAGCCGGUAAA
Rhof	Ras homolog gene family member f	NM_175092	#1 - GAUGCGAGGUGCACUCUAU #2 - CGUCGGUGUUUGAGAAGUA #3 - ACACAUUUCUGCCGAGGGA #4 - AGAUAGUGAUCGUAGGUGA
Rock1	Rho-associated coiled-coil containing protein kinase 1	NM_009071	#1 - GCAAAGAGAUUGUUAGAAU #2 - AGACACAGCUGUAAGAUUA #3 - UGUCGAAGAUGCCAUGUUA #4 - GACCUUCAAGCACGAAUUA
Spire1	Spire homolog 1 (*Drosophila*)	NM_176832	#1 - GGAAACACCUACGAACGUG #2 - GAAAUUAGACGGAGCAGAC #3 - GGACGACAUUCGGUGCAAA #4 - GCAUACAUUUCUGACCAAA
Spire2	Spire homolog 2 (*Drosophila*)	NM_172287	#1 - GGACGCACAUGAACUUAUC #2 - GAGCGUGGAUGUCCUCAAU #3 - CAAGAAGUAUGGACACAUC #4 - CAAAGAACACUGCACGAGA
Rhoq	Ras homolog gene family member Q	NM_145491	#1 - GAAACUAGCAAAAGAGAUA #2 - UAGCAAGACUGAAUGACAU #3 - UAAUAGGAACUCAGAUUGA #4 - GCUAAAGGAAUAUGCGCCA
Rhou	Ras homolog gene family member U	NM_133955	#1 - GAAGUGGGUUCCAGAGAUU #2 - CGACGUCACUGCCCAAAGG #3 - GUACAUCCCUACGGCCUUC #4 - CGUCAAAGUGCUCAUAGAA
Rhov	Ras homolog gene family member V	NM_145530	#1 - CGAUGUCAAUGUACUAAUU #2 - CUAUCGGCCUACAGCACUA #3 - CGCAGAAGAACUUGAAGGA #4 - CGAAUCGAGCUUUGGGACA

Continued on next page

Gene	Protein	NCBI Reference	Sequence
Rac1	RAS-related C3 botulinum substrate 1	NM_009007	#1 - GGACGAAGCUUGAUCUUAG #2 - AGACGGAGCUGUUGGUAAA #3 - GAUCGGUGCUGUCAAAUAC #4 - GCAAAGUGGUAUCCUGAAG
Rac2	RAS-related C3 botulinum substrate 2	NM_009008	#1 - AUGUGAUGGUGGACAGUAA #2 - CCACUGUAUUUGACAACUA #3 - GGCCAAGGAUAUUGAUUCA #4 - GGAUAUUGAUUCAGUCAAG
Rac3	RAS-related C3 botulinum substrate 3	NM_133223	#1 - GAAGUGCACUGUAUUCUAG #2 - GAAUAUAUCCCCACAGUUU #3 - UGACAAGGAUACGAUUGAA #4 - GUGGAUGGGAAGCCAGUUA
Rhobtb1	Rho-related BTB domain containing 1	NM_001081347	#1 - GAGCAUCGAUGGUGAAGUU #2 - GAAAGCCAAUCGGAUCAAA #3 - CCAGGGAUGUCGUCGAUGA #4 - CUACGAGACCAGCGUGUUU
Rhobtb2	Rho-related BTB domain containing 2	NM_153514	#1 - GAAAUCACAUCUGCGCAAU #2 - GCGCUAUGCUGACCUGGAA #3 - UGAAAGAAGAGGACCACUA #4 - CCCGAGAUGUGGUAGAUGA
Rhobtb3	Rho-related BTB domain containing 3	NM_028493	#1 - GUAAUUAUAUGGAAGCCAA #2 - CCGGAAAUGUCGCUGUUUA #3 - GGAUAACUAUAUUCCAGUG #4 - CCACUAACUACCUCAUAUU
Rhoh	Ras homolog gene family member H	NM_001081105	#1 - GAAUACGGGUGUAGACGUC #2 - AAGAACAAAUGGAUUAGUG #3 - GGAGCAACCUACCCUGUAC #4 - GUACAGCAGGUAUUUGAAU
Rnd1	Rho family GTPase 1	NM_172612	#1 - GAACAGACCUGAGCACUCU #2 - CAACUACAUUCAAGAAGGA #3 - CGACUCAGAUGCGGUAUUG #4 - GCAGAAAUCUACCUGGAGG

Continued on next page

Gene	Protein	NCBI Reference	Sequence
Rnd2	Rho family GTPase 2	NM_009708	#1 - UGAGGGAGCUAUCCAAGCA #2 - GGAGCUGUGUCCUACGUUG #3 - GGACAUGCGGACUGACCUG #4 - CACAGUGGCUUCUCUCGGC
Rhod	Ras homolog gene family member D	NM_007485	#1 - GGGAAGACGUCACUGAUGA #2 - GGAUUACUCAGAAUUGUUG #3 - GAUGAAGGGUAAACCUGUG #4 - GCAAGAUAGACCUGCGUAA
Iqgap2	IQ motif containing GTPase activating protein 2	NM_027711	#1 - CAGAACAAGUCGACGAAAU #2 - AGGCACACGUGGACCGUUA #3 - AAUCAUGGCUCACGGGAGA #4 - AGGUGAAAGUGAACGUGAA
Actr2	Actin-related protein 2	NM_146243	#1 - UUUGUAUGCUCAAGGUUUA #2 - UCACAUUUGCCCAGUAUAU #3 - AGACAGUUCGCAUGAUUAA #4 - UGGUGUAACUGUUCGAUAA
Actr3	Actin-related protein 3	NM_023735	#1 - AUACAGAGCCACAGUUUAU #2 - CAAGUUAUUACACACCAUA #3 - GUUCAACCAUGUUCAGGGA #4 - GGCGUCCUCUCUACAAGAA
Arpc5	Actin related protein 2/3 complex subunit 5	NM_026369	#1 - GUGUGGACCUCCUAAUGAA #2 - UGGACGAAUAUGACGAGAA #3 - ACACAAAGAGCCAGGCAGU #4 - UUUGAGAGCCCAUCUGACA
Arpc4	Actin related protein 2/3 complex subunit 4	NM_026552	#1 - GAACUGCUAUUACAGCCUG #2 - UAUCGUAGCUGAGGAGUUC #3 - GCAGGCCGAUGAAAUUGAG #4 - GAGAUGAAGCUGUCGGUCA
Arpc2	Actin related protein 2/3 complex subunit 2	NM_029711	#1 - UAUCUGCACUACCACAUUA #2 - GAGCAGUUAUCCAUUAUAG #3 - UCUAAGGCCUAUAUUCAUA #4 - GAGCUGAUGAGUUGUUAAA

Continued on next page

Gene	Protein	NCBI Reference	Sequence
Arpc3	Actin related protein 2/3 complex subunit 3	NM_019824	#1 - ACACCAAGCUCAUCGGUAA #2 - GGACUGAGGCUGUGUGAGA #3 - ACACGGACAUUGUGGAUGA #4 - GCAUACCACUCUUCUCUCA
Tagln2	Transgelin 2	NM_178598	#1 - GAAAGAACAUGGCUUGUGU #2 - GCCGAGCGCUAUGGCAUUA #3 - GUUCUGUGCAAGCUUAUUA #4 - CAAGAGGGCAAGAACGUGA
Flna	$\alpha-$Filamin	NM_010227	#1 - GCUCAGAGGUAGACGUGGA #2 - CCAGCAAGGUGAAGGCGUU #3 - CAGAGUAACAGGUGACGAU #4 - CAUUGAGGGUCCAUCUAAA
Dsp	Desmoplakin	XM_896350	#1 - UCAAAGUCCUGGAGCAAGA #2 - GCAUCCAGCUUCAGACAAA #3 - ACACCAACAUCGCUCAGAA #4 - GUGCAGAACUUGGUAAACA
Ptma	Prothymosin alpha	NM_008972	#1 - GCGGGUAGCUGAGGAUGAU #2 - GACCGAGGAGGAUGACUAG #3 - GGAUACCAGCUCCGAGAUC #4 - AUGACGAUGUGGACACCAA
Tpm1	Tropomyosin 1 alpha	NM_024427	#1 - UGAAGUCACUGGAGGCUCA #2 - GGACAAAUACUCCGAGGCU #3 - AGAGAGAUCAGUAACCAAA #4 - GAUCAGACUUUACUGGAGC
Cfl1	Cofilin 1, non-muscle	NM_007687	#1 - AGACAAGGACUGCCGCUAU #2 - GGUGGCAGCGCCGUCAUUU #3 - GUUCGCAAGUCUUCAACAC #4 - GAGAAUGCACCCCUCAAGA
Actb	$\beta-$Actin	NM_007393	#1 - GUAAAGACCUCUAUGCCAA #2 - CUAUGUUGCUCUAGACUUC #3 - CGAUAUCGCUGCGCUGGUC #4 - GCUAUGCUCUCCCUCACGC

Continued on next page

Gene	Protein	NCBI Reference	Sequence
Diap1	Diaphanous homolog 1 (*Drosophila*)	NM_007858	#1 - GUACAGCUGUGCGUGUUUG #2 - GAAGUUGUCUGUAGAGGAA #3 - GGAACAGUAUAACAAACUA #4 - GAAACCAGCAUGAGAUUAU
Diap3	Diaphanous homolog 3 (*Drosophila*)	NM_019670	#1 - GGACAAAUUUGCCAGUAUA #2 - UAAAUGCUCUCGUUACAUC #3 - CGACAGAUCUCACCUCAGG #4 - GAGAAGAUUGAAUUGGUUA
Fmnl1	Formin-like 1	NM_001077698	#1 - GGACGUCGUUUCCAUCGAG #2 - GCCAGGCCAUCGAGACGUA #3 - GCACCGAUUUGAAAAGCUA #4 - GGGUUUAAGAGGCGAGUUC
Fmnl2	Formin-like 2	NM_172409	#1 - GGCGACAAGUUAAAGAUAA #2 - CAACUUCACGCAAUUAUAG #3 - GCGACAAGCUGCAAGUACA #4 - GAAGGCGUGUUCAAGAAUC
Fhod1	Formin homology 2 domain containing protein 1	NM_177699	#1 - GAACCCAGCUAACGCUCUA #2 - GAGCGGUCCUAGAGCCUUA #3 - CGAAAGUCCUUGAGACGGA #4 - CGACACGUCAGAUGAGAUA
Fhod3	Formin homology 2 domain containing protein 3	NM_175276	#1 - ACACAGAGCUAUUGGUUUA #2 - CCAUUAAGGUGGACACUUC #3 - GGACCGCAUUGUCAAAUCA #4 - GUCCAUCGGAGGAUAAUUA
Rhob	Ras homolog gene family member B	NM_007483	#1 - GGAGGACUACGAUCGUUUA #2 - GAAGUGGGUGCCCGAGGUA #3 - GCAUCCAAGCCUAUGACUA #4 - CGUGUUCAGUAAAGACGAA
Rock2	Rho-associated coiled-coil containing protein kinase 2	NM_009072	#1 - CAAUGAAGCUUCUUAGUAA #2 - GAACGAGGAUGUUAGAAAU #3 - GCGGAAAGCUGAUCAUGAA #4 - GAUGAUGGCUAGACACAAA

Continued on next page

Gene	Protein	NCBI Reference	Sequence
Rhoj	Rras homolog gene family member J	NM_023275	#1 - GCACUUGCUUGGACUAUAC #2 - GCAAUGGACAUGAGGAGAA #3 - GCGCAGUGCUACUUGGAAU #4 - CACGGCUGCUGUGCAAUUA
Rhog	Ras homolog gene family member G	NM_019566	#1 - CGUCAUCUGUUUCUCCAU #2 - CAACACCGAUAAAGCGUGG #3 - CCAGUCCACCCUCCUAUGA #4 - GGGCGCACCGUGAACCUAA
Rnd3	Rho family GTPase 3	NM_028810	#1 - GAACGUGAAAUGCAAGAUA #2 - AGACUCCUGUGUCAUAUGA #3 - AAUCGACACACAAAGAAUA #4 - CGGAGCAGCCACUUACAUA
Arpc1b	Actin related protein 2/3 complex subunit 1B	NM_023142	#1 - GCACGGACCGCAAUGCCUA #2 - GAACAAGGACCGUACACAG #3 - AAGCAGAGCUCCCAGCGUG #4 - UGGCAACCCUGGCCUCUGA
Lmo2	LIM domain only 2	NM_001142335	#1 - UGAAAGCCAUCGACCAGUA #2 - UGUAUCACCUGGAGUGUUU #3 - GGUGACAGAUACCUUCUCA #4 - CGACAUAGUGUGUGAACAA
Grid2ip	Glutamate receptor, ionotropic, delta 2 (Grid2) interacting protein 1	NM_133355	#1- CAACAAGAGUUUCGGCUUC #2 - GCACAGCGUUUGCGUCGGA #3 - GGACGGUUCGAGUUUAUAA #4 - GGACCGGUCUGGAUCGAAU
Fhdc1	FH2 domain containing protein 1	NM_001033301	#1 - GGAGCUACAUUCAAUAUUA #2 - CAAGAGACAUCGAGAUUAU #3 - GAUCAGAGACGCUUCGAGA #4 - GCCGUAGGAUUUAAACUGU
Inf2	Inverted formin, FH2 and WH2 domain containing	NM_198411	#1 - GGACAGAGCACCCACCUAC #2 - GGAAGAAACGUCCCUCAAG #3 - GCAACUGCCAGCAAUCCUA #4 - CUCGAGUUCUCUAGCAAUA

Continued on next page

Gene	Protein	NCBI Reference	Sequence
Arpc1a	Actin related protein 2/3 complex, subunit 1A	NM_019767	#1 - CAACAUGUCUGCUAUGGAA #2 - GAACAUAAUGGGCAUAUCA #3 - GCCCGAUGCUCUUUAACUA #4 - GAAGUGGACAAGCAAGAUU
WAS	Wiskott-Aldrich syndrome	NM_000377	#1 - CGAGAACCAGCGACUCUUU #2 - GCUGGCCACUGCAGUUGUU #3 - GAACAUACCCUCCACCCUC #4 - CCUCUAAACUUAUCUACGA
Wasl	Wiskott-Aldrich syndrome-like	NM_028459	#1 - GAACGAGUCUCUCUUCUCC #2 - GGAACAAGAGCUAUACAAU #3 - GCAGAUCGGAACUGUAUGU #4 - GAGCAAAGCCAUUCAUUCC
Wasf1	WAS protein family, member 1	NM_031877	#1 - CCUAUUCCAUUGCAAGAAA #2 - CUACAGGUUUGAUAGAGAA #3 - UCAAUGAAGCACACAGUUU #4 - GGACGGAUCGUACUCACUC
Wasf2	WAS protein family, member 2	NM_153423	#1 - CCAAAUAGAGGGAAUGUGA #2 - GAAAAGAGGCACUCAAAUU #3 - UUAACAAUCUCAGUCCUUA #4 - GUUGACCGAGUACAAGUUA
Wasf3	WAS protein family, member 3	NM_145155	#1 - CAGCACAGAUAAUUGAAUA #2 - CAGAAGACAUAUUUGGUGA #3 - ACACGGAUCCCUCUUACUU #4 - ACCCAUAAGUGAUGCGAGA
Wash	WAS protein family homolog	NM_001037757	#1 - GAAUACGGCUCCAUCUUUA #2 - GCAAAGGUAUCUCUGGAAA #3 - CAUCCUACCUACCCGAUUU #4 - UCGCAGACGACCUGAUGUA
Whamm	WAS protein homolog associated with actin, golgi membranes and microtubules	NM_001004185	#1 - AAGGAUCACUGCCGAGAAA #2 - GCAGUUAGAUGUUGUGGAU #3 - GGAUAGACCAUGAACGCCA #4 - CAUUUAGAGACAUGCGAGA

Continued on next page

Gene	Protein	NCBI Reference	Sequence
Jmy	Junction-mediating and regulatory protein	NM_021310	#1 - GCACAAGACUAUAGAAAGC #2 - GAUCGACGCUCUAUGUUAC #3 - GCUCCACUGUUGACUAGUA #4 - UAGAGCCCAUCAUACAAUA
Cttn	Cortactin	NM_007803	#1 - CGAGAGAGCUCAGCGGAUG #2 - CCAGUAAUAUCCGUGCUAA #3 - GAAAGAUUACUCCAAAGGU #4 - CUAUAAGACUGGUUUCGGA
Hcls1	Hematopoietic cell specific Lyn substrate 1	NM_008225	#1 - GGGCAAAUAUGGAGUUGAG #2 - GCUAUAGCCCUGUAUGAUU #3 - CAACCACGGCGUAUAAGAA #4 - GGAGCGAAAGGCUGUGGUA
Cobl	Cordon-bleu WH2 repeat	NM_172496	#1 - AAUCAGAGAUGAGGUGUUA #2 - GAUACUAGCUCUCUAACCA #3 - GGAGGAUACUGAUGAAUGG #4 - CAAAUACGUUGAUUGGGUC
Lmod1	Leiomodin 1 (smooth muscle)	NM_053106	#1 - GAGAAGGUCAUCAGAGGUA #2 - UGCAAUUGCUAUCAUGUUA #3 - CAAAGUAGCUAAGUACCGG #4 - GCCGAAACAUGGACAAGCA
Lmod2	Leiomodin 2 (cardiac)	NM_053098	#1 - GAGAGGCGCUGAUGGCGUA #2 - GAAUGAGUAUGACGAGUAU #3 - CAGACAUGCUCAAGGUUAA #4 - CCUGAUACGACAGAAGUUA
Lmod3	Leiomodin 3 (fetal)	NM_001081157	#1 - CGAAUCUGCUUACCAGGAA #2 - CAAUGUCGCCUACCUUAAA #3 - GAUGAGAGCGUAGCGUUUG #4 - GAACUCCUAGCCAACUUAU
Ctnna2	Catenin (cadherin associated protein), alpha 2	NM_145732	#1 - CAACCGAGAUUAUGUAUUU #2 - GCAAACCGAUUUAAAGAGU #3 - GGUGAAAGCGUCUUAUGUA #4 - UGGUGGAACGUUAGCGAAA

Continued on next page

Gene	Protein	NCBI Reference	Sequence
Ctnna1	Catenin (cadherin associated protein), alpha 1	NM_009818	#1 - GUAAAGGGCCGUCUAAUAA #2 - GACCAAUGUCCCUCUAUUA #3 - GGACUUGCGUAGACAGCUU #4 - GCGUGAAGCUUGUCCGAAU
Ctnna3	Catenin (cadherin associated protein), alpha 3	NM_177612	#1 - GAUCAUAAAUGCUGCACUU #2 - GCUAAGAAGCCCUUGAUUA #3 - GCAUACCACUGAUGUAAUC #4 - UGACGGAGUACAUGAGUAA
Ctnnb1	Catenin (cadherin associated protein), beta 1	NM_007614	#1 - GAUCUUAGCUUAUGGCAAU #2 - GCAAGUAGCUGAUAUUGAC #3 - CAGCUGGCCUGGUUUGAUA #4 - GAACGCAGCAGCAGUUUGU
Cdh1	Cadherin 1	NM_009864	#1 - GCUCAAGAAUCUCUCAUUU #2 - CCAAGUACAUCCUCUAUUC #3 - GCGCUGAGAUGGACAGAGA #4 - GAAGAUCACGUAUCGGAUU
Cdh2	Cadherin 2	NM_007664	#1 - CCAAUCAACUUGCCAGAAA #2 - AAAGGAAAGUUCAGUAUGA #3 - GGACAUCAAUGGCAAUCAA #4 - GAUCAAAGCCUGGGACGUA
Cdh3	Cadherin 3	NM_007665	#1 - GGGAGAAGAUUGUCAAGUA #2 - GCUAACACAUGACUCAGAU #3 - ACAACUACCUUAACGAGUG #4 - ACGUAUGACUUGCAUCUUU
Lrrc58	Leucine rich repeat containing 58	NM_177093	#1 - ACAAUAACUUGCUGACUUA #2 - UAAAGAAAUCCCACCAGAA #3 - AAAGUGUGGUGGAGUCUAU #4 - GCAAGGACCAUUAAGAUCC
Acta1	Actin, alpha 1, skeletal muscle	NM_009606	#1 - GCAAUGAGCGUUUCCGUUG #2 - CAGCCUUCCUUUAUCGGUA #3 - CAGCUGAACGUGAGAUUGU #4 - CGGGAGAAGAUGACUCAAA

Continued on next page

Gene	Protein	NCBI Reference	Sequence
Actg2	Actin, gamma 2, smooth muscle, enteric	NM_009610	#1 - GAUCCUAACUCUCAAGUAC #2 - GACGGGAUCUCACAGACUA #3 - GAAAUUGUACGAGACAUCA #4 - CAACAUACAAUUCCAUCAU
Actc1	Actin, alpha, cardiac muscle 1	NM_009608	#1 - UAAAUACUCUGUCUGGAUU #2 - CUAUGAGGGUUAUGCCUUA #3 - GCAUUCAUGAAACUACUUA #4 - GGAUCUAGCUGGUCGGGAC
Acta2	Actin, alpha 2, smooth muscle, aorta	NM_007392	#1 - GCACCACUCUUUCUAUAAC #2 - GGACGUACAACUGGUAUUG #3 - GAUAGAACACGGCAUCAUC #4 - CGGCUUCGCUGGUGAUGAU
Actbl2	Actin, beta-like 2	NM_175497	#1 - GUAGGGACCUGACUGAUUA #2 - GAACGCAAGUAUUCGGUUU #3 - GAUAAUGGGUCAGGGAUGU #4 - CCAAGUACCAUGAAAAUUA
RAB27A	Rab27a, member RAS oncogene family	NM_023635	#1 - GGAGAGGUUUCGUAGCUUA #2 - GGAUGGAGAUUACGAUUAC #3 - GAAUCCACCUGCAGUUAUG #4 - AAACAUAAGCCACGCGAUU
Jup	Junction plakoglobin	NM_010593	#1 - CAAGAAGACUACCACCUAU #2 - UCACCAAGCUGCUCAACGA #3 - CGUAGAAUCUGUCCUGUUC #4 - GAGUGUAGAUGACGUCAAC
Ctnnd1	Catenin (cadherin associated protein), delta 1	NM_001085453	#1 - GAUAUUGGUAGGAUUGUUA #2 - CCGAAAGGCUCGUGAUAUG #3 - GCACUUAUGCUACCGCAAU #4 - GAGCAUGAGCGAGUAGUAA
Vcl	Vinculin	NM_009502	#1 - CGAGAUCAUUCGUGUGUUA #2 - GCCAAUAAAUCGACAGUGG #3 - GGGAUUACCUCAUUGACGG #4 - AAGAUGAGUGCUGAAAUUA

Continued on next page

Gene	Protein	NCBI Reference	Sequence
Vim	Vimentin	NM_011701	#1 - GACCAGAGAUGGACAGGUG #2 - GAACACUCCUGAUUAAGAC #3 - GAGAGAAACUAACCUGGAG #4 - UCACGAUGACCUUGAAUAA
Nckipsd	NCK interacting protein with SH3 domain	NM_030729	#1 - UAGCCUUGGUGGCCUAUUA #2 - GAACUCGUGCGGAGAAACA #3 - GAACACCGAGCGUCUCUAC #4 - GGUCUAAGCCAUGAGUUAU
Gsn	Gelsolin	NM_146120	#1 - GGUCAAAGGACGCCGUGUA #2 - CAACAGGAUCGGACGCUUU #3 - UGUGGCAUCUGGAUUCAAA #4 - GCGCGUACCUUUCGAUGCU
Coro6	Coronin 6	NM_139128	#1 - CCAAAUUUCUAGCCAUUAU #2 - GAACAGCAAUGGUAGCCUG #3 - GAUAAAGGCCCUCCGAGAU #4 - GAACCACCUUUCGUGCAUU
Coro1a	Coronin, actin binding protein 1A	NM_009898	#1 - UGACAGCUCUAUCCGGUAU #2 - CAAGAGGGUUGGCAUCGUG #3 - UGCAUUAUCUUUCCAUGUU #4 - CAAGCGAGUUCGUGUCAUC
Coro1b	Coronin, actin binding protein 1B	NM_011778	#1 - GACAAGAGCGUCCGAAUCA #2 - UACAUCCACUUCCUGAAUA #3 - GUAAACAACGGGACCUGAA #4 - AUUCGAGUGUCCCGAGUUA
Coro2a	Coronin, actin binding protein 2A	NM_178893	#1 - GAAAGUUGGACCCUCACUA #2 - GCAAGAUUCGGAUUGUUGA #3 - GGAUCGGUAUCAUGCCAAA #4 - GAGGGAACGUCUUGGACAU
Wipf1	WAS/WASL interacting protein family, member 1	NM_153138	#1 - CGAAGUGGAUCCAACAGAA #2 - GGAAGCCGACCACCGAUUU #3 - CAAGACGUAUCCCAGCAAA #4 - CAACAUUUGCACUCGCUAA

Continued on next page

Gene	Protein	NCBI Reference	Sequence
Nck2	Non-catalytic region of tyrosine kinase adaptor protein 2	NM_010879	#1 - CCAACUAUGUGGAGCGUAA #2 - GUGAAGGGCUCCCGUGUCA #3 - GAGGAAUGCUGCCAACAGG #4 CAAGUUCGCCUACGUAGCA
Pak1	p21 protein (Cdc42/Rac)-activated kinase 1	NM_011035	#1 - GAAAUUACGGAGCAUAGUG #2 - UCUAAGAAGACCUCCAAUA #3 - UAACACCACUCCGCCAGAU #4 - CGAAGAAAGAGCUGAUUAU
Tmod1	Tropomodulin 1	NM_021883	#1 - GACGAGAGCUGGAGAAAUA #2 - GAGAAGAUCUGGUUCCCUA #3 - GCAAUGACCCUGUGGCGUU #4 - CUUAACAACAUCCGGAAUA
Tmod2	Tropomodulin 2	NM_016711	#1 - AUAAUGACCUGGUUCGAAA #2 - GAGGAGAACUCAAGGAUCC #3 - GGACAAGAGUGGCAGCUGC #4 - AAUGACACCUUGACGGAGA
Tmod4	Tropomodulin 4	NM_016712	#1 - GAGAUGCCCUAUUGCAGUA #2 - GGUACAGCCUGACAAGUAU #3 - UCAAAGAGCGUGAUGACUU #4 - CUAAAGAGGGUACGGAGUA
Tpm2	Tropomyosin 2, beta	NM_009416	#1 - GGACUCAGACCGCAAAUAU #2 - GCAUUCAGCUCGUAGAGGA #3 - GGACAACGCACUCAAUGAC #4 - CGAAGAAGAGAUCAAACUU
Tpm3	Tropomyosin 3, gamma	NM_022314	#1 - GGAUCCAGCUGGUUGAAGA #2 - CAAGUAUUCGGAAGCUUUA #3 - GAACUAGCAACCAUGCAGA #4 - GCACCAAAGAGGAGCAUCU
Tpm4	Tropomyosin 4	NM_001001491	#1 - GGACCAGACACUAAACGAA #2 - CUGACGAAGCCGACCGCAA #3 - AUGAGGAGGUUGCUCGUAA #4 - GUAAUAGAGAACCGAGCCA
Rab3GEP	Rab3GEP	NM_178690	GCGAGAAGACGACACCUUUU

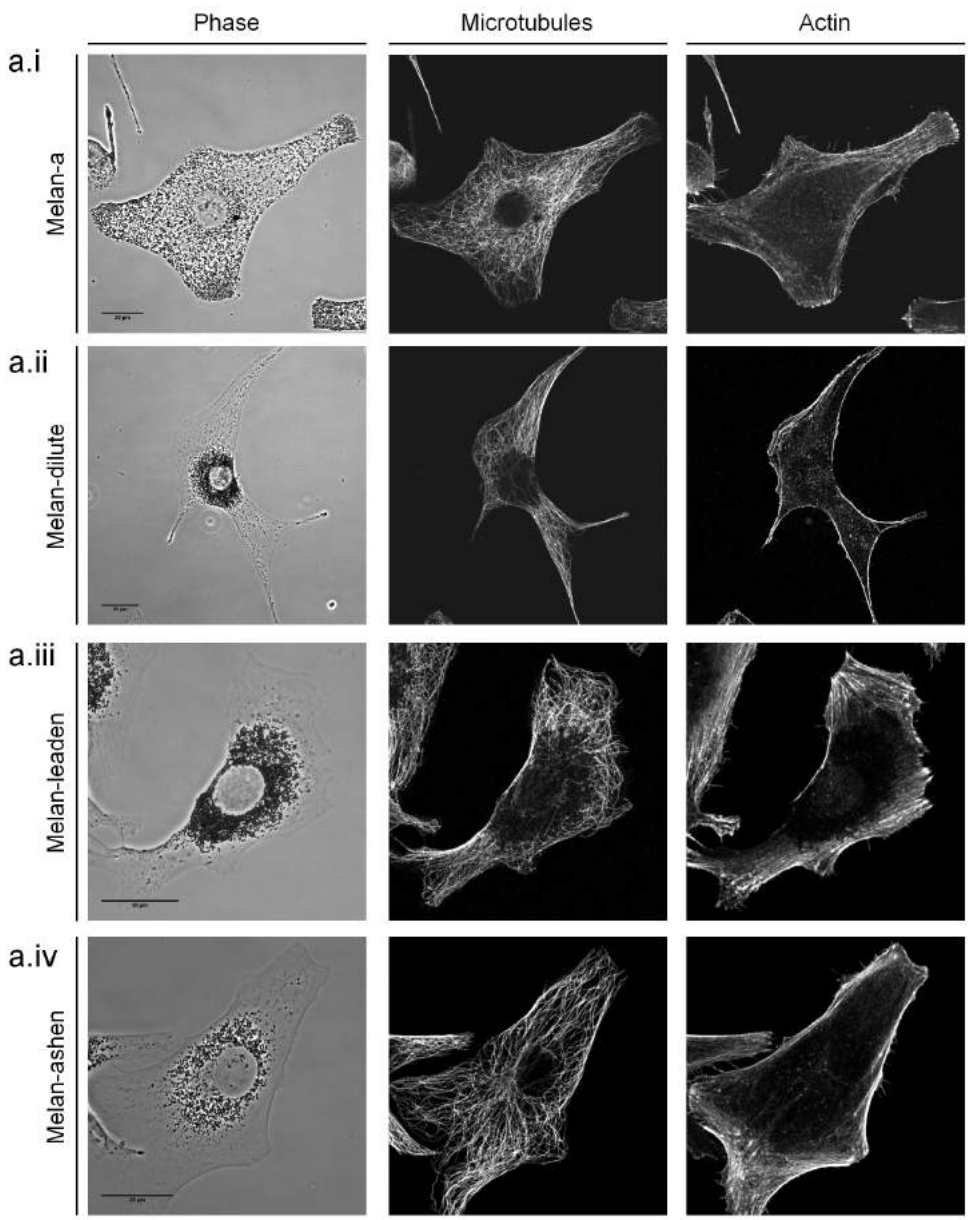


Figure 7.1 - Murine melanocyte cell lines used in this study. Representative images of cultured melanocytes showing distribution of melanosomes (via phase contrast), microtubules (via anti-tubulin antibody) and actin filaments (via phalloidin staining) in either wildtype melanocytes (a.i), melan-d1 which lack myosin-Va (a.ii), melan-leaden which lack melanophilin (a.iii) and melan-ash with lack Rab27a (a.iv). Note that the melanosomes in all three mutant melanocyte cell lines (melan-d1, melan-leaden, melan-ash) are clustered around the perinuclear area in contrast with the wildtype phenotype, where the melanosomes are dispersed throughout the cytoplasm.

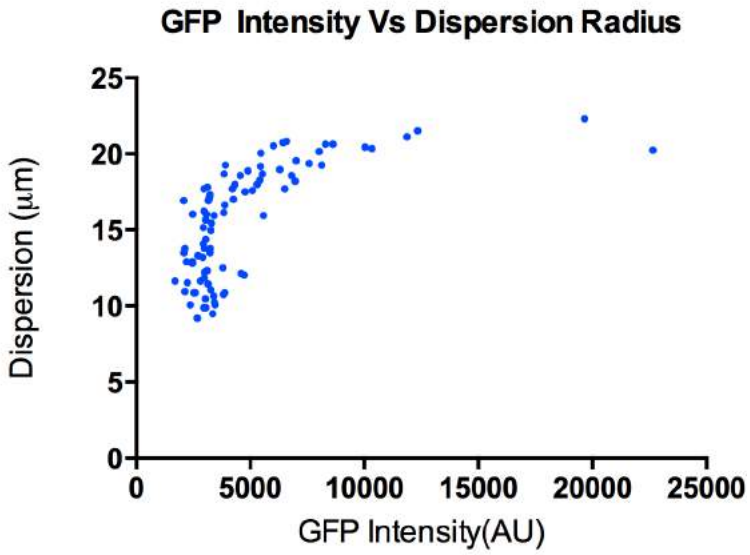


Figure 7.2 - GFP-myosin-Va intensitiy Vs melanosome dispersion radius. The fluorescence intensity of melan-dilute cells expressing GFP-myosin-Va plotted against the dispersion radius to determine if there is a correlation between signal intensity and the level of rescue observed.

Bibliography

Aamodt, E. J. and J. G. Culotti (1986). Microtubules and microtubule-associated proteins from the nematode Caenorhabditis elegans: periodic cross-links connect microtubules in vitro. *J. Cell Biol. 103*(1), 23–31.

Abella, J. V. G., C. Galloni, J. Pernier, D. J. Barry, S. Kjær, M.-F. Carlier, and M. Way (2016). Isoform diversity in the Arp2/3 complex determines actin filament dynamics. *Nat. Cell Biol. 18*(1), 76–86.

Alexandrov, K., H. Horiuchi, O. Steele-Mortimer, M. C. Seabra, and M. Zerial (1994). Rab escort protein-1 is a multifunctional protein that accompanies newly prenylated rab proteins to their target membranes. *EMBO J. 13*(22), 5262–5273.

Ali, M. Y., G. G. Kennedy, D. Safer, K. M. Trybus, H. L. Sweeney, and D. M. Warshaw (2011). Myosin Va and myosin VI coordinate their steps while engaged in an in vitro tug of war during cargo transport. *Proc. Natl. Acad. Sci. U.S.A. 108*(34), E535–541.

Ali, M. Y., E. B. Krementsova, G. G. Kennedy, R. Mahaffy, T. D. Pollard, K. M. Trybus, and D. M. Warshaw (2007). Myosin Va maneuvers through actin intersections and diffuses along microtubules. *Proc. Natl. Acad. Sci. U.S.A. 104*(11), 4332–4336.

Allan, V. J. (2011). Cytoplasmic dynein. *Biochem. Soc. Trans. 39*(5), 1169–1178.

Ammer, A. G. and S. A. Weed (2008). Cortactin branches out: roles in regulating protrusive actin dynamics. *Cell Motil. Cytoskeleton 65*(9), 687–707.

Ancans, J., D. J. Tobin, M. J. Hoogduijn, N. P. Smit, K. Wakamatsu, and A. J. Thody (2001). Melanosomal pH controls rate of melanogenesis, eumelanin/phaeomelanin ratio and melanosome maturation in melanocytes and melanoma cells. *Exp. Cell Res. 268*(1), 26–35.

Anderson, K. I., Y. L. Wang, and J. V. Small (1996). Coordination of protrusion and translocation of the keratocyte involves rolling of the cell body. *J. Cell Biol. 134*(5), 1209–1218.

Ando, H., Y. Niki, M. Ito, K. Akiyama, M. S. Matsui, D. B. Yarosh, and M. Ichihashi (2012). Melanosomes are transferred from melanocytes to keratinocytes through the processes of packaging, release, uptake, and dispersion. *J. Invest. Dermatol. 132*(4), 1222–1229.

Andreas, P. and H. Nilsson (2011). Skin Biopsies as Tools to Measure Fish Coloration and Colour Change. In U. Khopkar (Ed.), *Skin Biopsy - Perspectives*. InTech.

Arai, T. and Y. Kaziro (1976). Effect of guanine nucleotides on the assembly of brain microtubles: ability of 5'-guanylyl imidodiphosphate to replace GTB in promoting the polymerization of microtubules in vitro. *Biochem. Biophys. Res. Commun. 69*(2), 369–376.

Asbury, C. L. (2005). Kinesin: world's tiniest biped. *Curr. Opin. Cell Biol. 17*(1), 89–97.

Aspengren, S., D. Hedberg, and M. Wallin (2006). Studies of pigment transfer between Xenopus laevis melanophores and fibroblasts in vitro and in vivo. *Pigment Cell Res. 19*(2), 136–145.

Aspengren, S., L. Wielbass, and M. Wallin (2006). Effects of acrylamide, latrunculin, and nocodazole on intracellular transport and cytoskeletal organization in melanophores. *Cell Motil. Cytoskeleton 63*(7), 423–436.

Aspenstrom, P., A. Fransson, and J. Saras (2004). Rho GTPases have diverse effects on the organization of the actin filament system. *Biochem J 377*(Pt 2), 327–337.

Au, J. S.-Y. and J.-D. Huang (2002). A tissue-specific exon of myosin Va is responsible for selective cargo binding in melanocytes. *Cell Motil. Cytoskeleton 53*(2), 89–102.

Baetz, K., S. Isaaz, and G. M. Griffiths (1995). Loss of cytotoxic T lymphocyte function in Chediak-Higashi syndrome arises from a secretory defect that prevents lytic granule exocytosis. *J. Immunol. 154*(11), 6122–6131.

Bagshaw, R. D., J. W. Callahan, and D. J. Mahuran (2006). The Arf-family protein, Arl8b, is involved in the spatial distribution of lysosomes. *Biochem. Biophys. Res. Commun. 344*(4), 1186–1191.

Banaszynski, L. A., C. W. Liu, and T. J. Wandless (2005). Characterization of the FKBP·Rapamycin·FRB Ternary Complex. *J. Am. Chem. Soc. 127*(13), 4715–4721.

Barber, R. D., D. W. Harmer, R. A. Coleman, and B. J. Clark (2005). GAPDH as a housekeeping gene: analysis of GAPDH mRNA expression in a panel of 72 human tissues. *Physiological Genomics 21*(3), 389–395.

Basrur, V., F. Yang, T. Kushimoto, Y. Higashimoto, K.-i. Yasumoto, J. Valencia, J. Muller, W. D. Vieira, H. Watabe, J. Shabanowitz, V. J. Hearing, D. F. Hunt, and E. Appella (2003). Proteomic analysis of early melanosomes: identification of novel melanosomal proteins. *J. Proteome Res. 2*(1), 69–79.

Belmont, L. D. and T. J. Mitchison (1996). Identification of a protein that interacts with tubulin dimers and increases the catastrophe rate of microtubules. *Cell 84*(4), 623–631.

Benson, M. A., S. E. Newey, E. Martin-Rendon, R. Hawkes, and D. J. Blake (2001). Dysbindin, a Novel Coiled-coil-containing Protein That Interacts with the Dystrobrevins in Muscle and Brain. *J. Biol. Chem. 276*(26), 24232–24241.

Berg, J. S., B. C. Powell, and R. E. Cheney (2001). A Millennial Myosin Census. *Mol Biol Cell 12*(4), 780–794.

Bergeland, T., J. Widerberg, O. Bakke, and T. W. Nordeng (2001). Mitotic partitioning of endosomes and lysosomes. *Curr. Biol. 11*(9), 644–651.

Berson, J. F., A. C. Theos, D. C. Harper, D. Tenza, G. Raposo, and M. S. Marks (2003). Proprotein convertase cleavage liberates a fibrillogenic fragment of a resident glycoprotein to initiate melanosome biogenesis. *J. Cell Biol. 161*(3), 521–533.

Berzat, A. C., J. E. Buss, E. J. Chenette, C. A. Weinbaum, A. Shutes, C. J. Der, A. Minden, and A. D. Cox (2005). Transforming activity of the Rho family GTPase, Wrch-1, a Wnt-regulated Cdc42 homolog, is dependent on a novel carboxyl-terminal palmitoylation motif. *J. Biol. Chem. 280*(38), 33055–33065.

Besse, F. and A. Ephrussi (2008). Translational control of localized mRNAs: restricting protein synthesis in space and time. *Nat. Rev. Mol. Cell Biol. 9*(12), 971–980.

Bielli, A., P. O. Thörnqvist, A. G. Hendrick, R. Finn, K. Fitzgerald, and M. W. McCaffrey (2001). The small GTPase Rab4a interacts with the central region of cytoplasmic dynein light intermediate chain-1. *Biochem. Biophys. Res. Commun. 281*(5), 1141–1153.

Blajeski, A. L., V. A. Phan, T. J. Kottke, and S. H. Kaufmann (2002). G(1) and G(2) cell-cycle arrest following microtubule depolymerization in human breast cancer cells. *J. Clin. Invest. 110*(1), 91–99.

Block, S. M., L. S. Goldstein, and B. J. Schnapp (1990). Bead movement by single kinesin molecules studied with optical tweezers. *Nature 348*(6299), 348–352.

Booth, A. E. G. (2012). *Identifying a targeting factor for Rab27a*. Ph.D., Imperial College London.

Borisy, G. G. and E. W. Taylor (1967). The mechanism of action of colchicine. Binding of colchincine-3h to cellular protein. *J. Cell Biol. 34*(2), 525–533.

Borovansky, J., P. Hach, and J. Duchon (1977). Melanosome: an unusually resistant subcellular particle. *Cell Biol. Int. Rep. 1*(6), 549–554.

Bovellan, M., Y. Romeo, M. Biro, A. Boden, P. Chugh, A. Yonis, M. Vaghela, M. Fritzsche, D. Moulding, R. Thorogate, A. Jegou, A. J. Thrasher, G. Romet-Lemonne, P. P. Roux, E. K. Paluch, and G. Charras (2014). Cellular control of cortical actin nucleation. *Curr. Biol. 24*(14), 1628–1635.

Brady, D. C., J. K. Alan, J. P. Madigan, A. S. Fanning, and A. D. Cox (2009). The Transforming Rho Family GTPase Wrch-1 Disrupts Epithelial Cell Tight Junctions and Epithelial Morphogenesis. *Mol Cell Biol 29*(4), 1035–1049.

Brouhard, G. and D. Sept (2012). Microtubules: sizing up the GTP cap. *Curr. Biol. 22*(18), R802–803.

Brouhard, G. J., J. H. Stear, T. L. Noetzel, J. Al-Bassam, K. Kinoshita, S. C. Harrison, J. Howard, and A. A. Hyman (2008). XMAP215 is a processive microtubule polymerase. *Cell 132*(1), 79–88.

Brown, C. L., K. C. Maier, T. Stauber, L. M. Ginkel, L. Wordeman, I. Vernos, and T. A. Schroer (2005). Kinesin-2 is a motor for late endosomes and lysosomes. *Traffic 6*(12), 1114–1124.

Bryan, J. and L. Wilson (1971). Are Cytoplasmic Microtubules Heteropolymers? *PNAS 68*(8), 1762–1766.

Bubb, M. R., A. M. Senderowicz, E. A. Sausville, K. L. Duncan, and E. D. Korn (1994). Jasplakinolide, a cytotoxic natural product, induces actin polymerization and competitively inhibits the binding of phalloidin to F-actin. *J. Biol. Chem. 269*(21), 14869–14871.

Bubb, M. R., I. Spector, B. B. Beyer, and K. M. Fosen (2000). Effects of jasplakinolide on the kinetics of actin polymerization. An explanation for certain in vivo observations. *J. Biol. Chem. 275*(7), 5163–5170.

Budi, E. H., L. B. Patterson, and D. M. Parichy (2008). Embryonic requirements for ErbB signaling in neural crest development and adult pigment pattern formation. *Development 135*(15), 2603–2614.

Bultema, J. J., A. L. Ambrosio, C. L. Burek, and S. M. Di Pietro (2012). BLOC-2, AP-3, and AP-1 proteins function in concert with Rab38 and Rab32 proteins to mediate protein trafficking to lysosome-related organelles. *J. Biol. Chem. 287*(23), 19550–19563.

Burakov, A., E. Nadezhdina, B. Slepchenko, and V. Rodionov (2003). Centrosome positioning in interphase cells. *J Cell Biol 162*(6), 963–969.

Burridge, K. and E. S. Wittchen (2013). The tension mounts: Stress fibers as force-generating mechanotransducers. *J Cell Biol 200*(1), 9–19.

Buss, F., G. Spudich, and J. Kendrick-Jones (2004). Myosin VI: cellular functions and motor properties. *Annu. Rev. Cell Dev. Biol. 20*, 649–676.

Byers, H. R., M. Yaar, M. S. Eller, N. L. Jalbert, and B. A. Gilchrest (2000). Role of cytoplasmic dynein in melanosome transport in human melanocytes. *J. Invest. Dermatol. 114*(5), 990–997.

Cai, Q., L. Lu, J.-H. Tian, Y.-B. Zhu, H. Qiao, and Z.-H. Sheng (2010). Snapin-regulated late endosomal transport is critical for efficient autophagy-lysosomal function in neurons. *Neuron 68*(1), 73–86.

Campellone, K. G., N. J. Webb, E. A. Znameroski, and M. D. Welch (2008). WHAMM is an Arp2/3 complex activator that binds microtubules and functions in ER to Golgi transport. *Cell 134*(1), 148–161.

Campellone, K. G. and M. D. Welch (2010). A Nucleator Arms Race: Cellular Control of Actin Assembly. *Nat Rev Mol Cell Biol 11*(4), 237–251.

Canny, J. (1986). A Computational Approach to Edge Detection. *IEEE Transactions on Pattern Analysis and Machine Intelligence PAMI-8*(6), 679–698.

Caplow, M., R. L. Ruhlen, and J. Shanks (1994). The free energy for hydrolysis of a microtubule-bound nucleotide triphosphate is near zero: all of the free energy for hydrolysis is stored in the microtubule lattice. *J. Cell Biol. 127*(3), 779–788.

Caplow, M. and J. Shanks (1996). Evidence that a single monolayer tubulin-GTP cap is both necessary and sufficient to stabilize microtubules. *Mol Biol Cell 7*(4), 663–675.

Carter, A. P. (2013). Crystal clear insights into how the dynein motor moves. *J. Cell. Sci. 126*(Pt 3), 705–713.

Casey, P. J. and M. C. Seabra (1996). Protein prenyltransferases. *J. Biol. Chem. 271*(10), 5289–5292.

Certain, S., F. Barrat, E. Pastural, F. Le Deist, J. Goyo-Rivas, N. Jabado, M. Benkerrou, R. Seger, E. Vilmer, G. Beullier, K. Schwarz, A. Fischer, and G. de Saint Basile (2000). Protein truncation test of LYST reveals heterogenous mutations in patients with Chediak-Higashi syndrome. *Blood 95*(3), 979–983.

Chan, D. C., A. Wynshaw-Boris, and P. Leder (1995). Formin isoforms are differentially expressed in the mouse embryo and are required for normal expression of fgf-4 and shh in the limb bud. *Development 121*(10), 3151–3162.

Chang, F. K., N. Sato, N. Kobayashi-Simorowski, T. Yoshihara, J. L. Meth, and M. Hamaguchi (2006). DBC2 is essential for transporting vesicular stomatitis virus glycoprotein. *J. Mol. Biol. 364*(3), 302–308.

Charras, G. T., C.-K. Hu, M. Coughlin, and T. J. Mitchison (2006). Reassembly of contractile actin cortex in cell blebs. *J Cell Biol 175*(3), 477–490.

Cheli, Y., F. Luciani, M. Khaled, L. Beuret, K. Bille, P. Gounon, J.-P. Ortonne, C. Bertolotto, and R. Ballotti (2009). {alpha}MSH and Cyclic AMP elevating agents control melanosome pH through a protein kinase A-independent mechanism. *J. Biol. Chem. 284*(28), 18699–18706.

Cheney, R. E., M. K. O'Shea, J. E. Heuser, M. V. Coelho, J. S. Wolenski, E. M. Espreafico, P. Forscher, R. E. Larson, and M. S. Mooseker (1993). Brain myosin-V is a two-headed unconventional myosin with motor activity. *Cell 75*(1), 13–23.

Chereau, D., M. Boczkowska, A. Skwarek-Maruszewska, I. Fujiwara, D. B. Hayes, G. Rebowski, P. Lappalainen, T. D. Pollard, and R. Dominguez (2008). Leiomodin is an Actin Filament Nucleator in Muscle Cells. *Science 320*(5873), 239–243.

Chesarone, M. A. and B. L. Goode (2009). Actin nucleation and elongation factors: mechanisms and interplay. *Curr. Opin. Cell Biol. 21*(1), 28–37.

Chhabra, E. S. and H. N. Higgs (2007). The many faces of actin: matching assembly factors with cellular structures. *Nat. Cell Biol. 9*(10), 1110–1121.

Chircop, M. (2014). Rho GTPases as regulators of mitosis and cytokinesis in mammalian cells. *Small GTPases 5*.

Cho, C., S. L. Reck-Peterson, and R. D. Vale (2008). Regulatory ATPase Sites of Cytoplasmic Dynein Affect Processivity and Force Generation. *J Biol Chem 283*(38), 25839–25845.

Cho, C. and R. D. Vale (2012). The mechanism of dynein motility: Insight from crystal structures of the motor domain. *Biochimica et Biophysica Acta (BBA) - Molecular Cell Research 1823*(1), 182–191.

Choy, R. M., J. M. Kollman, A. Zelter, T. N. Davis, and D. A. Agard (2009). Localization and orientation of the gamma-tubulin small complex components using protein tags as labels for single particle EM. *J. Struct. Biol. 168*(3), 571–574.

Chretien, D., F. Metoz, F. Verde, E. Karsenti, and R. H. Wade (1992). Lattice defects in microtubules: protofilament numbers vary within individual microtubules. *J. Cell Biol. 117*(5), 1031–1040.

Chuang, Y.-y., A. Valster, S. J. Coniglio, J. M. Backer, and M. Symons (2007). The atypical Rho family GTPase Wrch-1 regulates focal adhesion formation and cell migration. *J. Cell. Sci. 120*(Pt 11), 1927–1934.

Chung, C. T., S. L. Niemela, and R. H. Miller (1989). One-step preparation of competent Escherichia coli: transformation and storage of bacterial cells in the same solution. *Proc. Natl. Acad. Sci. U.S.A. 86*(7), 2172–2175.

Cichorek, M., M. Wachulska, A. Stasiewicz, and A. Tyminska (2013). Skin melanocytes: biology and development. *Postepy Dermatol Alergol 30*(1), 30–41.

Clancy, B. and L. J. Cauller (1998). Reduction of background autofluorescence in brain sections following immersion in sodium borohydride. *J. Neurosci. Methods 83*(2), 97–102.

Conde, C. and A. Caceres (2009). Microtubule assembly, organization and dynamics in axons and dendrites. *Nat. Rev. Neurosci. 10*(5), 319–332.

Conti, M. A. and R. S. Adelstein (2008). Nonmuscle myosin II moves in new directions. *J Cell Sci 121*(1), 11–18.

Cooper, G. M. (2000). Structure and Organization of Actin Filaments.

Cooper, J. A. (1987). Effects of cytochalasin and phalloidin on actin. *J. Cell Biol. 105*(4), 1473–1478.

Corti, B. (1774). Osservazione Microscopische sulla Tremella e sulla Circulazione del Fluido in Una Planto Acquaguola. *Lucca, Italy: Appresso Giuseppe Rocchi*.

Costin, G.-E., J. C. Valencia, K. Wakamatsu, S. Ito, F. Solano, A. L. Milac, W. D. Vieira, Y. Yamaguchi, F. Rouzaud, A.-J. Petrescu, M. L. Lamoreux, and V. J. Hearing (2005). Mutations in dopachrome tautomerase (Dct) affect eumelanin/pheomelanin synthesis, but do not affect intracellular trafficking of the mutant protein. *Biochem. J. 391*(Pt 2), 249–259.

Cottingham, F. R. and M. A. Hoyt (1997). Mitotic spindle positioning in Saccharomyces cerevisiae is accomplished by antagonistically acting microtubule motor proteins. *J. Cell Biol. 138*(5), 1041–1053.

Coy, D. L., W. O. Hancock, M. Wagenbach, and J. Howard (1999). Kinesin's tail domain is an inhibitory regulator of the motor domain. *Nat. Cell Biol. 1*(5), 288–292.

Cramer, L. (2008). Organelle Transport: Dynamic Actin Tracks for Myosin Motors. *Current Biology 18*(22), R1066–R1068.

De Brabander, M. J., R. M. Van de Veire, F. E. Aerts, M. Borgers, and P. A. Janssen (1976). The effects of methyl (5-(2-thienylcarbonyl)-1h-benzimidazol-2-yl) carbamate, (R 17934; NSC 238159), a new synthetic antitumoral drug interfering with microtubules, on mammalian cells cultured in vitro. *Cancer Res. 36*(3), 905–916.

Dehring, D. A. K., F. Clarke, B. G. Ricart, Y. Huang, T. S. Gomez, E. K. Williamson, D. A. Hammer, D. D. Billadeau, Y. Argon, and J. K. Burkhardt (2011). Hematopoietic lineage cell-specific protein 1 functions in concert with the Wiskott-Aldrich syndrome protein to promote podosome array organization and chemotaxis in dendritic cells. *J. Immunol. 186*(8), 4805–4818.

Dekker-Ohno, K., S. Hayasaka, Y. Takagishi, S.-i. Oda, N. Wakasugi, K. Mikoshiba, M. Inouye, and H. Yamamura (1996). Endoplasmic reticulum is missing in dendritic spines of Purkinje cells of the ataxic mutant rat. *Brain Research 714*(1–2), 226–230.

Del Castillo, P., A. R. Llorente, and J. C. Stockert (1989). Influence of fixation, exciting light and section thickness on the primary fluorescence of samples for microfluorometric analysis. *Basic Appl Histochem 33*(3), 251–257.

Delgehyr, N., J. Sillibourne, and M. Bornens (2005). Microtubule nucleation and anchoring at the centrosome are independent processes linked by ninein function. *J. Cell. Sci. 118*(Pt 8), 1565–1575.

Dell Angelica, E. C., C. Mullins, S. Caplan, and J. S. Bonifacino (2000). Lysosome-related organelles. *FASEB J. 14*(10), 1265–1278.

Dell'Angelica, E. C. (2003). Melanosome biogenesis: shedding light on the origin of an obscure organelle. *Trends Cell Biol. 13*(10), 503–506.

DeLuca, J. G., C. N. Newton, R. H. Himes, M. A. Jordan, and L. Wilson (2001). Purification and characterization of native conventional kinesin, HSET, and CENP-E from mitotic hela cells. *J. Biol. Chem. 276*(30), 28014–28021.

Derivery, E., C. Sousa, J. J. Gautier, B. Lombard, D. Loew, and A. Gautreau (2009). The Arp2/3 activator WASH controls the fission of endosomes through a large multiprotein complex. *Dev. Cell 17*(5), 712–723.

Dessinioti, C., A. J. Stratigos, D. Rigopoulos, and A. D. Katsambas (2009). A review of genetic disorders of hypopigmentation: lessons learned from the biology of melanocytes. *Exp. Dermatol. 18*(9), 741–749.

Dettenhofer, M., F. Zhou, and P. Leder (2008). Formin 1-isoform IV deficient cells exhibit defects in cell spreading and focal adhesion formation. *PLoS ONE 3*(6), e2497.

Detter, J. C., Q. Zhang, E. H. Mules, E. K. Novak, V. S. Mishra, W. Li, E. B. McMurtrie, V. T. Tchernev, M. R. Wallace, M. C. Seabra, R. T. Swank, and S. F. Kingsmore (2000). Rab geranylgeranyl transferase alpha mutation in the gunmetal mouse reduces Rab prenylation and platelet synthesis. *Proc. Natl. Acad. Sci. U.S.A. 97*(8), 4144–4149.

Didsbury, J., R. F. Weber, G. M. Bokoch, T. Evans, and R. Snyderman (1989). rac, a novel ras-related family of proteins that are botulinum toxin substrates. *J. Biol. Chem. 264*(28), 16378–16382.

Diederich, S., L. Sauerhering, M. Weis, H. Altmeppen, N. Schaschke, T. Reinheckel, S. Erbar, and A. Maisner (2012). Activation of the Nipah virus fusion protein in MDCK cells is mediated by cathepsin B within the endosome-recycling compartment. *J. Virol. 86*(7), 3736–3745.

Diefenbach, R. J., E. Diefenbach, M. W. Douglas, and A. L. Cunningham (2002). The heavy chain of conventional kinesin interacts with the SNARE proteins SNAP25 and SNAP23. *Biochemistry 41*(50), 14906–14915.

Diefenbach, R. J., J. P. Mackay, P. J. Armati, and A. L. Cunningham (1998). The C-terminal region of the stalk domain of ubiquitous human kinesin heavy chain contains the binding site for kinesin light chain. *Biochemistry 37*(47), 16663–16670.

Dietrich, D., F. Seiler, F. Essmann, and G. Dodt (2013). Identification of the kinesin KifC3 as a new player for positioning of peroxisomes and other organelles in mammalian cells. *Biochim. Biophys. Acta 1833*(12), 3013–3024.

Dietrich, K. A., C. V. Sindelar, P. D. Brewer, K. H. Downing, C. R. Cremo, and S. E. Rice (2008). The kinesin-1 motor protein is regulated by a direct interaction of its head and tail. *Proc. Natl. Acad. Sci. U.S.A. 105*(26), 8938–8943.

Dogan, M. Y., S. Can, F. B. Cleary, V. Purde, and A. Yildiz (2015). Kinesin's Front Head is Gated by the Backward Orientation of its Neck Linker. *Cell Rep 10*(12), 1967–1973.

Doherty, G. J. and H. T. McMahon (2009). Mechanisms of endocytosis. *Annu. Rev. Biochem. 78*, 857–902.

Dominguez, R. (2009). Actin filament nucleation and elongation factors–structure-function relationships. *Crit. Rev. Biochem. Mol. Biol. 44*(6), 351–366.

Dominguez, R. and K. C. Holmes (2011). Actin Structure and Function. *Annual Review of Biophysics 40*(1), 169–186.

Dumont, A., E. Boucrot, S. Drevensek, V. Daire, J.-P. Gorvel, C. Poüs, D. W. Holden, and S. Méresse (2010). SKIP, the host target of the Salmonella virulence factor SifA, promotes kinesin-1-dependent vacuolar membrane exchanges. *Traffic 11*(7), 899–911.

Dunn, L. C. and L. W. Thigpen (1930). THE SILVER MOUSE A Recessive Color Variation. *J Hered 21*(12), 495–498.

Ebanks, J. P., R. R. Wickett, and R. E. Boissy (2009). Mechanisms regulating skin pigmentation: the rise and fall of complexion coloration. *Int J Mol Sci 10*(9), 4066–4087.

Echeverri, C. J., B. M. Paschal, K. T. Vaughan, and R. B. Vallee (1996). Molecular characterization of the 50-kD subunit of dynactin reveals function for the complex in chromosome alignment and spindle organization during mitosis. *J Cell Biol 132*(4), 617–633.

Eckley, D. M., S. R. Gill, K. A. Melkonian, J. B. Bingham, H. V. Goodson, J. E. Heuser, and T. A. Schroer (1999). Analysis of Dynactin Subcomplexes Reveals a Novel Actin-Related Protein Associated with the Arp1 Minifilament Pointed End. *J Cell Biol 147*(2), 307–320.

Eden, S., R. Rohatgi, A. V. Podtelejnikov, M. Mann, and M. W. Kirschner (2002). Mechanism of regulation of WAVE1-induced actin nucleation by Rac1 and Nck. *Nature 418*(6899), 790–793.

Edwards, S. R. and T. J. Wandless (2007). The Rapamycin-binding Domain of the Protein Kinase Mammalian Target of Rapamycin Is a Destabilizing Domain. *J. Biol. Chem. 282*(18), 13395–13401.

Evans, R. D., C. Robinson, D. A. Briggs, D. J. Tooth, J. S. Ramalho, M. Cantero, L. Montoliu, S. Patel, E. V. Sviderskaya, and A. N. Hume (2014). Myosin-Va and dynamic actin oppose microtubules to drive long-range organelle transport. *Curr. Biol. 24*(15), 1743–1750.

Even-Ram, S., A. D. Doyle, M. A. Conti, K. Matsumoto, R. S. Adelstein, and K. M. Yamada (2007). Myosin IIA regulates cell motility and actomyosin–microtubule crosstalk. *Nat Cell Biol 9*(3), 299–309.

Fagarasanu, A., M. Fagarasanu, G. A. Eitzen, J. D. Aitchison, and R. A. Rachubinski (2006). The peroxisomal membrane protein Inp2p is the peroxisome-specific receptor for the myosin V motor Myo2p of Saccharomyces cerevisiae. *Dev. Cell 10*(5), 587–600.

Faigle, W., G. Raposo, D. Tenza, V. Pinet, A. B. Vogt, H. Kropshofer, A. Fischer, G. de Saint-Basile, and S. Amigorena (1998). Deficient peptide loading and MHC class II endosomal sorting in a human genetic immunodeficiency disease: the Chediak-Higashi syndrome. *J. Cell Biol. 141*(5), 1121–1134.

Fan, J., A. D. Griffiths, A. Lockhart, R. A. Cross, and L. A. Amos (1996). Microtubule minus ends can be labelled with a phage display antibody specific to alpha-tubulin. *J. Mol. Biol. 259*(3), 325–330.

Farina, F., J. Gaillard, C. Guérin, Y. Couté, J. Sillibourne, L. Blanchoin, and M. Théry (2016). The centrosome is an actin-organizing centre. *Nat. Cell Biol. 18*(1), 65–75.

Fawcett, D. W. and K. R. Porter (1954). A study of the fine structure of ciliated epithelia. *J. Morphol. 94*(2), 221–281.

Feierbach, B. and F. Chang (2001). Roles of the fission yeast formin for3p in cell polarity, actin cable formation and symmetric cell division. *Curr. Biol. 11*(21), 1656–1665.

Figueiredo, A. C., C. Wasmeier, A. K. Tarafder, J. S. Ramalho, R. A. Baron, and M. C. Seabra (2008). Rab3gep is the non-redundant guanine nucleotide exchange factor for Rab27a in melanocytes. *J. Biol. Chem. 283*(34), 23209–23216.

Firestone, A. J., J. S. Weinger, M. Maldonado, K. Barlan, L. D. Langston, M. O'Donnell, V. I. Gelfand, T. M. Kapoor, and J. K. Chen (2012). Small-molecule inhibitors of the AAA+ ATPase motor cytoplasmic dynein. *Nature 484*(7392), 125–129.

Flannagan, R. S., V. Jaumouillé, and S. Grinstein (2012). The cell biology of phagocytosis. *Annu Rev Pathol 7*, 61–98.

Flyvbjerg, H., E. Jobs, and S. Leibler (1996). Kinetics of self-assembling microtubules: an "inverse problem" in biochemistry. *Proc. Natl. Acad. Sci. U.S.A. 93*(12), 5975–5979.

Forgacs, E., T. Sakamoto, S. Cartwright, B. Belknap, M. Kovács, J. Tóth, M. R. Webb, J. R. Sellers, and H. D. White (2009). Switch 1 mutation S217a converts myosin V into a low duty ratio motor. *J. Biol. Chem. 284*(4), 2138–2149.

Förtsch, J., E. Hummel, M. Krist, and B. Westermann (2011). The myosin-related motor protein Myo2 is an essential mediator of bud-directed mitochondrial movement in yeast. *J Cell Biol 194*(3), 473–488.

Frost, R., E. Norström, L. Bodin, C. Langhammer, J. Sturve, M. Wallin, and S. Svedhem (2013). Acoustic detection of melanosome transport in Xenopus laevis melanophores. *Anal. Biochem. 435*(1), 10–18.

Fujii, T., A. H. Iwane, T. Yanagida, and K. Namba (2010). Direct visualization of secondary structures of F-actin by electron cryomicroscopy. *Nature 467*(7316), 724–728.

Fuller, B. B., D. T. Spaulding, and D. R. Smith (2001). Regulation of the catalytic activity of preexisting tyrosinase in black and Caucasian human melanocyte cell cultures. *Exp. Cell Res. 262*(2), 197–208.

Gard, D. L. and M. W. Kirschner (1987). A microtubule-associated protein from Xenopus eggs that specifically promotes assembly at the plus-end. *J. Cell Biol. 105*(5), 2203–2215.

Gaskin, F., C. R. Cantor, and M. L. Shelanski (1974). Turbidimetric studies of the in vitro assembly and disassembly of porcine neurotubules. *J. Mol. Biol. 89*(4), 737–755.

Gaullier, J. M., A. Simonsen, A. D'Arrigo, B. Bremnes, H. Stenmark, and R. Aasland (1998). FYVE fingers bind PtdIns(3)P. *Nature 394*(6692), 432–433.

Gee, M. A., J. E. Heuser, and R. B. Vallee (1997). An extended microtubule-binding structure within the dynein motor domain. *Nature 390*(6660), 636–639.

Gennerich, A., A. P. Carter, S. L. Reck-Peterson, and R. D. Vale (2007). Force-induced bidirectional stepping of cytoplasmic dynein. *Cell 131*(5), 952–965.

Geron, E., E. D. Schejter, and B.-Z. Shilo (2013). Directing exocrine secretory vesicles to the apical membrane by actin cables generated by the formin mDia1. *Proc. Natl. Acad. Sci. U.S.A. 110*(26), 10652–10657.

Gibbons, I. R., J. E. Garbarino, C. E. Tan, S. L. Reck-Peterson, R. D. Vale, and A. P. Carter (2005). The affinity of the dynein microtubule-binding domain is modulated by the conformation of its coiled-coil stalk. *J. Biol. Chem. 280*(25), 23960–23965.

Gibbons, I. R. and A. J. Rowe (1965). Dynein: A Protein with Adenosine Triphosphatase Activity from Cilia. *Science 149*(3682), 424–426.

Gindhart, J. G. and L. S. Goldstein (1996). Tetratrico peptide repeats are present in the kinesin light chain. *Trends Biochem. Sci. 21*(2), 52–53.

Giot, L., J. S. Bader, C. Brouwer, A. Chaudhuri, B. Kuang, Y. Li, Y. L. Hao, C. E. Ooi, B. Godwin, E. Vitols, G. Vijayadamodar, P. Pochart, H. Machineni, M. Welsh, Y. Kong, B. Zerhusen, R. Malcolm, Z. Varrone, A. Collis, M. Minto, S. Burgess, L. McDaniel,

E. Stimpson, F. Spriggs, J. Williams, K. Neurath, N. Ioime, M. Agee, E. Voss, K. Furtak, R. Renzulli, N. Aanensen, S. Carrolla, E. Bickelhaupt, Y. Lazovatsky, A. DaSilva, J. Zhong, C. A. Stanyon, R. L. Finley, K. P. White, M. Braverman, T. Jarvie, S. Gold, M. Leach, J. Knight, R. A. Shimkets, M. P. McKenna, J. Chant, and J. M. Rothberg (2003). A protein interaction map of Drosophila melanogaster. *Science 302*(5651), 1727–1736.

Glater, E. E., L. J. Megeath, R. S. Stowers, and T. L. Schwarz (2006). Axonal transport of mitochondria requires milton to recruit kinesin heavy chain and is light chain independent. *J. Cell Biol. 173*(4), 545–557.

Goddette, D. W. and C. Frieden (1985). The binding of cytochalasin D to monomeric actin. *Biochem. Biophys. Res. Commun. 128*(3), 1087–1092.

Goh, W. I., T. Sudhaharan, K. B. Lim, K. P. Sem, C. L. Lau, and S. Ahmed (2011). RifmDia1 interaction is involved in filopodium formation independent of Cdc42 and Rac effectors. *J. Biol. Chem. 286*(15), 13681–13694.

Goldman, R. D. (1971). The role of three cytoplasmic fibers in BHK-21 cell motility. I. Microtubules and the effects of colchicine. *J. Cell Biol. 51*(3), 752–762.

Goley, E. D., S. E. Rodenbusch, A. C. Martin, and M. D. Welch (2004). Critical conformational changes in the Arp2/3 complex are induced by nucleotide and nucleation promoting factor. *Mol. Cell 16*(2), 269–279.

Gomez, T. S. and D. D. Billadeau (2009). A FAM21-containing WASH complex regulates retromer-dependent sorting. *Dev. Cell 17*(5), 699–711.

Gournier, H., E. D. Goley, H. Niederstrasser, T. Trinh, and M. D. Welch (2001). Reconstitution of human Arp2/3 complex reveals critical roles of individual subunits in complex structure and activity. *Mol. Cell 8*(5), 1041–1052.

Green, K. J., B. Geiger, J. C. Jones, J. C. Talian, and R. D. Goldman (1987). The relationship between intermediate filaments and microfilaments before and during the formation of desmosomes and adherens-type junctions in mouse epidermal keratinocytes. *J. Cell Biol. 104*(5), 1389–1402.

Green, K. J., J. C. Talian, and R. D. Goldman (1986). Relationship between intermediate filaments and microfilaments in cultured fibroblasts: evidence for common foci during cell spreading. *Cell Motil. Cytoskeleton 6*(4), 406–418.

Griffith, L. M., S. M. Downs, and J. A. Spudich (1987). Myosin light chain kinase and myosin light chain phosphatase from Dictyostelium: effects of reversible phosphorylation on myosin structure and function. *J. Cell Biol. 104*(5), 1309–1323.

Griffiths, G. M. (1996). Secretory lysosomes - a special mechanism of regulated secretion in haemopoietic cells. *Trends Cell Biol. 6*(9), 329–332.

Gross, S. P., M. C. Tuma, S. W. Deacon, A. S. Serpinskaya, A. R. Reilein, and V. I. Gelfand (2002). Interactions and regulation of molecular motors in Xenopus melanophores. *J. Cell Biol. 156*(5), 855–865.

Grummt, M., G. Woehlke, U. Henningsen, S. Fuchs, M. Schleicher, and M. Schliwa (1998). Importance of a flexible hinge near the motor domain in kinesin-driven motility. *EMBO J. 17*(19), 5536–5542.

Gundersen, G. G. and A. Bretscher (2003). Cell biology. Microtubule asymmetry. *Science 300*(5628), 2040–2041.

Guo, X., G. T. Macleod, A. Wellington, F. Hu, S. Panchumarthi, M. Schoenfield, L. Marin, M. P. Charlton, H. L. Atwood, and K. E. Zinsmaier (2005). The GTPase dMiro is required for axonal transport of mitochondria to Drosophila synapses. *Neuron 47*(3), 379–393.

Gupta, K. K., C. Li, A. Duan, E. O. Alberico, O. V. Kim, M. S. Alber, and H. V. Goodson (2013). Mechanism for the catastrophe-promoting activity of the microtubule destabilizer Op18/stathmin. *Proc. Natl. Acad. Sci. U.S.A. 110*(51), 20449–20454.

Gupta, V., K. J. Palmer, P. Spence, A. Hudson, and D. J. Stephens (2008). Kinesin-1 (uKHC/KIF5b) is required for bidirectional motility of ER exit sites and efficient ER-to-Golgi transport. *Traffic 9*(11), 1850–1866.

Gurland, G. and G. G. Gundersen (1995). Stable, detyrosinated microtubules function to localize vimentin intermediate filaments in fibroblasts. *J. Cell Biol. 131*(5), 1275–1290.

Gwynn, B., S. L. Ciciotte, S. J. Hunter, L. L. Washburn, R. S. Smith, S. G. Andersen, R. T. Swank, E. C. Dell'Angelica, J. S. Bonifacino, E. M. Eicher, and L. L. Peters (2000). Defects in the cappuccino (cno) gene on mouse chromosome 5 and human 4p cause Hermansky-Pudlak syndrome by an AP-3–independent mechanism. *Blood 96*(13), 4227–4235.

Ha, L., T. Ichikawa, M. Anver, R. Dickins, S. Lowe, N. E. Sharpless, P. Krimpenfort, R. A. Depinho, D. C. Bennett, E. V. Sviderskaya, and G. Merlino (2007). ARF functions as a melanoma tumor suppressor by inducing p53-independent senescence. *Proc. Natl. Acad. Sci. U.S.A. 104*(26), 10968–10973.

Hackney, D. D. and M. F. Stock (2000). Kinesin's IAK tail domain inhibits initial microtubule-stimulated ADP release. *Nat. Cell Biol. 2*(5), 257–260.

Hale, C. M., W.-C. Chen, S. B. Khatau, B. R. Daniels, J. S. H. Lee, and D. Wirtz (2011). SMRT analysis of MTOC and nuclear positioning reveals the role of EB1 and LIC1 in single-cell polarization. *J. Cell. Sci. 124*(Pt 24), 4267–4285.

Hall, P. A., P. H. McKee, H. D. Menage, R. Dover, and D. P. Lane (1993). High levels of p53 protein in UV-irradiated normal human skin. *Oncogene 8*(1), 203–207.

Halliburton, W. D. (1887). On Muscle-Plasma1. *The Journal of Physiology 8*(3-4), 133–202.

Hammer, J. A. r. and J. R. Sellers (2012). Walking to work: roles for class V myosins as cargo transporters. *Nat. Rev. Mol. Cell Biol. 13*(1), 13–26.

Hanson, J. and J. Lowy (1963). The structure of F-actin and of actin filaments isolated from muscle. *Journal of Molecular Biology 6*(1), 46–60.

Hara, M., M. Yaar, H. R. Byers, D. Goukassian, R. E. Fine, J. Gonsalves, and B. A. Gilchrest (2000). Kinesin participates in melanosomal movement along melanocyte dendrites. *J. Invest. Dermatol. 114*(3), 438–443.

Harada, A., Y. Takei, Y. Kanai, Y. Tanaka, S. Nonaka, and N. Hirokawa (1998). Golgi vesiculation and lysosome dispersion in cells lacking cytoplasmic dynein. *J. Cell Biol. 141*(1), 51–59.

Haviv, L., D. Gillo, F. Backouche, and A. Bernheim-Groswasser (2008). A cytoskeletal demolition worker: myosin II acts as an actin depolymerization agent. *J. Mol. Biol. 375*(2), 325–330.

Hearing, V. J. (2005). Biogenesis of pigment granules: a sensitive way to regulate melanocyte function. *J. Dermatol. Sci. 37*(1), 3–14.

Hetrick, B., M. S. Han, L. A. Helgeson, and B. J. Nolen (2013). Small molecules CK-666 and CK-869 inhibit actin-related protein 2/3 complex by blocking an activating conformational change. *Chem. Biol. 20*(5), 701–712.

Higgs, H. N. and K. J. Peterson (2005). Phylogenetic Analysis of the Formin Homology 2 Domain. *Mol Biol Cell 16*(1), 1–13.

Hill, M. A. and P. Gunning (1993). Beta and gamma actin mRNAs are differentially located within myoblasts. *J. Cell Biol. 122*(4), 825–832.

Hirokawa, N., Y. Noda, Y. Tanaka, and S. Niwa (2009). Kinesin superfamily motor proteins and intracellular transport. *Nat. Rev. Mol. Cell Biol. 10*(10), 682–696.

Hodges, A. R., E. B. Krementsova, and K. M. Trybus (2007). Engineering the Processive Run Length of Myosin V. *J. Biol. Chem. 282*(37), 27192–27197.

Hoepfner, D., M. v. d. Berg, P. Philippsen, H. F. Tabak, and E. H. Hettema (2001). A role for Vps1p, actin, and the Myo2p motor in peroxisome abundance and inheritance in Saccharomyces cerevisiae. *J Cell Biol 155*(6), 979–990.

Hoepfner, S., F. Severin, A. Cabezas, B. Habermann, A. Runge, D. Gillooly, H. Stenmark, and M. Zerial (2005). Modulation of receptor recycling and degradation by the endosomal kinesin KIF16b. *Cell 121*(3), 437–450.

Hofmann, I. and S. Munro (2006). An N-terminally acetylated Arf-like GTPase is localised to lysosomes and affects their motility. *J. Cell. Sci. 119*(Pt 8), 1494–1503.

Hollenbeck, P. J. and J. A. Swanson (1990). Radial extension of macrophage tubular lysosomes supported by kinesin. *Nature 346*(6287), 864–866.

Holleran, E. A., L. A. Ligon, M. Tokito, M. C. Stankewich, J. S. Morrow, and E. L. F. Holzbaur (2001). βIII Spectrin Binds to the Arp1 Subunit of Dynactin. *J. Biol. Chem. 276*(39), 36598–36605.

Holmes, K. C. (2008). Myosin Structure. In *Myosins*, Number 7 in Proteins and Cell Regulation, pp. 35–54. Springer Netherlands.

Holzinger, A. (2009). Jasplakinolide: an actin-specific reagent that promotes actin polymerization. *Methods Mol. Biol. 586*, 71–87.

Hoock, T. C., P. M. Newcomb, and I. M. Herman (1991). Beta actin and its mRNA are localized at the plasma membrane and the regions of moving cytoplasm during the cellular response to injury. *J. Cell Biol. 112*(4), 653–664.

Hotulainen, P., E. Paunola, M. K. Vartiainen, and P. Lappalainen (2005). Actin-depolymerizing Factor and Cofilin-1 Play Overlapping Roles in Promoting Rapid F-Actin Depolymerization in Mammalian Nonmuscle Cells. *Mol Biol Cell 16*(2), 649–664.

Howard, J., A. J. Hudspeth, and R. D. Vale (1989). Movement of microtubules by single kinesin molecules. *Nature 342*(6246), 154–158.

Hua, W., J. Chung, and J. Gelles (2002). Distinguishing inchworm and hand-over-hand processive kinesin movement by neck rotation measurements. *Science 295*(5556), 844–848.

Huang, L., Y.-M. Kuo, and J. Gitschier (1999). The pallid gene encodes a novel, syntaxin 13-interacting protein involved in platelet storage pool deficiency. *Nat Genet 23*(3), 329–332.

Hubbard, B. D. and E. Lazarides (1979). Copurification of actin and desmin from chicken smooth muscle and their copolymerization in vitro to intermediate filaments. *J. Cell Biol. 80*(1), 166–182.

Hume, A. N., L. M. Collinson, C. R. Hopkins, M. Strom, D. C. Barral, G. Bossi, G. M. Griffiths, and M. C. Seabra (2002). The leaden gene product is required with Rab27a to recruit myosin Va to melanosomes in melanocytes. *Traffic 3*(3), 193–202.

Hume, A. N., L. M. Collinson, A. Rapak, A. Q. Gomes, C. R. Hopkins, and M. C. Seabra (2001). Rab27a Regulates the Peripheral Distribution of Melanosomes in Melanocytes. *J Cell Biol 152*(4), 795–808.

Hume, A. N., A. K. Tarafder, J. S. Ramalho, E. V. Sviderskaya, and M. C. Seabra (2006). A coiled-coil domain of melanophilin is essential for Myosin Va recruitment and melanosome transport in melanocytes. *Mol. Biol. Cell 17*(11), 4720–4735.

Hume, A. N., D. S. Ushakov, A. K. Tarafder, M. A. Ferenczi, and M. C. Seabra (2007). Rab27a and MyoVa are the primary Mlph interactors regulating melanosome transport in melanocytes. *J. Cell. Sci. 120*(Pt 17), 3111–3122.

Hunt, A. J., F. Gittes, and J. Howard (1994). The force exerted by a single kinesin molecule against a viscous load. *Biophys J 67*(2), 766–781.

Hunter, A. W., M. Caplow, D. L. Coy, W. O. Hancock, S. Diez, L. Wordeman, and J. Howard (2003). The kinesin-related protein MCAK is a microtubule depolymerase that forms an ATP-hydrolyzing complex at microtubule ends. *Mol. Cell 11*(2), 445–457.

Hurford, M. T. and C. Sebastiano (2008). Hermansky-Pudlak Syndrome: Report of a Case and Review of the Literature. *Int J Clin Exp Pathol 1*(6), 550–554.

Hurley, J. H. (1999). Structure, Mechanism, and Regulation of Mammalian Adenylyl Cyclase. *J. Biol. Chem. 274*(12), 7599–7602.

Hutchins, J. R. A., Y. Toyoda, B. Hegemann, I. Poser, J.-K. Heriche, M. M. Sykora, M. Augsburg, O. Hudecz, B. A. Buschhorn, J. Bulkescher, C. Conrad, D. Comartin, A. Schleiffer, M. Sarov, A. Pozniakovsky, M. M. Slabicki, S. Schloissnig, I. Steinmacher, M. Leuschner, A. Ssykor, S. Lawo, L. Pelletier, H. Stark, K. Nasmyth, J. Ellenberg, R. Durbin, F. Buchholz, K. Mechtler, A. A. Hyman, and J.-M. Peters (2010). Systematic analysis of human protein complexes identifies chromosome segregation proteins. *Science 328*(5978), 593–599.

Hyman, A. A., D. Chretien, I. Arnal, and R. H. Wade (1995). Structural changes accompanying GTP hydrolysis in microtubules: information from a slowly hydrolyzable analogue guanylyl-(alpha,beta)-methylene-diphosphonate. *J. Cell Biol. 128*(1-2), 117–125.

Ikebe, M., D. J. Hartshorne, and M. Elzinga (1986). Identification, phosphorylation, and dephosphorylation of a second site for myosin light chain kinase on the 20,000-dalton light chain of smooth muscle myosin. *J. Biol. Chem. 261*(1), 36–39.

Imamula, K., T. Kon, R. Ohkura, and K. Sutoh (2007). The coordination of cyclic microtubule association/dissociation and tail swing of cytoplasmic dynein. *Proc. Natl. Acad. Sci. U.S.A. 104*(41), 16134–16139.

Introne, W., R. E. Boissy, and W. A. Gahl (1999). Clinical, molecular, and cell biological aspects of Chediak-Higashi syndrome. *Mol. Genet. Metab. 68*(2), 283–303.

Ishida, M., N. Ohbayashi, and M. Fukuda (2015). Rab1a regulates anterograde melanosome transport by recruiting kinesin-1 to melanosomes through interaction with SKIP. *Sci Rep 5*, 8238.

Ishikawa, R., T. Sakamoto, T. Ando, S. Higashi-Fujime, and K. Kohama (2003). Polarized actin bundles formed by human fascin-1: their sliding and disassembly on myosin II and myosin V in vitro. *J. Neurochem. 87*(3), 676–685.

Isogai, T., R. van der Kammen, and M. Innocenti (2015). SMIFH2 has effects on Formins and p53 that perturb the cell cytoskeleton. *Sci Rep 5*, 9802.

Itoh, T. and M. Fukuda (2006). Identification of EPI64 as a GTPase-activating protein specific for Rab27a. *J. Biol. Chem. 281*(42), 31823–31831.

Jackson, I. J. (1991). Mouse coat colour mutations: a molecular genetic resource which spans the centuries. *Bioessays 13*(9), 439–446.

Jackson-Grusby, L., A. Kuo, and P. Leder (1992). A variant limb deformity transcript expressed in the embryonic mouse limb defines a novel formin. *Genes Dev. 6*(1), 29–37.

Jahn, R. and D. Fasshauer (2012). Molecular machines governing exocytosis of synaptic vesicles. *Nature 490*(7419), 201–207.

Jaud, J., F. Bathe, M. Schliwa, M. Rief, and G. Woehlke (2006). Flexibility of the Neck Domain Enhances Kinesin-1 Motility under Load. *Biophysical Journal 91*(4), 1407–1412.

Johnson, K. A. and G. G. Borisy (1977). Kinetic analysis of microtubule self-assembly in vitro. *J. Mol. Biol. 117*(1), 1–31.

Johnson, K. A., M. A. Haas, and J. L. Rosenbaum (1994). Localization of a kinesin-related protein to the central pair apparatus of the Chlamydomonas reinhardtii flagellum. *J Cell Sci 107*(6), 1551–1556.

Johnston, G. C., J. A. Prendergast, and R. A. Singer (1991). The Saccharomyces cerevisiae MYO2 gene encodes an essential myosin for vectorial transport of vesicles. *J Cell Biol 113*(3), 539–551.

Johnston, S. A., J. P. Bramble, C. L. Yeung, P. M. Mendes, and L. M. Machesky (2008). Arp2/3 complex activity in filopodia of spreading cells. *BMC Cell Biol. 9*, 65.

Kaan, H. Y. K., D. D. Hackney, and F. Kozielski (2011). The structure of the kinesin-1 motor-tail complex reveals the mechanism of autoinhibition. *Science 333*(6044), 883–885.

Kanai, Y., Y. Okada, Y. Tanaka, A. Harada, S. Terada, and N. Hirokawa (2000). KIF5c, a novel neuronal kinesin enriched in motor neurons. *J. Neurosci. 20*(17), 6374–6384.

Kapitein, L. C., M. A. Schlager, W. A. van der Zwan, P. S. Wulf, N. Keijzer, and C. C. Hoogenraad (2010). Probing intracellular motor protein activity using an inducible cargo trafficking assay. *Biophys. J. 99*(7), 2143–2152.

King, S. J., C. L. Brown, K. C. Maier, N. J. Quintyne, and T. A. Schroer (2003). Analysis of the Dynein-Dynactin Interaction In Vitro and In Vivo. *Mol. Biol. Cell 14*(12), 5089–5097.

King, S. J. and T. A. Schroer (2000). Dynactin increases the processivity of the cytoplasmic dynein motor. *Nat Cell Biol 2*(1), 20–24.

Klein, C., N. Philippe, F. Le Deist, S. Fraitag, C. Prost, A. Durandy, A. Fischer, and C. Griscelli (1994). Partial albinism with immunodeficiency (Griscelli syndrome). *J. Pediatr. 125*(6 Pt 1), 886–895.

Klein, M. G., W. Shi, U. Ramagopal, Y. Tseng, D. Wirtz, D. R. Kovar, C. J. Staiger, and S. C. Almo (2004). Structure of the actin crosslinking core of fimbrin. *Structure 12*(6), 999–1013.

Klumpp, L. M., A. Hoenger, and S. P. Gilbert (2004). Kinesin's second step. *Proc Natl Acad Sci U S A 101*(10), 3444–3449.

Kobielak, A., H. A. Pasolli, and E. Fuchs (2004). Mammalian formin-1 participates in adherens junctions and polymerization of linear actin cables. *Nat. Cell Biol. 6*(1), 21–30.

Koka, S., C. L. Neudauer, X. Li, R. E. Lewis, J. B. McCarthy, and J. J. Westendorf (2003). The formin-homology-domain-containing protein FHOD1 enhances cell migration. *J. Cell. Sci. 116*(Pt 9), 1745–1755.

Kolega, J., L. W. Janson, and D. L. Taylor (1991). The role of solation-contraction coupling in regulating stress fiber dynamics in nonmuscle cells. *J. Cell Biol. 114*(5), 993–1003.

Kollman, J. M., A. Merdes, L. Mourey, and D. A. Agard (2011). Microtubule nucleation by gamma-tubulin complexes. *Nat. Rev. Mol. Cell Biol. 12*(11), 709–721.

Kollman, J. M., J. K. Polka, A. Zelter, T. N. Davis, and D. A. Agard (2010). Microtubule nucleating gamma-TuSC assembles structures with 13-fold microtubule-like symmetry. *Nature 466*(7308), 879–882.

Komarova, Y. A., A. S. Akhmanova, S.-I. Kojima, N. Galjart, and G. G. Borisy (2002). Cytoplasmic linker proteins promote microtubule rescue in vivo. *J. Cell Biol. 159*(4), 589–599.

Kon, T., K. Imamula, A. J. Roberts, R. Ohkura, P. J. Knight, I. R. Gibbons, S. A. Burgess, and K. Sutoh (2009). Helix sliding in the stalk coiled coil of dynein couples ATPase and microtubule binding. *Nat Struct Mol Biol 16*(3), 325–333.

Kon, T., M. Nishiura, R. Ohkura, Y. Y. Toyoshima, and K. Sutoh (2004). Distinct functions of nucleotide-binding/hydrolysis sites in the four AAA modules of cytoplasmic dynein. *Biochemistry 43*(35), 11266–11274.

Kondo, T. and V. J. Hearing (2011). Update on the regulation of mammalian melanocyte function and skin pigmentation. *Expert Rev Dermatol 6*(1), 97–108.

Korn, E. D., M. F. Carlier, and D. Pantaloni (1987). Actin polymerization and ATP hydrolysis. *Science 238*(4827), 638–644.

Korolchuk, V. I., S. Saiki, M. Lichtenberg, F. H. Siddiqi, E. A. Roberts, S. Imarisio, L. Jahreiss, S. Sarkar, M. Futter, F. M. Menzies, C. J. O'Kane, V. Deretic, and D. C. Rubinsztein (2011). Lysosomal positioning coordinates cellular nutrient responses. *Nat. Cell Biol. 13*(4), 453–460.

Kovar, D. R. and T. D. Pollard (2004). Insertional assembly of actin filament barbed ends in association with formins produces piconewton forces. *Proc. Natl. Acad. Sci. U.S.A. 101*(41), 14725–14730.

Kowalski, J. R., C. Egile, S. Gil, S. B. Snapper, R. Li, and S. M. Thomas (2005). Cortactin regulates cell migration through activation of N-WASP. *J. Cell. Sci. 118*(Pt 1), 79–87.

Kozielski, F., S. Sack, A. Marx, M. Thormählen, E. Schönbrunn, V. Biou, A. Thompson, E. M. Mandelkow, and E. Mandelkow (1997). The crystal structure of dimeric kinesin and implications for microtubule-dependent motility. *Cell 91*(7), 985–994.

Krause, M. and A. Gautreau (2014). Steering cell migration: lamellipodium dynamics and the regulation of directional persistence. *Nat Rev Mol Cell Biol 15*(9), 577–590.

Kuroda, T. S., H. Ariga, and M. Fukuda (2003). The Actin-Binding Domain of Slac2-a/Melanophilin Is Required for Melanosome Distribution in Melanocytes. *Mol Cell Biol 23*(15), 5245–5255.

Kurowska, M., N. Goudin, N. T. Nehme, M. Court, J. Garin, A. Fischer, G. de Saint Basile, and G. Menasche (2012). Terminal transport of lytic granules to the immune synapse is mediated by the kinesin-1/Slp3/Rab27a complex. *Blood 119*(17), 3879–3889.

Kuznetsov, S. A., G. M. Langford, and D. G. Weiss (1992). Actin-dependent organelle movement in squid axoplasm. *Nature 356*(6371), 722–725.

Lagal, V., M. Abrivard, V. Gonzalez, A. Perazzi, S. Popli, E. Verzeroli, and I. Tardieux (2014). Spire-1 contributes to the invadosome and its associated invasive properties. *J. Cell. Sci. 127*(Pt 2), 328–340.

Lammers, M., R. Rose, A. Scrima, and A. Wittinghofer (2005). The regulation of mDia1 by autoinhibition and its release by Rho*GTP. *EMBO J. 24*(23), 4176–4187.

Lane, P. W. and J. E. Womack (1979). Ashen, a new color mutation on chromosome 9 of the mouse. *J Hered 70*(2), 133–135.

Larijani, B., A. N. Hume, A. K. Tarafder, and M. C. Seabra (2003). Multiple factors contribute to inefficient prenylation of Rab27a in Rab prenylation diseases. *J. Biol. Chem. 278*(47), 46798–46804.

Lawrence, C. J., R. K. Dawe, K. R. Christie, D. W. Cleveland, S. C. Dawson, S. A. Endow, L. S. B. Goldstein, H. V. Goodson, N. Hirokawa, J. Howard, R. L. Malmberg, J. R. McIntosh, H. Miki, T. J. Mitchison, Y. Okada, A. S. N. Reddy, W. M. Saxton, M. Schliwa, J. M. Scholey, R. D. Vale, C. E. Walczak, and L. Wordeman (2004). A standardized kinesin nomenclature. *J. Cell Biol. 167*(1), 19–22.

Le Pape, E., K. Wakamatsu, S. Ito, R. Wolber, and V. J. Hearing (2008). Regulation of eumelanin/pheomelanin synthesis and visible pigmentation in melanocytes by ligands of the melanocortin 1 receptor. *Pigment Cell & Melanoma Research 21*(4), 477–486.

Leader, B. and P. Leder (2000). Formin-2, a novel formin homology protein of the cappuccino subfamily, is highly expressed in the developing and adult central nervous system. *Mechanisms of Development 93*(1–2), 221–231.

Ledbetter, M. C. and K. R. Porter (1963). A "Microtubule" in Plant Cell Fine Structure. *J Cell Biol 19*(1), 239–250.

Lee, S. A., R. Eyeson, M. L. Cheever, J. Geng, V. V. Verkhusha, C. Burd, M. Overduin, and T. G. Kutateladze (2005). Targeting of the FYVE domain to endosomal membranes is regulated by a histidine switch. *Proc. Natl. Acad. Sci. U.S.A. 102*(37), 13052–13057.

Leguy, R., R. Melki, D. Pantaloni, and M. F. Carlier (2000). Monomeric gamma -tubulin nucleates microtubules. *J. Biol. Chem. 275*(29), 21975–21980.

Leonhardt, R. M., N. Vigneron, C. Rahner, B. J. Van den Eynde, and P. Cresswell (2010). Endoplasmic reticulum export, subcellular distribution, and fibril formation by Pmel17 require an intact N-terminal domain junction. *J. Biol. Chem. 285*(21), 16166–16183.

Lerner, A. B., J. D. Case, and Y. Takahashi (1960). Isolation of melatonin and 5-methoxyindole-3-acetic acid from bovine pineal glands. *J. Biol. Chem. 235*, 1992–1997.

Leung, K. F., R. Baron, and M. C. Seabra (2006). Thematic review series: lipid posttranslational modifications. geranylgeranylation of Rab GTPases. *J. Lipid Res. 47*(3), 467–475.

Li, J. and B. Russell (2013). Phosphatidylinositol 4,5-bisphosphate regulates CapZB1 and actin dynamics in response to mechanical strain. *Am J Physiol Heart Circ Physiol 305*(11), H1614–H1623.

Liu, R., M. T. Abreu-Blanco, K. C. Barry, E. V. Linardopoulou, G. E. Osborn, and S. M. Parkhurst (2009). Wash functions downstream of Rho and links linear and branched actin nucleation factors. *Development 136*(16), 2849–2860.

Lo Presti, L., F. Chang, and S. G. Martin (2012). Myosin Vs organize actin cables in fission yeast. *Mol Biol Cell 23*(23), 4579–4591.

Lombillo, V. A., C. Nislow, T. J. Yen, V. I. Gelfand, and J. R. McIntosh (1995). Antibodies to the kinesin motor domain and CENP-E inhibit microtubule depolymerization-dependent motion of chromosomes in vitro. *J Cell Biol 128*(1), 107–115.

Lopes, V. S., J. S. Ramalho, D. M. Owen, M. O. Karl, O. Strauss, C. E. Futter, and M. C. Seabra (2007). The ternary Rab27a-Myrip-Myosin VIIa complex regulates melanosome motility in the retinal pigment epithelium. *Traffic 8*(5), 486–499.

Luduena, R. F., E. M. Shooter, and L. Wilson (1977). Structure of the tubulin dimer. *J. Biol. Chem. 252*(20), 7006–7014.

Maiti, S., A. Michelot, C. Gould, L. Blanchoin, O. Sokolova, and B. L. Goode (2012). Structure and activity of full-length formin mDia1. *Cytoskeleton (Hoboken) 69*(6), 393–405.

Mandelkow, E. M., E. Mandelkow, and R. A. Milligan (1991). Microtubule dynamics and microtubule caps: a time-resolved cryo-electron microscopy study. *J. Cell Biol. 114*(5), 977–991.

Mandelkow, E. M., R. Schultheiss, R. Rapp, M. Müller, and E. Mandelkow (1986). On the surface lattice of microtubules: helix starts, protofilament number, seam, and handedness. *J. Cell Biol. 102*(3), 1067–1073.

Manton, I. and B. Clarke (1952). An Electron Microscope Study of the Spermatozoid of Sphagnum. *J. Exp. Bot. 3*(3), 265–275.

Marks, M. S. and M. C. Seabra (2001). The melanosome: membrane dynamics in black and white. *Nature Reviews Molecular Cell Biology 2*(10), 738–748.

Martin, A. C., M. D. Welch, and D. G. Drubin (2006). Arp2/3 ATP hydrolysis-catalysed branch dissociation is critical for endocytic force generation. *Nat. Cell Biol. 8*(8), 826–833.

Martin, S. G. and F. Chang (2006). Dynamics of the formin for3p in actin cable assembly. *Curr. Biol. 16*(12), 1161–1170.

Marx, A., J. Müller, and E. Mandelkow (2005). The structure of microtubule motor proteins. *Adv. Protein Chem. 71*, 299–344.

Mas, J. S., I. Gerritsen, C. Hahmann, C. Jimenez-Cervantes, and J. C. Garcia-Borron (2003). Rate limiting factors in melanocortin 1 receptor signalling through the cAMP pathway. *Pigment Cell Res. 16*(5), 540–547.

Matesic, L. E., R. Yip, A. E. Reuss, D. A. Swing, T. N. O'Sullivan, C. F. Fletcher, N. G. Copeland, and N. A. Jenkins (2001). Mutations in Mlph, encoding a member of the Rab effector family, cause the melanosome transport defects observed in leaden mice. *Proc. Natl. Acad. Sci. U.S.A. 98*(18), 10238–10243.

Matsumura, F. (2005). Regulation of myosin II during cytokinesis in higher eukaryotes. *Trends in Cell Biology 15*(7), 371–377.

Mattila, P. K. and P. Lappalainen (2008). Filopodia: molecular architecture and cellular functions. *Nat Rev Mol Cell Biol 9*(6), 446–454.

Maurer, S. P., F. J. Fourniol, G. Bohner, C. A. Moores, and T. Surrey (2012). EBs Recognize a Nucleotide-Dependent Structural Cap at Growing Microtubule Ends. *Cell 149*(2-2), 371–382.

McCord, C. P. and F. P. Allen (1917). Evidences associating pineal gland function with alterations in pigmentation. *J. Exp. Zool. 23*(1), 207–224.

McGough, A., B. Pope, W. Chiu, and A. Weeds (1997). Cofilin Changes the Twist of F-Actin: Implications for Actin Filament Dynamics and Cellular Function. *J Cell Biol 138*(4), 771–781.

McNally, F. J. (2013). Mechanisms of spindle positioning. *J. Cell Biol. 200*(2), 131–140.

McNicol, A. and S. J. Israels (1999). Platelet dense granules: structure, function and implications for haemostasis. *Thromb. Res. 95*(1), 1–18.

Mejillano, M. R., B. D. Shivanna, and R. H. Himes (1996). Studies on the nocodazole-induced GTPase activity of tubulin. *Arch. Biochem. Biophys. 336*(1), 130–138.

Melendez, J., K. Stengel, X. Zhou, B. K. Chauhan, M. Debidda, P. Andreassen, R. A. Lang, and Y. Zheng (2011). RhoA GTPase is dispensable for actomyosin regulation but is essential for mitosis in primary mouse embryonic fibroblasts. *J. Biol. Chem. 286*(17), 15132–15137.

Mercer, J. A., P. K. Seperack, M. C. Strobel, N. G. Copeland, and N. A. Jenkins (1991). Novel myosin heavy chain encoded by murine dilute coat colour locus. *Nature 349*(6311), 709–713.

Mitchison, T. and M. Kirschner (1984). Dynamic instability of microtubule growth. *Nature 312*(5991), 237–242.

Mohri, H. (1968). Amino-acid Composition of "Tubulin" constituting Microtubules of Sperm Flagella. *Nature 217*(5133), 1053–1054.

Molli, P. R., D.-Q. Li, R. Bagheri-Yarmand, S. B. Pakala, H. Katayama, S. Sen, J. Iyer, J. Chernoff, M.-Y. Tsai, S. S. Nair, and R. Kumar (2010). Arpc1b, a centrosomal protein, is both an activator and substrate of Aurora A. *J. Cell Biol. 190*(1), 101–114.

Moores, C. A., M. Yu, J. Guo, C. Beraud, R. Sakowicz, and R. A. Milligan (2002). A mechanism for microtubule depolymerization by KinI kinesins. *Mol. Cell 9*(4), 903–909.

Motegi, F., R. Arai, and I. Mabuchi (2001). Identification of two type V myosins in fission yeast, one of which functions in polarized cell growth and moves rapidly in the cell. *Mol. Biol. Cell 12*(5), 1367–1380.

Mottaz, J. H. and A. S. Zelickson (1967). Melanin transfer: a possible phagocytic process. *J. Invest. Dermatol. 49*(6), 605–610.

Moua, P., D. Fullerton, L. R. Serbus, R. Warrior, and W. M. Saxton (2011). Kinesin-1 tail autoregulation and microtubule-binding regions function in saltatory transport but not ooplasmic streaming. *Development 138*(6), 1087–1092.

Müller-Reichert, T., D. Chrétien, F. Severin, and A. A. Hyman (1998). Structural changes at microtubule ends accompanying GTP hydrolysis: Information from a slowly hydrolyzable analogue of GTP, guanylyl (α,β)methylenediphosphonate. *Proc Natl Acad Sci U S A 95*(7), 3661–3666.

Murphy, M. E. and L. Cassimeris (2006). A novel cancer therapy approach targeting microtubule function. *Cancer Biol. Ther. 5*(12), 1721–1723.

Nagashima, K., S. Torii, Z. Yi, M. Igarashi, K. Okamoto, T. Takeuchi, and T. Izumi (2002). Melanophilin directly links Rab27a and myosin Va through its distinct coiled-coil regions. *FEBS Lett. 517*(1-3), 233–238.

Nagle, D. L., M. A. Karim, E. A. Woolf, L. Holmgren, P. Bork, D. J. Misumi, S. H. McGrail, B. J. Dussault, C. M. Perou, R. E. Boissy, G. M. Duyk, R. A. Spritz, and K. J. Moore (1996). Identification and mutation analysis of the complete gene for Chediak-Higashi syndrome. *Nat. Genet. 14*(3), 307–311.

Navarro, C., H. Puthalakath, J. M. Adams, A. Strasser, and R. Lehmann (2004). Egalitarian binds dynein light chain to establish oocyte polarity and maintain oocyte fate. *Nat. Cell Biol. 6*(5), 427–435.

Navone, F., J. Niclas, N. Hom-Booher, L. Sparks, H. D. Bernstein, G. McCaffrey, and R. D. Vale (1992). Cloning and expression of a human kinesin heavy chain gene: interaction of the COOH-terminal domain with cytoplasmic microtubules in transfected CV-1 cells. *J. Cell Biol. 117*(6), 1263–1275.

Newton, A. C. (1995). Protein Kinase C: Structure, Function, and Regulation. *J. Biol. Chem. 270*(48), 28495–28498.

Nilsson, H., M. Rutberg, and M. Wallin (1996). Localization of kinesin and cytoplasmic dynein in cultured melanophores from Atlantic cod, Gadus morhua. *Cell Motil. Cytoskeleton 33*(3), 183–196.

Nilsson, H. and M. Wallin (1997). Evidence for several roles of dynein in pigment transport in melanophores. *Cell Motil. Cytoskeleton 38*(4), 397–409.

Nylander, K., J. C. Bourdon, S. E. Bray, N. K. Gibbs, R. Kay, I. Hart, and P. A. Hall (2000). Transcriptional activation of tyrosinase and TRP-1 by p53 links UV irradiation to the protective tanning response. *J. Pathol. 190*(1), 39–46.

Oakley, B. R., C. E. Oakley, Y. Yoon, and M. K. Jung (1990). Gamma-tubulin is a component of the spindle pole body that is essential for microtubule function in Aspergillus nidulans. *Cell 61*(7), 1289–1301.

Odronitz, F. and M. Kollmar (2007). Drawing the tree of eukaryotic life based on the analysis of 2,269 manually annotated myosins from 328 species. *Genome Biol 8*(9), R196.

Ohbayashi, N., Y. Maruta, M. Ishida, and M. Fukuda (2012). Melanoregulin regulates retrograde melanosome transport through interaction with the RILP-p150glued complex in melanocytes. *J. Cell. Sci. 125*(Pt 6), 1508–1518.

Okazaki, K., M. Uzuka, F. Morikawa, K. Toda, and M. Seiji (1976). Transfer mechanism of melanosomes in epidermal cell culture. *J. Invest. Dermatol. 67*(4), 541–547.

Olmsted, J. B. and G. G. Borisy (1975). Ionic and nucleotide requirements for microtubule polymerization in vitro. *Biochemistry 14*(13), 2996–3005.

Otey, C. A., M. H. Kalnoski, and J. C. Bulinski (1988). Immunolocalization of muscle and nonmuscle isoforms of actin in myogenic cells and adult skeletal muscle. *Cell Motil. Cytoskeleton 9*(4), 337–348.

Palazzo, A., B. Ackerman, and G. G. Gundersen (2003). Cell biology: Tubulin acetylation and cell motility. *Nature 421*(6920), 230.

Palmisano, I., P. Bagnato, A. Palmigiano, G. Innamorati, G. Rotondo, D. Altimare, C. Venturi, E. V. Sviderskaya, R. Piccirillo, M. Coppola, V. Marigo, B. Incerti, A. Ballabio, E. M. Surace, C. Tacchetti, D. C. Bennett, and M. V. Schiaffino (2008). The ocular albinism type 1 protein, an intracellular G protein-coupled receptor, regulates melanosome transport in pigment cells. *Hum. Mol. Genet. 17*(22), 3487–3501.

Palumbo, A., F. Solano, G. Misuraca, P. Aroca, J. C. Garcia Borron, J. A. Lozano, and G. Prota (1991). Comparative action of dopachrome tautomerase and metal ions on the rearrangement of dopachrome. *Biochim. Biophys. Acta 1115*(1), 1–5.

Paschal, B. M., H. S. Shpetner, and R. B. Vallee (1987). MAP 1c is a microtubule-activated ATPase which translocates microtubules in vitro and has dynein-like properties. *J. Cell Biol. 105*(3), 1273–1282.

Pastural, E., F. J. Barrat, R. Dufourcq-Lagelouse, S. Certain, O. Sanal, N. Jabado, R. Seger, C. Griscelli, A. Fischer, and G. de Saint Basile (1997). Griscelli disease maps to chromosome 15q21 and is associated with mutations in the myosin-Va gene. *Nat. Genet. 16*(3), 289–292.

Paul, A. S., A. Paul, T. D. Pollard, and T. Pollard (2008). The role of the FH1 domain and profilin in formin-mediated actin-filament elongation and nucleation. *Curr. Biol. 18*(1), 9–19.

Paunola, E., P. K. Mattila, and P. Lappalainen (2002). WH2 domain: a small, versatile adapter for actin monomers. *FEBS Lett. 513*(1), 92–97.

Peckham, M., G. Miller, C. Wells, D. Zicha, and G. A. Dunn (2001). Specific changes to the mechanism of cell locomotion induced by overexpression of beta-actin. *J. Cell. Sci. 114*(Pt 7), 1367–1377.

Pellegrin, S. and H. Mellor (2005). The Rho family GTPase Rif induces filopodia through mDia2. *Curr. Biol. 15*(2), 129–133.

Peng, G. E., S. R. Wilson, and O. D. Weiner (2011). A pharmacological cocktail for arresting actin dynamics in living cells. *Mol. Biol. Cell 22*(21), 3986–3994.

Peng, J., B. J. Wallar, A. Flanders, P. J. Swiatek, and A. S. Alberts (2003). Disruption of the Diaphanous-related formin Drf1 gene encoding mDia1 reveals a role for Drf3 as an effector for Cdc42. *Curr. Biol. 13*(7), 534–545.

Perrin, B. J. and J. M. Ervasti (2010). The Actin Gene Family: Function Follows Isoform. *Cytoskeleton (Hoboken) 67*(10), 630–634.

Pevet, P. (2002). Melatonin. *Dialogues Clin Neurosci 4*(1), 57–72.

Pfender, S., V. Kuznetsov, S. Pleiser, E. Kerkhoff, and M. Schuh (2011a). Spire-type actin nucleators cooperate with Formin-2 to drive asymmetric oocyte division. *Curr. Biol. 21*(11), 955–960.

Pfender, S., V. Kuznetsov, S. Pleiser, E. Kerkhoff, and M. Schuh (2011b). Spire-Type Actin Nucleators Cooperate with Formin-2 to Drive Asymmetric Oocyte Division. *Curr Biol 21*(11), 955–960.

Pfister, K. K., P. R. Shah, H. Hummerich, A. Russ, J. Cotton, A. A. Annuar, S. M. King, and E. M. C. Fisher (2006). Genetic analysis of the cytoplasmic dynein subunit families. *PLoS Genet. 2*(1), e1.

Pierson, G. B., P. R. Burton, and R. H. Himes (1978). Alterations in number of protofilaments in microtubules assembled in vitro. *J. Cell Biol. 76*(1), 223–228.

Pollard, T. D. (1986). Rate constants for the reactions of ATP- and ADP-actin with the ends of actin filaments. *J. Cell Biol. 103*(6 Pt 2), 2747–2754.

Pollard, T. D., L. Blanchoin, and R. D. Mullins (2000). Molecular mechanisms controlling actin filament dynamics in nonmuscle cells. *Annu Rev Biophys Biomol Struct 29*, 545–576.

Potterf, S. B. and V. J. Hearing (1998). Tyrosine transport into melanosomes is increased following stimulation of melanocyte differentiation. *Biochem. Biophys. Res. Commun. 248*(3), 795–800.

Potterf, S. B., J. Muller, I. Bernardini, F. Tietze, T. Kobayashi, V. J. Hearing, and W. A. Gahl (1996). Characterization of a melanosomal transport system in murine melanocytes mediating entry of the melanogenic substrate tyrosine. *J. Biol. Chem. 271*(8), 4002–4008.

Pring, M., L. Cassimeris, and S. H. Zigmond (2002). An unexplained sequestration of latrunculin A is required in neutrophils for inhibition of actin polymerization. *Cell Motil. Cytoskeleton 52*(2), 122–130.

Pring, M., M. Evangelista, C. Boone, C. Yang, and S. H. Zigmond (2003). Mechanism of Formin-Induced Nucleation of Actin Filaments. *Biochemistry 42*(2), 486–496.

Provance, D. W., T. L. James, and J. A. Mercer (2002). Melanophilin, the product of the leaden locus, is required for targeting of myosin-Va to melanosomes. *Traffic 3*(2), 124–132.

Pruyne, D., M. Evangelista, C. Yang, E. Bi, S. Zigmond, A. Bretscher, and C. Boone (2002). Role of formins in actin assembly: nucleation and barbed-end association. *Science 297*(5581), 612–615.

Puri, N., J. M. Gardner, and M. H. Brilliant (2000). Aberrant pH of melanosomes in pink-eyed dilution (p) mutant melanocytes. *J. Invest. Dermatol. 115*(4), 607–613.

Qiu, W., N. D. Derr, B. S. Goodman, E. Villa, D. Wu, W. Shih, and S. L. Reck-Peterson (2012). Dynein achieves processive motion using both stochastic and coordinated stepping. *Nat Struct Mol Biol 19*(2), 193–200.

Quinlan, M. E., J. E. Heuser, E. Kerkhoff, and R. D. Mullins (2005). Drosophila Spire is an actin nucleation factor. *Nature 433*(7024), 382–388.

Quinlan, M. E., S. Hilgert, A. Bedrossian, R. D. Mullins, and E. Kerkhoff (2007). Regulatory interactions between two actin nucleators, Spire and Cappuccino. *J Cell Biol 179*(1), 117–128.

Quintyne, N. J., S. R. Gill, D. M. Eckley, C. L. Crego, D. A. Compton, and T. A. Schroer (1999). Dynactin Is Required for Microtubule Anchoring at Centrosomes. *J Cell Biol 147*(2), 321–334.

Rao, J. N., Y. Madasu, and R. Dominguez (2014). Mechanism of actin filament pointed end capping by tropomodulin. *Science 345*(6195), 463–467.

Rao, M. V., L. J. Engle, P. S. Mohan, A. Yuan, D. Qiu, A. Cataldo, L. Hassinger, S. Jacobsen, V. M.-Y. Lee, A. Andreadis, J.-P. Julien, P. C. Bridgman, and R. A. Nixon (2002). Myosin Va binding to neurofilaments is essential for correct myosin Va distribution and transport and neurofilament density. *J. Cell Biol. 159*(2), 279–290.

Raposo, G. and M. S. Marks (2002). The dark side of lysosome-related organelles: specialization of the endocytic pathway for melanosome biogenesis. *Traffic 3*(4), 237–248.

Raposo, G., D. Tenza, D. M. Murphy, J. F. Berson, and M. S. Marks (2001). Distinct protein sorting and localization to premelanosomes, melanosomes, and lysosomes in pigmented melanocytic cells. *J. Cell Biol. 152*(4), 809–824.

Reck-Peterson, S. L., A. Yildiz, A. P. Carter, A. Gennerich, N. Zhang, and R. D. Vale (2006). Single-molecule analysis of dynein processivity and stepping behavior. *Cell 126*(2), 335–348.

Redeker, V., R. Melki, D. Promé, J. P. Le Caer, and J. Rossier (1992). Structure of tubulin C-terminal domain obtained by subtilisin treatment. The major alpha and beta tubulin isotypes from pig brain are glutamylated. *FEBS Lett. 313*(2), 185–192.

Reilein, A. R., A. S. Serpinskaya, R. L. Karcher, D. L. Dujardin, R. B. Vallee, and V. I. Gelfand (2003). Differential regulation of dynein-driven melanosome movement. *Biochem. Biophys. Res. Commun. 309*(3), 652–658.

Reilein, A. R., I. S. Tint, N. I. Peunova, G. N. Enikolopov, and V. I. Gelfand (1998). Regulation of Organelle Movement in Melanophores by Protein Kinase A (PKA), Protein Kinase C (PKC), and Protein Phosphatase 2a (PP2a). *J Cell Biol 142*(3), 803–813.

Reppert, S. M., D. R. Weaver, V. M. Cassone, C. Godson, and L. F. Kolakowski (1995). Melatonin receptors are for the birds: molecular analysis of two receptor subtypes differentially expressed in chick brain. *Neuron 15*(5), 1003–1015.

Rice, S., A. W. Lin, D. Safer, C. L. Hart, N. Naber, B. O. Carragher, S. M. Cain, E. Pechatnikova, E. M. Wilson-Kubalek, M. Whittaker, E. Pate, R. Cooke, E. W. Taylor, R. A. Milligan, and R. D. Vale (1999). A structural change in the kinesin motor protein that drives motility. *Nature 402*(6763), 778–784.

Rief, M., R. S. Rock, A. D. Mehta, M. S. Mooseker, R. E. Cheney, and J. A. Spudich (2000). Myosin-V stepping kinetics: A molecular model for processivity. *Proc Natl Acad Sci U S A 97*(17), 9482–9486.

Rizvi, S. A., E. M. Neidt, J. Cui, Z. Feiger, C. T. Skau, M. L. Gardel, S. A. Kozmin, and D. R. Kovar (2009a). Identification and characterization of a small molecule inhibitor of formin-mediated actin assembly. *Chem. Biol. 16*(11), 1158–1168.

Rizvi, S. A., E. M. Neidt, J. Cui, Z. Feiger, C. T. Skau, M. L. Gardel, S. A. Kozmin, and D. R. Kovar (2009b). Identification and characterization of a small molecule inhibitor of formin-mediated actin assembly. *Chem. Biol. 16*(11), 1158–1168.

Roberts, A. J., T. Kon, P. J. Knight, K. Sutoh, and S. A. Burgess (2013). Functions and mechanics of dynein motor proteins. *Nat Rev Mol Cell Biol 14*(11), 713–726.

Roberts, A. J., B. Malkova, M. L. Walker, H. Sakakibara, N. Numata, T. Kon, R. Ohkura, T. A. Edwards, P. J. Knight, K. Sutoh, K. Oiwa, and S. A. Burgess (2012a). ATP-driven remodeling of the linker domain in the dynein motor. *Structure 20*(10), 1670–1680.

Roberts, A. J., B. Malkova, M. L. Walker, H. Sakakibara, N. Numata, T. Kon, R. Ohkura, T. A. Edwards, P. J. Knight, K. Sutoh, K. Oiwa, and S. A. Burgess (2012b). ATP-driven remodeling of the linker domain in the dynein motor. *Structure 20*(10), 1670–1680.

Robinson, R. C., K. Turbedsky, D. A. Kaiser, J.-B. Marchand, H. N. Higgs, S. Choe, and T. D. Pollard (2001). Crystal Structure of Arp2/3 Complex. *Science 294*(5547), 1679–1684.

Rodionov, V. I., F. K. Gyoeva, and V. I. Gelfand (1991). Kinesin is responsible for centrifugal movement of pigment granules in melanophores. *Proc. Natl. Acad. Sci. U.S.A. 88*(11), 4956–4960.

Rogers, S. L., I. S. Tint, P. C. Fanapour, and V. I. Gelfand (1997). Regulated bidirectional motility of melanophore pigment granules along microtubules in vitro. *Proc. Natl. Acad. Sci. U.S.A. 94*(8), 3720–3725.

Rohatgi, R., H.-y. H. Ho, and M. W. Kirschner (2000). Mechanism of N-Wasp Activation by Cdc42 and Phosphatidylinositol 4,5-Bisphosphate. *J Cell Biol 150*(6), 1299–1310.

Rohatgi, R., L. Ma, H. Miki, M. Lopez, T. Kirchhausen, T. Takenawa, and M. W. Kirschner (1999). The Interaction between N-WASP and the Arp2/3 Complex Links Cdc42-Dependent Signals to Actin Assembly. *Cell 97*(2), 221–231.

Romero, S., C. Le Clainche, D. Didry, C. Egile, D. Pantaloni, and M.-F. Carlier (2004). Formin is a processive motor that requires profilin to accelerate actin assembly and associated ATP hydrolysis. *Cell 119*(3), 419–429.

Rosa-Ferreira, C. and S. Munro (2011). Arl8 and SKIP act together to link lysosomes to kinesin-1. *Dev. Cell 21*(6), 1171–1178.

Rosenfeld, S. S., P. M. Fordyce, G. M. Jefferson, P. H. King, and S. M. Block (2003). Stepping and stretching. How kinesin uses internal strain to walk processively. *J. Biol. Chem. 278*(20), 18550–18556.

Rosenthal, C. K. (2013). Spindle positioning by membrane adjustment. *Nat Cell Biol 15*(8), 894–894.

Rossanese, O. W., C. A. Reinke, B. J. Bevis, A. T. Hammond, I. B. Sears, J. O'Connor, and B. S. Glick (2001). A role for actin, Cdc1p, and Myo2p in the inheritance of late Golgi elements in Saccharomyces cerevisiae. *J. Cell Biol. 153*(1), 47–62.

Rouiller, I., X.-P. Xu, K. J. Amann, C. Egile, S. Nickell, D. Nicastro, R. Li, T. D. Pollard, N. Volkmann, and D. Hanein (2008). The structural basis of actin filament branching by the Arp2/3 complex. *J. Cell Biol. 180*(5), 887–895.

Ruusala, A. and P. Aspenstrom (2008). The atypical Rho GTPase Wrch1 collaborates with the nonreceptor tyrosine kinases Pyk2 and Src in regulating cytoskeletal dynamics. *Mol. Cell. Biol. 28*(5), 1802–1814.

Sagot, I., A. A. Rodal, J. Moseley, B. L. Goode, and D. Pellman (2002). An actin nucleation mechanism mediated by Bni1 and profilin. *Nat. Cell Biol. 4*(8), 626–631.

Sakamoto, T., M. R. Webb, E. Forgacs, H. D. White, and J. R. Sellers (2008). Direct observation of the mechanochemical coupling in myosin Va during processive movement. *Nature 455*(7209), 128–132.

Salbreux, G., G. Charras, and E. Paluch (2012). Actin cortex mechanics and cellular morphogenesis. *Trends Cell Biol. 22*(10), 536–545.

Sandblad, L., K. E. Busch, P. Tittmann, H. Gross, D. Brunner, and A. Hoenger (2006). The Schizosaccharomyces pombe EB1 homolog Mal3p binds and stabilizes the microtubule lattice seam. *Cell 127*(7), 1415–1424.

Saras, J., P. Wollberg, and P. Aspenstrom (2004). Wrch1 is a GTPase-deficient Cdc42-like protein with unusual binding characteristics and cellular effects. *Exp. Cell Res. 299*(2), 356–369.

Schafer, D. A., S. R. Gill, J. A. Cooper, J. E. Heuser, and T. A. Schroer (1994). Ultrastructural analysis of the dynactin complex: an actin-related protein is a component of a filament that resembles F-actin. *J Cell Biol 126*(2), 403–412.

Scherer, J. and R. B. Vallee (2011). Adenovirus recruits dynein by an evolutionary novel mechanism involving direct binding to pH-primed hexon. *Viruses 3*(8), 1417–1431.

Schliwa, M. (1982). Action of cytochalasin D on cytoskeletal networks. *J. Cell Biol. 92*(1), 79–91.

Schliwa, M. and U. Euteneuer (1978). A microtubule-independent component may be involved in granule transport in pigment cells. *Nature 273*(5663), 556–558.

Schmidt, H., E. S. Gleave, and A. P. Carter (2012). Insights into dynein motor domain function from a 3.3 å crystal structure. *Nat Struct Mol Biol 19*(5), 492–S1.

Schmidt, V. A., L. Scudder, C. E. Devoe, A. Bernards, L. D. Cupit, and W. F. Bahou (2003). IQGAP2 functions as a GTP-dependent effector protein in thrombin-induced platelet cytoskeletal reorganization. *Blood 101*(8), 3021–3028.

Schneider, C. A., W. S. Rasband, and K. W. Eliceiri (2012). NIH Image to ImageJ: 25 years of image analysis. *Nat. Methods 9*(7), 671–675.

Schonichen, A. and M. Geyer (2010). Fifteen formins for an actin filament: a molecular view on the regulation of human formins. *Biochim. Biophys. Acta 1803*(2), 152–163.

Schroer, T. A. (2004). Dynactin. *Annu. Rev. Cell Dev. Biol. 20*, 759–779.

Schroer, T. A., J. B. Bingham, and S. R. Gill (1996). Actin-related protein 1 and cytoplasmic dynein-based motility - what's the connection? *Trends in Cell Biology 6*(6), 212–215.

Schuh, M. (2011). An actin-dependent mechanism for long-range vesicle transport. *Nat. Cell Biol. 13*(12), 1431–1436.

Sckolnick, M., E. B. Krementsova, D. M. Warshaw, and K. M. Trybus (2013). More Than Just a Cargo Adapter: Melanophilin Prolongs and Slows Processive Runs of Myosin Va. *J. Biol. Chem.*, jbc.M113.476929.

Scott, G., S. Leopardi, S. Printup, and B. C. Madden (2002). Filopodia are conduits for melanosome transfer to keratinocytes. *J. Cell. Sci. 115*(Pt 7), 1441–1451.

Seabra, M. C., E. H. Mules, and A. N. Hume (2002). Rab GTPases, intracellular traffic and disease. *Trends Mol Med 8*(1), 23–30.

Sedeh, R. S., A. A. Fedorov, E. V. Fedorov, S. Ono, F. Matsumura, S. C. Almo, and M. Bathe (2010). Structure, evolutionary conservation, and conformational dynamics of Homo sapiens fascin-1, an F-actin crosslinking protein. *J. Mol. Biol. 400*(3), 589–604.

Seeger, M. A. and S. E. Rice (2010). Microtubule-associated protein-like binding of the kinesin-1 tail to microtubules. *J. Biol. Chem. 285*(11), 8155–8162.

Selden, L. A., H. J. Kinosian, J. Newman, B. Lincoln, C. Hurwitz, L. C. Gershman, and J. E. Estes (1998). Severing of F-actin by the amino-terminal half of gelsolin suggests internal cooperativity in gelsolin. *Biophys J 75*(6), 3092–3100.

Semenova, I., A. Burakov, N. Berardone, I. Zaliapin, B. Slepchenko, T. Svitkina, A. Kashina, and V. Rodionov (2008). Actin dynamics is essential for myosin-based transport of membrane organelles. *Curr. Biol. 18*(20), 1581–1586.

Sharlow, E. R., C. S. Paine, L. Babiarz, M. Eisinger, S. Shapiro, and M. Seiberg (2000). The protease-activated receptor-2 upregulates keratinocyte phagocytosis. *J. Cell. Sci. 113 (Pt 17)*, 3093–3101.

Shati, A. A., A. M. Alsuheel, A. A. Alshehri, and M. Y. Otaif (2013). A novel RAB-27a mutation causing Griscelli syndrome type 2 with severe central nervous system involvement: Case report and review of literature. *IJMMS 5*(11), 467–470.

Sheets, L., D. G. Ransom, E. M. Mellgren, S. L. Johnson, and B. J. Schnapp (2007). Zebrafish melanophilin (Mlpha) facilitates melanosome dispersion by regulating dynein. *Curr Biol 17*(20), 1721–1734.

Sheng, Z.-H. and Q. Cai (2012). Mitochondrial transport in neurons: impact on synaptic homeostasis and neurodegeneration. *Nat. Rev. Neurosci. 13*(2), 77–93.

Shirsat, N. V., R. J. Pignolo, B. L. Kreider, and G. Rovera (1990). A member of the ras gene superfamily is expressed specifically in T, B and myeloid hemopoietic cells. *Oncogene 5*(5), 769–772.

Shoji, K., K. Ohashi, K. Sampei, M. Oikawa, and K. Mizuno (2012). Cytochalasin D acts as an inhibitor of the actin-cofilin interaction. *Biochem. Biophys. Res. Commun. 424*(1), 52–57.

Shutes, A., A. C. Berzat, A. D. Cox, and C. J. Der (2004). Atypical Mechanism of Regulation of the Wrch-1 Rho Family Small GTPase. *Current Biology 14*(22), 2052–2056.

Silvers, W. K. (1979). Dilute and Leaden, the p-Locus, Ruby-Eye, and Ruby-Eye-2. In *The Coat Colors of Mice*, pp. 83–108. Springer New York.

Sindelar, C. V., M. J. Budny, S. Rice, N. Naber, R. Fletterick, and R. Cooke (2002). Two conformations in the human kinesin power stroke defined by X-ray crystallography and EPR spectroscopy. *Nat. Struct. Biol. 9*(11), 844–848.

Smith, M. A., E. Blankman, M. L. Gardel, L. Luettjohann, C. M. Waterman, and M. C. Beckerle (2010). A Zyxin-Mediated Mechanism for Actin Stress Fiber Maintenance and Repair. *Dev Cell 19*(3), 365–376.

Soldati, T., M. A. Riederer, and S. R. Pfeffer (1993). Rab GDI: a solubilizing and recycling factor for rab9 protein. *Mol Biol Cell 4*(4), 425–434.

Soppina, V., S. R. Norris, A. S. Dizaji, M. Kortus, S. Veatch, M. Peckham, and K. J. Verhey (2014). Dimerization of mammalian kinesin-3 motors results in superprocessive motion. *Proc. Natl. Acad. Sci. U.S.A. 111*(15), 5562–5567.

Spillane, M., A. Ketschek, T. T. Merianda, J. L. Twiss, and G. Gallo (2013). Mitochondria coordinate sites of axon branching through localized intra-axonal protein synthesis. *Cell Rep 5*(6), 1564–1575.

Stearns, T., L. Evans, and M. Kirschner (1991). Gamma-tubulin is a highly conserved component of the centrosome. *Cell 65*(5), 825–836.

Stenmark, H. (2009). Rab GTPases as coordinators of vesicle traffic. *Nat Rev Mol Cell Biol 10*(8), 513–525.

Stenmark, H., R. Aasland, and P. C. Driscoll (2002). The phosphatidylinositol 3-phosphate-binding FYVE finger. *FEBS Letters 513*(1), 77–84.

Stephens, R. E. (1970). Thermal fractionation of outer fiber doublet microtubules into A- and B-subfiber components. A- and B-tubulin. *J. Mol. Biol. 47*(3), 353–363.

Stinchcombe, J. C. and G. M. Griffiths (2001). Normal and abnormal secretion by haemopoietic cells. *Immunology 103*(1), 10–16.

Stinchcombe, J. C., L. J. Page, and G. M. Griffiths (2000). Secretory Lysosome Biogenesis in Cytotoxic T Lymphocytes from Normal and Chediak Higashi Syndrome Patients. *Traffic 1*(5), 435–444.

Stossel, T. P., J. Condeelis, L. Cooley, J. H. Hartwig, A. Noegel, M. Schleicher, and S. S. Shapiro (2001). Filamins as integrators of cell mechanics and signalling. *Nat. Rev. Mol. Cell Biol. 2*(2), 138–145.

Stowers, R. S., L. J. Megeath, J. Gorska-Andrzejak, I. A. Meinertzhagen, and T. L. Schwarz (2002). Axonal transport of mitochondria to synapses depends on milton, a novel Drosophila protein. *Neuron 36*(6), 1063–1077.

Straub, F. (1942). Actin. *Stud. Inst. Med. Chem. Szeged.*(II), 3–15.

Strobel, M. C., P. K. Seperack, N. G. Copeland, and N. A. Jenkins (1990). Molecular analysis of two mouse dilute locus deletion mutations: spontaneous dilute lethal20j and radiation-induced dilute prenatal lethal Aa2 alleles. *Mol. Cell. Biol. 10*(2), 501–509.

Strom, M., A. N. Hume, A. K. Tarafder, E. Barkagianni, and M. C. Seabra (2002). A family of Rab27-binding proteins. Melanophilin links Rab27a and myosin Va function in melanosome transport. *J. Biol. Chem. 277*(28), 25423–25430.

Suetsugu, S., S. Kurisu, T. Oikawa, D. Yamazaki, A. Oda, and T. Takenawa (2006). Optimization of WAVE2 complex-induced actin polymerization by membrane-bound IRSp53, PIP(3), and Rac. *J. Cell Biol. 173*(4), 571–585.

Sugden, D. and S. J. Rowe (1992). Protein kinase C activation antagonizes melatonin-induced pigment aggregation in Xenopus laevis melanophores. *J. Cell Biol. 119*(6), 1515–1521.

Sun, C. X., M. A. Magalhaes, and M. Glogauer (2007). Rac1 and Rac2 differentially regulate actin free barbed end formation downstream of the fMLP receptor. *J Cell Biol 179*(2), 239–245.

Sun, H. Q., M. Yamamoto, M. Mejillano, and H. L. Yin (1999). Gelsolin, a multifunctional actin regulatory protein. *J. Biol. Chem. 274*(47), 33179–33182.

Suraneni, P., B. Rubinstein, J. R. Unruh, M. Durnin, D. Hanein, and R. Li (2012). The Arp2/3 complex is required for lamellipodia extension and directional fibroblast cell migration. *J. Cell Biol. 197*(2), 239–251.

Swank, R. T., S. Y. Jiang, M. Reddington, J. Conway, D. Stephenson, M. P. McGarry, and E. K. Novak (1993). Inherited abnormalities in platelet organelles and platelet formation and associated altered expression of low molecular weight guanosine triphosphate-binding proteins in the mouse pigment mutant gunmetal. *Blood 81*(10), 2626–2635.

Takenawa, T. and S. Suetsugu (2007). The WASP–WAVE protein network: connecting the membrane to the cytoskeleton. *Nat Rev Mol Cell Biol 8*(1), 37–48.

Tanaka, Y., Y. Kanai, Y. Okada, S. Nonaka, S. Takeda, A. Harada, and N. Hirokawa (1998). Targeted disruption of mouse conventional kinesin heavy chain, kif5b, results in abnormal perinuclear clustering of mitochondria. *Cell 93*(7), 1147–1158.

Tao, W., D. Pennica, L. Xu, R. F. Kalejta, and A. J. Levine (2001). Wrch-1, a novel member of the Rho gene family that is regulated by Wnt-1. *Genes Dev. 15*(14), 1796–1807.

Tarafder, A. K., G. Bolasco, M. S. Correia, F. J. C. Pereira, L. Iannone, A. N. Hume, N. Kirkpatrick, M. Picardo, M. R. Torrisi, I. P. Rodrigues, J. S. Ramalho, C. E. Futter, D. C. Barral, and M. C. Seabra (2014). Rab11b mediates melanin transfer between donor melanocytes and acceptor keratinocytes via coupled exo/endocytosis. *J. Invest. Dermatol. 134*(4), 1056–1066.

Tarafder, A. K., C. Wasmeier, A. C. Figueiredo, A. E. G. Booth, A. Orihara, J. S. Ramalho, A. N. Hume, and M. C. Seabra (2011). Rab27a targeting to melanosomes requires nucleotide exchange but not effector binding. *Traffic 12*(8), 1056–1066.

Tasken, K. and E. M. Aandahl (2004). Localized effects of cAMP mediated by distinct routes of protein kinase A. *Physiol. Rev. 84*(1), 137–167.

Theos, A. C., D. Tenza, J. A. Martina, I. Hurbain, A. A. Peden, E. V. Sviderskaya, A. Stewart, M. S. Robinson, D. C. Bennett, D. F. Cutler, J. S. Bonifacino, M. S. Marks, and G. Raposo (2005). Functions of adaptor protein (AP)-3 and AP-1 in tyrosinase sorting from endosomes to melanosomes. *Mol. Biol. Cell 16*(11), 5356–5372.

Theos, A. C., S. T. Truschel, G. Raposo, and M. S. Marks (2005). The Silver locus product Pmel17/gp100/Silv/ME20: controversial in name and in function. *Pigment Cell Research 18*(5), 322–336.

Thormählen, M., A. Marx, S. Sack, and E. Mandelkow (1998). The coiled-coil helix in the neck of kinesin. *J. Struct. Biol. 122*(1-2), 30–41.

Tomita, Y., T. Suzuki, Y. Tomita, and T. Suzuki (2004). Genetics of pigmentary disorders, Genetics of pigmentary disorders. *American Journal of Medical Genetics Part C: Seminars in Medical Genetics, American Journal of Medical Genetics Part C: Seminars in Medical Genetics 131C, 131C*(1, 1), 75, 75–81, 81.

Tran, P. T., P. Joshi, and E. D. Salmon (1997). How tubulin subunits are lost from the shortening ends of microtubules. *J. Struct. Biol. 118*(2), 107–118.

Trokter, M., N. Mücke, and T. Surrey (2012). Reconstitution of the human cytoplasmic dynein complex. *Proc. Natl. Acad. Sci. U.S.A. 109*(51), 20895–20900.

Trybus, K. M. (2008). Myosin V from head to tail. *Cell Mol Life Sci 65*(9), 1378–1389.

Tuma, M. C., A. Zill, N. Le Bot, I. Vernos, and V. Gelfand (1998). Heterotrimeric kinesin II is the microtubule motor protein responsible for pigment dispersion in Xenopus melanophores. *J. Cell Biol. 143*(6), 1547–1558.

Tzima, E., P. J. Trotter, M. A. Orchard, and J. H. Walker (2000). Annexin V relocates to the platelet cytoskeleton upon activation and binds to a specific isoform of actin. *Eur. J. Biochem. 267*(15), 4720–4730.

Ubersax, J. A. and J. E. Ferrell Jr (2007). Mechanisms of specificity in protein phosphorylation. *Nat Rev Mol Cell Biol 8*(7), 530–541.

Ushakov, D. S. (2009). Structure and function of the essential light chain of myosin. *BIOPHYSICS 53*(6), 505–509.

Vale, R. D., T. S. Reese, and M. P. Sheetz (1985). Identification of a novel force-generating protein, kinesin, involved in microtubule-based motility. *Cell 42*(1), 39–50.

Valencia, J. C., H. Watabe, A. Chi, F. Rouzaud, K. G. Chen, W. D. Vieira, K. Takahashi, Y. Yamaguchi, W. Berens, K. Nagashima, J. Shabanowitz, D. F. Hunt, E. Appella, and V. J. Hearing (2006). Sorting of Pmel17 to melanosomes through the plasma membrane by AP1 and AP2: evidence for the polarized nature of melanocytes. *J. Cell. Sci. 119*(Pt 6), 1080–1091.

van der Kant, R., A. Fish, L. Janssen, H. Janssen, S. Krom, N. Ho, T. Brummelkamp, J. Carette, N. Rocha, and J. Neefjes (2013). Late endosomal transport and tethering are coupled processes controlled by RILP and the cholesterol sensor ORP1l. *J. Cell. Sci. 126*(Pt 15), 3462–3474.

Vancoillie, G., J. Lambert, A. Mulder, H. K. Koerten, A. M. Mommaas, P. Van Oostveldt, and J. M. Naeyaert (2000a). Cytoplasmic dynein colocalizes with melanosomes in normal human melanocytes. *Br. J. Dermatol. 143*(2), 298–306.

Vancoillie, G., J. Lambert, A. Mulder, H. K. Koerten, A. M. Mommaas, P. Van Oostveldt, and J. M. Naeyaert (2000b). Kinesin and kinectin can associate with the melanosomal surface and form a link with microtubules in normal human melanocytes. *J. Invest. Dermatol. 114*(3), 421–429.

Vancoillie, G., J. Lambert, Y. Vander Haeghen, W. Westbroek, A. Mulder, H. K. Koerten, A. Mieke Mommaas, P. Van Oostveldt, and J. M. Naeyaert (2000). Colocalization of Dynactin Subunits P150glued and P50 with Melanosomes in Normal Human Melanocytes. *Pigment Cell Research 13*(6), 449–457.

Varga, V., J. Helenius, K. Tanaka, A. A. Hyman, T. U. Tanaka, and J. Howard (2006). Yeast kinesin-8 depolymerizes microtubules in a length-dependent manner. *Nat Cell Biol 8*(9), 957–962.

Vartiainen, M. K., T. Mustonen, P. K. Mattila, P. J. Ojala, I. Thesleff, J. Partanen, and P. Lappalainen (2002). The three mouse actin-depolymerizing factor/cofilins evolved to fulfill cell-type-specific requirements for actin dynamics. *Mol. Biol. Cell 13*(1), 183–194.

Vaughan, P. S., P. Miura, M. Henderson, B. Byrne, and K. T. Vaughan (2002). A role for regulated binding of p150glued to microtubule plus ends in organelle transport. *J Cell Biol 158*(2), 305–319.

Verhey, K. J., D. L. Lizotte, T. Abramson, L. Barenboim, B. J. Schnapp, and T. A. Rapoport (1998). Light Chain– dependent Regulation of Kinesin's Interaction with Microtubules. *J Cell Biol 143*(4), 1053–1066.

Verkhovsky, A. B., T. M. Svitkina, and G. G. Borisy (1997). Polarity sorting of actin filaments in cytochalasin-treated fibroblasts. *J. Cell. Sci. 110 (Pt 15)*, 1693–1704.

Vicente-Manzanares, M., X. Ma, R. S. Adelstein, and A. R. Horwitz (2009). Non-muscle myosin II takes centre stage in cell adhesion and migration. *Nat Rev Mol Cell Biol 10*(11), 778–790.

Vilfan, A. (2008). Myosin V passing over Arp2/3 junctions: branching ratio calculated from the elastic lever arm model. *Biophys. J. 94*(9), 3405–3412.

Vitre, B., F. M. Coquelle, C. Heichette, C. Garnier, D. Chrétien, and I. Arnal (2008). EB1 regulates microtubule dynamics and tubulin sheet closure in vitro. *Nat. Cell Biol. 10*(4), 415–421.

Vizcarra, C. L., B. Kreutz, A. A. Rodal, A. V. Toms, J. Lu, W. Zheng, M. E. Quinlan, and M. J. Eck (2011). Structure and function of the interacting domains of Spire and Fmn-family formins. *Proc Natl Acad Sci U S A 108*(29), 11884–11889.

Vogel, C. and E. M. Marcotte (2012). Insights into the regulation of protein abundance from proteomic and transcriptomic analyses. *Nat. Rev. Genet. 13*(4), 227–232.

Voter, W. A. and H. P. Erickson (1984). The kinetics of microtubule assembly. Evidence for a two-stage nucleation mechanism. *J. Biol. Chem. 259*(16), 10430–10438.

Wakatsuki, T., B. Schwab, N. C. Thompson, and E. L. Elson (2001). Effects of cytochalasin D and latrunculin B on mechanical properties of cells. *J. Cell. Sci. 114*(Pt 5), 1025–1036.

Walker, J. E., M. Saraste, M. J. Runswick, and N. J. Gay (1982). Distantly related sequences in the alpha- and beta-subunits of ATP synthase, myosin, kinases and other ATP-requiring enzymes and a common nucleotide binding fold. *EMBO J. 1*(8), 945–951.

Walker, M. L., S. A. Burgess, J. R. Sellers, F. Wang, J. A. Hammer, 3rd, J. Trinick, and P. J. Knight (2000). Two-headed binding of a processive myosin to F-actin. *Nature 405*(6788), 804–807.

Wallar, B. J., B. N. Stropich, J. A. Schoenherr, H. A. Holman, S. M. Kitchen, and A. S. Alberts (2006). The basic region of the diaphanous-autoregulatory domain (DAD) is required for autoregulatory interactions with the diaphanous-related formin inhibitory domain. *J. Biol. Chem. 281*(7), 4300–4307.

Wang, C. C., D. C. Chan, and P. Leder (1997). The mouse formin (Fmn) gene: genomic structure, novel exons, and genetic mapping. *Genomics 39*(3), 303–311.

Wang, F. S., J. S. Wolenski, R. E. Cheney, M. S. Mooseker, and D. G. Jay (1996). Function of myosin-V in filopodial extension of neuronal growth cones. *Science 273*(5275), 660–663.

Warshaw, D. M., G. G. Kennedy, S. S. Work, E. B. Krementsova, S. Beck, and K. M. Trybus (2005). Differential Labeling of Myosin V Heads with Quantum Dots Allows Direct Visualization of Hand-Over-Hand Processivity. *Biophys J 88*(5), L30–L32.

Wasmeier, C., M. Romao, L. Plowright, D. C. Bennett, G. Raposo, and M. C. Seabra (2006). Rab38 and Rab32 control post-Golgi trafficking of melanogenic enzymes. *J. Cell Biol. 175*(2), 271–281.

Watanabe, M., H. D. G. Fiji, L. Guo, L. Chan, S. S. Kinderman, D. J. Slamon, O. Kwon, and F. Tamanoi (2008). Inhibitors of Protein Geranylgeranyltransferase I and Rab Geranylgeranyltransferase Identified from a Library of Allenoate-derived Compounds. *J Biol Chem 283*(15), 9571–9579.

Watanabe, N., T. Kato, A. Fujita, T. Ishizaki, and S. Narumiya (1999). Cooperation between mDia1 and ROCK in Rho-induced actin reorganization. *Nat. Cell Biol. 1*(3), 136–143.

Wegner, A. and J. Engel (1975). Kinetics of the cooperative association of actin to actin filaments. *Biophys. Chem. 3*(3), 215–225.

Wei, M. L. (2006). Hermansky-Pudlak syndrome: a disease of protein trafficking and organelle function. *Pigment Cell Res. 19*(1), 19–42.

Weisenberg, R. C., G. G. Borisy, and E. W. Taylor (1968). The colchicine-binding protein of mammalian brain and its relation to microtubules. *Biochemistry 7*(12), 4466–4479.

Welch, M. D., A. H. DePace, S. Verma, A. Iwamatsu, and T. J. Mitchison (1997). The Human Arp2/3 Complex Is Composed of Evolutionarily Conserved Subunits and Is Localized to Cellular Regions of Dynamic Actin Filament Assembly. *J Cell Biol 138*(2), 375–384.

Welch, M. D. and R. D. Mullins (2002). Cellular Control of Actin Nucleation. *Annual Review of Cell and Developmental Biology 18*(1), 247–288.

Wendt, T., D. Taylor, K. M. Trybus, and K. Taylor (2001). Three-dimensional image reconstruction of dephosphorylated smooth muscle heavy meromyosin reveals asymmetry in the interaction between myosin heads and placement of subfragment 2. *Proc. Natl. Acad. Sci. U.S.A. 98*(8), 4361–4366.

White, B. H., R. D. Sekura, and M. D. Rollag (1987). Pertussis toxin blocks melatonin-induced pigment aggregation in Xenopus dermal melanophores. *J. Comp. Physiol. B, Biochem. Syst. Environ. Physiol. 157*(2), 153–159.

Wilson, S. M., R. Yip, D. A. Swing, T. N. O'Sullivan, Y. Zhang, E. K. Novak, R. T. Swank, L. B. Russell, N. G. Copeland, and N. A. Jenkins (2000). A mutation in Rab27a causes the vesicle transport defects observed in ashen mice. *Proc. Natl. Acad. Sci. U.S.A. 97*(14), 7933–7938.

Wloga, D., D. Dave, J. Meagley, K. Rogowski, M. Jerka-Dziadosz, and J. Gaertig (2010). Hyperglutamylation of tubulin can either stabilize or destabilize microtubules in the same cell. *Eukaryotic Cell 9*(1), 184–193.

Woehlke, G., A. K. Ruby, C. L. Hart, B. Ly, N. Hom-Booher, and R. D. Vale (1997). Microtubule interaction site of the kinesin motor. *Cell 90*(2), 207–216.

Woehlke, G. and M. Schliwa (2000). Walking on two heads: the many talents of kinesin. *Nat. Rev. Mol. Cell Biol. 1*(1), 50–58.

Woolner, S. and W. M. Bement (2009). Unconventional myosins acting unconventionally. *Trends Cell Biol. 19*(6), 245–252.

Woźniak, M. J. and V. J. Allan (2006). Cargo selection by specific kinesin light chain 1 isoforms. *EMBO J 25*(23), 5457–5468.

Wright, B. D., M. Terasaki, and J. M. Scholey (1993). Roles of kinesin and kinesin-like proteins in sea urchin embryonic cell division: evaluation using antibody microinjection. *J Cell Biol 123*(3), 681–689.

Wu, J.-Q. and T. D. Pollard (2005). Counting cytokinesis proteins globally and locally in fission yeast. *Science 310*(5746), 310–314.

Wu, L.-G., E. Hamid, W. Shin, and H.-C. Chiang (2014). Exocytosis and endocytosis: modes, functions, and coupling mechanisms. *Annu. Rev. Physiol. 76*, 301–331.

Wu, X., B. Bowers, K. Rao, Q. Wei, and H. JA (1998). Visualization of melanosome dynamics within wild-type and dilute melanocytes suggests a paradigm for myosin V function In vivo. *J. Cell Biol. 143*(7), 1899–1918.

Wu, X., K. Rao, M. B. Bowers, N. G. Copeland, N. A. Jenkins, and J. A. Hammer (2001). Rab27a enables myosin Va-dependent melanosome capture by recruiting the myosin to the organelle. *J. Cell. Sci. 114*(Pt 6), 1091–1100.

Wu, X. S., A. Masedunskas, R. Weigert, N. G. Copeland, N. A. Jenkins, and J. A. Hammer (2012). Melanoregulin regulates a shedding mechanism that drives melanosome transfer from melanocytes to keratinocytes. *Proc. Natl. Acad. Sci. U.S.A. 109*(31), E2101–2109.

Xu, K., P. M. Schwarz, and R. F. Luduena (2002). Interaction of nocodazole with tubulin isotypes. *Drug Dev. Res. 55*(2), 91–96.

Xu, Y., S. Takeda, T. Nakata, Y. Noda, Y. Tanaka, and N. Hirokawa (2002). Role of KIFC3 motor protein in Golgi positioning and integration. *J. Cell Biol. 158*(2), 293–303.

Yadav, S. and A. D. Linstedt (2011). Golgi positioning. *Cold Spring Harb Perspect Biol 3*(5).

Yadav, S., M. A. Puthenveedu, and A. D. Linstedt (2012). Golgin160 recruits the dynein motor to position the Golgi apparatus. *Dev. Cell 23*(1), 153–165.

Yang, H.-C. and L. A. Pon (2002). Actin cable dynamics in budding yeast. *Proc. Natl. Acad. Sci. U.S.A. 99*(2), 751–756.

Yang, J. T., W. M. Saxton, R. J. Stewart, E. C. Raff, and L. S. Goldstein (1990). Evidence that the head of kinesin is sufficient for force generation and motility in vitro. *Science 249*(4964), 42–47.

Yang, W., C. Li, D. M. Ward, J. Kaplan, and S. L. Mansour (2000). Defective organellar membrane protein trafficking in Ap3b1-deficient cells. *J. Cell. Sci. 113 (Pt 22)*, 4077–4086.

Yayoshi-Yamamoto, S., I. Taniuchi, and T. Watanabe (2000). FRL, a novel formin-related protein, binds to Rac and regulates cell motility and survival of macrophages. *Mol. Cell. Biol. 20*(18), 6872–6881.

Ye, J., G. Coulouris, I. Zaretskaya, I. Cutcutache, S. Rozen, and T. L. Madden (2012). Primer-BLAST: a tool to design target-specific primers for polymerase chain reaction. *BMC Bioinformatics 13*, 134.

Yeoh, S., B. Pope, H. G. Mannherz, and A. Weeds (2002). Determining the differences in actin binding by human ADF and cofilin. *J. Mol. Biol. 315*(4), 911–925.

Yildiz, A., M. Tomishige, R. D. Vale, and P. R. Selvin (2004). Kinesin Walks Hand-Over-Hand. *Science 303*(5658), 676 –678.

Zanic, M., J. H. Stear, A. A. Hyman, and J. Howard (2009). EB1 Recognizes the Nucleotide State of Tubulin in the Microtubule Lattice. *PLoS One 4*(10).

Zelickson, A. S., D. B. Windhorst, J. G. White, and R. A. Good (1967). The Chediak-Higashi Syndrome: Formation of Giant Melanosomes and the Basis of Hypopigmentation1. *The Journal of Investigative Dermatology 49*(6), 575–581.

Zeth, K., M. Pechlivanis, A. Samol, S. Pleiser, C. Vonrhein, and E. Kerkhoff (2011). Molecular basis of actin nucleation factor cooperativity: crystal structure of the Spir-1 kinase non-catalytic C-lobe domain (KIND)•formin-2 formin SPIR interaction motif (FSI) complex. *J. Biol. Chem. 286*(35), 30732–30739.

Zheng, Y., M. K. Jung, and B. R. Oakley (1991). Gamma-tubulin is present in Drosophila melanogaster and Homo sapiens and is associated with the centrosome. *Cell 65*(5), 817–823.

Zheng, Y., M. L. Wong, B. Alberts, and T. Mitchison (1995). Nucleation of microtubule assembly by a gamma-tubulin-containing ring complex. *Nature 378*(6557), 578–583.

Zhou, F., P. Leder, and S. S. Martin (2006). Formin-1 protein associates with microtubules through a peptide domain encoded by exon-2. *Exp. Cell Res. 312*(7), 1119–1126.

Zhou, K., K. D. Sumigray, and T. Lechler (2015). The Arp2/3 complex has essential roles in vesicle trafficking and transcytosis in the mammalian small intestine. *Mol. Biol. Cell 26*(11), 1995–2004.

Zigmond, S. H., M. Evangelista, C. Boone, C. Yang, A. C. Dar, F. Sicheri, J. Forkey, and M. Pring (2003). Formin leaky cap allows elongation in the presence of tight capping proteins. *Curr. Biol. 13*(20), 1820–1823.